2nd INTERNATIONAL ENGINEERING SYMPOSIUM – IES2012

(KU-MU-NITK-HCMCUT Joint Symposium)

100th Anniversary Memorial Hall &
Faculty of Engineering (Building No.2)

Kumamoto University

March 5-7, 2012





Conveners

Shuichi TORII
Professor, Department of Mechanical System Engineering
Kumamoto University, Japan

&

Katta VENKATARAMANA
Professor, Department of Civil Engineering
NITK, Surathkal, India

Organized by
Graduate School of Science & Technology
Kumamoto University, Japan

PROCEEDINGS OF

2nd INTERNATIONAL ENGINEERING SYMPOSIUM – IES2012

(KU-MU-NITK-HCMCUT Joint Symposium)

Venue

100th Anniversary Memorial Hall & Faculty of Engineering (Building No.2)
Kumamoto University

Date

March 5-7, 2012

Conveners

Shuichi TORII
Professor, Department of Mechanical System Engineering
Kumamoto University, Japan

&

Katta VENKATARAMANA
Professor, Department of Civil Engineering
NITK, Surathkal, India

Organized by

Graduate School of Science & Technology
Kumamoto University
Kumamoto City, Japan

PREFACE

The 1st International Engineering Symposium (IES 2011) was organized very successfully at Kumamoto University during March 3-5, 2011 with more than 100 participants from India, Indonesia, Vietnam, Taiwan, Hong Kong and Japan. With the objective of continuing the interaction initiated between the researchers during IES2011, the **2nd International Engineering Symposium (IES 2012)** has been organized during March 2012 in similar lines. This symposium intends to provide a common platform for bringing together researchers for expanding academic collaboration.

This time, the event focuses on the joint symposium among the four collaborating academic institutions: Kumamoto University (KU), Manipal University (MU), National Institute of Technology Karnataka (NITK) and Ho Chi Minh City University of Technology (HCMCUT).

The researchers from abroad have been invited to visit Kumamoto University and get familiar with its educational and research activities. The event focuses on the current research and development of the participating institutions on topics of mutual interest, with special emphasis on "Science & Technology". The emerging technologies and scientific advancements are discussed during the symposium. Presentations feature new and innovative technologies in the relevant fields.

This proceedings volume contains the technical papers presented at the symposium. The topics include a wide spectrum of themes covering all major disciplines of science and engineering. The efforts by faculty, staff and students of Kumamoto University in organizing this event are greatly appreciated.

We sincerely hope that all the readers will find the contents of this proceedings volume useful and productive. We look forward to more intense academic collaborations and research interactions in the coming days, to achieve the common goal of technological advancement for global peace and prosperity.

Shuichi Torii
Katta Venkataramana
Conveners

IES2012 Program Schedule

Venue: Faculty of Engineering, Building No.2

March 5, 2012 (Monday)

10:00 –10:30	Registration
10:30 – 11:10	**Opening session** (*Welcome address, Introduction to KU, Group Photo*)
11:10 – 11:30	Tea Break
11:30 - 12:45	**Keynote Lectures *(K1)***
12:45 – 14:00	Lunch Break
14:00 – 17:00	**Campus Tour & Laboratory Visits**
17:00 – 17:30	Free Time
17:30 – 19:00	Welcome Reception

March 6, 2012 (Tuesday)

9:30 – 11:00	**Technical Sessions** *(M1,C1,B1,E1)*
11:00 – 11:30	Break
11:30 - 12:45	**Technical Sessions** *(M2,C2,B2,E2)*
12:45 – 14:00	Lunch Break
14:00 – 15:30	**Technical Sessions** *(M3,C3,B3,A1)*
15:30 – 16:00	Break
16:00 – 17:00	**Technical Sessions** *(C4,B4,A2)*
17:00 – 17:30	Free time
17:30 – 19:00	Symposium Dinner

March 7, 2012 (Wednesday)

9:00 – 17:00	**Field visits**

Lunch & Dinner Venue - FORICO Cafeteria

Notations:

K Keynote Lectures
M Technical Sessions (Mechanical Engineering & Related Fields)
C Technical Sessions (Civil Engineering, Earth Sciences & Related Fields)
A Technical Sessions (Architecture & Related Fields)
B Technical Sessions (Biotechnology, Chemical Engineering & Related Fields)
E Technical Sessions (Electrical, Electronics, Computer Engineering & Related Fields)

Contents

Keynote Lectures

K1-1 A Review of Applications of Computational Fluid Dynamics in Multi-Domain Engineering
N Yagnesh Sharma

K1-2 Rainwater harvesting as an adaptation measure to climate change: An implication for Ho Chi Minh City, Vietnam
Phu Le Vo, Vo Thi Thu Tinh, Phan Huynh Cam Tu, Ha Pham Thuy Dung, Nguyen Van Dien and Trinh Thi Bich Huyen

K1-3 Virtues of Earth Science and its Vistas in Engineering Applications - A Typical Analysis
D Venkat Reddy

Mechanical Engineering & Related Fields

M1-1 Design and Control of a Low Cost Wheeled Inverted Pendulum Robot
Jatheendranath and Prasad Krishna

M1-2 Development of the suitable combustor and combustion characteristic of biofuels
Shun Matsuda and Shuichi Torii

M1-3 A study of conversion diesel engine to fully biogas engine with electronically controlled
Nguyen Ngoc Dung, Vo Le Hoai Phuong, Phan The Anh and Tran Dang Long

M1-4 Numerical analysis of gas turbine HP stage blade cooling with new cooling duct geometries
Chandrakant R Kini, Satish Shenoy B and N Yagnesh Sharma

M1-5 Analysis of elliptical perforated tube muffler - *Sohei Nishimura , Yuya Nishimura*

M1-6 Study on the Air Ventilation Grille - *Yuya Nishimura, Sohei Nishimura*

M2-1 Electrochemical investigation of corrosion behaviour of mild steel by Thiourea derivatives in hydrochloric acid solution
S. Divakara Shetty

M2-2 Study of gaseous fuelled motorcycle with electronically controlled gas injection system
Truong Hoai Linh, Le Dang Khoa, Tran Dang Long and Nguyen Ngoc Dung

M2-3 Performance, emissions & cyclic combustion studies of CI engine using Jatropha B20 fuel *A.B.V. Barboza, C.V. Sudhir and N. Yagnesh Sharma*

M2-4 The obstacle effect to the mixing efficiency in X-shaped micro channel
Shu-Min Tu, Shuichi Torii and Yang-Cheng Shih

M2-5 Heat transfer enhancement of Al_2O_3 nanofluid dispersed in Ethylene Glycol
Hajime Yoshino and Shuichi Torii

M3-1 Heat transfer performance of a multiple-heat pipe cooling device using pure water and alumina (Al_2O_3) nanofluid respectively as working fluid
Dao Danh Tung and Shuichi Torii

M3-2 The effect of heat transfer plate attached acrylic blocks near the inlet & outlet area of plate heat exchanger
Takato Yamamoto and Shuichi Torii

M3-3 Thermal fluid flow transport characteristics in confined channels with turbulent dual jet impingement
Caner Senkal and Shuichi Torii

M3-4 Study of thermal fluid flow and Venturi effect
Giichi Nakamuta, Shuichi Torii

M3-5 Investigation of combustion furnace fuelled by compost
Shota Watanabe and Shuichi Torii

M3-6 Research on the energy utilization with bio oil
Kenichi Matsumoto and Shuichi Torii

Civil Engineering, Earth Sciences & Related Fields

C1-1 Performance of high strength concrete subjected to elevated temperatures
Kishor S. Kulkarni, Subhash C. Yaragal and K S Babu Narayan

C1-2 Earthquake vulnerability assessment of buildings in Guwahati
Ajit Kamath Manohar, Kaustav Sengupta, Tamizharasi G and Indrani Gogoi

C1-3 Magnetorheological dampers – An overview
Tamizharasi G, Ajit Kamath Manohar, Kaustav Sengupta, Katta Venkataramana and Umesh G

C1-4 Experimental investigations on the flexural strength of reinforced concrete beams
Poornachand Pandit, Akshatha Shetty, Katta Venkataramama, K.S.Babunarayan, Indrani Gogoi, Praveen B.B, Mahesha, Shivaprasad Naik and Arun Sedamkar

C1-5 Experimental Study on Deterioration Monitoring of Shirasu Concrete in Hot Spring Environment
Dhruva Narayana Katpady, Koji Takewaka, Toshinobu Yamaguchi, Yasuyuki Moritaka and Yuuki Tatara

C2-1 Estimation of aquifer parameters using inverse modeling by incorporating prior information about rainfall recharge factor as constraints - *M K Nagaraj*

C2-2 Comparative analysis of ET_o using AWS data - *B.M. Dodamani and Shwetha*

C2-3 *CUBE* based trip generation using iterative zone-reclassification, and distribution for Bangalore - *Varghese George, Subramanyam U. and Amit S. Mahendrakar*

C2-4 Road Development in Mangalore City – A Scenario
Chandan C Gowda, H C Chinnagiri Gowda and Arun Kumar G

C3-1 Characteristics of Malabar laterite as a building material-Field and Laboratory studies
Kasthurba A K

C3-2 Damage level prediction of non-reshaped berm breakwater using ANFIS
S. Mandal, Subba Rao, Harish N and Lokesha

C3-3 Wave run-up, run-down studies on reshaped berm breakwater with artificial armour units - *Prashanth J, Subba Rao, Kiran G Shirlal, Balakrishna Rao K and Vishwanath N*

C3-4 Spectral characteristics of sediments in the Ba Lat estuary (Northern Vietnam) in relation to sediment properties for remotely sensed tidal flats monitoring
Nguyen Thi Ngoc and Katsuaki Koike

C3-5 Solid waste management for residential and commercial areas in India
Dibya Jivan Pati

C4-1 Impacts of the land subsidence on sustainable urban development
Le Van Trung and Vuong Quoc Viet

C4-2 Flexural fatigue analysis of steel fibre reinforced concrete
Girish M G, A Chandrashekar and A U Ravi Shankar

C4-3 Microstructure analysis of concrete subjected to elevated temperatures using mercury intrusion porosimetry
Sharath S, Sandesh V, Subhash C Yaragal, K S Babu Narayan and K Suryanarayana

C4-4 Relation between UPV and residual strength of concrete subjected to heating and sudden cooling - *Shree Laxmi Prashant, Subhash C Yaragal and K S Babu Narayan*

C5-1 Coordinated traffic signaling for three major junctions of Mangalore City using TRANSYT-12 - *Varghese George and Hemanth K R*

Architecture & Related Fields

A1-1 A field study on the moderating effect of sound absorption on the noisy sound environment in nursery school classrooms
Kazuaki Sakoda Munehide Saito, and Keiji Kawai

A1-2 Community response to aircraft and road traffic noises in Da Nang City, Vietnam
Thu Lan Nguyen, Takashi Yano, Huy Quang Nguyen, Khanh Tuyen Nguyen, Hiroaki Fukushima, Keiji Kawai, Tsuyoshi Nishimura, and Tetsumi Sato

A1-3 A mapping of recognition structure based on human life history
Kaoru Ono and Yuji Hoshino

A1-4 The relevance of physical configuration to mental map of town
Deepika Shetty and B. S. Bhooshan

A1-5 Application of digital documentation techniques for conservation of a Buddhist Stupa through virtual reconstruction - *Kailash Rao M and Srikumar M. Menon*

A1-6 Bio aesthetic aspects of planning for residential gardens in Mysore City, Karnataka, India - *Padmashree Urs M.K*

A2-1 Wood: A natural choice as a green building material – A key to a sustainable future
Roshan S. Shetty

A2-2 Gated communities in India – An overview
Sanghamitra Roy

A2-3 Strengthening imageability of an old urban core - a pilgrimage
Soumi Muhuri

A2-4 Primitive invention of mankind - earth architecture; case study at Wayanad, S.India
Kala Choyimanikandiyil

Electrical, Electronics, Computer Engineering & Related Fields

E1-1 Maximin degree domination number in graphs
S. S. Kamath and Prameela Kolake

E1-2 Initial e-learning pilot system for secondary educational institutions in Tuvalu
Atufenua Maui , Tony Kwato'o, Royyana M. Ijtihadia, Ronald Vetter, Yoshifumi Chisaki and Tsuyoshi Usagawa

E1-3 20 μW, 500 kHz Continuous-Time Low-Pass Filter in 0.18 μm CMOS Process
Vasantha M.H. and Tonse Laxminidhi

E1-4 Preserving privacy in data streams query processing on synopses
An Ngoc Thien NGUYEN, Tran Khanh DANG, Nam THOAI and Ngoc Hieu DUONG

E2-1 Charging method for an electric vehicle using a computerized ultra fast charger at recharge stations in India
Hafeez Basha R, Raju A and Nikhil Prakash P

E2-2 Experimental Evaluation of Recovery Algorithms of TCP in Wireless Networks
Vikash Kumar, Annappa B and Mohit P. Tahiliani

E2-3 Machine learning based intrusion detection systems using RSC
Sanoop Mallissery and Shahana Sathar

E2-4 Complexity Analysis of Simulink Models to Improve the Quality of Outsourcing in an Automotive Company
Jeevan Prabhu, Alexander Serebrenik and Sanjay Singh

E2-5 Round Robin Approach to Intrusion Detection System on SNMP
Ekansh Jitendra Gupta, Mayank Nayar and Raunaq Akhauri

Biotechnology, Chemical engineering & Related fields

B1-1 Studies on the Production of Camptothecin from an Endophytic Fungi Fusarium Sp
Sogra Fathima B, Krishna Kumar A J and Raj Mohan B

B1-2 Isolation of halophilic bacteria for ectoine, xylanase, cellulase production from agro-wastes
Pooja Shivanand, Gopal Mugeraya and Hitesh Chhabra

B1-3 Research on wastewater treatment by expanded granular sludge bed (EGSB) reactor using Polyvinyl alcohol (PVA) carrier
Vu Dinh Khang and Nguyen Tan Phong

B1-4 BIC model coupled with DOE to simulate supercritical fluid extraction of 10-DAB III from Taxus Wallichiana Zucc
Nguyen Quang Duy, Chau Ngoc Do Quyen, Phan Dinh Tuan, Mitsuru Sasaki, Motonobu Goto and Le Thi Kim Phung

B1-5 Optimization of conditions for extraction of collagen from the skin of Pangasius hypophthalmus by response surface methodology
Le Thi Thu Huong, Phan Ngoc Hoa, Nguyen Hoang Dung and Phan Dinh Tuan

B2-1 Neural network modeling of urea release from briquettes
M Ramananda Bhat, D V R Murthy and M B Saidutta

B2-2 Use of granular activated carbon for the enhancement of phenol removal from wastewater by Electrocoagulation
Rajesh Pachimatla and B. Prasad

B2-3 Comparison of LAM-DONG and PHU-YEN diatomite as raw materials for filter aid manufacture
Tran Duy Hai and Mai Thanh Phong

B2-4 Application of ultrasound and hemicellulase preparation to acerola juice processing
Nguyen Thi Xuan Lan, Vuong Thi My Thanh and Le Van Viet Man

B3-1 Use of Koji in production of fish sauce from the waste of fishery processing plant
Do Minh Hien, Huynh T. Truc Hang, Huynh T. Viet, Phan N. Hoa, Nguyen T. Thu Ha, Nguyen T. Hang, Shindo Jo and Nguyen Hoang Dzung

B3-2 Comparative studies on the total anti-oxidant activity of certain plant species unique to Western Ghats of India
Farhana K, Pavithra G S and Raj Mohan B

B3-3 Removing of Nitrogen from Landfill Leachate by Single-Stage Using Anammox and Partial Nitritation (SNAP) with Acrylic Pile Fabrics as Biomass Carrier
Pham Van Sung and Nguyen Tan Phong

B3-4 Nitrogen Removal from Landfill Leachate by Single-Stage Using Anammox and Partial Nitritation (SNAP) with BioFix as Biomass Carrier
Dao Vinh Loc and Nguyen Tan Phong

B3-5 Efficiency Treatment of Two-Stage Vertical Constructed Wetland System Planted with Phragmites australis (Cav.) and Vetiveria zizanioides (L.) for Domestic Wastewater Treatment
Nguyen Tan Phong and Dao Khanh Chau

B4-1 Microwave-assisted extraction and identification of antioxidants from Nerium oleander and determination of its total activity
Pavithra G S, Farhana K and Raj Mohan B

B4-2 Effect of Culture Conditions on the Production of Laccase by an Unidentified Basidiomycete-F-35b
Gopal Mugeraya , Akshata Hoskeri and Harisha Poojary

B4-3 Detoxification of Phorbol esters from Jatropha Seed Cake by White Rot Fungi
Sampath S Muddada, Ramesh Ramanujam, Chaitanya Kilaparthi, Harisha Poojary and Gopal Mugeraya

KEYNOTE LECTURES

2nd International Engineering Symposium - IES 2012
(KU-MU-NITK-HCMCUT Joint Symposium) March 5-7, 2012, Kumamoto University, Japan

A Review of Applications of Computational Fluid Dynamics in Multi-Domain Engineering

Dr.N. Yagnesh Sharma [1]

1 *Professor, Department of Mechanical and Manufacturing Engineering, Manipal Institute of Technology, Manipal University, Manipal-576104. Karnataka,India. email : yagnesh.sharma@manipal.edu*

Abstract: The Computational Fluid Dynamics (CFD) has become one of the most useful tools of engineering analysis. There has been a huge number of applications addressed by CFD in various disciplines of engineering and science. Here, some of the interesting research applications are delineated from the research output of the author and his research scholars. Though CFD is a scale neutral approach to solve many fluid and heat transfer problems, the real fluid conditions such as turbulence require suitable modelling for amenable solution. The recent strides into LES and DNS methodologies in CFD have made real flow solution possible within the available computational resources.

Keywords*: CFD, turbomachinery, combustion, solar, multiphase, blade-cooling*

Introduction

During the last three and a half decades Computational Fluid Dynamics (CFD) has emerged as one of the most prominent tools of analysis for wide variety of engineering problems across almost all disciplines of engineering. In this computer generated numerical algorithmic approach, the rate equations of transport of mass, momentum, energy etc., in the form of governing partial differential equations are solved in an iterative manner by a numerical scheme through both time and space marching in three dimensional space

CFD has become possible to deploy due mainly to the availability of high speed computers on one hand and efficient algorithms on the other. The former, by an exponential growth and the latter by several thousand diligent CFD enthusiasts. The phenomenal explosion in CFD activity of course did come through in the late 1980's with the arrival of CRAY supercomputers. The exponential drop in computational cost with the rapid availability of faster computers is shown in Fig.1 from the work of Chapman and Dean (1979). In fact the computational cost has been reducing by a whopping factor of 10 every 8 years. During the last three decades there has been a huge accessibility to high speed computing with the arrival of PC and workstation based computer systems. Now-a-days, a good Laptop is more capable than the so called Mainframe computer of the past. It is pertinent to note that though the computational cost are exponentially decreased, the cost of performing accurate experiments for scaled models have been steadily increasing over the same period of time. But it is not to suggest that computational methods will replace experimental methods as a means to get design information. The need for experiments will probably remain till full scale models could be solved i.e. Direct Numerical Simulation (DNS) becomes economical for all kinds of fluid flows. Infact in the domain of multiphase flows, such as boiling and condensation, with respect to complex geometry, experimental methods remain primary source of information.

The greatest advantage of CFD is that this tool is scale neutral, as the fundamental laws of mass, momentum and energy do manifest such neutral scale information. This is vastly different from the early era of empirical correlations developed

painstakingly over a large number of experiments for sizing and design of equipments such as heat exchangers, cooling towers, pumps, turbines as well as large systems such as ships, aircrafts and rockets. The main difficulty with empirical design is that these correlations are applicable only to a limited range of scales of fluid velocity, temperature, time, length etc. In fact several laboratory scale models are tested before setting up an empirical design correlation. Though it is said that CFD is scale neutral it must be remembered that in flows involving turbulent aspect it is still not economically feasible to utilise computational models that are free of empiricism for most practical problems. But, it must be noted that with the rapid development of CFD even the most complex flows such as supersonic and hypersonic flow analyses are within the realm of reality.

Development of CFD

- Richardson (1910) introduces point iterative scheme for numerically solving Laplace bi-harmonic equations.
- Liebman(1918) presents an improved version of Richardson method. Improving the convergence of the solution.
- Courant Fredrick and Lewy(1928) developed uniqueness and existence of numerical solutions and are fathers of the well-established CFL criteria in CFD literature as regards to stability of numerical solution.
- Southwell(1940) developed a relaxation scheme for solving structural and fluid dynamics problem.
- During the world-war II John Von Neumann developed his method to establish stability of numerical methods. But did not publish it.
- Frankel(1950) presented the first version of SOR(successive over-relaxation) scheme for solving Laplace equation.
- Allen and Southwell(1955) applied Southwell scheme to solve incompressible viscous flow over a cylinder(By hand calculation!!).
- Peaceman and Rachford(1955) developed a new family of implicit method with alternate sweep direction(ADI scheme).
- Evan and Harlow(1957) developed at the particle in cell method(PAIC).
- Godunov(1959) proposed solution technique for multidimensional compressible fluid dynamic problems.
- Lax and Wendroff (1960) introduced a method of computing flow with shock discontinuity.
- Patankar and Spalding (1972) introduced "SIMPLE" algoritham to solve three dimensional parabolic flow problems

A huge surge in the literature pertaining to a plethora of CFD techniques happened in the late 1970's and thereafter and it would suffice to say that today we have a huge bank of excellent algorithms to solve almost any problem in CFD.

Governing Equations of CFD:

The beauty of CFD is that all the conservation laws that govern a fluid flow could be succinctly put simply as a Transport Equation given by

$$\frac{\partial}{\partial t}\rho\phi + div(\rho\phi \mathrm{u}) = div(\Gamma grad\phi) + S_\phi$$

i.e,

unsteady term+convective term=
diffusive term+source term

General Solution Approaches:

Finite Difference Schemes:

Solution obtained by point values at mesh grids and PDE transformed by replacing each differential term in the PDE by the appropriate finite difference approximation.

Advantages:

- The original approach for CFD.
- Easy to get higher order discretizations

Disadvantage:

- Impractical for unstructured meshes.

Finite volume Schemes:

Solution represented by Control volumes and PDE transformed by writing in volume integral form. Discretization based on evaluation of volume integral over small control volumes.

Advantages

- Conserves mass, momentum, and energy exactly.
- Applicable to any mesh topology with appropriate control volumes.

Finite Element Schemes.

Here the solution is represented by Local basis functions and PDE is transformed by multiplying a test function and integrating.

Advantages

- Applicable to any mesh topology with appropriate test and basis functions.

Comparison of Analytic, Experimental Computational Fluid Dynamics

Analytical Methods

Provides general idea of flow physics such as mechanisms for transition, separation, etc. This is an area where only analytical methods can give much insight. No closed form solution available for many practical situations of flow in multi dimensions. This method is restricted to simple geometry and physics and to linear problems only.

Experimental Methods

Modeling the prototype and using the scaling laws to group variables of flow to simulate and observe the intricacies of physics of flow. Many practical empirical correlations are deduced from carefully calibrated experiments. Capable of being quite realistic, but suffers from Scaling problems and also sometimes from high operating costs.

Numerical Methods

Since analytic approaches are hopelessly difficult to solve due to the problem complexity, and turbulent physics, only recourse is to go for Numerical methods of CFD. The Direct numerical simulation (DNS) is an area in which CFD capabilities exceed experimental capabilities, because the results of the computation are far more detailed than those of the experiment. Truncation errors, specifying proper boundary conditions and Computer costs are the limitations.

CFD Application in Different Domains of Engineering

A few specific number of CFD applications in different domains of Engineering will be dealt with briefly now.

1. Combustion Characteristics in a Gas Turbine Combustor: Flow and Temperature distribution in the Combustor

Sharma N.Y., and Som S.K., (2002), did numerical modeling of Gas turbine Combustor flow. Tolpadi, A.K., (1995), indicated the two phase calculation strategy for fuel-air mixture. The Computational model refers to a tubular gas turbine combustor in which the combustion occurs from a continuously injected liquid fuel spray (Fig.2). Fig.3 and Fig.4 show the velocity field and dimensionless temperature contours (T_g/T_a) respectively, within the combustor for a specific operating condition as obtained from the solution of the present numerical model. It is observed from Fig.3 that a central toroidal recirculating flow has been established near the axis in the primary zone of the combustor. The central recirculating zone is a consequence of the high radial pressure gradient associated with the strong inlet swirl and the subsequent expansion of air in the initial diffuser part of the combustor under the given operating conditions. Therefore the size and location of the zone depends mainly on the inlet air swirl and the divergence angle of the inlet diffuser part.
The recirculating flow helps to stabilize the flame near the axis close to the burner as evident from the high temperature contours shown in Fig.5. Thus the high temperature contours, depicting the flame, are located in the primary zone from where they spread downstream.

2. Application of CFD in Turbo Machinery studies: Effect of Change in Radial Gap on Impeller-Diffuser Flow Interaction and on the Flow Characteristics of a Centrifugal Fan

Karanth, K.V. and Sharma, N.Y., (2009) used CFD techniques to capture flow characteristics in a centrifugal fan. The flow in the region bounded by the impeller exit and the diffuser entry i.e. the radial gap space is generally considered to be highly complex. In this work, a numerical solution with moving mesh technique is made use of in predicting the real flow behavior, as exhibited when a target blade of the impeller is made to move past a target blade on the diffuser. It is found from the literature that the effect of the radial gap between the impeller and diffuser on the interaction as well as on the performance of the fan has not been the focus of attention in these works. Hence a numerical analysis has been carried out in this work to extensively explore and predict the flow behaviour due to the change in radial gap.

It is known that radial gap is required to avoid steep velocity gradients at the diffuser entry region. This allows non uniform flow to mix out and enter the diffuser with lower velocities. Also the flow emanating from the impeller has jets and wakes as clearly seen in the instantaneous velocity plots shown in Fig.5,6,7,8. When such a flow enters diffusing flow passages, the quality of flow differs widely and some of the blades of the diffuser may experience flow separation leading to rotating stall and poor performance**.**

At smaller radial gap (Rgr), the flow enters the stationary diffuser almost at the same velocity profile as it leaves the impeller and jets and wakes related to the impeller exit flow do not have a chance to even out. This causes lower diffusion leading to lower diffuser static pressure recovery coefficient, and hence to a lower fan efficiency as shown in Fig.9. The shifting of the design point operation at lower radial gap ratio of 0.05 may be attributed to the fact that the energetic fluid jetting from the impeller enters the diffuser and decelerates over the diffuser. As a result, a large recirculation zone is formed in many of the diffuser blade passages as seen in Fig.5. This will block the flow and hence for peak point operation a higher mass flow rate is required. Hence there is a perceptible shift in the design point operation for radial gap ratio of 0.05. However, when the radial gap is relatively larger, even though the jets and wakes related to the exit flow from the impeller gets evened out, the flow tends to stall in some of the vanes of the diffuser due to change in angle of incidence. This will have detrimental effect on the static pressure rise across the fan leading to poorer efficiency.

3. Application of CFD in numerical simulation of flow through abrasive water suspension jet nozzle

Deepak et al., (2011) have worked on abrasive flow analysis in a water jet nozzle. Abrasive Water Suspension Jet (AWSJ) is one of the variants of Abrasive water jet machining where abrasives are premixed with a suspended liquid to form a slurry. The slurry is pressurized and expelled through the nozzle in AWSJ process. The general nature of flow through the AWSJ nozzle exhibits wall shear stress, resulting in rapid wear of the nozzle which degrades the cutting performance. Nozzle replacement costs play a significant role in the economics of the machining process and improvements in its wear characteristics, are critical for the growth of AWSJ technology. Recently with the development of CFD general purpose code it has become possible to model and simulate the flow through the AWSJ nozzle in a more realistic manner, using two phase Eulerian flow model.

It is to be understood that due to relatively high pressure used, in the order of 1000 bar, the jet velocity correspondingly becomes quite high. The abrasive particles moving with the corresponding high velocity of flow cause severe wall shear. This causes erosion of the nozzle, due to which the effective diameter of the nozzle may change significantly resulting in reduced exit kinetic energy of the jet. This

will not only reflect on the life of the nozzle but also the reduced kinetic energy will affect the machining process. Hence it is interesting to evaluate the effect of the variation of inlet pressure of the abrasive water suspension, on the wall shear stress of the nozzle. Fig.10 shows the computational domain used in the numerical simulation.

Simulation was carried out by varying the inlet pressure from 50 bar to 400 bar and graph of inlet pressure and corresponding wall shear stress developed is shown in Fig.11 and the developed pressure gradients as contour plot is shown in Fig.12. It is found from the plot of wall shear stress developed along the length of the nozzle for various operating pressure conditions at inlet that there is direct relationship between wall shear stress and inlet pressure. As seen from Fig.11, higher the operating pressure, higher will be the wall shear stress developed all along the nozzle. This is true because in the nozzle, the pressure energy is converted to kinetic energy and hence increased velocity is manifested all along the converging duct which results in higher wall shear stress, due to higher velocity gradients. For any given inlet operating pressure the wall shear stress initially increases in the converging section of the nozzle. However the wall shear stress seems to peak near the critical section which is due to a sudden change in the velocity gradient corresponding to the change in area at the critical section. But the wall shear stress seems to attain near constant value along the focus tube as there is no significant velocity change in the constant diameter focus tube till the exit of the nozzle.

It is also seen from the Fig.11 that the velocity gradients will have slight instability when changing over from converging duct portion to straight duct portion of the nozzle as can be seen from the wiggles in the shear stress distribution curves in the vicinity of the critical section.

4. Gas Turbine Blade Cooling Studies

Chandrakant et al., (2011) and Morris W.D., Chang S.W. (1997), have analyzed the cooling in HP stage turbine blades. While the configuration of the internal cooling ducts in real gas turbine airfoil can be highly complicated, in the present analysis, a simplified geometric model with different ducts of varying geometry is being studied for the effective cooling consideration as shown in Fig.13. In general, the coolant air enters the cooling ducts from the blade root, flows through entire length of ducts and finally leaves from blade tip. The cooling process is entirely by internal convective cooling only. The cooling ducts having through ducts of circular cross section with hole radius of 1.5 mm and 2 mm, helicoidal ducts of pitch length of 4 mm with circular cross section with hole radius of 1.5 mm are considered.

Fig.14 shows the non-dimensional temperature distribution of the exposed blade surface along the span at 30 % of chord length. This non-dimensional temperature distribution is taken at this position for all the different cases for the purpose of comparison. It is seen from the figure that with circular cooling duct along the span, the non-dimensional temperature has lower bound value of around 0.31 and upper bound of 0.45 only. The corresponding helicoidal duct of same radius but with pitch length 6 mm shows significant drop in blade surface temperature change as shown in the Fig.15. The blade non-dimensional surface temperature change is from lower bound value of 0.36 to upper bound value of 0.54 along the span length.

This drastic cooling of turbine blade can easily be ascribed to large convective area available within the helicoidal duct corresponding to a pitch length of 6 mm. The advantage of the helicoidal cooling duct is accentuated more if we consider the same helicoidal duct with different pitch length of 4 mm. As seen in Fig.14, with 4 mm pitch length, the corresponding convective area for heat transfer increases even more than the previous case and is reflected as steep non-dimensional temperature change varying from 0.40 to 0.585.

5. Application of CFD for Natural circulation flow simulation in a solar water heater

Manjunath et al., (2011) and Gertzos, K.P. and Caouris, Y.G., (2007) have done research on solar water heating systems. Solar water heating system, passive or active, is very popular in the current context of increased energy demand for both domestic and industrial purposes. Unfortunately, most of the solar heating systems have low thermal performance and there is a need to focus research on the enhancement of their performance. CFD tools can be of immense help in such analyses.

Natural convection flow that occurs in passive solar water heaters is one of the phenomenon that is difficult to simulate. CFD simulation of a passive solar water heater using commercial CFD software FLUENT are shown in fig.16-18.

The simulation is carried out using SIMPLE algorithm for pressure velocity coupling and PRESTO scheme for pressure discretization. Second order upwind scheme is used for the discretization of momentum and energy equations. To effect the buoyancy driven flow, density of water is defined as a function of temperature by a polynomial function.

Fig.16 shows the overall computational domain considered for the analysis. Temperature contour plots for a heat flux of 800 W/m^2 are shown in fig.17 and the corresponding density profiles are shown in fig.18. This analysis can be used to analyze the effect of turbulators, fins and improved design of solar collectors on heat transfer enhancement.

Conclusion

The application of CFD to the following problems has been explained in this paper.

- Combustion Characteristics in a Gas Turbine Combustor
- Effect of Change in Radial Gap on Impeller-Diffuser Flow Interaction and on the Flow Characteristics of a Centrifugal Fan
- HP stage turbine blade cooling by innovative geometry
- CFD simulation for Natural circulation flow in a solar water heater.

References

[1] Chandrakant R Kini, Satish Shenoy B, and N Yagnesh Sharma (2011), A Computational Conjugate Thermal Analysis of HP Stage Turbine Blade Cooling with Innovative Cooling Passage Geometries, The 2011 International Conference of Mechanical Engineering, World Congress of Engineers, London, July 6-8.

[2] Chapman, Dean R (1979),Computational Aerodynamics Development and Outlook, AIAA J., vol. 17, no. 12, pp. 1293 -1313.

[3] Deepak. D, Anjaiah. D, N. Yagnesh Sharma, (2011), Numerical Analysis of Flow through Abrasive Water Suspension Jet: The Effect of Inlet Pressure on Wall Shear and Jet Exit Kinetic Energy, World Congress Engineering, London, United Kingdom, 6-8th July 2011,Vol 3, pp. 2004-2008.

[4] Deepak D, D. Anjaiah, N. Yagnesh Sharma, (2011), Numerical Analysis of Flow through Abrasive Water Suspension Jet: The Effect of Abrasive Grain Size and Jet Diameter Ratio on Wall Shear, International Journal of Earth Sciences and Engineering, Vol 04, pp. 78-83.

[5] Gertzos, K.P. and Caouris, Y.G., (2007), Experimental and computational study of the developed flow field in a flat plate integrated collector storage (ICS) solar device with recirculation. Experimental Thermal and Fluid Science, 31, pp.1133-1145.

[6] Karanth, K.V. and Sharma, N.Y., (2009), CFD Analysis on the Effect of Radial Gap on Impeller - Diffuser Flow Interaction as well as on the Flow Characteristics of a Centrifugal Fan, International Journal of Rotating Machinery, Volume 2009, Article ID 293508, 8 pages,doi:10.1155/2009/293508.

[7] Manjunath M.S, K.Vasudeva Karanth and N Yagnesh Sharma, (2011), Three Dimensional Numerical Analysis of Conjugate Heat Transfer for Enhancement of Thermal Performance using Finned Tubes in an Economical Unglazed Solar Flat Plate Collector, International Conference of Mechanical Engineering, World Congress of Engineers, London, July 6-8., vol 3, pp. 2245-2249.

[8] Morris W.D., Chang S.W. (1997), An experimental study of heat transfer in a simulated turbine blade cooling passage, Int. J. Heat and Mass Transfer, Vol. 40, pp. 3703-371.

[9] Sharma N.Y., and Som S.K., (2002), Influence of fuel volatility on combustion and emission characteristics in a gas turbine combustor at different inlet pressures and swirl, Journal of Power & Energy, IMechE(London),Vol.216.pp.257-268.

[10] Tolpadi, A.K., (1995), Calculation of Two Phase Flow in Gas Turbine Combustor, ASME J. of Engg. for Gas Turbine and Power, Vol. 117, p.695.

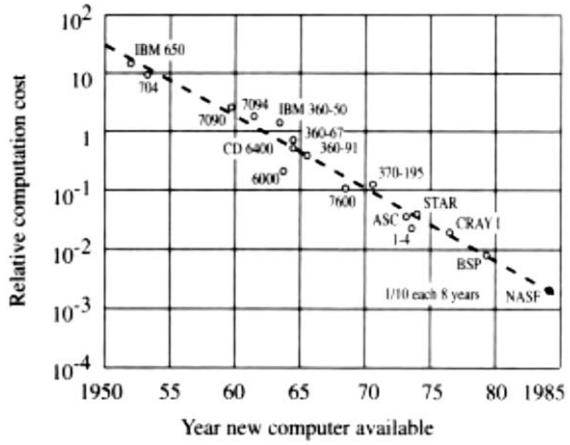


Fig.1 Variation of Relative cost over the years (Chapman and Dean,1979)

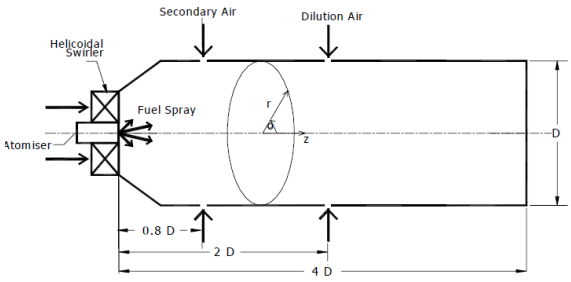


Fig.2: Computational domain for the Gas Turbine Combustor

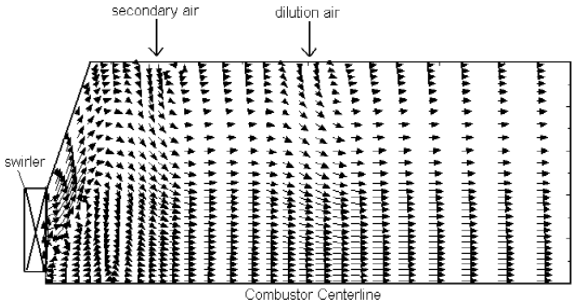


Fig.3: Velocity field in the Combustor

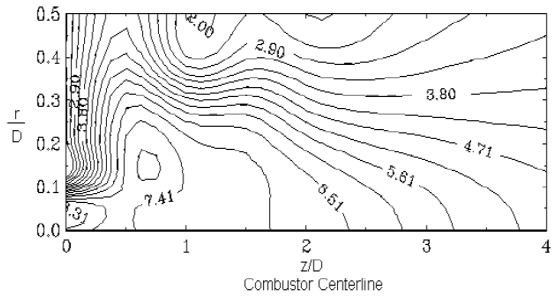


Fig.4: The non-dimensional temperature field in the combustor (Fuel: n hexane)

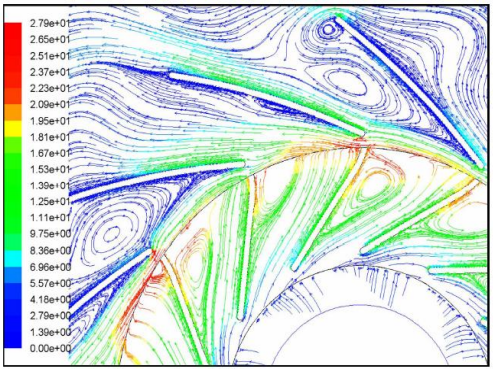
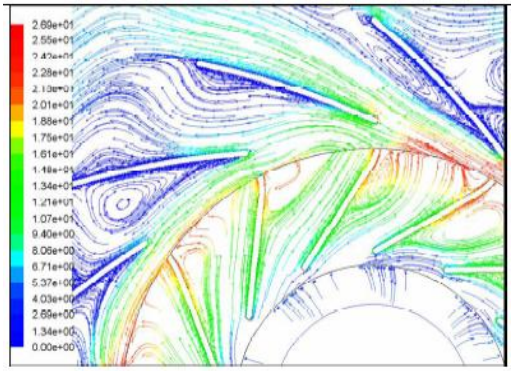
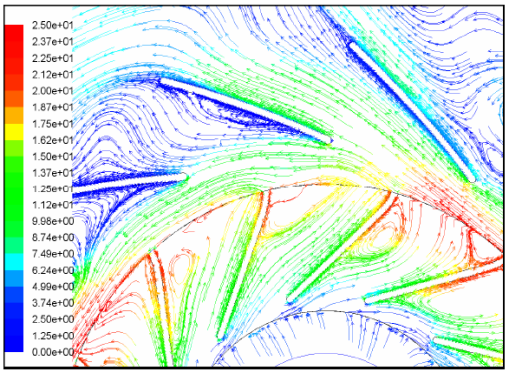


Fig.5: Instantaneous velocity plot for Configuration A (*Rgr*=0.05) – Impeller blades aligned with the



diffuser vanes.

Fig.6: Instantaneous Velocity plot for Configuration A (*Rgr*=0.1)– Impeller blades aligned with the



diffuser vanes.

Fig.7: Instantaneous Velocity plot for Configuration A (*Rgr*=0.15) Impeller blades aligned with the diffuser vanes.

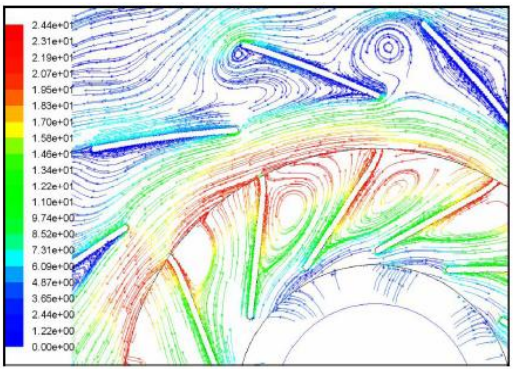


Fig.8: Instantaneous Velocity plot for Configuration A (*Rgr*=0.2) – Impeller blades aligned with the diffuser vanes.

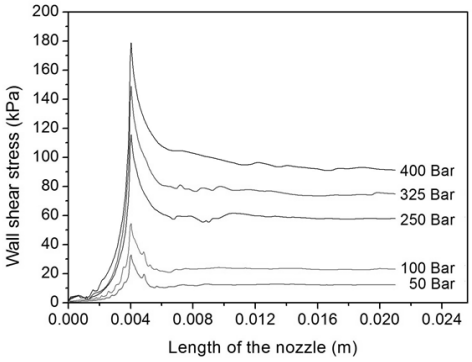


Fig.11: Plot of wall shear stress along the length of the nozzle

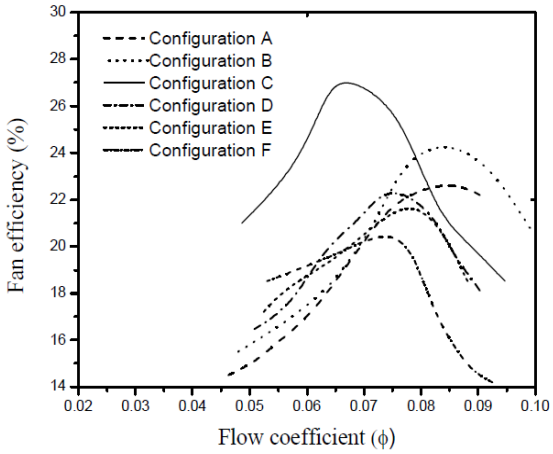


Fig.9: Performance of Centrifugal Fan (Efficiency vs. Flow Coefficient)

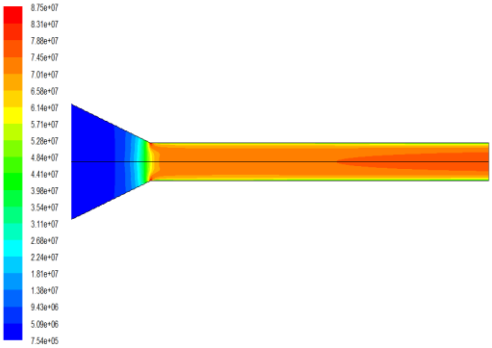


Fig.12: Plot of Pressure contours along the length of the Nozzle

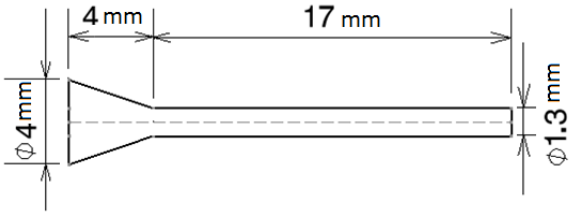


Fig.10 Nozzle used in AWSJ

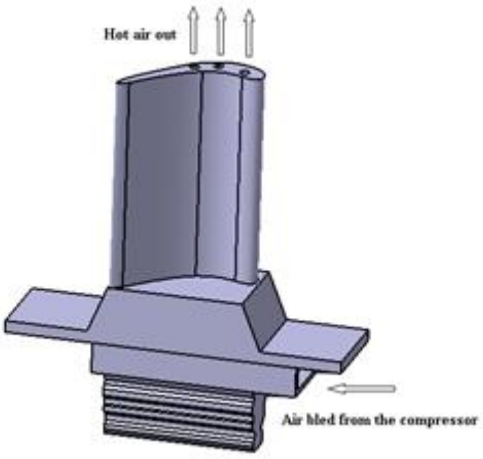


Fig.13: Schematic of turbine blade with cooling ducts

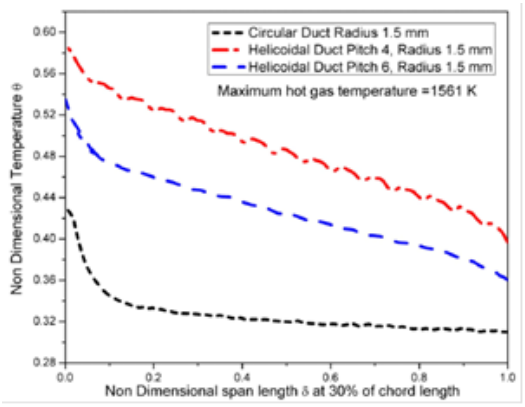


Fig.14: Non-dimensional Temperature variation along the span length of the blade

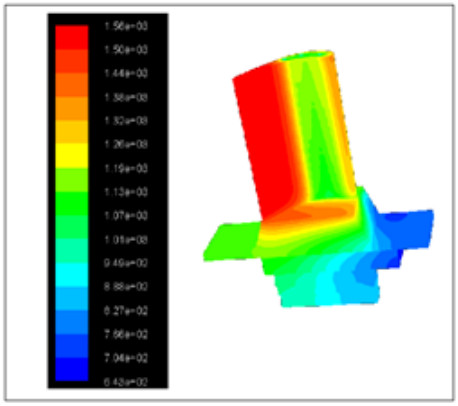


Fig.15: Temperature of blade surface having Helicoidal cooling duct of Pitch 6 mm and radius of 1.5 mm

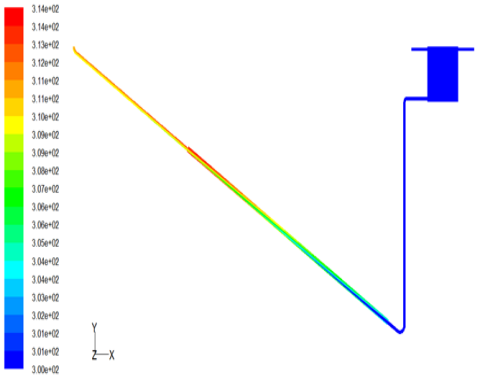


Fig.16: Temperature Contour plot for the overall computational domain

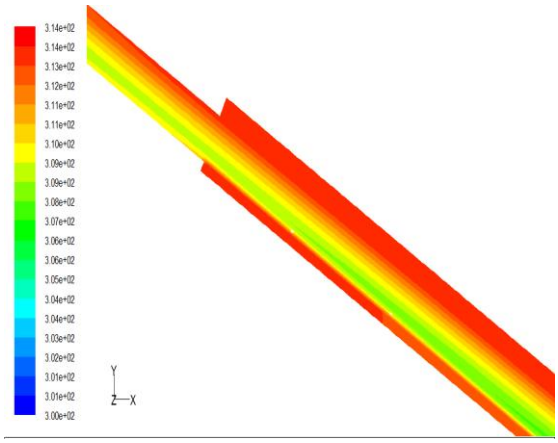


Fig.17: Temperature Contour plot at the exit of absorber tube

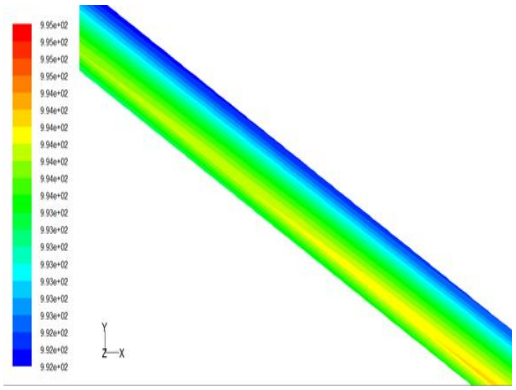


Fig.18: Density Contour plot at the exit of absorber tube

2nd International Engineering Symposium - IES 2012
(KU-MU-NITK-HCMCUT Joint Symposium) March 5-7, 2012, Kumamoto University, Japan

Rainwater Harvesting as an Adaptation Measure to Climate Change: An Implication for Ho Chi Minh City, Vietnam

Phu Le Vo(*), Vo Thi Thu Tinh, Phan Huynh Cam Tu, Ha Pham Thuy Dung, Nguyen Van Dien and Trinh Thi Bich Huyen

Faculty of Environment, Ho Chi Minh City University of Technology, Vietnam
(*) *Corresponding author:* volephu@hcmut.edu.vn

Abstract: Ho Chi Minh City, the Vietnam's largest city and biggest urban agglomeration, has experienced critical water shortage in which water use and management have placed constraints on its sustainable development. Parallel with the rapid growth of urbanization and population, the demand for water use has also increased dramatically. Though it is fortunate to be endowed with water resource, the City typifies the paradox of water availability and water stress. It is too much water and causes inundation in the wet weather with water scarcity during the dry season. Particularly, future water availability will be a striking challenge in the age of climate change. Given this context, rainwater is an alternative source in meeting accelerated water demand. However, this valuable and potential source was not received adequate attention by the local authority. The purpose of this paper is to exam the quality of rainwater harvested at household level. Furthermore, rainwater harvesting measures will be proposed to turn the present challenge into the future opportunity in the context of climate change.

Keywords*: Rainwater harvesting, climate change adaptation, water shortage, water quality, Ho Chi Minh City.*

Introduction

Since the renovation policy's launch in 1986, Ho Chi Minh City (HCMC) has undergone a remarkable economic growth associated with fast urban expansion over the past decades. Increasingly, it is now becoming the Vietnam's economic hub and the heart of the Mekong Delta region (Ha and Wong, 1999; Vo, 2008). Albeit creating many positive impacts and opportunities, its economic growth has had an adverse impact on the use of natural resources, including land use changes, air, water and soil degradation (O'Rourke, 2004).

Given this context, HCMC has been experiencing environmental challenges in which water use and management have placed constraints on its sustainable development. There is a fact that HCMC typifies the paradox of water availability and water stress (Vo and William, 2006). Seasonal fluctuations in annual precipitation result in variation of water quantity and quality in Vietnam's major urban centers, particularly in HCMC. Generally, Vietnam's rainfall is highly distributed in a short period of the year and causing water shortages and floods (Malano et al., 1999). During the rainy season, some areas of HCMC, particularly in peri-urban areas, experience stark inundation following intense rainfall associated with high tides. In contrast, the city's dwellers recently encountered water shortages during the dry season in recent severe drought years (Vo, 2008).

Further, HCMC is being ranked in the top ten (10) Asian coastal cities which are at risks to climate change impacts in terms of vulnerability, exposure and sensitivity (WWF, 2009). Recently, it was also identified as one of the top ten coastal municipalities to be highly inundated due

to coastal flooding and will be enormously affected by a projected 1 meter of sea level rise (Fuchs, 2010; Carew-Reid, 2007). These evidences spell that water is one of the most vulnerable resource, and will pose serious pressures on the sustainable management of water resource, both supply-side and demand-side. Therefore, the local authority would face with striking challenge in the practices of water management in the context of climate change.

Water Resource Management in a Changing Climate

Water is the life's most vital resource, but it is a scare resource. It is becoming scare not only the rising demand and population growth (Johnson et al., 2001), but also due to the ongoing global climate change (Vörösmarty et al., 2000; Falkenmark, 2009). Global demand for water is increasing, but the availability of desired water quantity and quality is decreasing.

With observational records and projections, it is reported that the world's freshwater resources are vulnerable and strongly impacted by climate change (Bates et al., 2008). Chandrappa et al. (2011) claimed that global climate change and environmental alterations have added pressures to hydro-meteorological risks in Asia. Despite many variations, the hydro-meteorological condition in Asia is at risks. While some Asian parts are receiving heavy rainfall, others are facing drought (Chandrappa et al., 2011).

Though climate change is just one of the pressures facing the world's water resources (Arnell, 1999), global warming is exacerbating water shortages in many Asian areas (ADB, 2009).

The recent ADB's report (2009) identified that Southeast Asian countries have experienced a downward trend in precipitation during 1960-2000. Together with Thailand, Vietnam is the second highest country with which has the ratio of annual freshwater withdrawal to total internal freshwater resources is 19.5% (ADB, 2009). Furthermore, the dry season is becoming hotter in recent years in Vietnam with an increase in average monthly temperature is 0.1-0.3^{0}C per decade (ADB, 2009).

As previous stated, HCMC has already faced with water shortages in the dry weather. Additionally, surface water source has been diminished in associated with the depletion of groundwater resource (Vo, 2008). The situation would be seriously exacerbated in the context of climate change.

It is recently reported that there will have changing trends in rainfall and drought periods in HCMC. The annual rainwater will decline in Eastern areas (coastal districts) and an increase of drought in the dry season during 1978-2007 (Ho Chi Minh DOST, 2011).

These indicate the vulnerability of HCMC to changes in water resources. Importantly, the services of water supply and sanitation will be affected due to sea level rise causing serious water disruption and urban inundation for up to 62% of the City's population by 2050 (World Bank, 2010).

Rainwater: The Promising Alternative Source for Climate Change Adaptation

The harvesting of rainwater refers to the collection of water from surfaces on which rain falls, and subsequently storing this water for later use. Rainwater harvesting can occur in multiple contexts and at a variety of scales. The collection of rainwater from the rooftops of buildings is suitable for urban areas and requires little investment or technology, as only roof gutters and storage tanks are needed to capture rainwater. Given the context of global water crisis, rainwater harvesting has received increasing attention worldwide as a modern, water-saving and simple technology.

Rainwater harvesting has been in practice for thousand years ago. According to Pandey et al. (2003) stated that rainwater was collected and utilized as an adaptation option to climate change by people living in various geographical and climatic

regions. Interestingly, rainwater was harvested for use in the dry Thar Desert of Southwest India in the city of Dholavira, even before the Indus Valley civilization (Pandey et al., 2003). Archaeological investigations found many ancient man-made earthworks of rainwater harvesting developed by Mayan people in South America, large-scale earthworks in the Bolivian Amazon, and check-dams (water-impounding structures) in Wadi Sana in United Arab Emirates dating back 15,000 years ago (Pandey et al., 2003).

Nowadays, rainwater harvesting systems have been booming in Queensland, New South Wales of Australia as an adaptive approach at household level to deal with water shortages and climate-related events (White, 2010; Chanan et al., 2010). Malaysia has introduced guidelines on rainwater harvesting since 1999 to cope with accelerating water demand (Nor et al., 2011). More importantly, harvesting rainwater has been addressed as one of the mainstream climate change adaptation projects in Barangay City Camp, the Philippines (Philippine Daily Inquirer, 2011). However, the utilization of rainwater and stormwater has been ignored for a long time in HCMC. Harvesting rooftop rainwater is only practiced in three outlying districts (Can Gio, Nha Be and District 7), accounting for 18.8% of total water supply sources (Vo, 2008).

Study Location and Methods

HCMC occupies a total area of 2,100 km^2 and is situated in the sub-equatorial and tropical zone. Thus, its climate is monsoonal with a high level of solar radiation, a relatively stable temperature, and with clearly divided rainy and dry seasons. The dry season is from November to April while the wet season lasts from May to October. Yearly average rainfall is about 1,950 mm. The rainy season accounts for 80–85% of yearly rainfall. High rainfalls occur in June and September. The highest annual rainfall was recorded in 1908 at 2,718 mm and in 1958 at 1,392 mm. The rainfall is not distributed evenly and tends to increase from the southwest to northeast (Vo, 2008).

- 48 samples of rainwater were collected at 16 districts for quality test. These districts are categorized in *outlying districts*: Can Gio, Nha Be and Hoc Mon; *inner districts*: Dist. 4, 5, 10, 11, Binh Thanh and Tan Binh; and *outer districts*: Dist. 6, 8, 9, 12, Thu Duc, Go Vap and Tan Phu. Rooftop rainwater was sampled in May, July and September 2011. Location of sampling rainwater is shown in Figure 1.
- Several physio-chemical and biological parameters were analyzed, including: pH, dissolved oxygen (DO), turbidity, hardness, total suspended solids (TSS), iron (Fe), chemical oxygen demand (COD) and total Coliform. Analyzed rainwater quality were compared with Vietnam National Standards, namely:

(i) *National Technical Regulation on Surface Water Quality*: QCVN 08:2008/BTNMT (prepared by MONRE).
(ii) *National Technical Regulation on Domestic Water Quality*: QCVN 02:2009/BYT (prepared by MOH).

- Quality of rainwater is then defined based on Water Quality Index (WQI) recently issued by Vietnam Environmental Protection Agency (VEPA) in July 2011 by applying calculation equation (1) and water use categories (Table 1):

$$WQI = \frac{WQI_{pH}}{100}\left[\frac{1}{2}\sum_{a=1}^{2} WQI_a \times \frac{1}{2}\sum_{b=1}^{2} WQI_b \times WQI_c\right]^{1/3} \quad (1)$$

Whereas:
WQI_a: WQI calculated for DO, COD
WQI_b: WQI calculated for TSS, turbidity
WQI_c: WQI calculated for total Coliform
WQI_{pH}: WQI calculated for pH.

Results and Discussion

Quality of the rainwater sampled

Water quality parameters are presented in Tables 2 and 3. In comparison with the two National Technical Regulations (QCVN 02:2009/BYT and QCVN 08:2008/BTNMT), the quality of rainwater collected at 16

surveyed districts can be summarized as follows:

- The concentration of hardness and iron from 16 rainwater samples meet the requirements of QCVN 02:2009/BYT (class II: maximum allowable levels for private and household water use from drilling bore wells, earth-wells, rainwater tanks, gutters) and QCVN 08:2008/BTNMT (class A1: domestic water supply purpose, irrigation, aquaculture and non-potable uses.
- pH of all rainwater samples meets the requirement of both National Technical Regulations, except samples at Districts 8, 11 and 12 have slightly acidity in July.
- The content of suspended solids (TSS) is satisfied with QCVN 08:2008/BTNMT (class A1), exceptionally the TSS level of collected sample at Nha Be district in September exceeds allowable level, two times higher than the regulated standard.
- The concentration of COD of almost harvested rainwater samples is very good level in May and July. However, COD content of rainwater sampled at districts 4, Binh Thanh, Hoc Mon and Nha Be exceeds permitted concentrations. Particularly, the collected rainwater sample at Nha Be district has high concentration of COD both in May and July (five times higher than National Regulation). One of the contributing factors for COD is the decomposition rate of organic matter.
- Measured turbidity level of rainwater samples at most districts exceeds permitted level in May (early period of the rainy season). The reason for this can be traced to the rate of deposition of dust, decay of accumulated organic debris and birds. These pollutants were flushed off by beginning rain events in May. The desired turbidity is better from July to September. In September, turbidity was measured at 10 of 16 districts falls under the regulated standard, except district 10 and Hoc Mon.
- Similarly, DO level in May also does not meet the acceptable limit of QCVN 08:2008/BTNMT, class A1. The level of DO is greater in July and September, except Nha Be.
- The high level of Coliform of rainwater samples collected in most districts was measured in May. Though the content of Coliform is decreased in July and September, but measured level is still much higher than acceptable limit of National Technical Regulation for domestic water supply (QCVN 02:2009, prepared by MOH) and surface water quality for class A1 (QCVN 08:2008, prepared by MONRE).

Water Quality Index of the Rainwater Harvested

Base on the WQI prepared by VEPA, the quality index of rainwater harvested is described in Figure 2. This shows that most rainwater samples have bad quality in May due to exceeding content of Coliform, turbidity. Only 6 collected rainwater samples are satisfied with domestic water supply source. Water quality is much better in July and September. There are 12 samples (in July) and 11 samples (in September) out of 16 rainwater collected that have quality ranging from good to very good, satisfying with domestic water supply purpose. However, several rainwater samples are not suitable for drinking and can be only used as non-potable purposes such as cleaning, flushing and gardening.

Harvesting Rainwater for Future Climate Change Adaptation in Ho Chi Minh City

As discuss above, rainwater in 16 surveyed districts in HCMC has good quality in the middle and late period of the rainy season (July and September). Exceptionally, microbiological and chemical quality of collected rainwater samples in peri-urban districts is not satisfied with National Regulation standards. Nevertheless, rainwater in urban areas can be reused for other urban non-potable purposes, including: washing, gardening, fire extinguishing, irrigation for large-scale agricultural practices in peri-urban areas, and aquifer recharge (with further appropriate treatment). The quality of rainwater depends on the design,

installation and maintenance of rainwater harvesting systems (RWH). Treated and clean rooftop harvested rainwater can even be used for replenish groundwater or stored in aquifers for later use.

Given scientific evidence that climate change eventually raises sea levels in HCMC, water will be one of the most vulnerable resources. Future water use and management is very dependent on how good management practices and policies are developed, both supply and demand sides. Therefore, there is a need for developing an effective policy for rainwater harvesting to adapt with climate change. Such a rainwater harvesting policy should take into account of the following measures:

- Advocating the utilization of rainwater as an alternative supply to augment water sources for the increasing demand.
- Developing a comprehensive guideline on harvesting rainwater at household level.
- Formulating the bylaws or compulsory regulations on rooftop rainwater collection and storage for that water on-site scale in new urban areas in associated with issuing development permits.
- Indicating time-frames for house owners to modify the roofs and grounds for all existing homes.

Conclusions

The above findings from this study show that rainwater quality in HCMC is suitable for many non-potable uses in urban area. This water source should be viewed as an alternative option for replenishing an increasing demand for water use. Although future research on rainwater quality is needed, rainwater harvesting is an implication for augmenting water source to deal with the future threats of climate change in HCMC. The need for rethinking and reshaping water policy is necessary. The formulation of rooftop rainwater reuse will be a critical component for sustainable water management in HCMC in the age of climate change.

Acknowledgements

The authors would like to sincerely thank you JICA-SUPREM Project for its generous sponsor to travelling cost for the authors and HCMUT for its fund enabling the implementation of this research. Any error or shortcomings remain the responsibility of the authors.

References

[1] ADB (2009), The Economics of Climate Change in Southeast Asia: A Regional Review, Asian Development Bank, Manila.
[2] Arnell, N (1999), Climate Change and Global Water Resources, Global Environmental Change, Vol. 9, pp. S31-S49.
[3] Bates, B et al (eds) (2008), Climate Change and Water, Technical Paper of the Intergovernmental Panel on Climate Change, IPCC Secretariat, Geneva.
[4] Carew-Reid, J (2007), Rapid Assessment of the Extent and Impact of Sea Level Rise in Vietnam, Climate Change Discussion Paper 1, International Centre for Environmental Management - ICEM, Queensland, Australia.
[5] Chandrappa, E, Gupta, S and Kulshrestha, U C (2011), Coping with Climate Change - Principles and Asian Context, Springer-Verlag, Berlin Heidelberg.
[6] Chanan, A, Vigneswaran, S and Kandasamy, J (2010), Valuing Stormwater, Rainwater and Wastewater in the Soft Path for Water Management: Australian Case Studies, Water Science and Technology, Vol. 62, No.12, pp. 2854-2861.
[7] Falkenmark, M (2009), Water and the Next Generation – Towards a More Consistent Approach *In* Biswas, A K, Tortajada, C and Izquierdo, R (eds) Water Management in 2020 and Beyond, Springer-Verlag, Heidelberg, pp. 65-87.
[8] Fuchs, R (2010), Cities at Risk: Asia's Coastal Cities in an Age of Climate Change, Asia Pacific Issues, July (96), pp. 1-12.
[9] Ha, H and Wong, T-C (1999), Economic Reforms and the New Master Plan of Ho Chi Minh City, Vietnam: Implementation Issues and Policy Recommendations, *GeoJournal*, 49, pp. 301-309.
[10] Ho Chi Minh City DOST (2011), Modeling factors for Land Use Planning, Water Resources and Urban Infrastructure under Climate Change.
[11] Johnson, N., Revenga, C. and Echeverria, J. (2001), Managing Water for People and Nature, Science, Vol. 292, No. 5519, pp. 1071-1072
[12] Lee, J Y et al (2011), Quality assessment of rooftop runoff and harvested rainwater from a building catchment, Water Science and Technology, Vol. 63, No.11, pp. 2725-2731.
[13] Malano, H M et al (1999), Management of Water Resources: *Can Australian Experiences be Transferred to Vietnam*? Water International, Vol. 24, No. 4, pp. 307-315.
[14] Nicholls, R J et al (2008), Ranking Port Cities with High Exposure and Vulnerability to Climate Extremes - Exposure Estimates. OECD, Paris.
[15] Nor, N M et al (2011), Rainwater Harvesting System for Link Houses, American Journal of Scientific Research, No. 19 (2011), pp. 51-57.
[16] O'Rourke, D (2004), Community-Driven Regulation: Balancing Development and the Environment in Vietnam. Urban and Industrial Environments. The MIT Press, Cambridge.

[17] Pandey, D N, Gupta, A K and Anderson, D M (2003), Rainwater Harvesting as an Adaptation to Climate Change, Current Science, Vol. 85, No. 1, pp. 46-59.
[18] Philippine Daily Inquirer (2011), Harvesting floodwaters tops climate change plans, Philippine Daily Inquirer, 18 July 2011, General Reference Center GOLD, Manila.
[19] Vörösmarty, C J et al (2000), Global Water Resources: Vulnerability from Climate Change and Population Growth, Science, Vol. 289, pp. 284-288.
[20] Vo, P L and Williams, M (2006), An Overarching Approach to Urban Water Resource Management in Ho Chi Minh City, Vietnam, Proc. 3rd Asia Pacific Association of Hydrology and Water Resources (APHW) Conference, Bangkok, Thailand, 16-18 October.
[21] Vo, P L (2008), Formulation of An Integrated Approach to Sustainable Water Management in Ho Chi Minh City, Vietnam, Ph.D Dissertation, Geographical and Environmental Studies, The University of Adelaide.
[22] White, I (2010), Rainwater harvesting: theorising and modelling issues that influence household adoption, Water Science and Technology, Vol. 62, No.2, pp. 370-377.
[23] World Bank (2010), Climate Risks and Adaptation in Asian Coastal Cities: A Synthesis Report, Washington, DC.
[24] WWF (2009), Mega Stress for Mega Cities: A Climate Change Vulnerability Ranking of Major Coastal Cities in Asia, WWF International, Gland, Switzerland.

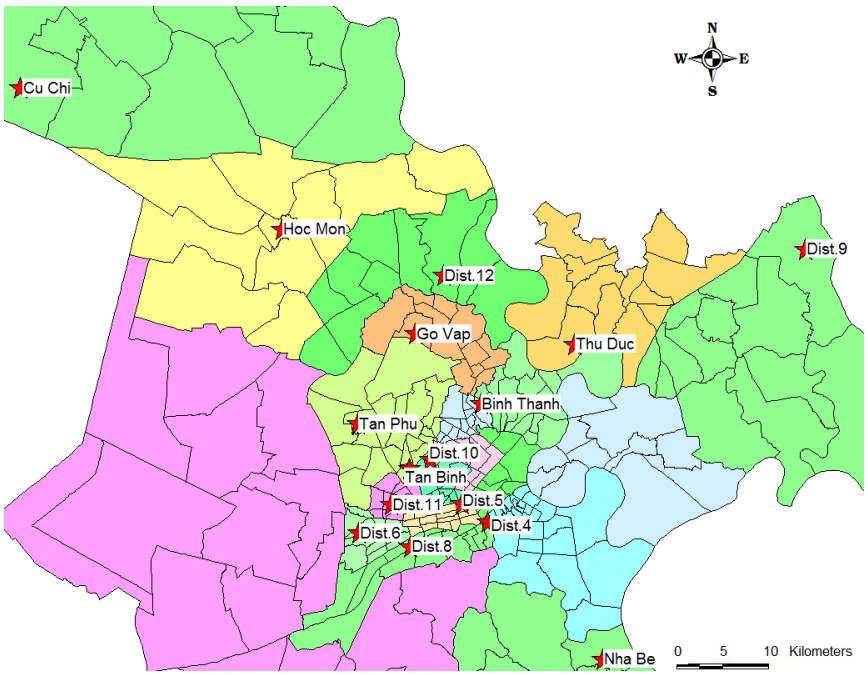


Fig. 1 Location of Rainwater Sampling

Table 1 WQI Vietnam, 2011

WQI	Water Use Purpose	Color
91-100	Domestic water supply purposes.	Blue
76-90	Use for domestic water supply but appropriate treatment is needed.	Green
51-75	Irrigation and other similar use purposes.	Yellow
26-50	Waterway transport and other similar use purposes.	Orange
0-25	Seriously polluted, future treatment solutions are needed.	Red

Table 2 Rainwater Quality: pH, DO, Hardness and Turbidity

District	Parameters											
	pH			DO (mg/l)			Hardness (CaCO3) (mg/l)			Turbidity (mg/l)		
	May	*Jul*	*Sep*	*May*	*Jul*	*Sep*	*May*	*Jul*	*Sep*	*May*	*Jul*	*Sep*
Dist. 4	6.50	6.17	7.90	5.00	4.40	6.00	30	10	6	11	6	2
Dist. 5	6.05	7.24	7.77	5.30	9.80	6.30	8	8	4	13	4	3
Dist. 6	6.60	7.23	7.29	3.90	9.90	5.80	60	8	24	30	2	0
Dist. 8	5.98	5.82	6.64	5.40	6.10	6.00	40	6	8	40	6	2
Dist. 9	6.78	7.14	6.90	7.40	8.30	5.60	20	4	16	0	1	0
Dist.10	6.40	7.39	7.96	5.50	7.10	6.00	44	30	20	4	3	30
Dist.11	6.70	5.95	7.40	5.70	5.80	5.70	44	4	10	14	2	0
Dist.12	6.35	5.61	6.95	5.70	6.30	6.00	20	4	4	5	3	0
Tan Binh	6.91	7.53	6.78	5.00	9.30	6.10	28	20	16	28	5	0
Binh Thanh	6.46	6.49	7.13	7.90	8.80	5.90	20	6	16	2	2	0
Thu Duc	7.70	6.33	7.77	6.10	5.50	6.10	20	6	4	8	8	0
Go Vap	6.52	6.03	7.56	6.90	7.00	6.40	14	6	4	3	7	0
Tan Phu	6.25	6.44	7.77	6.30	7.10	6.20	32	8	10	13	5	0
Cu Chi	7.28	6.19	7.60	7.50	8.00	6.00	20	6	8	5	2	0
Hoc Mon	6.44	6.88	7.78	6.80	7.30	5.60	20	12	10	6	7	7
Nha Be	6.60	6.19	7.73	4.00	5.90	5.80	54	16	8	8	4	1
QCVN 02:2009/BYT	**6 – 8.5**			**n.a**			**≤ 350**			**≤ 5**		
QCVN 08:2009/BT NMT (A1)	**6 – 8.5**			**≥ 6**			**n.a**			**n.a**		

Table 3 Rainwater Quality: TSS, Fe, COD and Coliform

District	Parameters										
	TSS (mg/l)			Fe (mg/l)			COD (mg/l)		Total Coliform (MPN/100ml)		
	May	*Jul*	*Sep*	*May*	*Jul*	*Sep*	*May*	*Jul*	*May*	*Jul*	*Sep*
Dist. 4	10.00	20	17.50	0.07	0.06	0.05	6.40	25.60	$567\ 10^3$	$46\ 10^3$	0
Dist. 5	17.50	5	1.11	0.15	0.01	0.02	6.40	1.60	$989\ 10^3$	0	0
Dist. 6	6.67	6.25	8.33	0.09	0.02	0.05	2.64	6.40	$398\ 10^3$	$2.3\ 10^3$	$46\ 10^3$
Dist. 8	20.00	6	11.11	0.25	0.09	0.09	1.42	3.20	$5\ 10^3$	360	$46\ 10^3$
Dist. 9	4.00	5	3.33	0.02	0.02	0.02	4.80	1.60	$151.5\ 10^3$	920	$1.5\ 10^3$
Dist.10	6.67	16	15.00	0.14	0.02	0.05	8.00	4.80	0	0	0
Dist.11	6.67	3	4.44	0.09	0.07	0.06	6.40	1.60	$131.5\ 10^3$	0	$21\ 10^3$
Dist.12	6.67	4.44	3.33	0.05	0.01	0.02	3.20	3.20	$54.5\ 10^3$	0	0
Tan Binh	8.00	6.25	2.22	0.05	0.57	0.25	6.01	6.40	74,333	360	$110\ 10^3$

Binh Thanh	11.11	4.44	6.10	0.09	N.D	0.02	16	1.60	2 10^3	0	4.3 10^3
Thu Duc	16.67	10	3.75	0.03	0.05	0.03	9.60	6.40	283.5 10^3	9.3 10^3	0
Go Vap	5.00	3.75	7.50	0.03	0.25	0.01	6.40	3.20	5.5 10^3	0	740
Tan Phu	1.67	4.44	4.44	0.05	0.00	0.02	1.90	6.40	0	2.3 10^3	0
Cu Chi	5.88	7.78	8.57	0.08	N.D	0.00	4.80	3.20	7.5 10^3	24 10^3	360
Hoc Mon	6.67	3	2.50	0.05	0.05	0.06	11.2	9.60	7 10^3	7.5 10^3	2.1 10^3
Nha Be	8.33	4.44	40	0.02	ND	0.01	16	51.20	30.5 10^3	0	21 10^3
QCVN 02:2009/BYT	**n.a**			**≤ 0.5**			**n.a**		**≤ 150**		
QCVN 08:2009/BT NMT (A1)	**≤ 20**			**≤ 0.5**			**≤ 10**		**≤ 2,500**		

Notes:

- n.a: Not regulated
- ND: Not detected

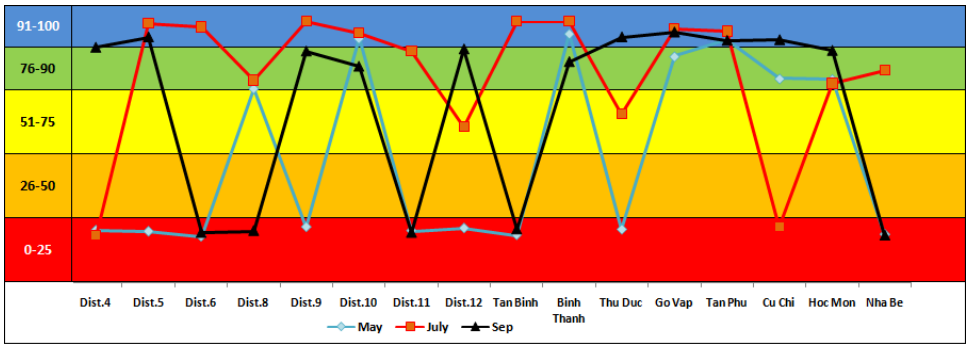


Fig. 2 WQI of Rainwater Harvested

Virtues of Earth Science and its Vistas in Engineering Applications - A Typical Analysis

D. VENKAT REDDY

Editor-in Chief, International Journal of Earth Sciences & Engineering (IJEE)
(Department of Civil Engineering, NITK Surathkal, India) Email:dvr1952@gmail.com

Abstract: Earth science is one of the frontline sciences. It has got greater role to play in various engineering applications and in turn in the national development. All civil engineering projects have to take into consideration one or the other geological aspects during planning. Practicing engineers face several geological challenges in the field almost every day. Engineering geology is a multidisciplinary subject having interrelations with other disciplines. Site selection, design and construction of onshore and off shore structures and all kinds of civil engineering constructions are influenced by the geological factors specific to the site. The sub-surface foundation condition in any engineering project always requires judicious interpretation of geological characteristics.

Key words: Earth Sciences, Engineering Geology, Geological Features, Engineering Applications

Introduction

The foundation of engineering geology was laid by William Smith, who was a professional civil engineer but has contributed immensely to geology due to his interest in earth sciences. He was the first person to introduce the term Engineering Geology; hence he is regarded as the "Father of Engineering Geology". The rapid industrialization all over the world also played a key role in the development of infrastructure by utilizing engineering geology for planning, from investigation stage to the maintenance stage. The civil engineer's responsibility is to define what kind of information he needs concerning the materials, surface and sub-surface conditions. It is an engineering geologist's responsibility to obtain and interpret that information. The responsibility of geologic interpretation rests with the geologists; similarly the responsibility of engineering interpretation and application rests with engineers. The geologists must assimilate the data and present conclusions and recommendations to the engineer in concise, practical form (Rogers Rhoades, 1946).

Earth Sciences - Engineering Applications

Geo sciences related to engineering geological inputs are required for engineering applications such as (i) Rock Types impact on Civil Engineering Projects (ii) Commercial / ornamental / decorative / constructional / infrastructural engineering (iii) Structural major and micro-discontinuities and impact on engineering projects (iv) Surface – subsurface - foundation engineering applications (v) Fluvial dynamics – water resource engineering (vi) Earth sciences in natural disasters engineering (vii) Coastal Geology and dynamics in coastal engineering applications.

(i) Rock Types impact on Civil Engineering Projects

Many engineering projects are related to the stability of rock types and their erosion vulnerability, physical, chemical and engineering properties. Rocks are broadly groped into three categories-igneous, sedimentary and a metamorphic rock. Most of the acidic igneous rocks have high strength for engineering utilization. An acidic

rock is a rock with high proportion of silica percentage (>60%). Granites, Granite porphyry rhyolites etc are examples of this category. Remote sensing technology utilizing in narrow spectral bands with EMR has proven capabilities for differentiation in engineering properties such as ductility, shearing strength, tensile strength (Shepherd and Walsh, 2002). The degree, extent and nature of rock weathering are among the most important geological factors to be considered during civil engineering constructions. Few case studies are presented below:

Obra Dam Project-India

For example, Obra Dam Project, Uttar Pradesh, India has experienced rock weathering problems. The bed rock in the area was highly weathered, fractured and brecciated, comprising of quartzite and banded quartzite. The other site, highly cavernous Kajarahat lime stone found solutions; cavities were discovered in these limestone formations that were resulted due to chemical weathering. This also gave rise to a two-fold problem of settlement of foundation structure and leakage of reservoir foundation through the left and right rims of reservoir. Extensive geotechnical measures were carried out for treatment of reservoir leakage (GSI, 1976). Dam construction on limestone formation requires additional care in establishing cavernous nature and extent. Weathering pattern and depth of weathering zone requires a detailed study before planning for major hydraulic structure in highly weathered rock formations (Anon 1975).

Parambikulam Aliyar Project-Tamil Nadu-India

Project area forms part of the Western Ghats and the rock types are biotitic gneisses of Archaean. The rocks are folded and faulted. Major shear zone extends continuously from the axis to the toe of the dam and further downstream into the tailing foundations with varying width. Highly weathered fractured and sheared zones facilitated the seepage through these zones. The extension of weathering below 18m depth, at the left flank of the dam necessitated the change in the alignment and design of the dam.(Venkat Reddy, 2010).

Rammam Hydroelectricity project, Darjeeling, West Bengal, India

Highly weathered gneisses and schists with ground conditions, heavy seepage week and roof collapse along weathered jointed intersections have been reported from the main tunnel of the Rammam Hydroelectricity project. Various remedial measures have been taken to control the weathered zones (Venkat Reddy, 1996).

Spectral Remote Sensing has proven capabilities in discriminating such various engineering properties of the rocks like brittleness, ductility, shearing strength, tensile strength etc., owing to it's very narrow spectral band width of EMR (Shepherd and Walsh, 2002).

(ii) Commercial / Ornamental / Decorative / Constructional / Infrastructural Engineering

The success of commercial stone industry primarily depends upon the production of defect free rock/stone blocks. Detection of defects in decorative and dimensional stones (commercial rock deposits) plays vital role in quality assessment. Indian granites (commercial rocks) are sought by many countries of the world because of variety of colors and good hardness due to which it takes mirror polish and visual appeal of numerous patterns and designs. Most of the commercial rock deposits are available in South India. Geological map of South India showing prominent commercial rock deposits presented in Fig. 1.

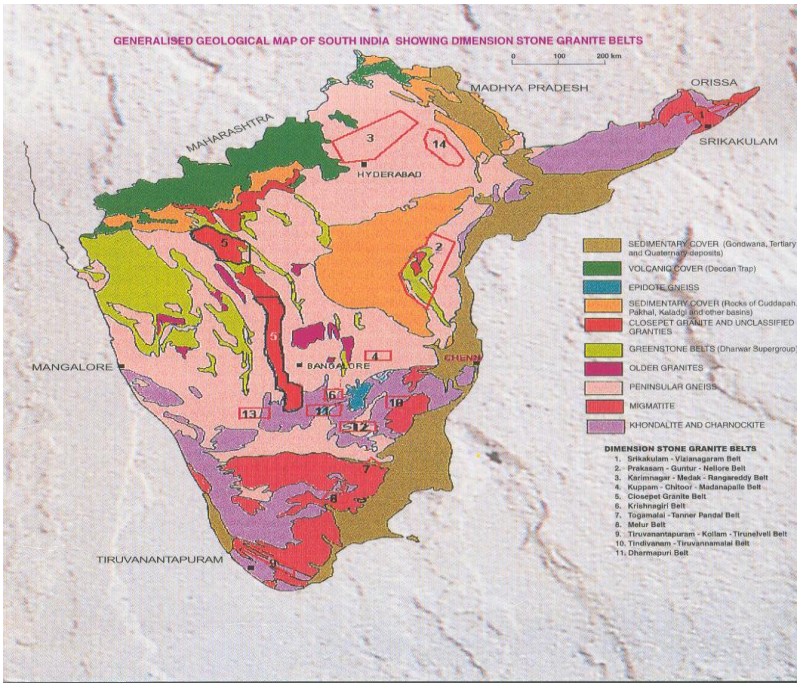


Fig.1: Geological Map of South India with commercial rock deposits (GSI, 1998)

All rocks are not suitable for constructional purposes. Natural/inherent defects in rock deposits will adversely affect the quality of the rock deposit. Major defects such as colour variation, textural variations, macro-micro discontinuities, inclusions, intrusions, alterations etc. Micro-petrographical analysis is required to assess the stress minerals, altered minerals etc. Typical micro-petrographic analysis of granite is shown in Fig.3. Altered feldspar minerals are noticed in Fig.2.



Fig.2: Micro - petrographic analysis of Granite-Karnataka, India

(iii) Structural major and micro - discontinuities and impact on engineering projects

Natural/inherent defects can be classified into two groups as major structural discontinuities and minor defects. Structural discontinuities are regional in magnitude and that affects whole body of granite pluton/rock. They are easily identified by aerial photographs or satellite imageries. Major lineaments are possible to be traced

out on satellite imagery or aerial photographs (Venkat Reddy, 1994).

Lineaments and Faults in Engineering:
Again, the lineaments, faults and the other tectonic features have direct bearing over various engineering applications like terrain stability, erosion vulnerability, ground water movement, migration of pollutants etc. Besides the already known ground based and optical remote sensing image based mapping techniques, the concept of shaded relief mapping using the ground based topo-surface data, the Shuttle Rader Topographic Mission (SRTM) data and satellite stereo image data have opened up major gate ways in mapping the faults presented in Fig. 2 (Ramasamy, 2006). SRTM shaded relief map – with lineaments, Salem district, Tamilnadu, India is presented in the Fig. 3.

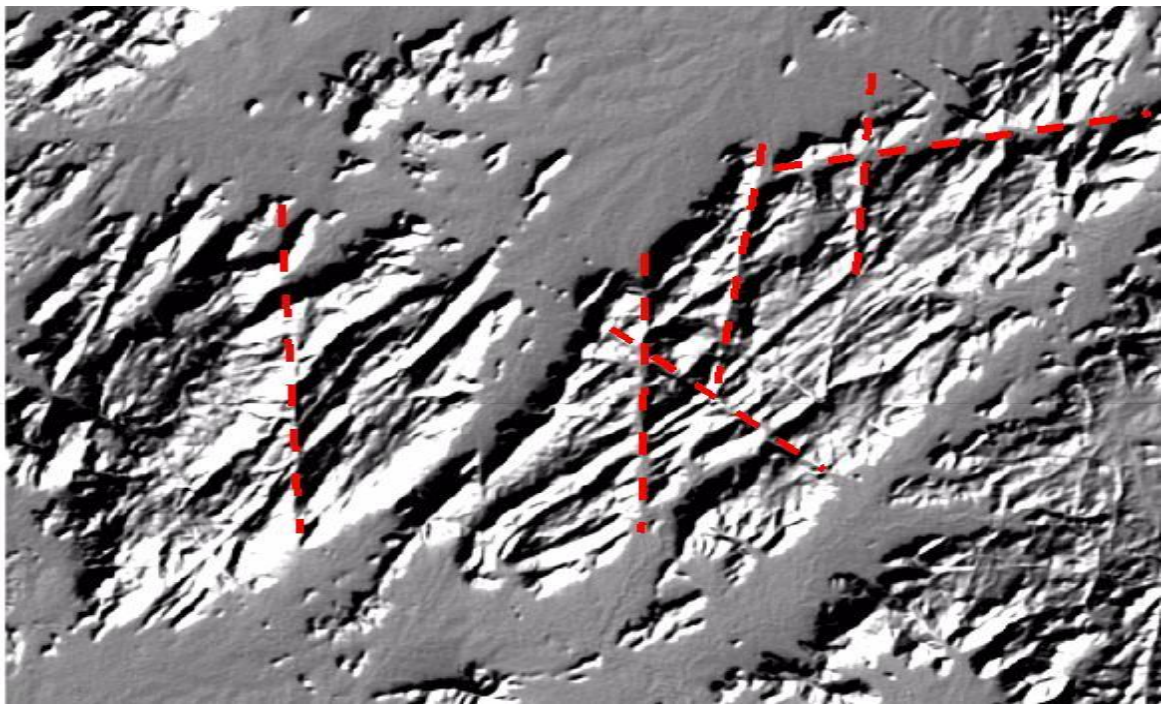


Fig. 3: SRTM Shaded Relief Map - Lineaments-Salem Area, Tamilnadu-India (Ramasamy, 2006)

(iv) Surface - sub surface –foundation engineering applications
The sub-surface foundation conditions are the vital engineering issues in which earth scientists play a significant role. Most of the foundations designs on hard crystalline rocks are firm for foundation. However highly weathered rocks, unconsolidated rocks, domal and anticlinal folds provide less stable basement. A detailed surface and sub-surface geological investigations are required for determining the site specific conditions. Space technology applications are useful for delineation of larger areas.

(v) Fluvial dynamics – water resource engineering
Fluvial geomorphic mapping of river system dynamics requires in depth study for understanding. Detailed study of river geomorphology bears baseline information on depositional environment, hydrologic dynamics. Water resources engineers before planning for major hydraulic structures requires in depth study in all aspects of river morphology, geological - hydrogeological systems, paleo –floor prone records, of the river system etc. A detailed analysis of fluvial dynamics of river basins has to be carried out before commencement of any specific hydraulic structure.

(vi) Earth sciences in natural disasters engineering

India has been prone vulnerable to natural disasters on account of its unique geo-climatic conditions. Floods, droughts, cyclones, earthquakes and landslides have been recurrent phenomena. About 60% of the landmass is prone to earthquakes of various intensities. Over 40 million hectares is prone to floods; about 8% of the total area is prone to cyclones.

Landslide and debris flows impact on engineering structures

Landslides are the major sliding activity of a rock mass or soil mass. All slopes have tendency to move. Landslides generally occur due to failure of the stability of hill slopes. However failure of slope mainly depends upon geology of the region, structural fractures, surface and ground water, stress in the rock mass and local seismicity. In our country parts of the Himalayan region are highly promotes small or large landslides and debris flows.

Himalayan region is more susceptible for Landslide activity and large number of Landslides have been reported in past. Malpa Landslide in Pithoragarh district of Uttarakhand (1998), 380 people were killed and entire village was washed away. September 20, 2008 Landslide in Shimla, (Himachel Pradesh) killed 26 persons and damage to road and bridges. The slide at Jhakri slide away NH-22 is shown in the Fig. 4 (Singh and Venkat Reddy, 2009).



Fig. 4: The slide at Jhakri, slide away NH-22 on 20th Sep 08, marked locations Above (for 120 meters)

Tsunamis

Understanding the origin and prediction of occurrence of tsunami is a challenging task being attempted very recently. In the deep waters of an ocean, they move as barely detectable ripples at hundreds of miles an hour. Near land, however, in shallow water they slow down. One wave after another pile up on top of its predecessor, creating a single wave that slowly surges towards shore, usually at few dozens of miles an hour. As this giant wave approaches, sediment and sand is sucked up, causing the seabed to drop and water to pour away. Once this starts to happen, you still have time before the main wave arrives–usually between 10 and 30 minutes (Kerr, 2005).

Such knowledge could have saved thousands on that Sunday (26th December, 2004 tsunami-of Asia).For this reason, tsunami awareness is now considered to be

of overriding importance for protecting life, particularly in areas that are more prone to see level changes. A tsunami detection system like one installed around the Pacific, can help, but the real need is for good education to respond to warnings provided.

(vii). Coastal Geology and Dynamics - in Coastal Engineering Projects

The Coastal areas stand as a testimony for the independent and interdependent dynamics of tectonic, Riverine, Physical oceanographic and Aeolian processes. As these processes and their time series modifications are embedded in the coastal geomorphic landforms (Vaidyanadhan and Ghosh, 1993). Understanding and mapping of such coastal geomorphic features can provide strong and scientific paths for the present and future engineering planning like site selection for harbors, measures for harbor sedimentation, sites for development of settlements and urbanization, development of beach resorts, inland water transport systems, sustainable aquaculture development, wetland management, coastal erosion issues and other ecosystem management, etc (Ramasamy & Venkat Reddy, 2009).

Conclusions

1. The geological aspects of the civil engineering site have to be studied in detail before commencement of the project.

2. Site selection, design and construction of public works such as roads, buildings, bridges, dams, reservoirs, tunnels, harbours etc are influenced by the local geological considerations.

3. Geological parameters have to be studied in detail before planning for major onshore and offshore structures.

4. A civil engineer must be in a position to understand the geological map of the project area with due practical knowledge for assessing and interpreting the data.

References

[1]. Anon (1975) **-** Geological Survey of India-Engineering Geology Case studies Miscellaneous Pub no. 129, pp.11-13.

[2]. Kerr, R.A (2005) South Asia tsunami – Failure to gauge the quake crippled the warning efforts, Science, 307 (5707), pp.301.

[3]. Ramasamy, SM. (2006), Remote Sensing and active tectonics of South India International Journal of Remote Sensing, Taylor and Francis, London, Vol. 27, No. 20, pp. 4397-4399.

[4]. Rogers Rhoades (1946), Geology in Civil Engineering – second pan American Congress of Mining Engineering and Geology Bureau of Reclamation-United States Department of Interior pp.1-10.

[5]. Singh. T.N and Venkat Reddy. D (2009), International Journal of Earth Sciences and Engineering, Natural disasters Vol. 01, No. 02, pp. 2-13, 2008.

[6]. Venkat Reddy. D (1996) Engineering Geology for Civil Engineers, Oxford and IBH Pub, New Delhi, India.

[7]. Venkat Reddy. D (2010), Engineering Geology-Vikas Publishers, New Delhi ,India.

MECHANICAL ENGINEERING
&
RELATED FIELDS

2nd International Engineering Symposium - IES 2012
(KU-MU-NITK-HCMCUT Joint Symposium) March 5-7, 2012, Kumamoto University, Japan

Design and Control of a Low Cost Wheeled Inverted Pendulum Robot

Jatheendranath[1], Prasad Krishna[2]

1 *Department of Mechanical Engineering, National Institute of Technology Karnataka, Surathkal, Mangalore 575025, India. email:krishnprasad@gmail.com*
2 *Department of Mechanical Engineering, National Institute of Technology Karnataka, Surathkal, Mangalore 575025, India. email:jatheendra@gmail.com*

Abstract: Self-balancing of robots is one of the fast emerging fields of robotics, mainly due to their high manoeuvrability and stability in uneven terrains. This paper deals with development and control of a low cost wheeled inverted pendulum robot. In order to reduce the cost, sensor fusion of a low cost gyroscope and accelerometer with Kalman filter was implemented for attitude determination. A PID controller was used for balancing and implemented in LabVIEW for quick prototyping. The prototype was interfaced with the computer using National Instrument Data Acquisition modules. Results of Calibration of Accelerometer and Gyroscope are reported. Balancing of the robot for a short duration was achieved. Methods to improve the system performance are also presented.

Keywords: Inverted pendulum, robot, gyroscope, accelerometer, Kalman filter

Introduction

Inverted pendulum robots are two wheeled robots whose centre of gravity lies above their pivot point. Because of this, they are inherently mechanically unstable. The balance and orientation of the robot is maintained by its control system which modulates the wheel torque and position according to the inclination of the robot.

The basic principle of dynamic balancing is to drive the wheels in the direction in which the body of the robot is falling. If the wheels can be controlled in such a way as to stay under the centre of gravity of the robot, it will remain balanced.

The robot has attitude sensors mounted on it which measures the inclination of the body. The change in orientation from vertical is sensed by the control system via feedback from these sensors. Then the control system counteracts the fall by actuating the wheel motors to move in the direction in which robot is falling. As a result, an opposing torque from the motors act on the body and it returns to set position. By this process, the robot maintains a dynamically stable vertical orientation.

One of the major advantages of two wheeled robots over four wheeled or legged robots is its manoeuvrability. They have virtually zero turning radius where as four wheeled robots need a turning radius more than their wheelbase.

The dynamic stability of the robots allows easy navigation on various terrains, turn sharp corners and traverse small steps or curbs. Motorized wheelchairs working on the same principle will have much better stability and manoeuvrability when compared to traditional ones. Two wheeled transporters like *Segway* work on this principle. Finally inverted pendulum robots form an excellent test bed for new control algorithms developed.

Objectives

Objective of the present work is to develop a low cost two wheeled inverted pendulum robot as a test bed for control algorithms. A working prototype is developed and a PID control system is implemented. Sensor fusion using Kalman filter is implemented for attitude measurement.

Literature review

In recent years, a rapid progress has been seen in the development of balancing robots. One of the first developments in this field was by Ha and Yuta (1996) of Intelligent Robot Laboratory, Institute of Information Sciences and Electronics, University of Tsukuba, Japan.

Another robot named *Joe* was developed at The Industrial Electronics Laboratory at the Swiss Federal Institute of Technology, Lausanne, Switzerland by Grasser et al. (2002). *Nbot* by Anderson (2003) is one of the robots responsible for the current popularity of balancing robots. Blankespoor et al. (2004) published a paper on experimental verification of the dynamic model for a quarter size self-balancing wheelchair. They developed a wheel chair which was capable of supporting a person in sitting and standing positions. A Linear Quadratic Regulator (LQR) controller was used to stabilize the wheelchair. Akesson et al. (2006) developed YAIP (Yet Another Inverted Pendulum Robot) as a flexible platform for teaching and research using low cost components. Takei et al. (2009) designed a wheeled inverted pendulum robot for baggage transportation. Change in centre of gravity because of the unknown weight of baggage was one of the main focuses of the project. They proposed a workaround for this by resetting the balance position at instances when the robot is stationary. Chiu (2010) developed a wheeled inverted pendulum using an adaptive output recurrent cerebellar model articulation controller. In another journal paper (2010) he introduced an intelligent back-stepping control for wheeled inverted pendulum. Grewal et al. (1991) presented a new approach for the development of large dimensional Kalman filters for calibration and alignment of complex inertial guidance systems. Haid and Breitenbach (2004) presented an algorithm using Kalman filter for correction of gyroscope drift. They fused a gyroscope output with a magnetic field sensor using a Kalman filter and found out that drift in gyroscope output can be minimized by this approach. Kumar and Jann (2004) developed a low cost inertial platform for an unmanned aerial vehicle. It used Kalman filter for sensor fusion and succeeded in eliminating drift and temperature variation effects. Luinge et al. (2005) used Kalman filter for combining the gyroscope and accelerometer data for orientation measurement of human body segments. Hyde et al. (2008) detailed their experience of using a composite filter for combining sensor data.

System modelling

Since the objective was to balance the robot in a plane, only two dimensional motion of the robot was considered for simplicity. The two drive motors are assumed to be identical and react to the input at the same rate. Since both motors were from the same manufacturer and have the same rating, the differences may be negligible. The Eq.1 and 2 represent the dynamics of the robot.

$$\frac{R}{K}\left(\frac{J}{r}+rm+\frac{rM}{2}\right)\ddot{x}+\frac{RrMl}{2K}\ddot{\theta}+\frac{K}{r}\dot{x}-K\dot{\theta}=v \quad (1)$$

$$(I+rMl+Ml^2)\ddot{\theta}+2\left(\frac{J}{r}+rm+\frac{rM+lM}{2}\right)\ddot{x}-Mgl\theta=0 \quad (2)$$

These can be expressed in state space form as shown in equation 3.

$$\begin{bmatrix}\dot{x}\\ \dot{\theta}\\ \ddot{x}\\ \ddot{\theta}\end{bmatrix}=\begin{bmatrix}0 & 0 & 1 & 0\\ 0 & 0 & 0 & 1\\ 0 & A_{32} & A_{33} & A_{34}\\ 0 & A_{42} & A_{43} & A_{44}\end{bmatrix}\begin{bmatrix}x\\ \theta\\ \dot{x}\\ \dot{\theta}\end{bmatrix}+\begin{bmatrix}0\\ 0\\ B_3\\ B_4\end{bmatrix}v \quad (3)$$

Sensor modelling

For the purpose of sensor fusion using Kalman filter, it is required to model the sensor system in discrete state space form.

For gyroscope, the bias voltage is subtracted from the output voltage and then divided by the sensitivity to get the

rate of rotation. This rate is integrated to get the rotation angle. Integration of gyroscope output can be represented by the Eq. 4&5.

$$\theta_{k+1} = \theta_k + (u_k - \beta_k)dt \quad (4)$$

$$\theta_{k+1} = \theta_k - \beta_k dt + u_k dt \quad (5)$$

This can be represented in state space form as shown in Eq. 6&7.

$$\begin{bmatrix}\theta \\ \beta\end{bmatrix}_{k+1} = \begin{bmatrix}1 & -dt \\ 0 & 1\end{bmatrix}\begin{bmatrix}\theta \\ \beta\end{bmatrix}_k + \begin{bmatrix}dt \\ 0\end{bmatrix}u_k \quad (6)$$

The angle is taken as output from the state

$$y_k = \theta_k$$

$$y_k = \begin{bmatrix}1 & 0\end{bmatrix}\begin{bmatrix}\theta \\ \beta\end{bmatrix}_k \quad (7)$$

For an accelerometer at an angle θ the component of acceleration due to gravity acting through the sensor will be gsinθ. The angle θ can be calculated from the accelerometer output by the following equation.

$$\theta = \sin^{-1}\left(\frac{V_{a-}V_{a0}}{K_a}\right) \quad (8)$$

Where K_a is the sensitivity of the accelerometer, V_a is accelerometer output voltage at angle θ and V_{ao} is output voltage at zero position

System Description

Major components of the system are a MEMS gyroscope, a MEMS accelerometer and a pair of geared dc motors.

The gyroscope used was a two axis Pitch-Roll rate gyroscope module (LPR530A) with selectable maximum sensing range of ±300 degrees per second or ±1200 degrees per second.

A three axis Low-G accelerometer module (MMA7361L) with a selectable acceleration range from ±1.5g or ±6g was used. It is a low power, low profile capacitive micro-machined accelerometer featuring signal conditioning, a 1-pole low pass filter and temperature compensation.

A pair of 200 rpm 12 Volt geared DC motors were used as actuators driven by a L298 Dual H-Bridge motor controller IC. Speed of motors were controlled by Pulse Width Modulated (PWM) signal generated by the LabVIEW program which runs a counter in NI PXI 6229 module with required duty cycle.

As a preliminary step to build the prototype, a 3D CAD model was developed using *Solidworks* and the dimensions of the structure were decided based on feasibility of full 180° movement about the pivot.

Main structural material of the robot was chosen to be plexi-glass(acrylic sheet) for its low cost, machinability and aesthetics. The dc motors were mounted on this using L brackets. The sensor PCB was mounted in the centre as shown in Figure 1.

Kalman filter & Sensor fusion

The system uses an accelerometer and gyroscope combination to measure the angle of tilt. The gyroscope measures the angular rate of motion. This output has to be integrated to get the angle of drift. The gyroscope provide accurate measurement in short term but as time progresses, errors accumulate due to integration and leads to drift in output. Another issue is that it doesn't have a set datum.

Even though the accelerometer readings may not be precise in short term due to noise components and other acceleration components, it gives sufficiently accurate results over a long period. So the accelerometer can be used to reset the gyroscope at the start-up and to rectify the drift. A signal level fusion technique using Kalman filter was employed to combine these two sensors.

The Kalman filter was introduced by R.E. Kalman (1960) in his paper describing a recursive solution to the discrete data

linear filtering problem. It is a set of mathematical equations that provides an efficient computational means to estimate the state of a process, in a way that minimizes the mean of the squared error. It supports estimations of past, present, and even future states, and it can do so even when the precise nature of the modelled system is unknown.

The Kalman filter uses a system's dynamics model, known control inputs to that system, and measurements (such as from sensors) to form an estimate of the system's state that is better than the estimate obtained by using any one measurement alone.

The filter uses the statistical characteristics of a measurement model to recursively determine estimates for fused data that are optimal in a statistical sense. The recursive nature of the filter makes it appropriate for use in systems without large data storage capabilities.

Gyroscope calibration

For calibrating the gyroscope, an optical encoder with a resolution of 1024 pulses/second was connected to the sensor board. NI PXI 6229 module was used for data acquisition and OriginPro software was used for data analysis. The mean of the static output was found to be 1.24861 with a standard deviation of 7.1396E-5 for a sample taken for 1245 seconds. At a sensitivity of 3.33V/°/s the maximum error in gyroscope output was 12 degrees (11.8%) while reversing at an angle of 100 degrees.

Accelerometer calibration

The accelerometer is calibrated by measuring its output in three different orientations - perpendicular to gravity (0 g), along gravity(g) and opposing gravity(-g). The sensitivity and zero output was determined as

$$K_a = 0.708V$$

$$V_0 = 1.28V$$

From Figure 2, it is evident that the accelerometer output follows the real motion quite accurately in the longer run. But the instantaneous values always show some deviation in random manner.

Kalman filter tuning

The Kalman filter was implemented by "Discrete Kalman filter VI" in LabVIEW. Gyroscope output is given as input (u(k)) and accelerometer output is given as output (y(k)) to the VI. The estimated output (yhat) gives the filtered angle. A second order stochastic noise model and the stochastic state space model developed in equation are also given as inputs to the VI as shown in Figure 5.

Filter tuning was done manually by modifying the noise model parameters and comparing the output with encoder reading. Best results were obtained for process noise covariance matrix value of 1E-4 and measurement noise covariance matrix 0.01. With these values the maximum error was reduced to about 2^o.

PID controller

The control algorithm used was Proportional Integral Derivative (PID) control because of its simplicity in tuning and implementation. The *Advanced PID VI* was used for generating the duty cycle in proportion to the angle of tilt. PID tuning was done manually by trial and error.

Results and discussions

Result of Sensor calibration

From Figure 2, it is evident that the accelerometer shows large errors on jerking motion of the body but comparatively error free at other times. The gyroscope on the other hand has higher errors throughout the measurement, but is not affected much by jerking motion as shown in Figure 3. These two sensors complement each other quite well in their characteristics. Kalman filtering gives better results than either of the sensors as shown in Figure 4. The maximum error was brought down from 12^o to 2^o.

Control system tuning results

The tuning of PID controller was done by varying the values of proportional, integral and derivative gains manually. The tuning

started with a small K_p value of .001 and was increased in steps. The final result is as shown in Figure 6. By the time K_p value reached 3.4, the robot was able to balance for about 6 seconds.
Beyond this further improvements could not be made on tweaking either proportional gain or differential gain. This was mainly due to slow response of the motors upon reversing and backlash in gears. The proposed solution is to use high response DC motors with quick reversing capabilities.

Conclusions

The following conclusions are deduced from this study:

- The sensors were calibrated and Kalman filtering was implemented.
- Prototype of the wheeled robot was fabricated and a simple PID control system was implemented.
- Balancing of the robot was achieved although for a short duration of time.

Further scope

The main obstacle for further improvement was poor reversal response of the motors. The delay in motor reversal and gear backlash proved to be detrimental in achieving the objectives completely. Use of high response DC motors with quick reversal capability is the major improvement required. This will provide scope for drastic improvement in performance.

Utilization of optimal control system like LQR in place of PID control is another improvement that can be implemented.

References

[1] Anderson, David P. (2005), nBot Balancing Robot, Website:www.geology.smu.edu/dpa-www/robo/nbot/.

[2] Au, K.W et al. (2001), Control of tilt up motion of a single wheel robot via model based and human based controller, Mechatronics, Vol. 11, pp. 451-473.
[3] Akesson, Johan et al. (2006), Design and Control of YAIP–an Inverted Pendulum on Two Wheels Robot, Proceedings of the 2006 IEEE International Conference on Control Applications, October 4-6, 2006.
[4] Blankspoor, Adam et al. (2004), Dynamic model for a quarter size self-balancing wheelchair, Proceedings of 2004 American control conference, June 30-July 2.
[5] Chiu, Chih Hui (2010), The Design and Implementation of a Wheeled Inverted Pendulum Using an Adaptive Output Recurrent Cerebellar Model Articulation Controller, IEEE transactions on industrial electronics, Vol.57, pp. 1814-1822.
[6] Chiu, Chih-Hui et al. (2010), Intelligent back-stepping control for wheeled inverted pendulum, Expert Systems with Applications, Vol. 38, No. 14, pp. 27-35.
[7] Grasser, Felix et al. (2002), JOE: A Mobile Inverted Pendulum, IEEE transactions on industrial electronics, Vol. 49, pp. 107-114.
[8] Grewal, S.M (1991), Application of Kalman Filtering to the Calibration and Alignment of Inertial Navigation Systems, IEEE Transactions on Automatic Control, Vol.36, No.1, pp. 4-13.
[9] Ha, Yun-Su and Yuta, Shin'ichi (1996), Trajectory tracking control for navigation of the inverse pendulum type self-contained mobile robot, Robotics and Autonomous Systems, Vol. 17, pp. 65-80.
[10] Haid, Markus et al. (2004), Low cost inertial orientation tracking with Kalman filter, Applied Mathematics and Computation, Vol.153, pp. 567–575.
[11] Hyde, R.A et al. (2008), Estimation of Upper-Limb Orientation Based on Accelerometer and Gyroscope Measurements, IEEE Transactions on Biomedical Engineering, Vol. 55, pp. 746-750.
[12] Kalman, R.E.,(1960), A New Approach to Linear Filtering and Prediction Problems, Transactions of ASME-Journal of Basic Engineering, 82 (Series D),35-45
[13] Kumar, N.S and Jann, T (2004), Estimation of attitudes from a low-cost miniaturized inertial platform using Kalman Filter-based sensor fusion algorithm, Sadhana, Vol. 29,No. 2, pp. 217–235.
[14] Li, Jingtao et al. (2008), Controller Design of a Two-Wheeled Inverted Pendulum Mobile Robot, IEEE International Conference on Mechatronics and Automation, 2008.
[15] Luinge, H.J (2005), Measuring orientation of human body segments using miniature gyroscopes and accelerometers, IEEE Transactions on Biomedical Engineering, Vol.43, pp. 273-282.
[16] Takei, Toshinobu et al.(2009), Baggage Transportation and Navigation by a Wheeled Inverted Pendulum Mobile Robot, IEEE transactions on industrial electronics, Vol. 56, pp. 3985-3994.



Fig.1 Two Wheeled Robot

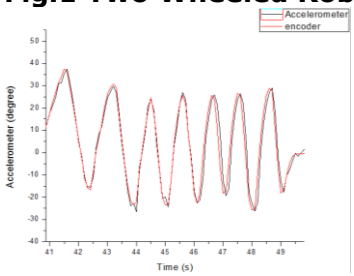


Fig.2 Accelerometer vs encoder

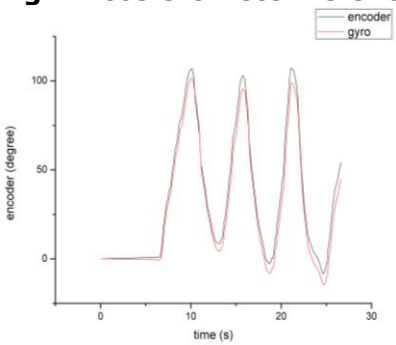


Fig.3 Gyroscope vs encoder

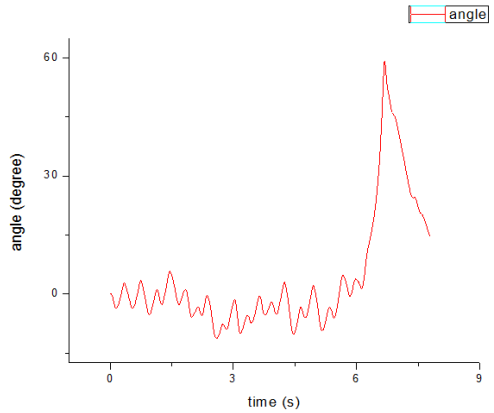


Fig.6 Angle of tilt while balancing

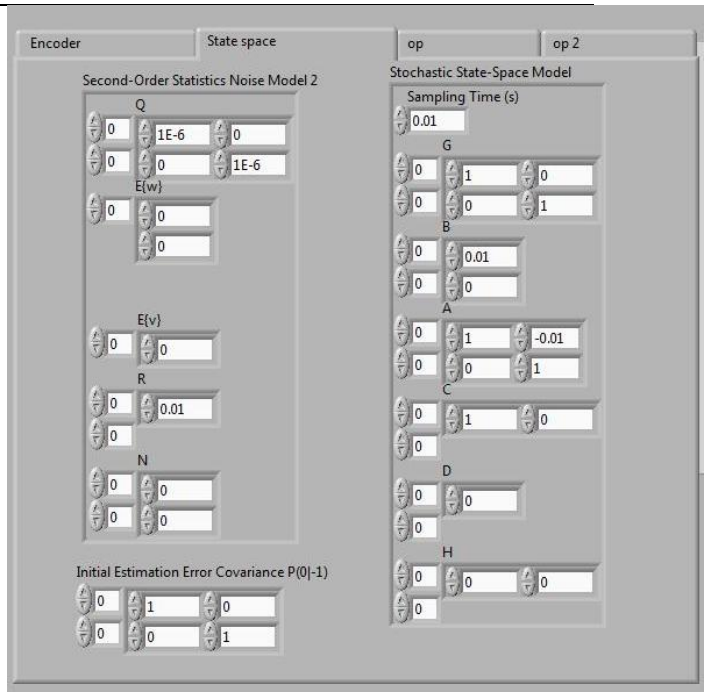


Fig.4 State space and stochastic noise models

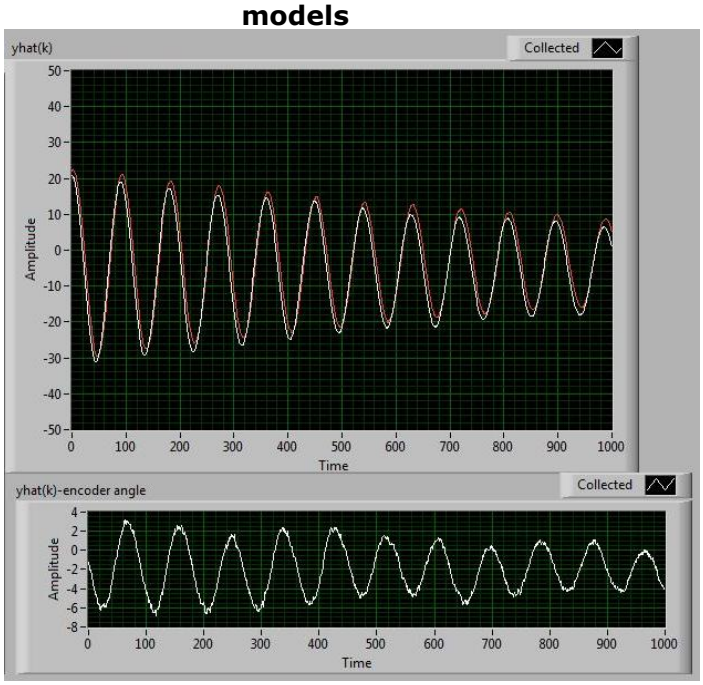


Fig.4 Kalman output vs encoder

2nd International Engineering Symposium - IES 2012
(KU-MU-NITK-HCMCUT Joint Symposium) March 5-7, 2012, Kumamoto University, Japan

Development of the suitable combustor and combustion characteristic of biofuels

Shun Matsuda, Shuichi Torii

Department of Mechanical System Engineering, Kumamoto University, Kurokami, 2-39-1, Kumamoto 860-8555, Kumamoto, JAPAN. E-mail: 088t3832@st.kumamoto-u.ac.jp

Abstract: Biofuels is made from biomass resource and it is a renewable energy source. Because it is contain of the energy from the sun. One of source of biomass is municipal solid waste. Thus it is used for biomass as part of waste reduction methods. The final goal of the study is to develop the combustor for the micro gas turbine using the biofuels. Here, emphasis is placed on maintaining the temperature in the furnace combustion and to maintain stable combustion extended periods. In the experiment, we investigate in the exhaust gas components, state of the temperature in the combustion furnace. Now, pyrolysis oil and pig manure is used to fuel. In case of combustion that mixed biomass with oil, it is important to maintain the stable combustion, analyze the constituent of exhaust gas, emit hot exhaust gas and remove the large sizes ashes in gas to drive a micro gas turbine.

Keywords: biomass, mixed combustion, exhaust gas, stable combustion

Introduction

In recent years, environmental and energy problems have steadily worsened. As one of solution, in this study is trying to use the energy from the combustion of biofuels. Biofuels are fuels derived from biomass which are attracting attention as a renewable fuel resource. Biomass has used the energy from the current ecosystem. Gases emitted by the consumption of biomass is absorbed again in the current ecological system has been constructed a circulation system. Therefore it is a renewable resource.

The purpose of this study is that to run a micro gas turbines using biomass fuels such as waste oil and waste liquid. In this experiments aims are reduction of emissions of toxic substances, hot gas emissions and the maintenance of steady state continuous combustion.

Methods

In this study, the experiments are performed as follows in the combustor. The experimental apparatus consists of fuel injection system and combustion chamber which have cyclone separator for

centrifugation. Fig.1 shows the fuel injection system. Two tanks is poured pig manure and pyrolysis oil. The fuel injector

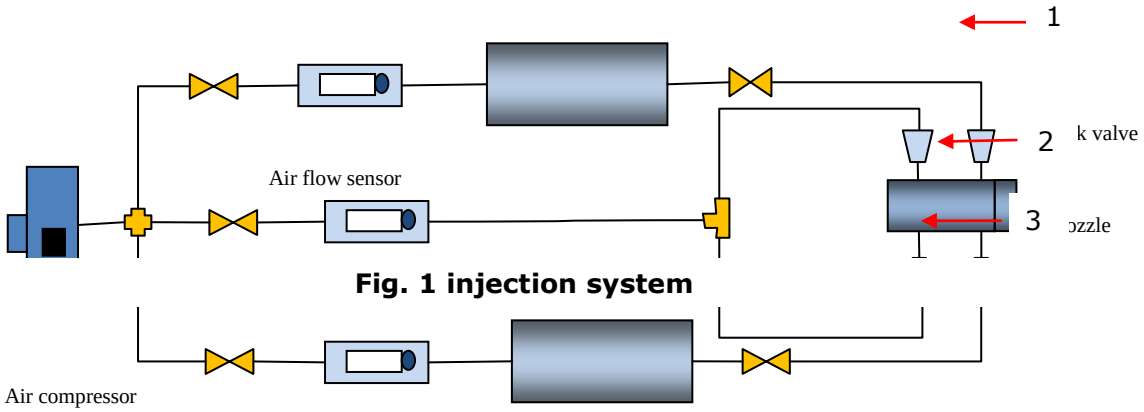


Fig. 1 injection system

is attached a swirl nozzle flow. Two tanks and nozzle attach to rubber heater. It is necessary to maintain at a high temperature fuel.[2] The fuel is mixed with the swirling flow, and it is injected from the nozzle.

Fig.2 shows the combustion chamber which is the shape of the cyclone separator. The combustion gas are subjected to the centrifugal motion in the combustion chamber which is the shape of the cyclonic separator, and separate out large solid particles, namely ash.[1] Position of thermo couple is three red allows.

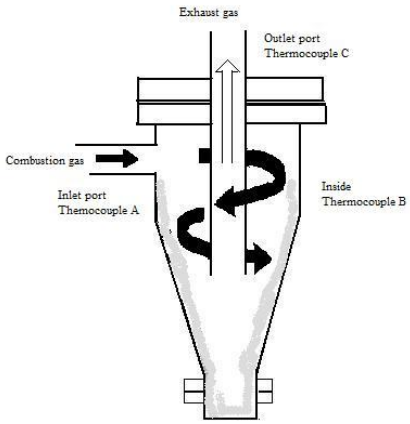


Fig. 2 combustion chamber

Fig.3 shows a joint of the combustion chamber and the fuel injection system. The unit uses a quartz glass tube connection, to confirm the combustion state.

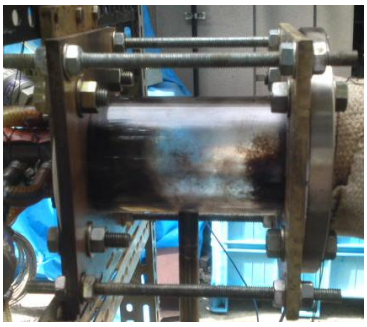


Fig. 3 joint of experimental apparatus

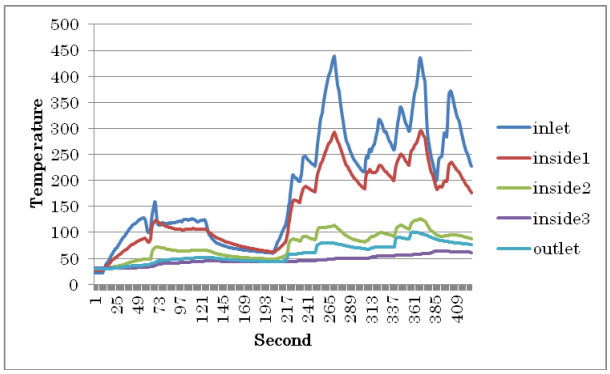


Fig. 4 result of experiment A

Result and discussion

Table 1 is amount of flow consumption fuel and air. The value is the average.

	Oil (l/min)	Air (l/min)	Liquid (l/min)	Rate of air/oil
A	0.35	20.00	0.46	57.14
B	0.65	17.91	0.80	27.56

Table 1 amount of flow consumption

Fig.4 and Fig.5 show the temperature distribution in the combustion furnace. Each experiment is not sustained long time and stable combustion. These results show what it doesn't lead to the continuation of the combustion.

On the other hand, temperature of outlet port is higher than it of inlet port 3.

And maximum heat loss is through from inside port 1 to inside port 2.

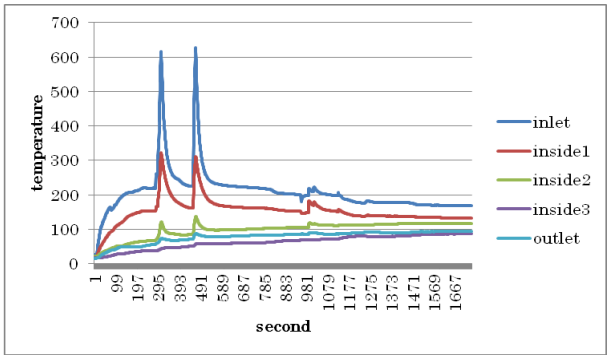


Fig. 5 result of experiment B

Conclusion

The following conclusions are deduced:

- Consider of amount of flow consumption. It needs to increase rate of flow air/oil.
- Decrease heat loss through from inlet port 1 to inlet port 2.

References

[1] Akira Ogawa, Ensihinbunriki(1980)
[2] Hideaki Tatibana, Misao Shioya, Keiji Wakai, Masaaki Fukushima, Technical development and future expectation of the pyrolysis for municipal post-use plastics (Journal of the japan institute of energy, 2007).

2nd International Engineering Symposium - IES 2012
(KU-MU-NITK-HCMCUT Joint Symposium) March 5-7, 2012, Kumamoto University, Japan

A Study of Conversion Diesel Engine to Fully Biogas Engine with Electronically Controlled

Nguyen Ngoc Dung[1] Vo Le Hoai Phuong[1] Phan The Anh[1] and **Tran Dang Long[1]**

1 *VNU-HCMC Key Lab for Internal Combustion Engine, Ho Chi Minh City University of Technology, 268 Ly Thuong Kiet street, district 10, Ho Chi Minh City, Vietnam. e-mail: dungnn2@hcmut.edu.vn*

Abstract: The using of biogas is growing very fast in the south region of Vietnam owing to its benefit in reducing environmental pollution and improving local economic. The main objective of this research was to convert a conventional direct-injection compression-ignition engine to a completely biogas engine. A prototype gaseous engine was modified from a direct-injection, 4-cylinder diesel engine. Injector nozzles were replaced by spark plugs and spark-ignition system with high-voltage was installed to ignite mixture. Biogas mixer system (venturi type) with electronically control was applied to replace diesel fuel system in order to supply gaseous fuel to the engine. In addition, engine management system with electronically controlled was used to control air-to-fuel ratio, ignition timing according to engine speed and load. The result showed that conversion biogas-based-diesel engine could operate fully with biogas (CH_4 62%) at high compression ratio (ε=17). The result from this research contributes for the development of high-efficiency biogas engines in Vietnam.

Keywords*: Biogas Engine, Venturi Mixer, High-Voltage Ignition System and High-efficiency.*

Introduction

The using of biogas is growing very fast in the south region of Vietnam owing to its benefit in reducing environmental pollution and improving local economic. Biogas is applying for home cooking, heating, and fuelled for internal combustion engine. By its advantages, central government has encouraged to apply biogas in the whole country as a positive way to solve the problem of energy security and environmental problem for Vietnam.

Binh Duong and Dong Nai provinces have high potential in applying biogas as an alternative fuel owing to its located of many big pig farms. According to government regulation, farm owners have to build biogas digesters to treat animal waste disposal and to protect local environment. The increases of biogas digesters contribute to the development of biogas application in local community, which help improve local economics and reduce environment pollution. However, the application of biogas in those provinces do not relevant to its potential and prospective owing to the limitation of research and technology transfer. The limitation of applying biogas may cause by the following reasons:

- Clean biogas: Most of biogas systems use directly raw biogas. The raw gas contains a large amount of H_2S. This is a harmful gas, which can cause corrosion metal surfaces and destroying engine and application system;
- Low biogas conversion efficiency: Biogas has been applying for internal combustion engine in order to supply energy for electric generator, water pump... Biogas engine has very low engine efficiency due to its converted from the spark-ignition engine. In addition, the engine is easily broken and corrosive by the raw biogas. Many

farmers stop using biogas engine due to its problems without technical support from the expert;

- Large application: Many big biogas digesters has been built and requested for large application. However, the research/system for large biogas application is lacked in Vietnam and required the action from researchers and the university;

Biogas has been applying for internal combustion engines widely in Vietnam. Biogas engine is converted from old spark-ignition engine (gasoline engine). The biogas-based-gasoline engine is contributing for economic development in rural area. Regularly, biogas engine is using for electric generator, water pump …and normally operates at low engine speed conditions (around 1500 rpm). Therefore, the conversion biogas-based-gasoline engine has low engine efficiency and generates low power output (<20 kW) compared to the original one (maximum power >60 kW). In order to get higher engine efficiency and higher power output, it required running engine at high-speed condition. However, the increase power output does not direct proportion to the engine speed or energy supply. Therefore, engine efficiency becomes worse at higher engine speed and increases tail pipe exhaust gas emissions.

Biogas-based-diesel engine may be a suitable solution to overcome the concern problems. At normal condition, conventional diesel operates at low and medium speeds and it has been widely applied for electric generator. Owning to similar characteristics, the conversion biogas-based-diesel engine for generator does not need too much change. In addition, the conventional diesel was manufactured with high compression ratio, high quality material; therefore, the conversion biogas engine is expected with higher thermal efficiency and longer using time. Furthermore, the biogas-based-diesel engine has the advantages that it can apply for various size of engine from small to big size (over 50 kW).

Popularly, there are three technologies to converse the conventional engine to the biogas engine [1-3]. Table 1 shows advantages and disadvantages of conversion method for biogas engine. According to this table, high efficiency biogas engine can be converted from compression ignition engine. The biogas-based-diesel helps reduce consumption of fossil fuel in operation and reduce contribution of CO_2 to the environment [4]. In addition, the application of high compression ratio spark-ignition biogas-engine for power generation will discard diesel-fuel dependence and has no soot in emission. So, the high-compression-ratio-spark-ignition-biogas-engine will overcome disadvantages of current conversion technologies [5,6]. The main objective of this research is to develop technology to convert diesel engine to biogas engine operating at high compression ratio. The conversion engine will operate at compression ratio higher than normal gas engine and expecting to generate high performance and high efficiency.

Conversion Engine

In order to convert diesel to biogas engine, the appropriate technologies are proposed to study as follow:

- Develop gas fuel system: In order to run with biogas, the conventional liquid fuel system is replaced by gas fuel system. Gas fuel system is calculated to control A/F ratio corresponding to engine load and speed.
- Design high voltage ignition system: Purified biogas with high methane concentration has different physical and chemical characteristics from gasoline and diesel fuel. This leads to different combustion characteristics such as in-cylinder pressure and rate of heat release. The conversion biogas engine is equipped with high voltage spark-ignition system. This special ignition system has a spark plug, ignition coil and electronic control unit and is designed by us for this study.
- Design and manufacture engine management system: Engine management system is very important to control engine with the variable of engine load and speed or the variable of biogas composition.

A direct-injection, water-cooled, natural aspiration, 4 cylinder diesel engine is used for this research. Engine has capacity 3,76

litter and compression ratio 17:1. In order to convert to spark-ignition biogas engine, injectors of the conventional engine are replaced by spark plugs. The position of fuel injection pump, crankshaft and camshaft sensors are used to determine the engine speed and control the advance ignition. The 50kVA electric generator was coupled to the engine via rubber coupling. Figure 1 shows principle of biogas-based-diesel engine.

Electric control biogas system, one of the most significant systems, ensures to supply adequately biogas for the engine. This system used a venturi mixing and the number and size of holes biogas supply are designed with the help of CFD software. Intake air flow rate and biogas flow rate are determined by the differential pressure of MAPs (Manifold Absolute Pressure). Thermocouples NTC are used to determine the intake air temperature and the biogas temperature to supply accuracy signals for ECU. In addition, the system has three stepper motors to control the intake air flow rate, the biogas flow rate and the A/F ratio. Throttle valve (4) controls air-fuel mixture to the engine and it was applied to manage the engine's operation stability. Biogas valve (7) controls the biogas flow rate to ensure the desired A/F ratio for the engine. The vacuum valve (2) controls the intake-vacuum-pressure and it is applied to increase the biogas flow rate to the engine when starting and the pressure of biogas sources is low. In addition to mechanical elements, a PID-feedback-controller is designed to achieve the desired A/F ratio through controlling concurrently the biogas valve and the intake air valve.

Electric control direct ignition system

For the purpose of completely eliminating diesel fuel and reduce soot emission, the engine used the direct ignition system to ignite air-fuel mixture in the end of compression period. Because, the compression ratio of the engine still remains at 17:1 so the direct ignition system has ability to ignite in high pressure, especially in cold start. A direct ignition CDI-DC model was developed to adjust the stored energy from 11,75mJ to 1.175mJ and change steplessly advanced ignition angle from 60^0BTDC to 15^0ATDC. Each of cylinders has bobine to create spark to ignite air-fuel mixture. Figure 3 shows direct ignition system design and manufacture by us.

Engine Management System

Engine management control system is designed to collect data and control engine with the variation of engine speed and load. Electronic control unit (ECU) was built with input specification (table 2), output specification (Table 3) and operation function (table 3).

The ECU was designed with processor AT89S53 of ATMEL and dsPIC30F4011 of Microchip because of its popularity and lower cost. Processor AT89S53 is used to collect and monitor engine operation parameters such as engine speed, temperature, pressure, battery voltage; and control step motor to open operation valve, spark ignition timing, relay and sonenoil valves. Processor dsPIC30F4011 is used to measure and calculate signal with high frequency such as intake mass flow, biogas flow, voltage and ampare of generator, calculating and control A/F ratio, spark ignition time. These processors are connected by using SPI, which can transfer data with speed 0,01 s (100 Hz). The purpose of separate and using 2 processor help system operate with high speed, real-time response and encrease ability to reduce noise.

Personal computer with human interface was used to store data and display control real-time control data. With active screen, people can adjusting parameters while engine is operating. Personal computer connect to ECU by RS-232. Human interface software was built based on LabVIEW. Operator can monitor and control A/F ratio, spark-ignition time and engine speed. The program permits to control engine operation follow ECU program or by modification program from personal computer.

Conclusions

Conversion biogas engine can

The following conclusions are deduced from this study:

- The conversion biogas engine operates with 100% biogas. Engine run well at low load condition.

- Biogas engine can operate at compression ratio 17. The engine is expected to work at higher load condition.
- Venturi mixture, spark-ignition system and engine management system can respond with engine load and speed.
- The conversion biogas engine does not contribute CO_2 to the environment.
- Using biogas engine could contribution for developing rural economic and encourage local people enhance to the issue of energy and environmental pollution.

Acknowledgements
The authors would like to thanks JICA SUPREM-HCMUT project (project B3-12) has provided financial support to carry out this research. Many thanks to Professor Shuichi Torii, Kumamoto University for his valuable advises for the project.

References
[1] Mitzlaff, Klaus Von, *Engine for biogas*, Deutsche Gesellschaft für Technische Zusammenarbeit (GTZ) GmbH, 1988.
[2] *DOE fundamentals handbook mechanical science* - Volume 2 of 2, U.S. Department of energy, DOE-HDBK, Washington DC, 1993.
[3] A.Chigier, *Progress in energy and combustion science*, An International Review Journal, Pregamon, U.S., 1999.
[4] *Biogas as Vehicle Fuel,* Trendsetter Report No. 3, Stockhom, October 2003.
[5] N. Mustafi, R. R. Raine and P. K. Bansal, *Biogas Fuel for Internal Combustion Engines*, Department of Mechanical Engineering, The University of Auckland, 2006.
[6] *Renewable energy in the U.S. biogas,* Swidish Trade Council, U.S., January 2008.

Table 1 Comparison of conversion technology for biogas engine

No	Based Engine	Conversion technology	Advantage	Disadvantage
1	Spark-ignition engine	No modification	- Simple and low cost. - Carbon neutral.	- Low engine efficiency
2	Compression ignition engine	Reduce compression ratio, set up ignition system	- Complicated, high cost. - Carbon neutral.	- Medium engine efficiency.
			- Simple, low cost	- Diesel knocking.

Table 2 Input signal of electronic control unit

No	Input	Purpose
1	Camshaft sensor	Determine engine speed, position of crank angle and combustion sequency of engine
2	Intake temperature	Adjusturement air intake
3	Biogas temperature	Adjusturement biogas intake
4	Water temperature	Monitor
5	Oil temperature	Monitor
6	Exhaust temperature	Monitor
7	Air pressure	Adjustement intake air
8	Biogas pressure	Adjusturement biogas flow
9	Oil pressure	Monitor
10	Intake flow	Control A/F ratio
11	Biogas flow	Control A/F ratio
12	Throttle position	Control engine speed
13	Position of control valve	Control A/F ratio
14	MAP	Control A/F ratio
15	Battery voltage	Monitor
16	Generator voltage	Monitor
17	Electric ampare	Monitor

Table 3 Output signal of electronic control unit

No	Output	Control object	Purpose
1	Throttle open position	Stepped motor control position	Control engine speed
2	Position of control valve	Stepped motor control valve position	Control A/F ratio
3	Position of MAP	Stepped motor control position of absolute valve	Control A/F ratio
4	Spark-igntion time	Control CDI-DC	Control engine speed and other
5	Biogas valve	Solenoid valve	Stop biogas inlet
6	Alarm	Alarm relay	Alarm signal
7	Emergency stop	Emergency relay	Contrl emergency stop

Table 4 Operation function of electronic control unit

No	Function	No	Function
1	Determine intake flow	8	Giám sát điện áp và dòng điện máy phát
2	Determine biogas flow	9	Monitoring misfire
3	Determine engine speed	10	Alarm
4	Determine difference among cylinders	11	Emergency stop
5	Determine crank angle position	12	Control A/F ratio
6	Monitoring temperature and pressure	13	Control advance spark igintion
7	Monitoring battery voltage	14	Control engine speed

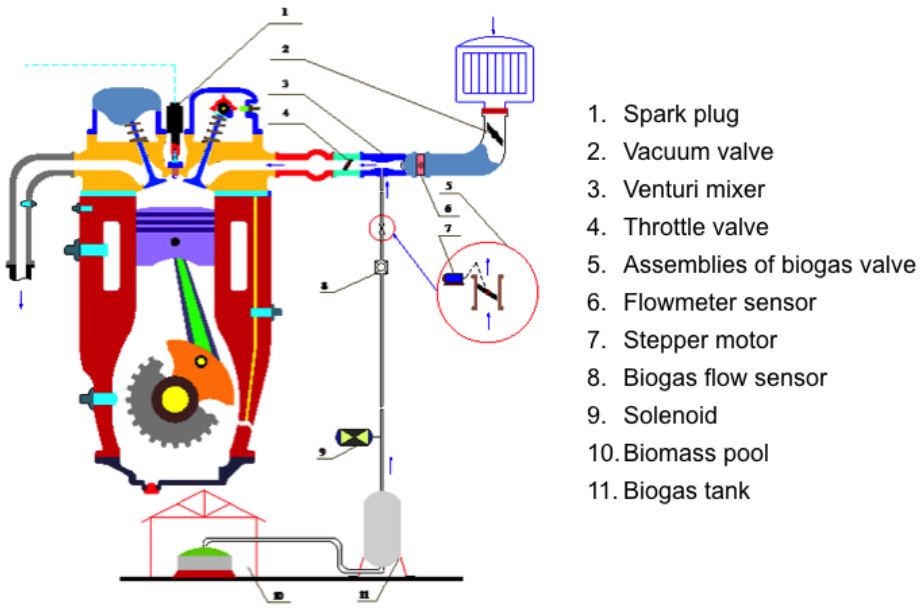


Fig.1 Schematic arragement of biogas-based-diesel engine

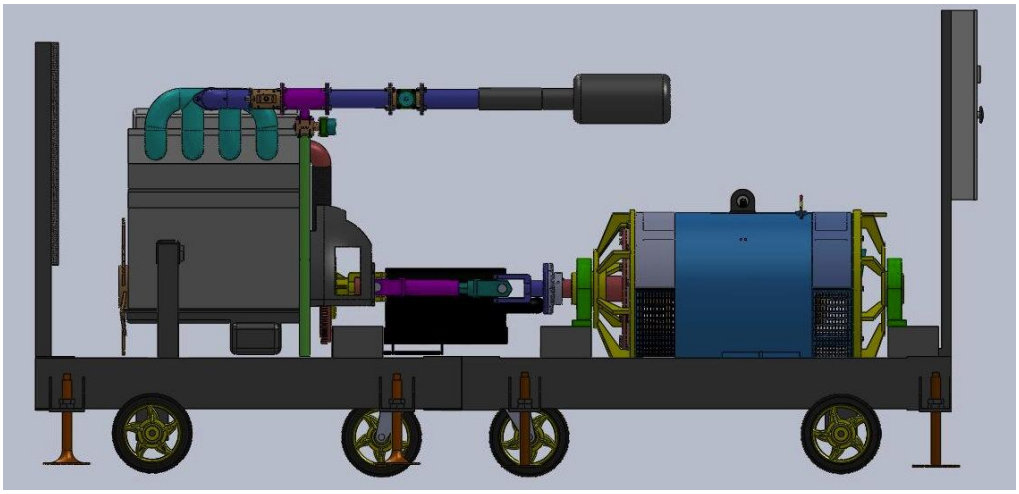


Fig.2 Design of manufactureing biogas generator



Fig.3 High voltage direct ignition system on conversion engine

2nd International Engineering Symposium - IES 2012
(KU-MU-NITK-HCMCUT Joint Symposium) March 5-7, 2012, Kumamoto University, Japan

Numerical Analysis of Gas Turbine HP Stage Blade Cooling with New Cooling Duct Geometries

Chandrakant R Kini [1] **Satish Shenoy B [2]** and **N Yagnesh Sharma [3]**

1 *Dept of Mechanical Engg.,MIT, Manipal University, Manipal, Karnataka State, India*
2 *Dept of Aeronautical and Automobile Engg., MIT, Manipal University, Manipal, Karnataka State, India.*
3 *Dept of Mechanical Engg., MIT, Manipal University, Manipal, Karnataka state, India. Email: nysharma@hotmail.com*

Abstract: The *turbine blades of HP stage are rather small to incorporate the blade cooling techniques efficiently. The current turbine entry temperature levels in advanced gas turbines exceed the melting point of the blade. So, along with high temperature material development, a novel cooling scheme must be developed for safe operation of HP stage. An effort has been made in this paper to computationally analyze the HP stage turbine blade for effective cooling using new duct within the blade. An helicoidal duct with circular cross-section has been analyzed corresponding to different duct diameters and pitch length of the helix. It is found from the analysis that helicoidal cooling duct with larger diameter and with lower pitch length provides a vastly improved cooling compared to straight ducted cooling ducts for the HP stage.*

Keywords*: HP Stage Turbine Blade Cooling, Innovative Cooling Geometries*

Introduction

Gas turbines are extensively used for aircraft propulsion, land-based power generation, and industrial applications. The gas turbine is a power plant, which produces a great amount of energy for its size and weight. Its compactness, low weight and multiple fuel application make it a natural power plant for many applications

Thermal efficiency and power output of gas turbines increase with increasing turbine entry temperature (TET). It is clear from Brayton cycle that the increase in pressure ratio increases the gas turbine thermal efficiency accompanied with increase in turbine firing temperature. The increase in pressure ratio increases the overall efficiency at a given temperature. However increasing the pressure ratio beyond a certain value at any given firing temperature can actually result in lowering the overall cycle efficiency [Horlock J H. (2001)].

As the TET increases, the heat transferred to the blades in the turbine also increases. The level and variation in the temperature within the blade material (which causes thermal stresses) must be limited to achieve reasonable durability goals. Also the temperatures are far above the permissible metal temperature due to which there is a need to cool the blades to operate without failure [Han J. et al. (2011)].

Therefore, along with high temperature material development, a sophisticated cooling scheme must be developed for HP stage turbine blade for continuous safe operation with high performance. Several research works are being carried out to address the above problems.

Problem statement and assumptions

The objective of the analysis is to study the effect of helicoidal cooling ducts on gas turbine blade cooling by varying the geometric parameters and comparing the same with circular cooling ducts. The following assumptions are made.

1. The computational domain is assumed to be made of solid-liquid interface with

conjugate heat transfer.
2. Steady incompressible flow for the fluid.
3. Flow is assumed to be turbulent with fully developed conditions.
4. Solution is marched in time and steady state is assumed to be obtained after all residuals are bought to prescribed constant values.

Numerical model

The commercial CFD software FLUENT (version 6.3.26) from Fluent, Inc. is employed for analysis. The simulation uses the segregated solver, which employs an implicit pressure-correction scheme. The SIMPLE algorithm is used to couple pressure and velocity. First order upwind scheme is selected for spatial discretization of the Reynolds Averaged Navier Stokes (RANS) equations as well as energy and turbulence equations. Converged results are obtained after the residuals were found to be less than the specified values. A converged result renders an energy residual of 10^{-6}, and momentum and turbulence kinetic energy residuals being 10^{-5}[Li X. et al. (2008)].

Flow equations

All the equations are presented in Cartesian tensor notation.

Mean flow equations:

Continuity:

$$\frac{\partial}{\partial x_i}(\rho U_i) = 0 \qquad (1)$$

Momentum Transport:

$$\frac{\partial}{\partial x_j}(\rho U_i U_j) = \frac{\partial P}{\partial x_i} + \frac{\partial}{\partial x_j}\left[\mu\left(\frac{\partial U_i}{\partial x_j} + \frac{\partial U_j}{\partial x_i}\right) - \rho\overline{u_i u_j}\right] \qquad (2)$$

Enthalpy:

$$\frac{\partial}{\partial x_j}(\rho U_i T) = \frac{\partial}{\partial x_j}\left[\frac{\mu}{\Pr}\frac{\partial T}{\partial x_j} - \rho\overline{u_i t}\right] \qquad (3)$$

Turbulence modeling equations

Zonal k-ε model: This consists of the high-Re k-ε in the fully turbulent core:

$$\frac{\partial}{\partial x_j}(\rho U_j k) = \frac{\partial}{\partial x_j}\left[\left(\mu + \frac{\mu_t}{\sigma_k}\right) - \frac{\partial k}{\partial x_j}\right] + P_k - \rho\varepsilon \qquad (4)$$

$$P_k = -\rho\overline{u_i u_j}\left(\frac{\partial U_i}{\partial x_j}\right) \qquad (5)$$

$$\frac{\partial}{\partial x_j}(\rho U_j \varepsilon) = \frac{\partial}{\partial x_j}\left[\left(\mu + \frac{\mu_t}{\sigma_\varepsilon}\right) - \frac{\partial \varepsilon}{\partial x_j}\right] + c_{\varepsilon 1}\frac{\varepsilon}{k}P_k - \rho c_{\varepsilon 2}\frac{\varepsilon^2}{k} \qquad (6)$$

Computational domain for the analysis

While the configuration of the internal cooling ducts in real gas turbine airfoil can be highly complicated, in the present analysis, a simplified geometric model with different ducts of varying geometry is being studied for the effective cooling consideration as shown in figure 7. In general, the coolant air enters the cooling ducts from the blade root, flows through entire length of ducts and finally leaves from blade tip. The cooling process is entirely by internal convective cooling only.

The cooling ducts having through ducts of circular cross section with hole radius of 1.5 mm and 2 mm, helicoidal ducts of pitch length of 4 mm and 6 mm with circular cross section with hole radius of 1.5 mm and 2 mm are considered.

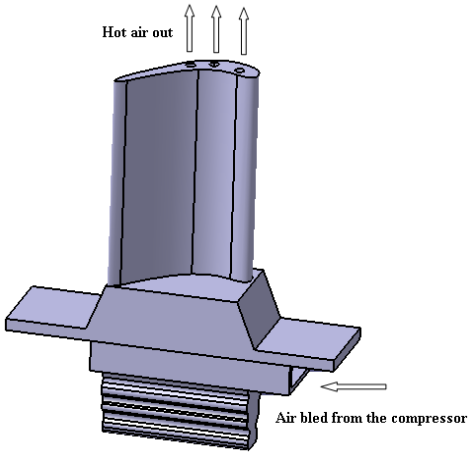


Fig. 1: Schematic of turbine blade with cooling ducts

Boundary Conditions

The required boundary conditions implemented in the study of blade profile and for inner cooling ducts are presented here. The boundary conditions are derived from the practical gas turbine operating conditions, corresponding to HP stage blade that are generally exposed to high

temperature and velocity. The through flow of hot gases over the turbine blade has a free stream temperature of hot gas as 1561 K and convective heat transfer coefficient of hot gas as 2028 W/m^{2}K. On the other hand the coolant air admitted at the duct of the blade root has an entry temperature of 644 K [Li X. et al. (2008)] and mass flow rate of 90 kg/hr. These settings are selected with a view to get a realistic representation of typical gas turbine operating conditions.

Table 1: Thermo physical properties of air at 644 K

Density	0.54 kg/m^3
Specific heat	1.06 kJ/kg K
Thermal conductivity	0.05 W/ m K
Kinematic Viscosity	59 × 10 $^{-6}$ m^2/s

Table 2: Thermal properties of blade material

Density	0.54 kg/m^3
Specific heat	1.06 kJ/kg K
Thermal conductivity	0.05 W/ m K
Kinematic Viscosity	59 × 10 $^{-6}$ m^2/s

Numerical grid, Meshing and Simulation Procedure

The information for geometric model for HP stage gas turbine was derived directly by measuring the coordinates of the blade profile using Coordinate Measuring Machine available in the Metrology Lab of Mechanical Engineering Department of MIT, Manipal. Gas turbine blades along with different cooling ducts configuration were modeled using the software CATIA (version V5 R14), which is an industry standard software for modeling.

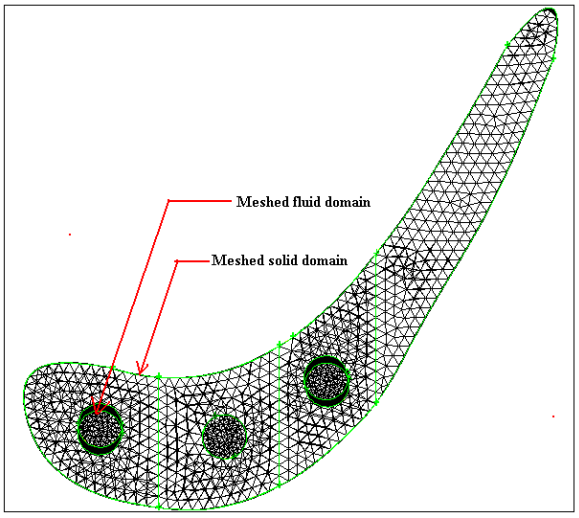


Fig. 2: Gas turbine blade modeled in CATIA and meshed in GAMBIT

To conduct numerical simulation, the computational domain as shown in figure 2, is meshed with control volumes built around each grid using GAMBIT (version 2.4.6), which is the preprocessor for FLUENT (version 6.3.26). The mesh for blade simulation is an unstructured type consisting of 2, 19,774 tetrahedral cells. But refined tetrahedral mesh was employed for cooling ducts as dimensions were very small, so as to extract good accuracy.

The grid independence test was performed to the quality of mesh for solution accuracy. The influence of further refinement did not change the result by more than 1.25 % which is taken here as appropriate mesh quality for computation.

Results and Discussions

The results of the thermal analysis in each case corresponding to parametric considerations of the geometry of the cooling duct are detailed below. The results analysis follows the cooling capabilities of helicoidal duct of various pitch lengths viz-a-viz the circular duct of same diameter.

The Non-dimensional temperature θ is defined as $\theta = \frac{T_\infty - T_L}{T_\infty - T_0}$ where T_∞ is hot gas temperature surrounding the blade profile

in a convective ambience, T_L is the temperature along the span length of the blade and T_o is temperature of the cooling air admitted to the cooling duct at the blade root. Similarly the Non-dimensional span length δ is defined as $\delta = \frac{L}{S}$ where L is the distance along the span length which the blade temperature is measured and S is overall span length

Case 1: Blade cooling with through duct of circular cross section of 1.5 mm radius and helicoidal duct of circular cross section and same radius with pitch length of 6 mm and 4 mm.

Figure 3 shows the non-dimensional temperature distribution of the exposed blade surface along the span at 30 % of chord length. This non-dimensional temperature distribution is taken at this position for all the different cases for the purpose of comparison. It is seen from the figure that with circular cooling duct along the span, the non-dimensional temperature has lower bound value of around 0.31 and upper bound of 0.45 only. The corresponding helicoidal duct of same radius but with pitch length 6 mm shows significant drop in blade surface temperature change as shown in the figure 3. The blade non-dimensional surface temperature change is from lower bound value of 0.36 to upper bound value of 0.54 along the span length.

This drastic cooling of turbine blade can easily be ascribed to large convective area available within the helicoidal duct corresponding to a pitch length of 6 mm. The advantage of the helicoidal cooling duct is accentuated more if we consider the same helicoidal duct with different pitch length of 4 mm. As seen in figure 9, with 4 mm pitch length, the corresponding convective area for heat transfer increases even more than the previous case and is reflected as steep non-dimensional temperature change varying from 0.40 to 0.585.

Figure 4 shows heat flux dissipated from cooled blade surface. It is clear that for circular ducted blade there is comparatively only negligible dissipation of thermal energy due to cooling of blade surface. Whereas for the helicoidal ducted blade as seen from the figure, a large flux dissipation occurs over the blade surface due to better cooling corresponding to the enhanced area available for helicoidal ducted blade. It is also possible that due to helicoidal nature of cooling duct, the heat dissipation rate is augmented because of turbulence that is brought about due to the path of the cooling duct. The combined effect is beneficial for maximum possible blade surface cooling.

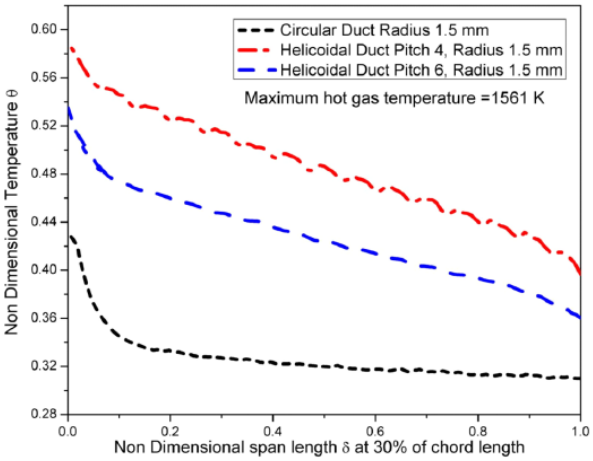


Fig. 3: Non-dimensional Temperature variation along the span length of the blade

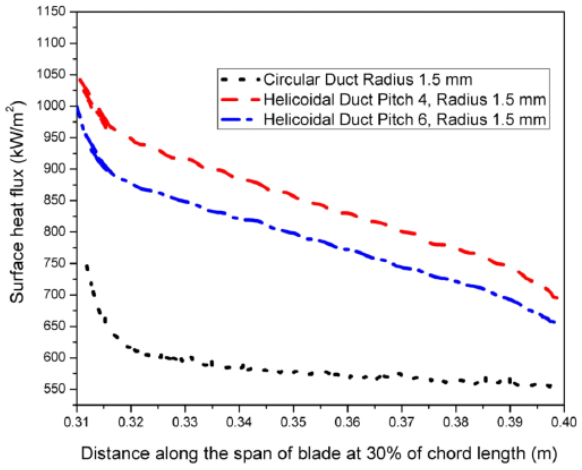


Fig. 4: Surface heat flux variation over the span of the blade

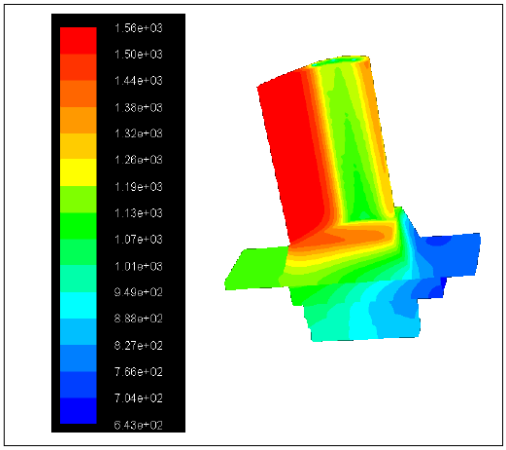


Fig. 5: Temperature of blade surface having Helicoidal cooling duct of Pitch 6 mm and radius of 1.5 mm

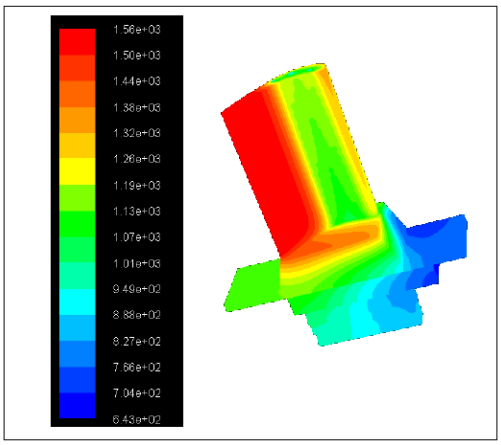


Fig. 6: Temperature of blade surface having Helicoidal cooling duct of Pitch 4 mm and radius of 1.5 mm

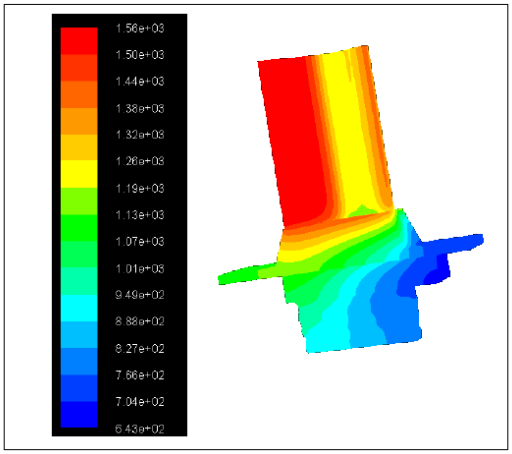


Fig. 7: Temperature of blade surface having Circular cooling duct of radius 1.5 mm

<u>Case 2: Blade cooling with through duct of circular cross section of 2 mm radius and helicoidal duct of circular cross section and same radius with pitch length of 6 mm .</u>

Since it is physically not possible to place a helicoidal duct of 2mm radius with pitch length of 4 mm inside the blade, this model is not taken for comparison purposes in this case. As seen in the figure 8 and 9 the phenomena explained for case 1 are manifested to almost the same extent for the level of cooling that is achieved when using larger cooling duct of 2 mm instead of 1.5 mm. In the case of circular duct there is negligible drop in temperature. But the gradient across the cooling surface is almost unchanged whereas for helicoidal cooling ducts with pitch length 6 mm it could be easily seen that there is reasonable change with respect to minimum and maximum possible surface temperature drop along the span length of the blade. This is due to the fact that by providing larger radius for the duct the effective convective area for the duct to exchange heat with the hot surface of the blade increases. And also possibly due to higher turbulence of the flow, as explained earlier.

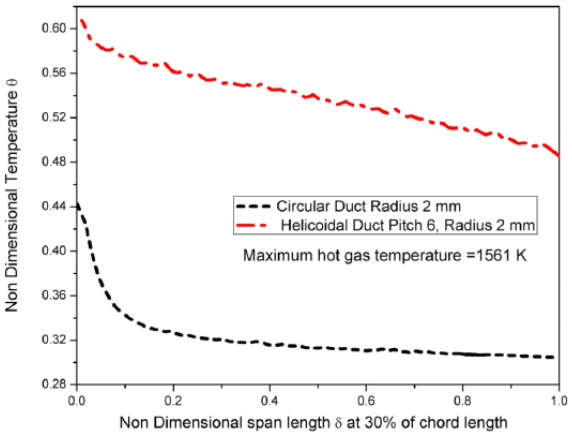


Fig. 8: Non-dimensional temperature variation along the span length of the blade

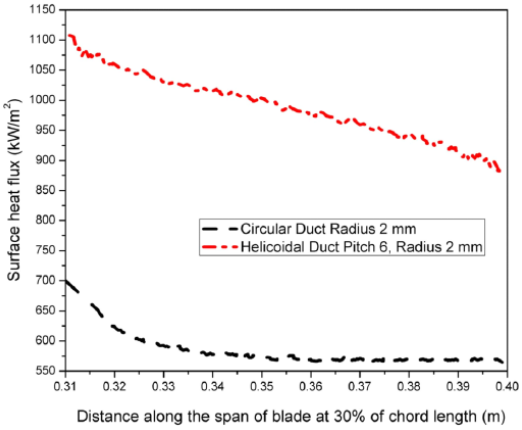


Fig. 9: Surface heat flux variation over the span of the blade

An interesting observation that can be made from figure 8 and 9 is that for helicoidal cooling ducts there is a minor fluctuation of temperature and heat flux over the span length of the blade. This is because of helicoidal nature of the cooling duct itself in which the duct passage is alternately will be in the vicinity of the leading and trailing surfaces of the blade, whereas at other positions the cooling duct is away from these two surfaces. Hence when the cooling duct is near to the surfaces there is enhanced cooling of the blade surfaces than when the cooling duct is positioned away from the two surfaces. This results in the fluctuations in the temperature profile as shown in the figure 8 and 9.

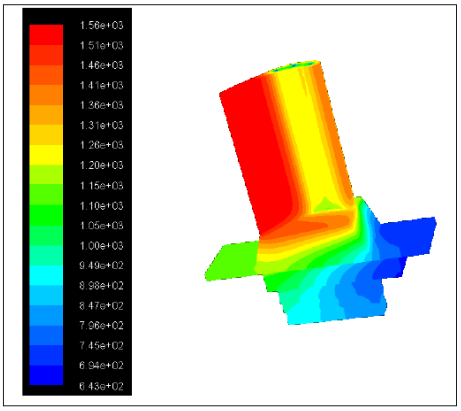


Fig. 10: Temperature of blade surface having Circular cooling duct of radius 2 mm

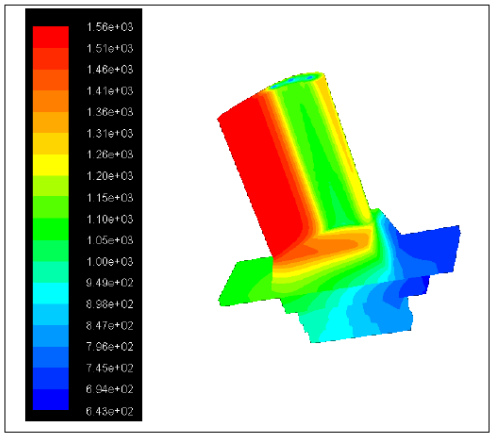


Figure 18: Temperature of blade surface having Helicoidal cooling duct of Pitch 6 mm and radius of 2 mm

The efficacy of using helicoidal cooling ducts is therefore justified but associated difficulties with respect to practical manufacturing of a turbine blade with helicoidal cooling ducts remains to be explored.

CONCLUSION

From present numerical analysis the following conclusions are derived.

- It is seen that an innovative helicoidal cooling passage, provides an augmented convective area for better heat dissipation.
- The helicoidal path also acts as a turbulators providing extended dissipation rates due to turbulence of flow.
- The diameter and pitch length plays a major role in optimizing the geometry of the helicoidal cooling passage.
- The temperature distribution shows wiggles in the solution due to proximity of the suction and pressure surfaces alternately for the helicoidal ducted passage

Acknowledgements

The Corresponding author wishes to gratefully acknowledge the financial support extended by the Manipal University, Manipal, India for sponsoring to this conference. The computational facilities were extended by Department of Mechanical Engineering, MIT,Manipal which is thankfully acknowledged

References

[1] Acharya, S., Dutta, S., Myrum, T.A., and Baker, R.S., (1993); "Periodically Developed Flow and Heat Transfer in a Ribbed Duct." International Journal of Heat and Mass Transfer, Vol. 36, No.8, pp. 2069-2082

[2] Chyu, M.K., and Naturajan. V (1995); "Surface heat transfer from a three-pass blade cooling passage simulator", J. Heat Transfer, Vol. 117, pp. 650–656.

[3] Kim, Y. W., Metzger, D. E., (1995); "Heat Transfer and Effectiveness on Film Cooled Turbine Blade Tip Models," J. Turbomachinery, Vol. 117, pp. 12-21.

[4] Prakash, C., and Zerkle, R., (1995); "Prediction of Turbulent Flow and Heat Transfer in a Radially Rotating Square Duct." ASME Journal of Turbomachinery, Vol. 114, No. 4, pp. 835-846.

[5] Dutta, S., Andrews, M.J., and Han, J.C., (1996); "Prediction of Turbulent Flow and Heat Transfer in Rotating Square and Rectangular Smooth Channels." International Gas Turbine & Aeroengine Congress & Exhibition, Birmingham, UK, June 10- 13, ASME Paper 96-GT-234

[6] Han, J., Ekkad, S. (2001); "Recent Development in Turbine Blade Film Cooling", Int. J. of Rotating Machinery, Vol. 7, pp. 21-40.

[7] Horlock, J.H. (2001); "Basic thermodynamics of turbine cools", J. Turbomachinery, Vol. 123, pp. 583-592.

[8] Li, X., Wang, T. (2008); "Computational Analysis of Surface Curvature Effect on Mist Film-Cooling Performance", J. Heat Transfer, Vol. 130, pp. 121901-10.

[9] Li, X.., Wang, T. (2008); "Two-Phase Flow Simulation of Mist Film Cooling on Turbine Blades With Conjugate Internal Cooling", J. Heat Transfer, Vol. 130, pp. 102901-8.

[10]http://new.bibus.cz/pdf/Special_Metals/Nikl/prehled/ nimonic-alloy_90_105.pdf

[11]http://www.engineeringtoolbox.com/airproperty-d_156.html

2nd International Engineering Symposium - IES 2012
(KU-MU-NITK-HCMCUT Joint Symposium) March 5-7, 2012, Kumamoto University, Japan

Analysis of elliptical perforated tube muffler

Sohei Nishimura[1], *Yuya Nishimura[2]*

1 *Kumamoto National College of Technology, 2627 Hirayama-Shin-Machi, Yatsushiro Kumamoto 866-8501 JAPAN, e-mail: nisimura@kumamoto-nct.ac.jp*
2 *Kumamoto National College of Technology 2659-2 Suya Koshi-shi, Kumamoto 861-1102 JAPAN, e-mail: nishimura@kumamoto-nct.ac.jp*

Abstract: Evidently, a perforated pipe is an essential component in muffler systems. It has the ability to reduce the power levels of noise sources generated by flow.

In this work, a method to derive the acoustic characteristic of elliptical perforated tube muffler with consideration of higher order mode is presented. Some comparisons between the experimental measurements and the predicted results were discussed. The mean flow velocity was not considered in this paper.

***Keywords**: muffler, perforated tubes, acoustic impedance, resonance frequency*

Introduction

Perforated tubes are a commonly used feature in muffler designs, mainly of their ability to reduce the acoustic power of the noise generated by flow significantly influenced by its velocity [1]-[5]. Contemporary automotive muffler chambers consist of more than one resonance room and expansion room jointed together in series, in which one or several perforated pipe is installed. When the dimension of each element is small comparable with the acoustic wavelength, the one-dimensional model four-pole parameter is frequently used. However, by the presence of a perforated pipe, the one-dimension frequency range will become extremely narrow due to the generation of higher order modes at low frequency range. In order to estimate the performance of mufflers in wide frequency range, the modelling or analysing of such an arrangement would require the acoustic characteristic including with the higher order modes effect.

In the present work, a method to derive the acoustic characteristic of an elliptical perforated tube muffler with a consideration the higher order mode effect is suggested. Some comparisons between the experimental measurements and the predicted results are also discussed. The mean flow velocity was not considered in this paper.

Analysis Methods

Model of analysis and boundary conditions

Consider the elliptic cylindrical cavity of eccentricity e_w and length ℓ having a thin perforated tube in elliptical form as shown in Fig. 1. The eccentricity of the input, perforated tube and the output are e_0, e_p and e_l, respectively. Assume that the acoustic impedance of perforated tube can be regarded as uniform over its surface.

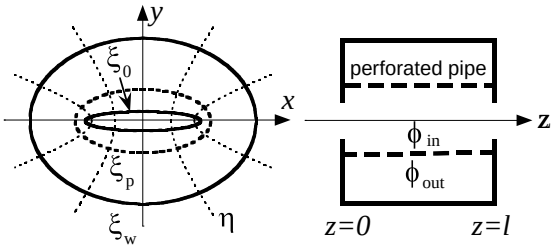


Fig.1 Perforated tube muffler model

The general solution of the wave equation in elliptical co-ordinates is a combination of some function as follows [6]

$$\phi(\xi,\eta,z) = A_0 \exp(\mu z) + B_0 \exp(-\mu z) \left(\sum_{m=0}^{\infty} C_m Ce_m(\xi,s)\, ce_m(\eta,s) + \sum_{m=0}^{\infty} S_{m+1} Se_{m+1}(\xi,s)\, se_{m+1}(\eta,s) \right) \quad (1)$$

Where $\phi(\xi,\eta,z)$ is the velocity potential, A_0, B_0, C_m and S_{m+1} are arbitrary constants determinable from the boundary conditions. Function $ce_m(\eta,s)$ and $Ce_m(\xi,s)$ are even and even modified Mathieu function of m-th order, $se_m(\eta,s)$ and $Se_m(\xi,s)$ are odd and odd modified Mathieu function of m-th order, respectively. The value of s is defined by the following equation.

$$s = \frac{q^2}{4} k^2 + \mu^2 \quad (2)$$

where q is the distance between the foci and the origin, $k = \omega / c$ with ω and c are the angular frequency and the sound velocity, respectively, μ is arbitrary constant.

Let the velocity potential inside the perforated tube be ϕ_{in} and that outside the tube be ϕ_{out}, respectively. Since the distribution of ϕ_{in} is symmetrical to the major and the minor axis, ϕ_{in} must be even and periodic in η, hence the general solution of ϕ_{in} becomes

$$\phi_{in} = A_i \exp(\mu z) + B_i \exp(-\mu z) \sum_{m=0}^{\infty} C_m Ce_m(\xi,s)\, ce_m(\eta,s) \quad (3)$$

Since ϕ_{out} has both symmetrical term and a unsymmetrical term, the general solution of ϕ_{out} becomes

$$\phi_{out} = A_0 \exp(\mu z) + B_0 \exp(-\mu z) \left(\sum_{m=0}^{\infty} C_m Ce_m(\xi,s)\, ce_m(\eta,s) + \sum_{m=0}^{\infty} S_{m+1} Se_{m+1}(\xi,s)\, se_{m+1}(\eta,s) \right) \quad (4)$$

The boundary conditions are as follows

[1] at $z = 0$, $V_z = -\frac{\partial \phi_{in}}{\partial z} = V_0 F_0(\xi,\eta)$ (5)

[2] at $z = l$, $V_z = -\frac{\partial \phi_{in}}{\partial z} = V_l F_l(\xi,\eta)$ (6)

[3] at $\xi = \xi_\omega$, $V_\xi = -\frac{\partial \phi_{out}}{\partial \xi} = 0$ (7)

[4] at $z = l$, $V_z = -\frac{\partial \phi_{out}}{\partial z} = 0$ (8)

Where V_z and V_ξ are the velocity components in the z, ξ directions, V_0 and V_l are the driving velocity at the input and the output piston,

$F\ \xi,\eta\ =1$ at the piston and $F\ \xi,\eta\ =0$ elsewhere,

Let the sound pressure and the volume velocity inside the perforated pipe be P_{in} and U_{in}, respectively. Let those outside the perforated pipe be P_{out} and U_{out} respectively. Then at the surface of perforated pipe $\xi=\xi_p$, the following relations are obtained

$$P_{in}=P_{out}+Z_{pipe}U_{out} \tag{9}$$

$$U_{in}=U_{out} \tag{10}$$

Where Z_{pipe} is the impedance of perforated pipe. Since the sound pressure P and volume velocity U are related to the velocity potential ϕ by $P=jk\rho c\phi$ and $U=\partial\phi/\partial\xi$, Eqs. (6) and (7) are then represented as

$$\text{[5] at } \xi=\xi_p,\ \phi_{in}-\phi_{out}=\frac{Z_{pipe}}{jk\rho c}\frac{\partial\phi_{out}}{\partial\xi} \tag{11}$$

$$\text{[6] at } \xi=\xi_p,\ \frac{\partial\phi_{in}}{\partial\xi}=\frac{\partial\phi_{out}}{\partial\xi} \tag{12}$$

In order to find ϕ_{in} and ϕ_{out} from Eqs.(5) to (12), let ϕ_{in}^a and ϕ_{out}^a be the solution of Eq.(3) and Eq.(4) obtained for the following boundary conditions:

$$\text{[1a] at } z=0,\ V_z=-\frac{\partial\phi_{in}^a}{\partial z}=V_0F_0\ \xi,\eta \tag{13}$$

$$\text{[2a] at } z=l,\ V_z=-\frac{\partial\phi_{in}^a}{\partial z}=0 \tag{14}$$

$$\text{[3a] at } \xi=\xi_\omega,\ V_\xi=-\frac{\partial\phi_{out}^a}{\partial\xi}=0 \tag{15}$$

$$\text{[4a] at } z=l,\ V_z=-\frac{\partial\phi_{out}^a}{\partial z}=0 \tag{16}$$

$$\text{[5a] at } \xi=\xi_p,\ \phi_{in}^a-\phi_{out}^a=\frac{Z_{pipe}}{jk\rho c}\frac{\partial\phi_{out}^a}{\partial\xi} \tag{17}$$

$$\text{[6a] at } \xi=\xi_p,\ \frac{\partial\phi_{in}^a}{\partial\xi}=\frac{\partial\phi_{out}^a}{\partial\xi} \tag{18}$$

and let ϕ_{in}^b and ϕ_{out}^b be the solution of Eq.(3) and Eq.(4) obtained for the following boundary conditions:

$$\text{[1b] at } z=0,\ V_z=-\frac{\partial\phi_{in}^b}{\partial z}=0 \tag{19}$$

$$\text{[2b] at } z=l,\ V_z=-\frac{\partial\phi_{in}^b}{\partial z}=V_lF_l\ \xi,\eta \tag{20}$$

$$\text{[3b] at } \xi=\xi_\omega,\ V_\xi=-\frac{\partial\phi_{out}^b}{\partial\xi}=0 \tag{21}$$

$$\text{[4b] at } z=0,\ V_z=-\frac{\partial\phi_{out}^b}{\partial z}=0 \tag{22}$$

$$\text{[5b] at } \xi=\xi_p,\ \phi_{in}^b-\phi_{out}^b=\frac{Z_{hole}}{jk\rho c}\frac{\partial\phi_{out}^b}{\partial\xi} \tag{23}$$

$$\text{[6b] at } \xi=\xi_p,\ \frac{\partial\phi_{in}^b}{\partial\xi}=\frac{\partial\phi_{out}^b}{\partial\xi} \tag{24}$$

then ϕ_{in} and ϕ_{out} can be obtained as $\phi_{in}=\phi_{in}^a+\phi_{in}^b$ and $\phi_{out}=\phi_{out}^a+\phi_{out}^b$, respectively.

At first, ϕ_{in} can be derive as following procedure. From (14) we have

$$B_i=A_i\exp\ 2\mu l \tag{25}$$

Substituting Eq. (25) into Eq. (3), we have

$$\phi_{in}^{a} = \sum_{m=0}^{\infty} A_i f\ z,\mu\ Ce_m\ \xi,s\ ce_m\ \eta,s \qquad (26)$$

where

$$f\ z,\mu = \exp\ \mu z + \exp\ 2\mu l\ \exp\ -\mu z \qquad (27)$$

Similarly, B_0 find from (16) and substituting into Eq.(4) we obtained

$$\phi_{out} = \sum_{m=0}^{\infty} C_m^0 f\ z,\mu\ Ce_m\ \xi,s\ ce_m\ \eta,s + \sum_{m=0}^{\infty} S_{m+1}^0 f\ z,\mu\ Se_{m+1}\ \xi,s\ se_{m+1}\ \eta,s \qquad (28)$$

and from (15) we have

$$\sum_{m=0}^{\infty} C_m^0 f\ z,\mu\ Ce_m^{'}\ \xi_\omega,s\ ce_m\ \eta,s + \sum_{m=0}^{\infty} S_{m+1}^0 f\ z,\mu\ Se_{m+1}^{'}\ \xi_\omega,s\ se_{m+1}\ \eta,s = 0 \qquad (29)$$

to make Eq.(29) always zero, it is necessary that

$$Ce_m^{'}\ \xi_\omega,s = \left.\frac{\partial Ce_m\ \xi,s}{\partial \xi}\right|_{\xi=\xi_\omega} = 0 \qquad (30)$$

and

$$Se_{m+1}^{'}\ \xi_\omega,s = \left.\frac{\partial Se_{m+1}\ \xi,s}{\partial \xi}\right|_{\xi=\xi_\omega} = 0 \qquad (31)$$

Letting the positive roots of Eq.(30) and Eq.(31) be $s_{m,i}$ and $\overline{s_{m+1,i}}$ $i = 0,1,2,\ldots$, respectively, and letting μ corresponding to $s_{m,i}$ and $\overline{s_{m+1,i}}$ be $\mu_{m,i}$ and $\overline{\mu_{m+1,i}}$ ϕ_{out}^{a} then ϕ_{out}^{a} and can be obtained as

$$\phi_{in}^{a} = \sum_{m=0}^{\infty}\sum_{i=0}^{\infty} A_{m,i} f\ z,\mu_{m,i}\ Ce_m\ \xi,s_{m,i}\ ce_m\ \eta,s_{m,i} \qquad (32)$$

$$\phi_{out}^{a} = \sum_{m=0}^{\infty}\sum_{i=0}^{\infty} C_{m,i} f\ z,\mu_{m,i}\ Ce_m\ \xi,s_{m,i}\ ce_m\ \eta,s_{m,i} + \sum_{m=0}^{\infty}\sum_{i=0}^{\infty} S_{m+1,i} f\ z,\overline{\mu_{m+1,i}}\ Se_{m+1}\ \xi,\overline{s_{m+1,i}}\ se_{m+1}\ \eta,\overline{s_{m+1,i}} \qquad (33)$$

Next, derive $A_{m,i}$ from Eq.(17) and considering (18) we have

$$C_{m,i} f^{'}\ z,\mu_{m,i}\ Ce_m\ \xi,s_{m,i}\ ce_m\ \eta,s_{m,i}\ \Big|_{z=0} = -V_0 F_0\ \xi,\eta \qquad (34)$$

By multiplying both sides of Eq.(34) by $Ce_m\ \xi,s_{m,i}\ ce_m\ \eta,s_{m,i}\ \cosh 2\xi - \cos 2\eta$ and integrating with respect to ξ from 0 to ξ_ω and with respect to from 0 to 2π we can determine the constant $C_{m,i}$. Thus ϕ_{in}^{a} becomes

$$\phi_{in}^{a} = \sum_{m=0}^{\infty}\sum_{i=0}^{\infty} \frac{V_0}{\dfrac{\mu_{m,i}\sin h\mu_{m,i}l}{\cosh \mu_{m,i}(l-z)} + Z_{m,i}\dfrac{\overline{\mu_{m+1,i}}\sinh \overline{\mu_{m+1,i}}l}{\cosh \overline{\mu_{m+1,i}}(l-z)}} \times H_{m,i}^{0}\ 1+Z_{m,i}\ \Theta_m\ \xi,\eta,s_{m,i} \qquad (35)$$

where

$$Z_{m,i} = \frac{Z_{pn}\ c_2 + Z_{pn}}{c_1 + Z_{pn}\ c_1 - c_2 - Z_{pn}} \qquad (36)$$

$$Z_{pn} = \frac{Z_{pipe}}{jk\rho c} \qquad (37)$$

$$C_1 = \frac{Ce_m\ \xi_p,s_{m,i}}{Ce_m^{'}\ \xi_p,s_{m,i}} \qquad (38)$$

$$C_2 = \frac{Se_{m+1}\ \xi_p,\overline{s_{m+1,i}}}{Se_{m+1}^{'}\ \xi_p,\overline{s_{m+1,i}}} \qquad (39)$$

$$\Theta_m(\xi,\eta,s_{m,i}) = Ce_m(\xi,s_{m,i})\,ce_m(\eta,s_{m,i}) \quad (40)$$

$$g(\xi,\eta) = \cosh 2\xi - \cos 2\eta \quad (41)$$

$$H^u_{m,i} = \int_0^{\xi_u}\int_0^{2\pi}\Theta_m(\xi,\eta,s_{m,i})\,g(\xi,\eta)\,d\xi d\eta \Big/ \int_0^{\xi_w}\int_0^{2\pi}\Theta^2_m(\xi,\eta,s_{m,i})\,g(\xi,\eta)\,d\xi d\eta \quad (42)$$

Similarly, by using Eqs.(19)-(24), ϕ^b_{in} can be obtained as

$$\phi^b_{in} = \sum_{m=0}^{\infty}\sum_{i=0}^{\infty}\frac{-V_l}{\frac{\mu_{m,i}\sin h\mu_{m,i}l}{\cosh\mu_{m,i}z} + Z_{m,i}\frac{\overline{\mu_{m+1,i}}\sinh\overline{\mu_{m+1,i}}l}{\cosh\overline{\mu_{m+1,i}}z}} \times H^l_{m,i}(1+Z_{m,i})\,\Theta_m(\xi,\eta,s_{m,i}) \quad (43)$$

where $H^l_{m,i}$ is defined by Eq.(41) in which ξ_0 is replaced by ξ_l. Thus, from Eq.(35) and Eq.(43), we obtaind ϕ_{in} as

$$\phi_{in} = \phi^a_{in} + \phi^b_{in} = \sum_{m=0}^{\infty}\sum_{i=0}^{\infty}\left(\frac{H^0_{m,i}V_0}{\frac{\mu_{m,i}\sin h\mu_{m,i}l}{\cosh\mu_{m,i}(l-z)} + Z_{m,i}\frac{\overline{\mu_{m+1,i}}\sinh\overline{\mu_{m+1,i}}l}{\cosh\overline{\mu_{m+1,i}}(l-z)}} - \frac{H^l_{m,i}V_l}{\frac{\mu_{m,i}\sin h\mu_{m,i}l}{\cosh\mu_{m,i}z} + Z_{m,i}\frac{\overline{\mu_{m+1,i}}\sinh\overline{\mu_{m+1,i}}l}{\cosh\overline{\mu_{m+1,i}}z}}\right)(1+Z_{m,i})\,\Theta_m(\xi,\eta,s_{m,i}) \quad (44)$$

Therefore, the sound pressure at the input becomes

$$P_0 = jk\rho c\phi_{in}\big|_{z=0} = jkZ_w\sum_{m=0}^{\infty}\sum_{i=0}^{\infty}GT_{m,i}Q^0_{m,i}U_0 - GS_{m,i}Q^l_{m,i}U_l(1+Z_{m,i})\,\Theta_m(\xi,\eta,s_{m,i}) \quad (45)$$

where

$$GS_{m,i} = \frac{1}{\mu_{m,i}\sin h\mu_{m,i}l + Z_{m,i}\overline{\mu_{m+1,i}}\sinh\overline{\mu_{m+1,i}}l} \quad (46)$$

$$GT_{m,i} = \frac{1}{\mu_{m,i}\tan h\mu_{m,i}l + Z_{m,i}\overline{\mu_{m+1,i}}\tanh\overline{\mu_{m+1,i}}l} \quad (47)$$

$$\mu_{m,i} = \frac{1}{a_w}\sqrt{\lambda^2_{m,i} - ka_w{}^2} \quad (48)$$

$$\overline{\mu_{m+1,i}} = \frac{1}{a_w}\sqrt{\overline{\lambda^2_{m+1,i}} - ka_w{}^2} \quad (49)$$

$$\lambda_{m,i} = 2\sqrt{s_{m,i}}/e_w \quad (50)$$

$$\overline{\lambda_{m+1,i}} = 2\sqrt{\overline{s_{m+1,i}}}/e_w \quad (51)$$

$$\Theta_m(\xi,\eta,s_{m,i}) = Ce_m(\xi,s_{m,i})\,ce_m(\eta,s_{m,i}) \quad (52)$$

$$Q^u_{m,i} = \frac{S_w}{S_0}\int_0^{\xi_u}\int_0^{2\pi}\Theta_m(\xi,\eta,s_{m,i})\,g(\xi,\eta)\,d\xi d\eta \Big/ \int_0^{\xi_w}\int_0^{2\pi}\Theta^2_m(\xi,\eta,s_{m,i})\,g(\xi,\eta)\,d\xi d\eta \quad (53)$$

$$g(\xi,\eta) = \cosh 2\xi - \cos 2\eta \quad (54)$$

$U_0 = V_0S_0$ and $U_l = V_lS_l$ are volume velocity at input an output, S_0, S_l and S_w are cross-sectional area of input, out-

put and chamber, respectively, $Z_w = \rho c / S_w$, a_w is major semi-axis of elliptical chamber, $Z_{m,i}$ is given in Eq. (36), the term related to the acoustic impedance of perforated pipe.

Similarly, the sound pressure on the output side ($z = l$) is given by the following equation

$$P_l = jk\rho c\phi_{in}\big|_{z=l}$$

$$= jkZ_w \sum_{m=0}^{\infty}\sum_{i=0}^{\infty} GS_{m,i}Q_{m,i}^{0}U_0 - GT_{m,i}Q_{m,i}^{l}U_l$$

$$1 + Z_{m,i}\ \Theta_m\ \xi, \eta, s_{m,i} \quad (55)$$

Conclusion

The derivation of the input and output sound pressure for the elliptical perforated tube muffler has been presented by solving the wave equation considering the higher order mode effects. The input and output pressure are given by Eq.(45) and Eq.(55), respectively.

References

[1] J.W Sullivan, M.J Crocker, Analysis of concentric tube resonators having un-partitioned cavities. Journal Acoustic Society of America, 64 (1978), 207-215.

[2] J.W Sullivan, A method for modeling perforated tube muffler components. 1. Theory. Journal Acoustic Society of America, 66 (1979), 772-788.

[3] K.S Peat, A numerical decoupling analysis of perforated pipe silencer elements,. Journal of Sound and Vibration 123 (1988), 199-212.

[4] H. Luo, C.C Tse, Y.N Chen, Modeling and applications of partially perforated intruding tube mufflers. Applied Acoustics 44 (1995), 99-116.

[5] C.N Wang, A numerical scheme for the analysis of perforated introding tube muffler components. Applied Acoustic 44 (1995), 275-286, 1995.

[6] N. W. McLachlan, Theory and application of Mathieu functions. Oxford at the Clarendon Press, 1947.

2nd International Engineering Symposium - IES 2012
(KU-MU-NITK-HCMCUT Joint Symposium) March 5-7, 2012, Kumamoto University, Japan

Study on the Air Ventilation Grille

Yuya Nishimura [1] , Sohei Nishimura[2]

1 *Kumamoto National College of Technology 2659-2 Suya Koshi-shi, Kumamoto 861-1102, JAPAN. e-mail: nishimura@kumamoto-nct.ac.jp*
2 *Kumamoto National College of Technology 2627 Hirayama-Shin-Machi, Yatsushiro Kumamoto 866-8501 JAPAN, e-mail: nisimura@kumamoto-nct.ac.jp*

Abstract: A conceptual model for manufacturing the new type of soundproofing ventilation grille unit is presented. The central problem is in designing the shape and dimension of this unit and the placement of these input and output opening in such a way as to maximize ventilation as well as preventing outside noise from entering the home. In this work, a method to predict the insertion-loss of ventilation grille unit is proposed by solving the wave equation, considering the resonance frequencies of higher-order mode.

***Keywords**: Ventilation, Higher-order mode, Insertion loss*

Introduction

Numerous studies on assessing the acoustic performance of vented facades to inner rooms have been published. However, there are still limited researches on the particular case of housing in tropical and developing country where the noise propagation needs to be prevented and the natural ventilation is demanded. As shown in Fig.1, ventilation grille consisted of several slits opening side by side in a wall is widely used in tropical climates countries.



Fig.1
Ventilation grille used in tropical climates countries

However, the annual increase in traffic noise in developing tropical countries has rendered this kind of ventilation grille to be useless because it serve a direct pathway for traffic noise to enter the home. In this report we deal with a ventilation grille consisted of several slits opening side by side in a wall. A method to predict the sound propagation in ventilation grille unit is proposed by solving the wave equation, considering the resonance frequencies of higher-order mode.

METHOD OF ANALYSIS

Model of the ventilation grille is shown in Fig.2. A section area $S_w = a \times b$ and depth *L* of rectangular cavity that has *N* inputs and *M* outputs at both side. Here, we present the theoretical calculation of the sound pressure inside the ventilation grille including the effects of higher-order mode wave for a simple case where no acoustic material is used.
Wave equation in term of the velocity potential is given by

$$\left(\frac{\partial^2}{\partial x^2}+\frac{\partial^2}{\partial y^2}+\frac{\partial^2}{\partial z^2}\right)\mathrm{F}=\frac{1}{c^2}\frac{\partial^2}{\partial t^2}\mathrm{F} \qquad (1)$$

where c is sound velocity, Let $\Phi = \sqrt{2}\,\phi \exp(j\,\omega t)$ ($j^2 = -1, w = k\,c, k$: wave

number) then the complete solution of Eq.(1) is given by

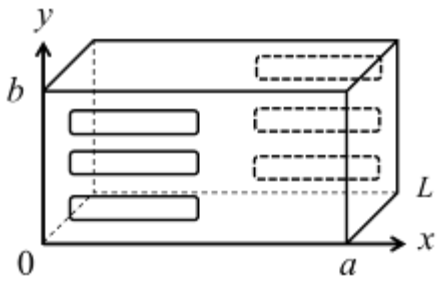


Fig.2 Model of ventilation grill

$$f = \left(Ae^{mx} + Be^{-mx} \right)\left(C\sin ax + D\cos ax \right) \left(E\sin\sqrt{s^2 - a^2}\,y + F\cos\sqrt{s^2 - a^2}\,y \right) \quad (2)$$

where *A*, *B*, *C*, *D*, *E* and *F* are arbitrary constants determinable from the boundary conditions, a, s and m are the constants.

Let $V_x = -\partial f / \partial x$, $V_y = -\partial f / \partial y$ and $V_z = -\partial f / \partial z$ is the velocity components in the x, y and z directions, respectively. At the left and the right side of the ventilation grill as shows in Fig. 2, the boundary conditions are

[1] $V_x = 0$ at $x = 0$ (3)

[2] $V_x = 0$ at $x = a$ (4)

[3] $V_y = 0$ at $y = 0$ (5)

[4] $V_y = 0$ at $y = b$ (6)

At the front side of ventilation grille, the velocity component in z direction be the sum of *N* inputs which has a velocity $V_0^{(i)}$ $(i = 1, ..., N)$, respectively.

[5] at $z = 0$

$$V_z = V_0^{(1)} F_0^{(1)}(x, y) + V_0^{(2)} F_0^{(2)}(x, y) + \cdots + V_0^{(N)} F_0^{(N)}(x, y) = \sum_{i=1}^{N} V_0^{(i)} F_0^{(i)}(x, y) \quad (7)$$

where $F_0^{(i)}(x, y) = 1$ at the input section area and $F_0^{(i)}(x, y) = 0$ elsewhere.

Similarly, At the back side of ventilation grille, the velocity component in *z* direction be the sum of *M* output which has a velocity $V_L^{(i)}$ $(i = 1, ..., M)$, respectively.

[6] at $z = L$

$$V_z = V_L^{(1)} F_L^{(1)}(x, y) + V_L^{(2)} F_L^{(2)}(x, y) + \cdots + V_L^{(M)} F_L^{(N)}(x, y) = \sum_{i=1}^{M} V_L^{(i)} F_L^{(i)}(x, y) \quad (8)$$

where $F_L^{(i)}(x, y) = 1$ at the output section area and $F_L^{(i)}(x, y) = 0$ elsewhere.

In order to find f from Eqs.(3) to (8), let f_a be the solution of Eq.(2) obtained for the following boundary conditions:

[1] at $x = 0$, $-\partial f_a / \partial x = 0$ (9)

[2] at $x = a$, $-\partial f_a / \partial x = 0$ (10)

[3] at $y = 0$, $-\partial f_a / \partial y = 0$ (11)

[4] at $y = b$, $-\partial f_a / \partial y = 0$ (12)

[5] at $z = 0$,

$$-\partial \phi_a / \partial z = \sum_{i=1}^{M} V_0^{(i)} F_0^{(i)}(x, y) \quad (13)$$

[6] at $z = L$, $-\partial f_a / \partial z = 0$ (14)

and let f_b be the solution of Eq.(2) obtained for the following boundary conditions:

[1] at $x = 0$, $-\partial f_b / \partial x = 0$ (15)

[2] at $x = a$, $-\partial f_b / \partial x = 0$ (16)

[3] at $y = 0$, $-\partial f_b / \partial y = 0$ (17)

[4] at $y = b$, $-\partial f_b / \partial y = 0$ (18)

[5] at $z = 0$, $-\partial f_b / \partial z = 0$ (19)

[6] at $z = L$,

$$-\partial \phi_b / \partial z = \sum_{i=1}^{M} V_L^{(i)} F_L^{(i)}(x, y) \quad (20)$$

then f can be obtained as $f = f_a + f_b$.

At first, f_a can be derive as following procedure. From (9) we have

$$\frac{\partial}{\partial x}\left(C\sin ax + D\cos ax \right)\Big|_{x=0} = 0$$

$$\therefore \quad C = 0 \qquad (21)$$

from(10)

$$\frac{\partial}{\partial x} D\cos \alpha x \Big|_{x=a} = 0$$

$$\therefore \quad \alpha = m\,\frac{\pi}{a} \qquad m = 0,1,2,\cdots,L \qquad (22)$$

Substituting Eqs. (21) - (22) into Eq. (2)

$$f = \sum_{m=0}^{\infty}\left(Ae^{mz} + Be^{-mz} \right)\cos\left(m\frac{p}{a} \right) \left(E\sin\sqrt{s^2-\alpha^2}\,y + F\cos\sqrt{s^2-\alpha^2}\,y \right) \qquad (23)$$

from Eq. (11)

$$\frac{\partial}{\partial y}\left(E\sin\sqrt{s^2-\alpha^2}\,y + F\cos\sqrt{s^2-\alpha^2}\,y \right)\Big|_{y=0} = 0$$

$$\therefore \quad E = 0 \qquad (24)$$

and from Eq. (12)

$$\frac{\partial}{\partial y}\left(F\cos\sqrt{s^2-\alpha^2}\,y \right)\Big|_{y=b} = 0$$

$$\therefore \sqrt{s^2-\alpha^2} = n\frac{\pi}{b} \quad n = 0,1,\cdots,L \qquad (25)$$

Substituting Eqs. (24) and (25) into Eq. (23), we have

$$\phi_a = \sum_{m=0}^{\infty}\sum_{n=0}^{\infty}\left(Ae^{\mu_{m,n}z} + Be^{-\mu_{m,n}z} \right)\cos\left(\frac{m\pi y}{a} \right)\cos\left(\frac{n\pi y}{b} \right) \qquad (26)$$

where

$$\mu_{m,n} = \sqrt{\left(m\pi/a\right)^2 + \left(n\pi/b\right)^2 - k^2} \qquad (27)$$

from Eq. (14)

$$\frac{\partial}{\partial z}\left(Ae^{\mu_{m,n}z} + Be^{-\mu_{m,n}z} \right)\Big|_{z=L} = 0$$

$$\therefore \quad B = Ae^{2\mu_{m,n}L} \qquad (28)$$

Substituting into Eq. (26)

$$\phi_a = \sum_{m=0}^{\infty}\sum_{n=0}^{\infty} e^{\mu_{m,n}L}\cosh\ \mu_{m,n}(z-L)\ C_{m,n}^{a} \cos\left(\frac{m\pi y}{a} \right)\cos\left(\frac{n\pi y}{b} \right) \qquad (29)$$

from Eq. (13)

$$-\frac{\partial}{\partial z}\sum_{m=0}^{\infty}\sum_{n=0}^{\infty} e^{\mu_{m,n}L}\cosh\ \mu_{m,n}(z-L)\ C_{m,n}^{a} \cos\left(\frac{m\pi y}{a} \right)\cos\left(\frac{n\pi y}{b} \right)\Big|_{z=0} = \sum_{i=1}^{N} V_0^{(i)} F_0^{(i)}(x,y) \qquad (30)$$

By multiplying both sides of Eq.(30) by $\cos(m\pi x/a)\cos(n\pi y/b)$ and integrating with respect to *x* from 0 to *a* and with respect to *y* from 0 to *b* we can determine the constant $C_{m,n}^{a}$.

$$\sum_{m=0}^{\infty}\sum_{n=0}^{\infty} e^{\mu_{m,n}L}\sinh\ \mu_{m,n}L\ C_{m,n}^{a} \int_0^a\int_0^b \cos\left(\frac{m\pi x}{a} \right)^2 \cos\left(\frac{n\pi y}{b} \right)^2 dx\,dy = \sum_{i=1}^{N}\int_0^a\int_0^b V_0^{(i)} F_0^{(i)}(x,y) \cos\left(\frac{m\pi x}{a} \right)\cos\left(\frac{n\pi y}{b} \right) dx\,dy$$

$$\sum_{m=0}^{\infty}\sum_{n=0}^{\infty} e^{\mu_{m,n}L}\sinh\ \mu_{m,n}L\ C_{m,n}^{a}\left(\frac{ab}{4} \right)$$

$$= \sum_{i=1}^{N} \int_0^a \int_0^b V_0^{(i)} F_0^{(i)}(x,y) \cos\left(\frac{m\pi x}{a}\right)\cos\left(\frac{n\pi y}{b}\right)dx\,dy \quad (31)$$

let $\theta_{m,n}$ is the right term of Eq.(31)

$$\theta_{m,n} = \sum_{i=1}^{N} \int_0^a \int_0^b V_0^{(i)} F_0^{(i)}(x,y) \cos\left(\frac{m\pi x}{a}\right)\cos\left(\frac{n\pi y}{b}\right)dx\,dy$$
$$= \sum_{i=1}^{N} \int_{a_{00}^{(i)}}^{a_{01}^{(i)}} \int_{b_{00}^{(i)}}^{b_{01}^{(i)}} V_0^{(i)} \cos\left(\frac{m\pi x}{a}\right)\cos\left(\frac{n\pi y}{b}\right)dx\,dy$$
$$= \sum_{i=1}^{N} \int_{a_{00}^{(i)}}^{a_{01}^{(i)}} \int_{b_{00}^{(i)}}^{b_{01}^{(i)}} \frac{U_0^{(i)}}{S_0^{(i)}} \cos\left(\frac{m\pi x}{a}\right)\cos\left(\frac{n\pi y}{b}\right)dx\,dy \quad (32)$$

where $U_0^{(i)}$ is the volume velocity at the output defined by $U_0^{(i)} = V_0^{(i)} S_0^{(i)}$.

Next, find $C_{m,n}^{a}$ from (31) and substituting to (29), then ϕ_a is obtained as

$$\phi_a = \frac{4}{S_w}\sum_{m=0}^{\infty}\sum_{n=0}^{\infty} \frac{\cosh\ \mu_{m,n}(z-L)}{\mu_{m,n}\sinh\ \mu_{m,n}L}\theta_{m,n} \cos\left(\frac{m\pi y}{a}\right)\cos\left(\frac{n\pi y}{b}\right) \quad (33)$$

Similarly, by using Eqs. (15) - (20), f_b can be obtained as

$$\phi_b = \frac{4}{S_w}\sum_{m=0}^{\infty}\sum_{n=0}^{\infty} \frac{\cosh\ \mu_{m,n}z}{\mu_{m,n}\sinh\ \mu_{m,n}L}\lambda_{m,n} \cos\left(\frac{m\pi x}{a}\right)\cos\left(\frac{n\pi y}{b}\right) \quad (34)$$

where

$$\lambda_{m,n} = \sum_{i=1}^{M} \int_{a_{L0}^{(i)}}^{a_{L1}^{(i)}} \int_{b_{L0}^{(i)}}^{b_{L1}^{(i)}} \frac{U_L^{(i)}}{S_L^{(i)}} \cos\left(\frac{m\pi x}{a}\right)\cos\left(\frac{n\pi y}{b}\right)dx\,dy \quad (35)$$

as mentioned above, ϕ is the sum of ϕ_a and ϕ_b, then we obtain

$$\phi(x,y,z) = \phi_a + \phi_b$$
$$= \frac{4}{S_w}\sum_{m=0}^{\infty}\sum_{n=0}^{\infty}\left\{\frac{\cosh\ \mu_{m,n}(z-L)}{\mu_{m,n}\sinh\ \mu_{m,n}L}\theta_{m,n} + \frac{\cosh\ \mu_{m,n}z}{\mu_{m,n}\sinh\ \mu_{m,n}L}\lambda_{m,n}\right\} \cos\left(\frac{m\pi x}{a}\right)\cos\left(\frac{n\pi y}{b}\right) \quad (36)$$

The sound pressure at the input is given by $P_0 = jk\rho c\phi(x,y,0)$ becomes

$$P_0 = j\frac{4k\rho c}{S_w}\sum_{m=0}^{\infty}\sum_{n=0}^{\infty} \left\{\frac{\cosh\ -\mu_{m,n}L}{\mu_{m,n}\sinh\ \mu_{m,n}L}\theta_{m,n} + \frac{1}{\mu_{m,n}\sinh\ \mu_{m,n}L}\lambda_{m,n}\right\} \cos\left(\frac{m\pi x}{a}\right)\cos\left(\frac{n\pi y}{b}\right) \quad (37)$$

The sound pressure at the output is given by $P_L = jk\rho c\phi(x,y,L)$

$$P_L = j\frac{4k\rho c}{S_w}\sum_{m=0}^{\infty}\sum_{n=0}^{\infty} \left\{\frac{1}{\mu_{m,n}\sinh\ \mu_{m,n}L}\theta_{m,n} + \frac{\cosh\ \mu_{m,n}L}{\mu_{m,n}\sinh\ \mu_{m,n}L}\lambda_{m,n}\right\} \cos\left(\frac{m\pi x}{a}\right)\cos\left(\frac{n\pi y}{b}\right) \quad (38)$$

Therefore, average sound pressure at the output piston becomes

$$\bar{P}_L = \sum_{i=1}^{M} \frac{1}{S_L^{(i)}} \int_{a_{L0}^{(i)}}^{a_{L1}^{(i)}} \int_{b_{L0}^{(i)}}^{b_{L1}^{(i)}} P_L\,dx\,dy$$

$$= j\frac{4k\rho c}{S_w}\sum_{m=0}^{\infty}\sum_{n=0}^{\infty}\left\{\frac{1}{\mu_{m,n}\sinh\ \mu_{m,n}L}\theta_{m,n} + \frac{\cosh\ \mu_{m,n}L}{\mu_{m,n}\sinh\ \mu_{m,n}L}\lambda_{m,n}\right\}\Delta_{m,n} \quad (39)$$

where

$$\Delta_{m,n} = \sum_{i=1}^{M}\frac{1}{S_L^{(i)}}\int_{a_{L0}^{(i)}}^{a_{L1}^{(i)}}\int_{b_{L0}^{(i)}}^{b_{L1}^{(i)}} \cos\left(\frac{m\pi x}{a}\right)\cos\left(\frac{n\pi y}{b}\right)dx\,dy \quad (40)$$

Expanding (A-39) with m=0 and n=0, average sound pressure at the output becomes

$$\bar{P}_L = j\frac{4k\rho c}{S_w}\left[\frac{1}{\sin(kL)}\left(-\sum_{i=1}^{N}U_0^{(i)} + \cos(kL)\sum_{i=1}^{M}U_L^{(i)}\right) + \sum_{\cdot}^{\cdot}\left\{\frac{1}{\mu_{m,n}\sinh\ \mu_{m,n}L}\theta_{m,n}\Delta_{m,n} + \frac{\cosh\ \mu_{m,n}L}{\mu_{m,n}\sinh\ \mu_{m,n}L}\lambda_{m,n}\Delta_{m,n}\right\}\right] \quad (41)$$

where

$$\theta_{m,n} = \sum_{i=1}^{N}\int_{a_{00}^{(i)}}^{a_{01}^{(i)}}\int_{b_{00}^{(i)}}^{b_{01}^{(i)}}\frac{U_0^{(i)}}{S_0^{(i)}} \cos\left(\frac{m\pi x}{a}\right)\cos\left(\frac{n\pi y}{b}\right)dx\,dy \quad (42)$$

$$\lambda_{m,n} = \sum_{i=1}^{M}\int_{a_{L0}^{(i)}}^{a_{L1}^{(i)}}\int_{b_{L0}^{(i)}}^{b_{L1}^{(i)}}\frac{U_L^{(i)}}{S_L^{(i)}} \cos\left(\frac{m\pi x}{a}\right)\cos\left(\frac{n\pi y}{b}\right)dx\,dy \quad (43)$$

$$\Delta_{m,n} = \sum_{i=1}^{M}\frac{1}{S_L^{(i)}}\int_{a_{L0}^{(i)}}^{a_{L1}^{(i)}}\int_{b_{L0}^{(i)}}^{b_{L1}^{(i)}} \cos\left(\frac{m\pi x}{a}\right)\cos\left(\frac{n\pi y}{b}\right)dx\,dy \quad (44)$$

$$\mu_{m,n} = \sqrt{\left(\frac{m\rho}{a}\right)^2 + \left(\frac{n\rho}{b}\right)^2 - k^2} \quad (45)$$

the symbol $\dot{\sum}$ means $\sum_{m=0}^{\infty}\sum_{n=0}^{\infty}$ without m=n=0.

The first term on the bracket represents the sound pressure of the plane wave and the second one represents the sound pressure components of the higher-order mode wave, respectively. From Eq.(41) $\bar{P}_L$ become great when at the following resonance frequencies of

$$\sin(kL) = 0 \quad \therefore \quad f = \eta\frac{c}{2L} \quad (\eta = 1, 2, 3....) \quad (46)$$

$$\mu_{m,n}\sinh\ \mu_{m,n}L = 0$$

$$\therefore f_{m,n} = \frac{c}{2\pi}\sqrt{\left(\frac{m\pi}{a}\right)^2 + \left(\frac{n\pi}{b}\right)^2 - \left(\frac{\eta\pi}{L}\right)^2} \quad (\eta = 0, 1, 2...) \quad (47)$$

An experiment was conducted using the reverberation chamber method to verify the actual sound attenuation characteristics. Fig.3 shows the experimental setup.

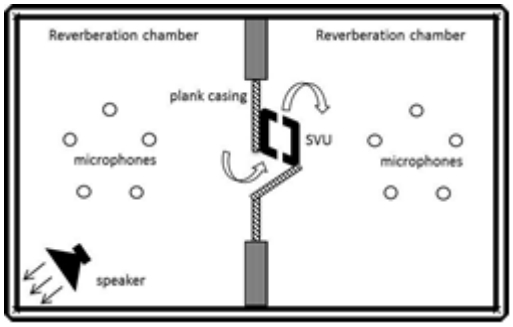


Fig.3 Measurement system based on the reverberation chamber method.

The volumes of reverberation chambers are 98m^3 and 179 m^3. The ventilation grille unit is installed at the aperture by a casing composed of a plank. The sound source is a loudspeaker fed by pink noise, and five microphones located in each chamber measure the spatially averaged sound pressure. The pressure levels in the sending chamber were 100 -105 dB to

achieved pressure level of 70 – 80 dB in the receiving room. The actual sound attenuation of ventilation grille will be estimated by the difference from the measurement results with and without ventilation grille unit inserted between two reverberation chambers. Some experiments were conducted using the reverberation chamber method. The same dimension of ventilation grille unit (a=48cm, b=7.5cm, L=29cm) with openings of input and output were used in the experiments. Fig.4 shows the measured results the unit when using an input and output having a shape as shown inside of the figure.

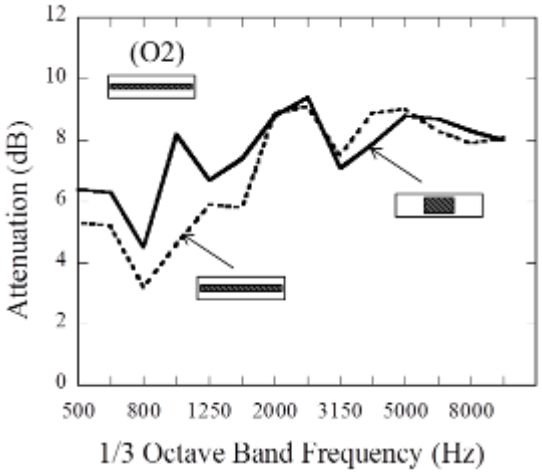


Fig.4 Measurement result based on the reverberation chamber method with change of input shapes.

The ratio of cross section area between the unit and input, output is 0.25. The sound propagating through air ventilation grille unit is a combination of plane wave and higher-order mode waves. Thus, a selection of input and output shapes that minimize those wave components as much as possible is very important.

CONCLUSIONS

A method to predict the sound propagation in ventilation grille unit is proposed by solving the wave equation, considering the resonance frequencies of higher-order mode. In order to maximize the soundproofing capability, it is necessary to decide the position of each input and output defined by Eq.(43)-Eq.(45). This technology will be present in an upcoming report.

References

[1] Daniel, R, Raichel, "The Science and Applications of Acoustics", Modern Acoustics and Signal Processing
[2] H.Y.T. Phan, T. Yano, H.A.T. Phan, T. Nishimura, T. Sato, Y. Hashimoto"Community response to road traffic noise in Hanoi and Ho Chi Minh City"Applied Acoustics, 71(2), pp.107-114, 2010
[3] H.A.T. Phan, T. Yano, H.Y.T. Phan, T. Nishimura, T. Sato, Y. Hashimoto "Annoyance caused by road traffic noise with and without horn sounds" Acoust.Sci. & Tech., 30(5), pp.327-337, 2009.9
[4] H.Y.T. Phan, T. Yano, H.A.T. Phan, T. Nishimura, T. Sato, Y. Hashimoto"Community response road traffic noise in Vietnam: Social surveys in Hanoi and Ho Chi Minh City" Proc. of The 37th International Congress and Exposition on Noise Control Engineering (internoise 2008), Shanghai, CD version, 2008.10
[5] Y.S. Choy, L. Huang "Multiple drumlike silencer for low frequen-cy duct noise reflection" Applied Acoustics, Volume 70, Issues 11-12, December 2009, Pages 1422-1430

2nd International Engineering Symposium - IES 2012
(KU-MU-NITK-HCMCUT Joint Symposium) March 5-7, 2012, Kumamoto University, Japan

Electrochemical Investigation of Corrosion Behaviour of Mild Steel by Thiourea Derivatives in Hydrochloric Acid Solution

S. Divakara Shetty

Department of Mechanical & Manufacturing Engineering, Manipal University, Manipal 576104, Karnataka, India. e-mail:sdsmanipal@yahoo.com

Abstract: Inhibition is one of the mechanisms used for mitigating the metallic corrosion especially in acid environment. In the present work an attempt has been made to study the inhibiting effect of N-benzyl-N/-phenyl thiourea and N-cyclohexyl-N/-phenyl thiourea on the corrosion of mild steel in 0.1 M HCl solution has been investigated using potentiostatic polarization technique. Results obtained reveal that these compounds act as efficient anodic inhibitors for the corrosion of mild steel in the range of temperature studied. Good inhibition efficiency (> 97 %) was evidenced from these compounds even at elevated temperatures. The adsorption of these compounds on the mild steel surface was found to obey Temkin's adsorption isotherm and the inhibition is governed by chemisorption mechanism.

Keywords*: Corrosion, Mild steel, Hydrochloric acid, Adsorption isotherm, Activation energy, and Potentiostatic polarization.*

Introduction

The use of inhibitors is a simple approach for giving protection against metallic corrosion, especially in acid media [2]. The effect of inhibitors adsorbed on metallic surface in the acid solution is to slow down the cathodic reaction as well as the anodic dissolution of the metal. Such effect is obtained by forming barriers of diffusion or by means of the blockage of the reaction sites [5]. Most of the efficient inhibitors used in industry are organic compounds having multiple bonds in their molecules and mainly contain nitrogen, sulphur and oxygen atoms through which they are adsorbed on the metal surface. Among these, thiourea and its derivatives have been used extensively as corrosion inhibitors for various steels in acid media [3,4,11].

The study of corrosion of mild steel in acid media is of both academic and industrial concern that has received a considerable amount of attention. Hydrochloric acid is known to be the working horse in the pre - treatment of mild steel components. The use of hydrochloric acid in pickling of metals, cleaning of scales, acidizing of oil and gas wells is more economical, efficient and trouble free compared to other mineral acids [10]. The great advantage of this acid over the other acid in cleaning and pickling operations lies in its ability to form metal chlorides which are extremely soluble in aqueous phase, compared to sulfate, nitrate, phosphate, etc. This high rate of solubility of chloride salts causes the least polarizing affect and does not hamper the rate of reaction [13]. Substituents to thiourea increase further its electron densties for their adsorption on the metal surface. Hence, in the present investigation N - benzyl - N/ - phenyl thiourea (BPTU), and N - cyclohexyl - N/ - phenyl thiourea (CPTU) were tried as inhibitors on the corrosion of mild steel in HCl solution at different temperatures and inhibitor concentrations by using potentiostatic polarization technique.

Experimental

The mild steel specimen of chemical composition (Wt %): C: 0.205; Si: 0.06; Mn: 0.55; S: 0.047; P: 0.039 and balance Fe was used in this study.

Table1. Elemental analysis of the compounds studied

Inhibitors	Molecular formula	Calculated (Found)%				
		C	H	N	O	S
BPTU	$C_{14}H_{14}N_2S$	69.39 (69.26)	5.82 (5.79)	11.56 (11.60)	-	13.23 (13.19)
CPTU	$C_{13}H_{18}N_2S$	66.63 (66.50)	7.74 (7.71)	11.95 (11.90)	-	13.68 (13.62)

The specimen of 12 mm diameter and 10 mm length was polished successively with 1/0 - 5/0 grade emery papers, thoroughly cleaned with soap water, rinsed with distilled water and then with alcohol and dried in air. The specimen was tightly fitted to one end of the Teflon holder, which exposes a polished surface area of 0.786 cm^2.

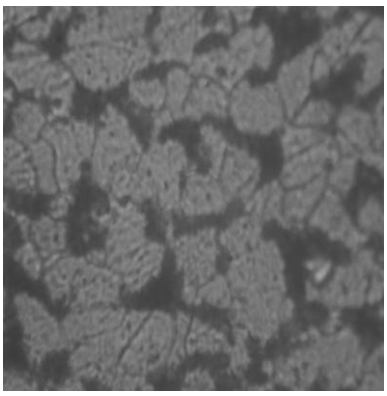


Fig.1 Microstructure of mild steel specimen

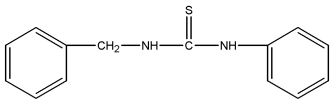
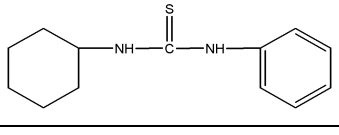
Table 2. Physical properties of inhibitors studied

Inhibitors	Molecular weight	Melting point (^{0}C)
BPTU	242.34	158
CPTU	234.37	149

The microstructure of mild steel specimen used for electrochemical studies is shown in Fig. 1. N - benzyl - N/ - phenyl thiourea (BPTU), and N - cyclohexyl - N/ - phenyl thiourea (CPTU)), were synthesized by following the reported procedure [9]. The compounds were purified by ethanol and their purity was checked by elemental analysis and melting point [Table 1 & 2]. The molecular structures of the compounds studied are given in Table 3. AR grade HCl and double distilled water were used to prepare 0.1 M HCl solution for all experiments.

Electrochemical studies were performed by using a Wenking potentiostat (LB95L) and a three electrode cell containing 400 ml of electrolyte at room temperature with and without inhibitors. A platinum foil was used as auxiliary electrode and a saturated calomel electrode (SCE) was used as reference electrode. The latter was connected through a Luggin's capillary to the cell.

Table 3. Name and structural formula of the thiourea derivatives

N - benzyl - N/ - phenyl thiourea (BPTU) 
N - cyclohexyl - N/ - phenyl thiourea (CPTU) 

The steady state open circuit potential (OCP) with respect to saturated calomel electrode was noted at the end of 25 - 30 minute. Tafel extrapolation studies were made from -250 mV Vs. OCP to +250 mV Vs. OCP with a scanning rate of 20 mV /

min from the cathodic side and the corrosion currents were noted. The plots of potential Vs. log I were drawn and the corrosion current density (i_{corr}) and corrosion potential (E_{corr}) were determined from the point of intersection of extrapolated linear anodic and cathodic regions. The experiments were repeated for 40 and 50 °C. The temperatures were accurately maintained (within ± 1 °C). The results were also confirmed by using linear polarization technique. The corrosion rates (CR) were calculated using the equation,

$$Corrosion\ rate(CR), mpy = \frac{(0.129 \times Eq.Wt \times i_{corr})}{D} \quad (1)$$

where, i_{corr} is the corrosion current density in μA/cm^2, Eq. Wt is the specimen equivalent weight [taken as 27.925 grams] and D is the specimen density taken as 7.86 g/cc.

Results and Discussion

The inhibing effect of BPTU, and CPTU on the corrosion of mild steel at different temperatures and inhibitor concentrations, studied by potentiodstatic polarization technique is presented in Table 4. The percentage inhibition efficiency (%IE) and the degree of surface coverage (θ) of mild steel were calculated by using the following relations,

$$\%IE = \left[\frac{i_{corr} - i_{corr(inh)}}{i_{corr}}\right] \times 100 \quad (2)$$

where i_{corr} & $i_{corr(inh)}$ are the current densities in the absence and presence of inhibitors respectively.

$$\theta = \left[\frac{i_{corr} - i_{corr(inh)}}{i_{corr}}\right] \quad (3)$$

The effectiveness of the inhibitors on the corrosion of mild steel were observed by a drastic reduction in corrosion current , and a positive shift in corrosion potential (Fig. 2). The shift in corrosion potential (E_{corr}) towards the anodic side indicates that the compounds studied act as efficient anodic inhibitors for mild steel in HCl solution. It is observed from the results [Table 4] that IE of the compounds increases with increase inhibitor concentration at all temperatures up to a critical concentration. The increase in IE may be due to blocking effect of the metal surface by both adsorption and film formation mechanism, which decreases the effective area of attack.

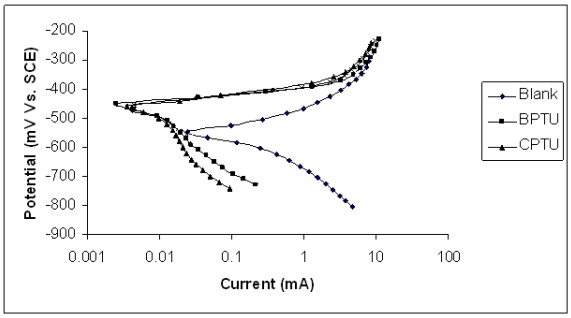


Fig.2 Potenstatic polarization curves for mild steel in 0.1 M HCl in the absence and presence of 0.0004 mol/L of inhibitors at 28 °C

The effect of temperature on IE is shown in Table 4. It is observed that %IE of did not change significantly with the increase in temperature from 28 °C to 50 °C. This indicates that the compounds investigated were insensitive to temperature in HCl medium. The excellent performance exhibited by the compounds may be due to the presence of protonated form of N and S atoms of the compounds which makes them adsorbed quickly on the metal surface, thus forming an insoluble stable film on the surface of the mild steel. Since sulphur is less electronegative than nitrogen and has two electron pairs available for co-ordination, the bonding between the inhibitor molecule and the mild steel surface probably occurs through a sulphur atom.

The values of thermodynamic parameters for the adsorption of inhibitors can provide valuable information about the mechanism of corrosion inhibition. The free energy of adsorption (ΔG_{ads}), the equilibrium constant (K) and the activation energy (E_a) at different temperatures were calculated by using the following equations,

$$\Delta G_{ads} = -RT \ln(55.5K) \quad (4)$$

where R is the universal gas constant in J/k/mol, T is the temperature in Kelvin and 55.5 is the concentration of water in mol /L.

Table 4. Tafel extrapolation results for the corrosion of mild steel in 0.1 M HCl at different temperature

C	28 ^{0}C			40 ^{0}C			50 ^{0}C		
(mol/L)	E_{corr} (mV)	*CR* (mpy)	*IE* (%)	E_{corr} (mV)	*CR* (mpy)	*IE* (%)	E_{corr} (mV)	*CR* (mpy)	*IE* (%)
Blank	-540	291.55	-	-538	428.57	-	-533	548.11	-
BPTU									
0.0001	-500	4.37	98.50	-488	9.64	97.75	-500	15.07	97.25
0.0002	-487	3.70	98.73	-482	8.57	98.00	-498	13.70	97.50
0.0003	-480	3.21	98.90	-471	7.80	98.18	-488	12.72	97.68
0.0004	-483	3.35	98.85	-470	7.93	98.15	-481	12.93	97.64
CPTU									
0.0001	-480	4.52	98.45	-475	9.86	97.70	-487	15.18	97.23
0.0002	-472	3.82	98.69	-468	8.79	97.95	-474	13.81	97.48
0.0003	-470	3.50	98.80	-468	8.23	98.08	-462	12.99	97.63
0.0004	-473	3.62	98.76	-470	8.36	98.05	-461	13.26	97.58

$$K = \theta / C(1-\theta) \quad (5)$$

where θ is the degree of surface coverage on the metal surface, C is the concentration of inhibitor in mol /L.

$$\ln(r_2/r_1) = -E_a \Delta T / (R \times T_1 \times T_2) \quad (6)$$

where r_1 and r_2 are the corrosion rates at temperatures T_1 and T_2 respectively and ΔT is the difference in temperature (T_1-T_2).

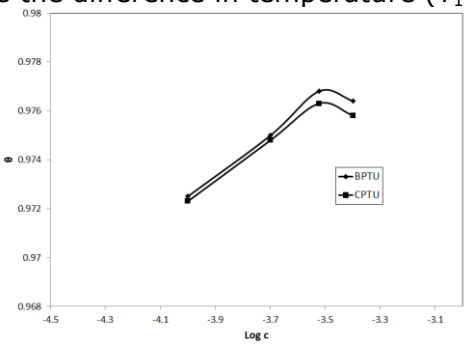
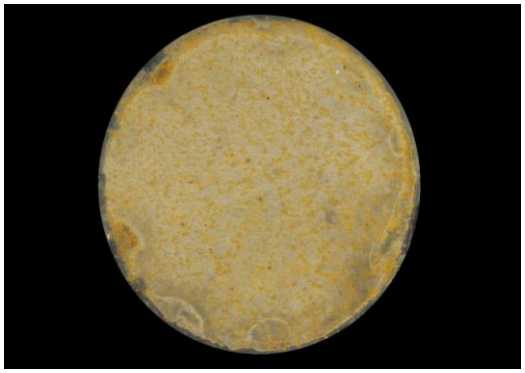
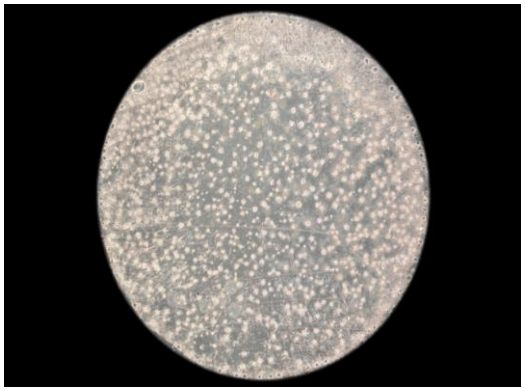


Fig.3 Temkin's adsorption isotherm plots for mild steel in 0.1 M HCl with inhibitors at 28°C.

The values of ΔG_{ads} for the compounds studied at different temperatures were more than 40 kJ/mol [Table 5], indicating that the inhibition in HCl medium is governed by chemisorption mechanism [7, 12]. The negative values of ΔG_{ads} indicated spontaneous adsorption and a strong interaction of inhibitor molecules with the mild steel surface [8]. The higher values of E_a in the inhibited solution of HCl, indicates that the compounds were more effective at lower temperatures [6].



(a)



(b)

Fig. 4 Photographs of mild steel surface exposed to corrodent: (a) 0.1 M HCl and (b) with 0.0004 mol/L of BPTU at 28 °C.

Table 5. Activation energy (E_a) and free energy of adsorption (ΔG_{ads}) for mild steel in 0.1 M HCl in the absence and presence of 0.0004 mol/L of inhibitors.

System	E_a (kJ/mol)	$-\Delta G_{ads}$ (kJ/mol)		
		28°C	40°C	50 °C
0.1 M HCl	24.38	-	-	-
BPTU	52.96	40.70	41.07	41.71
CPTU	51.02	40.42	40.84	41.56

To understand the mechanism of corrosion inhibition, the adsorption behavior of the organic adsorbates on the metal surface must be known. The degree of surface coverage (θ) values for different concentrations of inhibitors from the acid were tested graphically by fitting to various isotherms. The θ shows a linear relationship with log C [Fig.3], indicating that the adsorption of the compounds on the mild steel surface obeys Temkin's adsorption isotherm. The applicability of Temkin's adsorption isotherm verifies the assumption of a monolayer adsorption on a uniform homogeneous metal surface with an interaction in the adsorption layer[1].

The photographs of the mild steel sample corroded in 0.1 M HCl at 28 °C in the absence and presence of 0.0004 mol/L of BPTU (as a typical example) are shown in Fig. 4. The main mechanism of acid corrosion in HCl medium may be due to the anodic dissolution either at the grain boundaries or at the metal - media interface. The corrosion by pitting along with uniform attack is also noticed (Fig.4a) at the selected points on the metal surface. It is clearly indicative from the photograph (Fig.4b) that corrosion is inhibited to a large extent.

Conclusions

The polarization results reveal that the compounds investigated act as efficient anodic inhibitors for the corrosion of mild steel in HCl medium. The compounds inhibit the corrosion mild steel by adsorption on the metal surface. The IE values were nearly constant in the range of temperature studied. The adsorption of the compounds on the mild steel surface obeys Temkin's adsorption isotherm and the inhibition is governed by chemisorption mechanism. The protective effect of BPTU and CPTU were not lost even at the elevated temperature.

References

[1]A.E.Stoyanova, E.I. Sokolova, S.N. raicheva, Corros. Sci., 39 (1997) 1595.
[2]F. Bentiss, M. Traisnel and M. Legrenee, Br. Corros. J., 35 (2000) 315.
[3]Frighani, C. Monticilli, G. Brunoro and Z. Zucchini, Br. Corros. J., 23 (1988)7.
[4]I Singh, Corrision, 49 (1993) 473.
[5]J. L. Mora - Mendoza, J. G. Chacon-Nava, G. Zavala - Olivares, M. A. Gonzalez – Nunez and S. Targoose, Corros. Eng., 58 (2002) 608.
[6]M. A. Quraishi and H. K. Sharma, Indian J. Chem. Technol., 11 (2004) 331.
[7]M. A. Quraishi, D. Jamal and R. N. Singh, Corrosion, 58 (2002) 201.
[8]M. Elachari, M. S. Hajji, M. Salem, S. Kertit, J. Aride, R Choudert and Essassi, Corrosion, 52 (1996) 103.
[9]M. L. Moore and F. S. Crossly in "Organic Synthesis", Ed. E. C. Horning, Vol.3, John Wiley and Son's New York (1962) p.599.
[10]R. M. Hudson and C. J. Warning, Metal Finishing, 78 (1980) 21.
[11]Reeta Agarwal and T. K. G. Namboodhiri, Corros. Sci., 30 (1990) 37.
[12]S. Vishwanatham and Emranuzzaman, Indian J. Chem. Technol., 5 (1998) 246.
[13]V. V. Batrakov and N. I. Nanmova, Electrokhim, 15 (1970) 551.

2nd International Engineering Symposium - IES 2012
(KU-MU-NITK-HCMCUT Joint Symposium) March 5-7, 2012, Kumamoto University, Japan

Study of Gaseous Fuelled Motorcycle with Electronically Controlled Gas Injection System

Truong Hoai Linh[1] Le Dang Khoa[1] Tran Dang Long[1] and **Nguyen Ngoc Dung[1]**

1 *Key-Lab for Internal Combustion Engine, Ho Chi Minh City University of Technology*
268 Ly Thuong Kiet, Dist. 10, Ho Chi Minh City, Vietnam.
Email : hoailinhcm2007@yahoo.com

Abstract: The using of gaseous fuels (biogas/LPG) is growing very fast in Vietnam owing to its benefit as a promising alternative fuel in reducing environmental pollution and responding to crude oil exhaustion. The main objective of this research was to enlarge application of gaseous fuels for motorcycle. A prototype gaseous motorcycle was made based on a 110cm^3 class gasoline-fuel scooter. Gas injector was installed to intake manifold. Gas fuel quantity and injection time were calculated and controlled by central electronically controlled unit (ECU) based on intake pressure manifold, throttle position and engine speed. Experimental results from a chassis dynamometer for motorcycle using LPG showed that the fuel consumption decreased by 12%; the emission components such as CO, CO_2, HC and NO_x decreased by 80%, 20%, 30% and 30%, respectively. . However, motorbike acceleration was slightly decreased at high load condition when it fuelled with gaseous fuel. Considering the use of bi-fuel system for hybrid motorcycles, electronically controlled fuel injection systems and ignition control are very important. The results of this research contribute for the development and application of gaseous fuels in Vietnam.

***Keywords**:* Gaseous Fuels, Motocycle, Emission Reduction, Combustion Characteristics.

1. Introduction

Nowadays, the effects of climate change on human life have increasingly the concern problems. Major explanation is the rising of greenhouse gas that emits into the atmosphere from the different kinds of source such as factories, vehicles, and cattle farms. Among them, exhaust gas emission from the transportation is considering one of major source contribution to the increase of the greenhouse gaseous.

In Vietnam, the increase of economy contributes to the rapid increase transportation means, especially personal vehicles. The issues on exhaust gas emission become seriously important in the whole country. Among transportation means in Vietnam, motorcycle is one of the most important means, contributions for economics development.

Beside the advantages, personal motorcycle is considering the biggest emitted emission source to the environment. In 2011, Vietnam has about 34 million motorcycles, it accounts for approximately 95% of all vehicles. According to the forecast for the next few years on the use transportation means in Vietnam, the motorcycle is still the priority choice of most people. The poor of Vietnam's road infrastructure is impossible to satisfy the large number of vehicles and leads to higher traffic density.

Heavy traffic condition in big city causes vehicles regularly operating in low load conditions. This operating condition causes an increase of brake specific fuel consumption and exhaust gas emissions compared to the optimal working regime [1].

Reducing motorcycle emission is a big issue at moment in Vietnam. Many researchers have focus on improving engine combustion efficiency or apply

exhaust gas recirculation system. Among them, the application of gaseous fuel for motorcycle is still limited.

Biogas and liquefied petroleum gas (LPG) are the two promising fuel in applying for motorcycle in Vietnam. Biogas digester now is built all over the country in order to treatment animal waste and improve local environment. Biogas has been applied for various purposes such as lighting, fuelled for internal combustion engine and home cooking. The application of biogas for motorcycle is one of most promising solution owing to its carbon neutral. However, biogas fuel contains small amount of H_2S, which is cause a corrosion and damage engine component. One other hand, liquefied petroleum gas may preferable for motorbike application. The composition of LPG is mostly propane (C_3H_8) and butane (C_4H_{10}). The number of carbon atoms of LPG is fewer than gasoline, so the amount of carbon dioxide (CO_2) will emit less. Additionally, the propane-butane ratio in LPG also affects significantly to the emission compositions of vehicle. Specifically, LPG contains higher butane component, the NOx level is lower while the higher propane component will reduce CO [2]. That is the reason why the fuel conversion systems for engine using LPG are widely applied around the world.

Most commercial LPG engines use a mixer to supply gaseous fuel into intake manifold upstream of throttle valve [3]. However, for the mixer, it is difficult to achieve low emission standards, as it cannot control the air-fuel ratio precisely [4]. As for the electronic control injection unit is entirely possible to overcome the above disadvantage and increase the responsibility for each mode of vehicle speed and load to reduce emissions and fuel consumption.

For the LPG engine, the power output of engine is report to be decreased owing to the volumetric efficiency decreases. LPG is used in the gaseous form on the spark ignition engine; the volumetric efficiency of engine is lower than usage of gasoline 4-7% [5]. In addition, the engine uses LPG in gaseous state, which allows the mixing of LPG with intake air better, and form homogeneous combustion mixture easily, so the engine will run more stably and smoothly. Thus, the engine life will be prolonged. Another concerned problem of using LPG on motorcycle is LPG tank pressure, which is high; hence, the ensuring of safe operation is very important.

Based on the advantage and disadvantage of applying LPG as a alternative fuel on engines as similar as the evaluation of feasibility and using encouragement effectively LPG on motorcycle, the main objectives of this research is to study emission and performance characteristics by using LPG for motorcycles. Furthermore, the research also focuses on evaluating the dynamic ability of vehicle via acceleration time. Resulting from this research contributing for the development of applying alternative fuel in Vietnam.

2. Experimental setup and procedure

2.1. Experimental setup

2.1.1. Motorcycle using gasoline-LPG

The motorcycle using gasoline-LPG is converted based on scoter model of Honda with electronically fuel injection system. Table 1 shows some typical specifications of original motorcycle. The LPG injection system is set up in order to operate parallel with original gasoline injection system. Figure 1 described schematic arrangement of combine gas-liquid fuel system on conversion motorcycle. According to this figure, gasoline and LPG are injected by separate injector and not mixed-together in combustion mixture. Specifically, the vehicle has two fuel modes. Firstly, the vehicle uses gasoline entirely. Secondly, motorcycle engine operate with gasoline on idle and start state; on the other state, the vehicle uses entirely by LPG. Because it is difficult to start engine by LPG as the engine is cold and the idle speed of engine is higher than usage of gasoline, this will cause the difficulties in the controlling of vehicle. Engine compression ratio, fuel injections time and spark ignition time are kept as original. Because of higher octane number, the remain spark ignition and injection time may affect knocking phenomena when motorcycle is fuelled with LPG.

The LPG supply system applies the sequential injection method, which is

controlled by electronic. Amount of LPG injected into the intake manifold of engine will be adjusted to suit for the speed and load of engine and controlled by the ECU via the injection time and duration. LPG injector is installed to inject LPG gas directly on the intake manifold. A small hole in intake manifold is drilled for packing up injector-nozzle, than it is connected to LPG gas injector. Location of injector-nozzle is very important and strongly affected to engine performance. The location downstream of throttle valve is great for mixing gaseous LPG with intake air because of high turbulent. On the other hand, if the LPG is injected into the position upstream of throttle valve, the acceleration ability of vehicle will be reduced by the higher flow loss.

The LPG tank with a capacity of 10 liters can contain a maximum quantity of about 5 kg liquid-vapor LPG at a pressure of 8 bar. With this amount of LPG, the vehicle can run up to 320 km. The LPG tank is made of alloy steel to withstand the maximum pressure of 15 bars and put inside the personal items containing chamber of motorcycle. Figure 2 shows the location of LPG tank on motorcycle. The advantage of this design is to not affect motorcycle overview and do not need so much modify motorcycle frame. Due to the weight of LPG tank exceeds the limited weight of chamber, composite material is applied to reinforce the outside of chamber to increase the bearing capacity.

In this study, LPG is injected in gaseous form into the intake manifold of engine. LPG is decompressed from 8 bar to 0.6 bar via pressure regulator and then through to injector. At the pressure of 0.6 bar close to atmospheric pressure, LPG has been vaporized completely. Therefore, it is not necessary to install vaporizer in LPG supply system. This helps reduce cost for fuel conversion system.

The electronic control system of engine is installed an ECU which is connected to the vehicle's original ECU. This ECU is developed by ourselves. The ECU receives the signal of injection time and duration from the original ECU of vehicle to control gasoline and LPG injection. The gasoline and LPG injection time are similar but the LPG injection duration is the consequence of the original gasoline injection duration multiplied by an adjusted factor. This adjusted factor ensures the smoothly accelerating of vehicle and minimized emissions. Besides, the controller also acts automatically transferring from gasoline mode to LPG and reversing via engine speed signal.

All experiment were carried our on chassis dynamometer. The chassis dynamometer can generate and simulate operating conditions for motorcycles and measures the dynamic ability, the emission and fuel consumption of motorcycle in different load modes.

2.2. Experimental procedure

The motorcycle is installed on the chassis dynamometer, the LPG and gasoline tank of motorcycle are removed and placed on electronic scales to measure fuel consumption. Exhaust probe is inserted into exhaust pipe of vehicle to measure emissions. Motorcycle is warmed until the cooling water temperature of engine is stable and followed step start measuring. Measurement procedure is including: measuring emissions, fuel consumption and capacity of acceleration.

- Measuring emissions and fuel consumption of vehicle with using 100% gasoline and 100% LPG at mode of load 4kW; vehicle speed 20, 30, 40, 50 km/h.
- Measuring the acceleration ability of vehicle with using 100% gasoline and 100% LPG at mode of load 0 and 4kW; 100% throttle.

3. Results and discussion

3.1. Vehicle performance

3.1.1. Fuel consumption

Figure 3 shows the variation of fuel consumption with the vehicle speed. Generally, the fuel consumption increases as the vehicle speed increases. The fuel consumption of motorcycle with using LPG is less than usage of gasoline at all speeds. It can be seen from the explanation that the specific calorific value of LPG is higher than gasoline and its combustion efficiency is better. At the speed of 20, 30 and 50 km/h, fuel consumption reduced by 9%, 13% and 8%, respectively. In particular, at speed 40 km/h, fuel consumption

reduced by 19%. Fig.4 shows fuel consumption of vehicle when it runs in Japan 10 cycles on chassis dynamometer. Result shows that the vehicle with using LPG saves fuel about 12%.

3.1.2. Accelerating time

Based on the graph of Fig.5 shows that in both idle and load modes, the acceleration time of vehicle with using LPG is always higher than usage of gasoline. This shows that the power of engine with using LPG is lower than usage of gasoline. The reason explained that the energy density of gaseous LPG is lower than gasoline. Furthermore, the volume of gaseous LPG is larger than the volume of gasoline at the same weight and same condition, so the volumetric efficiency of engine is reduced. This causes the decreasing of engine power.

In both load modes of 0 kW and 4 kW, the acceleration time of vehicle with using LPG is higher than usage of gasoline by 35.6% and 56.9%, respectively. This shows that the decreasing of engine power at the load state is higher than no-load state. The acceleration time of vehicle with using gasoline at 4kW state is 10% higher than 0kW state. As for LPG, this value is 40%.

3.2. Emissions performance

3.2.1. Carbon monoxide (CO)

Carbon monoxide does not directly cause greenhouse effect but it occupies a part of air pollution. To minimize the damage of CO to environment, hence the decrease of CO content from vehicles is very important. The Experimental result of motorcycle with using LPG has showed that the CO content drops significantly. Fig.6 shows the variation of CO concentration with vehicle speed. Result shows that the CO concentration in exhaust gas of LPG is always stable and lower than gasoline. It decreases about 80% on average value. The decreasing of CO due to the combustion mixture is homogeneous. Because gasoline is injected in liquid state, so the mixing of gasoline with air is less homogeneous than the mixing of gaseous LPG with air. Moreover, higher vehicle's speed the shorter mixture's formation time, so the homogeneity of mixture will decrease. From the graph shows the CO content in exhaust gas of gasoline is always higher than LPG and increases gradually with vehicle speed. Formation of homogeneous mixture for the reducing of emissions is the advantage of LPG.

3.2.2. Carbon dioxide (CO_2)

Carbon dioxide is one of the components causing the greenhouse effect. A major solution for reducing the CO_2 content of vehicle is the usage of fuel contained a little carbon atoms. LPG is such fuel; its carbon-hydrogen ratio is lower than gasoline. Fig.6 shows the variation of CO_2 concentration with the vehicle speed. Generally, the concentration of CO_2 and the vehicle speed increase together. The CO_2 concentration in exhaust gas of LPG is lower than gasoline. It decreased by 20% on the average value. Particularly, at the speed of 20 and 30 km/h, which the vehicle operates regularly, it reduced by 30%.

3.2.3. Hydrocarbon (HC)

Existence of HC in exhaust gas indicates that the combustion is incomplete. The main reason for the incomplete combustion and formation of HC are lower temperature, lack of oxygen and non-homogeneity of mixture [6]. However, the laminar speed of LPG is higher than gasoline, so the combustion gas temperature rises highly in the early period of combustion [7]. At the same time, the mixture of LPG with air is more homogeneous than gasoline with air. Therefore, the HC concentration in the exhaust gas of LPG is lower than gasoline. Furthermore, LPG exists a gaseous state in atmospheric condition, so there is no liquid fuel condensation on the intake manifold. This helps reduce the HC component in exhaust gas. Fig.6 shows the variation of HC concentration with vehicle speed. The HC concentration in exhaust gas of LPG is lower than gasoline at all the vehicle speeds, it decreased by 30% on the

average value; at the speeds 20, 30, 40 and 50 km/h, it decreased by 45%, 37%, 29% and 5%, respectively.

3.2.4. Nitrogen oxides (NOx)

Formation of NOx increases in high temperature and pressure environment. In this experiment, the mixture of LPG is modified in the lean combustion region, so the combustion temperature is low. Fig.6 shows the variation of NOx concentration with the vehicle speed, it tends to increase with the vehicle speed. It is entirely reasonable, as the ability of cooling for the engine is reduced when the vehicle speed increases. Thereby, the ignition chamber temperature will rise highly. The result also shows that NOx concentration in the exhaust gas of LPG is lower than gasoline about 30% on the average value.

3.3. Driving performance

The graph of Fig.7 shows that the vehicle acceleration time from 0 to 300m with using LPG is higher than the usage gasoline about 16.5%.

In the range from 0 to 100 m, the slope of the speed curve of the vehicle with using LPG is smaller than the usage gasoline. The meaning that the acceleration capacity of the vehicle with using gasoline is better in the first 100 m. During the next 200 m, the slope of the speed curve of gasoline and LPG are approximate, so the acceleration capacity of the vehicle will not be much different. However, the acceleration capacity of vehicle is so unimportant in urban with the high traffic density.

4. Conclusion

This research focuses on testing the conversion gasoline to multi-fuel motorcycle. The following points are drawn from the research:

- The motorcycle runs well in both modes of liquid and gaseous fuels.
- The gasoline-LPG parallel fuel system for the motorcycle is stable. When the motorcycle uses LPG, so the fuel consumption and emissions reduces. At the same time, the engine power will reduce. However, the acceleration ability is still guaranteed.
- Motorcycle fuelled with LPG gas demonstrated good result responding to global warming and air pollution.

Acknowledgment

This research is supported from project T-KTGT-2010-37 at VNU-HCMC Key-Lab for Internal Combustion Engine. The authors would like to thanks JICA-Suprem project at HCMUT for their valuable support. Resulting of this project is developed from project B2-9.

5. References

[1] BUI VAN GA, Combustion of LPG-air Lean mixture and its application on motorcycle engines. The ASEM workshop on EU/ASIA Science and Tcchnology co-operation on clean technology. Hanoi, 3-4 November,2004.

[2] G.H. Choi, S.C. Bael, S.B. Han, Y.J. Chung, A study on the characteristics of combustion with butane and propane in A retrofitted diesel engine, IMechE Proc. Part D J. Automob. Eng. 218 (2004) 915–920.

[3] Y. Lee, C. Kim, S. Oh, K. Kang, Effect of injection timing on mixture distribution in a liquid-phase LPG injection engine for a heavy-duty vehicle, JSME Int. J. Ser. B 47 (2004) 410–415.

[4] H. Kwak, C. Myung, S. Park, Experimental investigation on the time resolved THC emission characteristics of liquid phase LPG injection (LPLi) engine during cold start, Fuel 86 (2007) 1475–1482.

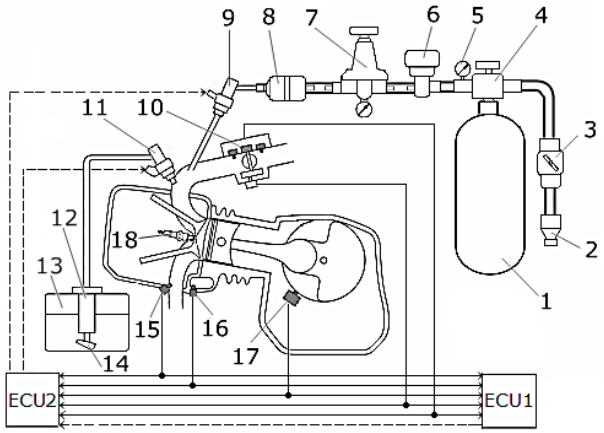
[5] M.I. Karamangil, Development of the auto gas and LPG-powered vehicle sector in Turkey: A statistical case study of the sector for Bursa, Energy Policy 35 (2007) 640–649.

[6] W.W.Pulkrabek, Engineering fundamentals of the internal combustion engine, Library of Congress Cataloging in Publication Data, 1997.

[7] John B. Heywood, Internal Combustion Engine Fundamentals, Mc-Graw Hill, USA (1988), 402-406.

Tab. 1 Specifications of tested motorcycle

Model	Lead Honda
Net weight	115 kg
Dimensions	1835/670/1125 mm
Transmission	CVT
Engine type	4-stroke SI
Bore	50 mm
Stroke	55 mm
Displacement	108 cm^3
Compression ratio	11.0:1
Cooling system	Water cooled
Max.power output	6.4 kW (7500 rpm)
Max.engine torque	9.2 Nm (6000 rpm)
Fuel system	Fuel-injected



1. LPG tank
2. Intake probe
3. Intake valve
4. Handling valve
5. Pressure gauge
6. Solenoid valve
7. Pressure regulator
8. LPG filter
9. LPG injector
10. Throttle unit
11. Gasoline injector
12. Gaoline pump
13. Gasoline tank
14. Gaoline filter
15. O_2 sensor
16. Water temp sensor
17. Crankshaft sensor
18. Bugi

Fig.1 Diagram of Fuel system

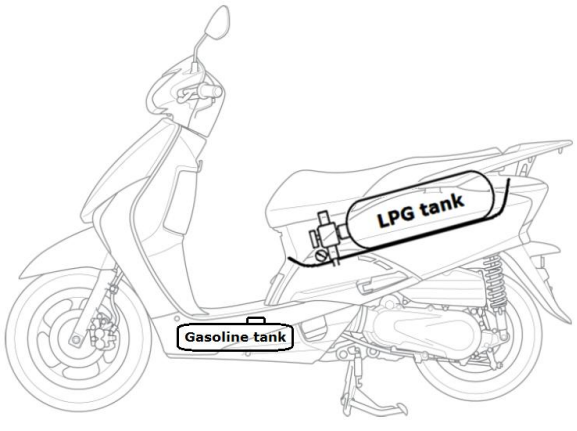


Fig.2 Position of LPG & gasoline tank

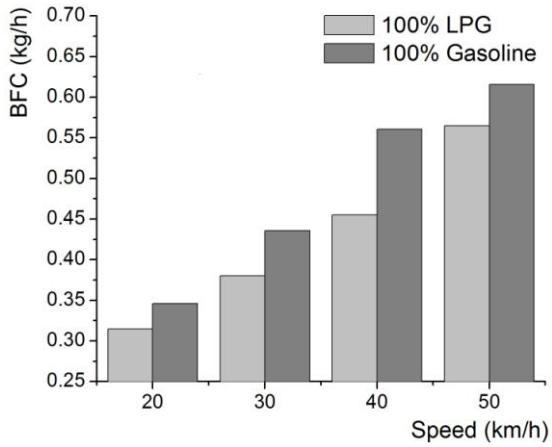


Fig.3 Comparison of brake fuel consumption

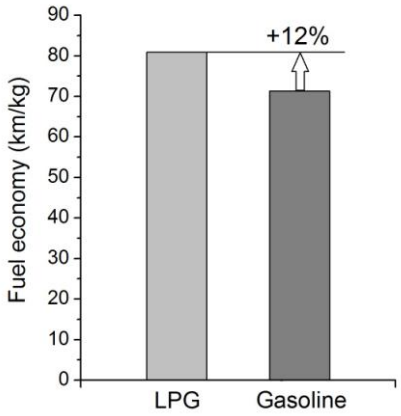


Fig.4 Comparison of fuel economy

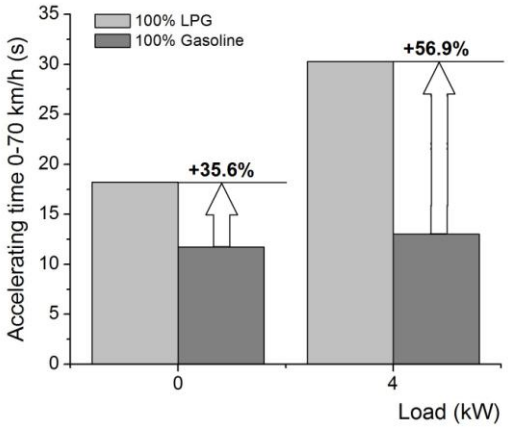


Fig.5 Comparison of accelerating time

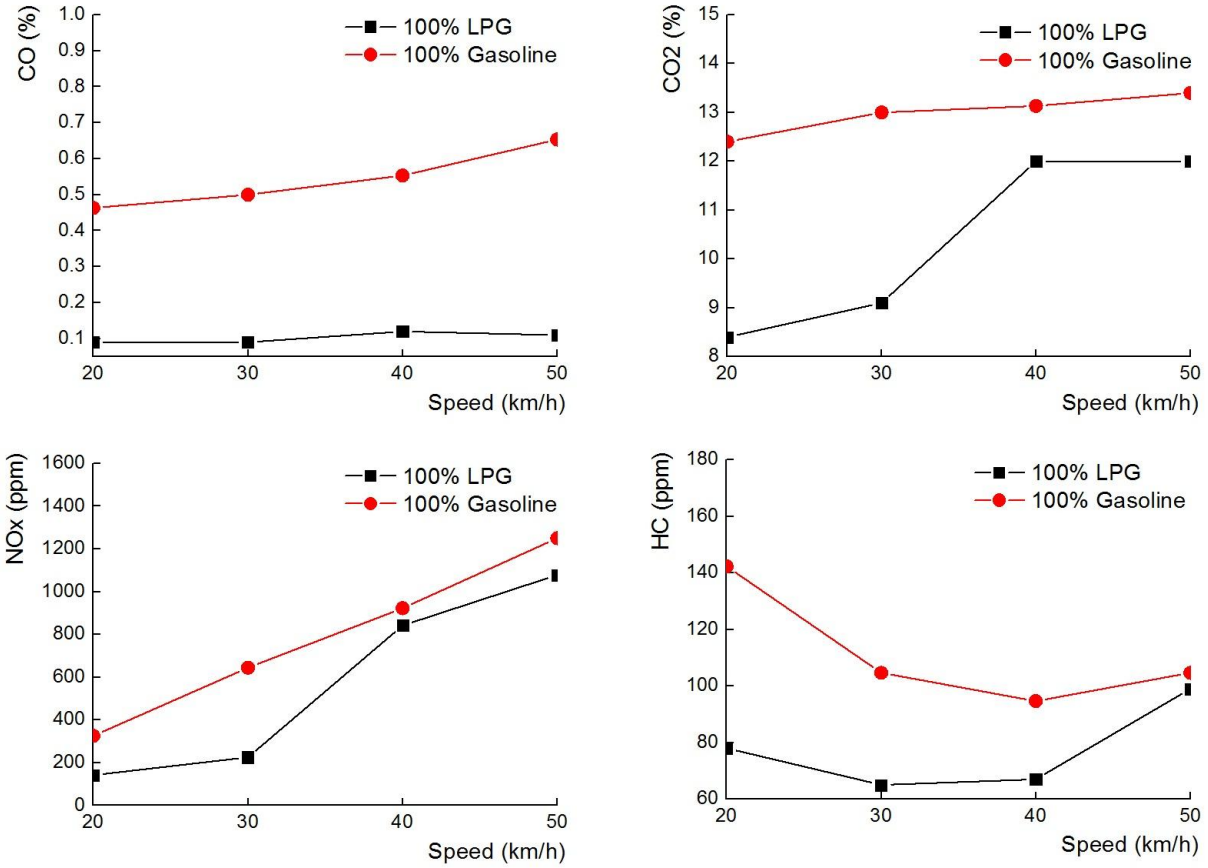


Fig.6 Comparison of emission

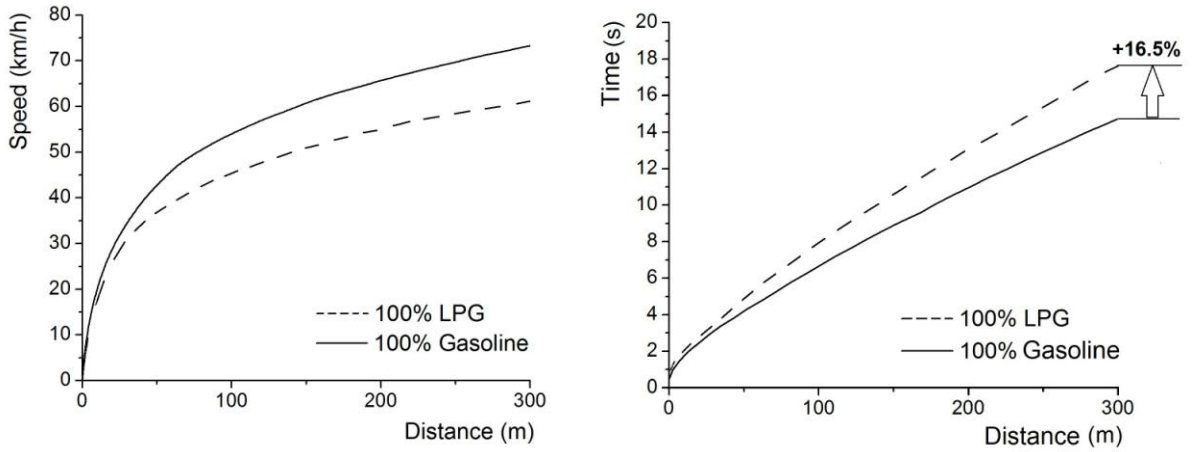


Fig.7 Comparison of driving performance

2nd International Engineering Symposium - IES 2012
(KU-MU-NITK-HCMCUT Joint Symposium) March 5-7, 2012, Kumamoto University, Japan

Performance, Emissions & Cyclic Combustion Studies of CI engine using Jatropha B20 Fuel

A.B.V. Barboza [1], C.V. Sudhir[2], N.Yagnesh Sharma[3]

1. *Department of Mechanical & Manufacturing Engg., Manipal University, Manipal, India. e-mail:barboza.augustine@gmail.com*
2. *Department of Mechanical & Industrial Engg., Caledonian College of Engg., Oman. e-mail:sudhir@caledonian.edu.om*
3. *Department of Mechanical & Manufacturing Engg., Manipal University, Manipal, India.(Corresponding Author) e-mail:nysharma@hotmail.com*

Abstract: Experiments were conducted on a single cylinder, constant speed, vertical, water cooled CI engine fuelled with methyl esters of Jatropha oil blended with petroleum diesel for 20% volume ratio (B20). Injection timing and injector opening pressure (IOP) were changed to study their influence on performance, emissions and combustion parameters. Pressure Vs. crank angle data for 500 cycles were recorded for each operating conditions which was later analyzed to estimate the cyclic variations in combustion parameters using a computer program. It was observed that advancing the injection timing and increasing the IOP up to 220bar resulted in improved performance and reduced cyclic variations in peak heat release rate but at the cost of higher rate of pressure rise. On the emissions front an inverse behaviour was observed between smoke opacity and NOx emissions with advanced injection timing and increased IOP.

Keywords*: Injection Timing, Injector Opening Pressure, Coefficient of Variation*

Introduction

The twin crisis of rapid depletion of fossil fuel based reserves and rising emissions have compelled the scientific community to look for alternate fuels for I.C. engines. CI engine being widely used in several sectors is an indispensable prime mover of the economy of a nation. Among the various alternate fuels identified, biodiesel produced from different vegetable oils is being widely considered as a viable substitute for a CI engine [F. Ma and M. A. Hanna (1999)].

Several experimental studies have shown that 20% volume blend of biodiesel derived from different vegetable sources with diesel (B20 fuel) has resulted in the best performance amongst all other blends [A.K. Agarwal and L.M. Das(2001)& B.K. Barnwal and M. P. Sharma (2005)]. Biodiesel produced from non edible oils such as Jatropha Curcas is quite economical considering its cheaper input cost. Experimental studies carried out using Jatropha oil either in the raw form or as a blend or as an ester reveal that jatropha to be a reasonable substitute for diesel fuel. [K.Pramanik (2003) & J.N.Reddy and A. Ramesh (2006)].

The cycle by cycle (CBC) variations in combustion characteristics of I.C. engines have been recognized as a limiting factor on engine performance and emissions. [J.B. Heywood (1988)].The CBC variations can be analyzed by sampling the combustion pressure data for a number of consecutive cycles. Kouremenos et.al. (1992) have concluded that more than 400 cycles form a reasonable level for a statistical analysis. Muammer Ozkan (2007) in his comparative CBC study using biodiesel and diesel reports that biodiesel would be an alternative fuel for a diesel engine with respect to CBC variations.

This paper throws light on the effect of engine operating variables such as IOP and injection timing on brake thermal efficiency, emissions such as oxides of nitrogen & smoke opacity. Also cyclic variations in combustion parameters such as peak heat release rate and peak rate of pressure rise in a CI engine operating on B20 fuel derived from Jatropha biodiesel are presented.

.

METHODOLOGY

Experiments were conducted on a single cylinder, four stroke, naturally aspirated, open chamber, water cooled, 5.2 kW peak output CI engine test rig. The engine was loaded using a directly coupled eddy current dynamometer. The engine and the dynamometer are interfaced to a control panel which is connected to a NI USB-6210 hardware and the same can be connected to a computer through a USB port. The specifications of the set up are given in Table 1. A PCB Piezotronics Inc. built piezo electric pressure transducer was installed in the engine cylinder which can measure the pressure trace in the cylinder with 1°crank angle resolution. The NI hardware can record 500 cycles of pressure crank angle data for each loading condition.

The whole set of experiments was carried out at the rated engine speed of 1500 rpm and a compression ratio of 17.5:1. The experiments were conducted at three injection timings of 20°BTDC 23°BTDC, 26°BTDC and four IOP's of 180,200,220& 240bar.

The properties of B20 fuel derived from jatropha oil and diesel are shown in Table 2. A separate Visual Basic computer program has been written in MS Excel which uses the pressure crank angle data recorded for 500 cycles to calculate average value and coefficient of variation (COV) of peak heat release rate and peak rate of pressure rise. An AVL 437-C Smoke meter is used to measure smoke opacity and MRU GmBH make Delta 1600L five gas analyzer is used for measuring the concentrations of NOx emissions.

TABLE 1 ENGINE DETAILS

Engine	Four stroke, single cylinder, constant speed, water cooled diesel engine
BHP	7BHP (5.2kW) @ 1500 rpm
Bore x Stroke	87.5 x 110 mm
Compression Ratio	17.5:1
Dynamometer	Eddy current type
Interfacing with computer	NI-USB 6210 hardware

TABLE 2 PROPERTIES OF DIESEL AND B20 FUEL

Properties	Diesel	B20
Density at 40ºC (kg/m^3)	828	835
Kinematic Viscosity at 40ºC (mm^2/sec)	2.71	3.36
Calorific Value (kJ/kg)	43172	42617
Flash Point (ºC)	53	75
Fire Point (ºC)	58	86

RESULTS AND DISCUSSIONS

Brake Thermal Efficiency

Figure 1 depicts the variation in brake thermal efficiency with injector opening pressure for the three injection timings at full load condition.

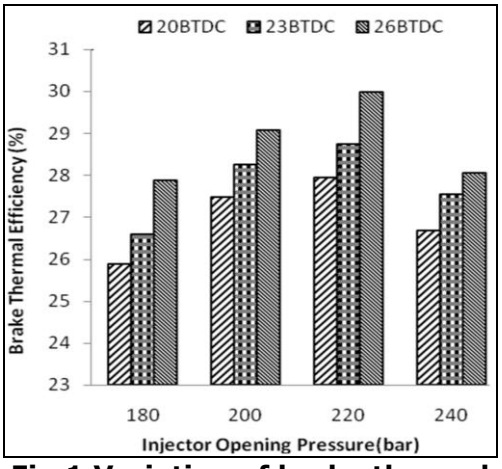


Fig.1 Variation of brake thermal efficiency with IOP at full load.

As shown in figure 1 there is a steady increase in brake thermal efficiency as the injection timing is advanced and as the

IOP is increased to 220 bar. The efficiency is relatively highest at 220 bar for an advanced injection timing of 26ºBTDC. At these operating conditions the efficiency is 29.97% which is 3.1% and 7.53% higher as compared to IOP's of 200bar and 180bar respectively Similarly as compared to injection timings of 23ºBTDC and 20ºBTDC, at 220bar the efficiency is higher by 4.28% and 7.25 respectively.
The superior performance at 220bar may be attributed to two factors. First direct fuel injection type diesel engines are more sensitive to fuel spray characteristics than indirect type diesel engines. Second B20 fuel has higher viscosity as compared to petroleum diesel and because of this the spray characteristics are greatly affected since the viscous nature of the fuel minimizes the fineness of atomization. Hence increasing the IOP from the rated value of 200bar to 220bar might have resulted in better fuel spray characteristics leading to proper mixture formation and more or less complete combustion of the mixture as compared to other IOP's tested. However increasing the IOP to 240bar at 26ºBTDC results in decrease in efficiency which is lower by 6.8%. This may be attributed to the reduced momentum of the fuel droplets to penetrate through the charge resulting from a very fine spray of the injected fuel at higher IOP.
Among the 3 injection timings tested the advance timing of 26ºBTDC exhibited consistent and better performance probably due to starting the combustion earlier compensates the effect of slow burning of jatropha derived B20 fuel due to its higher viscosity.

OXIDES OF NITROGEN:

Figure 2 illustrates the variation of Nitrogen Oxides emissions (NOx) with IOP for the three injection timings at full load condition.
As depicted in figure 2 NOx emissions not only increase with the increase in IOP and also as the injection timing is advanced. The higher percentage of oxygen present in the molecular structure of biodiesel may be a contributing factor for the formation of NOx emissions.

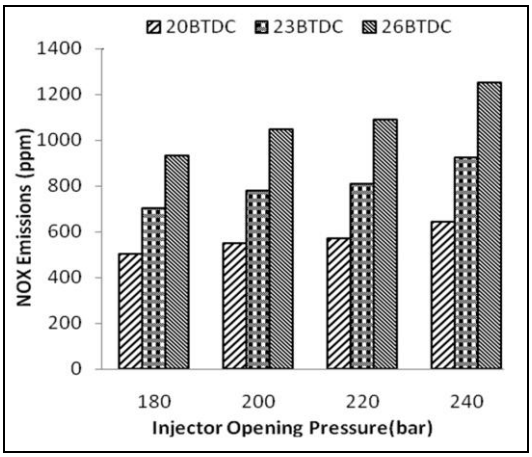


Fig.2 Variation of NOx emissions with IOP at full load.

It can be observed that for all the four IOP's tested NOx emissions recorded are the highest at 26ºBTDC followed by 23ºBTDC and 20ºBTDC. This may be attributed to rise in cylinder gas temperature caused by increased amount of premixed mass burning with the injection advance. At 20ºBTDC NOx emissions are the lowest probably due to lower combustion temperature and pressure resulting from poor combustion. The above fact is further substantiated by the higher exhaust gas temperatures recorded with ignition retard as compared to ignition advance.

For the three injection timings tested the NOx emissions recorded were highest for an IOP of 240bar followed by 220bar, 200bar and 180bar. The rise in NOx emissions with increasing IOP may be attributed to higher combustion temperatures resulting from considerable portion of the combustion occurring in the initial phase on account of smaller ignition delay. It was observed that changes in injection timing have a greater influence on NOx emissions as compared to changes in injector opening pressure.

SMOKE OPACITY:

Smoke opacity is the measure of extinction of light between a light source and a photovoltaic receiver. Figure 3 illustrates the variation of smoke opacity with IOP for the three injection timings at full load condition.

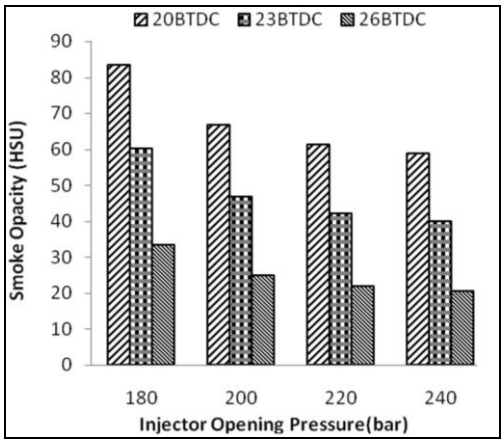


Fig.3 Variation of smoke opacity with IOP at full load.

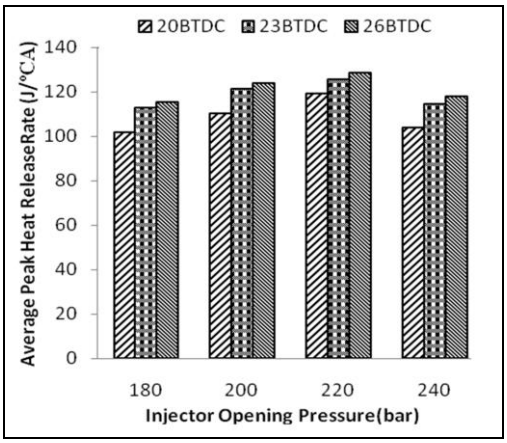


Fig.4 Variation of average peak heat release rate with IOP at full load.

As depicted in the above figure, unlike the NOx emissions smoke opacity increases not only with the reduction in IOP but also as the injection timing is retarded. It was observed that the changes in injection timing have a greater influence on smoke opacity as compared to changes in IOP This is probably due to the fact that at retarded injection timing of 20ºBTDC large amount of injected fuel does not burn as expected leading to incomplete combustion which was visible as thick smoke in the exhaust with high exhaust gas temperature.

It can be inferred from figure 3 that there is a steady fall in smoke opacity with the increase in IOP. This is the result of the improved spray pattern leading to better mixture formation and combustion.

PEAK HEAT RELEASE RATE:

The heat release rate was determined by analyzing the pressure history in the cylinder using single zone model with the first law of thermodynamics [C.V. Sudhir et.al. (2007)]. The average pressure data from 500 consecutive cycles were used for calculating the combustion parameters. The variation of average values of peak heat release rate for 500 cycles with IOP for the three injection timings at full load condition is depicted in figure 4. As depicted in the figure the peak heat release rate increases as the injection timing is advanced. The peak heat release rate values at 26°BTDC are 115.13J/°CA, 122.99J/°CA, 128.59J/°CA & 117.99 J/°CA for IOP's of 180bar, 200bar, 220bar and 240 bar respectively. This is probably due to the increase in ignition delay since the fuel is injected earlier in the compression process at lower temperature and pressure. This leads to a greater accumulation of the fuel resulting in more prominent initial phase of combustion. This also means that the diffusion combustion phase becomes less significant thereby resulting in lower smoke as shown in figure 3. The peak heat release rate is relatively higher at an IOP of 220 bar as compared to other injector opening pressures for the three injection timings tested. This may be attributed to improved premixed heat release resulting from better fuel atomization. The peak heat release rate reduces as the IOP is increased to 240 bar leading to lower efficiency as stated earlier.

The cyclic variations in peak heat release rate as indicated by its covariance at full load condition are depicted in figure 5. The COV values are relatively lower for an injection timing of 26°BTDC followed by 23°BTDC and 20°BTDC, indicating a fair degree of consistency with regard to peak heat release rate as the injection timing is advanced. The lowest covariance value is 1.78% which occurs at 26°BTDC for an IOP of 220 bar. The COV values are relatively higher for IOP's of 180 bar and 240 bar for the three injection timings indicating improper degree of atomization of fuel droplets.

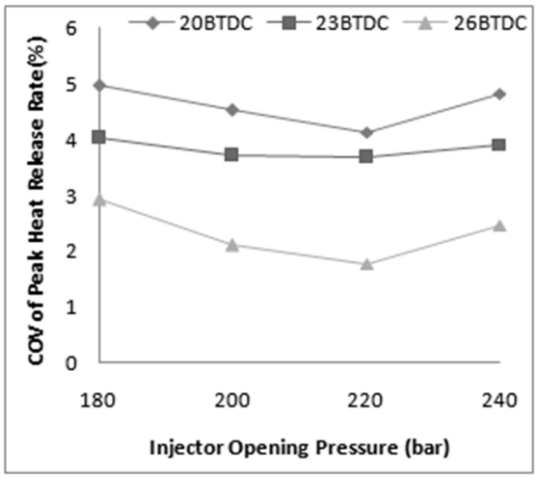


Fig.5 Variation of COV of peak heat release rate with IOP at full load.

The heat release rate curves determined by analyzing the average pressure data from 500 cycles at 26ºBTDC for the 4 IOP's at full loading condition is depicted in figure 6.

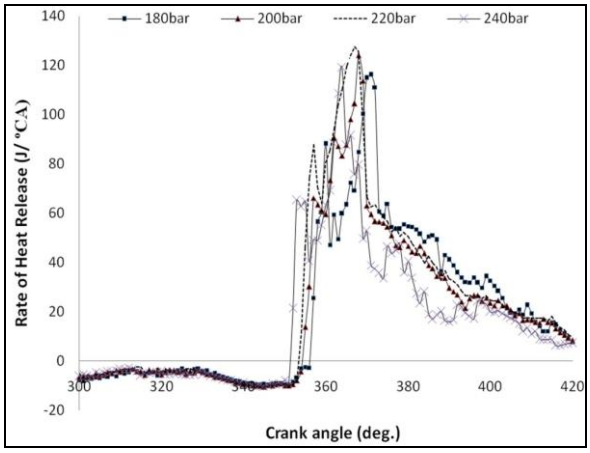


Fig 6 Rate of Heat Release – Crank angle diagram at 26ºBTDC at full load

The peak heat release rate is lower at IOP's of 180 bar & 240 bar as compared to IOP's of 200bar & 220 bar. Though the premixed heat release phase is more prominent at an IOP of 240 bar as compared to other IOP's partly due to ignition advance the diffusion combustion phase is less significant as the smaller size fuel droplets will have reduced momentum to penetrate through the charge. The heat release rate curves are more or less uniform for IOP's of 200bar and 220bar, the later resulting in highest peak heat release rate. The location of peak heat release rate moves towards TDC as the IOP is increased from 180 bar to 240 bar.

PEAK RATE OF PRESSURE RISE:

Figure 7 illustrates the variation of average values of peak rate of pressure rise for 500 cycles with Injector Opening pressure (IOP) for the three injection timings at full load condition. The advanced injection timing of 26ºBTDC and an IOP of 240 bar results in highest rate of pressure rise with a magnitude of 3.24bar/ºCA.

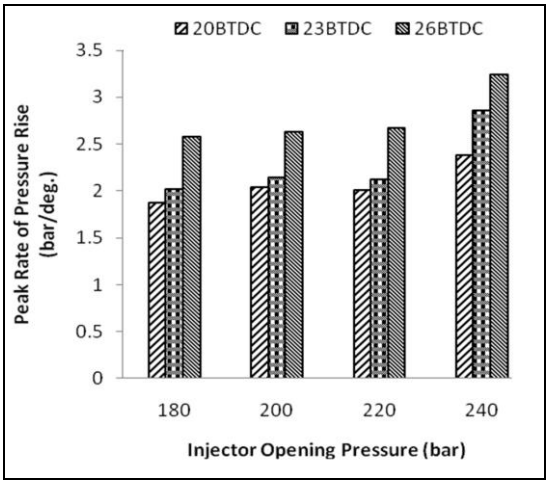


Fig.7 Variation of average peak heat release rate with IOP at full load.

In general the peak rate of pressure rise increases with the increase in IOP and as the timing is advanced. This may be attributed to the increase in ignition delay which would lead to higher pressure rise rate since a greater amount of fuel is being burnt in the uncontrolled combustion phase. Moreover the IOP of 240 bar results in faster combustion of the fuel in this phase due to a greater degree of atomization of the fuel droplets leading to rapid increase in rate of pressure rise. The above fact is further substantiated by the pressure rise rate curves for the average of 500 cycles at 26ºBTDC for the 4 IOP's at full loading condition as depicted in fig. 8.

It can be inferred from figure 8 that the crank angle of occurrence of peak rate of pressure rise occurs much earlier than TDC

as the IOP is increased The pressure rise rate curves are relatively smoother at IOP's of 200bar and 220 bar as compared to 180bar and 240 bar. At 240 bar the pressure rise rate curve increases at a rapid rate as compared to other operating conditions owing to rapid combustion.

The cyclic variations in peak rate of pressure rise as depicted in figure 9 exhibit relatively large cyclic variations at retarded and advanced injection timings and more or less an increasing trend can be observed with regard to cyclic variations as the IOP increases.

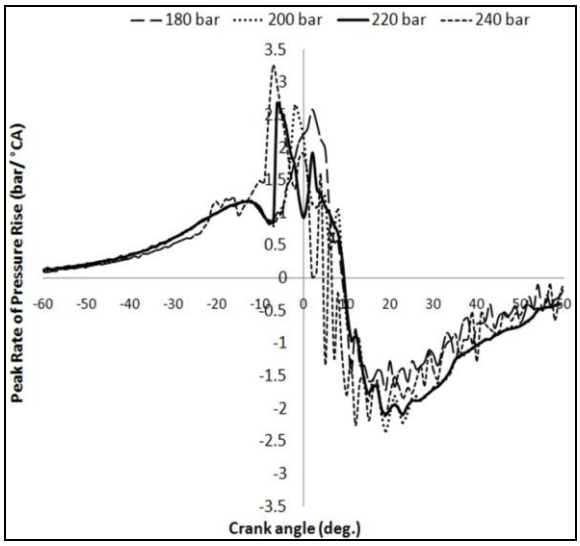


Fig. 8 Rate of pressure rise at 26ºBTDC at full load.

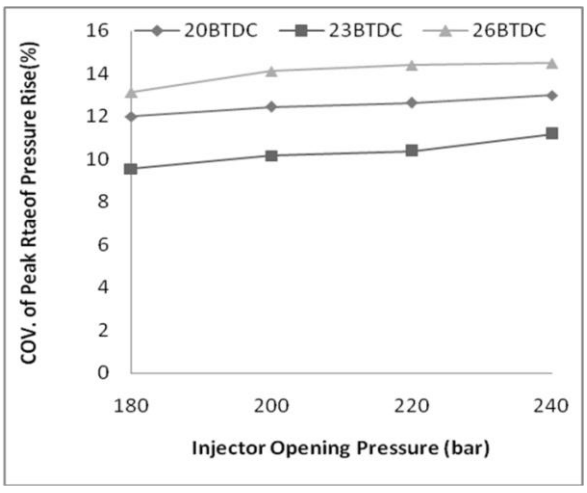


Fig.9 Variation of COV of peak rate of pressure rise with IOP at full load

Conclusions

The following conclusions are deduced from this study:

- Brake thermal efficiency and peak heat release rate increase as the injection timing is advanced and IOP is increased up to 220 bar, with lowest cyclic variations in peak heat release rate.
- Cyclic variations in peak rate of pressure rise increase as the injection timing is advanced and IOP is increased.
- An inverse behaviour was observed between smoke opacity and NOx emissions as the injection timing was advanced and IOP was increased.

References

[1] A.K. Agarwal and L.M. Das(2001), "Biodiesel development and characterization for use as a fuel in compression ignition engines, ASME Journal of Engineering for Gas Turbine and Power, vol.123, pp.440-447.

[2] B.K. Barnwal and M P Sharma (2005), "Prospects of biodiesel production from vegetable Oils in India, Renewable & Sustainable Energy Reviews, vol.9, pp.363-378.

[3] C.V.Sudhir, P.Mohanan & N.Y.Sharma (2007), Combustion Studies on CI Dual Fuel Engine with Petroleum Diesel Blends of Esterified Waste Frying Oil and LPG as Fuel, Paper No.108, ICET, Malaysia.

[4] D.A. Kouremenos, C.D. Rakopoulos and K.G. Kotsos (1992), "A stochastic – experimental investigation of the cyclic pressure variation in a DI single cylinder diesel engine", International Journal of Energy Research, vol. 16, pp.865-877.

[5] F. Ma and M. A. Hanna (1999), "Biodiesel production: A review", Journal of Bioresource Technology, vol.70, pp.1-15.

[6] J.B.Heywood (1988), "Internal Combustion Engine Fundamentals," McGraw-Hill Book Company, New York.

[7] J.N. Reddy and A. Ramesh (2006), "Parametric studies for improving the performance of a jatropha oil fuelled compression ignition engine", Renewable Energy, vol.31, pp.1994-2016.

[8] K. Pramanik (2003), "Properties and use of jatropha curcas oil and diesel fuel blends in compression ignition engine", Renewable Energy, vol.28, pp.239-248.

[9] M. Ozken(2007), "Comparative study of the effect of biodiesel and diesel fuel on a compression ignition engine's performance, emissions and its cycle by cycle variations", Energy & Fuels, vol.21, pp.3627-3636.

2nd International Engineering Symposium - IES 2012
(KU-MU-NITK-HCMCUT Joint Symposium) March 5-7, 2012, Kumamoto University, Japan

The obstacle effect to the mixing efficiency in X-shaped micro channel

Shu-Min Tu[1] Shuichi Torii[2] and **Yang-Cheng Shih[3]**

1 *Department of Mechanical System Engineering, Kumamoto University, Kurokami, 2-39-1, Kumamoto 860-8555, Japan. e-mail:toshumin@hotmail.com*
2 *Department of Mechanical System Engineering, Kumamoto University, Kurokami, 2-39-1, Kumamoto 860-8555, Japan. e-mail: torii@mech.kumamoto-u.ac.jp*
3 *Department of Energy and Refrigerating Air-Conditioning Engineering National Taipei University of Technology, Taiwan. e-mail:f10958@ntut.edu.tw*

Abstract: The study of fluid flow and heat transfer in micro scale is important to mechanical engineering, such as MEMS, medicine and bioengineering, information technology, air condition and refrigeration system. The obstacle effect is been considered as a method to increased the mixing efficiency in a mixer, particularly in micro scale. The main concern of this paper is to investigate the obstacle effect to the mixing performances in the X-shaped micro-channels. Two kinds of obstacles (diamond and circular shaped cylinder) in three kinds of positions were tasted in this paper. As the working fluid, water, is injected to micro-channel at different mass flow rate, over a wide range of flow condition, $0.48 < Re < 688$, have been discussed. The results show that, when the obstacle enhances the unsteady flow, the mixing efficiency will be increase. If the obstacle can not increases the unsteady flow, no matter how many obstacles arranged in micro channel, it will only increases the pressure drop, no benefit for mixing performance. It is clear that the obstacle effect plays an important role on the mixing performances in the X-shaped micro-channels.

***Keywords**: X-shaped micro-channels, obstacle effect, mixing performance*

Introduction

The study of obstacle effect in micro-channels concentrates on enhancing mixing performance such as increase the vortex, folded fluids to generate chaotic advection, and increase the interfacial area within the micro-channel to break up and recombine the flow.

Vadim N. Gamezo and Takanobu Ogawa [1] had study the flame acceleration and DDT in channels with obstacles: Effect of obstacle spacing. They study flame acceleration and deflagration-to-detonation transition (DDT) in obstructed channels using 2D reactive Navier–Stokes numerical simulations. The results showed that: First, more obstacles per unit length create more perturbations that increase the flame surface area more quickly, and therefore the flame speed grows faster. Second, DDT occurs more easily when the obstacle spacing is large enough for Mach stems to form between obstacles. L.K.H. Leung and D.C. Groeneveld [2] had study the Prediction of the obstacle effect on film-boiling heat transfer. They used three types of obstacles with the same blockage-area ratio of 37.8% to study on the obstacle effect. The results showed that the obstacles exhibited a strong enhancement effect on the film-boiling heat-transfer coefficient at locations downstream of the obstacles. A comparison between predictions of the correlation for the spacing-device effect and experimental data showed an under-prediction of the heat-transfer rate at locations downstream of the obstacle. The under-prediction is due mainly to the rewetting of the heated surface at the location of an obstacle, beyond which the developing film-boiling effect becomes dominant. The agreement between

prediction and data is significantly improved after accounting for the critical heat flux enhancement and developing film-boiling effects in the calculations.
In this present paper, we discuss the obstacle effect by changing the obstacle position and numbers. A 2-D modelling approach is adopted to examine the complex flow on the X-type micro-mixer. Our goal is to design a mixer by studying the effects of obstacle. Since mixing in a passive mixer occurs primarily by diffusion, reducing the mixing area is generally beneficial for faster mixing.

Numerical Simulation
The micro mixer designs were modeled and simulated by using the CFD FLUENT software (ANSYS, Inc.). To minimize effects of meshing on mixing, the mesh density was increased until grid-independent (as show in Figure 1). Six different structured grid systems, wherein the number of grids ranged from 7190 to 57408, were tested for each micro-channel. Finally, from the results of the grid-independence test, 42536 was selected (relative error in velocity equal to 0.006%) as the optimal number of grids.
The following assumptions were imposed in the formulation of the problem solving based on the characteristics of the flow: incompressible, continuum, no-slip boundary condition, laminar and a fully developed convection with constant fluid properties (H_2O water) in the upstream region. The governing equations include continuity, momentum, and energy equations, which obey the principle of conservation that can be expressed in the following general form,

$$\frac{\partial}{\partial t}(\rho\phi) + \nabla \bullet (\rho\vec{V}\phi - \Gamma_{\phi,eff}\nabla\phi) = S_\phi \qquad (1)$$

ρ is the density, ϕ is the dependent variable, $\vec{V}$ is the velocity vector, $\Gamma_{\phi,eff}$ is the effective diffusion coefficient, and S_ϕ is the source term. The diffusion-convection term of Eq. (1) is discretized by the second-order upwind scheme and the implicit method is used to discretize the transient term. After Eq. (1) is discretized, the general discretized equation can be written as (2),

$$a_p\phi_p = \sum a_{nb}\phi_{nb} + b \qquad (2)$$

where a_p and a_{nb} are discretized coefficients, and b is the discretized source term. In Eq. (2), subscript p represents the grid point under consideration and *nb* indicates the neighbors of grid point p. By employing the iterative scheme of a point implicit (Gauss-Seidel) linear equation solver in conjunction with an algebraic multigrid (AMG) method, the pressure and velocity, fields can be solved from Eq. (2).
During the iterative procedure, the SIMPLEC (Semi-Implicit Method for Pressure - Linked Equations - Consistent) algorithm was employed to solve the pressure-velocity coupling equations. The boundary condition of both outlets pressure was set to be 0 Pa. The solutions are considered to have attained convergence when the value of the relative residual is at most 10^{-6}.
In order to understand the mixing performance on different designed conditions, we defined the mixing efficiency equation (temperature based) as below:

$$M_{eff} = 1 - \frac{1}{L}\int_0^L \left|\frac{T_{Outlet} - T_{Ave}}{T_{Max} - T_{Ave}}\right| \mathrm{dx} \qquad (3)$$

In the above equation, L is the channel diameter, T_{Outlet} is the outlet temperature, T_{Max} is the maximum temperature, and T_{Ave} is the average temperature. We input the same working fluid (water) but different temperature (290K and 300K individually) in the two inlets, so the fluid properties are the same. In Eq (3), T_{Max} is fixed as 300K, T_{Ave} is based on the ideal condition, 295K; so when T_{Outlet} close to 295K, $\frac{1}{L}\int_0^L \left|\frac{T_{Outlet} - T_{Ave}}{T_{Max} - T_{Ave}}\right| \mathrm{dx}$ close to 0, M_{eff} closed to 1, represent the well mixing. On the contrary; when T_{Outlet} close to 300K, $\frac{1}{L}\int_0^L \left|\frac{T_{Outlet} - T_{Ave}}{T_{Max} - T_{Ave}}\right| \mathrm{dx}$ close to 1, M_{eff} closed

to 0, represent the bad mixing performance.
In the simulation, the dimension of x-direction was 2 mm with *Lc*, 4 mm with *Lm* and 2mm with *Ld*; the converge and diverge angles are fixed at 90°, the pipe spacing with 1mm was employed in this topic (Figure 2). The mass flow rate ranging from 0.00141 Kg/s (Re = 0.48) to 0.70522 Kg/s (Re = 688) were assumed in two inlets. The Reynolds number in Eq. (4) is valid for the common channel, whereas the X-shaped micro-channels have two inlets and both the inlet channels are characterized by half the Reynolds number.

$$\mathrm{Re} = \frac{\rho v d}{\mu} \qquad (4)$$

Two series of simulations were conducted: One supplied the same mass flow rate in both Inlet 1 and Inlet 2 but it was increased for each case (Case 1, Case 2, Case 4 and Case 7), and the other supplied a different mass flow rate to Inlet 1 and Inlet 2 (Case 3, Case5 and Case6) in order to understand the mixing preference (See Table 1).

Results

The simulation results of all models are shown in Figure 3 and Figure 4 In case 2, with the same supplied mass flow rate in Inlet 1 and Inlet 2 as 0.007 Kg/s, the two diamond obstacles has the highest pressure drop to the others. Compare to the different obstacle, the diamond obstacle has the higher pressure drop than the circular obstacle (Fig. 3). But for the velocity distribution, the diamond obstacle, circular obstacle, and no obstacle are all almost the same.
In case 1 (0.000705 kg/s) and case 2 (0.00705kg/s), the two different temperature water can mix to the average temperature (295K). As Shakhawat [3] declared at a very low Reynolds number, micro mixers can be classified into two categories: active and passive. Active micro mixers use additional structures or external sources to stir the fluids. Passive micro mixers do not require external energy: the mixing process relies entirely on molecular diffusion. Therefore, in these two cases, with slow flaw velocity, all the mixing efficiencies are equal 1.
In Case 4, with a higher mass flow rate in both inlets at 0.07 Kg/s, the two temperature water directly pass through the converging, mixing and diverging areas without mixing, as shown in figure 5. This phenomenon appears for all models, it shows that with too great a Reynolds number there is no difference in obstacle effect, the mixing mechanism becomes dominated by convection rather than diffusion. As Robin Liu [4] revealed, mixing in the straight channel decreases rapidly with an increasing Reynolds number due to the corresponding decrease in residence time.

In Case 7, with the mass flow rate at both inlet of 0.352 Kg/s, the performance of mixing becomes worse or undivided, With the obstacle in channel, the flow is unsteady (Figure 6). In the micro channel, in order to let the fluid pass through the channel more smoothly, the entrance has to add more pressure to resist the friction of the wall. With the greater aspect ratio, greater velocity gradient, and greater shear stress, the effect of the pressure becomes more conspicuous. Therefore, instability occurs during low pressure drops and a high velocity. Many investigations had focus on the early transition form in micro-channels. Mehendale [5] noted that for the early transition form laminar to turbulent flow in micro-scale tubes, the properties of the liquid change markedly as the fluid flows along the channel so that Reynolds number at the channel exit could be twice that at the inlet. Therefore, the early transition to turbulence might be partially attributed to the variation in Reynolds number. In the other way, the unsteady flow also increased the mixing efficiency.

Conclusion

The results show that, when the obstacle enhances the unsteady flow, the mixing efficiency will be increase. If the obstacle can not increases the unsteady flow, no matter how many obstacles arranged in micro channel, it will only increases the pressure drop, no benefit for mixing performance. It is clear that the obstacle

effect plays an important role on the mixing performances in the X-shaped micro-channels.

References

[1] Vadim N. Gamezo, Takanobu Ogawa, Elaine S. Oran (2008), Flame acceleration and DDT in channels with obstacles: Effect of obstacle spacing, JOURNAL of Combustion and Flame, iod: 10.1016

[2] L.K.H. Leung, D.C. Groeneveld, J. Zhang (2005), Prediction of the obstacle effect on film-boiling heat transfer, JOURNAL of Nuclear Engineering and Desing, 687-700

[3] Shakhawat Hossain, Mubashshir A Ansari, Afzal Husain, and Kwang-Yong Kim (2010). Analysis and optimization of a miceomixer with a modified Tesla structure. Chemical Engineering Journal 158 305-314.

[4] Robin H. Liu, Mark A. Stremler, Kendra V. Sharp, Michael G. Olsen, Juan G. Santiago, Ronald J. Adrian, Hassan Aref, and David J. Beebe (2000), Passive mixing in a three-dimensional serpentine microchannel. Journal of Microelectromechanical Systmes. VOL. 9, NO. 2.

[5] Mehendale, S.S., Jacobi, A.M., Shah, R.K (1999), Heat exchangers at micro- and meso-scales. In: Proceedings of the International Conference on Compact Heat Exchangers and Enhance Technology for the Process Industries, Banff, Canada, 55–74

Tab. 1 Mass flow rate in each case (Kg/s)

	Inlet 1	Inlet 2	Total
Case 1	0.00070	0.00070	0.00141
Case 2	0.00705	0.00705	0.01410
Case 3	0.00705	0.07052	0.07757
Case 4	0.07052	0.07052	0.14104
Case 5	0.00705	0.35261	0.35966
Case 6	0.07052	0.35261	0.42313
Case 7	0.35261	0.35261	0.70522

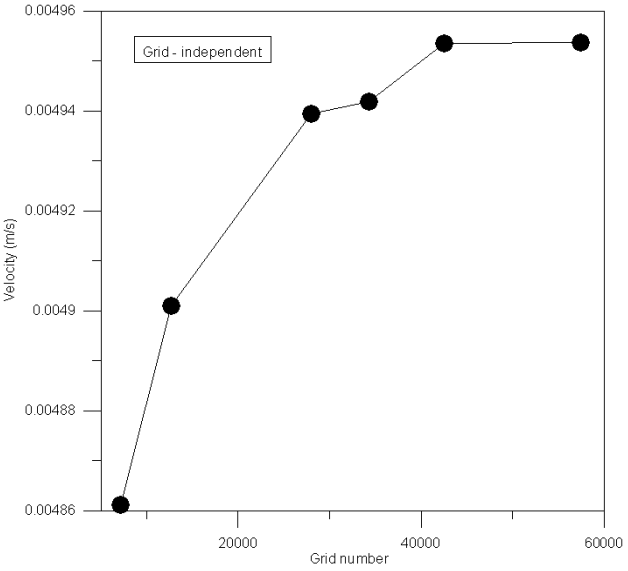


Fig. 1 Grid-independence in X-shaped micro-channel

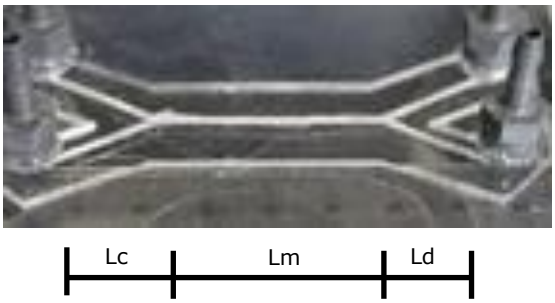


Fig. 2 X-shaped micro-channels

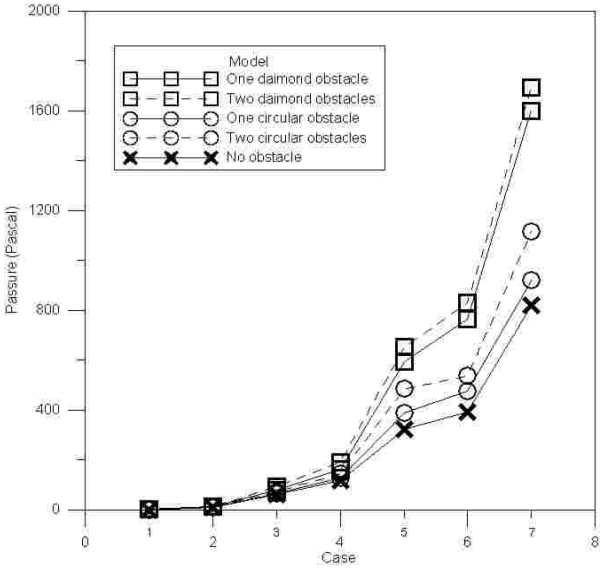


Fig. 3 Pressure drop in all models

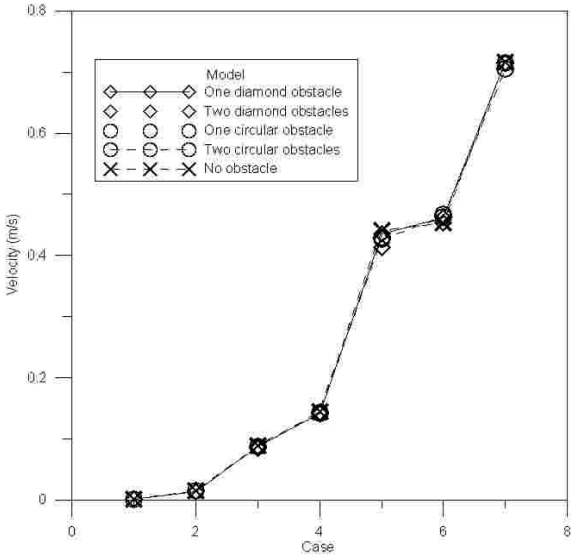


Fig. 4 Velocity in all models

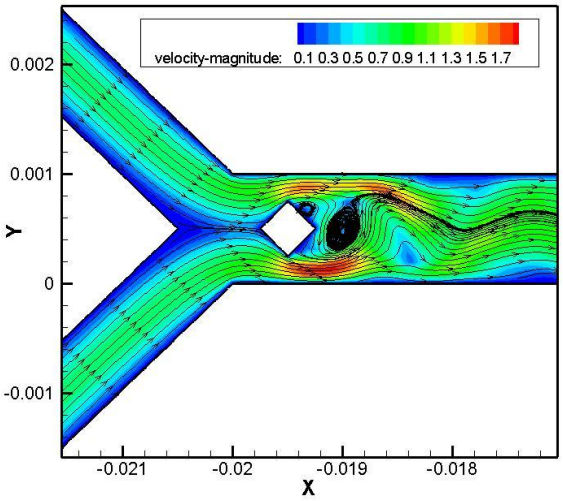


Fig. 6 Velocity magnitude in one diamond obstacle case 7

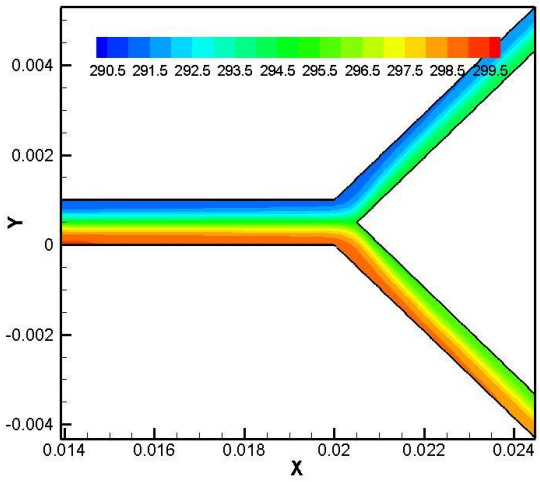


Fig. 5 Temperature distribution in one diamond obstacle case 4

2nd International Engineering Symposium - IES 2012
(KU-MU-NITK-HCMCUT Joint Symposium) March 5-7, 2012, Kumamoto University, Japan

HEAT TRANSFER ENHANCEMENT OF AL_2O_3 NANOFLUID DISPERSED IN ETHYLENE GLYCOL

HAJIME YOSHINO [1] and **SHUICHI TORII** [2]

1 *Graduate School of Science and Technology, Kumamoto University, Kurokami, 2-39-1, Kumamoto 860-8555, Japan. e-mail:111d8551@kumamoto-u.ac.jp*
2 *Graduate School of Science and Technology, Kumamoto University, Kurokami, 2-39-1, Kumamoto 860-8555, Japan. e-mail: torii@mech.kumamoto-u.ac.jp*

Abstract: In general heat transfer fluids, such as water, oil and ethylene glycol mixture are used in several industrial field. But traditional heat transfer fluids are inherently poor heat transfer fluids. There is a strong need to develop advanced heat transfer fluids. The aim of the present study is to disclose the thermal fluid flow transport phenomenon of nanofluids in the heated horizontal circular tube. Al_2O_3 particles dispersed in ethylene glycol are used as the working fluid. It is found from the study that (1) the viscosity of nanofluids increase in accordance with an increase of the volume fraction of the nanoparticles, (2) heat transfer enhancement is caused by suspending nanoparticles.

Keywords*: nanofluids, viscosity, Convective Heat Transfer*

Introduction

The working fluids with low thermal conductivity such as water or ethylene glycol suppress development of compact and higher performance heat exchangers. A new way to enhance thermal conductivity of the fluid is to suspend small solid particles in a fluid. Fluid including nanoparticles is called nanofluid. The nanofluid is found to possess long time stability and large efficient thermal conductivity[1]. Heat transfer performance for the nanofluid is superior to that of the original pure fluid. This is because the suspended ultrafine particles cause a substantial enhancement of the thermal conductivity of the mixture and improve its capability of energy change. Among numerous studies, Xuan and Li[2] measured convective heat transfer coefficient of Cu/water nanofluids of 0.3% in volume fraction to 2.0% at constant heat flux, and reported a substantial heat transfer enhancement. The purpose of this study is to disclose the thermal fluid flow transport phenomenon of nanofluid by measuring the effective viscosity and the convective heat transfer performance.

Experimental Method

Nanofluid which mixed Al_2O_3 nanoparticle and ethylene glycol is used in this study. Table 1[3] show physical property of Al_2O_3 nanoparticle and table 2 show the pH value, zeta potential and particle diameter. The dispersibility of particle in the nanofluid is measured by light scattering method. The dispersibility of particle in the nanofluid become worse in accordance with an increase of the volume fraction of the nanoparticles.

The experimental apparatus employed here is illustrated in Fig. 1. It consists of a closed flow loop, a heating unit, a cooling part, and a measuring and control unit. A straight stainless tube with 1000 mm in length, 3.96 mm in inner diameter, and 0.17 mm in thickness is employed as the test section and electrodes for the direct electric current heating are installed at both ends. The power supply is adjustable. The test tube is surrounded by a thick thermal insulation material to suppress heat loss along the test section. The six K-type thermocouples, which are welded on the outer surface of the test tube, are used to measure the local wall temperature along the heated surface of

the tube, and the other thermocouples are inserted into the flow at the inlet and outlet of the test section to measure the bulk temperature of working fluid. The viscosity is generally one of important physical properties. In this study, capillary viscometer is employed to measure the viscosity of nanofluids. The testfluids are diluted by adding pure water. The ratio of Al_2O_3 / ethylene glycol nanofluid to pure water is 1 to 1.

Table 1 Physical property of nanoparticles

Average particle diameter [nm]	31
Particle shape	Sphere
Specific particle surface area [m^2/g]	55
Crystal structure	Cubic crystal and Orthorhombic crystal
Density [g/cm^3]	3.5
Bulk density [g/cm^3]	0.31
Purity [%]	99.9
pH	6.5
Absorb amount of water [%]	1.6

Table 2 The pH value, zeta potential and particle diameter

Volume fraction [vol%]	pH	zeta potential [mV]	Particle diameter [nm]
0.1	4.76	23.83	121.8
1	4.14	26.29	127.4
5	4.33	24.94	129.5

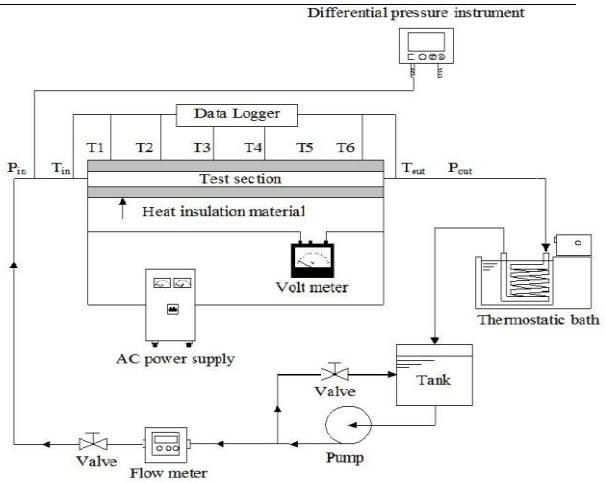


Fig.1 Schematic illustration of assembly

Results and discussion

Figure 2 depicts the viscosities for Al_2O_3 nanofluids, which are normalized by that of the pure water. The result show that the viscosity ratio of nanofluids increases in accordance with an increase of the volume fraction of the nanoparticles.

Heat transfer performance is illustrated in Fig. 3 in the form of Nusselt number (Nu) versus Reynolds number (Re) with Al_2O_3 nanofluid, as the parameter. The results show that nanofluids, containing only a small amount of nanoparticles, have substantially higher value of Nusselt number than the same liquids without nanoparticles. And the Nusselt number of nanofluids increase in accordance with an increase of the Reynolds number. For all test fluids, the Nusselt number increase drastically between Re=1200 and Re=1400.

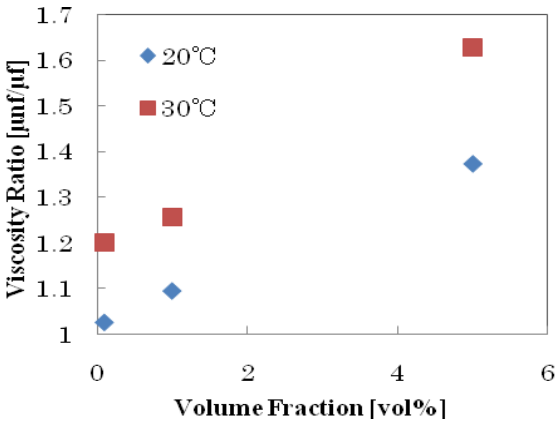


Fig.2 Viscosity ratio of nanofluids

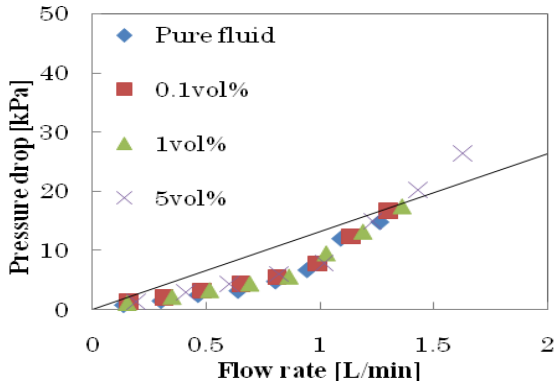


Fig.3 Pressure drop of nanofluids

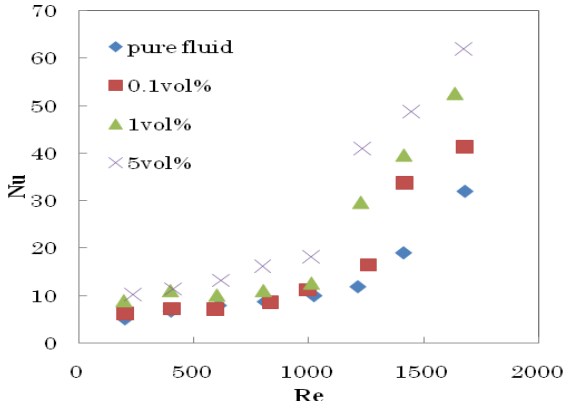


Fig.4 Relation between Nusselt number and Reynolds number for nanofluid and pure fluid

Conclusions

The following conclusions are deduced from the experimental results:

- Heat transfer enhancement is caused by suspending nanoparticles.
- The viscosity of nanofluids increase in accordance with an increase of the volume fraction of the nanoparticles.
- The dispersibility of particle in the nanofluid become worse in accordance with an increase of the volume fraction of the nanoparticles.

References

[1]Khanafer, K., Vafai, K. and Lightstone, M., International Journal of Heat and Mass Transfer, 46 (2003) 3639-3653.
[2]Xuan, Y. and Li, Q., Journal of Heat Transfer, 125 (2003) 151-155.
[3]http://www.cik.co.jp/product/nanotek/japanese/index.html

2nd International Engineering Symposium - IES 2012
(KU-MU-NITK-HCMCUT Joint Symposium) March 5-7, 2012, Kumamoto University, Japan

Heat Transfer Performance of a Multiple-Heat Pipe Cooling Device Using Pure Water and Alumina (Al_2O_3) Nanofluid respectively as Working Fluid

DAO DANH TUNG [1] **SHUICHI TORII [2]**

1 *Department of Mechanical System Engineering, Kumamoto University, Kurokami, 2-39-1, Kumamoto 860-8555, Japan. e-mail:daodanhtung@gmail.com*
2 *Department of Mechanical System Engineering, Kumamoto University, Kurokami, 2-39-1, Kumamoto 860-8555, Japan. e-mail:Torii@kumamoto-u.ac.jp*

Abstract: This experimental study is performed to investigate heat transfer performance of a multiple-heat pipe cooling device in the condition of different fill charge ratios and different constant heat fluxes. Here, pure water and alumina (Al_2O_3) nanofluid are employed respectively as working fluid. The heat pipe is composed of a heating section, a cooling section and an adiabatic section. The heating and cooling sections are the same size and both are connected by four circular parallel tubes. Here the corresponding external dimensions are 45mm in length, 45mm in width and 8mm in thickness, and the internal dimensions are 42mm, 42mm and 5mm respectively. The adiabatic section is consisted of four parallel circular tubes whose dimension is ϕ6 (external diameter) x ϕ5 (internal diameter) x 45 (length) mm. A series of experiments with different fill charge ratios and constant heat fluxes was carried out to measure temperature of the heat pipe. It is found that heat transfer performance as well as effective thermal conductivity of the heat pipe is affected by various operating conditions and the employed working fluids.

Keywords*: Multiple-heat pipe, heat transfer performance, fill charge ratio, nanofluid, heat flux, effective thermal conductivity.*

Introduction

As we have been known, during working process, there are a lot of equipment or parts - heating elements in machines generating a certain heat amount. These heating elements need to be cooled, that is maitaining their temperature at an appropriate value in order to make sure their initial designed technical features as well as their long life. In addition, due to requirment of users, some products have size becoming smaller with every passing day, but the power must be maitained constantly. This makes a high amount of heat generating in a small area - a high heat flux in side of these heating elements. In the cases of low heat flux, one can cool them by conventional cooling methods such as fans; heat sinks, conventional copper cooling fins, ... But in the cases of high heat flux, one generally use circular cooling water system. This method proves affectivly, but it is not always capable, especially with electrical or electronic devices. Thus, making an appropriate cooling device is very essential. Now there are a number of different cooling devices that are being used to cool heating elements, and the most common device is a heat pipe. It works base on boiling heat transfer and condensation heat transfer principle. Working fluid inside the heat pipe absorbs heat and boils at a certain pressure value in the heating area, after boiling, working fluid becomes vapor and evaporates to the ready cooled area and the vapor transports latent heat to this section and is condensed to working fluid again. After that, working fluid travels back to the heating area by capillary principle with a wick composed of a porous substance. This

device was suggest by Peterson, 1994; Faghri, 1995; Boo, 1998.

Although developed and applied very popularly, this type of heat pipe still has some weakness. They need a complicated structure – wick to take working fluid back of heating area. Therefore, its performance will be decreased due to blending between condensed working fluid and evaporating vapor. In addition, with this design, it is difficult to manufacture a fine product.

In order to overcome these weaknesses, in 1998, Akachi suggested "The loop type capillary heat pipe" this is a self- oscillating heat pipe with three sections: a heating section; an adiabatic section and a cooling section. This type of heat pipe is usually made by closed circuit cooper with calculated internal diameter. Inside of this heat pipe is also charged with fixed amount of working fluid. This heat pipe has no wick at all. With the study of Akachi in 1990 and Koizumi in 1992, this heat pipe is desirable with high performance.

With the same purpose to develop heat pipe, this study developed a new heat pipe with very simple structure as presented above. The heat pipe has been developed by no researcher. In this research, the heat transfer performance was investigated with the different fill charge ratios and different constant heat fluxes with the use of two working fluids – pure water and alumina (Al_2O_3) nanofluid respectively.

Experimental Apparatus and Method

Experimental apparatus

A schematic diagram of experimental apparatus is described in Fig 1. In this figure, the multiple-heat pipe is made in Laboratory of Kumamoto University – Japan, and it is heated on the heating section by the heater block made by copper containing 5 heaters (Made by HAKKO - Japan) inside with the use of a thermo-glue (made by AINEX Japan) between two surfaces to improve heat transfer (5 heaters are not shown in this figure). 5 heaters are connected with the transformer (made by YAMABISHI - Japan) and its voltage and power are measured by the Digital multi-meter (AC/DC POWER HITESTER 3334 made by HIOKI – Japan).

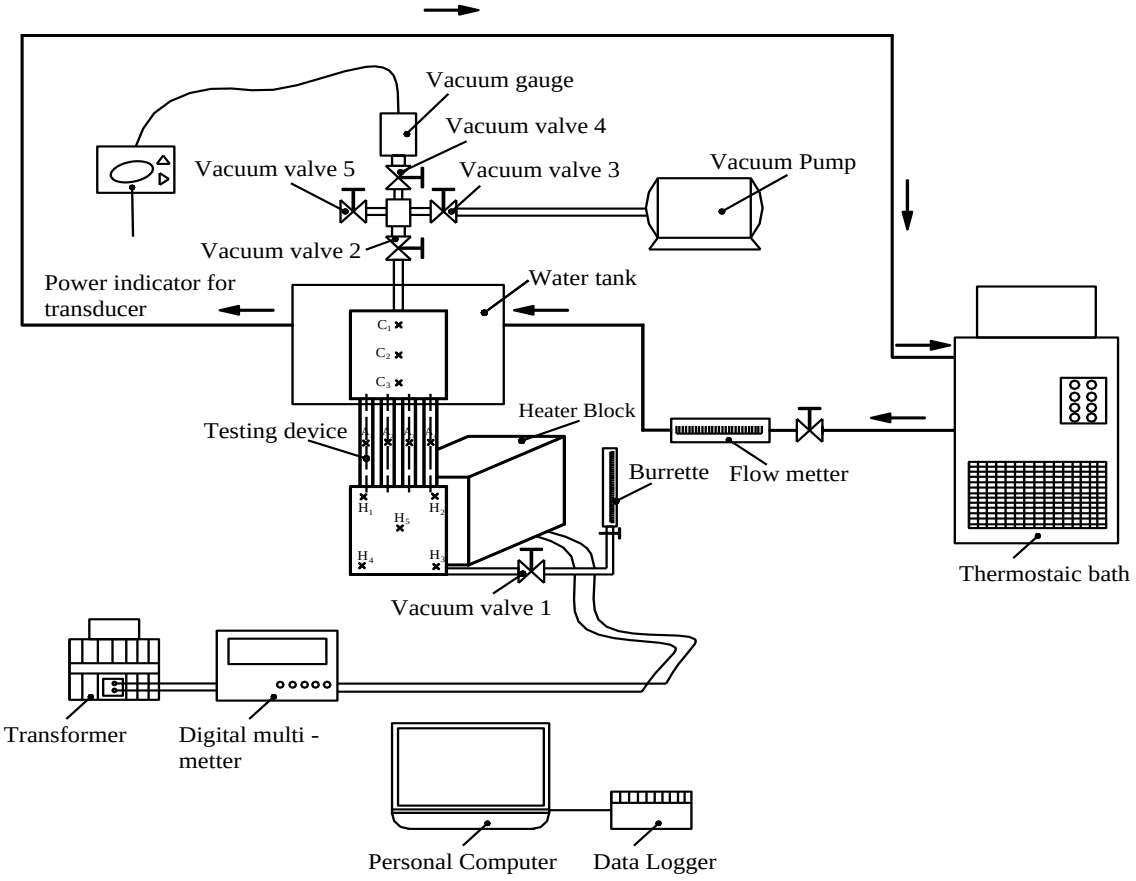


Fig.1 Schematic diagram of experimental apparatus

An accurate amount of working fluid is filled inside of the heat pipe by the burette (made in USA). Vacuum pressure inside the heat pipe is produced by the vacuum pump (GHD-030 made by ULVAC KIKO – Japan) with the measurement by the vacuum gauge and the Power indicator transducer (TPR-10 made by Diavac Limited – Japan). All vacuum valves are made by Swagelok – Japan. The cooling section of the heat pipe is cooled by cooling water set at 20^0C by the thermostatic bath (NCC-1100 made in Japan) with the flow measurement by the flow meter (RK400 made by KOFLOC – Japan). The temperature of the heater block and the heat pipe is measure by thermocouples type K with the aid of the data logger (KEYENCE NR-250 made in Japan) and the Personal Computer. The working fluid in this experimental study is pure water and alumina (Al_2O_3) nanofluid .

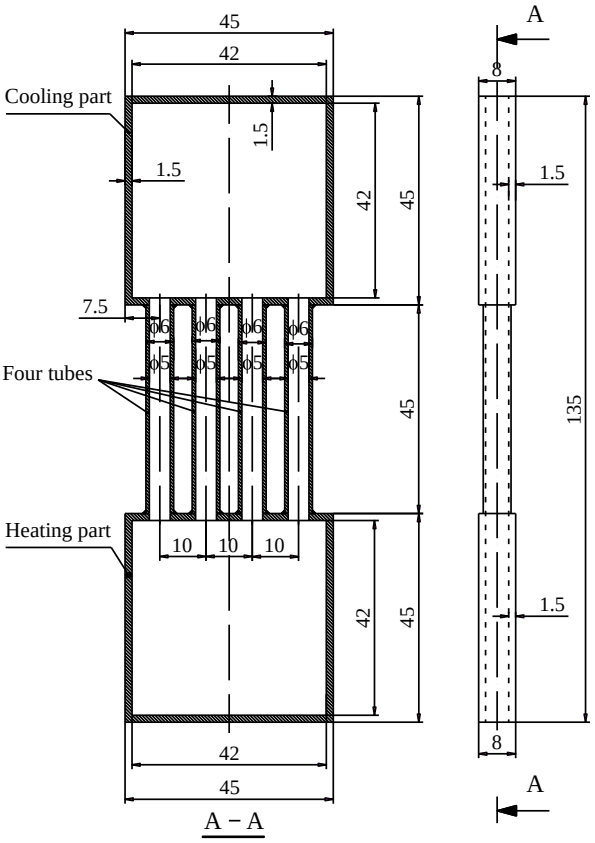


Fig.2 Structure of the multiple-heat pipe cooling device

adiabatic section and heating section are insulated with glass fiber to prevent heat loss, the cooling section is inserted to a water tank made by plastic to contain cooling water flowed circularly from the thermostatic bath. In order to fill in the working fluid and make vacuum pressure, each link part was manufactured

Experimental method

In this experiment, the working fluid was pure water and alumina (Al_2O_3) nanofluid respectively. The volume ratio – f_{cr} (fill charge ratio) between fill charge of working fluid volume and internal heating section volume were 30%; 40%; 50%; 60%; 70%; 80%; 90% and 100%. The corresponding constant heat fluxes of the heating session for each case of fill charge ratio were 5W/cm^2 (50kW/m^2); 10W/cm^2 (100kW/m^2); 15W/cm^2 (150kW/m^2); 20W/cm^2 (200kW/m^2); 25W/cm^2 (250kW/m^2). After getting results and comparing heat transfer performance of the heat pipe with the use of pure water, we could obtain the variation of heat transfer performance of the heat pipe with the change of the fill charge ratio. The angle between heat pipe axis and vertical direction was 0^0. As shown in Fig 1, the temperature of each section of the heat pipe was measured with K thermocouples as follows: for the heating section: point H_1, H_2, H_3, H_4, H_5; for cooling section: point C_1, C_2, C_3. The entry temperature of the cooling water was set at 15^0C using the controlled thermostatic bath and cooling water was supplied to the water tank at a rate of 3.5 l/min. After filling an adequate amount of pure water in the heat pipe, the vacuum pressure would be established by vacuum pump and its value was maintained at 7400 Pa for all cases. In order to get accurate vacuum pressure value, the vacuum pressure value was read on the power indicator transducer after 20 minutes and when changing from one fill charge ratio to another, the working fluid was filled in when all the apparatus system was 25^0C. Temperature was measured until the experiment reached steady state and the steady state time is at least 30 minutes. After finishing the experiment with the use of pure water, the experiment was performed with the use of alumina (Al_2O_3) nanofluid, the fill charge ratio were also 30%; 40%; 50%; 60%; 70%; 80%; 90% and 100% and the constant heat flux was tried testing with

10W/cm^2. Then, two results between the use of pure water and nanofluid were compared.

Experimental Results and Discussion
The effect of fill charge ratio and heat flux on temperature of the heat pipe

Figure 3 shows the temperature variation in the heating section and the cooling section at all of the fill charge ratios - f_{cr} from 30% to 100% at 10% intervals. We can see the temperature changes around a certain value. This can be explained easily as follows: when the heat pipe is heated, the temperature of heating section is increased and the working fluid becomes vapor and it would be evaporated to the cooling section. The heating section reaches the highest temperature when the working fluid evaporates totally. When the vapor meets the cooling section, it would transport heat to cooling section and condense into working fluid. Therefore, the temperature of the cooling section would be increased. When the condensed fluid travels back the heating section, it would receive heat from the heating section and make the temperature of the heating section decrease. At the same time, the cooling section is cooled by circulated cooling water contained in water tank.

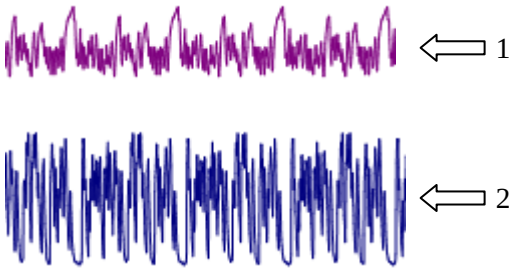


Fig.3 Temperature form of the heating section (1) and the cooling section (2)

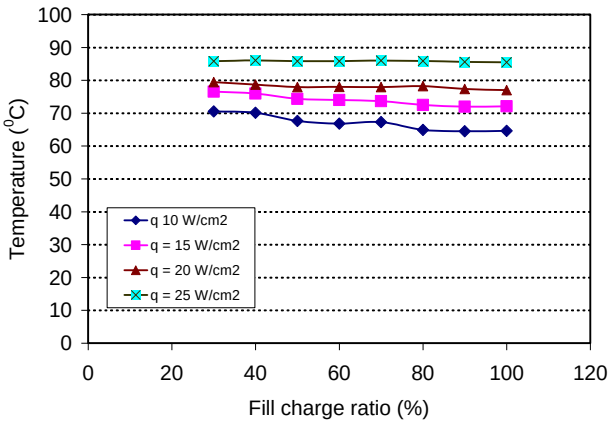


Fig.4 Mean temperature of the heating section versus fill charge ratio

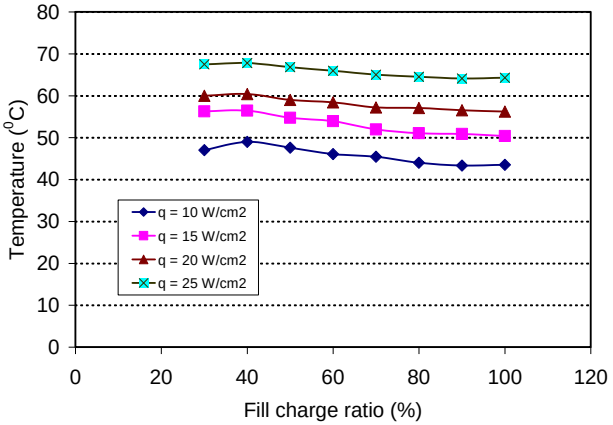


Fig.5 Mean temperature of the cooling section versus fill charge ratio

Figure 4 and 5 are the relationship between mean temperature of the heating section and the cooling section of the multiple-heat pipe cooling device with fill charge ratio, as shown in these figures, for the heating section, the higher the fill charge ratio, the lower the mean temperature at low heat fluxes – until 20W/cm^2 (200kW/m^2), but when the heat flux reaches higher value – 25W/cm^2 (250kW/m^2), mean temperature of the heating section does not have much variation corresponding with the variation of fill charge ratio. In addition, even applied a high heat flux but temperature of the heating section is still under 86^{0}C, this is a safe temperature for many parts or equipment in industrial fields. On the other hand, for the cooling section, the variation trend is different – the higher the fill charge ratio, the lower the mean temperature.

Heat transfer characteristic of the multiple-heat pipe cooling device

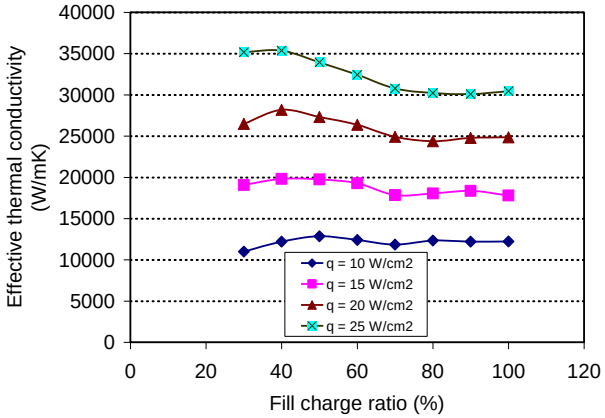


Fig.6 Effective thermal conductivity of the heat pipe versus fill charge ratio

Figure 6 shows the variation of effective thermal conductivity k_{eff} as a function of fill charge ratio f_{cr}. Effective thermal conductivity was calculated as follows:

$$Q = N.A.q' = N.A.k_{eff}\frac{T_H - T_C}{L}$$

$$\Rightarrow \quad k_{eff} = \frac{Q.L}{N.A.(T_H - T_C)}$$

Where, Q is total heat load, q' is heat flux from the heating section to the cooling section, L is length from the center of the heating section to the center of the cooling section, that is, the approximate distance between T_H measuring point and T_C measuring point. N is number of tubes of the adiabatic section (N = 4). A is flux area of the inner part of a tube in the adiabatic section. To get mean temperature T_H of the heating section and T_C of the cooling section, temperatures were measured and averaged. The local temperature of the heat pipe was measured by K thermocouples, points H_1; H_2; H_3; H_4; H_5 for the heating section and C_1; C_2; C_3 for the cooling section. These points were depicted in Fig 1.

As shown in figure 16, effective thermal conductivity k_{eff} increases when heat flux of the heat pipe increases, this illustrations that the heat pipe has capability to increase heat transfer speed when heat flux increases. But it is does not mean that the effective thermal conductivity of the heat pipe has capability to increase freely. This can be seen easily that the effective thermal conductivity of the heat pipe increases until applied the limited heat flux, in other world, the temperature of the heating section is not allowed to exceed dangerous value. And also from this figure, it can bee seen that the effective thermal conductivity in the case of heat flux q = 10W/cm^2 (100 kW/m^2), the effective thermal conductivity increases when fill charge ratio increase, but from 15W/cm^2 (150kW/m^2) and over of heat flux, effective thermal conductivity reaches highest around 40% of fill charge ratio and decreases when fill charge ratio increases up to 100%.

From the result shown in figure 16, the effective thermal conductivity of the heat pipe in the case of f_{cr} = 40% and q = 25W/cm^2 (250kW/cm^2) is almost 88 times greater than that of copper. Thus, this type of heat pipe has excellent transport characteristics even structure is very simple

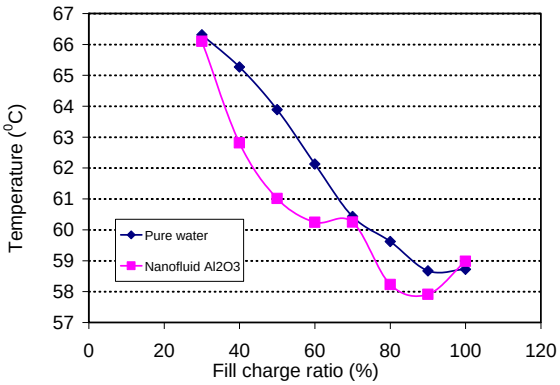


Fig.7 Mean temperature of the heating section versus fill charge ratio with the use of pure water and alumina (Al_2O_3) nanofluid respectively

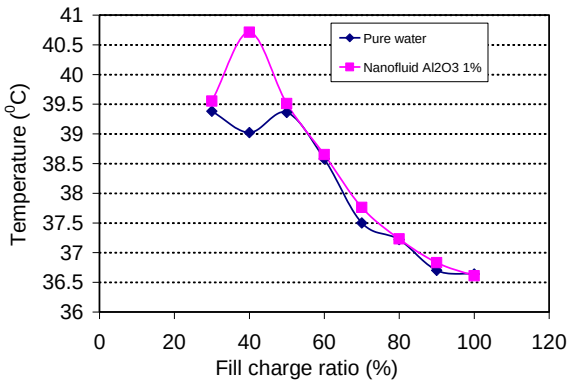


Fig.8 Mean temperature of the cooling section versus fill charge ratio with the use of pure water and alumina (Al_2O_3) nanofluid respectively

Figures 7 and 8 show mean temperature of The heating section and the cooling section of the multiple-heat pipe with the use of pure water and alumina (Al_2O_3) nanofluid respectively at 10W/cm^2 of heat flux, this is the initial result with the use of alumina (Al_2O_3) nanofluid for this heat pipe. As shown in these figures, mean temperature of the heating section of the multiple-heat pipe with the use of nanofluid is lower than that of the use of pure water. In contrast, mean temperature of the cooling section of the multiple-heat pipe with the use of nanofluid is higher than that of the use of pure water. This demonstrates that heat transfer performance of the multiple heat pipe using alumina (Al_2O_3) nanofluid is enhanced comparing with using pure water.

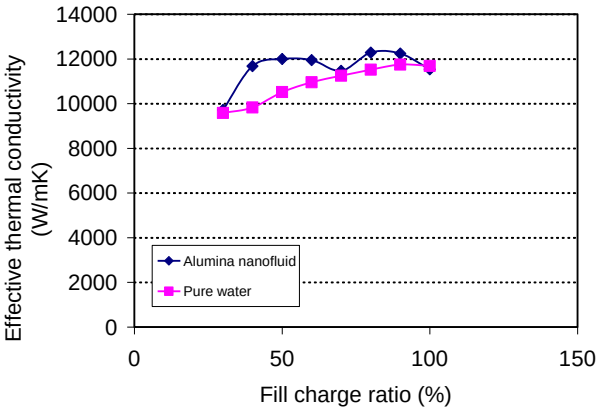


Fig.9 Effective thermal conductivity of the heat pipe versus fill charge ratio with the use of pure water and alumina (Al_2O_3) nanofluid respectively

Figure 9 shows the effective thermal conductivity of the multiple-heat pipe using pure water and alumina (Al_2O_3) nanofluid respectively. As shown in this figure, effective thermal conductivity of the multiple heat pipe using alumina (Al_2O_3) nanofluid is higher than that if using pure water.

Conclusion

From the observation of the results in this study, the following are main conclusions:

- With this type of heat pipe, from 30% to 100% of fill charge ratio at 10% intervals, when applied low heat flux – 10W/cm^2, the higher the fill charge ratio, the higher the heat transfer performance. When applied higher heat fluxes – from 15W/cm^2 and over, the highest effective thermal conductivity of the multiple-heat pipe appears around 40% of fill charge ratio of working fluid.
- This multiple-heat pipe has capability increasing heat transfer performance corresponding with the increase of heat flux.
- Mean temperature of the heating section of this multiple-heat pipe if used pure water just reaches 86^{0}C even applied high heat flux – 25w/cm^2.
- The heat transfer performance of this multiple-heat pipe is enhance when working fluid – pure water is replaced by alumina (Al_2O_3) nanofluid at 10W/cm^2

References

[1] Seok Hun Yoon., Cheol Oh., Jae Hyuk Choi., 2002 "A study on heat transfer characteristics of a self – oscillating heat pipe" KSME International Journal, Vol. 16 No. 3, pp. 354 – 362.
[2] Peterson G. P., 1994, "An introduction to heat pipe," John Wiley & Sons, Inc.
[3] Faghri A., 1995, "Heat pipe science and technology," Taylor & Francis.
[4] Boo J. H., 1998, "Fundamental principle and design sequence of heat pipes," Proceedings of the KSME 1998 annual meeting, pp. 3 – 18.
[5] Akachi H., 1988, "The loop type capillary heat pipe," Japanese patent (A), 1988 – 318493.
[6] Akachi H., 1990, "Structure of heat pipe," United States patent, Patent No. 4921041.
[7] Koizumi, 1992, "A cooler and thermal control device," Japanese patent (A), 1992 20788.

2nd International Engineering Symposium - IES 2012
(KU-MU-NITK-HCMCUT Joint Symposium) March 5-7, 2012, Kumamoto University, Japan

THE EFFECT OF HEAT TRANSFER PLATE ATTACHED ACRYLIC BLOCKS NEAR THE INLET & OUTLET AREA OF PLATE HEAT EXCHANGER

Takato Yamamoto [1] and **Shuichi Torii** [1]

1 *Department of mechanical engineering, Kumamoto University, Kumamoto, JAPAN*
E-mail: 084t3848@st.kumamoto-u.ac.jp

Abstract: The aim of this study is to consider the effect of acrylic blocks which is attached to separate herringbone plate. Experimental apparatus consists of the commercial plate heat exchanger, in which the plate which wanted to examine is sandwiched by two side walls made of flat plate. Water is used to simulate the working fluid in the vertical heat exchanger channel. A downward stream of cold water flows the vertical plate one side, while hot water flows upward along the other side wall of the vertical plate. The fluid temperature and pressure drop are measured at the test section inlet and outlet channels with the aid of thermocouples and differential pressure gauges, respectively. The overall heat transfer coefficient and frictional pressure drop were obtained by measuring temperature and pressure drop between inlet and outlet channels.

Keywords*: plate heat exchanger, pressure drop, heat transfer*

Introduction

In general, the plate heat exchanger is comparatively efficient in various heat exchangers and it is widely used for many industrial applications. The plate heat exchanger consists of the thin plate, the frame, and the gasket in which the plate shape is a key factor for the heat transfer enhancement. [1] An improvement of heat transfer performance of the plate heat exchanger is achieved by attachment of turbulent promoters in channel because of amplification of turbulence, while the frictional pressure drop increases. It is important to develop the plate, which suppresses the frictional pressure drop and at the same time promotes the heat transfer rate.

The aim of the present study is to improve heat transfer and pressure drop performance of plate heat exchanger in which the plate employed here is made of titanium and aluminum. In order to improve the performance, it is important to develop optimum acrylic blocks pattern. In this study, the single plate of the plate heat exchanger is used and the performance in the presence of the blocks which five kinds of plate are examined. The plate surface patterns which are separate herringbone is used and the characteristics of heat transfer and pressure drop are measured.

Experimental apparatus and Method

Fig.1 depicts the experimental apparatus which consists of test section, hot water loop and cold water loop. Water is used as the working fluid in the plate heat exchanger. Thermal energy of the hot water is transferred to the cold one through the titanium plate in the test section. Here hot and cold water is supplied by the independent loops, i.e., hot and cold water loops, respectively. The hot and cold water loops consist of a pump, a tank, a valve and a flow meter, respectively. The water tank in the hot water loop is heated by a pipe heater for adjusting the working fluid temperature, while the corresponding cold water loop is maintained at the constant temperature with the aid of the chiller-unit.

The test section in which thin titanium plate surface with concavity and convexity is sandwiched by two flat plate. The downstream of cold water in one channel is heated by the upstream of hot water in the other channel. That is the vertical counter-flow is formed in the test section. The test section is insulated to reduce heat losses. Cross section of the channel is 150 mm in width and the channel spaces in hot side and cold side are 3 mm. Each connection port is 20 mm in diameter. The thermocouples and differential pressure gauges are set up at 100 mm and 200 mm from each port, respectively. The fluid temperature and pressure drop are measured at the test section inlet and outlet of each channel with the aid of K type thermocouples and pressure gauges, respectively. The overall heat transfer coefficient and frictional pressure drop are estimated by measuring the water temperature, pressure drop and the water flow rate.

Figure 2 depicts the size and shape of the heat transfer plate. Dimension of the titanium plate is 400 mm length, 170 mm width and 0.5 mm thickness, as shown in Fig. 2. The most of heat transfer area shape is separate herringbone. The acrylic blocks with a rectangular cross section of 2 mm height, 5 mm wide and 20 mm long are periodically attached on surface of heat transfer plate and two sides and channel plate. The block pattern is vertical, horizon, radiation, radiation horizon and the block pitch is 5mm or every 10 degree. The volume flow rate is ranged from 1.0 to 7.0 l/min. The fluid temperature of cold side inlet and hot side inlet are 293.15 K and 303.15 K, respectively. The temperature and pressure drop of inlet and outlet of hot side and cold side in the test section are measured.

The overall heat transfer coefficient and frictional pressure drop are calculated by the measured flow rate, fluid temperature and pressure drop. The fluid properties are calculated at the averaged temperature of inlet and outlet bulk fluid. Heat transfer rate that the hot water exchanges the cold one is estimated as:

$$Q_h = W_h c_{p,h}(T_{h,i} - T_{h,o}) \quad (1)$$

$$Q_c = W_c c_{p,c}(T_{c,o} - T_{c,i}) \quad (2)$$

$$Q_{ave} = (Q_h + Q_c)/2 \quad (3)$$

The overall heat transfer coefficient between the hot and cold sides is expressed as

$$k = Q_{ave}/(A\Delta T_m) \quad (4)$$

where A is heat transfer surface area. The log mean temperature difference, ΔT_m, is determined from the inlet and outlet temperature of two counter flow channels, as

$$\Delta T_m = (\Delta T_1 - \Delta T_2)/\ln(\Delta T_1/\Delta T_2) \quad (5)$$

where

$$\Delta T_1 = T_{h,i} - T_{c,o} \text{ and } \Delta T_2 = T_{h,o} - T_{c,i} \quad (6)$$

The pressure drop measured in the experiment includes the frictional pressure drop, the pressure drop between inlet and outlet ports in the test section and the elevation pressure drop. The frictional pressure drop to be obtained is calculated by subtracting both pressure drop between two ports and elevation pressure drop from the measured pressure drop as:

$$\Delta P_f = \Delta P_{exe} - \Delta P_{port} \quad (7)$$

Here the pressure drop between two ports is proposed by Shah and Focke [6]. They reported that it is approximately 1.5 times the velocity head as:

$$\Delta P_{port} = 1.5(\Delta_m U_{2port}/2) \quad (8)$$

The Reynolds number based on the hydraulic diameter, Dh, of the channel is calculated as follows:

$$Re = (U \cdot D_h) / \nu \quad (9)$$

$$D_h = (4 \cdot A') / L \quad (10)$$

where U is the flow velocity, $A'$is the viscosity of water, A' is the cross section of the channel and L is the wetted perimeter of the channel.

Results and Discussion

The heat transfer results are summarized in Fig. 3 in the form of the overall heat transfer coefficient versus Reynolds number. As the block pattern is same, blocks attached on channel plate is better than heat transfer plate in the overall heat transfer coefficient. The overall heat transfer coefficient for the "horizon" pattern is the highest of the all pattern. This is because the flow is disturbed by the presence of the blocks, resulting in enhancement of heat transfer performance.

Fig. 4 depict the frictional pressure drop versus Reynolds number on hot side. It is

observed that the frictional pressure drop for blocks attached on channel plate is higher than the heat transfer plate. block attachment interval involves frictional pressure drop. If block interval is narrow, frictional pressure drop increase.

Conclusions

The experimental measurement has been performed on overall heat transfer coefficient and frictional pressure drop in narrow channel. Consideration is given to the effect of attachment blocks on overall performance. The conclusions are summarized as follows:

- Overall heat transfer coefficient for the blocks attached on channel is higher than the heat transfer plate employed here. The corresponding frictional pressure drop is substantially high. On the contrary, an amplification of frictional pressure drop is suppressed for the blocks attached in heat transfer plate.
- Frictional pressure drop performance is affected by the block interval. Blocks pattern which attached near the ribs of heat transfer plate, is higher than other.

References

[1] R. K. Shah and W. W. Focke, Plate Heat Exchanger and Their Design Theory, Heat Transfer Equipment Design, R. K. Shah, E. C. Subbarao and R. A. Mashelkar, eds., (1988), pp.227-254, Hemisphere.

[2] O. N. Sara, T. Pekdemir, S. Yapici and M. Yilmaz, Enhancement of heat transfer from a flat surface in a channel flow by attachment of rectangular blocks, *International Journal of Energy Research*, 25 (2001), pp. 563-576

[3] G. Tanda, Heat transfer in rectangular channels with transverse and V-shaped broken ribs, *International Journal of Heat and Mass Transfer*, 47 (2004), pp. 229-243

[4] D. Cavallero and G. Tanda, An experimental investigation of forced convection heat transfer in channels with rib turbulators by means of liquid crystal thermography, *Experimental Thermal and Fluid Science*, 26 (2002), pp. 115-121

[5] T. A. Rush, T. A. Newell and A. M. Jacobi, An experimental study of flow and heat transfer in sinusoidal wavy passages, *International Journal of Heat and Mass Transfer*, 42 (1999), pp. 1541-1553

[6] Y. Islamoglu and C. Parmaksizoglu, The effect of channel height on the enhanced heat transfer characteristics in a corrugated heat exchanger channel, Applied Thermal Engineering, 23 (2003), pp. 979-987

[7] P. Naphon, Heat transfer characteristics and pressure drop in channel with V corrugated upper and lower plates, *Energy Conversion and Management*, 48 (2007), pp. 1516-1524

[8] D. H. Han, K. J. Lee, Y. H. Kim, Experiments on the characteristics of evaporation of R410A in brazed plate heat exchangers with different geometric configurations, Applied Thermal Engineering, 23 (2003), pp. 1209-1225

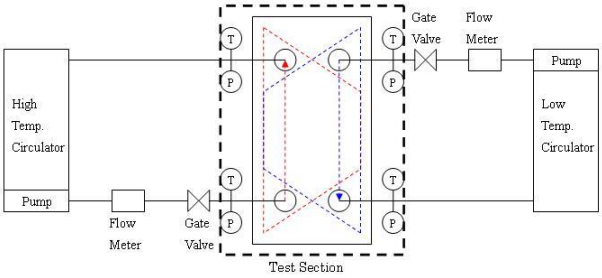


Fig. 1 Schematic of experimental apparatus

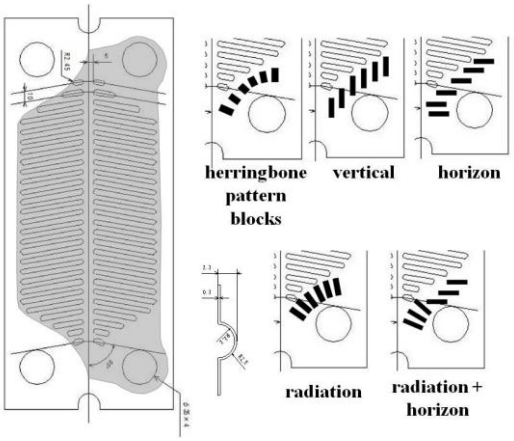


Fig. 2 Heat transfer plate & block pattern

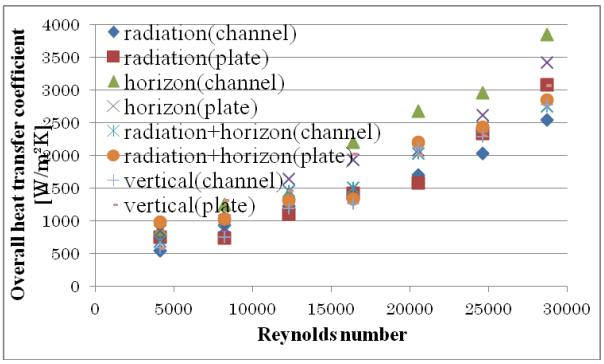


Fig. 3 Overall heat transfer coefficient variation with Reynolds number

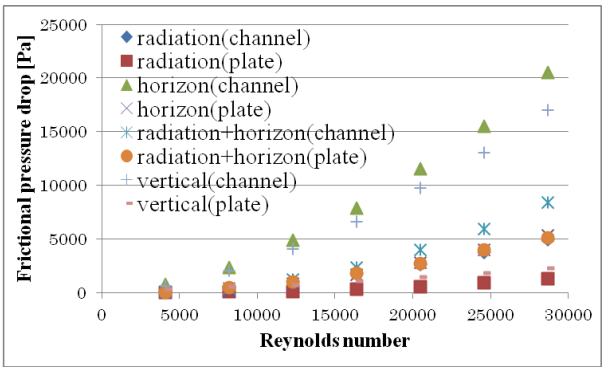


Fig. 4 Frictional pressure drop with Reynolds number on hot side

2nd International Engineering Symposium - IES 2012
(KU-MU-NITK-HCMCUT Joint Symposium) March 5-7, 2012, Kumamoto University, Japan

THERMAL FLUID FLOW TRANSPORT CHARACTERISTICS IN CONFINED CHANNELS WITH TURBULENT DUAL JET IMPINGEMENT

Caner SENKAL [1] **Shuichi TORII [1]**

1 *Department of Mechanical System Engineering, Kumamoto University, Kurokami, 2-39-1, Kumamoto 860-8555, Japan. e-mail:abc_10@kumamoto-u.ac.jp*

Abstract: Present study deals with the fluid flow and thermal fields in a two dimensional channel with inclined upper wall surface in which circular dual turbulent jet impinges on constant heat flux bottom wall surface. Numerical simulations are performed to determine the velocity and temperature profiles. Parameters used in numerical simulations are Reynolds number (2000≤Re≤10000), angle of inclined upper wall (0o ≤ θ ≤ 10o), inner jet to outer jet velocity ratio(0≤VR≤2)and the separation distance from nozzle tip to target impingement surface. Results showed that inclination angle of the upper wall enhanced heat transfer on the heated plate in the vicinity of channel outlet. Velocity ratio strongly effects heat transfer rate on the stagnation region.

Keywords*: electronics cooling,turbulence,jet*

Introduction

Jet impingement cooling is a promising and reliable cooling system due to its high heat transfer rates. There are vast various industrial applications of impingement cooling such as thermal management of electronic components, gas turbine blade cooling, glass manufacturing and annealing of metals. Because of the most of the industrial applications involved turbulent flow condition, investigating and understanding turbulent confined jets impinges on to a heated plate is important. Z.H. Lin et.al.[1] investigated heat transfer behavior of confined single slot jet experimentally. Their parameters were Reynolds number and separation distance to the heated plate. They concluded that separation distance does not effects local and average Nusselt number distribution on the heated plate. P. Hrycak[2] investigated circular impinging jet which diameter ranging between 3.18mm to 12.7mm. He reported that Nusselt number has a tendency to peak out about seven diameters away from the target plate, for tube-type nozzles. C. L. Huang et.al.[3] studied axisymmetric round jet impingement with confinement in the Reynolds range of 973-14051 including flow transition from laminar to turbulent. They reported that confinement does not have an effect on the stagnation region Nusselt number. The local Nusselt numbers in the 0<r/d<3 region for the their confined jet cases are smaller than those for the unconfined jet case; while the Nusselt numbers in the 3<r/d<5 region for their studied confined jet cases are larger than those for the unconfined jet cases. Sung and Mudawar[4] examined hybrid cooling schemes of micro channel and jet impingement. They predicted both single phase and two phase slot and series of circular jet numerically and experimentally. They achieved high cooling fluxes as much as 1127 W/cm2 and reported that superior cooling performance is achieved by optitum selection of micro channel height. Celik N. et. al.[5] carried out experiments to investigate heat transfer and flow field characteristics of coaxial jets parameterized by Reynolds number ranging from 5000 to 25000. They found that maximum stagnation point heat transfer yielded for the inner nozzle to outer nozzle ratio d/D = 0.55. On the other hand flatter heat transfer coefficient is obtained when decreasing d/D. They also reported that coaxial jets with high d/D ratio are preferable for cooling broad expanse of surfaces.

Although conventional jets are examined extensively by many researched stated above, there is still lack of knowledge of coaxial jets in literature. This study deals with heat transfer behavior and flow field of coaxial jet which impinges onto a constant heat flux surface. In order to achieve this goal numerical method is adopted. Effects of four main parameters (Reynolds number (2000≤Re≤10000), velocity ratio (0≤VR≤2), separation distance (2≤H≤8), inclination of the upper wall(0≤θ≤10)) are investigated.

Computational Modelling

Numerical simulations are performed using Star CCM+, commercial CFD software. The SST k-ω turbulence model was utilized for the numerical analysis. The use of this turbulence model was based on provided a good correlation with experimental results reported by other researches (Zu et.al.[6]). Two dimensional structured uniform mesh is illustrated in figure 1. Half of the computational domain is taken into consideration due to the symmetrical geometry.

The following assumptions are made to model the coaxial confined jet and channel:

- Two dimensional turbulent flow
- Fluid is incompressible
- Steady-State
- Constant Fluid Properties
- Negligible radiative and natural convection heat transfer

To describe forced convective heat transfer, the continuity, momentum and energy equations are required. With the assumptions described above, the governing equations are as follows:

Continuity:

$$\frac{1}{r}\frac{\partial}{\partial r}(\rho r V_r) + \frac{\partial}{\partial z}(\rho V_z) = 0 \quad (1)$$

r - Momentum:

$$\rho\left(V_r\frac{\partial V_r}{\partial r} + V_z\frac{\partial V_r}{\partial z}\right) = -\frac{\partial p}{\partial r} + \mu\left[\frac{\partial}{\partial r}\left(\frac{1}{r}\frac{\partial}{\partial r}(rV_r)\right) + \frac{\partial^2 V_r}{\partial z^2}\right] \quad (2)$$

z- Momentum:

$$\rho\left(V_r\frac{\partial V_z}{\partial r} + V_z\frac{\partial V_z}{\partial z}\right) = -\frac{\partial p}{\partial z} + \mu\left[\frac{1}{r}\frac{\partial}{\partial r}\left(r\frac{\partial V_z}{\partial r}\right) + \frac{\partial^2 V_z}{\partial z^2}\right] + \rho g_z \quad (3)$$

Energy:

$$\rho C_p\left(V_r\frac{\partial T}{\partial r} + V_z\frac{\partial T}{\partial z}\right) = k\left[\frac{1}{r}\frac{\partial}{\partial r}\left(r\frac{\partial T}{\partial r}\right) + \frac{\partial^2 T}{\partial z^2}\right] \quad (4)$$

Boundary conditions are depicted in figure 1.

A structured mesh with 3861 cells is adopted to solve the governing equations. The computational domain was descritized into rectangular faces. Grid independency study is performed. The local Nusselt number on the impingement plate for three different cell number is compared with successive grid refinement. Results showed that Nusselt number change between the grid number 3861 and 5973 is below %5.9 so 99 x 39 grid (total 3861 cells) is used for the computation. Grid refinement study is depicted in figure 2.

The solution was declared convergent when the maximum residual for each of the state variables was smaller than a convergence criterion of ε. Convergence criteria selected for the governing equations are 10^{-3} for continuity, momentum, and 10^{-6} for the energy equation.

Results

Prandtl number is taken 0.71 in this study and air is chosen as working fluid. Once the flow and thermal fields are obtained, the local Nusselt number can be calculated with the following equation:

$$Nu_x = (h_x \times D)/k \quad (5)$$

where h_x represents the local heat transfer coefficient on the target surface.

Effects of Reynolds number

Reynolds number was in the range of 2000 ≤ Re ≤ 8000 in the simulations. When the Reynol number is increased, heat transfer phenomena on the impingement plate enhanced dramatically as it is expected. Nusselt number distribution on the plate for three Reynolds number is depicted in figure 3.

For Reynolds number Re= 3000 and Re= 5000 it is observed that after the working fluid of inner nozzle impinges on the impingement plate it forms a wall jet

towards outer nozzle impingement. Nu number tends to increase to the outer nozzle impingement area because of this wall jet and then Nu number decreased along impingement plate until outlet gradually except in the vicinity of the outlet. Reverse flow is observed in the vicinity of the outlet for the Re number 3000 and 5000 so Nu number on the plate in the neighbourhood of outlet is increased sharply due to this reverse flow to the channel. However, for the case of Re=8000, reverse flow is not as effective as the other two cases.

Effects of Velocity Ratio (VR)

Velocity Ratio which is the ratio of inner nozzle velocity to outer nozzle velocity was in the range of $0 \leq VR \leq 2$. VR=0 is the situation that there is no inner nozzle working fluid injection to the channel and VR=2 corresponds to outer nozzle exit velocity magnitude of working fluid is just half of the inner nozzle velocity. Stagnation point Nusselt number of impingement plate is minimum for the case VR=0 due to the absence of inner nozzle injection. It is observed for VR=2 that the difference of the first peak and second peak of Nusselt number is decreased compared to the peak values for Re=3000 case. In order to obtain more uniform velocity distribution on the heated plate, inner nozzle velocity should set higher then outer nozzle velocity.

Effects of Separation Distance

Four different separation distance was taken into consideration, say H=2D,4D,6D,8D as D is the inner nozzle diameter. Stagnation point heat transfer rate is the most high for the case H=2. It is observed that the Nu number is high for H=2 among other cases until the horizontal position $r \approx 0.031$m on the impingement plate. For the cases H=4,6,8, there was no reverse flow into the computational domain hence the Nu number in the close vicinity of the outlet was stable. For H=8, heat transfer rate was almost constant along the heated plate. Nusselt distribution for four different separation distance case is depicted in figure.

Effect of inclination of the Upper Wall

Inclination of the upper wall is varied between $0^o \leq \theta \leq 10^o$ in simulations. While inclination of the upper wall was changed, other parameters (Re, VR, H) is kept constant. Results showed that inclination of the upper wall did not effect stagnation point heat transfer significantly, whereas, Nusselt number in the vicinity of domain outlet is increased for the cases of inclination 5^o and 10^o due to the accelerated flow by the upper wall but the Nu increment is not much compared to the case $\theta = 0^o$.

Conclusion

Numerical simulations has been employed to investigate two-dimensional, incompressible thermal-fluid flow of a dual turbulent jet with an inclined upper wall surface. Consideration is given to the influences of the velocity ratio, the Reynolds number, the nozzle height and the inclination angle of the upper plate on the flow pattern and the heat transfer performance in the channel. The results are summerized as follows:

When a dual turbulent jet is introduced into the two-dimensional channel, the flow pattern, isotherms, and heat transfer performance are affected by the velocity ratio, the nozzle height, and the Reynolds number. Heat transfer performance along the heated wall is amplified with an increase in the velocity ratio and the Reynolds number. On the contrary, a substantial reduction in the heat transfer rate, for VR=0.0, occurs in the stagnation zone, because the absence of the inner nozzle injections causes the recirculation in the corresponding region due. The heat transfer rate in the stagnation zone is attenuated by increasing the nozzle to impinging plate distance. In particular, the effect of the inclination angle in the downstream region, especially at the vicinity of outlet. The streamwise reduction in the heat transfer rate for $\theta = 0.0^o$ is suppressed by the presence of the inclined confinement surface and its value is intensified by the inclination angle.

References

[1]Lin Z. H., Chou Y.J. Hung Y. H., Heat transfer behaviors of a confined slot jet impingement, Int. J. Heat Mass Transfer. Vol. 40, No. 5, pp. 1095-1107, 1997
[2]Hrycak P. , Heat transfer from round impinging jets to a flat plate, Int. Journal of Heat and Mass Transfer/a. Vol. 26. No:12. pp. 1857-1865. ,1983
[3]Huang C. L. , Shieh Y. R. Hung Y. H. Local Thermal Characteristics of a Confined Round Jet Impinging onto a Heated Disk, IEEUCPMT Electronic Packaging Technology Conference, 1997
[4]Sung M., Mudawar I., Single-Phase and Two-Phase Hybrid Cooling Schemes for High-Heat-Flux Thermal Management of Defense Electronics, Journal of Electronic Packaging, Vol:131, 2009
[5]Celik N. Eren H., Heat transfer due to impinging co-axial jets and the jets fluid flow characteristics, Experimental Thermal and Fluid Science 33 715–727, 2009
[6]Zu Y. K., Yan Y.Y, Maltson J., Numerical Study on Stagnation Point Heat Transfer by Jet Impingement in a Confined Narrow Gap, Journal of Heat Transfer, ASME, Volume:131, 2009
[7]Chattopadhyay H., Numerical investigations of heat transfer from impinging annular jet, Int. J. Heat Mass 47 3197-3201, 2004.

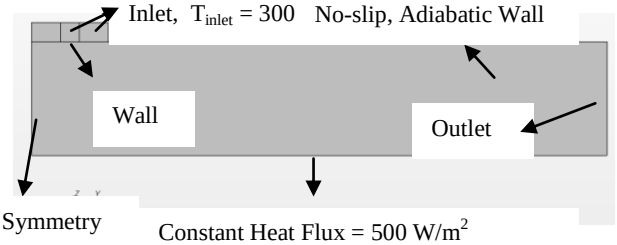


Fig.1 Boundary Conditions

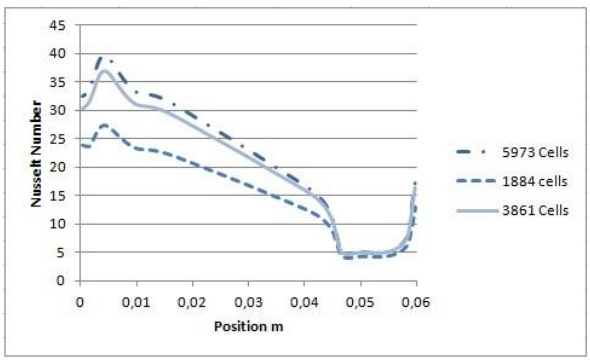


Fig.2 Grid Refinement

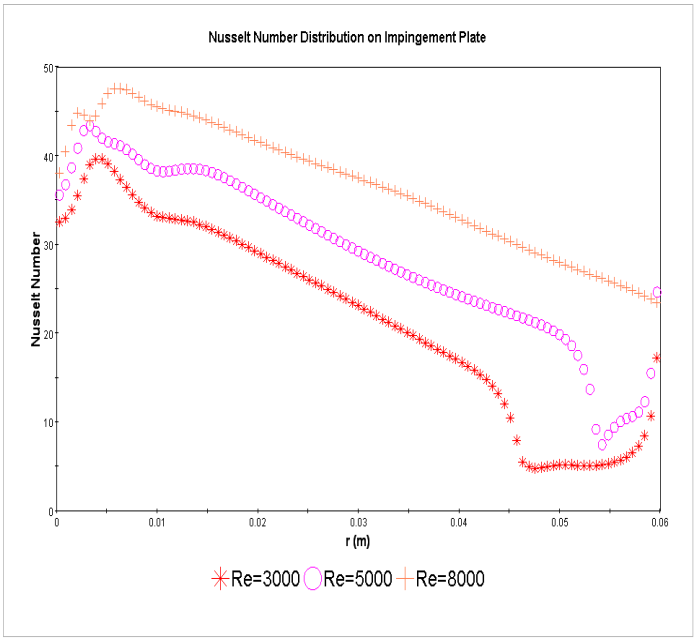


Fig.4 Nusselt Number Distribution for three different Reynolds number

2nd International Engineering Symposium - IES 2012
(KU-MU-NITK-HCMCUT Joint Symposium) March 5-7, 2012, Kumamoto University, Japan

STUDY OF THERMAL FLUID FLOW AND VENTURI EFFECT

Giichi Nakamuta, Shuichi Torii

Department of Mechanical System Engineering, Kumamoto University, Kurokami,2-39-1, Kumamoto 860-8555, Japan. e-mail:117d8531@st.kumamot-u.ac.jp

Abstract: The aim of this study is to utilize solar panels for a power source of a refrigerator on a car. Warming solar panels make efficiency of power generation worse. So we studied the cooling of the back of solar panels using venturi effect. In this study, the aluminum plate warmed by a silicon- rubber heater was used in place of a solar panel. There are three case of test section. Case1 doesn't have the cooling mechanism using venturi effect. Case2 has the mechanism. Case3 has the mechanism and micro fins on under face of the plate. Temperatures of three cases are compared in the various reynolds number.
If reynolds number is higher than 27000, temperatures of Case2 are higher than Case1. Temeratures of Case2 and Case3 are almost the same.

***Keywords**: Solar Panel, Aluminum Plate, Air Flow, Venturi Effect*

Introduction

In recent years, solar panel is expected to be one of things what solve the environmental problem. The aim of this study is to utilize solar panels for a power source of a refrigerator on a car. Warming solar panels make efficiency of power generation worse. So we studied the cooling of the back of solar panels using blow.

PRINCIPLE OF COOLING

Figure.1 shows the outline of the solar panel. On the surface of the solar panel, two projections which have each one hole are made. The hole leads to back of the solar panel. Space is made between back of the solar panel and the refrigerator. The two holes and the space are connected. When the head wind blows on the surface of the solar panel, the air pressure between the projections goes down by acceleration of the air current. This negative pressure between the projections makes the air flow in the space in accordance with the Bernoulli's theorem. This air flow takes the heat of back of the solar panel through the holes of the projections.

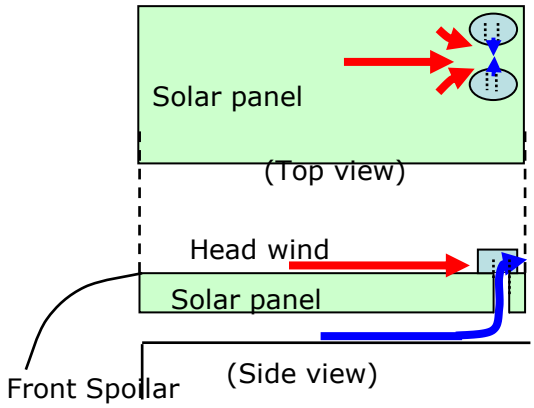


Figure.1 Cooling Mechanisum

EXPERIMENTAL METHOD

Figure.2 shows an outline of the experimental device.

Figure 3 shows front view of the test section of Case1. The test section of case1 has no space to draw in atmospheric air under the aluminium plate. The top view of the pipe in the test sections (all cases) is showed at Figure.4, but test section of

Case1 has no air passage leading to back face of the aluminium plate. Temperatures of the aluminium plates are measured.

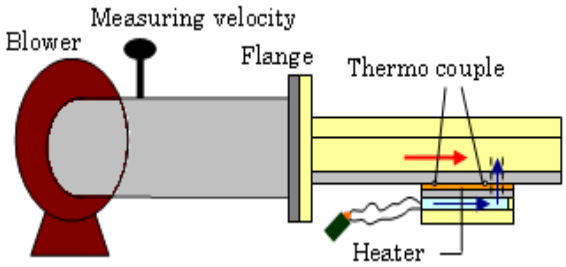


Figure.2 Experimental Apparatus

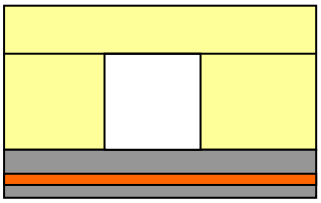


Figure.3 Front View of Case1

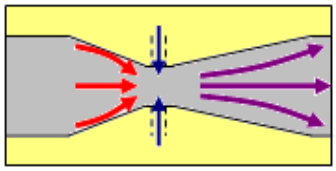


Figure4 Top View of test section

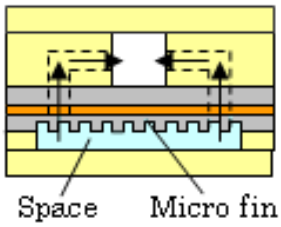


Figure.5 Front View of Case3

Figure.5 shows front view of test section of Case3. There is a space leading to the atmosphere and the pipe over the aluminum plate. Air is blown on the top surface of the aluminium plate in the test section through the pipe. The electric power of the heater is 9.56 W. This is calculated by the radiation of the sun.

Temperatures of the aluminium plate are measured by thermocouple at various Reynolds numbers in the pipe .

Besides that, the flow of the air in the space is measured and visualized by smoke.

RESULT AND DISCUSSION

Figure.6 shows the temperatures of aluminium plates of each cases at various Reynolds numbers in the pipe. Temperature of Case1 is the lowest , if Reynolds number of the pipe is lower than about 5000. If Reynolds number is 5000 to27000, temper-atures of three cases are almost same. If Reynolds is over 27000, temperatures of Case2 and Case3 are lower than Case1. Temperatures of Cas2 and Case3 are almost same at all Reynolds numbers.

Figure 7 shows Reynolds numbers of blow in the pipe and space under the aluminium pipe. It shows two Reynolds numbers are proportional.

Figure 8 shows smoke is drawn into the space according to venture effect. So, it is confirmed that atmospheric air is drawn in the space.

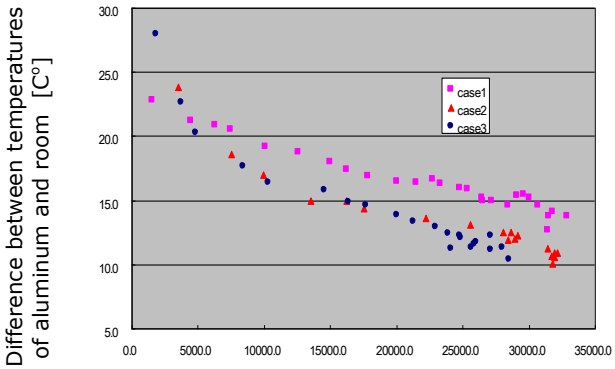


Figure.6 Relation of Reynolds Number and Temperature

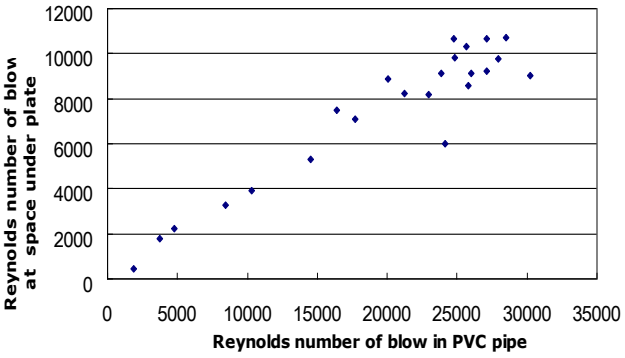


Figure.7 Relation of Reynolds numbers in Two Segment



Figure.8 Visualization of Flow under the Plate

Conclusion

- The refrigerator using venturi effect at this study has good effect , if Reynolds number in PVC pipe is more higher than 27000.
- But, micro fins don't have no effect.
- It is made sure that atmospheric air is drawn in the space under the plate by visualization using smoke.

2nd International Engineering Symposium - IES 2012
(KU-MU-NITK-HCMCUT Joint Symposium) March 5-7, 2012, Kumamoto University, Japan

Investigation of Combustion Furnace Fuelled by Compost

SHOTA WATANABE[1] **SHUICHI TORII [2]**

1 *Graduate School of Science and Technology, Kumamoto University, Kurokami, 2-39-1, Kumamoto 860-8555, Japan. e-mail:118d8553@st.kumamoto-u.ac.jp*
2 *Department of Mechanical System Engineering, Kumamoto University, Kurokami, 2-39-1, Kumamoto 860-8555, Japan. e-mail:torii@mech.kumamoto-u.ac.jp*

Abstract: In Japan, The livestock waste is changed to the compost actively because of the law about livestock wastes and its production increases rapidly in recent years. But now the compost have been excess of supply. Therefore a new method to use the compost is required. Combustion system consists of four main components: combustion furnace, burner, blower, and compost feeder. The burner is used for preheating. Composts fed by the compost feeder are transformed to the combustion furnace with the air. Composts are burned in the furnace. It are results that when the burner is started and composts put into the furnace, the temperature rises to over 600℃ smoothly. But after the burner is stopped, it falls rapidly and is not stability. From this, it can be said that it is necessary for stable combustion to more preheat.

Keywords*: compost, combustion, furnace,*

Introduction

In Japan, the law about livestock wastes have been enforced in 1999. The livestock waste is changed to the compost actively because of the law and its production increases rapidly in recent years. The compost had been used as a fertilizer. But now, chemical fertilizer have taken the place of it. Therefore the compost is left too much because the use of it is a little. So a new method to use the large compost is required quickly. The authors propose the method which a mixture of the compost and the air is burned in the Compost Furnace and the heat from it is used in various scenes.The purpose of this investigation is to observe the condition of stable combustion and found out the relationship with fed compost rate and stable combustion temperature.

Experiment method

Fig. 1 shows the Compost Combustion Furnace system. It consists of four main components: combustion furnace, burner, blower, and compost feeder. The burner is used for preheating. Composts fed by the compost feeder are transformed to the combustion furnace with the air from the blower. Composts are burned in the furnace. The combustion gas is discharged from the furnace chimney. The thermocouple measures the temperature in the furnace. The lacation of the thermocouple is top of the furnace, middle of the furnace, bottom of the furnace and the inside of the chimney. In this experimentation, the time of preheat is 30 min. Fed compost rate is changed variously (170 g/min, 240 g/min, 310 g/min, 380 g/min, 400 g/min, 550 g/min ,630 g/min, 740 g/min) 740 g/ min is maximum rate of Compost Feeder and 170 g/min is it's minimam rate. The temperature when the combustion is stable is found out in each situantion.

Results and Discussion

Table 1 shows condition of combustion and stable combustion temperature in each situation. Fig. 2 shows compost before combustion and Fig. 3 shows compost after stable combustion. Fig. 4 shows the relationship with the fed compost rate and stable combustion temperature. The

condition of combustion is stable in all situations. One of reasons of this fact is enough preheating. Fig. 2 and Fig.3 prove that the compost is completely burned. The stable temperature is between about 500 ℃ and about 700 ℃. The stable combustion temperature rise as the fed compost rate is increased. From this, it can be said that maximum rate of Feeder makes highest temperature combustion possible.

Conclusions

The following conclusions are deduced from the experimental results:

- The combustion is stable over full range of Compost Feeder's feed.
- The stable combustion temperature rise as the fed compost rate is increased.

References

[1] Ministry of Agriculture, Forestry and Fisheries of Japan, The law of livestock wastes, Website: http://www.maff.go.jp/j/chikusan/kankyo/taisaku/t_mondai/03_about/index.html

Table 1 Condition of combustion and temperature

Fed compost [g/min]	Condition of combustion	Temperature [℃]
170	stable	506
240	stable	485
310	stable	594
380	stable	534
400	stable	536
550	stable	594
630	stable	721
740	stable	720

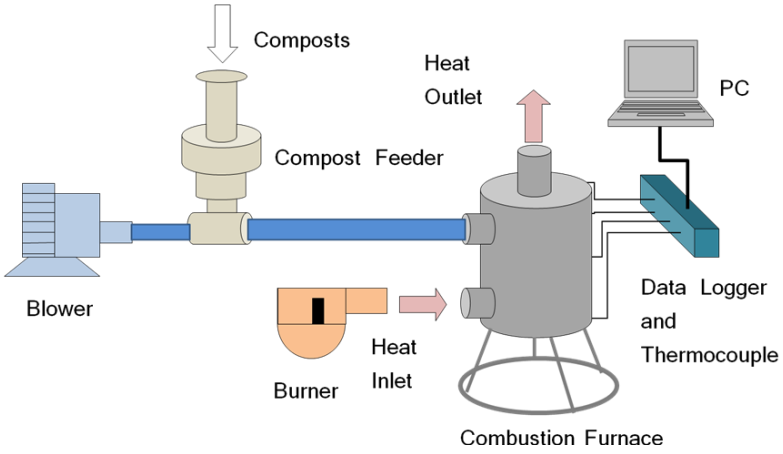


Fig. 1 Combustion system



Fig. 2 Compost (before combustion)



Fig. 3 Compost (after combustion)

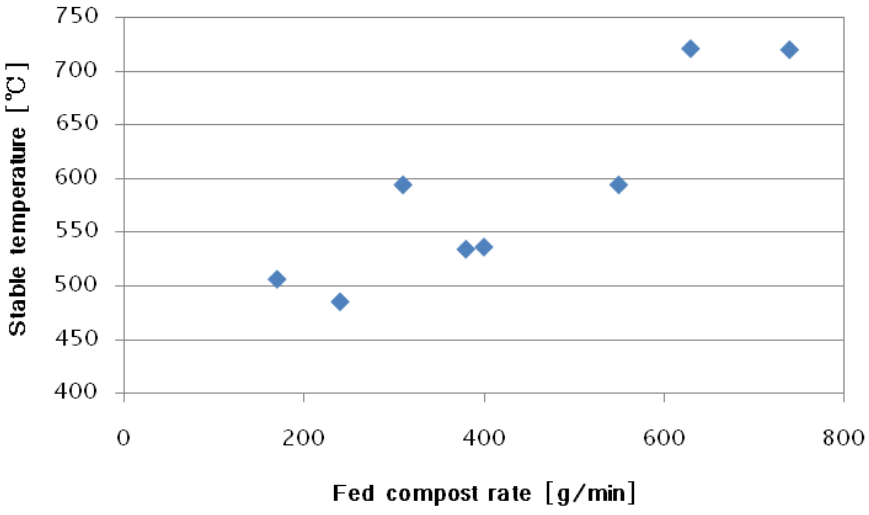


Fig. 4 The relationship with the fed compost rate and stable combustion temperature

2nd International Engineering Symposium - IES 2012
(KU-MU-NITK-HCMCUT Joint Symposium) March 5-7, 2012, Kumamoto University, Japan

Research on the energy utilization with bio oil

Kenichi Matsumoto [1] and Shuichi Torii [1]

1 Department of Mechanical System Engineering, Kumamoto University, Kurokami, 2-39-1, Kumamoto 860-8555, Japan. e-mail:058t2536@kumamoto-u.ac.jp

Abstract: In this paper, bio oil is focused. In recent years, global warming problems and energy problems are being discussed actively in environmental problems, and bio oil is considered that it can use in place of petroleum as fuel because bio oil is carbon neutral and renewable energy. But bio oil has some problems and it can not use for the mechanical devices directly as alternative fuel in place of kerosene or heavy oil. So I researched the conditions when we use bio oil as fuel for commercial firing equipment. It was found that (1) About 80℃ bio oil kinematic viscosity equal with normal temperature heavy oil, (2) Bio oil has high moisture content and we must heat quickly when we use bio oil, (3) Bio oil has possibility that can use with commercial burner. (4) It is necessary to high temperature to atomization the bio oil finely.

***Keywords**: Bio oil, Calorific value, Kinematic viscosity, Moisture content, Atomization,*

Introduction

In this paper, I studied the Bio oil. In recent years, global warming problems and energy problems are being discussed actively in environmental problems. As a means to solve this problem, we can use carbon neutral material as fuel. Carbon neutrality is the concept that when we produce something, the amount of carbon dioxide emissions equals the amount of carbon dioxide absorption and carbon neutral material is organic renewable resources. Bio oil is one of the carbon neutral material fuel and it is expected the practical application in place of exhaustible resource such as petroleum. Because it is liquid condition at normal temperature, so it is easy to carry. And it has high yield. Fig. 1 shows the bio oil. But bio oil has some problems and it can not use for the mechanical devices directly as alternative fuel in place of kerosene or heavy oil. For example, its calorific value is about half as much as crude oil, and it has high viscosity, and it is acidic at normal temperature. Because of such problems, constant burning is difficult when we use bio oil as fuel for commercial firing equipment. Therefore the purpose of this study is to examine the bio oil physical property values and to improve the commercial firing equipment in order to burn constantly with bio oil and to analyze the combustion system.

Experimental methods

I examined bio oil physical property values such as viscosity or moisture content before the burner improvement.

This research burning system is shown in Fig. 2. Explanations of main devices are below.

・Commercial firing equipment(Kato pilot burner, Model : GPN-8) : Normally this burner use gas oil and A-heavy oil and kerosene as fuel. This general purpose firing equipment burns fuel by bringing into the form of a spray. But bio oil has high viscosity and it set in the fuel hose and gear pump. Therefore bio oil can't bring into the form of a spray well. The viscosity can be reduced by heating the bio oil. So I measured the bio oil viscosity from 40℃ till 100℃. Ribbon heater is wound in burner piping in order to promote atomization

・ Furnace : There is a smokestack

behind the furnace and it exhaust the combustion gas.

- Thermocouple : Ten thermocouples are set in the furnace and those can measure the firing equipment flame temperature. The positions are shown in Fig. 3. Temperature is recorded on PC through Date Logger. In this way, we can know whether the flame is burning stably or not.

Results and discussions

Table 1 shows the bio oil physical property values that I measured. Because 40 ℃ bio oil kinematic viscosity is 168mm^2/s, and 10℃ A-heavy oil kinematic viscosity is 10mm^2/2, it was found that if the bio-oil heated above 80 ℃, it can dramatically reduce the kinematic viscosity, and it can be used as a fuel without clogging the gear pump. Also it was found that there is a need to shorten the heating time not to increase the kinematic viscosity with reduced moisture content.

Operation to lower the viscosity by heating the bio oil and hose pipe insulation, and heating the piping inside the burner, it was succeeded in about one minute burning. For longer combustion, it seems to need more bio oil atomization. The temperature of the heater way down by the operation of the burner, it needs raising the heater temperature more for atomization.

Conclusions

The following conclusions are deduced from this study:

- Bio oil has possibility that can use as fuel for commercial burner.
- Bio oil high viscosity can reduce by heating it and about 80℃ kinematic viscosity is close to normal oil.
- Bio oil has high moisture content and there is a need to shorten the heating time not to increase the kinematic viscosity.
- Bio oil has not high heat value and it is necessary to high temperature to atomization finely.



Fig. 1 Bio oil

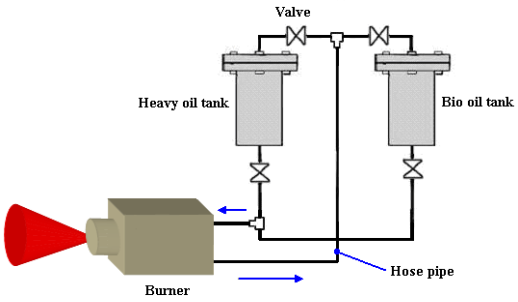


Fig. 2 Burning system

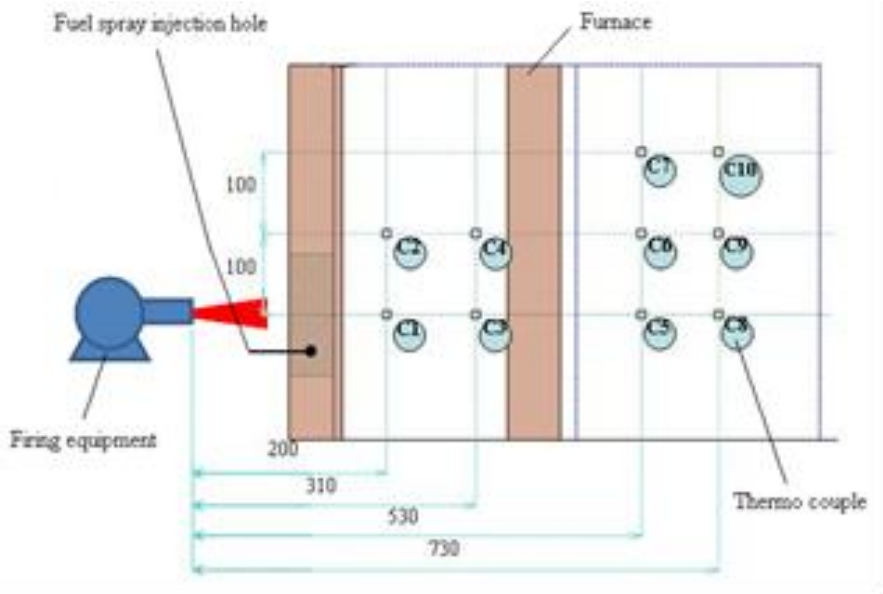


Fig. 3 Placement of each device [Unit : mm]

Table 1 Bio oil physical property values

Measurement item		Unit	Bio oil	
Heat value		J/g	17701	18008
Density	80℃	g/cm^3	1.2290	1.2282
	100℃		1.2212	1.2209
Viscosity	80℃	mPas	13.5	13.1
	100℃		7.44	7.00
Kinetic viscosity	80℃	mm^2/s	11.0	10.7
	100℃		5.73	5.70
Moisture content	20℃	%	38.35	39.85

CIVIL ENGINEERING, EARTH SCIENCES & RELATED FIELDS

2nd International Engineering Symposium - IES 2012
(KU-MU-NITK-HCMCUT Joint Symposium) March 5-7, 2012, Kumamoto University, Japan

Performance of High Strength Concrete subjected to Elevated Temperatures

Kishor S. Kulkarni, Subhash C. Yaragal and **K S Babu Narayan**

Department of Civil Engineering, National Institute of Technology Karnataka, Surathkal, Mangalore 575 025, India.
email: kishorsk1@rediffmail.com, *subhashyaragal@yahoo.com, shrilalisuta@gmail.com*

Abstract: High Performance Concrete (HPC) is a novel construction material with improved properties like higher strength, longer durability, and higher workability etc. than conventional concrete. The use of HPC has been used extensively throughout the world, predominately in the high rise buildings, bridges, oil, nuclear and power industries. With development in concrete and application of HPC, the understanding of its behavior when subjected to accidental fire is needed to ensure its serviceability. This study reports the residual compressive strength and sorptivity coefficient of HPC when subjected to elevated temperatures. The range of temperatures studied are 150 ^{0}C, 300 ^{0}C, 450 ^{0}C, 600 ^{0}C, 750 ^{0}C and 900 ^{0}C, with a retention period of 2 hours. After exposure to elevated temperatures their appearance, colour, and cracks were observed physically examined. Further, destructive tests were conducted to assess the residual compressive strength. The behavior of HPC at elevated temperature is presented in this paper.

***Keywords**:* High Performance Concrete, Elevated Temperatures, Residual Compressive Strength, Sorptivity coefficient.

Introduction

High Performance Concrete (HPC) has been used more widely in recent years for the construction of important concrete structures, tunnels, power industries, offshore structures and high rise buildings. Fire accidents, sabotages or natural hazards are the situations where HPC is likely to get exposed to elevated temperatures.

With development in materials and application of HPC, understanding of its behavior when subjected to fire is needed to guarantee its safe application. Although concrete is generally believed to be a bad conducting material, many recent past studied have shown extensive changes in microstructure of concrete leading to loss in strength, more so with high strength concrete (HSC).

Experimental study

The effect of elevated temperatures on compressive strength and sorptivity coefficient of HPC is reported in this Investigation. The materials used and their physical properties are discussed below.

Materials used:

Cement:
Ordinary Portland cement (OPC) conforming to IS 12269-1987. The specific gravity of cement was found to be 3.07.

Fine aggregate (FA):
Fine aggregate (sand) obtained from Local River source. The grading of fine aggregate conforms to Zone III of IS 383-1970. The specific gravity of sand was found to be 2.65 and fineness Modulus was 2.38. The water absorption was found to be 1.5 percent.

Coarse aggregate (CA):
The siliceous coarse aggregate of 12.5 and 20 mm size form local quarrying. The specific gravity was found to be 2.67 and fineness modulus of coarse aggregate was 7.15. The water absorption was found to be 0.5 percent.

Super-palsticizer:
Sulphonated napthalene polymer based high range water reducing admixture (HRWRA) 'CONPLAST 430' of FOSROC used. The specific gravity of HRWRA was 1.18. The optimum dosage was determined by marsh cone test method.

Preparation and testing of specimen:

M80 grade HPC was produced with pumpable workability. The mix proportion is as shown in table 1. The concrete mixing was done as per the ASTM C 192- 90 a (1994). Then concrete cubes of size 100 X 100 X 100 mm were cast and cured in water for 28 days. After 28 days of curing specimen were taken out, air dried, exposed to designated elevated temperatures and retained for 2 hours. The muffle furnace time temperature build up curve is as shown in Figure 1.

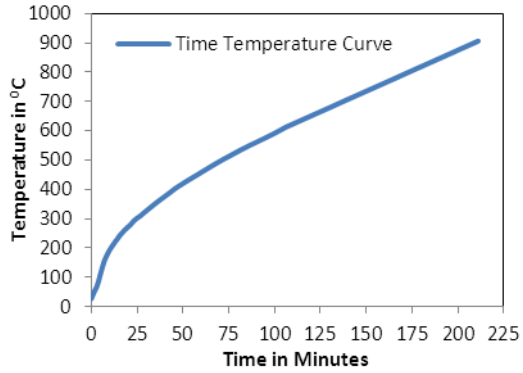


Fig. 1 Furnace time temperature build up curve.

After exposure to designated temperature the specimen were allowed to cool in the furnace to the room temperature. Then the physical observation was made, crack width measurement, difference in weight noted and one set of cubes tested for compressive strength, another set of tested for sorptivity.

The sorptivity test determines the rate of capillary –rise absorption by a concrete specimen. Measurement of capillary sorption were carried out using specimen pre-conditioned in the oven at 105 ^{0}C. Then specimens were cooled for room temperature, to achieve unidirectional flow the specimen's sides were coated with paraffin. The figure 2 shows the test set up made for the sorptivity.

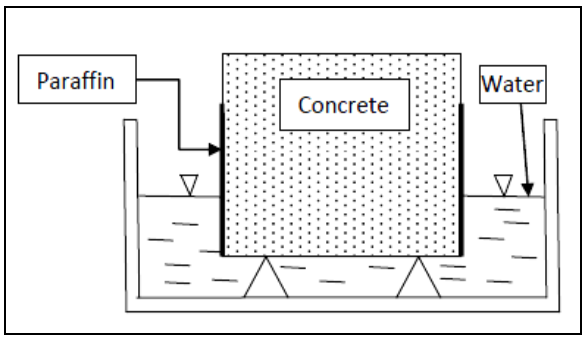


Fig. 2 Test set up for the sorptivity

At certain times the masses were measured using weighing balance, and then amount of weight observed was calculated and normalized with respect to cross-sectional area of specimen exposed to water at various times, such as 0, 5, 10, 20, 30, 60, 180, 360 and 1440 min. The rate of capillary rise absorption or sorptivity coefficient (k) was obtained by following equation,

$$\frac{Q}{A} = k\sqrt{t} \qquad (1)$$

Where,
Q - Amount of water absorbed (cm^3)
A - Cross- section of the specimen exposed to water surface (cm^2)
t - time (sec)

To determine the sorptivity coefficient, Q/A was plotted against the square root of time ($\sqrt{t}$), and then k was calculated from the slope of the linear relationship between Q/A and $\sqrt{t}$ (Demirel, B and Kelestemur, O, 2010)

Experimental results and discussion

Physical observations:
The variation in colour is observed with respect to temperature exposed. At 150^{0}C, the concrete colour doesn't change

noticeably. When temperatures is increased to 300 ^{0}C - 450 ^{0}C the colour changes from normal to pink or red, whitish grey around 600 ^{0}C -750 ^{0}C, and buff at 900 ^{0}C.

No visible cracks and spalling were found up to 450 ^{0}C, visible cracks were observed at 600 ^{0}C and these cracks were more pronounced (visible) in the case of specimens subjected to 750^{0}C and 900^{0}C. The crack width was measured by Direct Measurement Microscope (Elcometer 900, X50 magnification-MM). The maximum crack widths were found to be 0.3 mm, 0.4 mm for 600 ^{0}C, 900 ^{0} C exposed specimen respectively. The figure 3 shows the crack pattern at various temperatures. Above 750 ^{0}C the spalling was observed, corners were damaged and very sensitive to handle.

Loss in weight after exposure to elevated temperatures:

The weights of the specimen before and after exposure to elevated temperatures were taken for weight loss evaluation. As the temperature increases, continuous increase in weight loss is observed. Figure 4 shows variation of average percentage loss in weight with elevated temperatures. The total 6.36% weight loss observed at 900 ^{0}C temperature. From figure 5, it is observed that 58.41% of total weight loss occurs when exposed to 300^{0}C. The remaining 41.59% weight is lost gradually up to 900^{0}C.

Loss in strength after exposure to elevated temperatures

From figure 6, it is observed that at 300 ^{0}C the strength of specimen is increased by 3 %. This may be due to the high pressure stem curing (Autoclaving) effect (Neville, A, M, 1998). Then residual strength of concrete is decrease continuously with the increase in temperatures. At 450 ^{0}C, 600 ^{0}C, 750 ^{0}C and 900 ^{0}C respectively 23%, 46%, 60% and 80% of loss in compressive strength is observed.

Sorptivity test:

Figure 7 shows sorptivity coefficient of concrete cubes subjected to elevated temperatures. The sorptivity coefficient increases as the temperature increases. Up to 300 ^{0}C the coefficient is relatively same as unexposed specimens. Later the coefficient is observed to increase with increase in temperature, which means porosity of specimen increases. Figure 8 presents a plot between sorptivity coefficient and compressive strength of concrete. The regression analysis was carried out and best fit polynomial of second order proposed as below.

$$f_{ck} = 0.89 \times k^2 - 15.69 \times k + 84.28 \quad (2)$$

Where,
f_{ck}- *compressive strength of concrete*
k – sorptivity coefficient x 10^{-3} (cm/s$^{1/2}$)

Comparison of present work:

The figure 9 shows comparison of Normal Strength Concrete (NSC) and High Strength Concrete (HSC) at elevated temperatures. It has been observed that the behaviour of HSC is different from NSC in the temperature range of room temperature to 450 ^{0}C. Difference between the two is observed to is narrow down from 450 ^{0}C as reported by Cheng et al, (2004).

Conclusions

From this investigation the following conclusions were drawn:

- The weight loss is observed more up to 300 ^{0}C because of evaporation of free water, than due to degradation in the C-S-H gel.
- The critical degradation in strength is observed above 300 ^{0}C.
- Sorptivity coefficient is shown to give quantitative approach to determine the residual compressive strength at elevated temperatures.
- The behavior of HSC is different than the NSC at elevated temperatures.

References

[1] Aitcin, P.-C., (1998), High Performance Concrete, E&FN SPON, New York.
[2] ASTM Designation C192-90a, (1994), Standard Practice for Making and Curing Concrete test Specimens in the Laboratry.
[3] Cheng, F, P et al. (2004), Stress-Strain Curves for High Strength Concrete at Elevated Temperatures", Journal of Material Civil Engineering, Vol. 16, No. 1, pp. 84-90.
[4] Demirel, B, and Keleştemur, O, (2010), Effect of Elevated Temperature on the Mechanical Properties of Concrete Produced with Finely Ground Pumice and Silica Fume, Fire Safety Journal, Vol. 45, No. 6-8, pp. 385-391.
[5] Farhad, A, and Morteza, B, (2011), Constitutive Relationship for Normal and High- Strength Concrete at Elevated Temperatures, ACI Material Journal, Vol. 108, No. 4, pp. 355-364.
[6] IS 383-1970, Specifications for coarse and fine aggregates from natural sources for concrete, BIS, New Delhi.
[7] IS 12269 – 1987, Specifications for 53 Grade ordinary Portland cement, BIS, New Delhi.
[8] Neville, A M, (1995), Properties of Concrete, Pearson Education, South Asia.
[9] Yaragal, S, C et al. (2010), Studies on Normal Strength Cubes subjected to Elevated temperatures", Journal of Structural Fire Engineering, Vol. 1, No. 4, pp. 248-262.

Table 1 Details of design mix for one cubic meter of concrete

OPC (kg)	FA (kg)	CA (kg)		Water (kg)	Super-palsticizer (kg)	Mix proportion by weight
		12.5 mm	20 mm			C:FA:CA:w/c
500	546	642	642	130	10.62	1:1.09:2.57:0.26

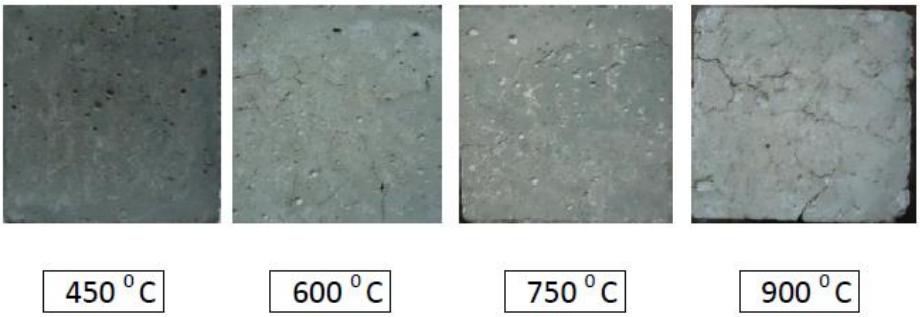


Fig. 3 Exposed concrete surface at different temperatures.

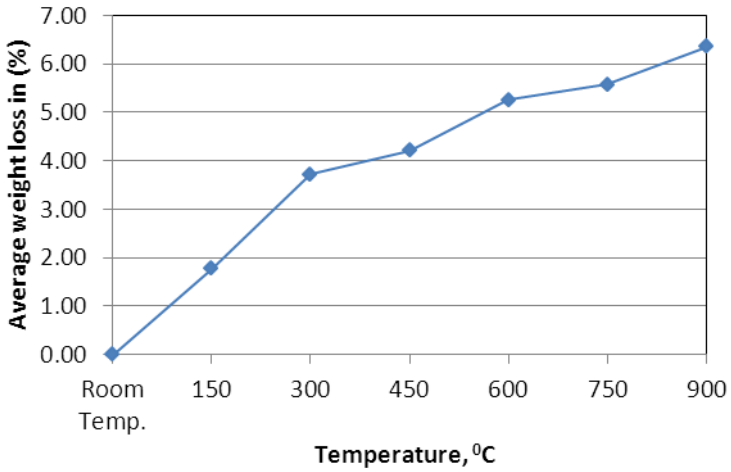


Fig. 4 Variation of percentage loss in weight with elevated temperatures

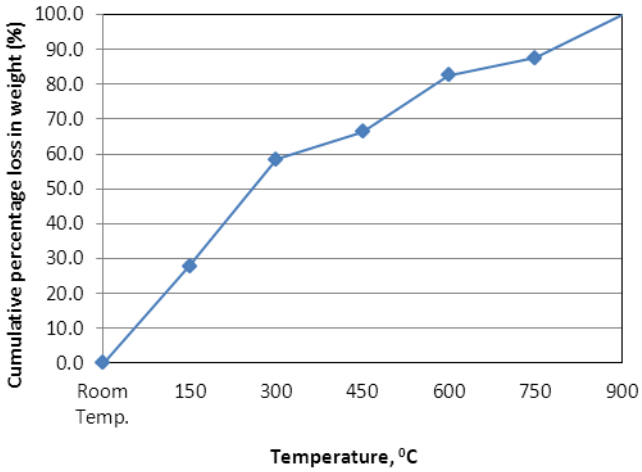


Fig. 5 Cumulative percentage loss in weight with elevated temperatures

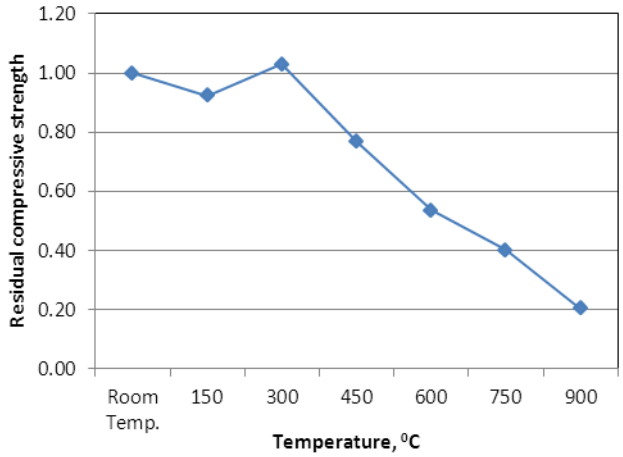


Fig. 6 Residual compressive strength of concrete cubes subjected to elevated temperatures.

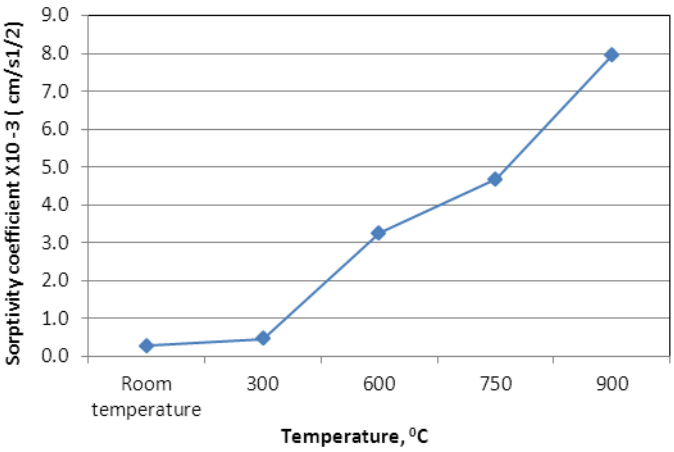


Fig. 7 Sorptivity coefficient of concrete cubes subjected to elevated temperature

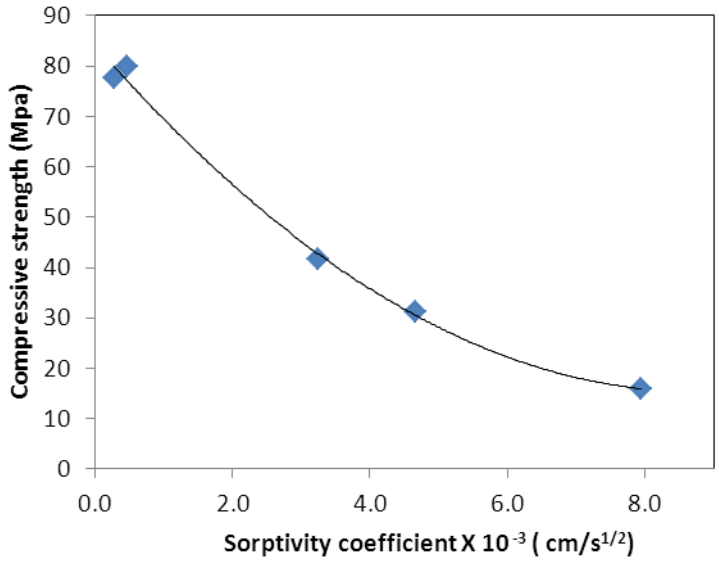


Fig. 8 Relation between Sorptivity coefficient and compressive strength of concrete

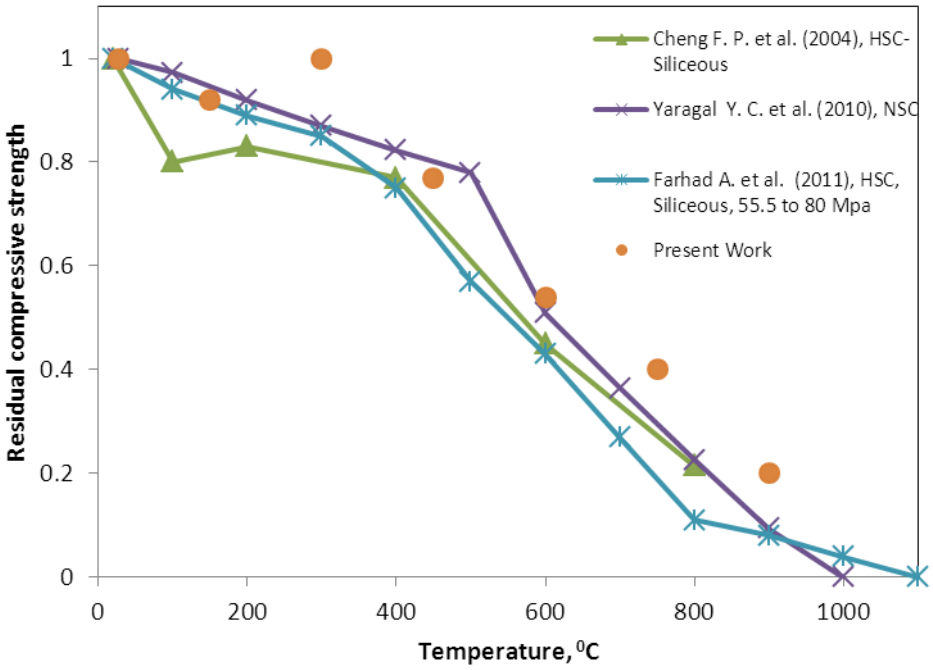


Fig.9 Comparison of present work with other researchers

2nd International Engineering Symposium - IES 2012
(KU-MU-NITK-HCMCUT Joint Symposium) March 5-7, 2012, Kumamoto University, Japan

Earthquake Vulnerability Assessment of Buildings in Guwahati

Ajit Kamath Manohar[1], Kaustav Sengupta[1], Tamizharasi G[1] and Indrani Gogoi [2]

1 *Department of Civil Engineering, National Institute of Technology Karnataka, Surathkal, Mangalore 575025, India.email:sengupta88@gmail.com*
2 *Department of Civil Engineering, Assam Engineering Institute, Guwahati, India. e-mail:gogoi.indrani@gmail.com*

Abstract: The high frequency of damaging earthquakes in India demonstrates the seismic vulnerability in India. This has jeopardized the existing building stock and necessitated its vulnerability assessment. Guwahati is a city in the north-eastern part of India which falls under the zone 5 of the earthquake zonation map of India according to IS 1893-2002. This paper presents a vulnerability assessment of various buildings in Guwahati, and indicates the degree of vulnerability of the buildings, and the measures that can be taken to prevent the potential damages.

Keywords*: Rapid Visual Screening, Vulnerability, Seismic Performance*

Introduction

Natural disasters like earthquakes, floods, tsunamis etc. are unpredictable and cause loss of human lives and properties. With an increasing population and rapid urbanization of major cities in India, vulnerability assessment of manmade structures like buildings, bridges and dams etc. has become necessary so that effective measures can be taken by the administrative bodies for disaster mitigation. Guwahati is a growing city in the north-eastern part of India, which falls under Zone 5 of the earthquake zonation map of India (IS 1893: 2002). The growing vulnerability emphasizes the need to incorporate earthquake resistant features in constructions practices. Earthquake vulnerability assessment can be carried out primarily in two steps – (i) a preliminary evaluation and (ii) a detailed evaluation. Rapid Visual Screening (RVS) is a method that can be adopted for preliminary investigation. In the paper, RVS has been performed on the various buildings in Guwahati, and performance score for each building has been calculated based on the parameters affecting the seismic behaviour.

Vulnerability Assessment Methodology

A. Rapid Visual Screening

The RVS method was originally developed by the Applied Technology Council (ATC) in the late 1980's and published in 1988 in the FEMA 154 report. It is a very quick way of assessing the building vulnerability based on visual screening, where a "sidewalk survey" is carried out by an experienced screener, who visually examines the building to identify features that affect the seismic performance of the building, such as the building type, seismicity, soil conditions and irregularities. This enables users to classify surveyed buildings into two categories: those acceptable as to "risk to life safety" or those that may be seismically hazardous and should be evaluated in more detail by a design professional, experienced in seismic design. Evaluation in this first level does not require any analysis. The visual survey of a building can be completed in less than 30 minutes and can be accomplished from the street without entering into a building. This survey is carried out based on the criteria proposed by Arya (2000) where the screening is done based on Seismic

intensity, Building types and damageability grades proposed by him.

B. Evaluation of Performance Scores

A performance score is calculated for each building based on numerical values on the RVS form corresponding to the features of the building (Srikanth et al. 2010). This performance score mainly depends on soil type, building condition, architectural and earthquake resistance features. The performance score indicates the seismic vulnerability of a building and may be further compared to a "cut-off" score to determine whether a building has potential vulnerabilities that should be evaluated further by an experienced engineer. The parameters used for evaluation of performance score are building height, frame action, pounding effect, structural irregularity, short columns, heavy overhang, soil conditions, falling hazard, apparent building quality, diaphragm action etc. Using the surveyed data, performance score or PS of the buildings has been calculated using the expression (Jain, 2010) as given below

$$PS = (BS) - \Sigma [(VSM) \times (VS)] \quad (1)$$

Where VSM represents the Vulnerability Score modifiers and VS represents the Vulnerability Score that is multiplied with VSM to obtain the actual modifier to be applied to the BS or Basic Score. The vulnerability scores that are dependent on various features such as presence of basement, number of storeys, apparent quality, asymmetric location of staircase, (with respect to plan), re-entrant corners, open storeys, substantial overhangs and short columns. A RVS format as shown in Fig. 3 can be used by Screeners for assessment at site. Vulnerability Scores (VS) and Vulnerability Score Modifiers can be assigned as shown in the format given in Table 3 and 4 (Jain, 2010 and Srikanth et al. 2010) for RCC and masonry buildings respectively.

C. Observations

The buildings in Guwahati are predominantly masonry as well as RCC, with a small percentage of wooden buildings. Since the number of wooden buildings were less their results were not compared with other buildings. But most of the wooden buildings need detailed investigations. Fig.1 shows the percentages of different kinds of buildings surveyed in that particular region. The percentage of buildings falling beyond cut-off scores for RCC and Masonry type buildings for different base scores are shown in Fig.2.

D. Discussions

The performance scores of the buildings were calculated and based on some of the minimum requirements cut-off scores is also calculated. The buildings that falls below cut-off scores needs further assessment for both RCC and masonry kind of buildings. But almost all the masonry buildings in that particular region require further assessment for assessing its vulnerability.

E. Theory of Cut-off Scores

Any structure built is expected to satisfy the requirements of safety. The least requirement that any structure should satisfy is that collapse should be prevented during the event of the most severe earthquake that can occur during the life of the structure, that is, Maximum Considered Earthquake according to IS 1983 – 2002. Cut – off score for a structure can be looked upon as a rating which indicates the minimum requirements of the structure. Failures of structures during past earthquakes have taught us a lot of lessons, regarding the necessity of the earthquake resistant requirements of buildings.

From these observations, the minimum requirements can be arrived upon:

1. RCC buildings:
   - Simple plan (as much symmetrical as possible).
   - No load discontinuities (soft storeys should be avoided).
   - Good quality of construction and strict adherence to the detailing requirements.
2. Masonry buildings:
   - Simple plan (as much symmetrical as possible).
   - Tying up of the walls.
   - Presence of a horizontal tied band all around the walls.

Therefore, to find the cut – off scores, the following minimum requirements are assumed to be present in a structure. The cut – off scores can be summarized as follows:

Table 1 Cut-off score for RCC structures

No. of storeys	Base Score	Cut – Off Score
1 or 2	100	83
3	90	57
4	75	39
5	65	22
>5	60	17

Table 2 Cut – Off Scores for Masonry structures

No. of Storeys	Base Score	Cut – Off Score
1 or 2	100	73
3	85	47
4	70	27
5	50	5

Conclusions

The following conclusions are deduced from this study:

- A Rapid Screening Methodology is described in the paper using a RVS format which can be effectively used by screeners for a rapid assessment of seismic vulnerability of a building.
- A format for Performance score evaluation is presented for RCC and masonry type buildings.
- As the codal provisions become more stringent with every revision, these structures may not meet the demands in the years to come.
- Guwahati being in highly seismic zone and due to frequent occurrence of earthquakes, the construction practices are generally seismic resistant.
- Some of the buildings considered in the present study are old and in need of repair, retrofitting and restoration to comply with the service requirements of the revised code.

Acknowledgement

Prof. Jayanta Pathak of Assam Engineering College, Guwahati, Assam, India is acknowledged for funding the rapid visual screening under research funded by Directorate of Science & Technology (DST) *Sanction no. DST/23(437)/SU/2004.* The students of Assam Engineering Institute who had laboriously carried out the RVS are acknowledged.

References

[1] Arya, A.S. (2000). Rapid Visual Screening of masonry buildings (All Seismic Zones). Disaster Risk Management – Document Series http://www.ndmindia.nic.in

[2] Arya, A.S. (2000). Rapid Visual Screening of RCC Buildings. Disaster Risk Management – Document Series. http://www.ndmindia.nic.in

[3] IS 1893: Part 1: 2002 (2007). Criteria for Earthquake Resistant Design of Structures - Part 1: General Provisions and Buildings, Bureau of Indian Standards, New Delhi.

[4] IS 13828: 1993 (2008), Improving earthquake resistance of low strength masonry buildings – Guidelines, Bureau of Indian Standards, New Delhi.

[5] IS 4326: 1993 (2008) Code of practice for earthquake resistant design and construction of buildings, Bureau of Indian Standards, New Delhi.

[6] SP 6: Part 6: 1972 (2001). Handbook for structural engineers - Application of plastic theory in design of steel structures.

[7] IS 13920: 1993 (2008), Ductile detailing of reinforced concrete structures subjected to seismic forces - Code of practice, Bureau of Indian Standards, New Delhi.

[8] Srikanth T., Kumar R. P., Singh, A. P., Rastogi, B. and Kumar, S. (2010) "Earthquake Vulnerability Assessment of Existing Buildings in Gandhidham and Adipur Cities Kachchh, Gujarat (India)", European Journal of Scientific Research , Vol.41 No.3, pp.336-353, ISSN 1450-216X, http://www.eurojournals.com/ejsr.htm

[9] Jain, S.K. (2010), Seismic Assessment & Retrofitting of RC Frame Buildings, Rebuild, Vol. 4, 1, pp. 6-8.

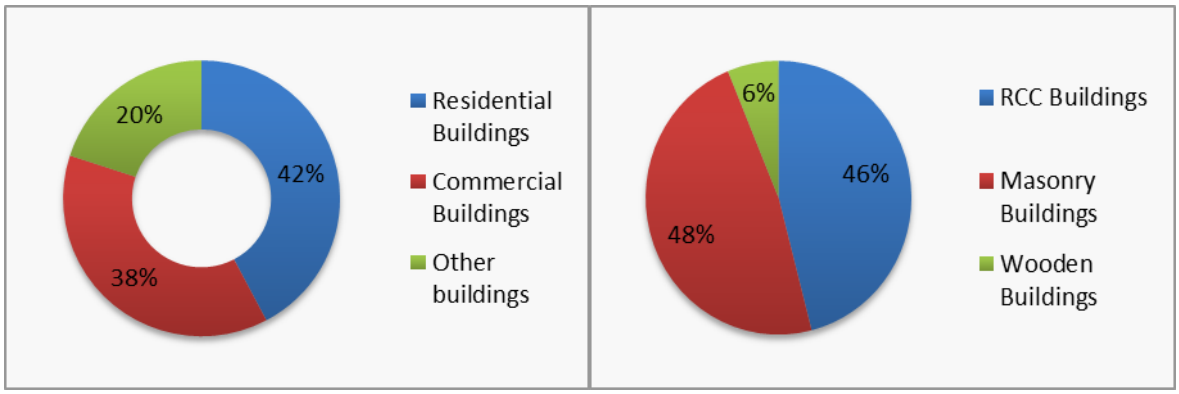


Fig.1 Percentage of buildings surveyed

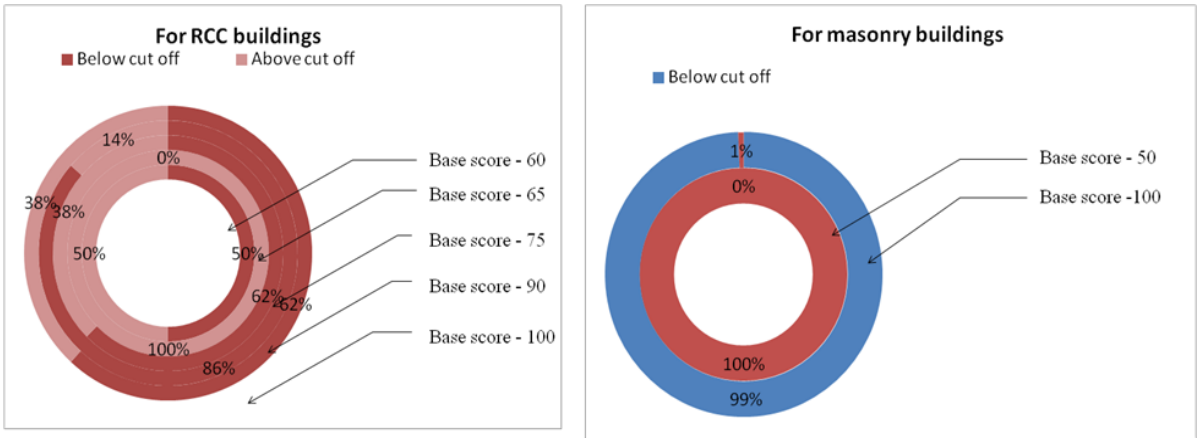


Fig.2 Percentage of buildings falling beyond Cut – off score

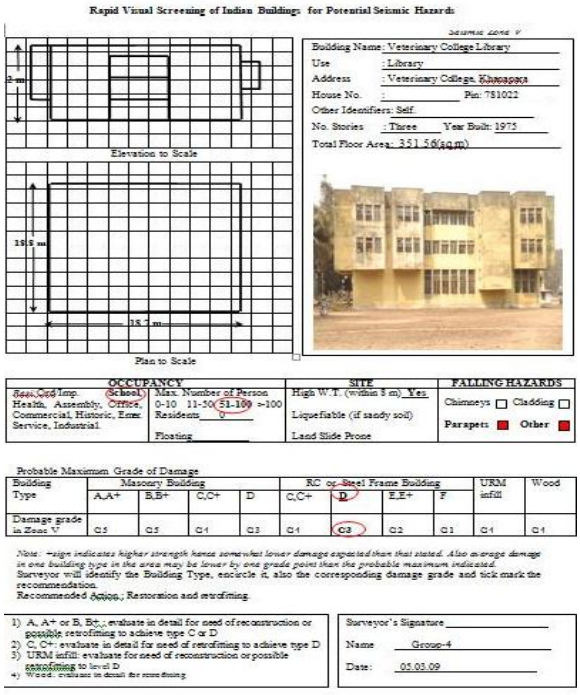


Fig.3 An example of Rapid Visual Screening done in the city of Guwahati

Table 3 Performa for Evaluation of Performance Score for RCC Buildings

RAPID VISUAL SCREENING OF EARTHQUAKE SAFETY						CALCULATION SHEET RC FRAME	
Falling hazards identifier 'F'		Stories				Seismic Zone V	Base Score
Marquees/hoardings/roof signs		1 or 2				100	
AC units/grillwork		3				90	
Elaborate parapets		4				75	
Heavy elevation features		5				65	
Heavy canopies		>5				60	
Substantial balconies							
Heavy cladding							
Structural glazing							
Vulnerability Score (VS)						Vulnerability Score Modifier (VSM)	VS×VSM
NUMBER OF STOREYS	1or2						
Soft storey	0	-15	-20	-25	-30	Absent =0 Present=1	
Vertical irregularities, setbacks, building on slopes	-10	-10	-10	-10	-10	Absent =0 Present=1	
Plan irregularities	-5	-5	-5	-5	-5	None=0 Moderate=1 Extreme=2	
Heavy overhangs	-5	-10	-10	-15	-15	Absent =0 Present=1	
Apparent quality	-5	-10	-10	-15	-15	Good=0 Moderate=1 Poor=2	
Short columns	-2	-5	-5	-5	-5	Absent = 0 Present=1	
Poundings	0	-2	-3	-3	-3	Absent = 0 Unaligned floors= 2 Poor apparent quality of adjacent building = 2	
Soil conditions	10	10	10	10	10	Medium = 0 Hard =1 Soft = -1	
Frame action	10	10	10	10	10	Absent = 0 Present =1 Not sure = 0	
Water tank at roof capacity	0	-3	-4	-5	-5	Absent = 0 Capacity < 5000l= 0.5 Capacity > 5000l=1	
Location of water tank	0	-3	-4	-5	-5	symmetric=0 unsymmetrical=1	
Basement-full or partial	0	3	4	5	5	Absent = 0 Present =1	
						∑ (VSMXVS) =	
Performance Score = Base Score - ∑ (VSMXVS) =							

Table 4 Performa for Evaluation of Performance Score for Masonry Buildings

Falling hazards identifier 'F'		Stories			Seismic Zone V	Base Score
Marquees/hoardings/roof signs		1 or 2			100	
AC units/grillwork		3			85	
Elaborate parapets		4			70	
Heavy elevation features		5			50	
Heavy canopies						
Substantial balconies						
Heavy cladding						
Structural glazing						
Vulnerability Score (VS)					Vulnerability Score Modifier (VSM)	VS×VSM
Number of Storeys	1 or 2					
Structural irregularity	-10	-10	-10	-10	Absent =0 present=1	
Apparent quality	-10	-10	-10	-10	Good=0 Moderate=1 Poor=2	
Soil conditions	10	10	10	10	Medium = 0 Hard =1 Soft = -1	
Poundings	0	-3	-5	-5	Absent = 0 Normal apparent condition of adjacent building=1 Poor apparent condition of adjacent building=2	
	Openings					
Wall openings	-5	-5	-5	-5	Small(< 1/3)=0 Moderate(1/3to2/3)=1 Large(> 2/3)=2	
Orientation of openings	-2	-5	-5	-5	Regular = 0 Irregular=1	
Diaphragm action	-10	-15	-15	-15	Present/unsure=0 Lack of diaphragm action=1	
Basement-full or partial	0	3	4	5	Absent = 0 Present =1	
	Other features					
Horizontal bands	20	20	20	20	Absent =0 present=1	
Arches	-10	-10	-10	-10	Doesn't exist/unsure=0	
Random rubble stone masonry walls					Remedial measures exist=0 Don't exist=1	
Water tank at roof capacity					Absent = 0 Capacity<5000L= 0.5 Capacity>5000L=1	
Location of water tank					Symmetric=0 Unsymmetrical=1	
Basement-full or partial					Absent = 0 Present =1	
		∑ (VSMXVS) =				
Performance Score = Base Score - ∑ (VSMXVS) =						

2nd International Engineering Symposium - IES 2012
(KU-MU-NITK-HCMCUT Joint Symposium) March 5-7, 2012, Kumamoto University, Japan

Magnetorheological Dampers – An overview

Tamizharasi G [1] Ajit Kamath Manohar [1] Kaustav Sengupta [1]
Katta Venkataramana [1] and Umesh G [2]

1 *Department of Civil Engineering, National Institute of Technology Karnataka, Surathkal, Mangalore 575025, India. e-mail : k_ajit90@yahoo.co.in*
2 *Department of Physics, National Institute of Technology Karnataka, Surathkal, Mangalore 575025, India.*

Abstract: Disasters such as earthquakes, cyclones, floods and other similar phenomena cause large-scale damage to lives and environment. The most remarkable challenge in civil engineering is to protect the structures from these hazards and a lot of research is being carried out world-wide in this field. This paper discusses a semi-active control device which can operate under very low power requirement. Magnetorheological (MR) damper is one of the new technologies designed using MR fluids to produce controllable dampers to serve this purpose. Specially, MR fluid technologies are reliable, inexpensive, and relatively insensitive to temperature fluctuations. This type of damper has high dynamic range, low power requirements, large force capacity and robustness. In this paper, behaviour of MR fluid and its application in making MR damper have been discussed.

Keywords: *Magnetorheological (MR) dampers, MR fluid, Semi-active control device.*

Introduction

Evaluation of new construction technologies are in need of the hour for protecting civil engineering structures from natural disasters such as earthquakes and severe winds. During these natural disasters, structures will be subjected to huge lateral forces causing severe vibrations. These vibrations can be controlled by providing some energy dissipating devices which can modify the structural characteristics such as its rigidity, mass, damping or vibration mode shape and by the use of passive or active control forces. Passive control systems do not require any external energy source to power them, but, they are unsuitable to adapt to structural changes or varying usage patterns. Shear walls or braces may be looked upon as examples. Active control systems use an external power source that controls the actuators that apply load to the structure in a prescribed manner. But, active control systems have the inherent problems of instability. Therefore, an intermediate form of a control system like semi–active control system that combines the properties of both passive and active control systems is being looked upon as a better alternative. It would require a low power source as well as the properties of a stable damping device. The MR Damper is one such semi–active control system that is being recommended to dissipate structural vibrations.

A MR Damper or MR shock absorber is a damper filled with MR fluid, a smart material, which is controlled by a magnetic field, usually using an electromagnet. This allows the damping characteristics of the shock absorber to be continuously controlled by varying the power of the electromagnet. The initial discovery and development of MR fluids can be credited to Jacob Rabinow at the US National Bureau of Standards in the late 1940s.

MR Fluid

MR fluid is a kind of smart material which contains suspended liquid that is made of magnetic particle and carrier fluids. Its

rheological characteristic will vary in the presence of magnetic field. When subjected to a magnetic field, the fluid greatly increases its apparent viscosity, to the point of becoming a viscoelastic solid. Importantly, the yield stress of the fluid when in its active state can be controlled very accurately by varying the magnetic field intensity. In the absence of magnetic field, MR fluid is a liquid having characteristic similar to that of carrier fluid. But if the applied magnetic field is strengthened, its rheological characteristic has rapid change. Within few milliseconds, it exhibits the properties similar to solid. Response times of 6.5ms have been recorded (Kciuk and Turczyn, 2006).

This transform property from liquid to solid makes MR fluid to have tremendous applications in the industry. Usually MR fluid is applied in vibration isolator, damper, clutch and aerospace material.

MR Fluid Components

The three major components of MR Fluid are: Basic fluid or carrier fluid, metal particles and stabilizing additives.

The ***base fluid*** acts as the function of the carrier in which the magnetic particles are suspended. MR fluids behave similar to base fluid in accordance with their chemical composition. The common carrier fluids used for making the MR fluid are hydrocarbon oils, mineral oils or silicon oils. The criterion for selection depends upon the working temperature range of the oils, and is also influenced by the settling characteristics in the oils. The viscosity of carrier fluid depends on the concentration of metal particles suspended in it. The viscosity will be high even in the off-state because of the presence of metal particle. Silicone oil can be used as a carrier fluid because of its greater viscosity at low shear rate, high temperature range of about -50 to 200°C, lower settling rate with higher viscosity (Jolly, 1998).

The ***metal particles*** form a chain-like structure under the influence of magnetic field as shown in Fig.1. This change in rheological behaviour by forming the chain-like structure offers resistance to the flow of fluid which is called MR effect. Mostly the metal particles are made of carbonyl iron, or powder iron, or iron/cobalt alloys to achieve a high magnetic saturation. The amount of metal powder in MR fluid can be from 20 to 40% by volume (Dyke et al. 1997). The particle size may be around μ-meter range, typically from 3 to 5 microns. The viscosity of MR fluid in off-state will be higher if the size and quantity of the particles are large. Since the ultimate strength of the MR fluid depends on the saturation magnetization of the suspended particles, the selected particles should have large saturation magnetization.

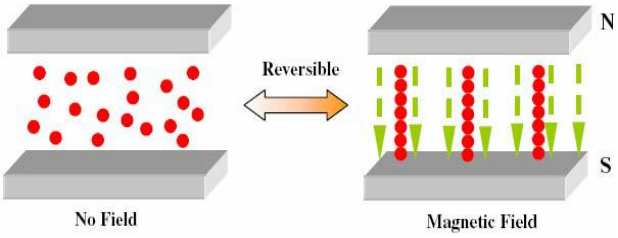


Fig.1 Mechanism of MR Fluid
(Chen and Tian, 2006)

Carbonyl iron powder can be used because of its low coercivity and high saturation magnetization (2.1Tesla, at room temperature) that can develop yield stresses of about 100 kPa (Olabi and Grunwald, 2007; Muhammad et al. 2006). Carbonyl iron particles are obtained by thermal decomposition of iron pentacarbonyl ($Fe(CO)_5$). Since it is preferred to have non-abrasive particles in MR fluid based devices, spherical and highly pure carbonyl iron particles can be used as a dispersion phase in MR fluids. Iron–cobalt alloys have a higher saturation magnetization, but, it has a higher bulk density of 8.1 g/cc, which will reduce the cohesive properties of the MR fluid. Ceramic iron alloys have a low saturation magnetization of 0.4 – 0.6 Tesla.

The ***stabilizing additives*** are suspending agents that discourage gravitational settling and promote particle suspension, enhance lubricity, modify viscosity, and inhibit wear. In carriers like silicone oil, the use of lecithin, Oleic Acid acts as a well

dispersed suspending agent (Lopez-Lopez et al. 2008).

All three components define the magneto-rheological behaviour of the MR fluid. The total density of the fluid may be around 3–4 g/cc. The change of any one of the MR component may cause the changes in rheological behaviour.

Rheological Properties of MR Fluids

MR fluids are the suspensions of micron sized magnetized particles suspended in carrier fluid. The carrier fluid acts as a dispersed medium that ensures the homogeneity of particles in the fluid. In order to prevent the gravitational settling and to promote the stable particle suspension additives (stabilizers and surfactants) are used (Kciuk and Turczyn, 2006). Table 1 shows the properties of MR fluid.

Table 1 Properties of MR Fluid (Kciuk and Turczyn, 2006; Carlson 1995)

Property	Typical value
Initial Viscosity	0.2 – 0.3 Pa.s (at 25° C)
Density	3 – 4 g/cm^3
Magnetic field strength	150 – 250 kA/m
Yield point τ_0	50 – 100 kPa
Reaction time	Few milliseconds
Typical supply voltage and current intensity	2 – 25 V, 1 – 2 A
Work temperature	-40 to 150 ° C

Behaviour of MR Fluid: In the absence of magnetic field, MR fluid behaves like a Newtonian fluid. But as soon as the field is applied, the MR fluid shows the characteristics of Bingham fluids. It has been recognised that the Bingham model can be used in describing the rheological features of an MR fluid (Jolly et al, 1998; Olabi and Grunwald, 2007).

A **Bingham plastic** is a non-Newtonian fluid whose yield stress must be exceeded before flow can begin i.e., at zero shear rate there is some resistance to flow. The condition, at which the maximum stress can be applied without causing continuous movement, is the yield stress and this is a function of the magnetic field strength. Then total yield stress is given by (Kciuk and Turczyn, 2006; Olabi and Grunwald, 2007; Yan et al. 2007):

$$\tau = \tau_0 (H) + \eta \Upsilon \qquad (1)$$

Where

τ_0 – yield stress caused by applied magnetic field, (Pa)
H – magnetic field strength (A/m)
Υ – shear rate (s^{-1})
H – plastic viscosity (Pa.s)

Fig.2 shows the typical relationship between shear stress and shear rate for a Bingham fluid and compared with a Newtonian fluid.

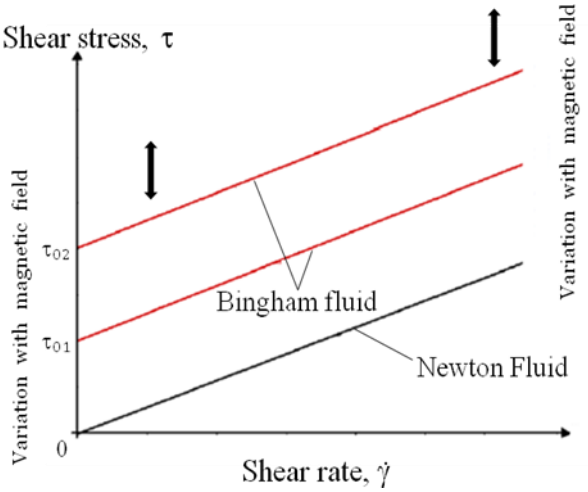


Fig.2 Shear stress versus shear rate for Newton and Bingham model of MR Fluid (Olabi and Grunwald, 2007).

Herschel-Bulkley model can be used as an alternative to Bingham plastic model which accounts for the post-yield shear thinning behaviour of MR fluids, as shown in Fig.3.

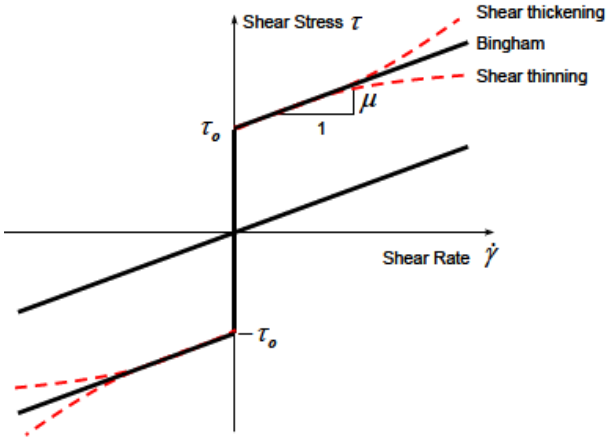


Fig.3 Visco-plastic models often used to describe MR fluids (Goncalves, 2005)

The Herschel-Bulkley model can be expressed as (Goncalves, 2005; Wang and Liao, 2011; Resiga et al, 2007)

$$\tau = \pm \tau_0 + K|\Upsilon|^{\frac{1}{m}} \quad (2)$$

Where, *K* and *m* are fluid parameters. For $m > 1$ equation (2) represents a shear thinning fluid while shear thickening fluids are described by $m < 1$. It can be noted that for $m = 1$, the Herschel-Bulkley model reduces to the Bingham plastic model.

Sensitivity to temperature: MR fluid is stable over broad range of temperature with only slight variations in yield stress in the range of -40 to 150 degree Celsius (Carlson, 1995; Wang and Liao, 2011; Kciuk and Turczyn, 2006). The value of yield stress reduces slightly due to the slight change in the volume fraction that can be neglected since it is very small.

Comparison with ER and Ferro fluids: MR materials are more advantageous than ER materials, because the change in rheological behaviour is very larger and MR materials are about 20 to 50 times stronger. MR materials are less sensitive to moisture and contaminants and hence they can be used in any contaminated environment. In addition, they are unaffected by the surface chemistry of surfactants, require only less power (50W) and voltage (12-24V) for MR material activation than ER materials (Kciuk and Turczyn, 2006).

The main difference between MR fluids and ferrofluids are the size, the quantity and the quality of the iron particles (Olabi and Grunwald, 2007). The variation of properties of both the fluids is given in Table 2.

Table 2 MR fluid versus Ferrofluid (Olabi and Grunwald, 2007)

Representative feature	MR Fluid	Ferrofluid
Energy factor	>1	<1
Maximum yield stress	100 kPa	10 kPa
Particle size	Some μm	Some nm
Particle material	Carbonyl iron	Iron oxide
Fraction by volume	20 to 40%	Up to 10%
Stability	Medium	Good
Functionality	Controllable shear stress	Controllable liquid flow

Operational Modes of MR Fluids

An MR fluid can be used in any one of three main modes of operation: Flow mode, direct shear mode, squeeze flow mode (Poynor, 2001; Goncalves, 2005; Wang and Liao, 2011). The flow mode, direct shear mode and its combination can be used to develop all kinds of linear and rotary MR dampers while the squeeze flow mode is only used to develop linear MR dampers with limited amplitudes.

Flow mode (Fig.4a) can be used in dampers and shock absorbers, by using the movement to be controlled to force the fluid through channels, across which a magnetic field (H) is applied. ***Shear mode*** (Fig.4b) is particularly useful in clutches and brakes, in places where rotational motion must be controlled. ***Squeeze-flow mode*** (Fig.4c), on the other hand, is most suitable for the applications of small, millimeter order movements but involving large forces. From these three modes, flow

mode can be used to make the MR Damper (Wang and Liao, 2011).

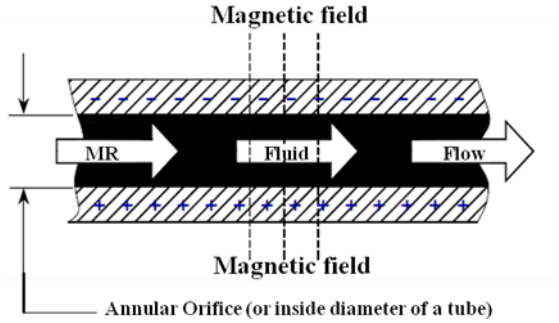


Fig.4a Flow mode, (Poynor, 2001)

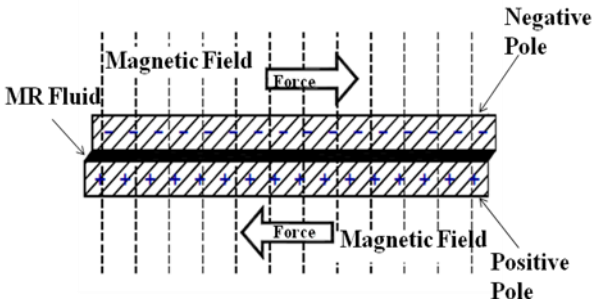


Fig.4b Direct shear mode, (Poynor, 2001)

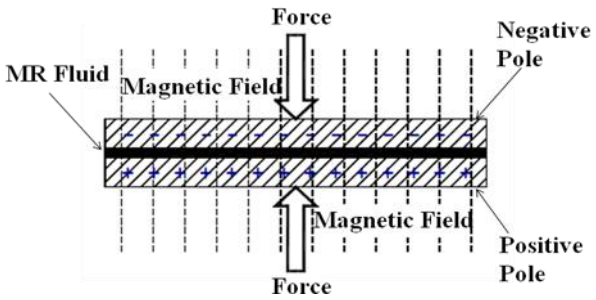


Fig.4c Squeeze film mode, (Poynor, 2001)

MR Damper

MR Damper is a device in which damping is given by means of shear stress of MR fluid. It has the property that the damping character changes as soon as it comes in contact with the external magnetic field. It acts as a semi-active control device that has the capability of generating greater magnitude of forces for large-scale applications with lower power requirement. Interestingly, MR damper offers highly reliable operation with their performance of being insensitive to temperature and impurities (Wang and Liao, 2011; Carlson, 1995).

Operational Principle

The operational principle of the cylindrical MR damper is shown in Fig 5. The MR fluid is filled in the gap between the fixed outer cylinder and inner cylinder which can move with a velocity of *v*. In the absence of magnetic field, MR fluid cannot restrict the relative motion between the fixed outer and inner cylinder. However, when the electric current passes through the solenoidal coil, the magnetic flux path is formed and the particle will gets aligned to form a chain-like structure in the direction of the magnetic field. These chain-like structures restrict the motion of the MR fluid, thereby increasing the shear stress of the fluid.

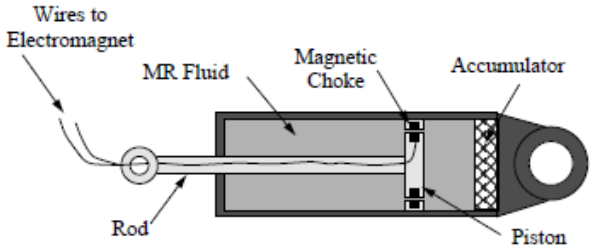


Fig.5 Operational Principle of MR Damper (Yan et al, 2007; Dyke et al, 1996)

The damping can be achieved by utilizing the shear force of MR fluid. The damping values can be adjusted continuously by changing the external magnetic field strength (Yan et al, 2007, Dyke et al, 1996).

Types of MR Damper

There are three types of MR dampers such as the mono tube, the twin tube, and the double-ended MR damper (Poyner, 2001; Ashfak et al. 2009). Initially, Mono tube MR damper (Fig.6) is the most common type of damper that can be in any orientation and compact in size. It has only one reservoir for MR fluid and an accumulator mechanism to accommodate the change in volume due to piston rod movement. Secondly, Twin tube MR damper (Fig.7) is the one that has two fluid reservoirs, one inside the other. The inner reservoir guides the piston rod whereas the outer reservoir accommodates the changes in the volume due to the piston rod movement. A foot valve is provided at the bottom of the inner reservoir in order to regulate the

flow of fluid between the two reservoirs. Finally, double-ended damper (Fig.8) which has a piston rod of equal diameter protrudes from both ends of the damper housing. An accumulator mechanism is not required since there will be no change in volume as the piston rod moves relative to the damper body.

Conclusions

This paper has discussed the design of MR damper using MR fluid. MR fluid has the characteristics of becoming solid under the application of magnetic field. These characteristics pave the way for making the MR damper. This kind of damper plays an important role in reducing the structural vibrations.

References

[1] Ashfak A et al. (2009), "Design, Fabrication and Evaluation of MR Damper", University of Kerala, India. World Academy of Science, Engineering and Technology 53 2009. pp 358-363.
[2] Carlson J.D et al. (1995), "Commercial Magnetorheological Fluid Devices", Lord Corporation, Cary, USA. 5th Int. Conf. on Electro-Rheological, Magneto-Rheological Suspensions and Associated Technology Sheffield, 10-14 July 1995.
[3] Chen L and Tian J, (2006), "Distributed Magnetorheological (MR) Fluid Damper for Active Structural Vibration Control", Adelaide University, Australia.
[4] Dyke S.J. et al. (1996), "Modelling and Control of Magnetorheological Dampers for Seismic Response Reduction", Dept. of Civil Engg, Washington University.
[5] Dyke S.J. et al. (1997), "On the Efficacy of Magnetorheological Dampers for Seismic Response Reduction", ASME Design Engineering Technical Conferences, California. DETC97VIB3828.
[6] Goncalves F.D. (2005), "Characterizing the Behaviour of Magnetorheological Fluids at High Velocities and High Shear Rates", Virginia Polytechnic Institute, Virginia.
[7] Jolly M R. et al. (1998), "Properties and Applications of Commercial Magnetorheological Fluids", Thomas Lord Research Centre, Cary.
[8] Kciuk M. and Turczyn R. (2006), "Properties and Application of Magnetorheological fluids", Poland. Journal of Achievements in Materials and Manufacturing Engineering, Vol.18. Issue 1-2. pp. 127-130.
[9] Lopez-Lopez M T. et al. (2008), "Preparation of well-dispersed magnetorheological fluids and effect of dispersion on their magnetorheological properties". *www.springerlink.com/index/vp2266243u4850pw.pdf* . pp.787-796.
[10] Muhammad A. et al. (2006), "Review of magnetorheological (MR) fluids and its applications in vibration control", College of Shipbuilding Engineering, China. Journal of Marine Science and Application, Vol.5.No.3. pp. 17-29.
[11] Olabi A.G. and Grunwald A. (2007), "Design and application of magneto-rheological fluid", Dublin City University, Ireland. Materials and Design 28 (2007), pp. 2658–2664.
[12] Poynor J.C., (2001), "Innovative Designs for Magneto-Rheological Dampers", Virginia Polytechnic Institute, Virginia.
[13] Resiga D.S et al. (2007), "A Rheological Model for Magneto-Rheological Fluids", 3rd German-Romanian Workshop on Turbomachinery Hydrodynamics. pp141- 158.
[14] Wang D.H. and Liao W.H., (2011), "Magnetorheological fluid dampers: a review of parametric modelling", Smart Mater. Struct. 20 (2011) 023001. pp 1-34.
[15] Yan Y et al. (2007), "Analysis of magnetorheological fluid damper", Chongqing Institute of Technology, China. pp 263-265.

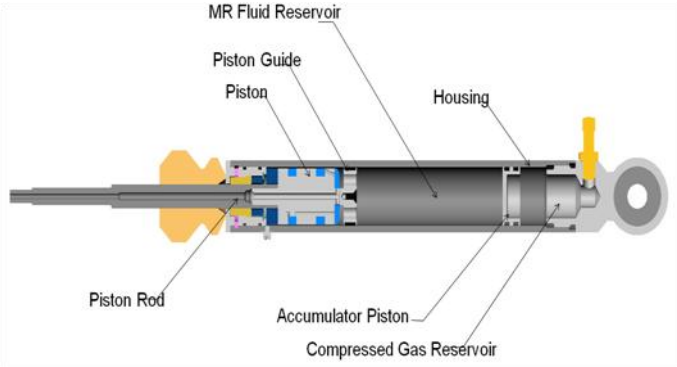


Fig.6 Mono tube MR damper (Poynor, 2001)

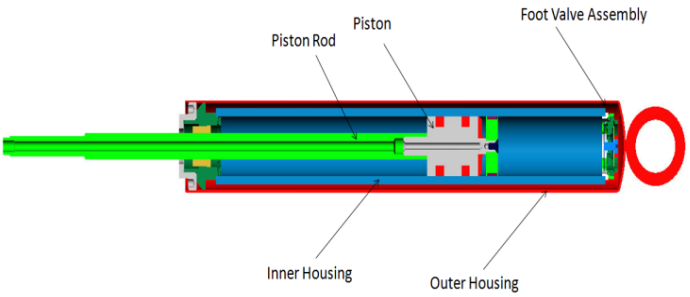


Fig.7 Twin tube MR damper (Poynor, 2001)

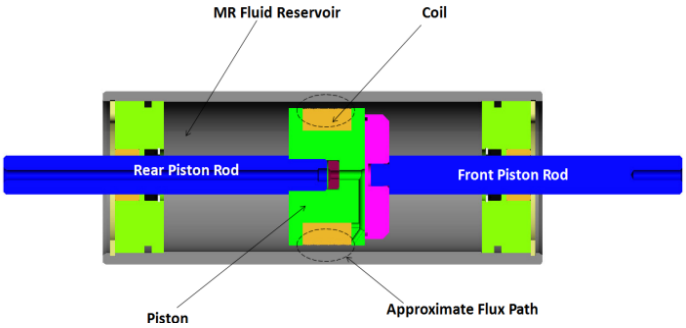


Fig.8 Double-ended MR damper (Poynor, 2001)

2nd International Engineering Symposium - IES 2012
(KU-MU-NITK-HCMCUT Joint Symposium) March 5-7, 2012, Kumamoto University, Japan

Experimental investigations on the flexural strength of reinforced concrete beams

Poornachand Pandit[1] Akshatha Shetty[1], Katta Venkataramama[1], K.S.Babunarayan[1], Indrani Gogoi[2], Praveen.B.B[1], Mahesha[1], Shivaprasad Naik[1] and Arun Sedamkar[1]

1 *Department of Civil Engineering, National Institute of Technology Karnataka, Surathkal, Mangalore 575025, India. email:poornachandra16@gmail.com, ven.nitk@gmail.com, shrilalisuta@gmail.com,akshathashetty16@gmail.com*
2 Assam Engineering Institute Chandmari, Guwahati-781003 India. *email: indranigogoi@yahoomail.com*

Abstract: Structural stability is majorly influenced by strength of concrete. Flexural strength is a measure of the tensile strength of concrete, in other words it is a measure of a resistance against failure in bending. The main aim of this study is to analyse the strength, experimentally, of corroded beams using both Ordinary Portland Cement (OPC). Beam specimens are prepared using M_{20} grade concrete for OPC. Beam specimens casted are tested as vertical cantilever beam in specially prepared loading set up and load deflection behaviour is studied.

Keywords*: Load-Deflection curve, Ultimate load, Deflection, Corrosion rate*

Introduction

Flexure or bending is commonly encountered in structural elements such as beams and slabs which are transversely loaded. Corrosion is one of the important factors that reduces the cross-sectional area of the steel, thereby reducing the load carrying capacity of the structure and induces brittle failure of structures without prior warning. Hence, these effects of corrosion need to be studied for better performance of structures (Staton Walker et al.1998). The studies become more important especially in corrosive environment such as coastal regions, where structures are exposed to the environment having high humidity and salt content. The moment carrying capacity of an under-reinforced concrete beam depends mostly on the strength of reinforcing steels. Therefore, loss of reinforcing steel may be critical and requires special consideration. Corrosion is one of the important causes of steel area loss (Castro et al. 1997). General corrosion, which appears uniformly along the length of the reinforcement, will have two effects: firstly, it will reduce the cross-sectional area of the steel and secondly, it will create local discontinuities in the steel surface. These effects reduce the tensile capacity of the steel in proportion to the loss of its cross-sectional area. Thus, as the corrosion products increase, the cross-sectional area of steel decreases and hence, in addition to the bond deterioration, the ultimate moment capacity of structure also decreases, till the area of the steel becomes so small that it can no longer withstand the load and hence results in the collapse of the structure (Ahmad, 2003).

Experimental Program

Material properties:

1. **Cement:** Ordinary Portland Cement (43 Grade) cement was used in the present investigation. The results confirm the requirement as per IS 10262:1982.
2. **Fine Aggregate:** Physical tests on fine aggregates were conducted. The results are tabulated in Table 1.

3. **Coarse Aggregate:** The size of the aggregate used was 20mm downsize and 12.5mm down size angular type coarse aggregate. Physical tests on coarse aggregates were conducted. Test results and combined sieve analysis are tabulated in table 2.
4. **Reinforcing steel:** For 12mm, 16mm and 20mm diameter of bars obtained yield strength was 470MPa, 470MPa and 480MPa respectively.
5. **Water:** In this experiment normal potable water is used.

Concrete Mix design:
The mix proportion used for M_{20} grade of OPC concrete was 1:2.24:3.67 and water cement ratio has been taken as 0.5. The slump obtained was between 80 to 120mm.

Reinforcement details:
Two series of reinforced concrete cantilever beams of cross section 300mm x 400mm and 2150mm length has been casted, which is having a shear span of 1750mm and 400mm bearing length. Beams with an effective cover of 30mm are designed based on the sizes of the components in RCC Building as per IS 456:2000. In series-1, beams are prepared with concrete made of Ordinary Portland Cement. Beams are provided with two 20mm diameter and one 16mm diameter at top and same reinforcement is provided at bottom. Shear reinforcement of 12 mm diameter TMT bars with a spacing of 150mm c/c for a length of 1650mm from the free end and 12 mm diameter TMT bars with a spacing of 75mm c/c for a length of 500mm for remaining length of beam to ensure that flexural failure would dominate over shear failures shown in the Fig.1.

Corrosion Rate Measurements:
To study the existing corrosion level of the beam specimens, initial current density was measured using the corrosion measuring system "Gill AC". Controlled beams were not subjected to corrosion ones. These beam specimens were divided into number of grids to locate the guard ring probe to polarize the definite area on concrete rebar as shown in the Fig.2. At each node, corrosion current density was measured by LPR technique. These beam specimens were tested with the corroded beams for different levels of corrosion. The current density for each specimen is shown in the Table 3.

Testing Setup:
Flexural testing of the cantilever beam was carried out under the specially prepared loading frame. Loading set up was constructed in the existing reaction bed at laboratory to test the beam as a vertical cantilever by applying point load at the free end of the beam in transverse direction. To achieve the fixity at the fixed end of the beam, heavy duty hydraulic jack was used against the steel column section at the other side of the beam. Full fixity was achieved at the bottom end of the beam by adjusting the movement of the hydraulic jack arm.
The loading frame was designed as a steel space frame, Built up section made up of two ISMC-100 sections with face to face was used to construct the loading frame. 16 mm diameter hilty bolts of 40kN capacities were grouted on the reaction bed to fix the loading frame to the reaction bed. The loading frame was designed to carry a 100kN concentrated load, which is the expected reaction from the beam element.
All beams are tested as cantilever beam in a 15 tonne capacity steel testing frame made up of rolled steel joists, the beam having a span of 1750mm was fixed at one end for a bearing length of 400mm. The span and load points were kept constant for all the beams. The concentrated load is applied on the free end of a beam. The load spreader arm, wherever used is a rolled steel joist which is supported on the rollers kept on the loading points. Over the load spreader arm the proving ring of 20 tonnes capacity which is used to measure the applied load, is placed over which the hydraulic jack of 20 tonnes was fixed to the rolled steel joist of the loading frame. The pump of a hydraulic jacks operated by a hand lever. Fig.3 shows the loading details of the beam specimen.

Theoretical Calculations:
In the present study three control specimens prepared with OPC mix were

tested as a cantilever beam, in the specially prepared loading set up, to determine the flexural capacity. Hydraulic jack was used to fix the beam bottom to the reaction bed.

ultimate moment capacity of Beam

$$M_u = C_{uc}(d - 0.416\,x_u) + C_{us}(d - d')$$

$$M_u = 0.543\ f_{ck} \times x_u \times b(d - 0.416\,x_u) + 462.131 \times 320$$

$$M_u = 128.154\ kN - m$$

Therefore Ultimate load $W_u = \frac{M_u}{l}$

$$\frac{128.154}{1.75} = 73.23kN$$

Experimental Results:

For control beam (CB) specimens results are as given below in Table 4 and load deflection curve are shown in Fig.4.

Concluding Remarks:

Beam specimens are prepared to study the flexural strength of the beam with OPC Concrete. The initial corrosion current density has been determined for controlled beam by using ACM instrument. The results show that there is 31.3% variation in the theoretical values of ultimate load (kN) compared to experimental Observations.

In this paper the results for only control specimens have been presented. Experiments are presently being carried out on beams with different levels of corrosion.

References

[1] Ahmad S, (2003), Reinforcement corrosion in concrete structures, its monitoring and service life prediction––a review, Journal of Cement & Concrete Composites. 25, pp. 459–471.

[2] Castro, P., Weva and Balancim, M. (1997). Corrosion of reinforced concrete in a tropical marine environment and in accelerated tests. Construction and Building Materials, 11(2), pp. 75-88.

[3] IS 456:2000, Plane and reinforced concrete – code of practice, Bureau of Indian Standards, New Delhi.

[4] IS: 10262 (1982), Recommended guidelines for concrete mix design, Bureau of Indian Standards, New Delhi.

[5] Staton walker, and D L Bloem,(1998),Studies of Flexural strength of concrete, Part 3, NRMCA Publication No. 75.

Acknowledgement:

The Partial financial support from BRNS research project Sanction No. 2009/36/115-BRNS/3371 is gratefully acknowledged.

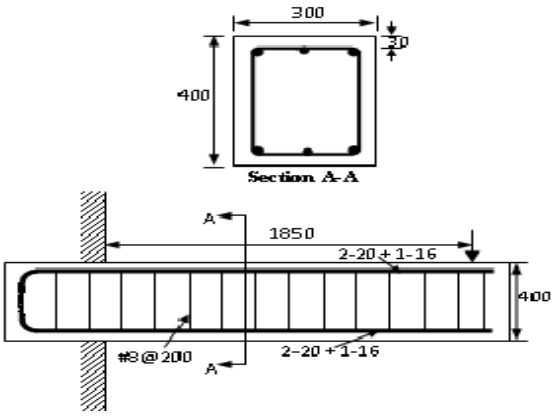


Fig.1 Reinforcement details of beam specimens



Fig.2 Beam specimen marked in to number of grids to measure corrosion current density.



Fig.3 Loading of the beam specimen

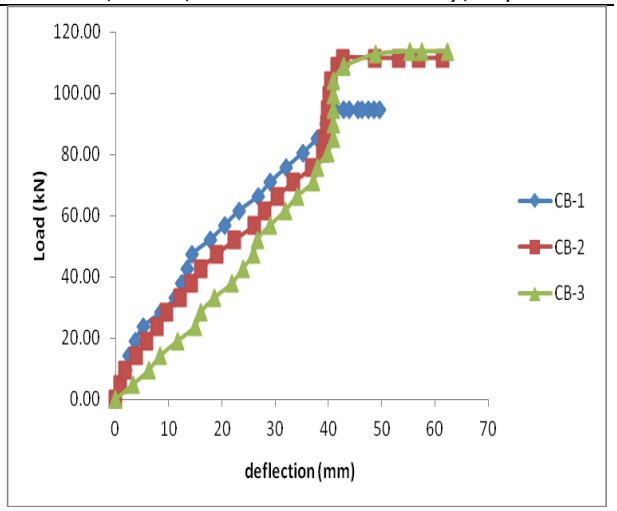


Fig.4 Variation of deflection(mm) with Load (kN) for controlled beam Specimen

Table 1 Test results of fine aggregates used for OPC concrete mix

Characteristics of fine aggregate (natural river sand)		
1	Specific gravity	2.56
2	Water absorption	2.61%
3	Moisture content	2.0%
4	Grading	Zone-II

Table 2 Test results of coarse aggregate of 20mm down size used for OPC mix

Characteristics of Coarse aggregate of 20mm down size		
1	Specific gravity	2.66
2	Shape	Angular
3	Water absorption	0.5%
4	Moisture content	Nil

Table 3 Corrosion current density of Control Specimens

Beam	**Corrosion current density, i_{corr} (mA/cm^2)**					
	Grid Number					
	1	**2**	**3**	**4**	**5**	**Avg**
CB -1	0.0039	0.0038	0.0041	0.0038	0.0038	0.0039
CB -2	0.0039	0.0038	0.0038	0.0039	0.0045	0.004
CB- 3	0.0039	0.0038	0.0038	0.0039	0.0039	0.0039

Table 4 Load- Deflection Results

Beam Specimens	**Ultimate Load (kN)**	**Ultimate load (kN) (Average)**	**Deflection (mm)**	**Defection (mm) (Average)**
CB-1	94.68		49.64	
CB-2	111.5		61.44	
CB-3	113.61	**106.597**	62.4	57.83

2nd International Engineering Symposium - IES 2012
(KU-MU-NITK-HCMCUT Joint Symposium) March 5-7, 2012, Kumamoto University, Japan

Experimental Study on Deterioration Monitoring of Shirasu Concrete in Hot Spring Environment

Dhruva Narayana Katpady[1] Koji Takewaka[2] Toshinobu Yamaguchi[3] Yasuyuki Moritaka[4] Yuuki Tatara[5]

1 *Department of Ocean Civil Engineering, Kagoshima University, Korimoto, 1-21-40, Kagoshima 890-0065, Japan. email:dnkata@gmail.com*
2 *Department of Ocean Civil Engineering, Kagoshima University, Korimoto, 1-21-40, Kagoshima 890-0065, Japan. email: takewaka@oce.kagoshima-u.ac.jp*
3 *Department of Ocean Civil Engineering, Kagoshima University, Korimoto, 1-21-40, Kagoshima 890-0065, Japan. email: yamaguch@oce.kagoshima-u.ac.jp*
4 *Department of Ocean Civil Engineering, Kagoshima University, Korimoto, 1-21-40, Kagoshima 890-0065, Japan.*
5 *Department of Ocean Civil Engineering, Kagoshima University, Korimoto, 1-21-40, Kagoshima 890-0065, Japan.*

Abstract: Sulfate attack on concrete occurs due to a chemical breakdown mechanism where sulfate ions attack components of the cement paste. The compounds responsible for sulfate attack are water-soluble sulfate containing salts, such as alkali-earth (calcium, magnesium) and alkali (sodium, potassium) sulfates that are capable of chemically reacting with components of concrete. In this study, monitoring of sulfate attack on Shirasu concrete is carried out by modelling the conditions which represents the hot spring area where the abutments and piers using Shirasu concrete were constructed. The area is famous for hot springs in Kagoshima prefecture, Japan, and the highest water temperature at a certain depth below the ground is of the order of 130^0C with high concentrations of sulfates. A laboratory setup is made which represents the actual site area and the specimens are immersed in the actual hot spring water extracted. Two monitoring methods are used for evaluating the sulfate attack of concrete. One is an electro-chemical method for detecting corrosion of reinforcing steel in concrete due to sulfate, and the other is the method using a monitoring sensor developed to evaluate the sulfate penetration depth. The degree of deterioration of Shirasu concrete due to hot spring water is compared with the control concrete made with blast furnace slag cement which is well known to be durable under the chemical attacked environment.

Keywords: *Sulfate attack, Shirasu, Electro-chemical method, Monitoring sensor, Corrosion, Blast furnace slag.*

Introduction

External sulfate attack is a chemical breakdown mechanism where sulfate ions from an external source attack components of the cement paste. Such attack can occur when concrete is in contact with sulfate containing water e.g. seawater, swamp water, ground water or sewage water. The often massive formation of gypsum and ettringite formed during the external sulfate attack may cause concrete to crack and scale. However, both laboratory studies and examinations of field concrete show that external sulfate attack is often manifested, not only by expansion or cracking, but also by loss of cohesion and strength.

In a hot spring area of Kirishima in Kagoshima prefecture, bridge pier constructions are carried out using Shirasu concrete. In the area, the hot spring water is contaminated by sulfates with high concentration. As the pier foundations are laid deep underground, the temperature around the foundation also rises due to hot springs. At the foundation, the highest

temperature is of the order of 130^0C. Both the temperature and high concentrations of sulfates in water are said to have deteriorating effect on concrete.
Previous studies have proved that the behavior of Shirasu concrete is very good compared to normal one and also has high resistance for chemical attack. In the present study, an attempt has been made to evaluate the sulfate attack on Shirasu concrete quantitatively by using two monitoring methods, one of which is electro-chemical method for detecting corrosion of reinforcing steel in concrete due to sulfate, and another is the method using a monitoring sensor developed to evaluate the sulfate penetration depth. Shirasu concrete specimens are submerged in the actual hot spring water extracted from the hot spring in Kirishima area and then monitored for sulfate attack. Comparative study has been made with concrete using blast furnace slag cement as control.

Shirasu and Shirasu concrete
Kyushu Island is a typical volcanic zone in Japan, and especially, over the southern part of this island, a great quantity of pyroclastic flow deposits vomited from the volcano about 20000 years ago have been distributed widely and quickly. The quantity of the deposit is estimated to be more than 300 billion ton. This pyroclastic flow deposit is called Shirasu which is one of the local names and means "White sand" in Japanese. It is porous material with large amount of very fine particles. It has high quantity of volcanic glasses and has been confirmed to show pozzolanic reaction. Concrete using Shirasu as fine aggregates is named as Shirasu Concrete [Takewaka et al, 2004].

Experimental investigation methodology
In the study, Shirasu having specific gravity of 2.2 is used in concrete as fine aggregate. The mix proportion of Shirasu concrete is shown in Table 1. Shirasu concrete (here-in after called "Shirasu concrete") of water binder ratio of 50%, with Low heat Portland cement has been used in the experiments. In another case, concrete having water cement ratio of 50% with type B of blast furnace slag cement (here-in after called "BB Concrete") is also used. A target slump of both concretes is 10 cm.

(1) Outline of specimens
Two types of concrete specimens having 200×200mm of cross section and 250mm of length are prepared for the experiment. One is the specimen to examine protection ability of concrete against the corrosion with 4 steel bars with 13mm diameter, of which two are normal deformed reinforcing steel bars (IR) and others are the polished round bars on which surface iron oxide cover (SR) is removed. These bars are set in concrete having 2 and 5 cm of the cover thickness, as shown in Fig.1. A reference electrode is inserted at the center of the specimens to monitor the natural potential of each steel bar. Another type of concrete specimen, which is shown in Fig 2, is also prepared to monitor the penetration depth of the aggressive chemicals in the hot spring water to corrode the steel in concrete. In the specimen, a monitoring sensor is inserted at the center and the output is taken out by electrical wires. Fig.3 shows the assembly of a sensor. The sensor is made of polymer cement mortar of 51mm diameter and 60mm length, with stainless steel rod of 50mm length attached at one end. The polymer cement mortar section is wound by 4 iron wires of 0.1mm diameter at 5mm, 15mm, 30mm, and 45mm form the left end as shown in the figure. As the aggressive chemical diffuses into the specimen and reaches at the iron wire, it gets corroded and soon breaks. Therefore, when the electric resistance of the wire is monitored, the penetration depth of the aggressive chemical can be easily predicted.
These specimens are cured in water with temperature of 20℃ for 28 days and later submerged in the test solution.

(2) Exposure test method
Natural hot spring water with sulfate ion concentration of 206.9mg/kg and pH of 2.9 is used as the solution of the immersion test of the specimens. The chemical characteristics of the solution used are shown in Table 2.

For the test, three immersion conditions with 3 different solution temperatures of 20, 40 and 80 ℃ are arranged. These temperatures are maintained using heaters in the tank. Monitoring data is acquired automatically by data logger every hour for their functionality.

Results and discussion

(1) Change in compressive strength

Fig 4 shows the comparison between compressive strength of BB concrete and of Shirasu concrete immersed in the hot spring waters under the different temperature conditions during 1.25 and 2 years of exposure periods, together with the ones measured just before the immersion test.

The compressive strengths of both concretes clearly increase in the hot spring water compared with the ones before testing. This may be due to continuing latent hydration in BB concrete or pozzolanic reaction in Shirasu concrete even in the aggressive solution.

However, with increasing water temperature, the strengths relatively decrease in both concretes, though in all temperature conditions, Shirasu concrete has the higher strength than the BB concrete.

The longer the immersion period, the lower the strengths of both concretes clearly. It seems to be due to a chemical attack of the hot spring water. On the other hand, Shirasu concrete seems not to be so affected by the water temperature in the longer period, while BB concrete is continuously affected throughout the exposure period.

(2) Penetration depth of the aggressive chemicals

Fig.5 shows surface appearance of both concretes after 2 years of the exposure test. Efflorescence distributes on the wider area of the surface of Shirasu concrete than of BB concrete.

On the other hand, Shirasu concrete and BB concrete are monitored for penetration condition of aggressive chemicals at 4 cover thicknesses of 5mm, 15mm, 30mm and 45mm by using the sensor shown in Fig.3. Fig.6 shows the change of electric potential of iron wire set at the different cover thickness on the sensor in concrete with the exposure period. The concretes that are monitored are those which were exposed to the hot spring water with 80^0C.

In Shirasu concrete, the iron wires at all cover thickness are undisturbed and show 0mV throughout the exposure period. It is clearly evident that the concrete has the high resistance for ingress of the aggressive chemical. The BB concrete, however, behaves differently. Even though all iron wires of sensor in the concrete show the potential of 0mV until 708 days of exposure period, the iron wire at 5mm cover thickness shows increase in potential above zero over 708 days of the exposure period. It means that the diffusion of the aggressive chemicals reaches at 5mm inside of BB concrete at least on 708 days after starting the exposure.

(3) Quantitative analysis of sulfate ingress by EPMA

A quantitative analysis by using EPMA is carried out to evaluate the concentration of aggressive chemical penetrating into concrete. In this examination, the analysis focuses especially on sulfur content in concrete because a sulfate attack would be one of the most aggressive deterioration mechanisms due to the hot spring water.

The typical examples of EPMA analysis for both Shirasu and BB concrete in the hot spring water are shown in Fig.7. Based on the analysis results, Fig.8 depicts distributions of the sulfur concentration with depth in concrete exposed during 450 days and 2 years, based on the EPMA analysis results.

In the case of Shirasu concrete, a peak of the concentration is at around 2-3mm depth from the specimen's surface after 450 days of exposure time and at around 3.5-5mm after 2 years. At both peaks, the sulfur concentration is almost same and is about 1.75 mass %. For both exposure periods, the concentration reduces drastically to 1.0 mass %, which is almost same as the initial contents of sulfur in Shirasu concrete, at about 6-7mm depth. In contrast, the sulfur concentration in BB concrete reaches the highest level at depths of around 3-4mm after 450 days of the exposure period, and around 4-7mm after 2 years.

At both peaks, the sulfur concentration is almost same and is about 1.35 mass % which is less than the peak concentration in Shirasu concrete. However, the sulfur concentration in concrete within about 10 mm or less of depth is higher than 0.85 mass% which is the initial contents of sulfur in BB concrete.
From these results, it can be understood that Shirasu concrete has the higher ability to keep the penetration of sulfur or sulfate within only its surface area and protect them to penetrate into the inner area, compared with BB concrete.

(4)Monitoring of steel corrosion in concrete by half cell potential using embedded reference electrode

The half cell potential of the reinforcing steel bars is measured using an embedded type of reference electrode. The comparison of potential is done between 2 types of reinforcement bars (normal deformed steel bar and polished round bar) with 20mm and 50mm cover thicknesses each. Fig 9.shows changes in the potential of steel bar in Shirasu concrete and BB one with the exposure period.
In the case of all steel bars in BB concrete, the half cell potential drastically changes to negative direction until the exposure period of around 25 to 50 days, then keeps the potential of about -600 to -700mV with small change at longer exposure time, in spite of types of reinforcement bars, cover thickness and exposure temperature. On the other hand, in the case of Shirasu concrete, the behavior of potential change with exposure time is different depending on exposure temperature. In Shirasu concrete exposed in the 80℃, the measured data of half-cell potential on the embedded steel bars shows the same tendency as the one in BB concrete under same temperature condition. However, under the 20 or 40℃, the potential of steels in Shirasu concrete fluctuate between -200 and -400mV for about 1year, then change to keep stable condition at about -700mV.
Depending on ASTM C 876, a threshold potential for corrosion on steel in concrete is about -230+1.0(t-25), and here, "t" is temperature (℃). Therefore, , corrosion is expected in all case of steel bars shown above, except the steel in Shirasu concrete under 20 and 40℃ of temperature in early stage of the exposure test.

(5)Corrosion condition of steel bars in concrete

After the exposure test for 2 years, the test specimens are broken and steel bars are taken out to evaluate corrosion condition. Fig.10 shows rate of corrosion area on the bar surface. The corrosion areas of reinforcement bars in Shirasu concrete are almost negligible, though a bar under exposure temperature of 80℃ have small spot corrosion as shown in Fig.11(a). On the contrary, the corrosion clearly arises on the steel bars in BB concrete under the condition of 20℃ and 40 ℃ of exposure temperature (see in Fig.11(b)).
These results show that the corrosion is mild in case of Shirasu concrete when compared to BB concrete, and also have good relation with the estimation result obtained by the half cell potential measurement environment.

Conclusion

1. The monitoring sensor, which is developed to monitor the chloride penetration, can be effectively applied for determination of sulfate parameters in the hot spring water which corrodes the steel in concrete.
2. From past researches it is well known that Shirasu concrete is more durable than the ordinary concrete. From present research Shirasu concrete proves its high resistant nature in case of hot spring environment too.
3. From the results, Shirasu concrete has not allowed sulfate to penetrate deeper. This means that it is less porous, conforming internal pozzolanic reactions.

References

[1] Nishiyama, et al (2006), Properties of Concrete with both Shirasu and Sea Sand as Fine Aggregate, Proceedings of the Japan Concrete Institute, Vol.28 , No.1 pp.125-130.

[2] Okuji, et al (2004), Experimental Research on Applicability of Shirasu Concrete under High

Temperature Environment, Proceedings of the Japan Concrete Institute, Vol.26, No.1 , pp.681-686.
[3] Takewaka, et al (2001), Development of Non-Destructive Monitoring System for Evaluating Chloride Penetration Process into Concrete , Proceedings of the Japan Concrete Institute, Vol.23 , No.1, pp.1183-1188.
[4] Takewaka, et al (2004), State-of-Art-Report on Characteristics of SHIRASU Concrete and its Practical Use, Concrete Journal, Vol.42, No.3, pp.38-47 (in Japanese).

Table 1 Mix proportion of Shirasu concrete and BB concrete

Type of concrete	W/C (%)	Cement	s/a (%)	(kg/m^3)					SP (%)	Slump (cm)	Air (%)
				Water	Cement	Shirasu	Sand	CA			
Shirasu concrete	50	Low heat	34	195	390	478	—	1105	0.8	10	3.6

Table 2 Chemical characteristics of solution used for exposure test

pH	2.9
Constituents	mg/kg
Sulfate ion (SO_4^-)	206.9
Bisulfate ion (HSO_4^-)	8.8
Chloride (Cl^-)	66.1
Hydrogen sulfide (H_2S)	2
Carbon dioxide (CO_2)	65.1

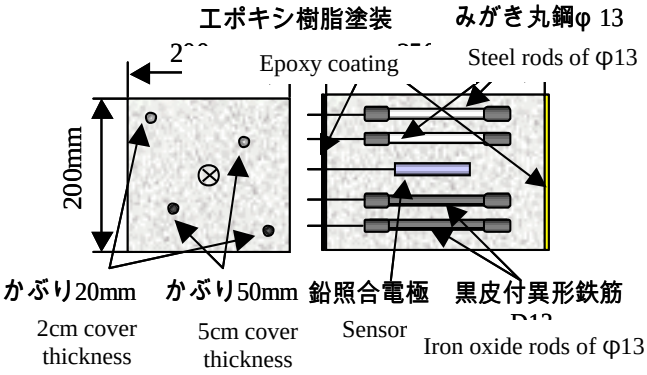


Fig.1 Laboratory setup of specimens

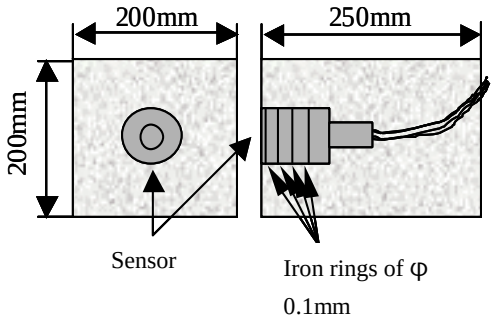


Fig.2 Sensor setup in specimens

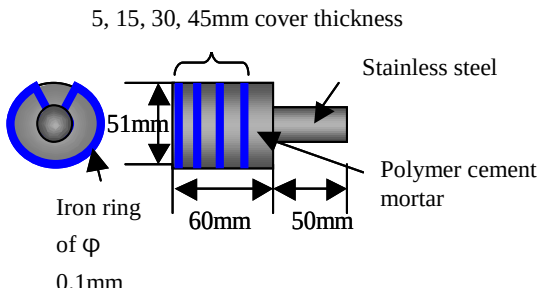


Fig.3 Assembly of sensor

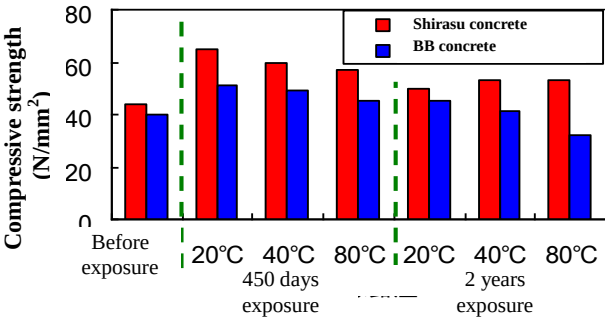


Fig.4 Compressive strength comparison



Shirasu BB concrete

Fig.5 Surface appearance of specimens exposed in hot spring water during 2years

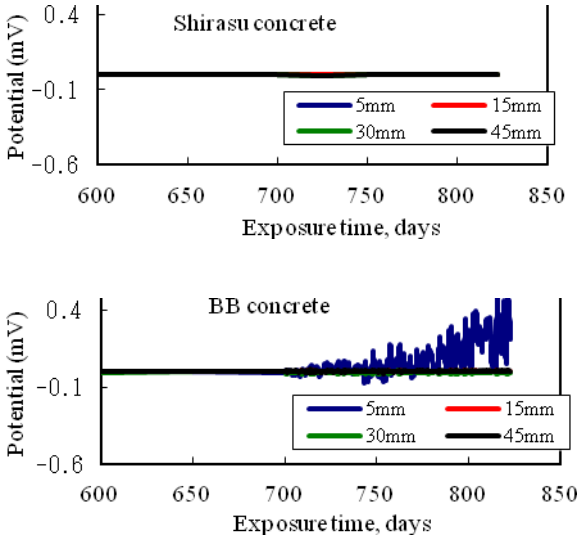
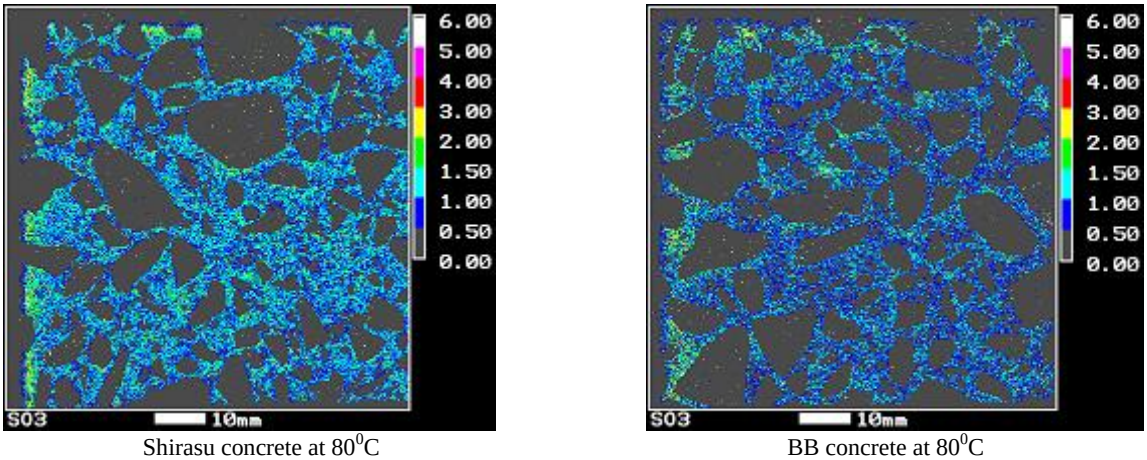


Fig.6 Potential at reinforcement bars at different cover thickness and age



Shirasu concrete at 80^{0}C BB concrete at 80^{0}C

Fig.7 EPMA analysis

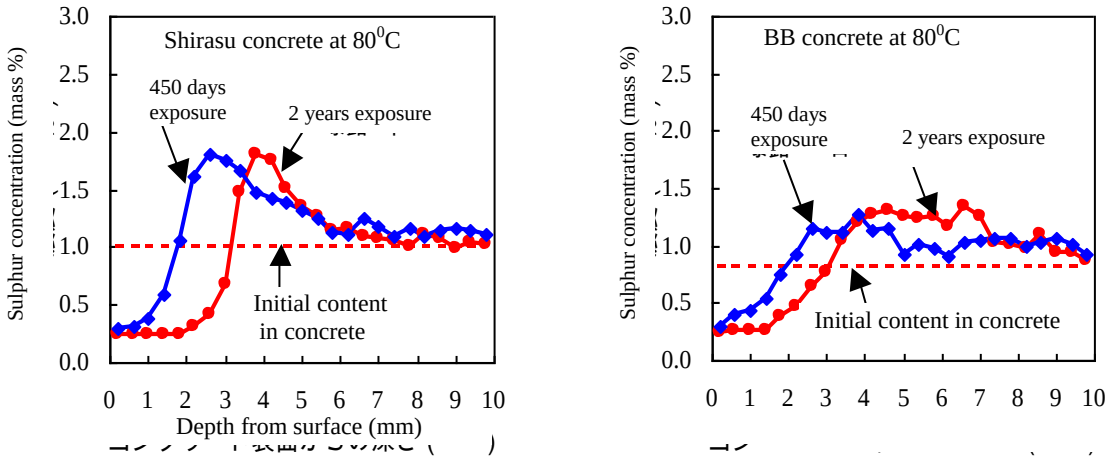
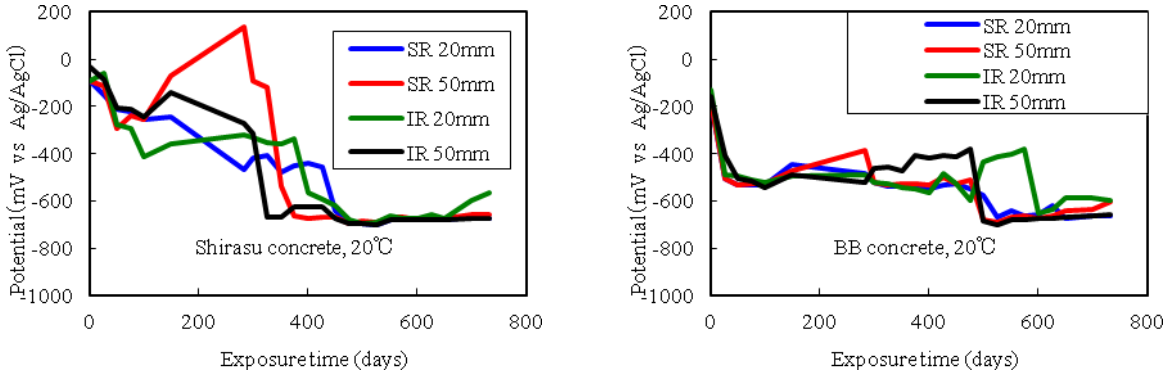


Fig.8 Distribution of sulphur concentration



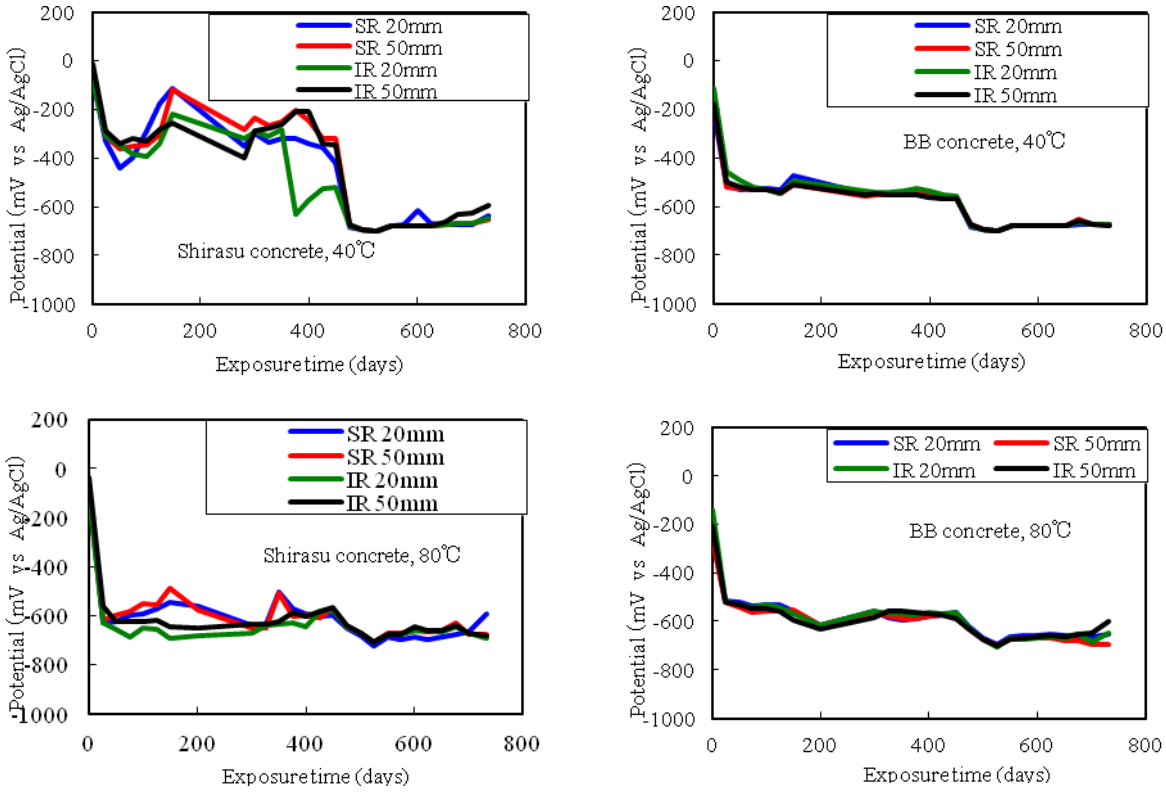


Fig.9 Relationship between half- cell potentials of steel in concrete with exposure period

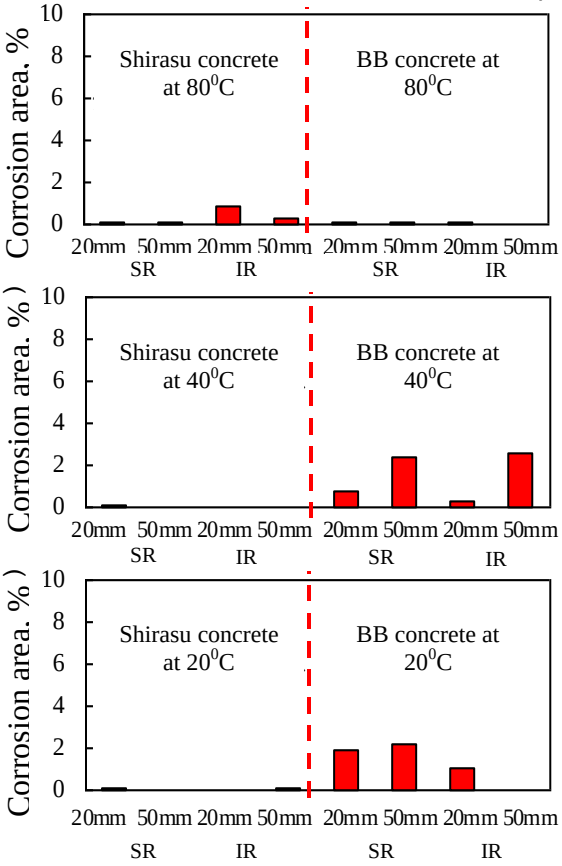
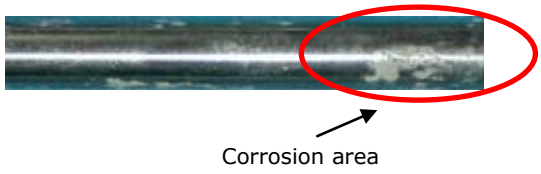


Fig.10 Rate of corrosion on steel bars



(a)In Shirasu concrete at 80°C and 20mm cover thickness



(b)In BB concrete at 20°C and 50mm cover thickness

Fig.11 Surface condition of steel bar in concrete for 2 years of exposure test.

2nd International Engineering Symposium - IES 2012
(KU-MU-NITK-HCMCUT Joint Symposium) March 5-7, 2012, Kumamoto University, Japan

ESTIMATION OF AQUIFER PARAMETERS USING INVERSE MODELING BY INCORPORATING PRIOR INFORMATION ABOUT RAINFALL RECHARGE FACTOR AS CONSTRAINTS

M K Nagaraj

Dept. of Applied Mechanics and Hydraulics, National Institute of Technology Karnataka Srinivasanagar, Surathkal, India 575025 Email: rajumkn@yahoo.com

Abstract: Groundwater resource estimation is an important issue and should be viewed in more comprehensive manner. In order to estimate groundwater resource accurately, the aquifer parameter values such as transmissivity, specific yield and rainfall recharge factor have to be known precisely. These parameters can be estimated by using inverse modeling, which is quite extensively used from past four decades. In any inverse problem, the convergence, uniqueness, stability and identifiability are the key issues to be considered. In the present study a parameter estimation model is developed which estimates transmissivity, specific yield and rainfall recharge factor simultaneously for a regional aquifer system. The aquifer is divided into zones and zonal parameters are estimated using water level fluctuation data. The present model used an out put error criterion where the objective is to minimize the weighted least square error between observed and computed water level changes on a seasonal basis. Gauss Newton algorithm is used for minimization and this method requires computation of first derivatives and in the present model parameter perturbation technique is adopted. The model also estimates parameter uncertainly using parameter covariance matrix.

In the present study, an aquifer system is considered where 30 parameters are simultaneously estimated with and without consideration of prior information about the parameters. From the study it is observed that the parameters are considerably better estimated when prior information is used.

It must be noted that in next two decades, groundwater plays a key role in water sector and hence accurate assessment of groundwater resource is solely depend on the accurate estimate of aquifer parameters. Thus during the period 2010-2025, the estimation of aquifer parameters with special reference to rainfall recharge is highly essential. This not only helps in accurate assessment of groundwater but also helps in taking appropriate decision in conjunctive use policy, urban planning etc.

***Keywords**: aquifer, parameter estimation, prior information*

Introduction

Estimation of aquifer parameters is highly essential to assess groundwater resources precisely. Inverse modeling is one of the successful tool which is quite extensively used to estimate aquifer parameters such as transmissivity, specific yield and rainfall recharge factor. In inverse modeling, estimation of these parameters with some prior information will not only significantly improve the parameter convergence but also helps in getting an improved error is uncertainty. In the present study a parameter estimation model is developed for a regional groundwater system, and the relative importance of incorporation of prior information is demonstrated.

Model Development

In the present study, parameter estimation model for regional groundwater system is developed for regional groundwater system. The model is based on output error criterion and weighted least square method is used for the objective function. The analysis model

uses a general two dimensional parabolic type partial differential equation using source/sink terms. The equation is solved by using Galerkin Finite Element method using linear triangular elements. Zonation approach is used for parameterization, where the region is divided into a number of homogeneous zones. The heterogenity of the system is represented by variation in the parameters between the zones.

The analysis model developed is coupled with an optimisation algorithm for the purpose of parameter estimation. The model uses weighted least square (WLS) method with Gauss-Newton algorithm for minimisation. The objective of the model is to estimate unknown parameters Tx(i), Ty(i) , Ty(i) and Fr(i), i = 1 Nz. Where Nz is the total number of zones in the region, Tx and Ty are the transmissivities in x and y direction, Sy is the specific yield and Fr is the rainfall recharge factor. In the present study a linear rainfall recharge model is used (Thus Fr indicates some percentage of rainfall that effectively contributes to the building of groundwater table) The unknown parameters are to be estimated such that computed values of field variable match well with corresponding observed values. The measurements that are considered in the present study are nodal water level change and zonal water level changes over a reach for a specified season. A season in the present study consists of two distinct seasons, one monsoon and one non-monsoon following the dominant rainfall trend prevalent in India The objective function is expressed by the following equation

$$Min\ E = \sum_{L=1}^{Ns} \sum_{i=l}^{M(L)} W_i L \left(S^{L}_{Oi} - S^{L}_{Ci} \right)^2 \qquad (1)$$

Where
Ns : Number of season used
S^{L}_{Oi}: Observed value (water level change) for season L
S^{L}_{Ci} : Computed value (water level change) for season L
M(L): Number of ith measurement for season L
WL: Weight for ith measurement for season L

In the present study, Gauss-Newton algorithm is used for the solution of WLS minimization problem. Output error criterion is considered for minimisation where a set of parameter values are initially assumed and is iteratively improved until the model response is close to that of field measurement.

This algorithm requires computation of sensitivity coefficients which are obtained by parameter Perturbation technique. In any inverse problem, parameter uncertainty is very important. The present model also estimates the parameter uncertainty using parameter covariance matrix. It must be noted that the parameter covariance matrix can be obtained by sensitivity matrix. It is obvious that in case of lower redundancy (ie when measurement points are relatively less) or higher level of noise in the field data, when parameters are estimated using inverse modeling, shows higher parameter uncertainty.

The parameter estimation model is used for different combination of zonation pattern in a regional groundwater system.

Model Application on a Regional Groundwater System

The parameter estimation model developed is applied on a regional groundwater system and its robustness is tested for uniqueness, idenitifiability and stability of parameter for a synthetic aquifer system. The study area consists of 50 km^2 with 5 zones each of area 10km^2. First the model is analysed for typical zonation based on some administrative units and later the same study area is zoned in a different manner based on aquifer parameters. The zonal draw downs on a seasonal basis is computed for both the cases. It must be noted that in the above study transmissivity values varied from 50 m^2/day to 250 m^2/day. Specific yield values varied from 2 % to 10 % and rainfall recharge factor is varied from 3 % to 15 %. The average annual draft is about 60 mm while the average rainfall is about 800 m.

The internal values of T, S_y, F_r are assumed as 1000, 0.5 and 0.5 respectively. The parameters are estimated by creating a noisy data randomly generated using zero mean and unit variance, with 0.05 m noise. 20 parameters are estimated using 40 measurements in two seasons. Table 1 shows the parameter convergence with and without prior information and Table 2 shows the parameter uncertainty and estimation error when prior information about rainfall recharge factor is incorporated.

It must be noted that in case b the prior information about only Rainfall rechrge is given while in case c prior information about all parameters are given. The prior information is given in the form of upper and lower bounds while correcting the parameter value in each iteration.

From the study, it is observed that when prior information about parameter are incorporated, convergence is considerably faster. The parameters are converged in about 40, 30 and 25 iteration respectively for cases a, b, c.

Conclusions

A parameter estimation model is developed for a regional aquifer system using an out put error criterion. The present model estimates transmissivity, specific yield and rainfall recharge factor on a zonal basis. In the present study, the role of incorportation of parameters information in inverse modeling is studied. 20 parameters are estimated using just 2 seasonal water level charges over 40 nodal point. From the study it is observed that when prior information about parameters are incorporated, the parameter convergence is relatively faster. The parameter also shows both lesser estimation error and uncertainty when prior information is incorporated. It is also observed that there is a significant improvement in parameter uncertainty, when compared to estimation error.

References

[1] Nagaraj. M.K., Sridharan. K, Sekhar.M (2001). Sequential estimation of aquifer parameter in a regional groundwater system. International Conference, ICCE, IISc., Bangalore, 589-593.
[2] Yeh W.W.G (1986). Review of parameter identification procedure in groundwater hydrology inverse problem. WRR 22(2), 95-108.
[3] Yunjunghyan K, Leek (1998). Model identification criteria for inverse estimation of hydraulic parameters. Groundwater 36(2), 230-239.

Table 1 Parameter Convergence

Iteration number	Objective function value		
	Without prior information (a)	With prior information	
		(b) (only rainfall recharge)	(c) (all parameters)
2	1000	700	500
4	500	450	50
6	100	80	10
8	20	22	4
10	10	15	1
15	2	10	0.05
20	0.6	3.0	0.04
25	0.25	0.50	0.022
30	0.08	0.05	0.022
35	0.008	0.05	0.022

Table 2 Estimation Error and Parameter Uncertainty

(a) Without prior information

Zone	Estimation error (%)				Uncertainty (%)			
	Tx	T_y	S_y	F_r	T_x	T_y	S_y	F_r
1	02	02	02	01	08	13	04	03
2	06	07	02	08	08	11	04	07
3	06	03	04	04	21	13	06	07
4	03	06	08	02	14	09	08	12
5	09	09	05	06	10	09	09	09

(b) With prior information about only Rainfall Recharge (Constraint only upper Limit)

Zone	Estimation error (%)				Uncertainty (%)			
	T_x	T_y	S_y	F_r	T_x	T_y	S_y	F_r
1	02	02	02	01	05	13	03	02
2	05	06	02	05	05	12	03	05
3	05	02	03	04	11	10	05	06
4	02	05	06	02	13	09	06	06
5	07	08	03	04	10	05	06	04

(c) With prior information about all parameters (Constraint only upper Limit)

Zone	Estimation error (%)				Uncertainty (%)			
	T_x	T_y	S_y	F_r	T_x	T_y	S_y	F_r
1	02	02	01	01	04	11	02	02
2	04	04	01	04	05	11	02	04
3	04	01	02	02	07	09	05	05
4	02	04	04	01	09	06	05	04
5	04	04	01	02	07	04	04	02

2nd International Engineering Symposium - IES 2012
(KU-MU-NITK-HCMCUT Joint Symposium) March 5-7, 2012, Kumamoto University, Japan

Comparative analysis of ET_o using AWS data

B.M.Dodamani [1] **Shwetha [2]**

1 *Department of Applied Mechanics & Hydraulics, National Institute of Technology Karnataka, Surathkal, Mangalore 575025, India. email:mani@nitk.ac.in*
2 *Department of Applied Mechanics & Hydraulics, National Institute of Technology Karnataka, Surathkal, Mangalore 575025, India. email:naksha7@gmail.com*

Abstract: Reference crop evapotranspiration (ET_o) is the most complex and important component of the hydrologic cycle. Earlier studies have evaluated various popular empirical evapotranspiration methods that belonged to three categories: (1) mass-transfer based methods, (2) radiation based methods, and (3) temperature-based methods. In this study, a cross comparison was made between four methods selected from two categories. ET_o methods namely: Hargreaves (temperature-based), Makkink and Priestley-Taylor (radiation-based) were evaluated with the FAO 56-PM method using weekly meteorological data from the 173 AWS stations distributed in Kerala and Tamil Nadu. Weather parameters as point data were converted into continuous surface data using spatial interpolation techniques. The applicability of the spatial model was tested using the statistical parameter RMSE, for this 5% of the total AWS stations were removed in weather parameter data sets and spatially interpolated using IDW interpolation technique to get values at removed stations and spatially distributed ET_o was estimated using ET_o spatial model and compared with the estimated ET_o at the removed stations. The range of ET_o during monsoon season by the FAO56-PM was varies from 1.75-7.49 mm/day, Priestley-Taylor method was varies from 2.16 – 7.63 mm/day, Makkink was from 1.64 – 7.19 mm/day and Hargreaves method was from 3.17 – 7.77 mm/day. The comparison was made on the basis of statistical analysis. The mean bias error (MBEs), for estimated ET_o by applying Priestley-Taylor, Hargreaves, Makkink methods, and compared to FAO-56 PM estimated values, were 0.642, 0.9224 and -0.135 mm/day respectively.

***Keywords**:* Reference Crop Evapotranspiration (ET_o), AWS, Weather parameters, FAO56 PM equation, Priestley-Taylor equation, Makkink equation, Hargreaves equation, GIS, Spatial Interpolation, Spatial model, RMSE.

Introduction

Water scarcity is a major problem, facing number of nations especially the third world countries in the present time. Irrigated agriculture accounts for about 70% of the available fresh water globally. Apart from precipitation, evapotranspiration (ET) is the most significant component of the hydrological budget. Irrigation water demand is usually determined through evapotranspiration (ET) estimation procedures. The evapotranspiration rate from a reference surface, not short of water, is called the reference crop evapotranspiration or reference evapotranspiration and is denoted as ET_o. Several models have been proposed by many authors to estimate monthly, weekly, daily and hourly ET_o, depending on the availability of weather parameters and these include Food Agriculture Organization Penman Monteith (FAO-PM), Kinberly-Penman, FAO Corrected Penman, Blanney-Criddle, Priestley-Taylor, FAO-Radiation, Hargreaves, and FAO-Blanney Criddle (Paul et al. 2004). Many of these models are subject to local calibration thereby making them to have limited global

acceptance. Due to the higher performance of FAO-PM model in different parts of the world when compared with other models, it has been accepted as the standard method of computing ET_o from meteorological data, since it has given comparable results with observed ET_o in different climatic regions of the world. (Allen, et al., 1998, Gavila et al., 2006).

In order to use FAO-PM model in computing daily ET_o, meteorological data are required such as daily maximum and minimum air temperature, solar radiation, wind speed, and relative humidity. These data can be obtained directly from automatic weather stations which are now in use in different parts of the world. However, in India and other developing countries, these automatic weather stations are available in some places, due to the high cost of acquiring and maintaining them. Similarly, in meteorological stations where analogue instruments are used, limited data are recorded due to obsolete or faulty equipment and lack of appropriate facilities. These hereby make it very difficult to estimate ET_o. In most cases, only the maximum and minimum air temperature are available. In such situation, the procedure for estimating ET_o outlined in Allen, et al., 1998 are used and has been found to produce accepted results (Droogers & Allen, 2002). Hargreaves method has been recommended for the computation of ET_o when only the maximum and minimum air temperature are available (Allen et al., 1998). The result obtained from the use of Hargreaves method has been reported to produce satisfactory results in computing weekly or monthly ET_o (Hargreaves and Allen, 2003)..

Most of the methods employ meteorological data observed at point locations to estimate ET_o. The complex spatial heterogeneity of the meteorological factors could not be considered in the conventional techniques. Therefore they may result in inaccurate estimations in large water sheds. In the past decade, with the support of Geographic Information System (GIS) it is found possible to estimate spatially distributed ET_o over an entire region (Tsanis & Noam 2003). Spatially distributed modeling involves calculation of every parameter influencing the estimation of ET_o, in each grid at a particular spatial resolution.

STUDY AREA

The study area lies between longitudes $75^0 0' 0''$ E and $80^0 20' 0''$ E and latitudes $8^0 0' 0''$ N and $14^0 5' 0''$ N, covers Tamil Nadu and Kerala states of India(Fig1). The region has four distinct seasons, South-West monsoon from June to September, North-East monsoon from October to December, the winter season from January to February and summer from March to May. The study is mainly concentrated on South-West monsoon season.

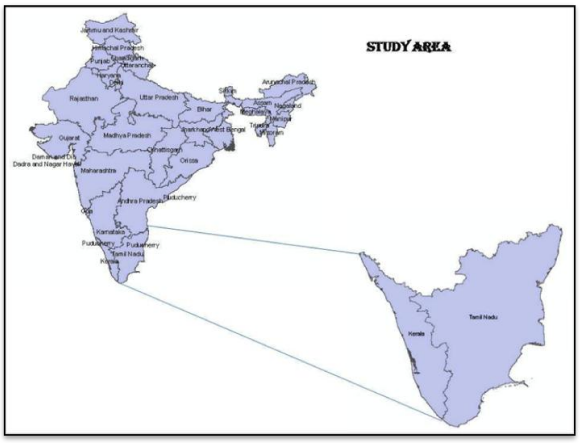


Fig 1. Stydy area

Tamil Nadu covers an area of 130,058 Sq Km, The geographical location of Tamil Nadu is such that the climatic condition shows only slight seasonal variations. Due to close proximity to the sea, the temperatures and humidity remain relatively high all the year round. The average annual rainfall in Tamil Nadu is 998mm. Kerala is a tiny strip of land Its land area is 38,863 sq km stretching 580 km in length and 30.130 km in breadth Kerala receives copious rain, average annual rainfall is 3000mm per year. The temperature in Kerala normally ranges from 28° to 32° C on the plains but drops to about 20° C in the highlands.

The climate data for this study were obtained from the 173 automatic weather stations located in Tamil Nadu, Kerala and some parts of Karnataka and Andhra Pradesh stations were also considered since nearest stations of these two states will influences on spatial interpolation.

Hourly values of data for a period of May 2010 to September 2010 were collected and then converted into required data using shell script. The weather parameters used were temperature, relative humidity, wind speed, solar radiation, sunshine duration and atmospheric pressure. Solar radiation and atmospheric pressure were calculated as per the guidelines of FAO Irrigation and drainage paper 56.

The FAO-PM method requires a numerous meteorological data, such as maximum and minimum air temperatures, relative humidity, solar radiation, and wind speed. To obtain such data is time consuming and complicated. If some of these data are not available, alternative methods must be used for ET_o estimation. Furthermore, rapid and reliable methods are needed for estimating ET_o for areas in which weather data are not available.

The FAO-PM method is the most reliable and universally accepted method because it is based on physical principles, and considers all the climatic factors, which affects ET_o. The Food and Agriculture Organization of the United Nations (FAO) has proposed FAO-PM method as the standard method for estimating ET_o, and for evaluating other methods (Slavisa Trajkovic, 2005). Since, the results of this method has given similar ET_o values compared to observed ET_o in different climatic regions of the world. The traditional method of using point values of the meteorological factors as inputs for the estimation of ET_o, for a large complex water shed provides a crude estimation of ET_o. The spatial variations of the meteorological factors is not considered in the traditional techniques. Therefore, they may result in an inaccurate estimations in large water sheds. Therefore it is necessary to get spatial distribution of ET_o for a large watersheds. Numerous methods have been developed for ET_o estimation out of which some techniques have been developed partly in response to the availability of data. Factors such as data availability, the intended use, and the time scale required by the problem must be considered when choosing the ET_o calculation technique.

FAO-PM method

Food Agriculture Organization (FAO) recommended the adoption of the Penman-Monteith combination method as a new standard for ET_o and advised procedures for calculation of the various parameters. The method overcomes shortcomings of the previous FAO Penman method and provides values more consistent with actual crop water use data worldwide.

estimate ET_o can be expressed as:

$$ET_o = \frac{0.408\Delta(R_n - G) + \gamma \frac{900}{T+273} u_2 (e_s - e_a)}{\Delta + \gamma(1 + 0.34u_2)} \quad 1$$

Where,

ET_o = reference evapotranspiration [mm day-1],

R_n = net radiation at the crop surface [MJ m-2 day-1],

G = soil heat flux density [MJ m-2 day-1],

T = mean daily air temperature at 2 m height [°C],

u_2 = wind speed at 2 m height [m s-1],

e_s = saturation vapour pressure [kPa],

e_a = actual vapour pressure [kPa],

(e_s-e_a) = saturation vapour pressure deficit [kPa],

Δ = slope vapour pressure curve [kPa °C-1],

γ = psychrometric constant [kPa °C-1].

The computation of all data required for the estimation of the ET_o followed the method and procedure given in the FAO paper 56.

Hargreaves Method

ET_o can be estimated using minimum climatological data. In a situation where solar radiation, wind speed, relative humidity and other data are completely absent, ET_o can also be estimated using the equation stated by Hargreaves and Samani (1982) and is given as:

$$ET_o = 0.0023 * 0.408(R_a)(TC + 17.8)\sqrt{(TD)} \quad 2$$

Where,

ET_o = Reference Crop Evapotranspiration (mm/day)

TD = Tmax-Tmin (^{0}C)

TC = average daily temperature (^{0}C)

R_a= Extraterrestrial radiation [MJ m-2 day-1]

Priestly Taylor Method

The Priestley-Taylor equation (Priestley and Taylor, 1972) is a modification of Penman's theoretical equation. An empirical approximation of the Penman combination equation is made by the Priestley-Taylor to eliminate the need for input data other than radiation.

$$ET_o = \alpha \frac{\Delta}{\Delta + \gamma} \left(R_n - G \right) \frac{1}{\lambda} \qquad 3$$

Where,

ET_o = Reference Crop Evapotranspiration (mm/day)

α =1.26

λ = latent heat of vaporization, 2.45 [MJ kg-1],

Δ = slope of saturation vapour pressure curve at air temperature T [kPa °C-1],

γ =psychrometric constant [kPa °C-1],

R_n = net radiation

G = soil heat flux density [MJ m-2 day-1],

Makkink Method

This is another simplified eqution combination of the original Penman equation; it disgrades the aerodynamic component and replaces the net radiation balance with incoming shortwave solar radiation (R_s). The equation is:

$$ET_o = 0.61 \left[\frac{\Delta}{\Delta + \gamma} \right] \cdot \left(\frac{R_s}{\lambda} - 0.12 \right) \qquad 4$$

Where,

ET_o = Reference Crop Evapotranspiration (mm/day)

Δ = slope of saturation vapour pressure curve at air temperature T [kPa °C-1],

γ = psychrometric constant [kPa °C-1],

λ = latent heat of vaporization, 2.45 [MJ kg-1],

R_s = the incoming solar radiation [MJ m-2 day-1].

Quantitative approaches to the evaluation of Priestley-Taylor, Makkink and Hargreaves method performances measures to be carry out. These ensure a rigorous comparison of the methods, an extended analysis was performed using different statistical indices for the estimated values. Intercepts (b) and slopes (a) for the least squared regression analysis also were calculated. It has been pointed out (Fox, 1981) that commonly used correlation measures, such as (R) and (R^2), and tests of statistical significance in general, are often inappropriate or misleading when used to compare methods. In this study, in addition to intercept, slope, and coefficient of correlation the following statistical analysis were also determined.

1. MBE is the mean bias error. The consistent deviation of analytical results from the true value caused by systematic errors in a procedure. Bias is the opposite but most used measure for trueness which is the agreement of the mean of analytical results with the true value, i.e. excluding the contribution of randomness represented in precision.

$$MBE = N^{-1} \sum_{i=1}^{N} \left(P_i - O_i \right) \qquad 5$$

2. Variance ($S_d^{2)}$ is the distribution of differences, simply expresses the variability of the difference between FAO-PM method (P_i) and other methods (O_i) values around the MBE.

$$S_d^{\,2} = (N-1)^{-1} \sum_{i=1}^{N} \left(P_i - O_i - MBE \right)^2 \qquad 6$$

3.RMSE is the average difference expressed by the root mean squared error. It is the best among overall measures of model performance because they summarize the mean difference between estimated by FAO-PM (O) and estimated by other methods (P). RMSE is practical as it shows the errors in the same unit and scale as the parameter itself and it can range from 0 to infinity and, of course, lower values are better.

$$RMSE = \sqrt{N^{-1} \sum_{i=1}^{N} \left(P_i - O_i \right)^2} \qquad 7$$

4.$RMSE_s$ the systematic component (Willmott, 1981) and it was computed in addition to RMSE. Systematic RMSE is determined by the distance between the linear regression best-fit line and 1:1 line. The systematic component is a measure of the space available for local adjustment. A good method is considered to have systematic RMSE close to RMSE.

$$RMSE_s = \sqrt{N^{-1}\sum_{i=1}^{N}(P_i^* - O_i)^2} \qquad 8$$

5.$RMSE_u$ is the unsystematic component (Willmott, 1981) and it is determined by the distance between the data points and the linear regression best-fit line, and it is representative of "noise" level in the method being tested and is a measure of the scatter about the regression line; it can be interpreted as a measure of the potential accuracy. A good method is considered to have a very low unsystematic RMSE.

$$RMSE_u = \sqrt{N^{-1}\sum_{i=1}^{N}(P_i - P_i^*)^2} \qquad 9$$

Where

P_i stands for estimated by FAO56 PM and P_i* stands for values estimated by the other (Hargreaves, Priestly Taylor and Makkink) methods.

RESULTS

Missing values in weather parameters data set were filled using regression equation. To achieve this, six nearest reference stations from each candidate station were selected. The parameters R^2 (coefficient of correlation) and b (slope) [The value of ($R^2 \geq 0.7$) and b value ($0.7 \leq b \geq 1.3$)] were used as criteria to select best nearby reference station. And both candidate and reference stations were found homogeneous, these conditions were satisfied between candidate and reference stations. Later, missing values in the candidate station were filled with respect to reference station using regression equation. Finally, the filled data set were used to estimate ET_o using different empirical methods, and also used as input for spatial interpolation to estimate spatial distribution of ET_o.

The range of ET_o during monsoon season by the FAO56-PM was varies from 1.75-7.49 mm/day, Priestley-Taylor method was varies from 2.16 – 7.63 mm/day, Makkink was from 1.64 – 7.19 mm/day and Hargreaves method was from 3.17 – 7.77 mm/day. The ET_o values for the station situated in hilly region of Tamil Nadu, found very less due to low temperature and high relative humidity. ET_o values were maximum in the first week of the month June and in the remaining months constant ET_o values were found when estimated with FAO-PM, Priestly Taylor and Makkink methods but Hargreaves equation over estimated ET_o, because it consider only temperature parameter but not the humidity.

The ET_o values for the station situated in coastal region of Tamil Nadu, were found maximum in this region, this is due to high temperature and high relative humidity and Hargreaves and Priestly Taylor methods yielded similar ET_o values compared to FAO-PM method, where as Makkink methods underestimated ET_o. This is due to temperature plays a major role in the coastal regions and temperature is main parameter required by Hargreaves equation.

The comparison was made on the basis of statistical analysis. Table 1 shows the statistical results. The mean bias error (MBEs), for estimated ET_o by applying Priestley-Taylor, Hargreaves, Makkink methods, and compared to FAO-56 PM estimated values, were 0.642, 0.9224 and -0.135 mm/day respectively.

Indices	Priestly-Taylor	Makkink	Hargreaves
R^2	0.850	0.699	0.320
MBE (mm/d)	0.642	-0.135	0.922
S_d^2	0.622	0.350	1.851
RMSE (mm/d)	0.756	0.506	1.235
RMSE(s) (mm/d)	4.096	4.487	7.604
RMSE(u) (mm/d)	3.671	4.374	8.141

Table 1. Statistical measures of different methods with FAO-PM method

To obtain spatially distributed ET_o, weather parameters data were spatially interpolated using Inverse Distance Weighted (IDW) technique. The maps of

spatially distributed ET_o over Kerala and Tamil Nadu states for 18 weeks of kharif season for the year 2010 were generated. The spatial processed results are continuous surfaces which contains values in all over their surface. Actually these are raster data that each cell corresponds to one value of ET_o. The spatial modeling of ET_o enables the understanding of the spatial variability of the ET_o for every 2 km grid. It provides the basis for spatial mapping of ET_o, for 18 weeks. In this study area average temperature varies from 17^0C minimum to 35^0C maximum. The net radiation depends on air temperature, land surface temperature, albedo, solar zenith angle, julian day and elevation. The typical ET_o values of specially distributed in the region is shown in Fig 2 & 3.

ET_o was found maximum in the coastal regions of Tamil Nadu. On contrary, minimum ET_o values were found in Kerala because of the low temperature, since it gets rain during southwest monsoon season. Generally ET_o will be minimum in the rainy season. It can be observed that ET_o in the plain area is almost higher than that in a hilly areas, because of low temperatures and high relative humidity at the higher elevation. The maximum value of 6.572 mm/day and 6.0925 mm/day and a minimum of 2.096 mm/day and 1.896 mm/day has been found in the months of June and September.

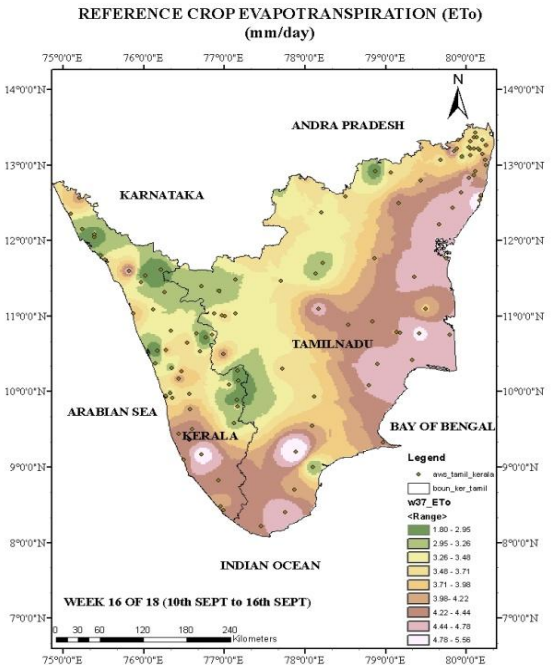


Fig 2. Spatial Distribution of ET_o of the 15th week

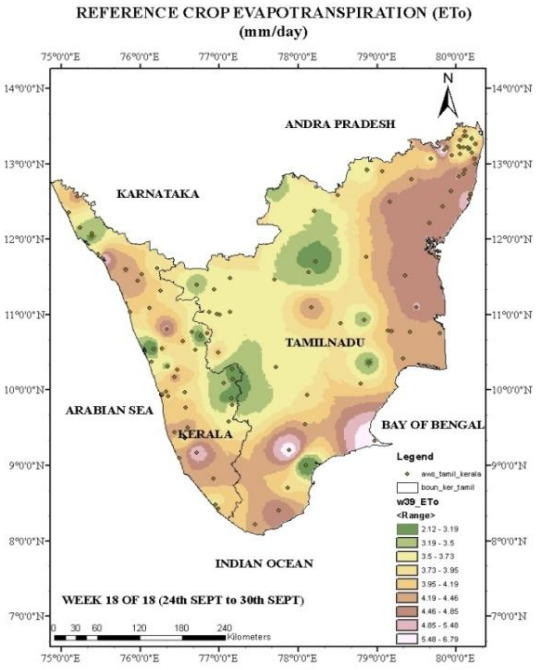


Fig 3. Spatial Distribution of ET_o of the 18th week

References.

1) Chard G. Allen, Luis S. Pereira, Dirk Raes, Martin Smith (1998) " Crop evapotranspiration - Guidelines for computing crop water requirements FAO Irrigation and Drainage paper 56", Food and Agriculture Organization of the United Nations.

2)Droogers, P., and Allen, R.G. (2002): Estimating reference evapotranspiration under inaccurate data condition. J. Irrig. Drain. Syst., 16(1), 33-45.
3) J. Fox. Statistical models for non-experimental data: A comment on Freedman. Journal of Educational Statistics, 1987 12:161-164.
4)Gavilan, P., Lorite, I.J., Tornero, S. and Berengena, J. 2006: Regional calibration of Hargreaves equation for estimating reference ET in a semiarid environment. *Agric. Water Manage.,* 81(3), 257-281.
5) Hargreaves, G.H., and Allen, R.G., 2003: History and evaluation of Hargreaves evapotranspiration equation. *J. Irrig. Drain. Eng.,* 129(1), 53-63.
6) Paul E Dodds, Wayne S Meyer and Annette Barton A Review of Methods to Estimate Irrigated Reference Crop Evapotranspiration acrossAustralia, CRC for Irrigation Futures Technical Report No. 04/05
April 2005
7)Trajkovic, S., and Kolakovic, S., 2009: Evaluation of reference evapotranspiration equations under humid conditions. *Water Resour. Manage.,* 23, 3057-3067.
8)Tsanis, I.K., and Naoum, S., "The Effect of Spatially Distributed Meteorological Parameters on Irrigation Water Demand Assessment", Advances in Water Resources, 26, 311-324, 2003.
9) Wlllmott, C. J. (1981). On the valldatlon of models. Phys. Geogr. 2: 184-194.

2nd International Engineering Symposium - IES 2012
(KU-MU-NITK-HCMCUT Joint Symposium) March 5-7, 2012, Kumamoto University, Japan

CUBE based Trip Generation Using Iterative Zone-reclassification, and Distribution for Bangalore

VARGHESE GEORGE [1] **SUBRAMANYAM U.V.** [2] and **Amit S. Mahendrakar** [3]

1 *Department of Civil Engineering, National Institute of Technology Karnataka, Mangalore – 575025, Karnataka, India. E-mail : varghese@nitk.ac.in*
2 *Former student, Department of Civil Engineering, National Institute of Technology Karnataka, Mangalore – 575025,Karnataka, India.*
3 *Former student, Department of Civil Engineering, National Institute of Technology Karnataka, Mangalore – 575025,Karnataka, India.*

Abstract: This study deals with the development of an approach to model trip-generation and distribution for the City of Bangalore using data compiled in 2002. Since the initial attempts at development of reliable trip-generation regressions using *SPSS* were un-successful, an iterative zone-reclassification approach was adopted in modelling the trip-productions and attractions. The reclassification of zones was performed based on the assumed influence of various groups of zones, the location of production and attraction centres and their nearness, and the improvement in the R-square value of regressions developed at each iteration. Finally, the 159 zones of the city were broadly categorized into twelve influence areas, and the trip-generation and distribution studies were performed using *CUBE* software. The predictions for the base year were verified with the actual data. Predictions for 2011 and 2021 were then performed.

Keywords*: modelling, transport, trip-generation, distribution, CUBE, Bangalore*

Introduction

Transportation occupies an important place in modern life and contributes to the economic, industrial, social and cultural development of any country. The ability to move people and goods from one location to another is the primary function of a transport system. The capabilities of modern transport technology have not been fully exploited to a large extent in Indian cities due to the limitations imposed by uncontrolled urban growth and rapid industrialization. Limitations in the availability of economic resources also have compounded the problems. The increasing accident rates, traffic delays and ineffective use of urban transport systems and poor accessibility form a major part of the problems faced by present urban transport systems.

In order to overcome these problems a systems approach is adopted in urban transport planning rather than relying on adhoc solutions to complex urban transport problems. The *transportation planning process* provides the basic framework for decision makers in the field of urban transport planning, in identifying strategies for improving the performance of urban transportation systems.

The modelling approach adopted in this study involves the use of the traditional 4-stage modelling process comprising – trip-generation, trip-distribution, modal split, and traffic assignment. However, trip-generation modelling exercises pose problems resulting in the inability to develop reliable regression equations. This study focuses on *SPSS* (Statistical Package for Social Sciences), and *CUBE* based trip-generation modelling using iterative zone-reclassification, and trip-distribution modelling for the City of Bangalore.

Literature Survey

Bruton (1985) provides an overview of studies performed at West Midlands in 1964, Greater Glasgow in 1964, Teesside

in 1965, Belfast in 1965, the SELNEC studies in 1965, Merseyside in 1966, West Yorkshire in 1967, and Tyneside in 1967. These investigations provided valuable information on the importance of land-use in the planning process.

In India, Chari (1985) performed a study on the importance of land-use models in traffic planning of Warangal city near Hyderabad. The studies indicated that land-use played a vital role in the location of basic industries in urban areas. Sarna et al. (1989) adopted the traditional four-stage transport planning process for the analyses and projection of urban transport demand for New Delhi. The study recommended the introduction of Mass Rapid Transit Systems including High Capacity Bus-ways in order to satisfy future demands.

Robillard (1975) formulated a linear regression model to estimate an O-D matrix that could produce estimated link-flows similar to those observed. Van Zuylen and Willumsen (1980) suggested an information minimization model and an entropy-maximization model for the estimation of O-D trip matrix. Wang et al. (2006) experimented with the concept of *entropy* as applied in the field of information theory to describe trip-distribution. Willumsen (1984) extended the static O-D matrix estimation problem and applied the maximum entropy approach in the O-D matrix estimation problem with multiple time-intervals.

Anderson and Olander (2002) examined the practically of using a single internal trip purpose to generate the production and attraction values for traffic analysis zones in small urban-community travel-models. Wong et al. (2005) performed a study on the estimation of the O-D matrix using a dynamic trip assignment model for congested highway networks of Hong Kong city. The studies concluded that assignment-based origin-destination (O-D) estimation problem formulated in an entropy-maximization model was necessary for congested traffic to estimate time-dependent O-D demand cost-effectively without neglecting congestion effect.

RITES (2003) adopted the multinomial logit-model approach for mode-choice modelling of trip-data collected as part of the Inter-modal Survey for Commuter Rail System in Bangalore in the year 2003 for Infrastructure Development Department of Karnataka. The models were calibrated for various modes such as cars, two-wheelers, and bus-trips using time and cost as variables.

Study Area Characteristics

Bangalore, known as the 'Silicon Valley' of India, is expanding at a rapid phase due to the rapid growth of the IT industry, and other industrial activities. The rapid growth of this city has resulted in overcrowding, traffic delays, congestion, and air and noise pollution.

The Bruhat Bengaluru Mahanagara Palike (BBMP), or in other words, the Greater Bangalore Development Corporation, presently occupies a vast area of 750 sq.km. The trips of this region are influenced by a number of factors such as zonal population, zonal employment and student-enrollment, nearness to production and attraction centers of the city, zonal-income, and land-use characteristics.

The lack of a reliable database on urban trip-making has resulted in haphazard urban development, and ineffective operation of public transport systems. The data collected and compiled by RITES Bangalore (2003), based on the Inter-modal Survey Conducted in 2002, made available for academic purposes, was used in this study.

Scope and Objectives

This work provides an overview on trip-generation and trip-distribution using *Cube* software for the City of Bangalore. The various steps in this work are as follows:

1. Data on population, employment, and student-enrolment of the zones in the city, road network and node-link diagrams, and origin-destination trip-matrices, are compiled.
2. Studies are performed on the development of regressions for trip-productions, and trip-attractions, using *SPSS*.

3. Re-grouping of the 159 zones of the city under various categories is performed, based on criteria explained in the methodology described below.
4. Regression analyses are again performed as in step 2 above, and the zones are further regrouped as in step 3 to ensure improvements in the R-square values of 12 families of relationships tested, including multi–linear regressions and power functions, in this iterative approach.
5. The final set of regressions developed, are used as input to the trip-generation module in *CUBE* software, and the trip-productions and attractions predicted are verified.
6. The trip-distribution exercise is the performed using the *CUBE* software, and the trips predicted are verified.

Basic Theory

The gravity model approach adopted in this work, derives its strength from the theory of *demographic gravitation* (Stewart, 1948), a concept of social-physics, where the motivational force for travel (F), can be expressed as a function of the populations (N_1 and N_2) at the origin and destination of trips, and the distance of travel (d), using the expression,

$$F = N_1 . N_2 / d^2 \quad (1)$$

Vorhees (1956) formulated the expression for the gravity model in the form,

$$Tij = O_i . D_j . f(C_{ij}) . K_{ij} / \Sigma [D_j . f(C_{ij}) . K_{ij}] \quad (2)$$

where, T_{ij} = number of trips predicted between the origin zone i and the destination zone j; O_i = number of trips produced at zone i; D_j = number of trips attracted by zone j. $f(C_{ij})$ = *deterrence-function* or *friction-factor*; C_{ij} = cost or impedance of travel time from i to j; and K_{ij} = zone-to-zone adjustment factor.

The CUBE software used in this work employs the BPR (1965) approach in the calibration of the gravity model. But this method is considered to perform computations for a production-constrained system (Black, 1981). Hence, the second phase of this approach utilizes a production-attraction balancing exercise. Also, in the initial phase of BPR calibration, the zone-to-zone adjustment factor (K_{ij}) is assumed to be unity.

The Methodology

1. Attempts at the development of trip-generation regressions for the entire 159 zones succeeded only in generating relationships with R-square values ranging between 0.058, and 0.084.
2. In the next step, the heart of the city including the *Vidhan Soudha* (Legislative Assembly Complex) was chosen as the major activity center, and the zones under the influence of this region was identified based on the assumed zonal-influences, proximity between production and attraction centers, and origin-destination data-compliance. In this step, 38 zones that were outside the influence-zone were eliminated. This resulted in a smaller OD matrix of 121x121 size, with trip-generation regressions with R-square values of around 0.125.
3. In the next step, the ratio between zonal-employment or population and the total-trips generated was considered, and the zones having a ratio greater than 4 to 5 were eliminated, reducing the matrix size to 90x90, yielding trip-generation equations of R-square values of about 0.48.
4. The 69 (38+31) zones eliminated in the previous two steps were grouped together, and a few more zones were eliminated based on criteria explained in step 2. This resulted in a matrix of 52x52 size yielding trip-generation equations of R-square values of about 0.65. This matrix was named as Category 1 (Indiranagar).
5. Zones that were found to occur repeatedly in various zone categories were eliminated by pair-wise comparison as far as possible. Thus categories 1 to 7 were identified. However, some of the zones are seen to occur in two categories. E.g., zones

7 and 98 of category 4 also appear in category 7.

6. Iterating the zone-reclassification described in steps 2, 3, and 4, the 159 zones were finally classified under twelve categories of OD matrices, yielding trip-generation equations of higher R-square values ranging between 0.75 and 0.99. Categories 8a (with 41 zones), 8b (with 9 zones), and 8c (with 4 zones) constitute the *central region*; categories 1 (with 16 zones), 2a (with 8 zones), 2b (with 6 zones), 3 (with 7 zones), 5 (with 25 zones), 6a (with 10 zones), and 6b (with 11 zones) comprise the *suburban region*; and categories 4 (with 28 zones) and 7 (with 13 zones) constitute the *outer region*. Table 1 provides details of the regressions developed for the suburban region of the city, while Table 2a and Table 2b give details on the analysis of prediction errors.

7. The trip-production and attraction models developed above were used as an input to the *CUBE* module for trip-generation and distribution. Additionally, the shortest path matrix, and the existing origin-destination (OD) matrix for the category of zones tested were also provided as inputs.

8. The trip-distribution was performed using *CUBE* for various forms of *friction-factors* in combination with various types of *level of service* (LOS) functions to obtain the best predictions. A compound deterrence function such as the Tanner's (1961) model, was also used.

9. The model predictions were verified with the actual trips for the base year 2002, and further predictions for 2011, and 2021 were performed.

Results and Discussions on Trip-generation Modelling for the suburban region

In Table 1, it is seen that in the case of zones in Category 6(a) under the suburban region, the trip-generation models with additive constants of reasonable magnitudes gave very high R-square values of about 0.99, ensuring better prediction accuracies. In the case of trip-predictions in Category 1 under the suburban region, the adjusted R^2 values for the models used in predicting trip-productions, trip-attractions, and total-trips were 0.87, 0.89, and 0.88 respectively.

The regression models for Category 1 were used to validate the trip generations of the zones in that category, for the base year data of 2002. See Table 2a. Here, it can be seen that the average error in the prediction of trip-productions, trip-attractions, and total-trips among the zones (AEZ) were 29.72%, 37.11%, 32.98% respectively. Additionally, Table 2b shows that the prediction errors at the category level (PEC) in the prediction of trip-productions, trip-attractions, and total-trips were -9.18%, -7.82 %, and -8.50 % respectively. This indicates that the trips predicted are under-estimated.

Results and Discussions on Trip-distribution Modelling for the suburban Region

Using the existing OD for the zones in the category tested, the shortest paths, and the trip generation models developed, the trip-distribution modelling was performed in *CUBE*. The results of the modelling exercise for trip-distribution performed using *CUBE* were analysed. Table 3a provides details of the best combinations of *friction-factors* and *level-of-service functions* used in modeling trip distributions for various categories. CUBE also performed the balancing of the productions and attractions.

The trip-distribution output provided by *CUBE* was then analyzed for the base year data of 2002. The trip-frequency distribution table for trip-distributions performed for the zones in Category 1, were compiled using the predicted trip-distributions, the actual OD, and the shortest path matrix. See Table 3b. The average of the predicted errors for trips classified under various distance ranges was found to be 7.94%. Fig.1 illustrates the trip frequency distribution. Since the prediction errors were found to be within a tolerance level of +/- 10%, the predicted trip-distributions were considered to be

acceptable. Similar predictions were made for 2011, and 2021.

Conclusions

The results of the trip-generation modeling exercise compiled under Table 1, Table 2a, and Table 2b indicate that trip-generation in the suburban area of Bangalore city is significantly influenced by the population, employment, and student enrolment in the zones. The trip-distribution performed using *CUBE*, closely followed the actual trips provided by the OD matrix for the base year data, as evident in Table 3b, and Fig.1.

Based on the above observations, it can be inferred that trip-distributions for the future can be performed with a reasonable level of accuracy for 2021 if the productions and attractions for 2021 are made available. The basic justification for this assumption is that the travel times remain almost stable in large cities although much changes take place in household income, family structure, land use, and labor participation (Levinson and Kumar, 1994; Barnes and Davis, 2000).

Acknowledgements

The authors acknowledge the kind gesture of RITES Bangalore, in providing the OD data, and the shortest path distances based on surveys performed in 2002 for 159 zones of the City of Bangalore. Acknowledgements are also due to the Ministry of Human Resource Development, Government of India, for providing financial resources for the purchase of *CUBE* software.

References

[1] Anderson, D.M. and Olander, P.J. (2002) Evaluation of Two Trip Generation Techniques for Small Area Travel Models, *Journal of Urban Planning and Development* 128(2): 77-88.

[2] Barnes, G. and Davis, G. 2000. Understanding Urban Travel Demand: Problems, Solutions, and the Role of Forecasting, University of Minnesota Center for Transp. Studies: Transp. and Regional Growth Study

[3] Black, John (1981) Urban Transport Planning, Croom Helm Ltd., St. John's Road, London SW-11.

[4] BPR (1965), Calibrating and testing a gravity model for any sized urban area, Rerport, Bureau of Public Roads (BPR), U.S. Department of Commerce, Washington DC.

[5] Bruton, M.J. (1985) A textbook on *Introduction to Transportation Planning.* London, UCL Press.

[6] Chari, S.R (1985) Application of Land Use Transport Models for location of Basic Industries in Urban Areas, *National Seminar on Metropolitan Transport in India,* New Delhi, March 1-2.

[7] Levinson, D. and A. Kumar 1994 The Rational Locator: Why Travel Times Have Remained Stable, J. of the American Planning Association, 60:3 319–332

[8] RITES (2003) Inter-modal Survey for Commuter Rail System, Bangalore, Prepared for Infrastructure Development Department of Karnataka and MTP Railway (Chennai), RITES India Ltd., Bangalore.

[9] Robillard, P. (1975) Estimating the O-D Matrix from observed link volumes *Transp. Res.* 9: 123-128.

[10] Sarna, A.C., Prakash, A., Mukhopadhaya, D., Bhatiya, N.L., Suthar, H.H. (1989) Planning of Mass Rapid Transit System-a Case Study of Delhi, *IRC Journal* 53(3): 553-587.

[11] Stewart, John Q., "Demographic Gravitation: Evidence and Applications," *Sociometry*, Vol. 11, No. 1/2. (Feb. - May, 1948), pp. 31-58.

[12] Tanner, J. C. (1961). Factors affecting the amount of travel, Road Research Technical Paper No. 5, Her Majesty's Stationery Office, London.

[13] Van Zuylen, H.J. and Willumsen, L.G. (1980) The most likely Trip Matrix estimated from traffic counts, *Transportation Research Part B* 14: 281-293.

[14] Voorhees, Alan M. (1956) *A General Theory of Traffic Movement,* Proceedings of the Institute of Traffic Engineers, New Haven, Connecticut.

[15] Wang, Dian-Hai, Yao, Rong-Han, and Jing, Chao (2006) Entropy Models of Trip Distribution, *Journal of Urban Planning and Development* 132:1 (29): 29-35. http:// dx.doi.org /10.1061/(ASCE)0733-9488(2006)132:1(29)

[16] Wong, K.I., Wong, S.C., Tong, C.O., Lam, W.H.K., Lo, H.K., Yang, H., and Lo, H.P. (2005) Estimation of Origin-Destination Matrices for a Multimodal Public Transit Network, *Journal of Advanced Transportation* 39(2):139-168.

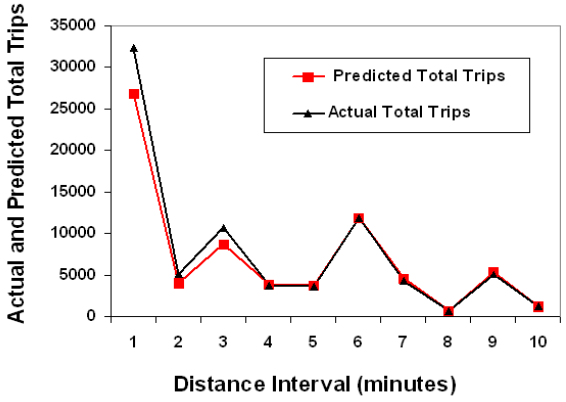


Fig. 1 Trip Frequency Distribution Curve for Zones in Category 1

Table 1 Summary of Regressions for Trip Generation for the Suburban Region

Category	Regression Function	TG	Additive Constant	Coefficients of Independent Variables			R^2 Value	F-test Value
				X	Y	Z		
1	Linear$^{\theta}$	A	-	0.075	-0.001	0.229	0.870	29.121
		B	-	0.070	0.008	0.250	0.891	35.387
		C	-	0.145	0.007	0.479	0.882	32.236
	Power	A	-	96.950	93.182	333.514	0.834	21.704
		B	-	59.477	150.013	335.090	0.833	21.631
		C	-	156.427	243.195	668.604	0.834	21.795
6(a)	Linear	A	-	0.053	0.021	-0.004	0.981	119.536
		B	-	0.053	0.021	-0.002	0.980	116.566
		C	-	0.106	0.042	-0.006	0.981	118.126
	Power$^{\theta}$	A	-54.852	1.18E-4	0.024	0.052	0.992	262.972
		B	-60.607	1.17E-4	0.027	0.053	0.992	256.709
		C	-115.459	2.36E-4	0.047	0.105	0.992	260.556

TG = Trip generation models developed; X = population; Y = employment; and Z = student enrolment;
F values mentioned above were considered for regressions with a minimum confidence level of 95%;
- denotes categories where the F-test, t-test and standard error values are not generated by SPSS, since the number of zone under these categories are lesser; and
θ denotes regression equation selected for performing trip-generation using *CUBE*.

Table 2a Validation for Trip-generation Models using Data for 2002 for Category 1 (Sub-urban Region-Partial List)

Zone No	Error in Predictions for Zones (%)		
	Trips Produced	Trips Attracted	Total Trips
67	27.70	19.57	23.36
69	36.81	32.21	34.48
74	54.37	50.85	52.65
75	16.08	11.17	13.69
152	9.30	5.34	7.29
Total	27.70	19.57	23.36
AEZ (%)	29.73	37.11	32.98
PEC (%)	-9.17643	-7.82456	-8.5005

Table 2b Prediction Errors at the Category Level for Trip-generation Models using Data for 2002 for All Zone Categories – Partial List

Category	Error in Predictions at the Category level - PEC (%)		
	Trips Produced	Trips Attracted	Total Trips
1	-9.176	-7.824	-8.500
2(a)	-4.345	-5.100	-4.590
6(a)	-0.016	-0.009	-0.029
7	-2.090	-1.289	-1.688
8(a)	-0.038	-0.050	0.000
8(b)	-0.125	0.082	-0.040

Table 3a Combinations of Friction-Factors and Level-of-Service factors Adopted for Trip Distribution (Partial List)

Category	Friction Factor Tested	Level of Service Tested
1	$1/s^2$	$1/s^2$
2a	$1/s^2$	$1/s^2$
6a	$1/s^2$	$1/[s^2.\ e^{s^2}]$
7	$1/s^2$	$^{\#}1/[s^2.e^{s2}]\{1/c_1+1/c_2\}$
8a	$1/s^2$	e^s

S = shortest path distance; and
A_1, C_1, C_2 =constants.
$^{\#}$ Tanner's Model (1961)

Table 3b Trip Frequency Distribution Table for the Category 1 (Sub-urban Region-Partial List)

Distance Interval (minutes)	Pre-dicted Total Trips	Actual Total Trips	Ave-rage Error (%)
1	26844	32383	17.1
2	4053	5043	19.6
3	8727	10702	18.5
10	1244	1200	3.70
Total			79.4
Average error in the distance intervals			7.94

2nd International Engineering Symposium - IES 2012
(KU-MIT-NITK Joint Symposium) March 5-7, 2012, Kumamoto University, Japan

Road Development in Mangalore City – A Scenario

Chandan C Gowda [1] **H C Chinnagiri Gowda** [2] and **Arun Kumar G**[3]

1 *Department of Civil Engineering, NMAM Institute of Technology, Nitte-574110, Karkala Taluk, Udupi District, Karnataka, India, Email; chandu627@gmail.com*
2 *Principal, Government Polytechnic Bantwal 574211, Karnataka, India Email: chinnagiri_hc@yahoo.co.in*
3 *Junior Engineer, Mangalore City Corporation, Mangalore-575002, Karnataka, India.*

Abstract: Road is one of the important connectivity for the development of the country. In a city like Mangalore which is the second most developing city in Karnataka state of India, having a population of around 700,000, a lot of development has taken place over a decade. Over the past 5 years there has been significant development of new, as well as existing roads. Most of the flexible pavements are being converted into rigid pavements and wider roads resulting in decrease of congestion and lesser accidents. It has also helped to achieve improvement in fuel economy and continuous flow of vehicles. This paper discusses about the road developments taken place in Mangalore over a decade regarding the total length of roads, types and width of roads and other related issues.

Keywords*: road developments, flexible pavement, rigid pavement*

Introduction

Roads play a vital role in economic development and social progress of the country. Mangalore, (12.87°N 74.88°E) running with most of its length along the coastal line is located between the Arabian Sea and the western ghat mountain ranges. Mangalore has an area of 132.45 km^2 with a tropical climate. The average temperature in summer is 38°C and in winter is 17°C. It receives rainfall from May 15th to October 15th with an average annual rainfall of 3479mm. Mangalore has an important necessity for connecting the rest of the state because Mangalore's port handles 75 per cent of India's coffee exports and the bulk of the nation's cashew exports. Moreover Mangalore, with abundant mineral transportation, high growth in agricultural and industrial production, need a well developed road network to cater to the intra-state and regional traffic.

Three National Highways pass through Mangalore viz NH-66 (17) linking Panvel and Kanyakumari, NH-75 (48) linking Mangalore and Bangalore, NH-175 (13) linking Mangalore and Solapur.

Different types of pavement are adopted for construction which provides smooth transportation of the vehicles. Over the years significant development is taking place for improving the type of pavements.

Pavements

Two types of pavements are adopted depending on the load distribution. They are

1. Flexible pavement and
2. Rigid pavement

Flexible Pavement

These are the pavements having negligible flexural strength. They consist of 3 layers i.e. surface course, base course and sub base course, below which the soil subgrade will be present.

Each layer receives loads from the above layer, spreads them out, and passes on these layers to the next layer below. The load transmission is by grain to grain transfer through the points of contact. Thus the stresses will be reduced, which are maximum at the top layer and minimum on the top of the subgrade. In order to take maximum advantage of this property, layers are usually arranged in the order of descending load bearing capacity with the highest load bearing capacity material on the top and the lowest load bearing capacity material at the bottom.

So maximum compaction is necessary for load distribution through a larger area. It depends on the materials used for construction as well. Bituminous pavement is an example for flexible pavement. Flexible pavements are so named because the total pavement structure deflects or flexes under loading.

In Mangalore, over a decade ago all the roads were of flexible pavements, whereas now both rigid and flexible pavements are being constructed.

The existing lengths of flexible pavement roads are as given in table 1.

Table 1: Details of flexible pavements

Road Width (In m.)	Flexible	Existing (In km.)	Proposed (In km.)	Total (In km.)
45	0	0	0	0
30	8	8	0	8
24	0	0	0	0
18	83	71	12	83
12	194	165	29	194
9	119	101	18	119
6	577	490	87	577
Total	981	835	146	981

The process of laying the flexible pavement involves many steps. The 2 types of laying of flexible pavements are ordinary asphalting and asphalting by using paver finish.

Ordinary asphalting

After surveying and designing, the site is levelled either by filling or cutting. In case of filling, the sand and soil are mixed in the ratio of 1:4 and is laid in layers; with each layer being 15cm till the required height is obtained. In case of cutting, the extra soil is removed up to the required depth. The ground is then checked for level. Hence the soil sub grade is prepared. In ordinary asphalting, following levelling of soil subgrade the preparation of sub base course is done. This involves spreading of grade II aggregate gravel of 63-45mm thickness. It is later compacted in layers for required thickness. Over this, a layer of murrum is spread and watered. The whole is compacted again. Then the road is allowed for vehicular movement for a period of 15 days for better compaction. Base course is prepared by spreading a layer of grade III aggregate gravel of 45-25mm thickness and it is compacted for required thickness. Over this a layer of murrum is spread, watered and compacted again. This is then allowed for vehicular movement for a period of another 15days for compaction. The sub base course and the base course together forms the water bound macadam (WBM Figure 1).

Then the cleaning of water bound macadam (WBM) surface is done using small picks and wire brushes. Finally dusting with compressed air to prepare the surface to receive bituminous treatment.



Figure 1: Sub base course- WBM

Over the prepared surface a tack coat is applied at the rate of 10kg/10 m^2 in which heated bitumen is sprayed with a spray set.

Finally the surface course is laid which includes a layer of 20mm thick wearing coat involving 20mm downsize aggregate gravel and another layer of 6mm thickness seal coat is applied for surface finish.

Paver finish asphalting

In Paver finish asphalting the sub base course consists of sub base and base course of ordinary asphalting. The procedure being the same.

Then surface dressing is done by using crushed stone chippings and bitumen at 18kg/10 $m^{2.}$ This is laid on prepared sub base surface. Base course of bituminous macadam (BM Figure 2) is laid over it for a thickness of 50mm and it is spread by using paver finish machine and compacted by using vibratory roller.



Figure 2: Base course of flexible pavement BM

The surface course of semi dense bituminous concrete (SDBC Figure 3) of 25mm thick is laid and levelled by using the paver machine and compacted by using vibratory roller.

Rigid pavement

Rigid pavements are the ones with no or very little flexural strength. These are made up of concrete, which maybe plain, reinforced or prestressed. The grade of concrete depends on the traffic density of the road. The concrete thickness varies from 6-11 inches. Rigid pavements have



Figure 3: Surface course- SDBC

slab action and transmits the wheel load stresses through wider area below.

The main point of difference between rigid and flexible pavement is that the critical condition of stress in the rigid pavement is the maximum flexural stress occurring in the slab due to the wheel load and temperature changes where as in flexible pavement it is the distribution of compressive stresses. Rigid pavements do not get deformed when the lower layer gets deformed.

Use of rigid pavements started in Mangalore over a decade ago. Rigid pavements are being used (for wider roads of 24m and 30m) because of its life span of minimum 30 years as compared to flexible pavements which has a maximum life span of 10 years. Table 2 shows the details of rigid pavements

In the process of laying rigid pavements the first step is same as that in flexible pavements i.e. either filling (Figure 4) or cutting depending on the site. Then a layer of dry lean concrete (DLC Figure 5) is provided for a thickness of 15cm which is also used as levelling coarse.

Table 2: Details of rigid pavements

Road Width (In m.)	Rigid	Existing (In km.)	Proposed (In km.)	Total (In km.)
45	53	0	53	53
30	60	50	10	60
24	54	46	8	54
18	0	0	0	0
12	0	0	0	0
9	0	0	0	0
6	0	0	0	0
Total	167	96	71	167



Figure 4: Sub grade preparation

On this layer of dry lean concrete (DLC) polythene sheet (Figure 6) is provided so as to retain the water in case of segregation.



Figure 5: Dry lean concrete

On this the final layer of concrete is placed and a smooth finish is given. The thickness of this layer is 27.5- 30cm.



Figure 6: Polythene sheet below fresh concrete to maintain W/C ratio



Figure 7: Finished rigid pavement

The major development of roads in Mangalore started due to the first US$20 million budget plan from the state government. Whereas now the second US$20 million budget plan is progressing with prime importance to the development of storm water drainage, footpath and remaining completion of roads. The total road length of different widths of roads existing and proposed is as shown in the table 3.

Table 3: Details of existing and proposed pavements

Road Width (In m.)	Existing (In km.)	Proposed (In km.)	Total (In km.)
45	0	53	53
30	58	10	68
24	46	8	54
18	71	12	83
12	165	29	194
9	101	18	119
6	490	87	577
Total	931	217	1148

Advantages of rigid pavement
It has good durability, longer life service of 30 years. It also withstands repeated flooding and sub surface water without deterioration.

Disadvantages
Loss of non-skid surface at the top. It needs an even subgrade with uniform settling. It may fault at transverse joints and requires frequent joint maintenance. The overall maintenance is costlier. Wear and tear of wheels is more. Initial and construction cost is more.

Advantages of flexible pavements
Pavement gets adjusted to limited differential settlement. It can be easily repaired. Maintenance is easy and not costlier. Additional thickness can be added by any time of necessity. Non-skid properties do not deteriorate. The movement of vehicles are quieter and smoother. Flexible pavement tolerates greater range of temperature variations.

Disadvantages
Loses some flexibility and cohesion as time proceeds. The pavements need resurfacing sooner than rigid pavement. Not chosen where water is expected. It produces more air and dust pollution than rigid pavements. Production is costlier.

Conclusions
The necessity of using rigid pavements over flexible pavements recently, is due to heavy rainfall which Mangalore experiences for about 6 months a year. This results in economy when compared to flexible pavement in the long run. The objectives are to deliver safer, quicker and easier travel. This will result in local, regional and national benefits for business, industry and tourism. Reduces traffic congestion at peak hours, saves travel time, saving in fuel consumption by vehicles and thereby reduction in pollution. Also the cost of maintenance is reduced there by the same can be utilized for the development of city.

2nd International Engineering Symposium - IES 2012
(KU-MU-NITK-HCMCUT Joint Symposium) March 5-7, 2012, Kumamoto University, Japan

CHARACTERISTICS OF MALABAR LATERITE AS A BUILDING MATERIAL - Field and Laboratory studies

Kasthurba A K
Department of Architecture, NIT Calicut, India
kasthurba@nitc.ac.in

Abstract: This paper describes a comprehensive investigation of laterite from four representative quarries in Malabar region of Kerala, to assess its quality as a building material. The objective of this work is to characterize laterite from major quarries of Malabar region in western India for building purposes based on field and laboratory studies. An attempt has been made in this study to bring out a basis for selection of laterite for construction purposes from quarries based on its morphological and textural features. A schematic model showing morphological and textural variation of laterite at different levels of the profile and its effect on engineering properties has been brought out to simplify the selection of laterite for building purpose from quarries. The impact of morphological characteristics of laterite based on engineering properties is explained with the help of schematic models.
Key words: laterite, building material, engineering properties, morphological characteristics

INTRODUCTION

Laterite stone blocks are being used as prime material for architectural applications in Malabar region of western India for ages, because of being abundant, relatively easy to cut and shape and showing good performance in many applications. Due to the wide variations in appearance (colour, texture and structure) of laterite, it is often challenging for the engineers to identify and select laterite for building applications. Testing of laterite is cumbersome, due to the laborious specimen preparation procedures. An attempt has been made in this study to bring out a basis for selection of laterite for construction purposes from quarries based on its morphological and textural features. The objective of this work is to characterize laterite from major quarries of Malabar region in western India for building purposes based on field and laboratory studies.

SELECTION OF QUARRIES

The Malabar region consists of northern part of Kerala State, located in west coast of India between 74°30' E to 77°E longitude and 10°N to 12°30' N latitude Representative laterite quarries were identified and selected from regions popular for laterite mining (based on large volume of quarrying) from Malabar region of Kerala. Four widely scattered active quarries were selected for the study, based on the large volume of laterite mining. Selected quarries were in a widely scattered area located in 3 districts of Kerala namely, Kannur, Kozhikode and Malappuram, as shown in Fig. 1. Laterite from these quarries were identified and named after their respective quarry regions as, UL – Ulikkal and PTA - Panayathamparampa from Kannur district, MU - Muchukunnu from Kozhikode district and PM - Perinkulam from Malappuram district. The in-situ characteristics of laterite like colour, texture, structure, hardness and morphological variations with depth of a profile were studied.

Freshly quarried laterite blocks as supplied commercially, were sampled from different depths of each quarry. Engineering properties of laterite significant for its building application such as compressive strength, specific gravity and water absorption of were determined in the laboratory using standard procedures.

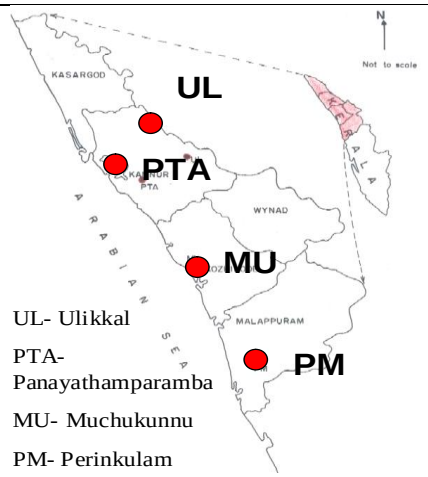


Fig. 1 Map showing location of selected quarries in three districts of Kerala

FIELD INVESTIGATIONS

Investigations were carried out on exposed laterite quarry profiles by examining the exposed vertical face. Distinct zones of morphological and textural variations were measured by tape and examined in the field with the help of an expert geologist. The hardness of different strata was measured using a Type P pendulum hammer (Proceq, 2005) at accessible locations. Readings were noted at 5 points, 50 cm apart along the horizontal plane at various levels as shown in Fig. 2.

Specimens were collected in the form of standard size blocks (390x190x190mm.) as per Indian standard codes for laterite stone masonry (IS 3620, 1979). Scratch test was conducted on specimen fragment (iron concretions) to determine the hardness based on mineral composition represented by the Moh scale of hardness (Reddy, 1996). The marked laterite block specimens were sealed and brought to laboratory for comprehensive characterization as a building material.

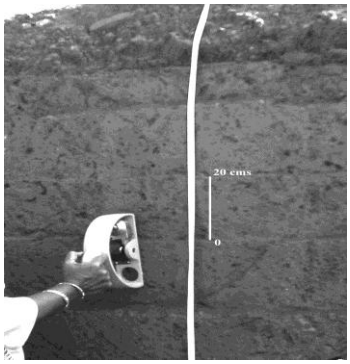


Fig. 2 Pendulum hammer reading being taken on the exposed face of the laterite quarry

LABORATORY INVESTIGATIONS

The compressive strength of laterite blocks of standard size were determined as per standards (ASTM C 170, 1990). Dressed and capped specimens were tested in saturated condition by loading in the direction perpendicular to the bedding plane until failure, as shown in Fig. 3.



Fig. 3. Compressive strength testing of laterite blocks

Large lumps were taken from the crushed specimen (after failure) to determine the physical properties, namely, specific gravity and water absorption as per standards (IS 1124-1974). Crushed aggregates passing through 40 mm and retained in 20 mm Indian standard sieve were used to determine physical properties.

RESULTS AND DISCUSSION

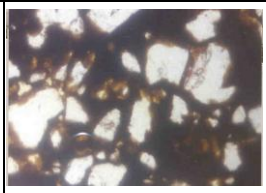
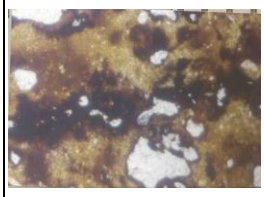
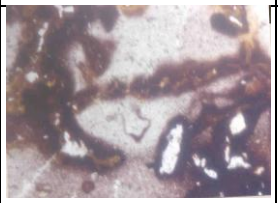
Textural variations, and the sample locations, are shown in Fig. 4. The depth wise variation in field characteristics and engineering properties are reported in Table1. The average values of 3 specimens are reported for each test. Detailed investigation was carried out for typical MU quarry profile to determine its field characteristics and geo-morphological variations.

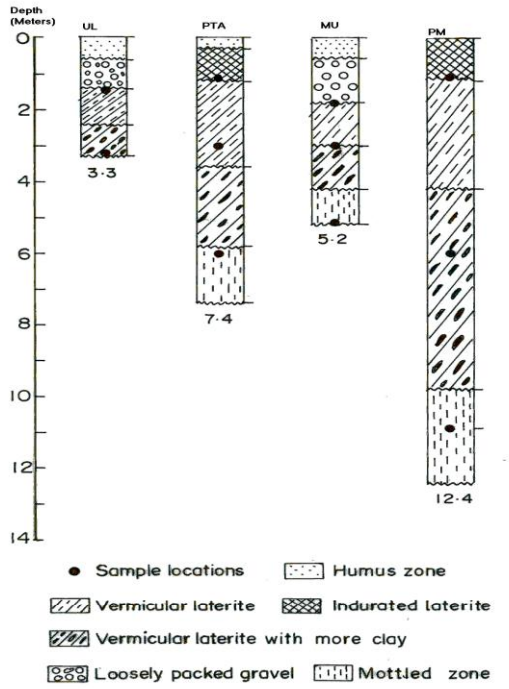
Characteristics of a Typical Laterite Profile (MU Profile)

The typical MU quarry selected for the study had a total depth of 5.2 m. Samples was taken from various depths of 1.8, 3.0 and 5.2 m from the top. Megascopic study was conducted using hand lens to study the structural and textural features. Microscopic study (thin section analysis) of the specimen was also conducted to

determine the mineral composition and its distribution in the matrix using a polarised microscope. The megascopic features and photomicrograph of the specimens from different strata of MU profile is given in Table 2.

Table 2. Megascopic and microscopic features of MU laterite profile

Depth (m)	Megascopic Study		Microscopic Study	
	Image Analysis	Remarks	Photomicrograph (40X)	Remarks
1.8		Dark brown to dark red, with yellow colour lining in the cavities		Ferruginous dense iron matrix with quartz grains embedded in it. Denotes highly matured laterite
3.0		Dark red to brown ferruginous materials filled with yellowish white clay		The matrix is essentially ferruginous. The matrix is more porous in nature
5.2		Red to pink streaks of iron minerals in a matrix of kaolinite mainly white and light yellow in colour		Dominated by the presence of clay minerals. Iron minerals are in the formation stage seen as thin channels in the clay matrix



UL-Ulikkal; PTA- Panayathamparampa; MU-Muchukunnu,; PM- Perinkulam

Fig. 4 Textural variations and sample locations of laterite profile of selected quarries

MORPHOLOGICAL VARIATIONS OF LATERITE PROFILE AND THEIR INFLUENCE ON ENGINEERING PROPERTIES

Based on scientific investigation of four representative quarries from predominant sources of laterite supply in Malabar region, it was found that laterite of different grades (based on compressive strength) were obtained from the same quarry from various depths. A schematic model has been brought out to simplify the selection of laterite for building purpose from quarries (based on morphological features of laterite within a profile). A schematic model showing morphological and textural variation of laterite at different levels of the profile and its effect on engineering properties (strength, hardness, specific gravity and water absorption are explained in Fig. 4.

Top portions of the profile contain high quantity of iron in crystalline and continuous form, resulting in dense packing. It is evident that higher

compressive strength and hardness of laterite from top layer of profile was due to the tight fit of iron mineral fabric. The dense ferruginous matrix offered high degree of resistance to failure. PM laterite belongs to this textural category, as shown in Fig. 5A. This laterite is often referred as matured type (by masons). MU laterite (Fig. 5B) has similar chemical composition and but shows variation in micro-texture due to embedding of quartz grains in the ferruginous matrix. PTA laterite belongs to the mottled variety where the ferruginous crystalline fabric is present as mottles/ streaks aligned in a clay matrix, as shown in Fig. 5C. This laterite is not matured; the ferruginous mottles attain continuity and induration by several wetting and drying cycles during the laterisation process. UL laterite is of intermediate type where the texture is a combination of mottled type and vermicular type.

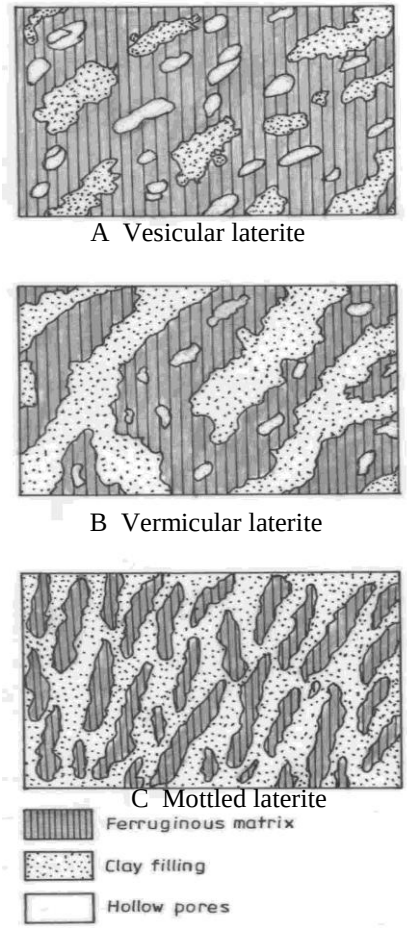


Fig.5 Schematic diagram depicting the morphological variation in specimens from different depths within a quarry

ANALYSIS OF RESULTS

The investigation of laterite for building purpose from Malabar region reveals that laterite shows a wide variation of engineering properties based on the geographic location and also within a quarry with depth. Hence, is not possible to define strength of laterite based on a region or quarry. However, a general guideline of selection of laterite for building purposes may be adopted based on this study. Even though profiles apparently appear unstratified, the morphological variations with depth can be distinguished by a close megascopic study. The thickness of concretionary laterite (suitable for building purpose) varies highly based on the region and depending on the formation. There is no good correlation between rebound number values obtained and the hardness categorization presented in Table 1. Presence of irregular cavities and clay

filled pores in laterite may be the reason for the disparity in the hardness values by rebound number. Hence field evaluation of laterite using pendulum hammer may not suitable for laterite.

The hard ferruginous vermicular laterite, dark reddish brown to red colour, occurs in the top portion of the profile, possesses high strength, specific gravity and low water absorption. This top portion of laterite, found to possess less clay content (yellowish white to white colour), can be categorised as good quality for building purposes. Specific gravity and compressive strength decrease with depth. The increase in water absorption of specimens with depth is seen in all laterite profiles. This may be attributed to the increase in clay content (Kaolinite) with depth as identified by the megascopic and microscopic study of the specimens presented in Table 2 (for MU). The decrease in strength and increase in water absorption with depth leads to a decline in the quality of laterite blocks of the deeper layers. This characteristic feature is common in all the four profiles studied. The high specific gravity and hardness of samples from top layers may be attributed to the presence of large quantity of iron (heavy minerals) in the top layers as seen by the megascopic studies. The dense and dark colour of laterite specimens from the top indicates the presence of mafic ferruginous minerals (goethite, magnetite and hematite) as seen from the megascopic study.

However, a minor deviation in this trend is observed in the behaviour of samples from top layers of PM and PTA profile (durricrust layer). The variation of compressive strengths of the specimens from the topmost durricrust layer may be due to presence of defects in the form of channels and pores, which causes an early failure of the specimen; this is in spite of high hardness and specific gravity of these specimens. Splits and cracks are also formed during the cutting and dressing operation of the durricrust laterite (hard and brittle in nature) than other types. The variation in compressive strength may be attributed to the presence of the micro-cracks during the specimen preparation. Hence, in such cases, laterite of good quality is taken from layers underlying the hard topmost layers. This is also a common selection procedure adopted by the practitioners.

SUMMARY

A general behavior of laterite for building purposes based on the study can be summarized as follows:

- Laterite is essentially heterogeneous, anisotropic rock consisting of hard ferruginous skeletal framework impregnated with soft clayey material. It contains lot of structural irregularities in the form of cavities and pores.
- The Malabar laterite can be categorized as weak rock (weaker than class B bricks of minimum strength 3.5 MPa) that can be used for low-rise buildings and partition walls.
- Laterite suited for construction purpose is mainly ferruginous in nature and of a vermicular type (continuous coherent mass).
- Compressive strength and specific gravity of laterite blocks decreases with the depth of quarry. The increase in water absorption of laterite samples of the deeper layers may be attributed to the increase in clay content (Kaolinite).
- Indurated laterite crusts seen at the top portion of laterite profile (as seen in PTA and PM laterite) are found to be brittle, and contain numerous structural irregularities as channels and pores. The strength of this laterite is found highly variable even though the specific gravity is high.
- Laterite of relatively good quality for building purpose (high compressive strength and low water absorption) was located in the top portion of profiles (below durricrust layer).

REFERENCES

1. **ASTM C 97** (2002) Standard test methods for water absorption and bulk specific gravity of dimension stone, ASTM, Philadelphia, USA.
2. **ASTM C170** (2004) Standard test method for compressive strength of

dimensional stone. ASTM, Philadelphia, USA.

3. **Karunakaran, C.** and **Roy, S.S**. (1981) Laterite profile development linked with polycyclic geomorphic surfaces in South Kerala, *Proceedings of international seminar on laterisation process, Trivandrum, India*, 221-231.
4. **Varghese, T.** and **Byju, G**. (1993), Laterite soils - Their Distribution, Characteristics and Management, *Technical Monograph No.1*, *State Committee on Science, Technology and Environment*, Government of Kerala, Thiruvananthapuram, India.
5. **Narayanaswamy** and **Rajendran, C.P.** (1987) A note on laterisation cycles associated with sedimentaries, Kasarkode district, Kerala, *Journal of Geological Society of India*, 30, October, 309- 314.
6. **IS 3620** (1979) Indian standard specification for laterite stone block for masonry, *Bureau of Indian Standards*, New Delhi, India.
7. **Reddy, D.V. (**1996) Decorative and dimensional stones of India, *CBS Publishers and distributors*, New Delhi
8. **Gribble, C.D.** (1988) Rutleys Elements of Mineralogy, 27th edition, *a Academic division of Unwin Hyman, London*
9. **Proceq.**(2005) http://www.proceq.com/english/produkte/betonpruefhammer.php.

Table 1 Variation in properties with depth of laterite profile

Field Investigations					Experimental Results				
Depth from top (m)	**Colour**	**Structure**	**Rebound Number**	**Remarks ***	**Depth (m)**	**Compressive Strength (MPa)**	**Specific gravity**	**Water absorption (%)**	**Hardness (Moh scale)**
UL Laterite									
1.8	Brownish Yellow	Vermicular	33-56	S	1.8	1.44	2.15	10.82	1-2
3.0	Whitish yellow	Vermicular	25-48	S	3.0	1.05	1.74	13.20	< 2
PTA Laterite									
1.0	Brownish red	Vesicular	40-62	H	1.0	2.42	2.67	9.74	3-4
3.0	Reddish brown	Vermicular	--	M	3.0	2.57	2.31	11.02	2-3
6.0	Red	Mottled	43-50	S	6.0	1.13	1.85	13.92	< 2
MU Laterite									
1.8	Brownish red	Vesicular	45-65	M	1.8	2.06	2.71	12.8	1-3
3.0	Yellowish red	Vermicular	38-54	M	3.0	1.86	2.07	14.30	< 3
5.2	Pink	Mottled	36-45	S	5.2	0.66	1.51	15.73	1-2
PM Laterite									
1.2	Reddish brown	Scoriacious	45-72	H	1.2	3.06	2.95	9.12	3-4
6.0	Brownish red	Scoriacious	--	M	6.0	3.19	2.23	10.20	3
10.8	Yellowish red	Vermicular	36-55	S	10.8	1.66	1.82	13.40	< 3

*Note: H – Hard; M – Medium; S - Soft

H = Hard - cannot break with hammer in one blow.

M = Medium hard - can break with hammer in one blow. S = Soft - can be broken with fingers

2nd International Engineering Symposium - IES 2012
(KU-MU-NITK-HCMCUT Joint Symposium) March 5-7, 2012, Kumamoto University, Japan

Damage level prediction of non-reshaped berm breakwater using ANFIS

S. Mandal[1], Subba Rao[2], Harish N[3] and Lokesha[4]

1 *Ocean Engineering Division, National Institue of Oceanography, Goa-403004, India. e-mail:smandal@nio.org,*
2 *Department of Applied Mechanics and Hydraulics, National Institute of Technology Karnataka, Surathkal, Mangalore 575025, India. e-mail:surakrec@gmail.com,*
3 *Department of Applied Mechanics and Hydraulics, National Institute of Technology Karnataka, Surathkal, Mangalore 575025, India. e-mail: harish.nitk@rediffmail.com,*
4 *Department of Applied Mechanics and Hydraulics, National Institute of Technology Karnataka, Surathkal, Mangalore 575025, India. e-mail: lokeshgouda@gmail.com*

Abstract: In the present study , the Adaptive Neuro Fuzzy Inference System (ANFIS) model is constructed using experimental data set to predict the damage level of berm breakwater. Experimental data for non-reshaped berm breakwater are collected from Marine Structures Laboratory, Department of Applied Mechanics and Hydraulics, NITK, Surathkal, India. The input parameters from experimental data are used to train the ANFIS model and results are determined in terms of statistical measures like mean square error, root mean square error, correlation coefficient and scatter index. The ANFIS results are compared with the Artificial Neural Network and concluded that ANFIS can be efficient tool in predicting the damage level of non reshaped berm breakwater.

***Keywords**: Berm Breakwater, Damage, ANFIS*

Introduction

Breakwaters are the structures constructed to provide protection to the port and harbor facility from dynamic forces of the ocean waves. They are used to protect beaches, cultivation land, and valuable habitats from erosion. From the past, physical models are developed and experiments are carried out to design safe breakwaters (Brunn P. et al. 1976, Baird and Hall 1984, Van der Meer 1988, Torum et al. 1999, 2003 and Subba Rao et al. 2004 and 2008) which are time consuming and expensive in terms of cost.

To minimize the cost and time in conducting the experimental work, the soft computing tools like Artificial Neural Network (ANN), Support Vector Machine (SVM), Adaptive Neuro Fuzzy Inference System (ANFIS), etc., are being widely used to predict outcome of the experimental results. These soft computing tools have been used in coastal field for prediction of experimental results. Mase et al. (1995) applied neural network technique to predict the stability and damage level of rubble mound breakwater. The predicted damage levels are matching with the measured damage levels by Vander Meer's (1988) and Smith et al (1992). Yagci et al. (2005) used neural network technique to predict the damage ratio of breakwater. Model estimations of damage ratios were matching with the predicted values by neural network method. The ANN application enables the consideration of wave period, wave steepness, and breakwater slope and wave height in estimating damage ratio. Kim and Park (2005) applied the artificial neural network method to design the rubble mound breakwater. According to them the neural network technique gave more accurate results than the conventional empirical model and the extent of accuracy was affected by structure of neural network. Kim et al., (2011) used Support Vector Regression to

predict the stability number of armor blocks of breakwaters. The proposed method proves to be an effective tool for designers of rubble mound breakwaters to support their decision process and to improve design efficiency. Balas et al., (2010) applied hybrid model for the preliminary design of rubble mound breakwater and a better agreement between the predicted and measured was obtained when compared to stability equations of Vander Meer's (1988) and ANN. Patil et al., (2011) used ANFIS model for predicting wave transmission coefficient of horizontally interlaced multilayer moored floating pipe breakwater and showed that ANFIS model outperformed ANN model for predicting wave transmission coefficient.

In the present paper, performances of the ANFIS for the prediction of damage level for non reshaped berm breakwater are investigated, and the results are compared with Artificial Neural Network.

Experimental Data

The experimental work was carried in Marine Structures Laboratory, Department of Applied Mechanics and Hydraulics, NITK, Surathkal, India. The wave flume is 50 m long, 0.71 m wide, 1.1 m deep, and has a 42 m long smooth concrete bed. Fig.1 shows a sketch of the wave flume.

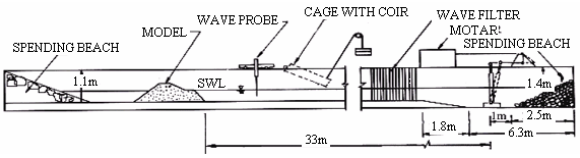


Fig.1 Experimental Set-Up

Four set of experiments were carried out for 3000 waves. In the first set of experiment, stability for different wave periods and height on conventional breakwater model with trapezoidal cross section with armour stone weight W50 = 74 gm was tested. In the second set of experiments, statically stable non-reshaped berm breakwater models were tested with the armour stones weight W50 = 52 gm which is about 30% less than 74 gm. They studied the influence of berm width on the stability of the breakwater, runup and rundown (Subba Rao et al., 2004). In the third set of experiments armor stones weight W50 = 58.6 gm which is about 20% less than 74 gm. The influence of tidal effect and stability were studied by changing the depth of water in front of the breakwater model. In the fourth set of experiments the influence of location of the berm and stability were studied by keeping the armor stones weight W50 = 52 gm, the weight used in conventional breakwater (Subba Rao et al., 2008). Range of experimental variables is shown in Table 1.

For the present analysis, experimental data are converted into non dimensional parameters like Wave Steepness (H_o/L_o), Surf Similarity(ζ), Relative berm width by water depth (B/d), Armor Stone Weight (W_{50}/ W_{50max}), Relative berm width (B/ L_o) and Relative berm location (h_B/L_o) and they are used for the analysis. 124 data sets are considered for the present study. From 124 data sets randomly 93 (80%) data sets are used for training the networks and 31 (20%) data sets are used for testing the models.

Table1. Range of Experimental Variables

Variables	Range
Wave height H (m)	0.10, 0.12, 0.14, 0.16
Wave period T (Sec)	1.6, 2.0, 2.6
Water depth above the bed level d (m)	0.25, 0.30, 0.35, 0.40
Armor stone weight W50 (gm)	52 to 74
Crest height above the seabed (m)	0.70
Berm width B (m)	0.60
Berm position above seabed hB (m)	0.32

Adaptive Neuro-Fuzzy Inference System

Adaptive Neuro Fuzzy Inference System (ANFIS) was first introduced by Jang 1993. It is a combination of least-squares and backpropogation gradient decent methods used for training Takagi-Sugeno type fuzzy inference system which is used for an effective search for the optimal parameters. It can provide a starting point

for constructing a set of fuzzy 'if-then' rules with appropriate membership functions to generate the fixed input-output pairs. ANFIS is a simple structure with effective learning algorithm and high speed. (Vairappan et al 2009). ANFIS training can use alternative algorithms to reduce the error of the training. The advantage of a hybrid approach is that it converges much faster, since it reduces the search space dimensions of the backpropagation method used in neural networks.

Architecture of ANFIS

A simple architecture of ANFIS with I-input variables O-output variables is shown in Fig.2. It consists of five layers and each layer is explained below.

Layer 1

Every node in this layer is an adaptive node with a node function

$$O_{1,i} = \mu A_i(x), \quad \text{for } i = 1, \qquad (1)$$

$$O_{1,i} = \mu B_{i-2}(x), \text{ for } i = 3,4 \qquad (2)$$

x (or y) is the input node and Ai (or Bi−2) is a linguistic variables associated with the membership function of a fuzzy set (A1,A2,B1,B2).Typical membership function:

$$\mu A(x) = \frac{1}{1+\left[\frac{c_i}{a_i}\right]^{2b_i}} \qquad (3)$$

where a_i, b_i and c_i is the parameter set. Parameters are called as premise parameters.

Layer 2

Each node in this layer is a fixed node, indicated by Π Norm. The output is the product of all the incoming signals.

$$O_{2,i} = w_i = \mu A_i(x) \cdot \mu B_i(y), \quad i = 1,2 \qquad (4)$$

output signal w_i represents the fire strength of a rule.

Layer 3

Each node in this layer is a fixed node N Norm. The ith node calculates the ratio of the firing strength to the sum of the firing strength.

$$O_{3,i} = \bar{w}_i = \frac{w_i}{w_1+w_2}, \quad i = 1,2 \qquad (5)$$

Output signal $\bar{w}_i$ is called normalized firing strengths.

Layer 4

Each node in this layer is an adaptive node, indicated by square node with a node function:

$$O_{4,i} = w_i f_i = w_i(p_i x + q_i y + r_i) \qquad (6)$$

where w_i is the normalized firing strength from layer 3. {pi, qi, ri} is the parameter set which are called as consequent parameters.

Layer 5

Each node in this layer is a fixed node, indicated by circle node which computes the overall output as the summation of all incoming signals:

$$\text{Overall output} = O_{5,1} = \sum_i \bar{w}_i f_i = \frac{\sum_i w_i f_i}{w_i} \qquad (7)$$

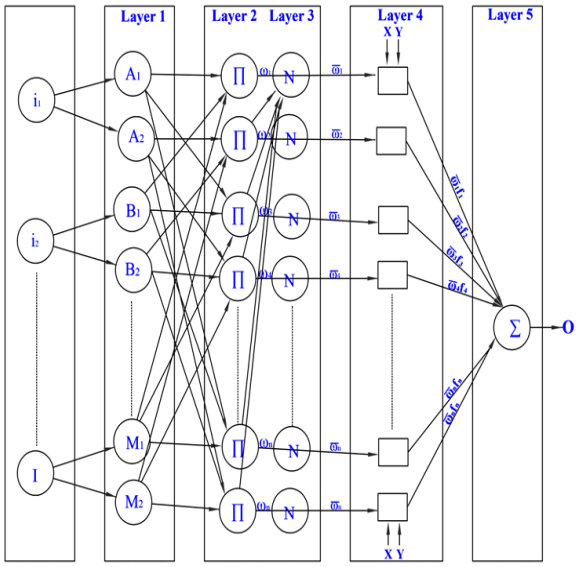


Fig.2 ANFIS structure

In the present study ANFIS structure consists of 64 fuzzy rules for 6 input parameters namely i1=Ho/Lo, i2=ζ, i3=B/d, i4=W50, i5= B/ Lo and i6= hB/Lo. And uses first order Sugeno model with 2 generalised gauss membership function is assigned for input parameters and is obtained by

$$f(x,\sigma,c) = e^{\frac{-(x-c)^2}{2\sigma^2}} \qquad (8)$$

where x is input parameters, c and σ are mean and variance respectively.

Results and Discussion

In the present study, Adaptive Neuro Fuzzy Inference System (ANFIS) is used to predict the damage level of non reshaped berm breakwater to reduce the time and cost for carrying the experimental work. The performance of the model is evaluated

using statistical measures which are defined as follows:

Mean Square Error

$$(\mathrm{MSE}) = \frac{1}{n}\sum_{i=1}^{n}\left|\frac{O_i - P_i}{P_i}\right|^2 \times 100 \quad (9)$$

Root Mean Square Error

$$(\mathrm{RMSE}) = \sqrt{\frac{1}{n}\sum_{i=1}^{n}\left(\frac{O_i - P_i}{P_i}\right)^2} \times 100\% \quad (10)$$

Correlation Coefficient

$$(\mathrm{CC}) = \frac{\sum_{i=1}^{n} P_i O_i}{\sqrt{\sum_{i=1}^{n} P_i^2 \sum_{i=1}^{n} O_i^2}} \quad (11)$$

Scatter Index

$$(\mathrm{SI}) = \frac{\sqrt{1/n\sum_{i=1}^{n}\left((P_i - \bar{P}_i) - (O_i - \bar{O}_i)\right)^2}}{\bar{O}} \quad (12)$$

where, O and P are observed and predicted damage level respectively, n is the number of data set used and $\bar{P}$ & $\bar{O}$ are average predicted and observed damage level respectively.

In this study, the ANFIS model is used to predict the damage level of non reshaped berm breakwater. Out of 124 experimental data set, 93 data set are used for training the model and 31 data set are used for testing the model.

The ANFIS model, with a combination of gradient descent algorithm and least squares algorithm is used for an effective search for the optimal parameters to yield good results. Based on this hybrid approach, correlations of training and testing are increased. Here, Sugeno first order with 64 fuzzy rules and 2 generalised 'gauss' membership function are used to train the model.

The results obtained during training and testing processes for input parameters are calculated by means of statistical measures like correlation coefficient, mean square error, root mean square error and scatter index values as shown in Table 2. The ANN model results are also shown in Table 2 (Mandal et al 2011) where CCs in two models are higher than 0.94 and 0.884 for trained and test data respectively. MSE and RMSE for all models are less than 5.8785, 2.424, 12.4118 and 3.523 for training and testing respectively. And SI is less than 0.00218 and 0.08617 for training and testing respectively for all the models. Fig.3 shows the correlation between the observed and predicted damage level for training and testing of ANFIS model. Fig 4 shows the testing performances for ANFIS model for prediction of damage level and it shows that observed and ANFIS model have similar outline which indicates better model for prediction.

The ANFIS model with 64 fuzzy rules and 2 generalized gauss membership function is used which reduces the processing time and gives better results for prediction of damage level than ANN model for all statistical criteria. The ANFIS model outperformed ANN model and provided the best performance, i.e., the lowest RMSE and highest CC for test output. Results of the study also indicate that the predictive capability of the ANFIS model used in this study is better when compared with ANN in damage level prediction.

Summary and Conclusion

In the present study, the ANFIS model is applied to predict the damage level of non reshaped berm breakwater. The experimental data generated by wave flume at Marine Structure laboratory, NITK, Surathkal, India is used in this study. From 124 data sets randomly 93(80%) data sets are used for training the network and 31(20%) data sets are used for testing the network.

Two models show good results in terms of statistical measures like mean square error, root mean square error, correlation coefficient and scatter index for observed and predicted damage level. Among these two models, ANFIS structure which uses first order Sugeno containing 64 rules and 2 generalized gauss membership functions yields better results compared to ANN model.

From the present study we can conclude that ANFIS model is an effective tool in predicting the damage level of non reshaped berm breakwater and fast in

predicting the damage values. Therefore it can be used as an alternative tool to determine the damage level of non reshaped berm breakwater.

References

[1] Baird W. F. and Hall H.R., 1984. The Design of breakwaters using quarried stones. Proc., 19th Int. Conf. On Coastal Engineering, pp.2580-2591.
[2] Brunn, P. and Johannesson P., 1976. Parameters affecting stability of rubble mounds. J. Waterways, Harbors and Coastal Engineering Division, 102, pp.141-163.
[3] Balas C. E., Koc M. L. and Tur R., 2010. Artificial neural networks based on principal component analysis, fuzzy systems and fuzzy neural networks for preliminary design of rubble mound breakwaters. J. Applied Ocean Research, 32, pp.425-433.
[4] Jang J.S.R., 1993. ANFIS: Adaptive Network Fuzzy Inference System. IEEE Transactions on Systems, Man, and Cybernetics 23 (3), pp. 665-685.
[5] Kim D. K., Kim D. H., Chang S.K., Lee J. J. and Lee D. H., 2010. Stability Number Prediction for Breakwater Armor Blocks USing Support Vector Regression. KSCE Journal of Civil Engineering, 15(2), pp. 225-230.
[6] Kim D.H and Park W.S., 2005. Neural network for design and reliability analysis of rubble mound breakwater. J. Ocean Engineering, 32, 1332-1349.
[7] Mase H., Masanobu S. and Tetsuo S., 1995. Neural network for stability analysis of rubble mound breakwater. J. of waterway, port, coastal and Ocean Engineering, 121(6), pp.294-299.
[8] Mandal S., Subba Rao, Harish N. Lokesha, 2011. ANN and SVM modeling in predicting damage level of non reshaped berm breakwater. Accepted in National conference on HYDRO-2011, 29-30 December 2011 at SVNIT, Surat, India.
[9] Patil S.G., Mandal S., Hegde A.V. and Alavandar S., 2011. Neuro-fuzzy based approach for wave transmission prediction of interlaced multilayer moored floating pipe breakwater. J. Ocean Engineering, 38, pp.186-196.
[10] Subba Rao, Pramod C. H. and Rao B.K., 2004. Stability of berm breakwater with reduced armor stone weight. J. Ocean Engineering, 31, pp.1577–1589.
[11] Subba Rao, Subrahmanya K., Rao B.K., and Chandramohan V. R., 2008. Stability aspects of nonreshaped berm breakwaters with reduced armour weight. J. Waterway, Port, Coastal, and Ocean Engineering, 134, pp.81-87.
[12] Smith W.G., Kobayashi N. and Kaku S., 1992. Profile changes of rock slopes by irregular waves. Proceedings of 23th International Conference Coast Engineering ASCE, New York, NY 1992. Pp.1559–1572.
[13] Torum A., Krogh S.R., Bjordal S., Fjeld S., Archetti R. and Jacobsen A., 1999. Design criteria and design procedure for berm breakwaters. Proc., Coastal Structures '99', Balkema, Rotterdam, pp.331-341.
[14] Torum A., Franziska K. and Andreas Menze 2003. On berm breakwaters stability, scour, overtopping. J. Coastal Engineering, 49, pp. 209-238.
[15] Van der Meer J. W., 1988. Deterministic and probabilistic design of breakwater armor layer. J. Waterways, Ports, Coastal and Ocean Engineering, 114, pp. 66-80.
[16] Vairappan C., Tamura H., Gao S. and Tan Z., 2009. Batch type local search-based Artificial Neuro-Fuzzy Inference Systems (ANFIS) with self-feedbacks for time series prediction. J. Neuro computing 72, pp. 1870-1877
[17] Yagci O., Mercan D.E., Cigizoglu H.K. and Kabdasli M.S., 2005. Artificial intelligence methods in breakwater damage ratio estimation. J. Ocean Engineering, 32, pp. 2088-2106

Table2. Statistical measures for different model

Model		MSE	RMSE	CC	SI
ANN	Train	5.879	2.424	0.94	0.0022
	Test	12.412	3.523	0.88	0.0197
ANFIS	Train	0.734	0.856	0.99	0.0007
	Test	3.638	1.907	0.91	0.0086

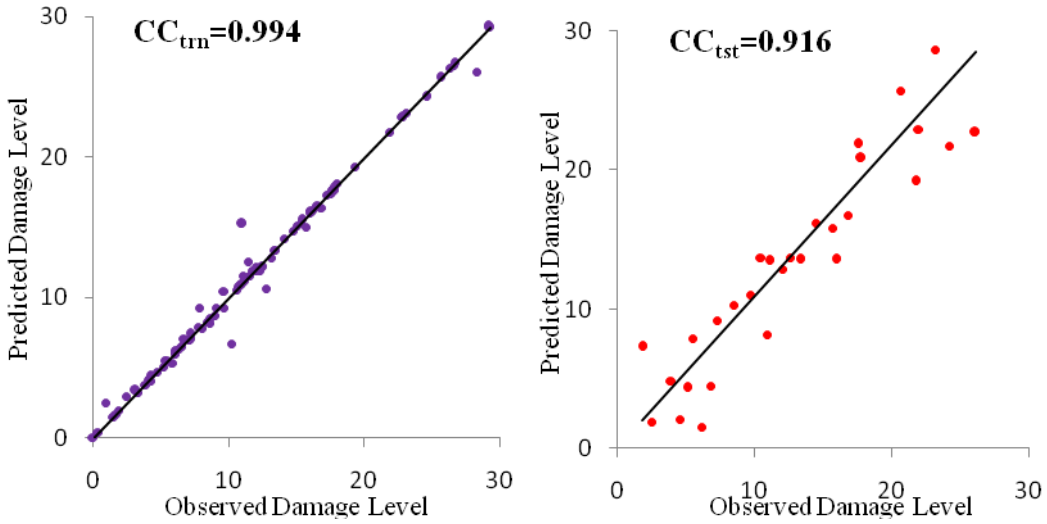


Fig. 3 Observed and predicted damage level by ANFIS method for train and test data.

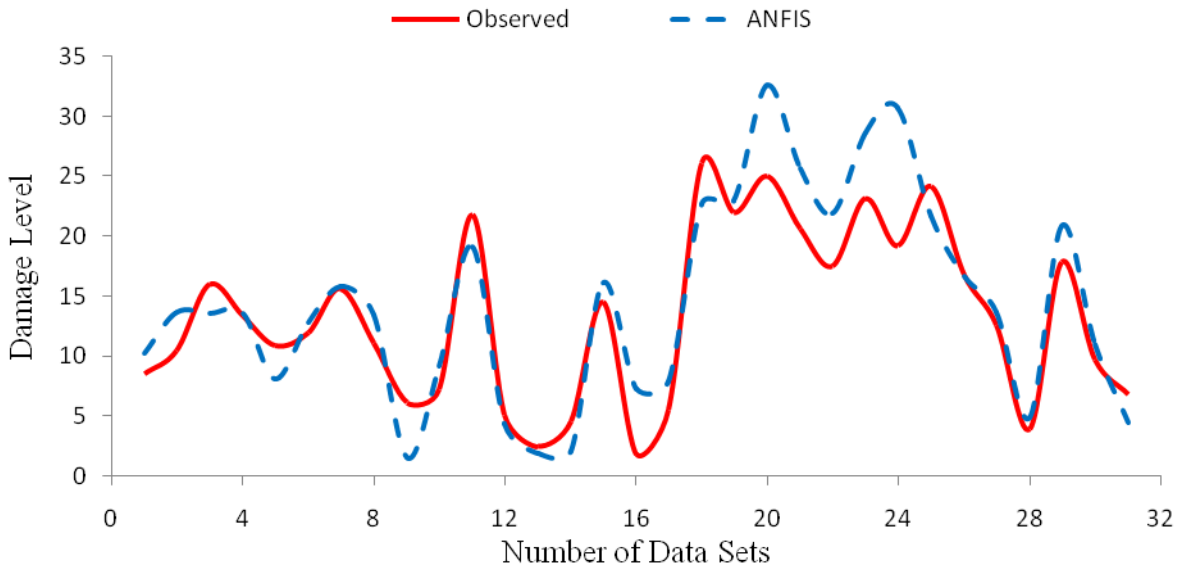


Fig. 4 ANN and SVM performances for damage level prediction for testing data.

2nd International Engineering Symposium - IES 2012
(KU-MU-NITK-HCMCUT Joint Symposium) March 5-7, 2012, Kumamoto University, Japan

Wave Run-Up, Run-Down studies on reshaped Berm Breakwater with artificial armour units

Prashanth J[1] Subba Rao[2] Kiran G Shirlal[3] Balakrishna Rao K[4] and Vishwanath N[5]

1 *Department of Applied Mechanics and Hydraulics, National Institute of Technology, Surathkal. Mangalore 575025, India. e-mail:prashnitk.hsn@gmail.com*
2 *Department of Applied Mechanics and Hydraulics, National Institute of Technology, Surathkal. Mangalore 575025, India. e-mail:surakrec@gmail.com*
3 *Department of Applied Mechanics and Hydraulics, National Institute of Technology, Surathkal. Mangalore 575025, India.*
4 *Department of Civil Engineering, Manipal Institute of Technology, Manipal 576104, India.*
5 *Department of Applied Mechanics and Hydraulics, National Institute of Technology, Surathkal. Mangalore 575025, India.*

Abstract: The objective of this study is to investigate the wave run-up, run-down characteristics of berm breakwater using concrete cube as artificial armour unit with reduced weight of the armour. The experiments are conducted under following conditions, berm widths 0.3m and 0.45m, water depths ranging from 0.35m to 0.45m, breakwater slope 1:1.5. Reduced weights (25% & 50%) of armour unit are used in berm breakwater. From the experimental study it is found that the wave run-up is more for longer period waves in comparison with the shorter period waves. It is found that berm width has a great influence on wave run-up and wave run-down and is found to decrease with the increase in berm width. Dimensionless wave run-up varied from 0.52 - 1.85. Dimensionless wave run-down varied from 0.45 - 1.35.

***Keywords**: Berm breakwater, wave run-up, wave run-down, wave steepness*

Introduction

The conventional rubble mound breakwaters needs very big size stones in large quantities. The berm breakwater has been adopted at several places as an economic solution when large cover blocks of natural stones are not available. Priest et al. (1964), Brunn and Johannesson (1976), and Ergin et al. (1989), showed that S-shaped rubble mound breakwaters (berm breakwaters) are more stable than conventional breakwaters under certain conditions. Subba Rao et al. (2008) conducted a series of experiments to study the stability of non-reshaped berm breakwaters. They found that the slope of breakwater has much influence on wave run-up and with the change of slope from 1:1.5 to 1:2 the run-up was reduced by 36%. Also with the increase in wave steepness, the wave run-up was found to decrease. The run-down was found to be more significant than the run-up when SWL was above the berm and run-down was less than run-up when SWL was below the berm (Subba Rao et al., (2006)). Pilarczyk (1990) found that run-up on slope decreases with increasing artificial berm width and the reduction rapidly falls off once a certain minimum width is exceeded : for $B > 0.25L_o$ for non breaking waves and for $B > 4H_s$ for strong breaking waves i.e. for $H_s/L_o > 0.03$. In the present paper wave run-up and run-down studies have been done for different wave parameters.

Details of Experimental Work

The present work involves an experimental study on the influence of change in different wave parameters and storm

duration on the wave run-up and run-down of the berm breakwater. Weight of armour unit used for berm breakwater and conventional breakwater are calculated using Hudson equation (CEM 2006) for a design wave height of 0.1m and are 106gm and 79.5gm respectively. The seaward slope of berm breakwater and conventional breakwater are 1:1.5 and 1:2 respectively. Fig. 1 shows the sectional elevation of the berm breakwater model studied. Geometrically similar scale of 1:30 is selected for the present investigation. In the present model, the primary layer is divided into three zones crest ward slope, berm and toe ward slope, and the units in these regions are coloured as white, red and grey respectively.

The armour weight obtained using Hudson equation for berm breakwater is reduced 50% for model A and 25% for model B; their weights corresponding to the reduction are 79.5gm and 53gm respectively. The armour layer thickness is calculated using layer coefficient as explained in the CEM (2006). A crest width of 0.15m or a minimum of three cubes width is provided. The model characteristics are given in Table 1. Table 2 gives the range of experimental variables considered for the study.

Wave Flume

Experiments were conducted by generating regular waves in a two-dimensional wave flume 50m X 0.71m X 1.1m as shown in Fig. 2. The ranges of wave height and periods that can be generated in this wave flume are 0.02m to 0.24m and 0.8s to 4s, respectively. The flume is provided with bottom hinged flap type wave generator. It has a smooth concrete bed for length of 42m. The wave generating chamber is 6m in length. Gradual transition is provided between the normal flume bed level and that of generating chamber by a ramp. The wave filter consists of a series of vertical asbestos cement sheets spaced at about 0.1m centre-to-centre parallel to the length of the flume. The far end of the flume has a wave absorbing beach with 1:12 slope consisting of rubble stones. Therefore, wave reflection in the flume is insignificant.

Wave run-up and wave run-down

Wave run-up is the phenomenon in which an incoming wave crest runs up along the slope up to a level that may be higher than the original wave crest. The vertical distance between still water level SWL and the highest point reached by the wave tongue is called the run-up (Fig. 3). Similarly wave run-down is the vertical lower level reached by backwash of a wave on a coastal structure (Fig. 3).

Results and Discussions

Effect of water depth on wave run-up

The variation of Wave Run-up (R_u/H_o) with Wave Steepness (H_o/L_o) for different water depths is shown in Fig. 4. It is seen that for both the models there is decrease in wave run-up with the increase in wave steepness. The wave run-up for model A ranges from 0.94 to 1.79 and for model B it varies from 0.52 to 0.99. From the graph it can be noticed that run-up for model A is high compared to model B. Also it can be noticed that the decreasing trend in model A is steep compared to model B. This may be due to the shorter berm in model A as compared to model B. The reduction in run-up is 46% in model B when compared with model A.

Effect of water depth on wave run-down

The variation of Wave Run-down (R_d/H_o) with Wave Steepness (H_o/L_o) for different water depths is shown in Fig. 5. It is seen that for both the models there is decrease in wave run-down with the increase in wave steepness. For model A wave run-down varies from 0.84 to 1.24 and for model B it varies from 0.45 to 0.81. It is seen from the graph that variation of run-down is gradual decrease with the increase in steepness. The run-down is low for model B than model A. The reduction in run-down is 50% with model B when compared to model A. The reduction may be due to the presence of longer berm in model B than model A.

Comparison of wave run-up and run-down with conventional rubble mound breakwater

From the graphs of wave run-up and run-down it can be observed that the run-up and run-down has decreased considerably in case of berm breakwater models when compared to conventional breakwater. The reduction is due to the presence of berm in berm breakwater model. There is 15.19% and 35.91% reduction in run-up for model A & model B compared to conventional breakwater respectively and 23.81% reduction in run-down for model B compared to conventional breakwater. The wave run-down is 14.17% high for model A when compared to conventional breakwater. This may be because of smaller weight armour units undergoing a large reshaping, which results in increased down rush of water.

Conclusions

The following conclusions are deduced from this study:

- As deep water wave steepness increases, wave run-up (R_u/H_o) decreases for all the variables considered in the present study. (R_u/H_o) ranges from 0.52 to 1.79.
- The wave run-down (R_d/H_o) decreases as deep water wave steepness increases, for all the variables considered in the present study (R_d/H_o) vary from 0.45 to 1.24.
- From the study it can be concluded that berm length has effect on wave run-up and wave run-down. With the increase in berm length both wave run-up and run-down reduces.
- The run-up and run-down values are reduced by 35.91% and 23.80% due to the presence of berm when compared model B with conventional rubble mound breakwater.
- The run-up and run-down values are reduced by 15.19% and 9.44% when compared model A with conventional rubble mound breakwater.

Acknowledgements

The authors are thankful to the Director of National Institute of Technology Karnataka, Surathkal, and Head of the Department of Applied Mechanics and Hydraulics for the facilities provided for the investigation and permission granted to publish the results. Also the authors would like to thank INCH, Ministry of Water Resources, GOI for providing financial support to carry out the work.

References

[1] Brunn P and Johannesson P (1976), Parameters affecting stability of rubble mounds, Journal of Waterway, Harbours and Coastal Engineering Division, ASCE, Vol. 102, pp. 141-163.

[2] Coastal Engineering Manual (CEM) (2006), Fundamental of Design, EM 1110-2-1100(Part-VI), U.S. Army Corps. of Engineers.

[3] Ergin A, Gunbak A R and Yanmaz A M (1989), Rubble mound breakwaters with S-shape design, Journal of Waterway, Port, Coastal, Ocean Eng., ASCE, 115(5), pp. 579-593.

[4] Pilarczyk K W (1990), Design of seawalls and dikes including overview of the revetments, Coastal protection, Balkema, Rotterdam.

[5] Priest M S, Pugh J W and Singh R (1964), Seaward profile for rubble mound breakwaters, Proc. 9th Int. Conf. on Coastal Engineering, ASCE, 553-559.

[6] Shore Protection Manual (1984), U.S. Army Coastal Engineering Research Center, Department of the Army, Corps of Engineers, U.S. Govt. Printing Office, Washington, DC.USA.Vol.1 and 2.

[7] Subba Rao, Balakrishna Rao K, Rajesh AVRP (2006), Stability aspect of berm breakwaters, Proceedings of National Conference on Hydraulics and Water Resources, HYDRO-2006.

[8] Subba Rao, Subrahmanya K, Balakrishna Rao K, Chandramohan V R (2008), Stability aspects of non-reshaped berm breakwaters with reduced armor weight, Journal of Waterway, Port, Coastal and Ocean Engineering, ASCE, March/ April 2008 Vol. 134, No. 2, pp. 81-87.

[9] Torum A (1998), On the stability of berm breakwaters in shallow waters and deep water, Proc. 26th Int. Conf. on Coastal Engineering, Copenhagen, Denmark, ASCE, pp. 1435-1448.

[10] Van der Meer J W (1992), Stability of the seaward slope of berm breakwaters, Journal of Coastal Engineering, 16, pp. 205-234.

Table 1 Model Characteristics

	Model A	Model B
Armour Weight	55.65 gm	79.5 gm
Thickness of armour layer	0.063 m	0.105 m
Size of the armour unit (D_{n50})	0.0285 m	0.0325 m
Berm Width (B)	0.30 m	0.45 m
Position of berm from sea bed	0.45 m	0.425 m

Table 2 Range of Experimental Variables

Variable	Expression	Range
Wave height	H	0.10,0.12,0.14,0.16m
Wave period	T	1.6, 2.0 & 2.6 sec
Storm duration	N	3000 waves
Angle of wave attack	θ	90^0
Water depth	D	0.35, 0.40, 0.45m
Primary armour layer thickness	t_p	0.1047m
Secondary armour layer thickness	t_s	0.0490m
Shape of the armour unit	-	Cube
Slope	-	1:1.5

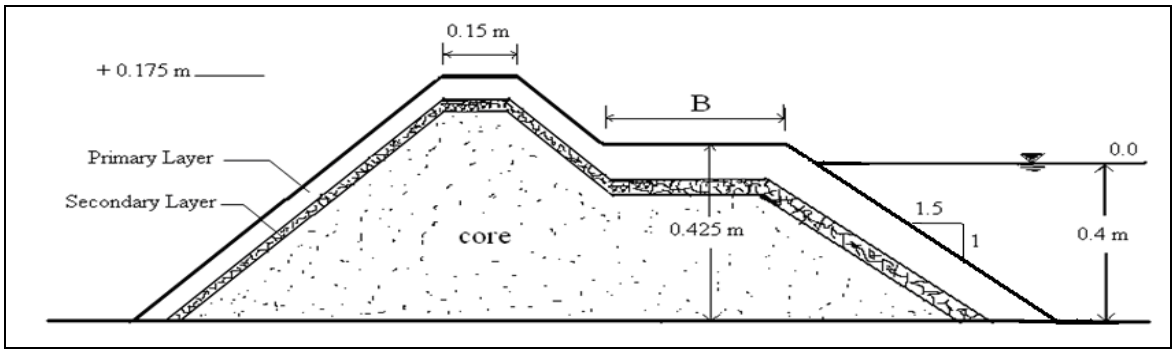


Fig.1 Cross-section of berm breakwater model

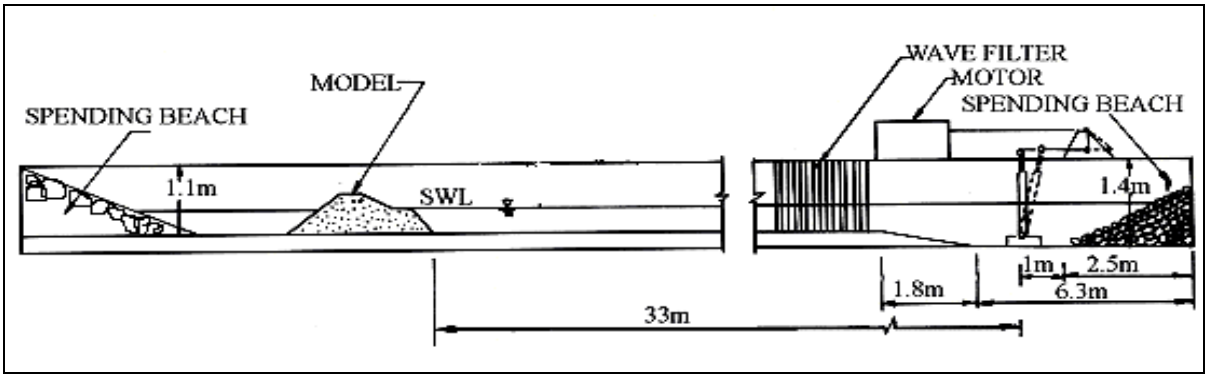


Fig.2 Details of experimental setup

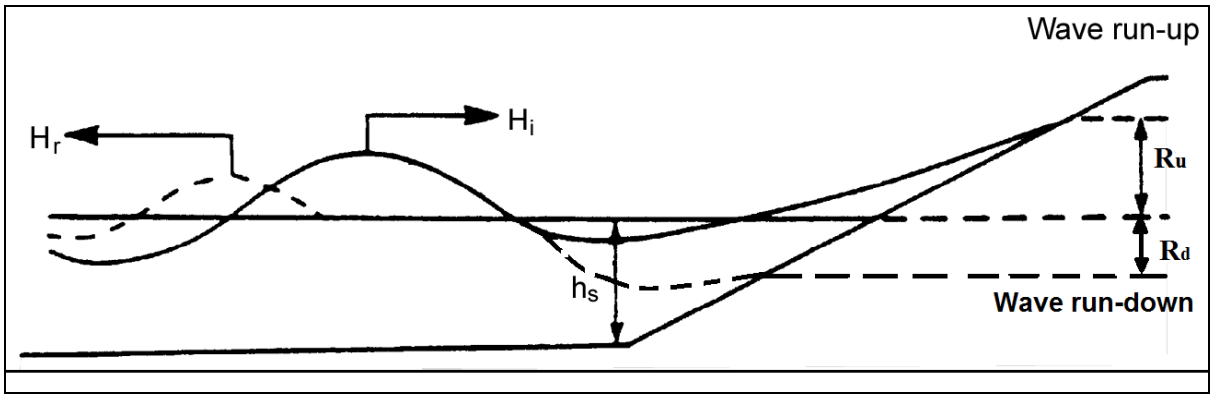


Fig.3 Wave run-up and Wave run-down

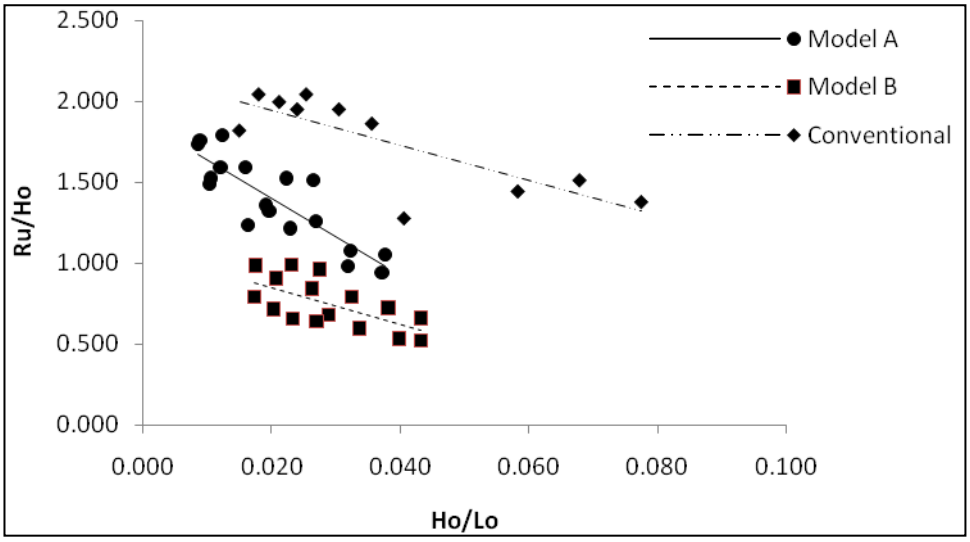


Fig.4 Variation of Wave Run-up with Wave Steepness

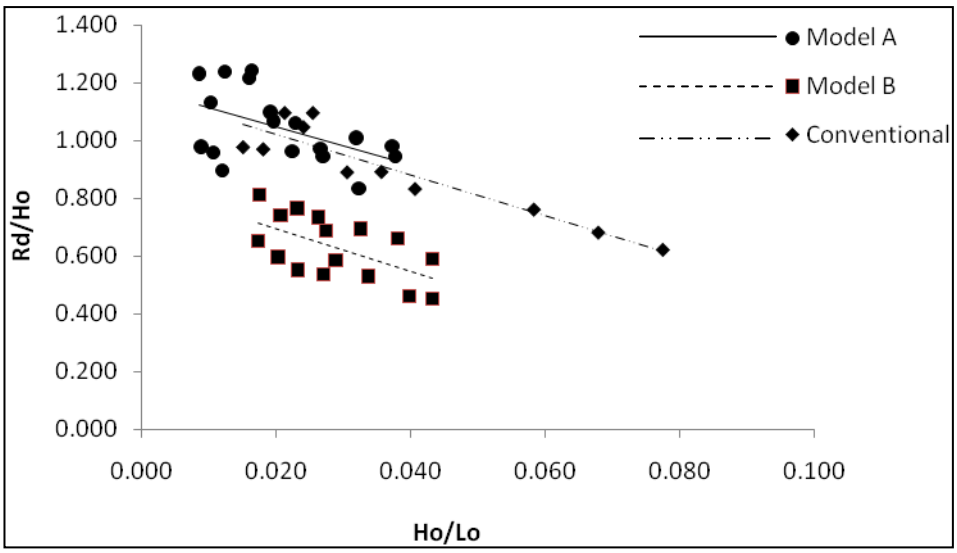


Fig.5 Variation of Wave Run-down with Wave Steepness

2nd International Engineering Symposium - IES 2012
(KU-MU-NITK-HCMCUT Joint Symposium) March 5-7, 2012, Kumamoto University, Japan

Spectral characteristics of sediments in the Ba Lat estuary (Northern Vietnam) in relation to sediment properties for remotely sensed tidal flats monitoring

Nguyen Thi Ngoc [1] and **Katsuaki Koike** [2]

1 *Department of Life and Environmental Science, Kumamoto University, Kurokami, 2-39-1, Kumamoto 860-8555, Japan. e-mail: nguyenngoc231@gmail.com*
2 *Department of Urban Management, Kyoto University, Katsura C1-2-215, Kyoto 615-8540, Japan. email: koike.katsuaki.5x@kyoto-u.ac.jp*

Abstract: Sediment properties such as grain size, water content, and chemical and mineral compositions are major factors that influence on reflectance spectra of sediments. This study investigates the correlation of laboratory measured reflectance spectra with grain size and water content of intertidal sediments in the Ba Lat estuary, Northern Vietnam. Statistic analysis was applied to data on reflectance, grain size, and water content of 101 sediment samples. The strongest negative linear correlation was found between a simulated ALOS (Advanced Land Observing Satellite) band 4 reflectance spectra and the sand content for both the dry and wet sediments with correlation coefficient of -0.78 and -0.71, respectively. Between the simulated ALOS band 4 reflectance spectra and the water content of overall sediments existed a non-linear relationship (r=0.55). However, variation of all the simulated ALOS band reflectance spectra with loss of water content of representative sediments showed a negative linear correlation, of which sandy mud sediment had highest correlation coefficient (r=-0.91) in the simulated ALOS band 4. The results suggested that ALOS band 4 was the most suitable to distinguish intertidal sediments in advanced studies on sediment classification using remote sensing.
***Keywords**: Reflectance spectra, intertidal sediments, sand content, water content, simulated ALOS band.*

Introduction

The optical reflectance of intertidal sediments is influenced by itself properties (e.g., grain size, mineral and chemical compositions, and cyanobacteria) and environmental factors (e.g., water content, topography, and roughness) (Asrar, 1989; Ryu et al., 2004). Grain size and water content are two critical factors that need to be considered in classifying intertidal sediments by using remote sensing.

The effect of grain size and water content on reflectance of intertidal sediments was reported in the earlier studies (Bryant et al., 1996; Rainey et al., 2000, 2003; Ryu et al., 2004; Van de Wal and Herman, 2007; Small et al., 2009). Ryu et al. (2004) suggested that Landsat ETM+ reflectance is more sensitive to the surface water content than interstitial water content and to 0.25 mm in grain size of sediment than 0.125 and 0.0625 mm. Through *in situ* and laboratory reflectance experiments, Rainey et al. (2000) clarified a positive linear relationship between reflectance in a simulated ATM (Airborne Thematic Mapper) band 9 and percentage sand, while a negative relationship between reflectance and interstitial water content. Small et al. (2009) showed distinct drying trajectories for different grain size of sediments and suggested that grain size distribution may be spectrally distinguishable from moisture content for both wet and dry samples, but dry samples are more suitable to this estimation. This viewpoint agrees to the

suggestion by Rainey et al. (2000) of a possibility for mapping intertidal sediment distribution by remotely sensing data under dry condition during the image acquisition.

Integrating satellite imagery analysis and interpretation of *in situ* and laboratory measured spectra is an effective method in detecting and monitoring surface tidal flats such as grain size distribution (Yates et al., 1993; Rainey et al., 2003; Ryu et al., 2004; Sørensen et al., 2006; Van der Wal and Herman, 2007), morphologic change (Ryu et al., 2008), surface roughness and sediment texture (Van der Wal et al., 2005). Remote sensing data have been used including Landsat 5 TM (Yates et al., 1993), Landsat ETM+ (Ryu et al., 2004, 2008; Sørensen et al., 2006), ATM (Rainey et al., 2003) and SAR (Synthetic Aperture Radar) (Van der Wal et al., 2005; Van der Wal and Herman, 2007). ALOS image was acquired corresponding with the period of sediment samples collection in the Ba Lat estuary. Therefore, the wavelength of ALOS band 1-4 was selected to calculate reflectance spectra of sediments. Then this study aims at clarifying two relationships of simulated ALOS band reflectance - grain size and simulated ALOS band reflectance-water content under a laboratory condition.

Study area

The Ba Lat estuary, an arrow-shaped jutting out into the sea, is the major and typical delta of the Red River system in Northern Vietnam (Fig. 1). About 31×10^6 m^3 of sediment occupying nearly 38% of the annual amount of sediment carried by the Red River system is discharged into the South China Sea through Ba Lat mouth (Duc et al., 2007). Ba Lat estuary belongs to a meso-tidal region with diurnal tide and a tidal range from 2.0 to 3.7 m.

This study focused on the tidal areas at the 2 m water depth composed of Con Lu and Con Vanh Islands formed by accretion, Con Mo and Con Vanh shoals - active bars - in front of Ba Lat mouth, and the Giao Xuan, Giao Lac, Giao An, Nam Thinh coastal areas. The Con Mo and Con Vanh shoals exhibited mainly well-sorted and relatively uniform sands (Duc et al., 2007). Mangroves grow naturally in the north of Con Lu and along the channel banks and were planted in the muddy flats from Giao An to Giao Xuan commune from 1997. Nearly all tidal flats covered by mangroves at Con Vanh, Con Ngan Islands have been converted to aquaculture ponds since the early 1980s. The muddy sand flats in the northeast and southwest parts are enclosed for clam (*Meretrix lyrata*) aquaculture.

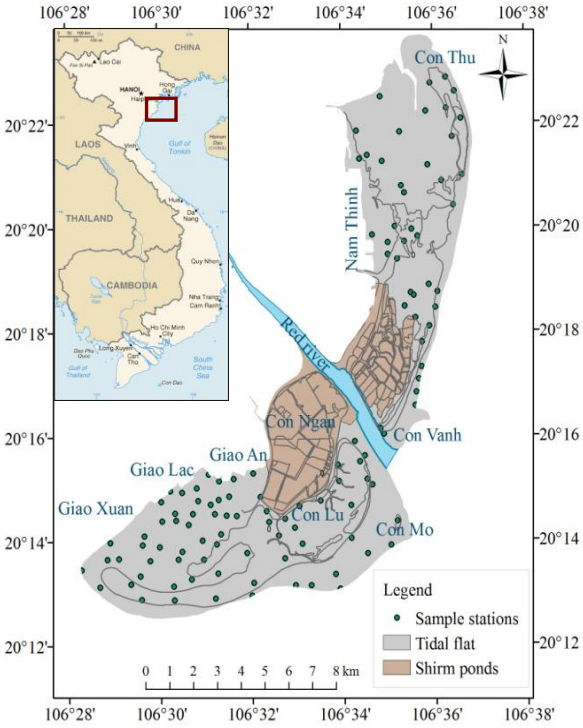


Fig.1 Location of sample points in Ba Lat estuary

Methods

Sampling and sediment grain size analysis

Field survey was carried out in June 2010 during a neap tide when the tidal flats were completely exposed. Sediment samples were collected from the surface to 1 cm depth in the tidal flats by plastic scoop and stored in plastic bag. Sediment samples then were transported to the laboratory and preserved in a freezer. Grain size of the sediment samples were analysed by a combination of two methods: sieve for sandy fraction (0.063-2.000 mm) and pipette for finer grained size (less than 0.063 mm), respectively. Content of sediment fractions was expressed as percentage of the total sample weight.

Spectral measurement

Analytical Spectral Devices (ASD) Field Spec®3 spectrometer with wavelength from 350 to 2500 nm was used to measure reflectance spectra of sediments. All spectral measurements were operated at room temperature in a dark room to control surrounding scattered light sources. Sediment spectra were collected at two states: wet and dry (in an oven at 105°C for 24 hours) with 10 times repeat.

Data analysis

Reflectance spectra were calibrated to absolute reflectance using the data of white reference panel. Simulated reflectance of ALOS band 1, 2, 3, and 4 were calculated by averaging reflectance spectra within the range of 420-500 nm, 520-600 nm, 610-690 nm and 760-890 nm, respectively. To evaluate relationships of reflectance - grain size and reflectance - water content, Spearman's correlation coefficient was calculated for each pair of variables.

Results

Sediment properties

Sediments in the Ba Lat estuary contained sand fraction (>0.063 mm) varying in wide range from 1 to 99% (64±37%, mean±1 SD). A total of 101 sediment samples were divided into four sediment groups by Folk's textural classification system (1968): sand, muddy sand, sandy mud, and mud and following in this order sand content decreased with percentage of 92-99 (97±2), 60-89 (75±9), 10-47 (26±11) and 1-10 (6±3), respectively. Water content of sediments varied from 2 to 94% (37±19%) and increased with decreasing of sand content (r=-0.82).

Correlation of reflectance spectra and sand content

Average reflectance was calculated for overall sediment samples and four separate sediment groups: sand, muddy sand, sandy mud, and mud. Simulated ALOS band 1-4 reflectance of dry sediments was 0.16, 0.23, 0.29 and 0.34 in average higher than those of wet sediments (0.07, 0.12, 0.16 and 0.19). All average reflectance lines showed a similar pattern of reflectance increasing from ALOS band 1 to band 4 (Fig. 2). Average reflectance of the mud group was higher than those of the other three groups in all the ALOS bands, especially when sediments were absolute dry. The spectral contrast was observed clearly between the mud group and the sand group.

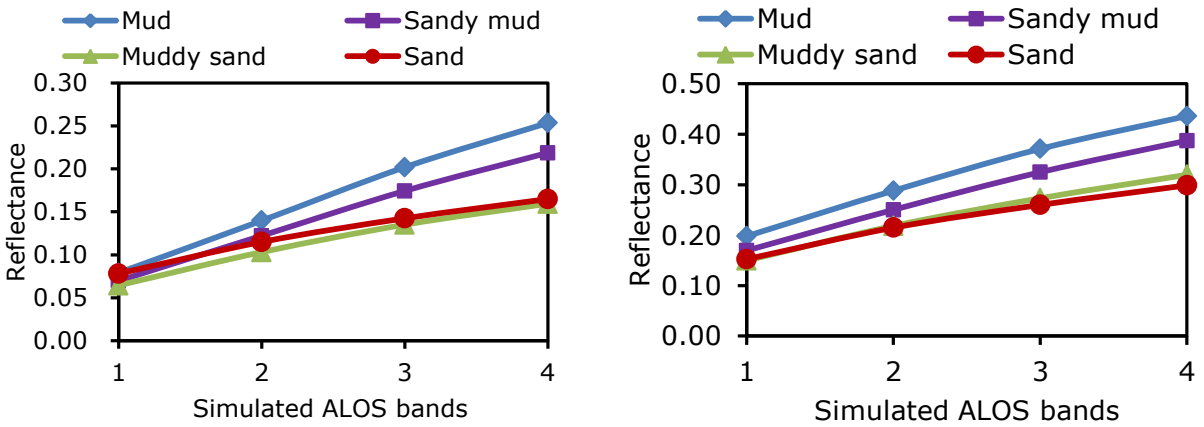


Fig. 2 Average reflectance in the simulated ALOS bands of four sediment groups under the wet (left) and dry (right) conditions

Table 1 shows correlation coefficients of the sand content and the simulated ALOS band 1-4 reflectance spectra for the wet and dry sediments. Generally, reflectance of both the dry and wet sediments in all the bandwidths decreased with an increase of sand content, except for the reflectance of simulated ALOS band 1 for wet sediments (r=0.19). Relationships between the sand content and all the simulated ALOS bandwidths of the dry sediments were stronger than those of the wet sediments.

There was the strongest negative linear correlation of the simulated ALOS band 4 reflectance and the sand content for the simulated ALOS band 4 reflectance and the dry sediments (r=-0.78) and a little weaker correlation observed between the sand content for wet sediments (r=-0.71).

Linear relationship between the simulated ALOS band 4 reflectance and the sand content (C_s) was given by regression Eq. (1) (R^2 = 0.66) and Eq. (2) (R^2 = 0.62) for the dry and wet sediments, respectively (Fig. 3).

$$R_{ALOS4\text{-}Dry} = 0.429 - 0.00137 \times C_s \quad (1)$$

$$R_{ALOS4\text{-}Wet} = 0.246 - 0.00088 \times C_s \quad (2)$$

Table 1 Correlation coefficients of simulated ALOS band reflectance and the sand content

Bandwidth	Dry sediments	Wet sediments
ALOS band 1	-0.41	0.19
ALOS band 2	-0.55	-0.42
ALOS band 3	-0.71	-0.65
ALOS band 4	-0.78	-0.71

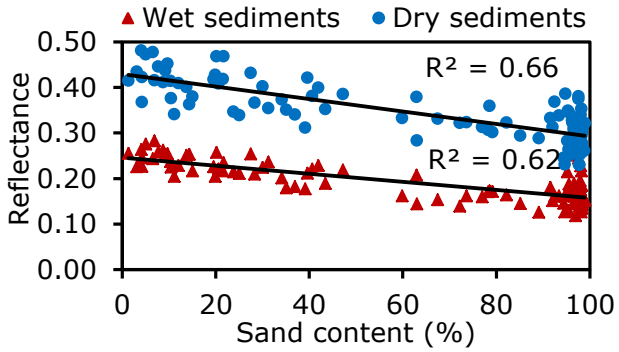


Fig. 3 Linear regression of the simulated ALOS band 4 reflectance and the sand content

We selected four representative samples for major types of sediments (mud, sandy mud, muddy sand and sand) in the Ba Lat estuary with sand content of 7.68, 40.61, 72.19, and 95.51% respectively to characterize the spectral contrast to grain size in detail. Change in the reflectance spectra of the representative samples was significant when these sediments were wet. Reflectance spectra decreased in the order of mud - sandy mud - muddy sand - sand in the 650 - 1150 nm wavelength (visible - near infrared region) and in the order of mud - sandy mud - sand - muddy sand in the 1300 - 2500 nm (shortwave infrared region). Under the dry condition, there was no significant difference in the reflectance in the visible - near infrared region, while slight decreasing of reflectance in the shortwave infrared bandwidth was observed in the reverse order (sand - muddy sand - sandy mud - mud) in the wet sediments. Maximum spectral contrast between the mud and sand was observed in the simulated ALOS band 4 under the wet condition with average reflectance of 0.24 and 0.14, respectively, on the contrary those for the dry mud and sand were similar (Fig. 4).

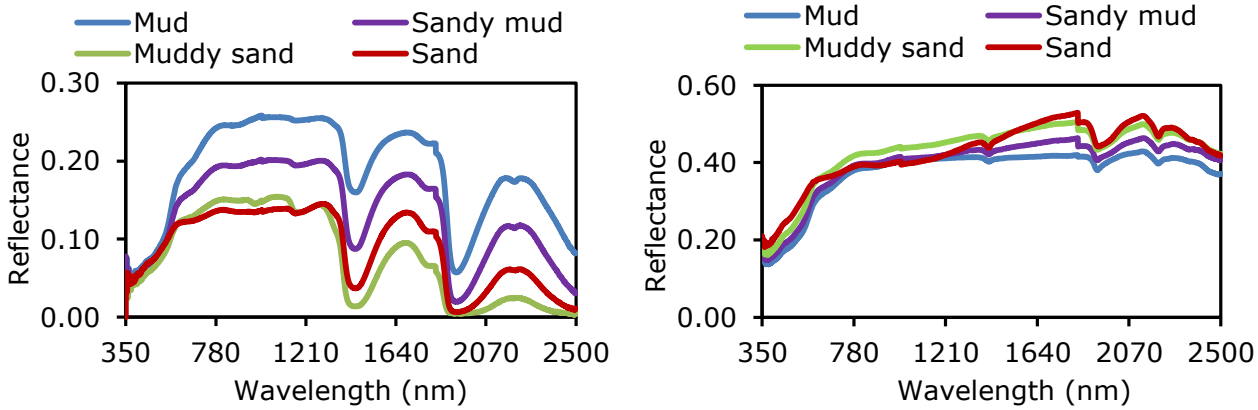


Fig. 4 Spectral curves of representative sediment samples under the wet (left) and dry (right) conditions

Correlation of reflectance spectra and water content

All the dry sediment samples showed higher reflectance than the wet sediment samples for all the ALOS bands as proven by Fig. 3. Between the simulated ALOS band 4 reflectance and the water content presented the best correlation (r=0.55) compare to correlations of the other ALOS bands and water content (Table 2). Non - linear correlation between the simulated ALOS band 4 reflectance and the water content (C_w) was described by a cubic polynomial function (R^2 = 0.59) as can be seen in Eq. (3). The regression model showed a decrease of the ALOS band 4 reflectance as the water content increased around 25%, especially significant reflectance drop in the 20-30 % range of water content. Then the ALOS band 4

reflectance increased with an increase of the water content in the range of 25-75%. Finally, the ALOS band 4 reflectance decreased when the water content increased from 75 to 94% (Fig. 5).

$$R_{ALOS4} = -0.000001\times(C_w)^3+0.000203\times(C_w)^2 -0.007022\times(C_w) + 0.234129 \quad (3)$$

Table 2 Correlation coefficients of simulated ALOS band reflectance and the water content

Bandwidth	Spearman's rho
ALOS band 1	-0.33
ALOS band 2	0.23
ALOS band 3	0.47
ALOS band 4	0.55

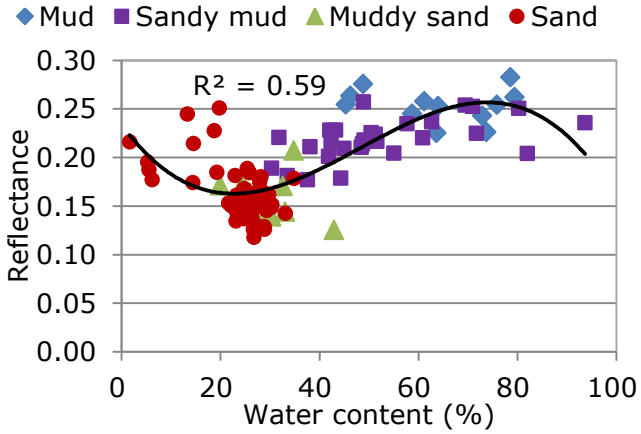


Fig. 5 Non-linear regression of the simulated ALOS band 4 reflectance and the water content

Reflectance variation with loss of water content of four representative sediments as mentioned above was tested. The most significant negative linear was found between the water content and the reflectance of ALOS band 4 (r = -0.91), and second correlation by the ALOS simulated band 3 (r = -0.88) for the sandy mud (Table 3).

Table 3 Correlation coefficients of simulated ALOS band reflectance and the water content for representative sediments

Bandwidth	Mud	Sandy mud	Muddy sand	Sand
ALOS band 1	-0.86	-0.87	-0.83	-0.84
ALOS band 2	-0.86	-0.87	-0.83	-0.84
ALOS band 3	-0.81	-0.88	-0.84	-0.85
ALOS band 4	-0.77	-0.91	-0.87	-0.86

Conversely, these correlations were the weakest for the mud samples with the r's of -0.81 and -0.77, respectively. In addition, the r's of the ALOS bands 1 and 2 simulated reflectance spectra with the water contents were the same regardless of sediment type (r = -0.86 for mud, r = -0.87 for sandy mud, r = -0.83 for muddy sand, and r = -0.84 for sand).

Discussion

This study presented the dependence of reflectance spectra on grain size and water content of the sediments in the laboratory. The strongest negative correlation was identified between the ALOS band 4 simulated reflectance and the sand content for overall wet and dry sediment samples (r = -0.71 to -0.78) in the Ba Lat estuary. This was enhanced in the spectral contrast between the sand and mud groups. Mud group showed higher average reflectance at all the ALOS bandwidths than the sand group. This result is opposite to a positive correlation between the reflectance and particle size reported in the previous researches on mapping intertidal sediment from remote sensing data (Gerbermann, 1979; Bryant et al., 1996; Rainey et al., 2000, 2003; Ryu et al., 2004). However, the evidence for negative relationship between the reflectance and grain size was found in the primary and recent works. Rainey et al. (2000) presented a case of intertidal sediments *in situ* which were completely saturated and obtained higher reflectance of the mud than the sand. Additionally, primary studies on the influences of grain size on mono-mineral powders (e.g., silicate rock and pyroxene) suggested that the reflectance in the visible and near-infrared generally decreases as the grain size increases (Adams and Filice, 1967; Hunt and Vincent 1968; Clark, 1999). Hapke (1993) and Clark (1999) interpreted that grain size controls amount of light scattered and absorbed by a grain; a larger grain size absorbs more light results in reflectance drop.

The water content has been considered as one of the most important parameter for classifying intertidal sediments by using remote sensing (Bartholdy and Folving, 1986; Yates et al., 1993; Rainey et al., 2000; Ryu et al., 2004). Earlier laboratory and *in situ* studies presented the negative reflectance - moisture correlation (Bryant et al., 1996; Rainey et al., 2000, 2003; Ryu et al., 2004; Kaleita et al., 2005; Van de Wal and Herman, 2007). In this study,

water content affected obviously on the reflectance spectra of the intertidal sediments. The reflectance of dry sediments was higher than wet sediments because of liquid water absorption. The negative reflectance - moisture correlation was observed when investigation of reflectance variation with the loss of water content for four representative sediments. The non-linear relationship between the simulated ALOS band 4 reflectance and the water content existed for overall sediment samples. The reflectance - water content relationship can clarify the spectral contrast between two sediment groups: mud and sand under the wet condition. All the sediments were wet but different in water content: the water content of the mud group (45-79, 64±12%) was much higher than the sand group (2-35, 23±7%) (Fig. 5). Rainey et al. (2000) found that the maximum spectral difference between the sand and mud exists when the sediments are at 25% saturation. As can be seen in Fig. 5 when water content varied from 25 to 75% that was almost similar in the water content of mud group (45-79, 64±12%) the reflectance increased with increase of the water content. While the average water content of sand group was less than 25% that remarked the reflectance decrease with increase of the water content.

Conclusion

The present study demonstrated clearly the correlation of reflectance spectra with the grain size and water content of the intertidal sediments in Ba Lat estuary. Reflectance of almost simulated ALOS bands showed negative correlations to both the grain size and water content of the sediment samples. Simulated ALOS band 4 reflectance had the closest linear relation to the sand content for dry sediments (r=-0.78) and the non-linear correlation with the water content (r=0.55), which suggests that the ALOS band 4 could be the most suitable band for detecting intertidal sediment distribution. In the context of reflectance based laboratory, this study discarded influence of surface water on the reflectance. Therefore, further studies on sediment classification by remote sensing technique need to consider the influence of surface water content on the reflectance of tidal flats.

References

[1] Adams, J B, and Filice, A L (1967), Spectral reflectance 0.4 to 2.0 microns of silicate rock powders, GR Journal, Vol. 72, pp. 5705-5715.
[2] Bartholdy, J, and Folving, S (1986), Sediment classification and surface type mapping in the Danish Wadden Sea by remote sensing, NSR Journal, Vol. 20, pp. 337-345.
[3] Bryant, R G et al. (1996), A preliminary investigation into the spectral characteristics of inter-tidal estuarine sediments, RS Journal, Vol. 17, pp. 405-412.
[4] Clark, R N (1999), Spectroscopy of rocks and minerals and principles of spectroscopy, In Remote sensing for Earth Sciences, Manual of remote sensing (ed. by Rencz, A. N.), John Wiley and Sons, New York, pp. 3-58.
[5] Duc, D M et al. (2007), Sediment distribution and transport at the nearshore zone of the Red river delta, Northern Vietnam, AES Journal, Vol. 29, pp. 558-565.
[6] Folk, R L (1968), Petrology of sedimentary rocks, Hemphill's, Austin, pp. 170.
[7] Gerbermann, A H (1979), Reflectance of varying mixtures of clay soil and sand, PERS Journal, Vol. 45, pp. 1145-1150.
[8] Hapke, B (1993), Introduction to the theory of reflectance and emittance Spectroscopy, Cambridge University Press, New York.
[9] Hunt, G R, and Vincent, R K (1968), The behavior of spectral features in the infrared emission from particulate surfaces of various grain sizes, GR Journal, Vol. 73, pp. 6039-6046.
[10] Kaleita, A L et al. (2005), Relationship between soil moisture content and soil surface reflectance, ASAE Journal, Vol. 48, pp. 1979-1986.
[11] Rainey, M P et al. (2000), The influence of surface and interstitial moisture on the spectral characteristics of intertidal sediments: Implications for airborne image acquisition and processing, RS Journal, Vol. 21, pp. 3025-3038.
[12] Rainey, M P et al. (2003), Mapping intertidal estuarine sediment grain size distributions through airborne remote sensing, RSE Journal, Vol. 86, pp. 480-490.
[13] Ryu, J H et al. (2004), A critical grain size for Landsat ETM+ investigations into intertidal sediments: a case study of the Gomso tidal flats, Korea, ECSS Journal, Vol. 60, pp. 491-502.
[14] Ryu, J H et al. (2008), Detecting the intertidal morphologic change using satellite data, ECSS Journal, Vol. 78, pp. 623-632.
[15] Small, C et al. (2009), Spectroscopy of sediments in the Ganges-Brahmaputra delta: Spectral effects of moisture, grain size and lithology, RSE Journal, Vol. 113, pp. 342-361.
[16] Sørensen, T H et al. (2006), Intertidal surface type mapping in the Danish Wadden Sea, MG Journal, Vol. 235, pp. 87-99.
[17] Van der Wal, D et al. (2005), Characterisation of surface roughness and sediment texture of intertidal flats using ERS SAR imagery, RSE Journal, Vol. 98, pp. 96-109.
[18] Van der Wal, D, and Herman, P M J (2007), Regression-based synergy of optical, shortwave infrared and microwave remote sensing for monitoring the grain size of intertidal sediments, RSE Journal, Vol. 111, pp. 89-106.
[19] Yates, M G et al. (1993), The use of satellite imagery to determine the distribution of intertidal surface sediments of The Wash, England, ECS Journal, Vol. 36, pp. 333-344.

2nd International Engineering Symposium - IES 2012
(KU-MU-NITK-HCMCUT Joint Symposium) March 5-7, 2012, Kumamoto University, Japan

Solid Waste Management for Residential and Commercial Areas in India

Dibya Jivan Pati

Manipal School of Architecture and Planning, Manipal University, Manipal, Karnataka- 576 104, India. e-mail: dibyajivan.arun4u@gmail.com

Abstract: Rapid urbanization and uncontrolled growth rate of population has lead solid waste generation and management more acute in India. This research presents a methodology for estimating solid waste generation, efficient collection system and strategies for their effective disposal and recycling in urban areas taking Cuttack as the study area. Willingness to pay for different Municipal Solid Waste (MSW) services helped to determine the extent of MSW management services. The proposed actions for enhancing better quality of environment through proper MSW management require detailed economic and operational feasibility analysis and depend on user charges from every household (h.h.) to make their implementation successful due to which solid waste management can be dealt as the best solution for urban scenarios in India.

***Keywords**: Waste generation, Collection, Recycling, Municipal solid waste, Management.*

Introduction

Waste management and disposal is a growing environmental concern in almost all cities in India. Proper disposal of urban waste is not always a solution for reducing its adverse effect, but also presents a large potential for resource recovery. People belonging to all background in many cities are still unaware of the environmental hazards associated with improper SWM. Improper SWM is also associated with the incidence of large number of diseases and making the surrounding unsuitable for inhabiting.

Background of the study

The greater the economic prosperity and higher the percentage of urban population, the greater amount of waste is produced. Generally, solid waste planners place too much emphasis on residential waste; this waste represents only about 30 percent of the overall municipal waste stream but often receives the lion's share of attention, Daniel Hoornweg (1999). India ranks third among Asian countries, next to China, where low income group are expected to generate around 0.7 kg/capita/day in the year 2025. This indicates the rapid generation of waste by an individual in India. To carry out a clear research, one such city has been picked up as study area – Cuttack, Odisha, with a vision towards the year 2030.

Aim and objectives

The main aim of the research is to prepare a municipal solid waste management (MSWM) plan for Cuttack municipal area. The objective is to analyse the quantum of waste generation, to plan an efficient collection system with required landfill and prepare appropriate strategies for recycling and disposing of useful waste.

Literature Review

Wastes are those which are of no use or have any value. Solid waste can be liquid, semi-solid, and solid or containerized gaseous material; e.g. toys, clothes, papers, scrap metals etc. Solid waste management (SWM) involves management of activities associated with generation, storage, collection, transfer and transport, processing and disposal of solid waste. Commonly called as 'Municipal Solid Waste' or MSW, they are classified into many categories like bio-degradable waste, non-biodegradable, recyclable and non-recyclable waste.

Functional elements of MSWM: -

Generation – In Indian cities, it's been seen that solid waste generation ranges from 200gms/capita/day in small city to 500gms/capita/day in metro. The amount of waste generated per capita is estimated to increase at a rate of 1% to 1.33% annually, Bhide A.D. and B.B.Sunderesan (1983).

Storage - In commercial areas wastes are stored within the premises and also same in industrial areas which are called primary storage. While in residential areas, the occupants take the waste from their own dustbin and transfer it into community storage bins called secondary storage.

Collection – Waste are generally transferred from small primary collection to large bins, called secondary collection. Primary collections are quite common in India.

Transportation – Problems has been seen in developing countries where 60% of wastes are collected to be transported to the disposal site but rest are left behind due to unavailability of fleet or absent of sufficient crews or worker.

Disposal - These days, new methods are being adopted. The disposals of garbage are done by Sanitary Land Fill (SLF). These are well designed and engineered with better facilities to reduce nuisance and health hazard to public and environment, Amalendu Bagchi (2004).

Concept of 3Rs

3Rs popularly known as reduce, reuse and recycle has the concept which itself goes beyond just better waste management. When we look at the 3R concept within the production cycle, we can see a number of ways in which 'reduce, reuse, recycle' aspects can be incorporated, Hari Srinivas (1997).

Case studies on best practices

1. Composting and vermin-composting, Phillipines -

The main objectives were to reduce production of solid waste by composting; to reduce the amount of waste for disposal by landfill, thereby minimizing pollution and to reduce disposal cost.

Types of composting method used:

a. Traditional method
b. Non-traditional method

Materials used: - Worms (African Night crawlers/Red wigglers), Bedding, Hammer mill/shredder (3hp), Food wastes, fruit/vegetable trimmings and peelings, Dry leaves and stems, Strainer / Sifter, Gardening gloves.

Composting bedding facility infrastructure

5 beds in 1 composting facility of 500 sq.m., 1 Facility = 5 beds, shredding area, stacking for raw materials, storage of harvest, Dimension of the pit: W – 9ft, L – 18 ft., H – 3ft

The result:

- Input = 400 kilos of yard waste and 2 kilos of worms
- Output = 350 kilos of compost

Benefits:

- Savings from dumping fee of 2,500/truck and operations cost of 2,500 (diesel, driver and helper)
- Income from compost at Rs.30/kilo (INR)
- Income from sale of worms =Rs.700/kilo
- Employment generation; and
- Environmental protection

Study area and Data collection

City of Cuttack is surrounded by two rivers – Mahanadi and Kathajodi Rivers. The average temperature range is 42°C to 10°C. Major soil types are alluvial, sandy and clayey.

Population under Cuttack Municipal Corporation is 6,55,000 (2008 census) with density of 2206/sqkm. Total area of Cuttack under municipality is 118.70 sqkm with 48 wards, under it, Census India (2001). Average household size is estimated to be 5.5 members per house, Census India (2001). Refer Fig.1 for land use map of Cuttack city under municipality and Fig.2 for Ward map.

Existing situation regarding SWM

- Provision of waste bins is not sufficient
- Despite the total amount of solid waste being generated is around 248 MT/day, they have no adequate garbage collection system, IIT Kharagpur (2006).
- Methods like storage system, segregation, door-to-door collection are still not practiced in many areas
- Modes of transport of garbage are wheelbarrows and tractor-trailers.

Data collection

Primary, secondary and visual surveys were carried out to find the complete data

which explains the current profile of Cuttack.

A survey Performa consisted of a set of objective questions based on the socio-economic, physical and environmental aspects related to the study area. The respondents were the household members and laborers working in relevant management system. The secondary survey is the most relevant data in this research study due to the need of environmental aspects of the area. The approach was made to the various organizations associated with MSWM. Various constraints were faced due to non-availability of certain data and the unwillingness of officials to part with sensitive data.

The primary and secondary survey helped to provide information to analyze the study area with the help of various tools and techniques taking at least five wards as core study area.

Waste Generation

Population: -

The population of city is estimated to be increasing about 58% from 2008 to 2030. The unavailability of land can be the reason for decreasing trend in growth rate. Population of Cuttack municipal area is given in Table 1 with projection. It's expected that the population will rise to 1115000 in 2030, IIT Kharagpur (2006).

Residential waste generation: -

Calculations were carried out for residential waste generation considering average weight of waste based on nature of dwelling units. Table 2 shows the estimated avg. wt. of waste generated.

Commercial waste generation: -

Same calculations were carried out in case of commercial areas with total number of shops at each ward level and then converted into amount of different waste being generated per day at city level which came to be 19267 kg/day.

Thus, the total waste generated based on residential and commercial waste for 2008 is 128.62 metric ton/day (MT/day).

Other waste generation: -

As per the Comprehensive Development Planning (CDP) of Cuttack of Development Planning Area, 2009, construction waste, hospital waste, sweeping waste and hotel/market general waste also contribute to other waste coming into total of 187.4 MT/day, i.e. 59.5% of total waste.

Thus, the total waste generated in 2008 at city level is estimated as 316 MT/day. And this value is projected to find the total estimated amount of waste generation in 2030 as 619.8 MT/day at Cuttack city level.

Waste Collection

As per the secondary survey, an interview was taken on municipal staffs to find the characteristics of the waste collection system in Cuttack which included number of permanent staffs, temporary staffs and vehicles used for transportation. The final dumping site is located at Chakradharpur which is 25km from Cuttack Municipal Corporation (CMC) office. Fig.3 shows the site for dumping. The location of dustbins, route of transportation and collection point were observed through primary surveys.

Willingness to separate and recycle: -

From primary survey it was found that there can be three categories of waste – Landfill, compost and recyclable waste. Fig.4 shows clear data of number of people willing to separate and recycle in 2008 and estimation of the same for the year 2030.

Willingness to pay: -

As per primary survey, the willingness to pay for door-to-door collection system has been analysed to find an appropriate amount of money to utilize for increasing manpower and providing vehicles for collecting garbage. Table 3 shows the categories of dwelling units where households are willing to pay an average price/month for different activities. Assuming the average user charge for daily collection to be Rs.10/month/family the annual charge would be Rs.120/month/family. And this data helped to find the Gross amount of money that could be collected through all the families as well as the shops in Cuttack. Table 4 shows the amount of money that could be collected for door-to-door collection.

Door-to-door collection (d2d)

Labor requirement: With certain assumptions, the number of laborers required to collect the waste were calculated considering data such as

number of buildings, speed of wheelbarrow, time for loading and unloading etc. Assuming the working hours to be 7am-11am, the number of labors requirement could be found out for every ward.

Cart/wheel barrows requirement: The number of carts can be calculated regarding the amount of waste to be collected. Since construction wastes are not expected to be collected through d2d collection, hence it has not been included here. The number of carts required was calculated by using standard capacity of one cart having 6cu.ft volume, *[www.epa.vic.gov.au/bus/erep/docs/waste materials-densities-data.pdf]* and can carry only MSW (domestic waste) of 100kg when fully loaded. So regarding this value, the required number of carts could be calculated.

Waste Disposal

Existing scenario: The secondary survey helped to list out the scenario of waste disposal by interviewing the CMC staffs. According to the visual survey, some observations have been noted - Only 60% of waste collection is achieved, the dumping was the only method, segregation of waste is not practiced, rag pickers collect few plastic and sell them for Rs.10/kg.

Estimate for Sanitary landfill area: Considering situation after 20 years, the total area for landfill was calculated as shown below: -

- Total Quantity of land fill waste to be collected after Door to door collection at present = 152335 kg/day
- Projected quantity of landfill waste for year 2030 = 294568 kg/day
- The averages (223451.4326 kg/day) of these two values are taken considering landfill life of 20 years.
- The standard density of waste after compaction is taken as 600 kg/cu.m.
- Thus, daily waste volume of landfill waste is estimated as 372cu.m.
- Considering 20 years, total volume of landfill waste is estimated as 2,715,600cu.m.
- Assuming the depth of the land fill = 4m (considering a safety of 2mt from ground water table) area for landfill is estimated as 678900 sq. mts.(For e.g. (824 x 824) sq. mts.) or 167 acres approx. The site has been proposed as per Cuttack CDP 2009, hence, it not the part of the research.

Estimates on area requirement for compost plants: According to the case study *on best practice*, the size of single compost bed could be ascertained with approximate volume – 486 cu.ft**.** Since, density of food waste when compacted = 1029 kg/cu.m. Thus, 14163 kg of compost waste can be composted in 486 cu.ft pit. Thus, assuming the decomposing of waste to be 30 days, the total number of pits required will be 120. Later the total area for compost plant was calculated by adding the area of all pits and area for drying the composted materials which is 1.5 times the area of total pits, i.e. 0.67 acres of land. NGOs are responsible for location of site.

Estimates on recyclable waste: According to the analysis through primary survey, the total waste including-paper, plastic, glass and metals came to be 37869 kg/day. This was further estimated for 2030 at city level, in which the total recyclable waste generated would be 73125 kg/day. Waste segregation centers at the ward level should be constructed taking into account the quantity of recyclable waste.

Proposals and cost benefit analysis

Tax collection by municipalities: An added tax could be specially considered for d2d collection. So as per the analysis from willingness to pay through primary survey a gross total of tax could be calculated. Hence the total money which can be collected by the Municipality is estimated as 1.15 crore/year. These can be used for activities like street cleaning, collection from community bins and mini ports, transfer of waste and landfill acquisition.

Cost benefit analysis on composting: Considering the average selling price of compost to be Rs. 2000/ton, construction waste – Rs. 1500000, implementation and machinery – Rs.400000 and other cost to be Rs.650000, the revenue generation is estimated as Rs.1104000 for 30 days which proves composting to be the most profitable operation.

Costs benefit analysis on Recycling:
Assuming the average selling price of each recycled materials, the total revenue generation could be estimated for the year 2020 as follows –
Recycled paper → Rs. 4, 68, 33, 150/year
Recycled plastic → Rs. 95, 99, 208/year
Recycled glass → Rs. 1, 05, 56, 859/year
Recycled metals → Rs. 6, 88, 83, 749/year

Collection Plan
After the thorough analysis, it is possible to propose for 100% efficient collection system. A scheme can be prepared based on alternate days for collection of different waste through a week. For each ward, according to the number of workers, the collection efficiency could be evaluated through number of containers requirement. Fig.5 shows the plan of collecting wastes through four trips in one colony.

Awareness
General recommendations and campaign should also be followed to create more awareness among the public. Police force should also be put among the part of such responsibilities and imposing certain penalty can also bring in control among the violators.

Conclusion
Major aspects that could be highlighted as follows:
- Estimating solid waste generation;
- d2d collection and strategies for effective disposal of waste & recycling;
- benefits from various methods of treatment;
- Participation of private companies and
- NGOs which plays a major role in efficient collection and disposal of MSW; and employment generation.

This research methodology could also be adopted in other Indian cites for effective planning of MSW management services.

Acknowledgements
Consultants at IIT, Kharagpur helped in producing relevant data on Cuttack. Municipality staffs provided necessary information during survey. Dr. D.Pandit helped in completing the research through his valuable suggestions.

References
[1] Amalendu Bagchi (2004), Design of Landfills and Integrated Solid Waste Management
[2] Bhide A.D. and B.B.Sunderesan (1983), Solid Waste Management in Developing countries
[3] IIT Kharagpur, 2006, CDP Cuttack
[4] Census India (2001)
[5] Daniel Hoornweg (1999), What a Waste!
[6] Hari Srinivas (1997), The 3R Concept and Waste Minimization
[7]www.epa.vic.gov.au/bus/erep/docs/wastematerials-densities-data.pdf

Table 1: Population of Cuttack

Year	City Population
1991	403418
2001	535139
2008	655000
2030 (estimate)	1115000

Table 2: Residential waste based on nature of dwelling units

No. of floors	% of h.h.	Estim.no. of buildings	Tot. waste gen. in kg / day
Slums	5.40	6431	2526.46
1storey	78.7	93677	73068.06
2storey	14.0	9269.44	12397.88
Multi st	1.93	957.5	2361.83
Total		110334.5	90354.24

Table 3: Average price/month

No. of floors	daily collection	odor free	clean city
1	6.0	8.4	7.7
2	7.00	9.56	7.86
Multi-st.	7.2	10.6	7.6

Table 4: Amount of money (in Rs/yr)

No. of floors	Rs./year/ building or shop	no. of bldgs/ shops (estim.)	Cuttack
One	120	93677	11241240
Two	216	9269	2002200
Multi-	288	957.5	275760
Com.	120	3533	423960
money for d2d/yr			13519200

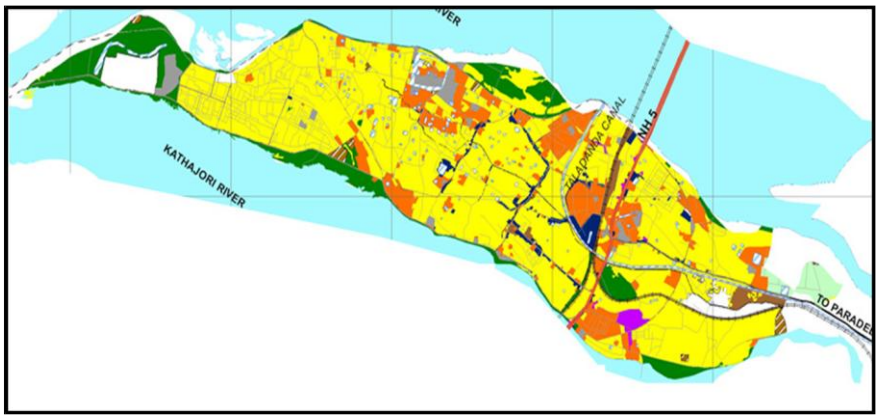


Fig. 1: Land use map of Cuttack city under Municipality

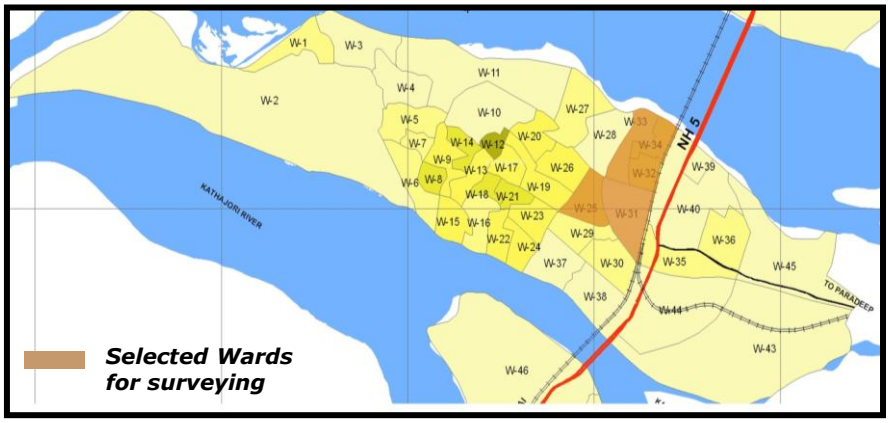


Fig. 2: Wards selected for survey and data collections



Fig. 3: Dumping site at Chakradharpur

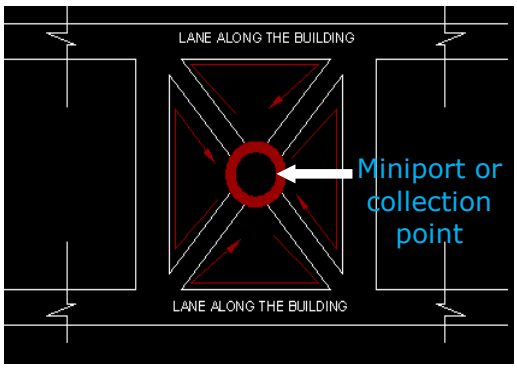


Fig.5: Plan for collecting wastes

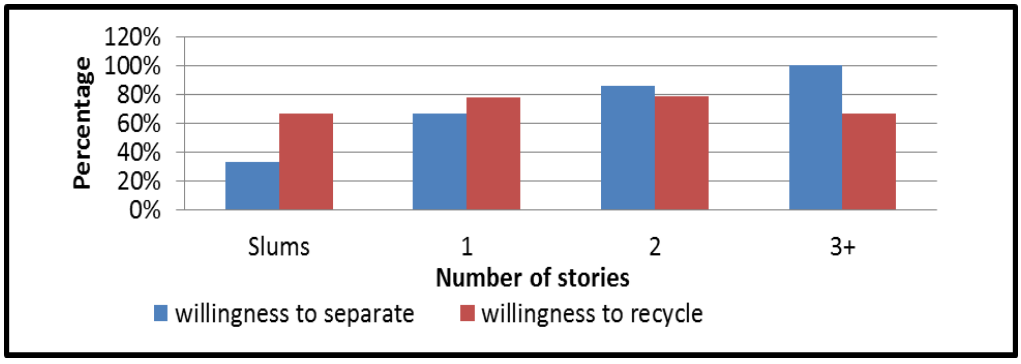


Fig.4: Graphical representation of number of people willing to separate and recycle

2nd International Engineering Symposium - IES 2012
(KU-MU-NITK-HCMCUT Joint Symposium) March 5-7, 2012, Kumamoto University, Japan

IMPACTS OF THE LAND SUBSIDENCE ON SUSTAINABLE URBAN DEVELOPMENT

Le Van Trung [1] **Vuong Quoc Viet [2]**

1 *Department of Environmental Management, Ho Chi Minh city University of Technology, Viet Nam. e-mail: lvtrungs@yahoo.com*
2 *Geomatics Center, Viet Nam National University's Information Technology Park, VietNam. email: quoc.viets@yahoo.com*

Abstract: This paper discusses the relation between land subsidence, ground water use and urban development activities. The spatial and temporal variations of land subsidence depend on the corresponding variations of the urban development (average velocity > 10mm/year) have resulted in tides moving into low-lying areas that were previously above high-tide levels. Each year, climate change could cause sea levels to rise by 3mm in the mean high tide level and this involved certain difficulties for tide line analysis, flood prevention plan and management.
This paper demonstrates the Permanent Scatterer InSAR (PSInSAR) Technique for land subsidence monitoring and the use of GIS for mapping susceptible areas for a study site. This solution aims to achieve the sustainable urban management.

***Keywords**: PSInSAR Technique, Land subsidence, Climate change, GIS*

Introduction

Ho Chi Minh City (former Sai Gon) is situated by the Sai Gon River in the centre of the Cuu Long delta and the South-eastern part of South Vietnam. HCM city has population 8 mil. people, 2095 km2 area and great potential for developing industry, exports, tourism and services. At present, however, residents of HCM city must confront flooding every year during the rainy season. Flooding may be caused by heavy rain, high tide, rain & tide, poor drainage, water release by hydroelectric dams and land subsidence combined with a global sea level rise. Flood prevention has been one of the biggest preoccupations of Ho Chi Minh City authorities and large-scale work are carrying out such as: construction of new sewers, repair of existing drainage systems, excavation of canals and reinforcement of the banks, demolition of housing built on piles,... Many projects have been implemented but in fact most of them are not effective, because urban development of HCM city and its surrounding areas has grown very rapidly in the sectors of industry, trade, transportation, real estate and many others from the year 1986 until now. This exponentially increase urban development introduce several environmental problems such as: extensive conversion of prime agricultural areas into residential and industrial areas; increase in groundwater extraction due to development of industrial activities and the high population increase; especially HCM City locates at the soft soil, the ground water use was in a large scale, ground water decreasing (>20m from 1990 until now) caused deform of soil which makes the ground level goes down. Land subsidence (average velocity > 6mm/year) has resulted in tides moving into low-lying areas that were previously above high-tide levels. Each year, climate change could cause sea levels to rise by 3mm and in the mean high tide level, water level in rivers is higher than the ground level. Most of the river area in HCM city becomes on-ground river and land subsidence makes the situation even worse. Figure 1 illustrates the rapidly growing urbanization and Figure 2 introduces the flood on low-lying land due

to the combined effect of tide and land subsidence

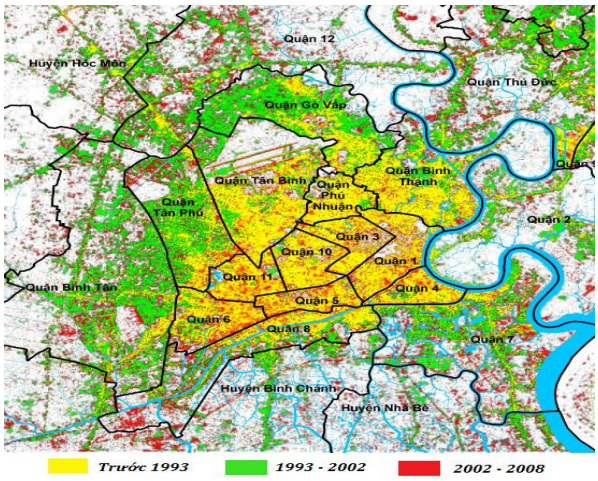


Fig. 1 Trend of the urbanization of city

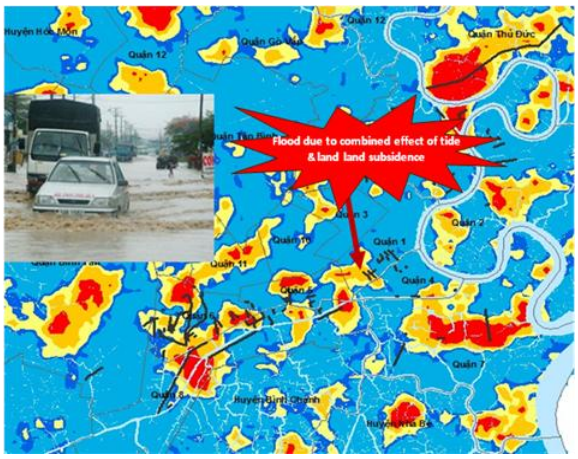


Fig. 2 Flooding-prone areas of the city

This paper will discuss current land subsidence that involved certain difficulties for flood prevention plan and management as well as what actions should be taken now to reduce risks of flood disasters that aims to achieve the sustainable urban management.

Status of land subsidence

Land subsidence due to excessive withdrawal of groundwater has become a worldwide problem in, for example, Tokyo, Japan (Yamaguchi 1969), Bangkok, Thailand (Bergado et al. 1987), Venice, Italy (Carbognin et al. 2000),… However, the land subsidence in HCM city was discovered in 2003, there were several areas appeared land subsidence especially around water pumping stations of district 6 (10 - 22cm), district 12 (20cm), district Binh Tan (3 - 30cm) and Binh Chanh (4 - 19cm). Rapid increase of ground water use started in 1990 when HCM City were urbanized with some new districts, people and the industries used ground water as the main water resource. Ground water exploitation was estimated at about 800,000 m^3/day (in 2008) and the expansion of surface water works in city has not met this rapid increase. Besides, until now free of charge ground water and uncontrolled exploitation has increasingly augmented the exploitation rate.

Evaluating the preliminary result in using Permanent Scatterer InSAR (PSInSAR) Technique showed that land subsidence started in the cities of Ho Chi Minh in the 1986s and was getting worse until now.

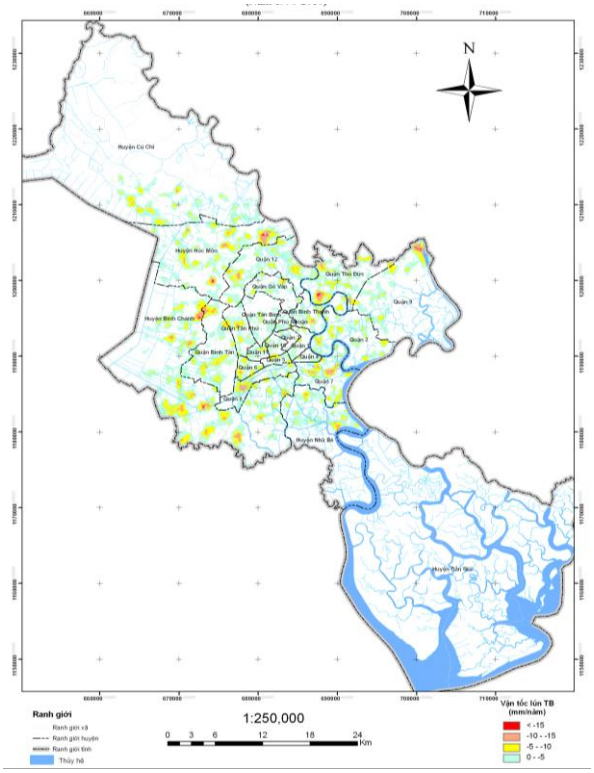


Fig. 3 Land deformation map of the city

In general the land subsidence exhibits spatial and temporal variations, with the rates of about 6 to 10 mm/year. A few locations can have the subsidence rates up to about 15 mm/year. Land subsidence leads to the permanent lower down of the ground elevation, and put heavy pressure on the solutions for flood prevention. Therefore, HCM city needs a new

assessment of land subsidence and sea level changes in flood prevention.

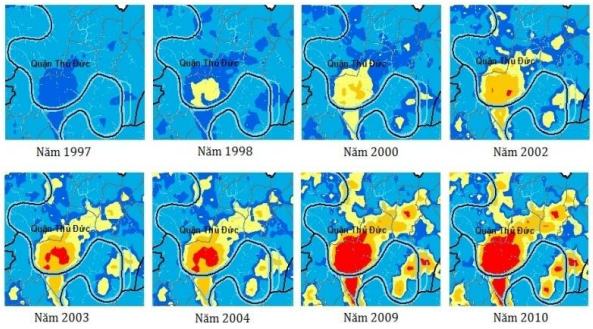


Fig. 4 Subsidence rates for different years

Over 140km2 of the area has suffered the land subsidence (0, 67% area of HCM city) with the maximum rate of subsidence is 10 -15 mm/year. Five districts with subsidence greater than 15mm/year and the subsidence region coincides with a groundwater depression cone. From 1997 to 2002, several subsidence areas have formed and widen, the total amount of subsidence had increased from 155mm in 2003 to 310mm by 2010.

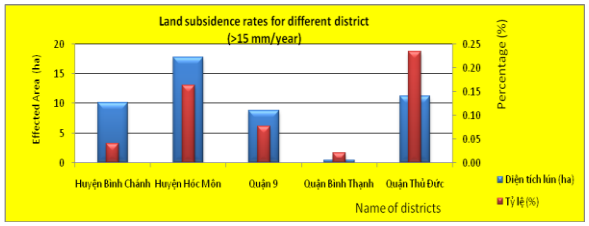


Fig. 5 Subsidence rates and affected area

Urban development and subsidence

Land subsidence in HCM city can be caused by the excessive groundwater extraction, load of buildings and constructions, and the combined effect of a large number of urbanized zones are situated at a very low elevation and along the canals with alluvium soil. Up to now, there is no information yet about the contribution of each factor on the subsidence at each location and their spatial (contribution) variation

The impact of land subsidence in HCM city could be seen in several forms, but almost subsidence are caused by human's activities, in which the groundwater large exploitation is the most important factor. HCM City locates at the soft soil and has the five aquifers, namely, (i) Holocene, (ii) Pleistocene, (iii) Upper Pliocene, (iv) Lower Pliocene and (v) Mesozoic. Three of five aquifers play an important role in water supply for this city: Pleistocene aquifer (20–50 m), upper Pliocene aquifer (50–100 m) and lower Pliocene aquifer (100–140 m). Until now, ground water level is decreasing (annual drawdown: 2m depth at the heavy ground water pumping stations) that may cause deform of soil due to ground water extraction. The ground level goes down at the rate of few 15mm per year that can be measured at the heavy ground water pumping stations

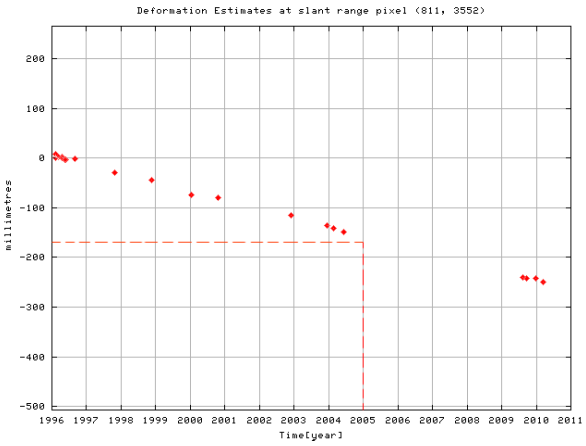




Fig. 6 Subsidence rates at pumping station

The increase in population and urban development activities in HCM city lead to increase in built-up areas, decrease in green areas and increase impervious surfaces that water cannot infiltrate. These surfaces are primarily associated with transportation (streets, highways, parking lots, sidewalks) and buildings,... In 1975, the green areas made up more than 40 percent of the HCM city's area and currently account for only 10 percent of the area (the inner city districts).

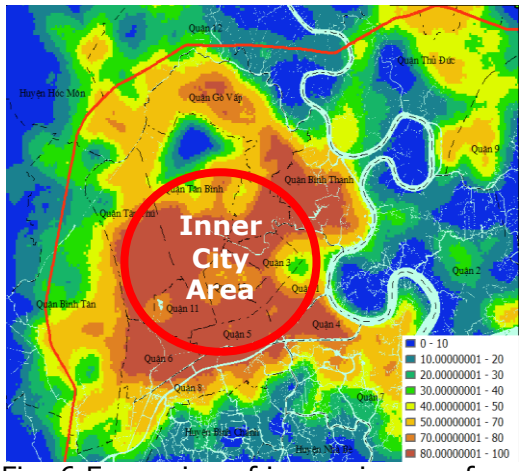


Fig. 6 Expansion of impervious surfaces

Five new districts have also been developed (1997) which also increase the coverage of built-up areas in the region and people and the industries used ground water as the main water resource in economic activities. Evaluating the preliminary results showed that land subsidence is usually associated with the relatively high rates of groundwater level change rates. The correlation between land subsidence and excessive groundwater taking in HCM city can be illustrated in Figure 7 that shows the maximum subsidence during the period of 1990-2000 is about 70 mm, while for the period of 2000 -2010 is about 150 mm.

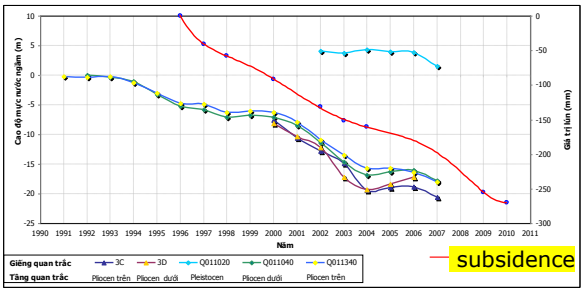


Fig. 7 Correlation between land subsidence and groundwater level change rates

In general, the subsidence rates in HCM city area during this period is about 26 -30 cm at several locations. Land subsidence made original levelling height lapse and deteriorates flood prevention situation through knocking down the ground elevation. Urban development in HCM city caused increases in built-up areas, population, industrial activities and groundwater extraction,... The lowering of the groundwater level is not only caused by extensive pumping but also by a decrease in groundwater recharge. The most effective means of subsidence reduction is to prohibit groundwater pumping in the subsidence region as well as undertaking aquifer restoration and artificial recharge. A comprehensive monitoring network coupled with an understanding of the ground conditions and subsidence mechanisms in HCM city and accurate researches must be done on land subsidence to identify the surface deformation for solving problems in flood prevention.

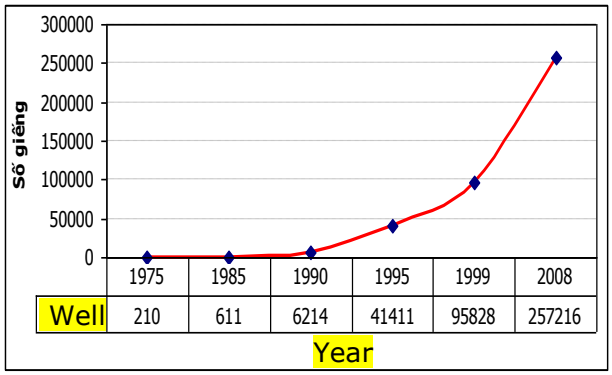


Fig. 8 Trend of ground water exploitation

HCM city dominantly consists of plains of which the percentages are 60 % is that ground elevation level is below +1.5m while current max tide level: +1.58 m. The effect of land subsidence and sea level rise will cause residents in many wards suffered water-logging of between 0.4-0.5m

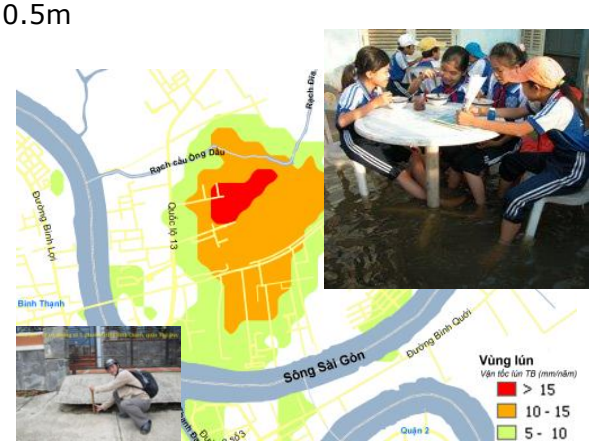


Fig. 9 Effect subsidence at flooding areas

Conclusions

The HCM City locates at the soft soil and the low elevation of the land, rivers and canals form a complex network that is affected by tide. This paper showed that impacts of the land subsidence on sustainable urban development and the following conclusions are deduced from this study:

.

- Over the period of 1997–2010, the land subsidence exhibits spatial and temporal variations, with the rates of about 6 to 15 mm/year.
- Land subsidence in HCM city can be caused by the excessive groundwater extraction, load of buildings and constructions, and the combined effect of a large number of urbanized zones are situated at a very low elevation and along the canals with alluvium soil.
- Land subsidence combined with a global sea level rise has been increased frequency of flooding, that residents in many wards suffered water-logging of between 0.4-0.5m however, the contribution of land subsidence to flooding has not been taken into much consideration.
- The impacts of urbanization on groundwater systems are predictable and should be considered in urban planning.
- HCM City needs to conduct a risk assessment and to complete the monitoring network covering subsidence zones for flood prevention plan that aims to achieve the sustainable urban development.

Acknowledgements
The authors thank Ho Chi Minh City University of Technology, Vietnam for technical support during this work and JICA - HCMUT Project provided financial support to carry out this research.

References

[1] Chen, Y.Q., G.B. Zhang, X.L. Ding, and Z.L. Li. *Monitoring Earth Surface Deformations with InSAR Technology: Principle and Some critical Issue.* Journal of Geospatial Engineering, 2000, 2(1): 3-21.

[2] Damoah-Afari P., Ding X.L. *Measuring Ground Subsidence in Shanghai using Permanent Scatterer InSAR technique*. The 26th Asian Conference on Remote Sensing, 2005.

[3] Ferretti, A., Prati, C., and Rocca, F.,. Nonlinear subsidence rate estimation using permanent scatterers in differential SAR interferometry. *IEEE Transactions on Geoscience and Remote Sensing*, 2000, Vol. 38, 2202-2212.

[4] Ferretti, A., Prati, C., and Rocca, F., Permanent scatterers in SAR Interferometry. *IEEE Transactions on Geoscience and Remote Sensing,* 2001,Vol. 39, 8-20

[5] Hasanuddin Z. ABIDIN, Heri ANDREAS, Irwan GUMILAR and Mohammad GAMAL, Yoichi FUKUDA and T. DEGUCHI. Land Subsidence and Urban Development in Jakarta (Indonesia). 7th FIG Regional Conference,2009

[6] Yueping Yin; Kaijun Zhang; Xiaochun Li Urbanization and land subsidence in China. The Geological Society of London, 2006

2nd International Engineering Symposium - IES 2012
(KU-MU-NITK-HCMCUT Joint Symposium) March 5-7, 2012, Kumamoto University, Japan

Flexural Fatigue Analysis of Steel Fibre Reinforced Concrete

Girish M G [1] **A Chandrashekar [2]** and **A U Ravi Shankar[3]**

1 *Department of Civil Engineering, Manipal Institute of Technology, Manipal 576104, India. e-mail:girishmurgod@gamil.com*
2 *Department of Civil Engineering, KVG College of Engineering, Sullia, D.K 574327, India. email:acs.nitk@gmail.com*
3 *Civil Engineering Department, National Institute of Technology Karnataka, Surathkal, Mangalore 575025, India. aur@nitk.ac.in*

Abstract: This paper presents the experimental investigation carried on Steel Fiber Reinforced Concrete (SFRC) subjected to repeated loading. The SFRC beam specimen of size 500mm x 100mm x 100mm containing mixed steel fibers of size 50mm x 2mm x 0.6mm and 0.5mmΦ× 30mm in different proportions were tested under two point flexural fatigue load at a frequency of 2Hz at various stress levels. The readings obtained from the flexural fatigue test were used to plot S-N diagram and also to perform statistical analysis using two parameter Weibull distributions.

***Keywords**:* Steel fiber reinforced concrete; flexural strength; fatigue failure of rigid pavements; Weibull Distribution.

Introduction

Structures such as deck slab of bridge, highway and airfield pavements are often exposed to repetitive (fluctuating) loads by moving traffic. This causes variation of stresses in the structural parts and the structural member fails at a smaller stress level than the stress level at static loading condition, Phull and Rao (2007). The phenomenon of early failure of structural components under repetitive loads is known as fatigue failure. The word fatigue is derived from the Latin word fatigare which means 'to tire', Suresh (2006). Fatigue is widely accepted terminology in engineering studies which deal with damage and failure of structure under dynamic or fluctuating loads. In this paper, the fatigue failure of steel fiber reinforced concrete pavement under repetitive flexural load is discussed.

The fatigue failures may be simple or compound and can occur in different forms. In rigid pavements, fatigue failure begins with initiation of micro-cracks within the concrete layer under the application of wheel load due to moving traffic. These cracks usually start from the bottom of the concrete layer and propagate up to surface, resulting deterioration of pavement due to decrease in flexural strength and subsequent loss of pavement materials through the developed cracks. Therefore fatigue is an important factor to be considered for designing of cement concrete pavement.

Systematic study carried by many researchers has shown that the incorporation of steel fibers into the concrete mix significantly improves flexural strength, Rollings (1989), Lok and Pei (1999), ductility, Bayasi (2001), high damage tolerance, Kuang (2009) and fatigue strength, Shi et al (1993), Singh et al (2005 and 2006), Chandrashekar et al. (2010) of concrete. The improvement in mechanical strength is due to either by fibers knitting the cracks together there by delaying the propagation of cracks or by transferring the force across the cracks.

In the present investigation for the analysis of flexural fatigue behavior of SFRC, cement concrete beams of dimension 500mm x 100mm x 100mm containing crimped steel fibres (fig.1) in

different proportions (Table1), were subjected to two point flexural repetitive loads at a frequency of two cycles per second. The grade of concrete used is M30. Prior to the fatigue test, fundamental tests such as compressive strength test, flexural test, tensile test and modulus of elasticity test on hardened concrete were also conducted.

Results and Discussion

Effect of fibers on compressive strength

Concrete containing steel fibers showed better compressive strength than the reference concrete (fig.2). The increase in compressive strength with respect to reference concrete (R) for HS1 is 8% and for HS2 is 18%. Between two fiber mixes, HS2 has improved strength of 8% when compared to HS1.

Effect of fibers on flexural strength

The flexural strength is an important factor in view of the fact that increase in flexural strength will improve the fatigue resistance of concrete. The incorporation of steel fibers into concrete improved the flexural strength of concrete (fig.3). This enhancement in strength is due to resistance offered by the fibers to crack propagation and also due to induced ductility by the fibers. The increase in flexural strength for HS1 and HS2 with respect to reference concrete is found to be 6% and 13% respectively.

Effect of fibers on tensile strength

The incorporation of steel fibers into concrete significantly increased the tensile strength of concrete (Fig.4). The increase in tensile strength when compared to reference concrete for HS1 is 28% and for HS2 is found to be 42%.

Effect of fibers on elasticity modulus

The inclusion of fibers into concrete considerably enhanced the elasticity modulus (Fig.5). The increase in elasticity modulus when compared to reference concrete for HS1 and HS2 is found to be 36% and 50% respectively.

Effect of fibers on fatigue strength

The fatigue behaviour of SFRC can easily be analysed using stress-life approach (originally proposed by Wohler in 1860s), Suresh (2006). In stress-life approach, the fatigue test results are represented by S-N plot, where S denotes the stress amplitude and N represents number of cycles to fatigue failure. S-N curve gives the basic information about the progressive failure of structure under repetitive loads. Table2 gives the results of two point flexural fatigue tests conducted on reference and steel fiber reinforced concrete and the same is pictorially represented using S-N plot (Fig.6-8). It is observed that at the higher stress amplitude the concrete specimens sustained fewer cycles to failure and as stress amplitude reduced the no. of cycles to failure also increased gradually. The regression equation generated from the S-N curve can be used to estimate fatigue cycles at various stress amplitudes. Although S-N curves are widely used in fatigue studies, it is known to be an empirical approach, Suresh (2006) and gives fundamental information only. Further, fatigue life test results are often scattered and the failure patterns are randomly distributed. Therefore, uncertainties of these types require use of some statistical approach for analysis. Weibull distribution is one such well known statistical method generally employed for the analysis of fatigue failure, Singh et al (2005 and 2006).

The cumulative distribution function F_N (n) of the Weibull probability can be expressed as

$$F_N(n) = 1-\exp\left[-\left(\frac{n-n_0}{\mu-n_0}\right)^{\alpha}\right] \qquad (1)$$

For $n \geq n_0$; $\alpha > 0$; and $\mu > n_0$, in which n specific values of the random variable, N; α=shape parameter or Weibull slope at stress level, S; μ=scale parameter or characteristic at stress level, S; and n_0=location parameter or minimum life at stress level, S.

The Weibull survival function is as given below.

$$L_R(n) = 1 - F_N(n) \qquad (2)$$

Substituting for F_N (n) and taking log on both sides the above equation is deduced as follows

$$\ln\left[\ln\left(\frac{1}{L_R(n)}\right)\right] = \alpha \ln(n) - \alpha \ln(\mu) \qquad (3)$$

The equation (3) represents the general form of straight line. A graph (fig.9) is plotted between $\ln\left[\ln\left(\frac{1}{L_R(n)}\right)\right]$ & $\ln(n)$ for all series of concrete, and a best fit straight line is drawn through the data. The slope of the line provides an estimate of the shape parameter α and the characteristic life μ can be obtained using the equation $B = \alpha \ln(\mu)$ where B is a constant of straight line obtained from graph. The values of α and μ so obtained are tabulated in the Table3. It is found that (fig.10) as the stress amplitude decreases the values of characteristic life μ increases significantly which indicates that a member can take more load repetition at lower stress. Further, the statistical model is validated using Kolmogorov–Smirnov goodness-of-fit test and the result of the test is given in the Table4. The model is found to be acceptable at 5% significance level.

Conclusions

The following conclusions are deduced from this study:

1. The inclusion of crimped steel fibers in the concrete matrix resulted in improvement in compressive and flexural strength. The increase in compressive strength is found to be 8% to 18% and enhancement in flexural strength is found to be 6% and 13% respectively.
2. The fibers enhanced the tensile strength and elasticity modulus considerably. The increase in tensile strength is found to be 28% to 42% and improvement in elastic modulus is found to be 36% to 50%.
3. The steel fibers in the concrete helps in bridging the cracks developed due to applied load thereby delaying the propagation of cracks and enhancing the fatigue resistance of concrete.
4. The variation of fatigue life at various stress levels can be well studied using S-N plot and further supported by two parametric Weibull distribution.

Acknowledgements

We would like to express our sincere gratitude to Ex-H.O.D of Civil Engineering Dept. NITKS for permitting us to use laboratory facilities to this research. We also like to thank the organisers of IES 2012, for providing us an opportunity to express our views. Finally we would like to express our sincere gratitude to MIT Manipal, for providing all sort of support.

References

[1] Bayasi, Z., Kaiser, H. (2001), Steel Fibers as Crack Arresters in Concrete, Indian Concrete Journal Vol. 75, No.3, pp.215-219.
[2] Chandrashekar A, Ravi Shankar A.U, and Girish M. G (2010), Fatigue Behaviour of Steel Fibre Reinforced Concrete with Fly Ash, Highway Research Journal, Vol. 3, No.2, pp. 9-22.
[3] IRC SP: 46-1997, Guidelines for Steel Fiber Reinforced Concrete for Pavements, Indian Roads Congress", New Delhi.
[4] Kuang J. S, Baczkowski B. J. (2009), Steel-Fibre-Reinforced Concrete Coupling Beams Subjected to Monotonic Loading, Magazine of Concrete Research, Vol. 61, No.1, pp. 35-41.
[5] Lok. T, Pei, J. (1999), Flexural Behaviour of Steel Fiber Reinforced Concrete, Journal of Materials in Civil Engineering, Vol. 10, No.2, pp.86-97.
[6] Phull Y R ,Jagannatha Rao P (2007), Assuring Fatigue Adequacy of Concrete Pavements: Some Essential Needs, Indian Highways March, pp 9-19
[7] Rollings, R. (1989), Developments in the Corps of Engineers Rigid Airfield Design Procedures, proceedings of the international conference on concrete pavement design, Purdue University, West Lafayette (IN), pp 405.
[8] Shi X. P, Fwa T.Fand Tan S.A (1993), Flexural Fatigue Strength of Plain Concrete, ACI material Journal V90,No.5,pp 435-440
[9] Sing, S.P., Mohammadi, Y. and Kaushik, S., K. (2005), Flexural Fatigue Strength and Failure Probability of Steel Fibrous Concrete Containing Mixed Fibres, IE Journal-CV, Vol.86, pp. 12-18.
[10] Sing, S.P., Mohammadi, Y. and Kaushik, S., K. (2006), Probability of Fatigue Failure of Steel Fibrous Concrete Containing Mixed Fibers, Asian Journal of Civil Engineering (Building and Housing), Vol. 7, No. 1, pp. 1-12.
[11] S Suresh (2006), Fatigue of Materials, 2nd ed., Cambridge University Press, New York.

Table 1 Description of specimen

Designation	Description	Flat Fibers	Wire Fibers
R	Reference concrete	Nil	Nil
HS1	SFRC	0.25%	0.25%
HS2	SFRC	0.50%	0.50%

Table 2 Fatigue life data

Designation	Sl. No↓/Stress Ratio→	0.85	0.8	0.75	0.7
R	1	90	1665	11150	35343
	2	156	2240	18680	45675
	3	265	3200	28935	73444
	4	308	4260	32849	83151
	5	360	5170	35118	100000
HS1	1	126	2356	10764	32413
	2	228	2413	11864	41373
	3	268	4135	26810	53264
	4	328	5600	49197	75756
	5	418	6337	51500	90300
HS2	1	158	2247	14105	28130
	2	190	3520	24500	37656
	3	235	4263	34750	48344
	4	328	4575	37900	67405
	5	418	10370	45617	86172

Table 3 Weibull parameters

Designation	Stress Level	α	μ	correlation coeff., R^2
R	0.85	1.526	284	0.961
	0.80	1.906	3879	0.988
	0.75	1.785	30144	0.938
	0.70	2.009	79161	0.965
HS1	0.85	1.933	322	0.975
	0.80	1.817	4957	0.897
	0.75	1.117	36691	0.893
	0.70	2.077	67957	0.974
HS2	0.85	2.186	307	0.954
	0.80	1.49	5951	0.875
	0.75	1.874	37158	0.959
	0.70	1.969	62389	0.983

Table 4 K-S test result

Series	Stress Ratio	D_t	D_c	Remark
R	0.85	0.2379	0.563	For all Values of X_i, since $D_t < D_c$, the Weibull distribution used for estimating fatigue life is significant and accepted. Where $D_t=\|F^+(X_i) - F_N(X_i)\|$; D_c from K-S statistical table for a sample size of 5 and at significance level of 5%.
	0.80	0.1775		
	0.75	0.2689		
	0.70	0.2021		
HS1	0.85	0.1909		
	0.80	0.2097		
	0.75	0.2322		
	0.70	0.1645		
HS2	0.85	0.1727		
	0.80	0.3088		
	0.75	0.2303		
	0.70	0.1513		





(a) 0.5mmΦ× 30mm (b) 50×2.5×0.5mm

Fig.1 Steel Fibers

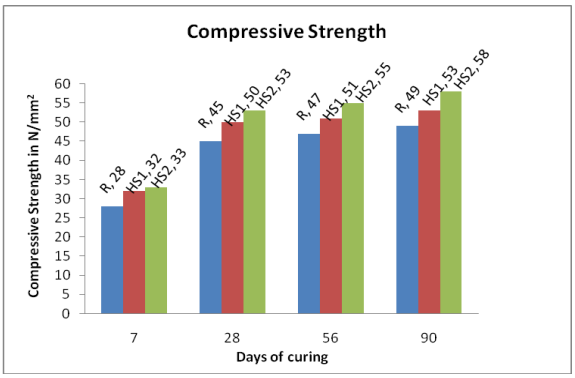


Fig.2 Compressive strength of concrete

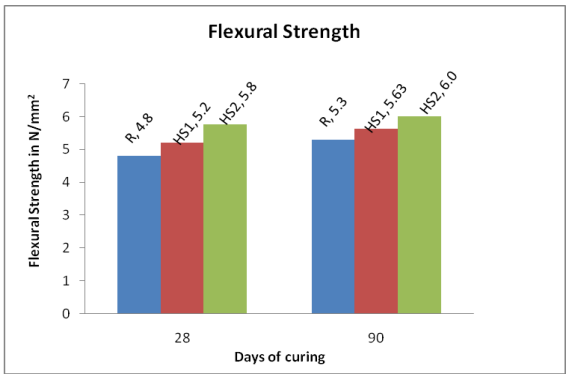


Fig.3 Flexural strength of concrete

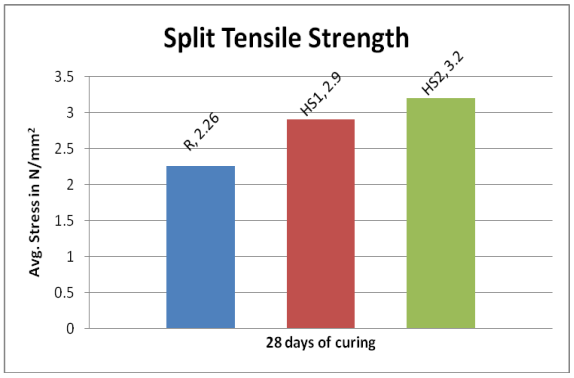


Fig.4 Tensile strength of concrete

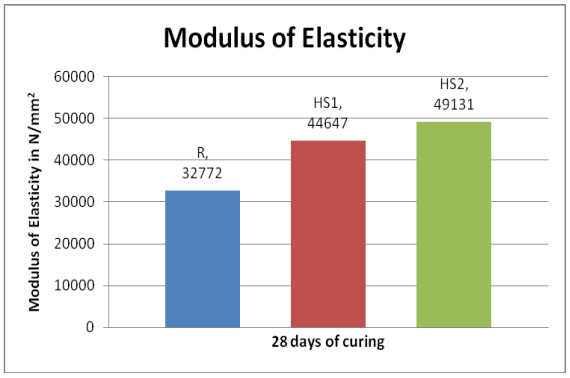


Fig.5 Elasticity Modulus of concrete

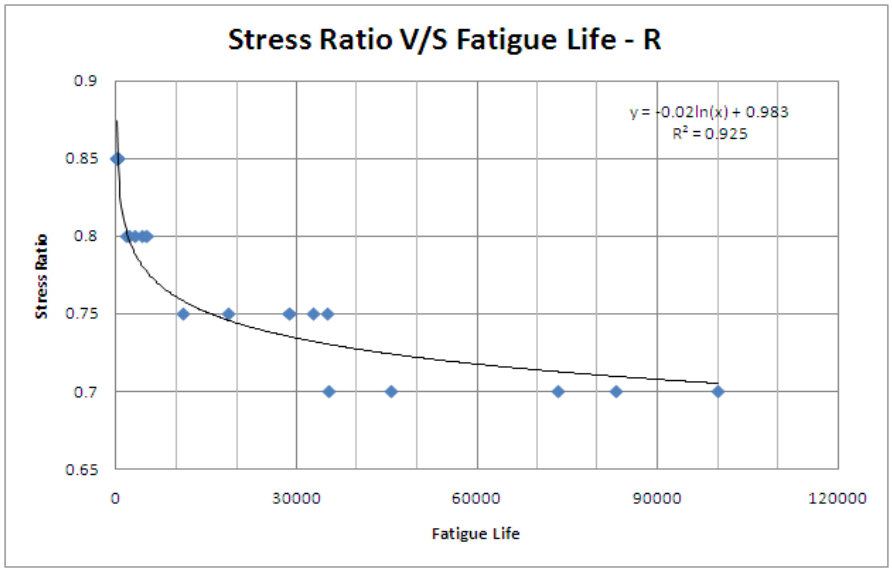


Fig.6 Fatigue life at different stress ratio

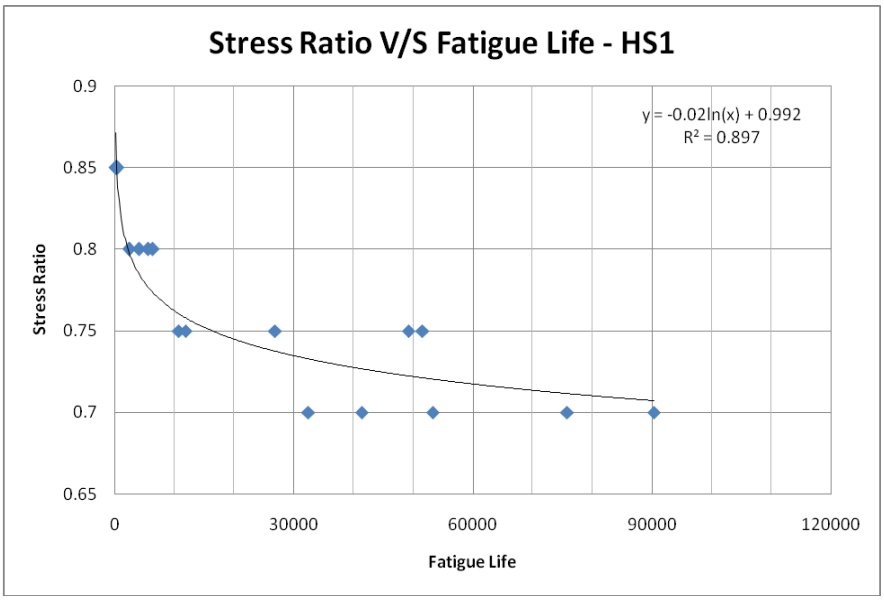


Fig.7 Fatigue life at different stress ratio

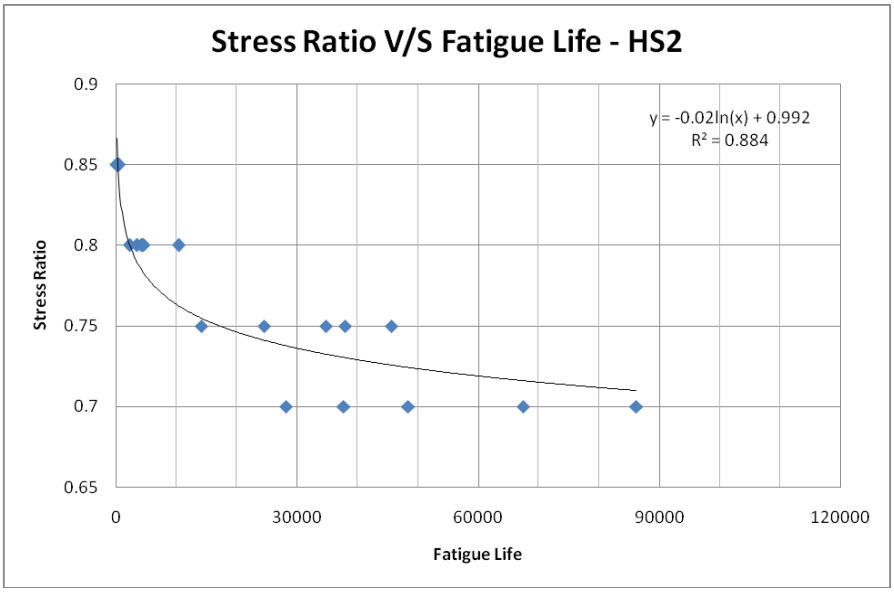


Fig.8 Fatigue life at different stress ratio

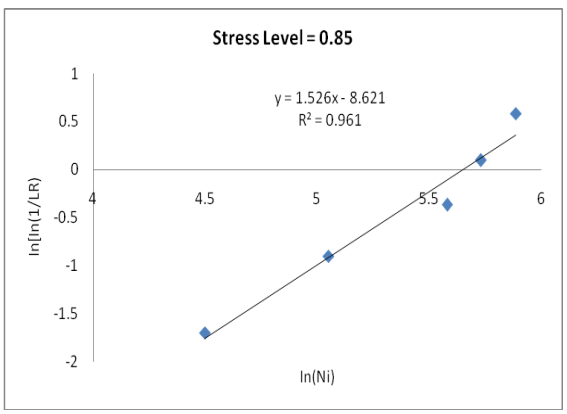


Fig.9 (specimen) Weibull parameter α and μ

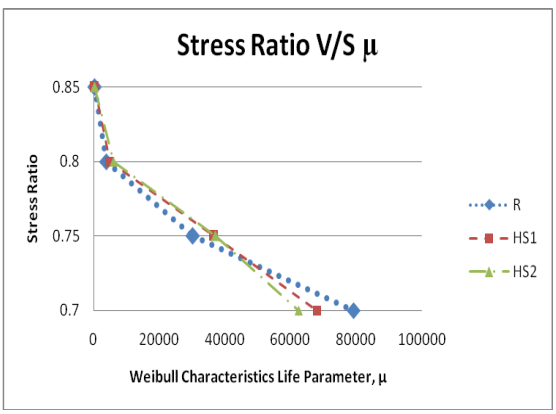


Fig.10 variation of μ and stress ratio

2nd International Engineering Symposium - IES 2012
(KU-MU-NITK-HCMCUT Joint Symposium) March 5-7, 2012, Kumamoto University, Japan

MICROSTRUCTURE ANALYSIS OF CONCRETE SUBJECTED TO ELEVATED TEMPERATURES USING MERCURY INTRUSION POROSIMETRY

Sharath S [1] Sandesh V [2] Subhash C Yaragal [3] K S Babu Narayan [4] and K Suryanarayana [5]

1 Department of Naval Architecture and Ocean Engineering, Osaka University, Japan. E-mail: sharath.2462@gmail.com
2 Chennai Petroleum Corporation Ltd, Manali, Chennai, India. E-mail: sandesh.nitk@gmail.com
3,4 Department of Civil Engineering, National Institute of Technology Karnataka (NITK) Surathkal, Mangalore 575025, India. E-mail: subhashyaragal@yahoo.com
5 Central Power Research Institute, Bangalore, India.

Abstract: Concrete is likely to get exposed to sustained elevated temperatures during fire accidents due to natural calamities such as earthquakes, typhoons, landslides etc. Concrete undergoes strength deterioration when exposed to fire loads. This study attempts to correlate the residual strength characteristics of normal strength concrete (M40) exposed to various elevated temperatures of 150°C, 300°C, 450°C, 600°C and 750°C for a retention period of two hours, to that of consequent changes in microstructure of concrete, measured as porosity using Mercury Intrusion Porosimetry (MIP). Further, attempts are also made to relate splitting tensile strength to the compressive strength of thermally deteriorated concrete. An equation is proposed for residual strength assessment from the MIP results.

Keywords*: Elevated Temperatures, Residual Strength, Concrete Cubes, Mercury Intrusion Porosimetry*

Introduction

Concrete is the most widely used construction material and has established itself as the most versatile construction material in all the disciplines of civil engineering owing to its high compressive strength and mouldability. However, structural concrete is found to undergo serious damages when it is subjected to elevated temperatures due to accidental fires (Georgali, 2005). The behavior of concrete when subjected to elevated temperatures has been studied since past few decades and studies indicate strength deterioration with the increase in exposure temperature (Campbell-Allen, 1965), (Arioz, 2007). Concrete is subjected to elevated temperature during an accidental event such as fire or when it is near to the reactors or furnaces or earth quake induced fire accidents. The strength deterioration of concrete is attributed to the coarsening of pore structure and opening of the capillaries, due to dehydration of the gel, that were initially filled by the hydration products.

The progress in the field of materials science has shown that the properties of a material originate from its internal structure (Mehta, 2000). In concrete, the reaction between the high-density cement particles and low-density water results in hydration product consisting of solid of intermediate density and a residual pore system. Pores are therefore inherited to hydration reaction. The characteristics of the pore system, which affect the properties of cement based materials are the porosity and pore structure (Abell et al, 1999). Porosity, which is a measure of degree of

porousness of materials is defined as the ratio of volume of pores to that of the total volume of material. The pore structure of concrete, perhaps more than any other characteristic of material affects the behavior of concrete. The pore structure of material can be represented through a relationship between cumulative pore volume and the pore radius known as pore size distribution. There are basically two types of pores i.e. gel pores and capillary pores. The engineering properties such as strength, permeability, resistance to aggressive environments of concrete are mainly a function of capillary porosity (Mehta, 2000). A study on similar lines was carried out by Chan et al (2000) to understand microstructure using Mercury intrusion porosimetry (MIP). MIP tests were carried out to measure changes in the pore size distribution in concrete.

In this paper, a non-destructive testing technique Mercury Intrusion Porosimetry (MIP) is used to analyse the microstructure of the concrete subjected to elevated temperatures and the distribution of pore sizes is assessed. This paper presents the results of changes in the microstructure and in turn the strength characteristics of the concrete specimens subjected to elevated temperatures of 150, 300, 450, 600 and 750°C for a retention period of two hours. Further, the compressive and split tensile strengths are related.

MIP Analysis

Mercury Porosimetry Analysis is the progressive intrusion of mercury into a pore structure of concrete specimen under stringently controlled pressures (Figure 1). From the pressure versus intrusion data, the instrument generates volume and size distributions using the Washburn equation. The governing equation for MIP analysis to obtain pore size distribution is shown in Eq.1.

$$D = \frac{-4\gamma\cos\theta}{P} \qquad (1)$$

where γ is the surface tension of mercury θ is the contact angle and P is the external pressure. By measuring the volume of mercury that intrudes into the sample material with each pressure change, the volume of pores in the corresponding size class is known. Figure 2 shows a mercury intrusion porosimeter.

Methodology and test procedure

1. The test was carried out on normal strength concrete (M40 grade) cube specimens of 100x100x100 mm size after 28 days curing. The concrete mix design for M40 was carried out as per revised IS 10262:2009. The mix proportions obtained are tabulated in Table 1.

2. After keeping the control specimens aside, the concrete specimens were subjected to elevated temperature (150 to 750°C) at an increment of 150°C in an electric furnace available at R & D centre, NITK as shown in Figure 3.

3. The retention time for each temperature was two hours followed by natural cooling for 24 hours.

4. Two sets (6 nos.) of specimen were tested to evaluate residual compressive (3 nos.) and split tensile strength (3 nos.) for control specimen and as well as for specimen subjected to elevated temperature.

5. After destructive testing, small pieces of specimen were kept in absolute alcohol to prevent further hydration for MIP analysis.

6. Mercury Intrusion Porosimetry test was performed on the preserved specimens.

7. The compressive and split tensile strengths were compared with the original strength of concrete specimen (un-exposed). Further, the residual strengths were compared using porosity obtained from MIP tests.

Results and discussions

There is a marked improvement in compressive strength of the concrete cube at the temperature of 150°C due to the autoclaving effect as reported in literature. From Table 2, it can be observed that the total loss of compressive strength in the specimen exposed to 750°C is about 73%

i.e., it can take only about 27% of the load when compared to a control specimen.
It can be observed from Figure 4 that the residual strength decreases as the specimen is exposed to elevated temperatures beyond 150°C. This reduction in strength follows a linear pattern till 450°C beyond which pattern followed is non-linear as predicted by other researchers. This is mainly due to extensive degradation of concrete specimens at temperatures beyond 450°C.

Compressive strength and split tensile strength are related by normalising the points to fit a linear equation as plotted in Figure 5. The relationship between compressive strength and split tensile strength is proposed as in Eq. 2.

$$Y = 0.0495X \quad (2)$$

where, Y and X represents split tensile and compressive strengths respectively.

From MIP analysis, it is observed that there is an increase in the number of pores in microstructure of concrete with an increase in exposure temperature. The cumulative pore volume increases with increase in temperature as presented in Figure 6.

It is also observed that with increase in exposure temperature volume of mercury intruded increases. Figure 7 shows that the number of pores for any given pore size increases with increase in exposure temperature.

The residual compressive strength decreases with the increase in volume of mercury intruded as shown in Figure 8. This is due to the increase in number of pores as well as their sizes at elevated temperatures.

Porosity obtained from MIP test can be used as an index relating compressive strength as shown in the Figure 9. Since there is extensive degradation of concrete specimen beyond 450°C, an equation is proposed to predict residual compressive strength from porosity up to 450°C. The proposed prediction equation is represented by Eq. 3. Further it is correlated with observed residual strength with an error in prediction limited to 5%. Table 3 shows the correlation.

$$Y = -0.858X \quad (3)$$

where,
Y=Predicted average residual compressive strength in MPa
X=Porosity in % obtained from MIP test

Conclusions

The following conclusions are deduced from this research work:

- There is a loss of about 73% in the compressive strength of specimen exposed to 750°C.
- A relationship is obtained relating residual compressive strength and residual split tensile strength.
- Number of pores and pore size in microstructure of concrete increases as the exposure temperature increases.
- A relationship is obtained relating porosity and residual compressive strength by limiting the error in prediction to 5%.
- Porosity can be used as an index to obtain residual compressive strength. Therefore by using a non-destructive testing technique strength characteristics of concrete can be obtained.
- Mercury Intrusion Porosimetry can be a reliable tool to assess the microstructure of concrete and determine strength characteristics.

Acknowledgements

The authors gratefully acknowledge Central Power Research Institute (CPRI), Bangalore for their kind permission in conducting MIP tests during this research.

References

[1] A.B. Abell, K.L. Willis and D.A. Lange (1999), "Mercury Intrusion Porosimetry and Image Analysis of Cement Based Materials", Journal of Colloid and Interface Science, 211, pp. 39-44.
[2] O. Arioz (November 2007), "Effects of elevated temperatures on properties of concrete", Fire Safety Journal, Volume 42, Issue 8, pp. 516-522.
[3] D. Campbell-Allen, E.W.E. Low and H.Roper (1965), "An investigation on the effect of elevated temperatures on concrete for reactor vessels", Nuclear Structural Engineering, 2, pp. 382-388.
[4] S.Y.N. Chan, Xin Luo and Wei Sun (2000), "Effect of high temperature and cooling regimes on the compressive strength and pore properties of high performance concrete", Construction and Building Materials 14 (2000) 261-266.
[5] Georgali B, Tsakiridis P.E (2005), "Microstructure of fire-damaged concrete-A case study", Cement & Concrete Composites, 27, pp. 255–259.

[6] V. Mehta (2000), "Study of Microstructure of concrete using Mercury Intrusion Porosimetry", Website:http://www.vishal-mehta.com/2_works/3_Research-thesis/2_Study-of-Microstructure-ofconcrete-using-Mercury-Intrusion-porosimetry.
[7] S.C. Yaragal et al (2010), "Studies on normal strength concrete cubes subjected to elevated temperatures", Journal of Structural Fire Engineering Vol. 1 Number 4.

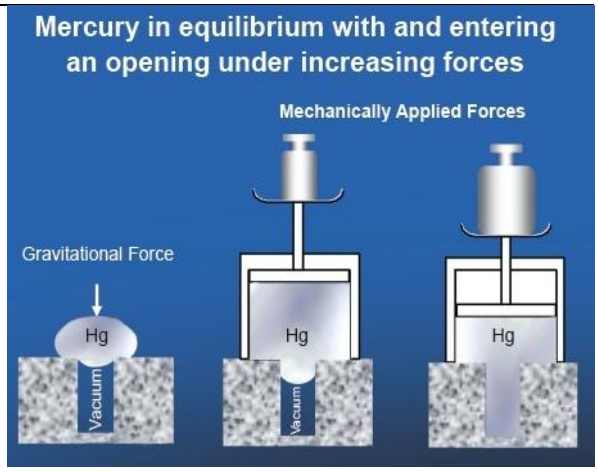


Fig.1 MIP Analysis

Since mercury does not wet most substances and will not spontaneously penetrate pores by capillary action, it must be forced into the pores by the application of external pressure.
http://www.micromeritics.com/Repository/Files/Mercury_Porosemitry_Theory_poster.pdf

Table 1
Concrete Mix Design Proportions

Water-cement ratio (w/c)	0.45
Cement (Ultra Tech 43)	1
Fine Aggregate (Zone-I grading)	1.525
Coarse Aggregate (50% 20mm+50% 10mm graded)	2.434
Slump (mm)	50



Fig. 2 Mercury Intrusion Porosimeter



Fig. 3 Electric heating furnace

Table 2
Compressive strength variation

Temperature (°C)	Sl. No	Load (KN)	Compressive strength (MPa)	Average Residual strength (MPa)	% Residual strength
Room	1	395	39.5	40.17	1.00
	2	410	41.0		
	3	400	40.0		
150	1	480	48.0	45.67	1.14
	2	430	43.0		
	3	460	46.0		
300	1	370	37.0	40.0	0.99
	2	410	41.0		
	3	420	42.0		
450	1	360	36.0	33.33	0.83
	2	320	32.0		
	3	320	32.0		
600	1	160	16.0	15.33	0.38
	2	140	14.0		
	3	160	16.0		
750	1	95	9.5	10.67	0.27
	2	105	10.5		
	3	120	12.0		

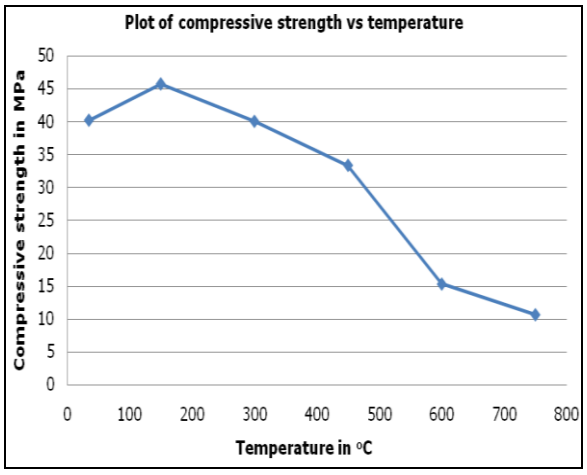


Fig. 4 Compressive strength variation

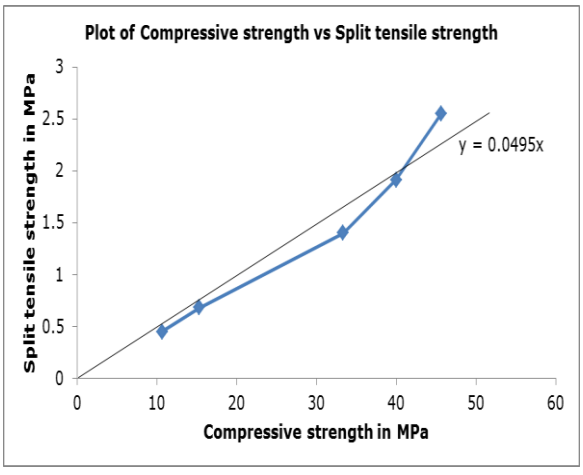


Fig. 5 Variation of compressive strength with split tensile strength

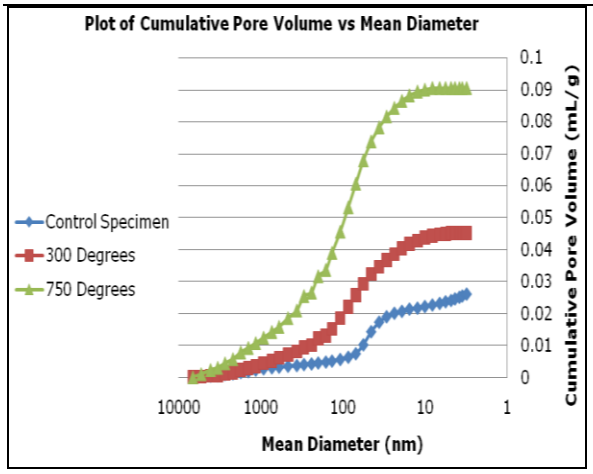


Fig. 6 Cumulative intrusion of mercury vs pore size

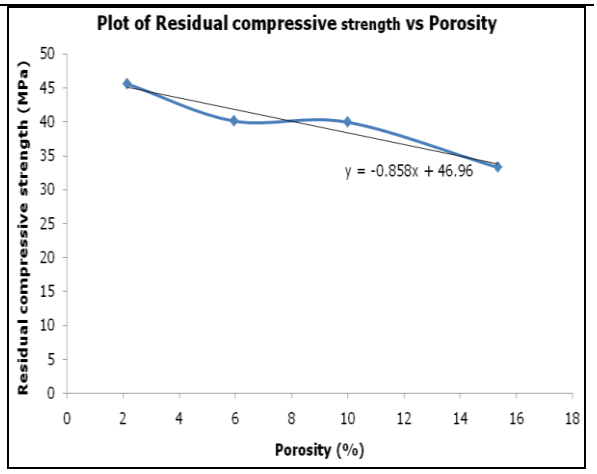


Fig. 9 Residual strength variation with porosity

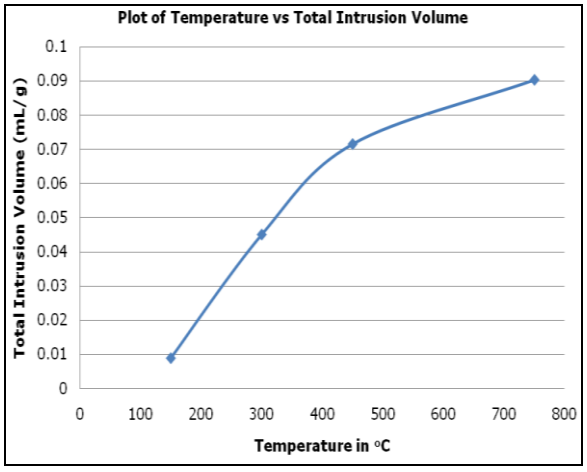


Fig. 7 Total intrusion volume of mercury vs temperature

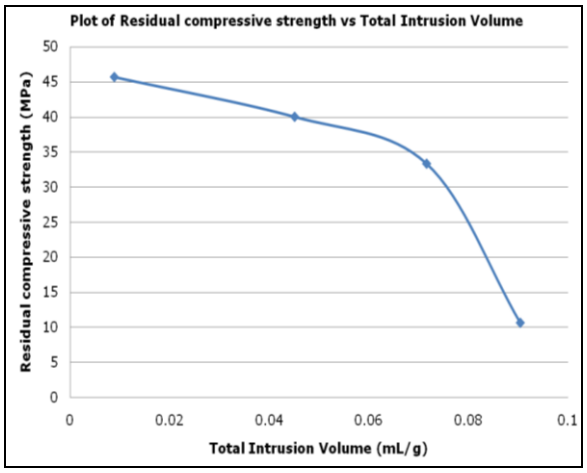


Fig. 8 Residual compressive strength variation with total intrusion volume of mercury

Table 3
Correlation of observed and predicted values of residual compressive strength

Temperature (°C)	Observed Residual strength (MPa)	Predicted Residual strength (MPa)	% error
Room	40.17	41.86	4.29
150	45.67	45.12	1.21
300	40.0	38.39	4.03
450	33.33	33.81	1.43

2nd International Engineering Symposium - IES 2012
(KU-MU-NITK-HCMCUT Joint Symposium) March 5-7, 2012, Kumamoto University, Japan

Relation between UPV and Residual strength of concrete subjected to heating and sudden cooling

Shree Laxmi Prashant [1] **Subhash C Yaragal** [2] and **K S Babu Narayan** [3]

[1]*Department of Civil Engineering, National Institute of Technology Karnataka, Surathkal, Mangalore 575025, India. email:* shrilaxmi.civil@gmail.com
[2,3]*Department of Civil Engineering, National Institute of Technology Karnataka, Surathkal, Mangalore 575025, India.*

Abstract: Concrete is a very popular and versatile construction material and finds its applications in most of the residential and commercial buildings. Concrete may be subjected to elevated temperatures during accidental fire or when it is in the vicinity of reactors and furnaces. Concrete is found to experience strength deterioration when subjected to elevated temperatures. The residual strength properties of the concrete depend on the method of cooling adopted. It is an usual practice to extinguish the fire by spraying water. This induces a thermal shock, leading to deterioration in strength of concrete. An experimental investigation is carried out to assess the deterioration of concrete due to heating and cooling of OPC concrete. The heating temperatures were 200°C to 800°C at an interval of 100°C and the cooling methods adopted were water quenching and furnace cooling. Residual properties such as compressive strength and UPV are reported. The UPV is found to deteriorate at a faster rate with the increase in exposure temperature as compared to the compressive strength.

Keywords: Elevated Temperatures, Residual UPV, Residual Strength, Sudden Cooling.

Introduction

Concrete is the most popularly used construction material and it finds its application in almost all the civil engineering disciplines. Its characteristics such as mouldability and high compressive strength have made it a versatile building material. Concrete offers good resistance to heat because of its low conductivity and incombustible nature and further, no toxic fumes are emitted from concrete surface when it is heated. Because of all these characteristics concrete can be rated as the best building material as far as resistance to heat is concerned.

Structural concrete is found to undergo deterioration when it is subjected to elevated temperatures due to accidental fires (Georgali B (2005)). The behaviour of concrete when subjected to elevated temperatures has been studied since past few decades and studies indicate strength deterioration with the increase in exposure temperature (Campbell-Allen D (1965), Khoury G A (1988), Arioz O (2007)).

The deterioration of strength when subjected to elevated temperatures is due to unequal volumetric changes between cement paste and aggregates coupled with deterioration of hydration products like calcium hydroxide and calcium silicate hydrates, (Guerrieri M et.al, (2009)). The deterioration of bond between cement paste and aggregates is responsible for strength loss of concrete (Campbell-Allen D (1965)). For exposure temperatures upto 400°C the strength deterioration is not significant, the compressive strength of concrete drops slightly first and then goes up a little. For exposure temperatures above 400°C the compressive strength tends to fall drastically and the residual strength after 800°C exposure may be only 20% of its ambient strength (Xiao J et.al (2004), Arioz O, (2007)). Decomposition of calcium hydroxide and calcium carbonate in the range of 430°C – 600°C has an additional effect on strength loss, (Peng G F (2006)). At 600°C the decomposition of C-S-H gel is associated with significant reduction in strength where the cement paste loses its binding property due to

release of physically and chemically bound water. This results in significant reduction of strength.

Concrete strength is affected not only during the heating phase but also during cooling. During a building fire it is an usual practice to extinguish the fire by spraying water, which makes the concrete to cool suddenly. The rapid cooling of heated concrete, similar to rapid heating can cause strength deterioration (Janotka I et.al (2005), Xin L (2000)). This is due to the phenomenon of rapid cooling connected with extreme shrinkage of the specimen and crack propagation leading to the final effect of strength loss. Lee J et.al. (2008) conducted experiments to investigate effect of different cooling regimes (slow cooling, natural cooling, and rapid cooling) on OPC concrete heated to target temperatures of 200, 400, 600 and 800°C. Water cooling caused severe deterioration of compressive and flexural strengths, while slow cooling showed lower deterioration of strength. Experiments carried out Chan S Y N et.al (2000) and Peng G F et.al (2008) on heated high performance and fiber reinforced concrete respectively have showed more deterioration of strength of subjected to thermal shock due to rapid cooling. Aerated concrete also experiences larger deterioration of strength due to sudden cooling (Tanacan L (2009)).

Ultrasonic pulse velocity is a popular NDT technique to assess the thermal deterioration of concrete. Several experimental studies have been carried out to investigate how the pulse velocity was affected by the damage of concrete caused by various high temperatures (Yiching L et.al (2011), Yang H et.al (2009)). Fairly accurate estimation of damage can be done with the help of UPV (Chung H W et.al (1985)). This paper reports a UPV study carried out to investigate the quality of concrete after subjected to elevated temperature and cooled naturally or suddenly. These results are compared with those obtained from actual destructive testing.

Experimental Investigation

Material Properties and Testing Methodology

Ordinary Portland Cement 43 grade with brand name ACC was used for preparing the concrete specimen. River sand conforming to zone 3 (I.S 383-1970 grading requirements) with specific gravity 2.65 was used. Coarse aggregates with specific gravity 2.77 satisfying I.S 383-1970 grading requirements for graded aggregates was used. The concrete was mixed in a concrete mixer and poured into moulds of size 100mm x 100mm x 100mm. After 24 hours the concrete cubes were demoulded and cured for 28 days under water.

Test Procedure

The concrete cubes were subjected to elevated temperature in an electric oven. Temperature range was 200°C to 800°C at an interval of 100°C. The time temperature build up of the furnace is shown in Fig.1. The temperature time gradient is steep upto 400°C around 20°C/min and flattens gradually above 400°C at rate of 7°C/min.

After the target temperature was reached the specimen were maintained at that temperature for duration of 3 hrs. For furnace cooling the furnace was switched off after exposure and the specimen were left in the furnace until the interior of the furnace reached room temperature. For sudden cooling the specimen were removed immediately after exposure and immersed in a small tub containing water at room temperature. The specimen were allowed to cool in the water till specimen cooled to the room temperature. The specimen were later removed from water, wiped dry with cloth and tested for UPV. UPV was measured by direct method. The direct method involves the determination of speed of an ultrasonic pulse generated in the direction of the receiver. The time of the wave following the shortest path (a straight line) to the receiver is recorded by the timing circuit of the measuring equipment.

The direct method is used for detection of cracks, in the assessment of the uniformity

of concrete and for estimation of the strength of concrete (Fig 2).

The ultrasonic pulse velocity (V) is given by

$V = L/t$ in km/s

Where L = length of the specimen (path length) in km

t = traveling time in seconds

After UPV the cubes were later tested for residual compressive strength in the compressive testing machine.

Results and discussions

Figs. 3 and 4 show the variation in residual strength ratio by destructive testing and residual UPV ratio for various exposure durations from 200°C to 800°C and subjected to sudden cooling and furnace cooling respectively. Residual strength and UPV ratios are obtained by dividing the residual strength or residual UPV with the original strength or UPV of the concrete before elevated temperature exposure.

Both the residual strength as well as the residual UPV ratio decreases with the increase in the exposure temperature for both the cooling conditions. However the variation of UPV is more as compared to the variation in residual strength ratio. This is because of large amount of cracking that has occurred as a result of high temperature exposure. Concrete experienced higher deterioration of strength and UPV when the concrete is cooled suddenly by quenching.

In Fig 3 for 200°C exposure the residual strength ratio is 0.83 while the residual UPV ratio is 0.89, the residual UPV ratio is higher than the residual strength ratio. For the exposure temperature of 300°C to 800°C the residual strength ratio is higher than the residual UPV ratio. This shows that the deterioration of UPV is more sensitive.

The concrete exposed to 300°C has the strength ratio of 0.81 and UPV ratio is 0.79. The concrete looses all the water contained in the capillary pores upto 300°C. The concrete also begins to lose the water contained in the gel. For the exposure temperature of 400°C and cooled suddenly by quenching the strength ratio is 0.6 and the corresponding UPV ratio is 0.67. This signifies that the concrete has started losing substantial amount of its strength and because of loss of gel water the cement paste loses its binding property hence the concrete loses its homogeneity.

For the concrete exposed to 500°C and above the deterioration of microstructure of concrete resulted in lower UPV values and the UPV ratio is 0.37, while the strength ratio is 0.6. At this temperature the CSH, the major product of hydration of cement starts decomposing. For the exposure temperature of 600 to 800°C the compressive strength and UPV deterioration is very severe. The UPV ratio is zero for these temperatures. This is because of large cracks that are developed as a result of deterioration of the interfacial transition zone and loss of bond between cement paste and aggregates.

Fig 4 shows the deterioration of UPV and strength ratio for the concrete exposed to elevated temperature and furnace cooled. For the exposure temperature of 200 - 500°C the strength and UPV follows the same trend. For 200 and 300°C the strength and UPV ratios are almost the same. Hence both the curves coincide.

For 400 and 500°C the UPV ratio curve slightly deviates from the strength ratio curve. The UPV ratio values are about 5-6% lower than the strength ratio. For 600°C however there is large deterioration of UPV ratio. The UPV ratio drops to 0.36 at 600°C exposure from 0.71 at 500°C. The CSH decomposes at this temperature; hence the concrete suffers extensive internal cracking. This fact is visible from the UPV deterioration curve and the UPV ratio is hence zero for 700 and 800°C exposed concrete.

Fig 5 shows the compressive deterioration of concrete with temperature and subjected to sudden and furnace cooling compared with few of the previous literature published. FC and SC represents the residual strength of concrete exposed to elevated temperature and furnace cooled and suddenly cooled by quenching in water. For the exposure temperature

upto 300°C, FC and SC reports lower residual strength than reported by previous researchers such as Savva A et.al (2005) and Handoo et.al (2002). The FC results are almost similar to those reported by Arioz (2007) and Poon C S et.al (2001). Sudden cooling of heated concrete by quenching in water has however resulted into higher deterioration of strength.

For 400 and 500°C exposure FC continues with the same trend of strength deterioration as for 200 and 300°C, the curve later becomes steeper for 600 to 800°C. These are however lower values as compared to those reported by Handoo et al (2002). For the exposure temperature of 500 to 800°C Poon (2001) has reported concrete strength to be affected more severely by the exposure temperature. FC curve is similar to the strength deterioration reported by Arioz (2007). The deterioration of SC is however more severe than FC but has retained higher percentage of strength than reported by Poon C S (2001) for the concrete exposed to 800°C.

Conclusions

1. Concrete suffers deterioration of strength and UPV when subjected to elevated temperature.
2. The deterioration of UPV is more severe than the compressive strength.
3. Sudden cooling induces thermal shock resulting in lower strength and UPV as compared to concrete cooled in furnace.
4. UPV provides a qualitative assessment of damage occurred to strength and transport properties of concrete. The residual UPV data can be used for planning of necessary repair and retrofitting work to be carried out to make the damaged concrete member serviceable.

References

[1] Arioz O (2007), Effects of elevated temperatures on properties of concrete, Fire Safety Journal, 42, 8, pp. 516-522.
[2] Campbell-Allen D, E. W. E. Low and H. Roper (1965), An Investigation on the Effect of Elevated Temperatures on Concrete for Reactor Vessels, Nuclear Structural Engineering, 2, pp. 382-388.
[4] Chan S Y N, Xin Luo, Wei Sun (2000) Effect of high temperature and cooling regimes on the compressive strength and pore properties of high performance concrete, Construction and Building Materials, 14, pp. 261-266.
[3] Chung H W and Law K S (1985), Assessing Fire Damage of Concrete by the Ultrasonic Pulse Technique, Cement, Concrete, and Aggregates, CCAGDP, Vol. 7, No. 2, pp. 84-88.
[5] Georgali B.,Tsakiridis P.E. (2005), Microstructure of fire-damaged concrete. A case study, Cement & Concrete Composites, 27, pp. 255–259
[6] Guerrieri M, Sanjayan J and Frank C (2009), Residual compressive behavior of alkali-activated concrete exposed to elevated temperatures, Fire and Materials, 33, pp. 51–62.
[7] Handoo S.K, Agarwal S, Agarwal S.K (2002), Physicochemical, mineralogical, and morphological characteristics of concrete exposed to elevated temperatures, Cement and Concrete Research, 32, 7, pp.1009-1018.
[8] Janotka I, Nurnbergerov T (2005), Effect of temperature on structural quality of the cement paste and high-strength concrete with silica fume, Nuclear Engineering and Design 235 2019–2032
[9] Khoury G A and Patrick J. E. Sullivan (1988), Research at Imperial College on the Effect of Elevated Temperatures on Concrete, Fire Safety Journal, 13, pp. 69 – 72.
[10] Lee J, Yunping Xi, William K (2008), Properties of concrete after High-Temperature Heating and Cooling, ACI Materials Journal, V. 105, No. 4, July-August 2008, pp. 334-341.
[11] Peng G F, Bian S H, Guo Z Q, Zhao J, X Peng, Yu-Chuang Jiang (2008), Effect of thermal shock due to rapid cooling on residual mechanical properties of fiber concrete exposed to high temperatures, Construction and Building Materials, 22, pp. 948–955.
[12] Peng G F, Yang W, Zhao J, Liu , Bian S H, Zhao L H (2006), Explosive spalling and residual mechanical properties of fiber-toughened high-performance concrete subjected to high temperatures, Cement and Concrete Research, 36, pp. 723–727.
[13] Poon C S, Salman A, Anson M, Wong Y L (2001), Strength and durability recovery of fire-damaged concrete after post-fire-curing, Cement and Concrete Research, Volume 31, 9, , pp. 1307-1318
[14] Savva A, Manita P, Sideris K.K. (2005) Influence of elevated temperatures on the mechanical properties of blended cement concretes prepared with limestone and siliceous aggregates, Cement & Concrete Composites, 27, pp. 239–248.
[15] Tanaçan L, Ersoy H Y, Arpacıoğlu Ü (2009), Effect of high temperature and cooling conditions on aerated concrete properties, Construction and Building Materials, 23, 3, pp. 1240- 1248
[16] xiao J, Gert K (2004), Study on concrete at high temperature in China—an overview, Fire Safety Journal, 39, pp. 89–103.
[17] Xin L, Sun W, Chan S Y N (2000), Effect of heating and cooling regi.mes on residual strength and microstructure of normal strength and high-performance concrete, Cement and Concrete Research, 30, pp. 379-383.
[18] Xu Y, Wong Y L, Poon C S, Anson M, (2003), Influence of PFA on cracking of concrete and cement paste after exposure to high temperatures Cement and Concrete Research, 33, pp.2009–2016

[19] Yang H, Lin Y, Hsiao C, Jian-YouLiu, "Evaluating residual compressive strength of concrete at elevated temperatures using ultrasonic pulse velocity, Fire Safety Journal 44 (2009) pp. 121– 130.

[20] Yiching L, Chiamen H, Hsuanchih Yang, Yu-Feng Lin, "The effect of post-fire-curing on strength–velocity relationship for nondestructive assessment of fire-damaged concrete strength", Fire Safety Journal 46 (2011) pp.178–185.

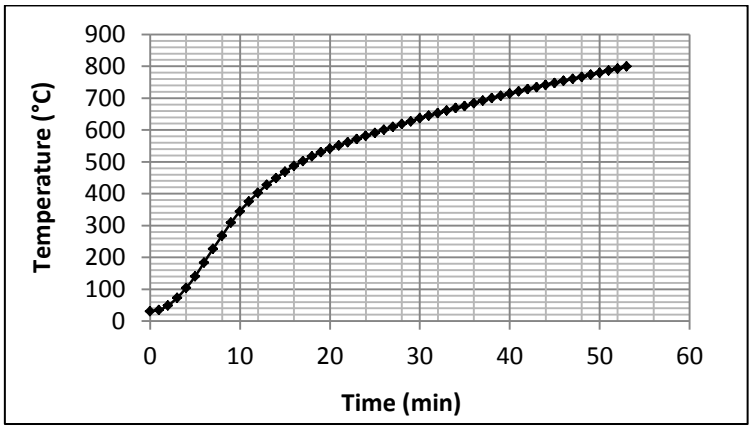


Fig. 1 Time Temperature Curve

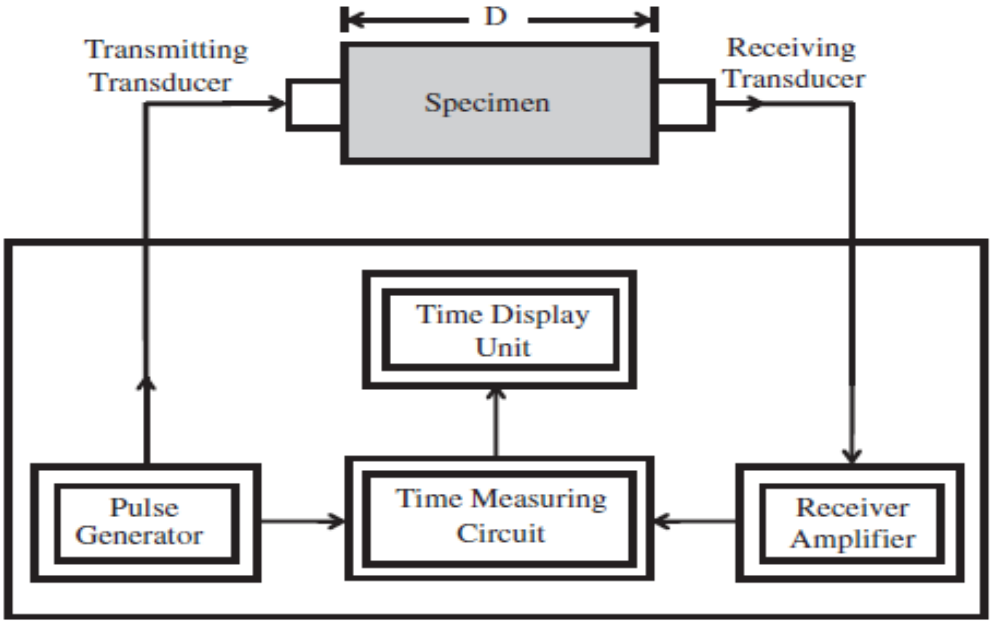


Fig. 2 Schematic diagram of pulse velocity measurement.

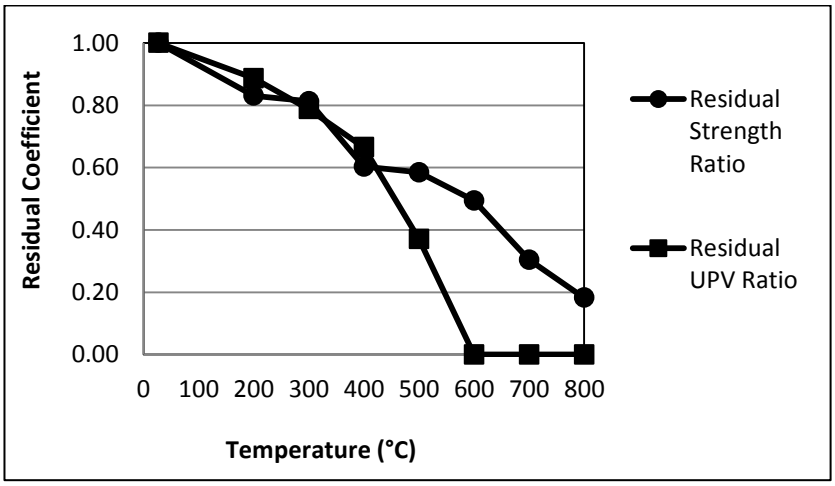


Fig. 3 Deterioration in strength by destructive testing and UPV for concrete heated and suddenly cooled

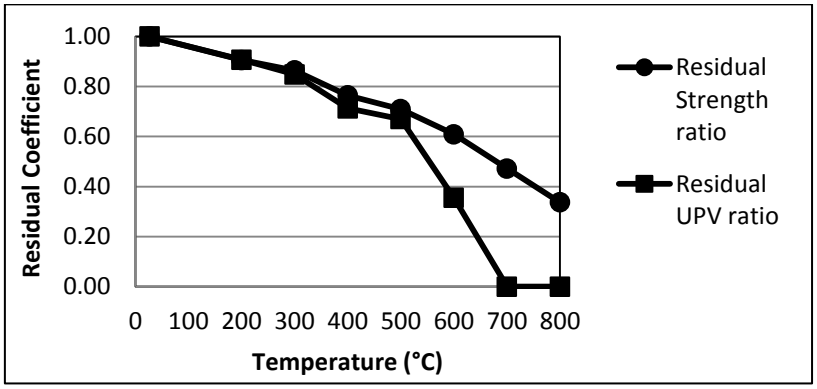


Fig. 4 Deterioration of strength by destructive testing and UPV for concrete heated and suddenly cooled

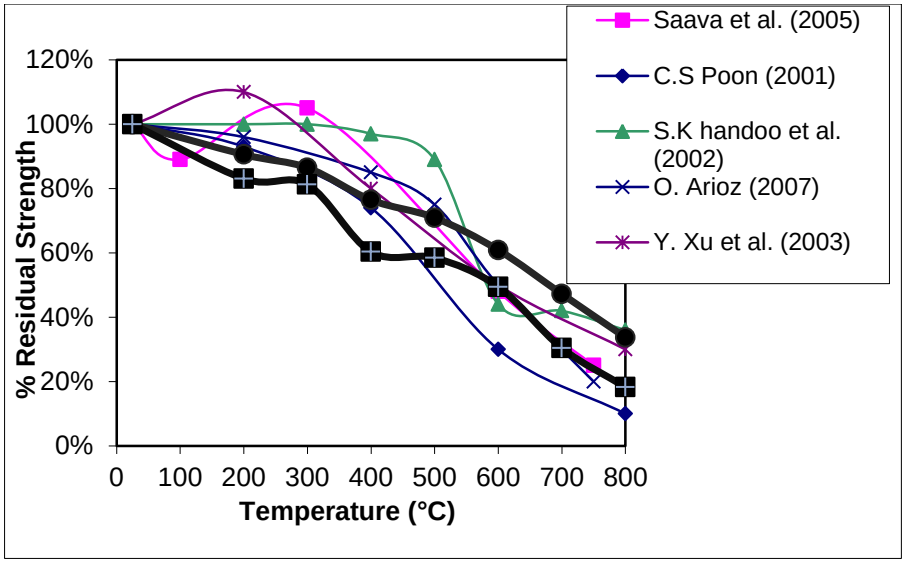


Fig. 5 Comparison of Residual Strength with other published literature

2nd International Engineering Symposium - IES 2012
(KU-MU-NITK-HCMCUT Joint Symposium) March 5-7, 2012, Kumamoto University, Japan

Coordinated Traffic Signaling for Three Major Junctions of Mangalore City Using *TRANSYT-12*

VARGHESE GEORGE [1] and **Hemanth K.R.** [2]

1 *Department of Civil Engineering, National Institute of Technology Karnataka, Mangalore – 575025, Karnataka, India. E-mail : varghese@nitk.ac.in*
2 *Former Student, Department of Civil Engineering, National Institute of Technology Karnataka, Mangalore – 575025,Karnataka, India.*

Abstract: The present work deals with the application of TRANSYT-12, for the design of a co-ordination of the signals on three main junctions of the signal system for Mangalore city. The road network loop connecting PVS Junction, Hampanakatta, and Jyothi Junction, joining back to PVS Junction was analysed. The other nodes representing Bunts Hostel Junction, Navbharath Circle, and Karnataka Bank Junction are considered for their contribution to the traffic network loop, in addition to the flows arriving from a number of give-ways. The existing scenario, with the present system of fixed time isolated signals was compared to the alternate scenario with the use of coordinated signals, and improvements in the existing network. It was found that the performance of traffic flow in the network could be improved considerably by adopting various remedial measures. Studies were also performed for the year 2012.

Keywords*: modelling, traffic, coordinated, signal, TRANSYT, Mangalore*

Introduction

Road-traffic congestions occur due to inefficiency of the road-network system in handling road traffic. Congestion results in huge losses to road-users, in addition to causing accidents, noise, and atmospheric pollution. Traffic engineers endeavor to ensure more orderly and less chaotic traffic flow in the road network.

In the 1980s, India witnessed large-scale urbanization, and rapid industrialization, coupled with the increasing travel demand of the emerging middle-class population that could afford to pay more. The number of motor vehicles registered a growth rate of around 10 per cent per annum. The growth of cars registered 7.5 percent, while that for buses, trucks, and two-wheelers stood at 5.3, 6.2, and 17.2 percentages (Kadiyali, 1987). This resulted in a chaotic situation, since most cities in India were not designed to handle the increasing number of vehicles. Traffic-delays, accidents, and increasing levels of pollution necessitate the use of better strategies to manage traffic flow.

The present work deals with the application of TRANSYT-12, a traffic network study tool, for the design of coordinated signal system for the central business district (CBD) of Mangalore city. The existing scenario, with the present system of fixed time isolated signals was compared to the alternate scenario with the use of coordinated signals, and improvements in the existing network. TRANSYT-12, a simulation based tool for modeling traffic flow in road networks, was used for this purpose. The study revealed that the performance of traffic flow could be improved considerably by adopting various remedial measures tested. Studies were also performed for the year 2012.

Literature Survey

A number of studies were performed world-wide on traffic signals and control systems. In India, Victor and Santhakumar (1987) examined the applicability of Gamma distribution to green time, in the

modeling of manually controlled T-junctions, and mid-block pedestrian crossings.

A number of adaptive signal control systems using artificial intelligence techniques such as expert systems, fuzzy logic, and neural networks were proposed (Gartner, 1983). Trabia, et al. (1999) performed the design and evaluation of a fuzzy-logic based traffic signal controller for isolated intersections. Nakatsuyama et al. (1984) used fuzzy logic to model the control of two adjacent intersections with one-way movements, while Chiu (1992) applied fuzzy logic for controlling multiple intersections in a network of two-way streets with no turning movements.

Bhattacharya and Virkler (2006) identified optimal signal co-ordination plans to minimize the total-delay to both vehicles and pedestrians for peak-hour traffic, using the signal optimization software Synchro 3.2. Yun, and Park (2006) performed studies on a stochastic traffic signal optimization method that consists of a heuristic simulation model and the microscopic simulation model CORSIM. Sarkar and Ahmad (2007) demonstrated the application of TRANSYT-10 on a stretch of a principal arterial road in Delhi, with the primary objective of synchronizing a series of traffic signals in an optimum manner.

Study Area, Scope and Objectives

This paper examines the issues related to traffic congestion in the central area of Mangalore. The three major signalized intersections (i.e., Hampankatta junction, Jyothi Junction, and PVS Junction), were proposed to be interconnected using a coordinated signal system. The other minor un-signalised manually controlled traffic junctions in this loop included Bunts Hostel Junction, Navbharath Junction, and Karnataka Bank Junction. See Fig.1.

Working of *TRANSYT*

The *TRANSYT* (Traffic Analysis Study Tool or Traffic Network Study Tool), was developed by D.I. Robertson of U.K. in 1969 (Vincent et al., 1980). This is an off-line computer program for determining and studying fixed time, and coordinated traffic signal timings in any network of roads for which the average traffic flows are known. The *traffic model* computes the *performance index (PI*) in monetary terms, which is a weighted sum of all vehicle delays and stops. An *optimizing routine* systematically alters the signal offsets and/or allocation of green-times, to search for the timings that reduce the *PI* to a minimum value. The approach adopted in this optimization is referred to as the *hill-climbing* technique.

TRANSYT can model give-way priority controls, signalised roundabouts, and flared approaches. It computes the performance index (*PI*) as a weighted combination of the *delay* and *stops* on all links of the network given as (*Binning, et al., 2003*):

$$PI = \sum_{i=1}^{N}(W.w_i.d_i + ((K/100).k_i.s_i)) \quad (1)$$

where N = number of links; W = overall cost per average PCU-hour of delay; K = overall cost per 100 PCU-stops; w_i = delay weighting on link i ; d_i = delay on link i ; k_i = stop weighting on link i ; and s_i = number of stops on link *i.*

TRANSYT computes the delays due to over-saturation, and other random delays using the expression (*Binning, et al., 2003*):

$$R+S=T/4\ \{[(f-F)^2 + (4f/T)]^{1/2} + (f-F)\} \quad (2)$$

where f = the average arrival rate on the link (PCU/hour); F = the maximum flow that can be discharged from the link (PCU/hour); and T = the duration of the flow condition for which signal timings are being considered (hours).

The *TRANSYT* signal optimizer attempts to minimize the *PI* by reducing the delay, and decreasing the number of stops.

Methodology

- Before working on *TRANSYT,* complete information on the network, with data on the connectivity of links, and nodes was obtained. The network was *created* in *TRANSYT,* and *run.*
- The link details such as, *link number*, *connected destination node*, *width of the lane* (m) *saturation flow* (PCU), *length of link* (m), *total flow in the link*

(PCU), *in flow* from *upstream links*, and *cruise speeds* (KMPH) were provided.

- Details on the un-signalised junction nodes were then provided.
- Information on the *give-way* links were then provided.
- The dimensional details of the roads and junctions in the form of AutoCAD drawings prepared by Dalal Consultants (2003), were collected from Traffic Management Report for Mangalore Town submitted to Karnataka Urban Development and Costal Environmental Projects, Govt of Karnataka.

  In order to represent the field conditions in a more realistic manner, some of the links are sub-divided into smaller links by using dummy nodes in between. These dummy nodes and connected links were used to represent minor non-signalized Junctions with inflows from side-nodes. Dummy nodes are also provided close to the Junction where the flows in the links have to be subdivided to represent the flows from the link turning to other direction. See Fig. 2.

  In a similar manner, the lengths of the links, the link-speeds, and the maximum link-flows in PCUs (passenger car units) were diagrammatically represented in *TRANSYT*.

  Also, other details such as the length and width of the road links, stop-line saturation flows for major links according to Webster and Cobbe (1966), uniform flow sources, up-stream links and link numbers, and the turning movements at junctions for the peak-hours were provided through the *TRANSYT* interface.

  The cost of delay was computed based on the weighted average income of Rs 12611 (or 280 USD @ 2007 exchange rate) for passengers travelling by various modes.

  The cost per stop for a standing delay of 60 seconds was computed as Rs 0.16 (or 0.0035 USD) for an average network vehicle speed of 25 kmph based on Khanna and Justo (2001).
- The flows and turning movements from other minor roads were ignored, and alternatively, equivalent *uniform flows* were assigned to the corresponding links.
- The output of the input data (in .prt format) was then cross-checked. This mainly consisted of all input data and *cost of delays* ($/hour), *cost of stops* ($ per hour), *performance Indices* ($/hour), *exit nodes*, *green times* (seconds), *total distance travelled* (PCU-km/hour), *mean journey speed* (km/h), *fuel-consumption predictions* (litres/hour), and *Flow pattern graphs* as specified in the input data.
- The *TRANSYT signal optimizer* then performed the minimization of the *PI*. The *CYCLOP cycle-optimisation* procedure was run to obtain the optimal signal timing, and the *NetCon* option was used to generate the graphical output of network.
- The *Graph generator* option was used to view the *graphs for performance indices, cyclic flows* and *uniform queues.*
- The output of the *flow-profile* graphs will reveal all the links that need to come under the coordinated signal system. This is indicated by the mean modulus error value (*MME*).

Results and Discussions on Analyses for 2007

The output of the *flow-profile* graphs provided details of the links with *MME* values that lay between 0 and 0.22. These low values, indicated that the flows need to be controlled using the coordinated signal system.

An inspection of the *cycle optimization profile* (*CYOP*) calculations related to the percentage of saturation, for the nodes indicated that the saturation is lesser for a higher cycle time of 180 seconds. The saturation levels were found to increase for higher cycle times.

TRANSYT indicated the over-saturated links with the symbol '<'. Some links had a

high percentage of saturation of about 258% indicating that the link capacities have exceeded. TRANSYT also gives details on the *cruise-delays* on the links.

However, the performance index is considered for final decision-making. The total performance index of the network ws found to have a higher value of 322393.4 Rs/h, and the network speed was found to be as low as 3.6 KMPH due to excess delays and stops in some of the links. Thus, the links that need to be improved were identified.

In order to reduce the *PI* values, the following treatments are tested for the related links and nodes:

1) Treatment of Junctions (including improvement of flares for a length of 15m at the junctions).
2) Treatment for lane widths or links (including increasing of half-a-lane width of 1.75 m for a length of 100 m to the right-turning or straight-traffic).
3) Providing free left turn using extra lanes if required (and imposing right-turn restrictions).
4) Providing free right turns/restricting right turns/providing flyovers.

When the first option was adopted, the performance index of the network decreased from 322393.4 Rs/h to 257378.8 Rs/h, and the network mean-journey speeds increased from 3.6 KMPH to 4.3 KMPH.

The second option saw the performance index decreasing to 163339.9 Rs/h, with the network mean-journey speeds increasing up to 6.3 KMPH.

The third option saw the performance index decreasing significantly to 47664.7 Rs/h, with the network speeds increasing to 13.8 KMPH. This was found acceptable, and the signal timings were noted. See Table 1 for details on the final signal timings after 3-stages of improvements. Table 2 gives details on the network performance after the three stages of improvements. Fig.3 illustrates the improvement in performance and fuel consumption at various stages of improvement in the network.

Results and Discussions on Analyses for 2012

The network was loaded for an increase of 36.57% for the 5-year period based on the history of growth of vehicles in the city. The analyses showed that it was required to provide flyovers at the major junction (Hampankatta), in addition to widening of the roads by at least 1 traffic lane width of 3.5m.

Conclusions

The use of *TRANSYT* was found to be of special benefit in devising strategies for short term and long treatment of junctions, and road links. It also provided a basis for computing costs due to fuel wastage. Further computations can also be made to estimate the degree of pollution caused due to traffic congestion.

Acknowledgements

The authors acknowledge the kind gesture of the Ministry of Human Resource Development, Government of India, for having provided the financial resources for the purchase of *TRANSYT* software used in this work.

References

[1] Bhattacharya, Prabhati and Virkler, Mark I. (2005) Optimization for Pedestrian and Vehicular Delay in a Signal Network, Transportation Research Record: J. Transportation Research Board, Vol. 1939, pp. 115-122, DOI: 10.3141/1939-14.

[2] Binning, James C., Mark Crabtree, and Graham Burtenshaw *(2003) "TRANSYT 12 User Guide"* Application Guide 48-Issue-D, TRL Ltd., Crowthorne.

[3] Chiu, S. (1992) Adaptive traffic signal control using fuzzy logic, In: Proceedings of the IEEE Intelligent Vehicles Symposium, pp. 98-107.

[5] Dalal Consultants and engineers Ltd (2003) "*Traffic Management Report for Mangalore Town*", submitted to the Karnataka Urban Infrastructure Development and Finance Corporation Ltd (KUIDFC Ltd), Government of Karnataka, by Dalal Consultants and Engineers Ltd, Mangalore.

[7] Gartner, N.H., (1983) OPAC: *"A Demand-responsive Strategy for Traffic Signal Control"*, Transportation Research Record, No. 906. Transportation Research Board, Washington, DC, pp. 75-81.

[10] Kadiyali, L R. (1987), "*Roads, transport demand forecast for 2000 A.D",* Journal of the Indian Roads Congress, Vol. 48-3. New Delhi.

[12] Khanna, S.K., and Justo, C.E.G. (2001) *Highway Engineering*, 8th Edition, Nem Chand and Bros. Civil Lines, Publishers, Roorkee.

[15] Nakatsuyama, M., Nagahashi, H., Nishizuka, N. (1984) Fuzzy logic phase controller for traffic junctions in the one-way arterial road, In: Proceedings of the IFAC Ninth Triennial World Conference. Pergamon Press, Oxford, pp. 2865-2870.

[16] Sarkar, P.K., and Ahmad, Syed Aqeel (2007) "*Traffic Management Through Signal Coordination by Using TRANSYT on an Urban Arterial of Delhi*". Indian Highway, march pp. 29-34.

[17] Trabia, Mohamed B., Kaseko, Mohamed S., and Ande, Murali (1999) A two-stage fuzzy logic controller for traffic signals, J. Transportation Research Part C, Vol. 7 pp. 353-367.

[18] Victor, D.J. and Santhakumar, S.M. (1987) "*Distribution of Green Time and Red Time at Police Controlled T-Junctions and Mid-Block Pedestrian Crossings*", Indian Highways, Indian Roads Congress, Vol.15, No.6, pp.18-25.

[19] Vincent, R.A., Mitchell, A.I. and Robertson, D.I. (1980) "*User Guide to TRANSYT Version 8*", TRRL Report 888, Crowthorne.

[20] Webster, F.V. and B.M. Cobbe (1966) Traffic Signals, Road Research Technical Paper No. 56, Road Research Laboratory (U.K.), H.M.S.O. London.

[21] Yun, Ilsoo and Park, Byungkyu Brian (2006) Application of Stochastic Optimization Method for an Urban Corridor, Proc. Winter Simulation Conference, L. F. Perrone, F. P. Wieland, J. Liu, B. G. Lawson, D. M. Nicol, and R. M. Fujimoto, eds., Phoenix, Arizona, pp 1493-99.

Table 1 Final Signal Timings - 2007

	Number of phases	Start of Stage 1	Start of Stage 2	Start of Stage 3
PVS (Node 10)	3	2	99	134
Joythi (Node 30)	3	29	101	164
Hampan-katta (Node 40)	3+1	109	31	93
* Stage 4 of Hampankatta Junction is a pedestrian phase.				

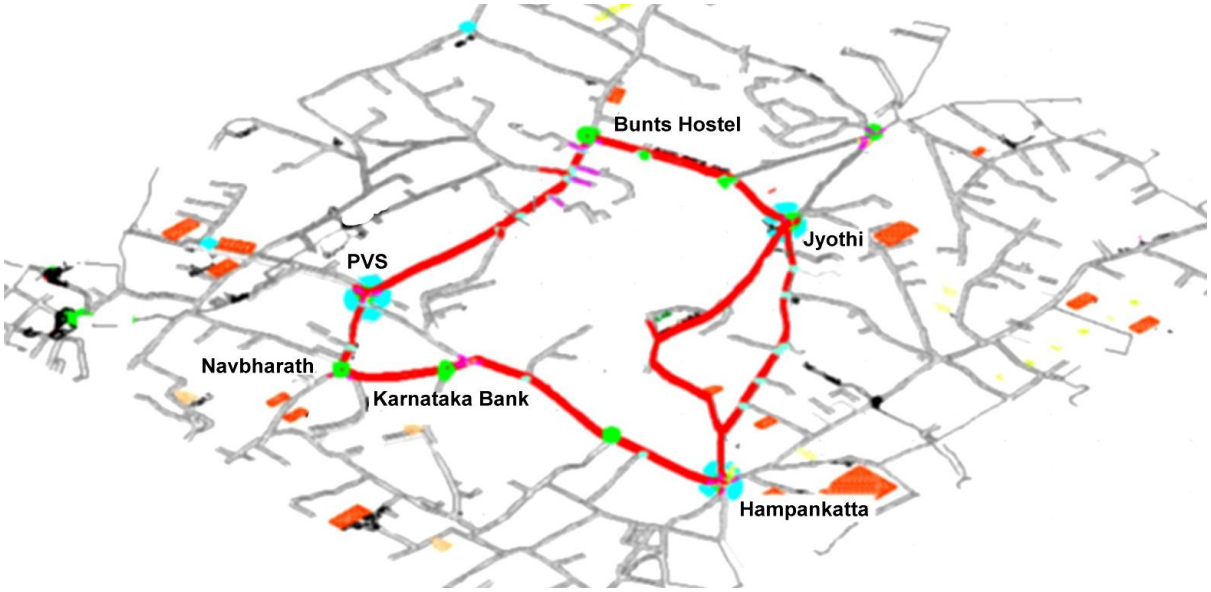


Fig. 1 Map of the Study Area

Table 2 Network Performance After 3-Stages of Improvement - 2007

	Total time spent delay (PCU-H/H)	Mean journey speed (KM/H)	Total random + over-saturation delay (PCU-H/H)	Total cost of delays (Rs/h)	Total fuel consumed liters per hour	Total performance Index (Rs/h)
Without any treatment	5404.2	3.6	4248.8	320131.4	6854.1	322393.4
After 3-stages of treatment	1397.1	13.8	450.3	45958.5	2201.5	47664.7
Percentage of improvement	74.15	283.33	89.40	85.64	67.88	85.22

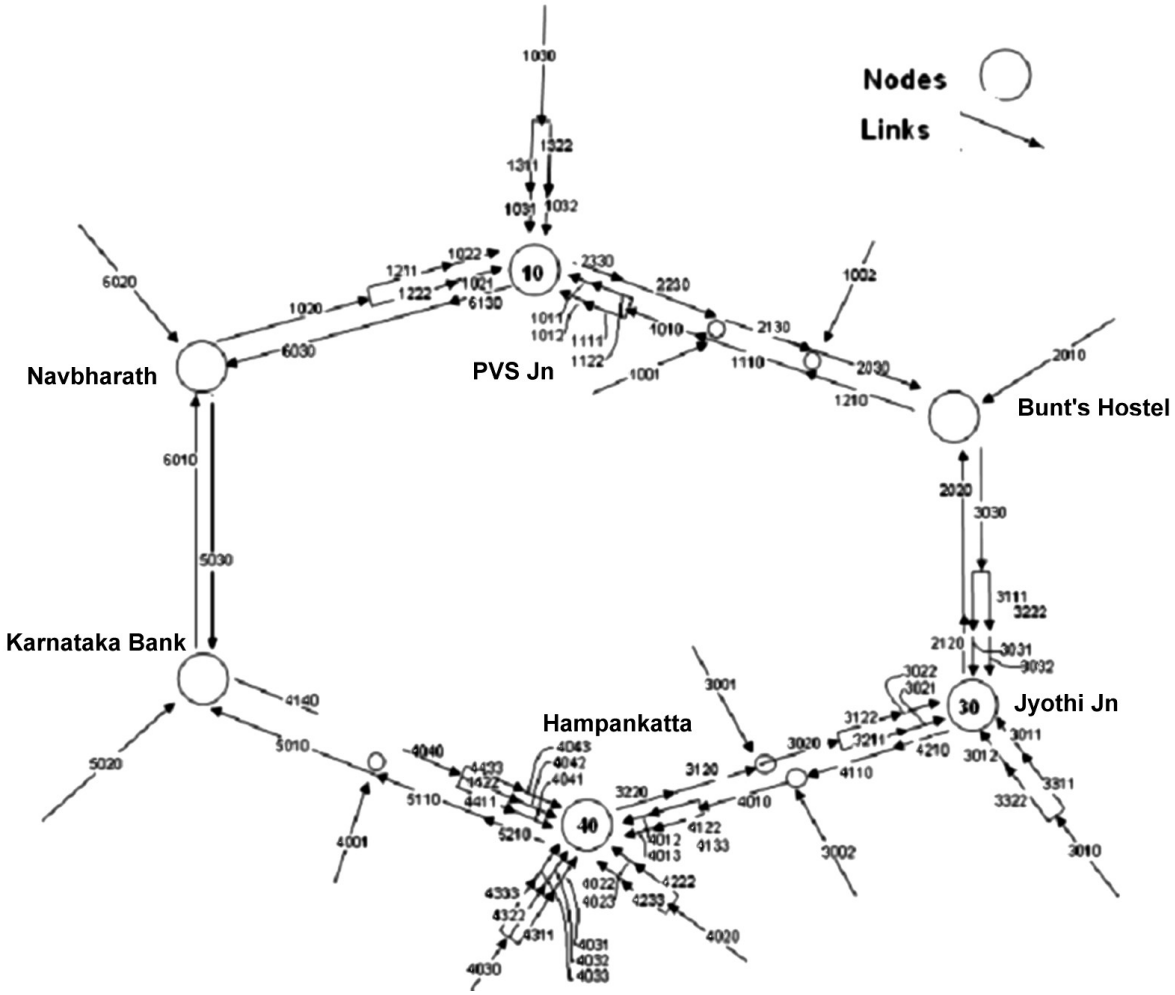


Fig. 2 Link – Node Numbering

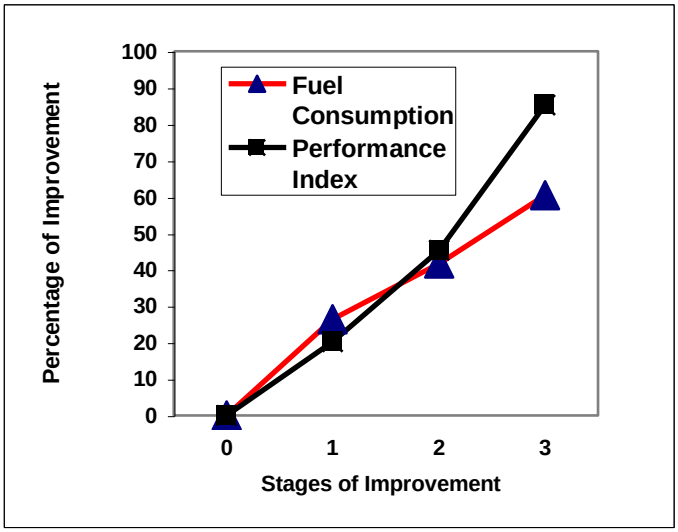


Fig. 3 Improvement in Performance and Fuel Consumption

ARCHITECTURE
&
RELATED FIELDS

2nd International Engineering Symposium - IES 2012
(KU-MU-NITK-HCMCUT Joint Symposium) March 5-7, 2012, Kumamoto University, Japan

A field study on the mitigation of noisy sound environment of nursery school classrooms by sound absorption

KAZUAKI SAKODA [1] **MUNEHIDE SAITO** [2] and **KEIJI KAWAI** [3]

1 *Graduate school of Science and Technology, Kumamoto University, Kurokami, 2-39-1, Kumamoto 860-8555, Japan. e-mail:118d8911@st.kumamoto-u.ac.jp*
2 *Graduate school of Science and Technology, Kumamoto University.*
3 *Graduate school of Science and Technology, Kumamoto University.*

Abstract: Acoustic environment in nursery schools is often so noisy with children's voices and activities that it could be harmful to health of children and teachers. In order to examine whether the sound absorption mitigates the noisy situation in classrooms, two types of experiments were carried out: one is a year-long experiment to examine long term effect, and another is a month-long experiment for a comparison of rooms of the same age group. The result of the year-long experiment indicated that the noise level reduced by 5dB in average after the installation of the sound absorber. The month-long experiment also indicated a noise reduction by the sound absorption by the comparison of the rooms of the same age condition. The level reduction in both of the experiments was greater than the expected physical reduction and this suggested that the voice of children became lower than that without sound absorption.

***Keywords**: Sound absorption, Acoustic environment, Pre-school, Classroom*

Introduction

Acoustic environment in nursery schools is generally noisy due to children's voices and activities and this could be harmful to physical and mental health of children and teachers. Several studies very high noise levels such as 85 dB in L_{Aeq} or than the 100 dB in L_{max} (Waye et al 2010, Grebennikov 2007). The acoustic environments of educational buildings could affect children's mental development and learning of language and reading (Vallet et al 2002). In order to mitigate the noisy situation of the indoor acoustic environment, sound absorption is considered to be a possible solution and this study aims to examine this effect. For this purpose, series of field experiment were carried out in which sound absorbing boards were installed in the classrooms of an actual nursery school.

Experiment

The experiments were carried out from April 2010 to August 2011 in a nursery school in Kumamoto city, Japan. In this nursery school, children from 0 to 5 years old are taken care of in six classrooms for each age. Sound absorbing boards, made of polyester, were hung on the ceilings of the classrooms using nylon strings (Fig. 1). Three conditions of absorbing area, namely about 0, 40 and 80 % of the ceiling area, were assigned for each of the room. Table 1 shows dimensions of the classrooms and conditions of absorbing area. The original surface materials of the classrooms were not apparently sound absorptive with wooden flooring, wooden or gypsum boards, glass windows with wooden or aluminium sashes, and gypsum boards ceilings.

Experiment 1, conducted from April 2010 to March 2011, examined the long term effect of the sound absorption by alternating three absorption conditions every three or four months in each of the classrooms. The three absorption conditions alternated either in an ascending order from 0 % to 80 % (rooms A, C and E) or in a descending order from 80 % to 0 % (rooms B, D, F).

Table 1 Dimension of classrooms and Conditions of sound absorption

Classrooms	Age	Volume (m^3)	Surface (m^2)	Conditions of absorber (sound absorbing area [m^2])				
				Experiment 1			Experiment 2	
				Period 1 - 1 (Apr. - Jul.)	Period 1 - 2 (Sep. - Nov.)	Period 1 - 3 (Dec. - Mar.)	Period 2 - 1 (2010 / 2011)	Period 2 - 2 (2010 / 2011)
A	5	137	173	0% (0)	40% (17)	80% (34)	0% / 40%	40% / 80%
B	4	141	176	80% (34)	40% (17)	0% (0)	80% / 40%	40% / 0%
C	3	102	148	0% (0)	40% (15)	80% (33)	40% / 40%	40% / 40%
D	2	102	148	80% (33)	40% (15)	0% (0)	-	-
E	1	99	139	0% (0)	40% (14)	80% (28)	-	-
F	0	97	137	80% (28)	40% (14)	0% (0)	-	-

Experiment 2 compares the effect of three absorber conditions by using three classrooms each of which contains children in the same age group. It conducted in August 2010 and 2012 when the children from three to five years old are mixed and then divided into three classes in August. Experiment 2 was conducted using three classrooms each of which contains a mix-age class of about 20 children of from three to five years old. Three conditions of absorbing area were assigned for each of the rooms in former two weeks (Period 1-1) in 2010. After that, all the rooms were set to the same ratio of 40 % in latter two weeks (Period 1-2). On the other hand, all the rooms were set to the same ratio in former two weeks (Period 2-1) in 2011. And the conditions were assigned each of the rooms in latter two weeks (Period 2-2).



Fig.1 Installation of sound absorbing boards

Acoustic Characteristics

To obtain the acoustical characteristics of the six classrooms, impulse responses were measured for each of the rooms using the maximum length sequence (MLS) signals. MLS signals were produced by an omni-directional speaker, received at four points per room, and processed into impulse responses.

Fig. 2 shows reverberation time (RT) of the rooms with each absorption conditions. (The room's names are not indicated.) The RT of 1 kHz band without sound absorption was 0.57-0.75 and these values are considered to be too long compared to the recommended value (0.6s) of WHO environmental noise guideline for the speech intelligibility in classrooms. After the installation of the sound absorption at 40 % cover ratio, the RT became 0.34-

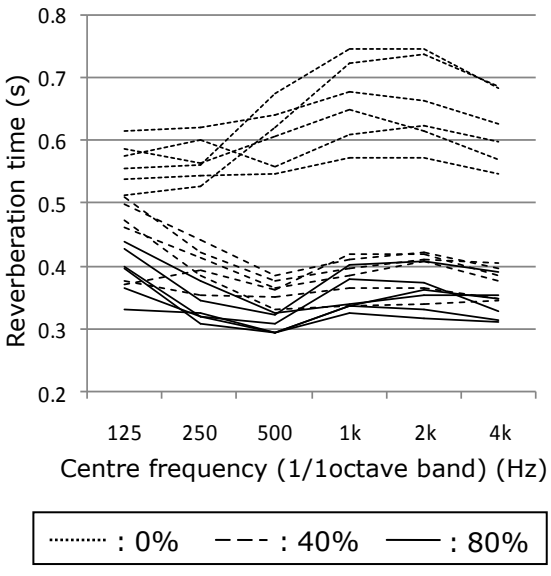


Fig.2 Reverberation time of the rooms

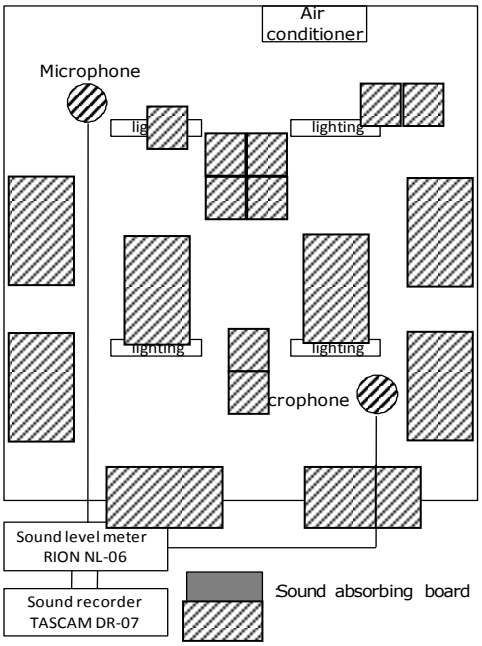


Fig.2 Arrangement of measuring instruments

0.42 s and the RT at 80 % cover ratio was 0.32-0.41 s. The little difference of RTs between 40 % and 80 % may be due to the installation of sound absorbing board only to the ceiling, which cause less diffused sound field and the reflection between the side walls without sound absorber might be left longer.

Average absorption coefficient was estimated from the RT using Eyring's formula. The average absorption coefficient of the rooms at 0, 40, and 80 % cover ratio was around 0.16, 0.26, and 0.28 s, at 1 kHz band, respectively.

Noise measurement

The indoor sound was recorded to measure noise levels in classrooms. Since the sound levels could be affected by the distance between a microphone and sound sources. In order to reduce the effect of the distance-dependent energy of direct sounds from the sound source, two microphones, both hung 30 cm bellow the ceiling with several meters distance each other, were used for recording the sound simultaneously (Fig. 3). Then, simultaneous sound pressure levels were calculated every 100 millisecond from the two recorded sound sequences, and these values can be regarded as the sound levels of far from the sound sources and thus can be regarded as the levels less affected by the direct sounds.

The noise levels in classrooms widely fluctuate depending on the children's activity. Thus, three time period were selected for the analysis: lunch time that was one of the periods in a day when children's voice was loudest, reading time in which the teacher reads a book to the children, and napping time as back ground noises.

Results and discussion

Experiment 1

Fig. 3 shows the result of noise measurement in lunch time and reading time. The noise levels (LAeq) fluctuated due to the daily difference of activity but, in general, they decreased in the rooms of ascending order (A, C, and E) of sound absorption and increased in the rooms of descending order (B, D and F). Then average values of L_{Aeq} for each of the absorption conditions were calculated (Fig. 4). The difference between 0% and 80% was 5-6 dB in the rooms of ascending order while that was 3-4 dB in the rooms of descending order. These level differences are grater than the expected physical noise attenuation (2.4 dB) by sound absorption of 80% cover ratio assuming a diffused sound field. This suggests that voice level of children and teachers became lower in the absorptive rooms due to the improved speech intelligibility by sound absorption.

Experiment 2

The measurement was conducted in 3 days in both of Period 1-1 and Period 1-2, and 8 days in both of Period 2-1 and Period 2-2. The lunch time L_{Aeq} is shown in Fig. 6. In Period 1-1, average L_{Aeq} without sound absorption (room A) were around 75 dB and 6-8 dB higher than those in the rooms with sound absorption (rooms B and C), which were 67-69 and 69-72 dB, respectively. In period 1-2, the L_{Aeq} were 71-75, 67-73, and 70-74 dB in room A, B and C, respectively. Thus, the level difference between the rooms decreased to around 3 dB. In Period 2-1, the level difference between rooms was around 2 dB. After that, in Period 2-2, it became 5 dB. These results suggest that the sound

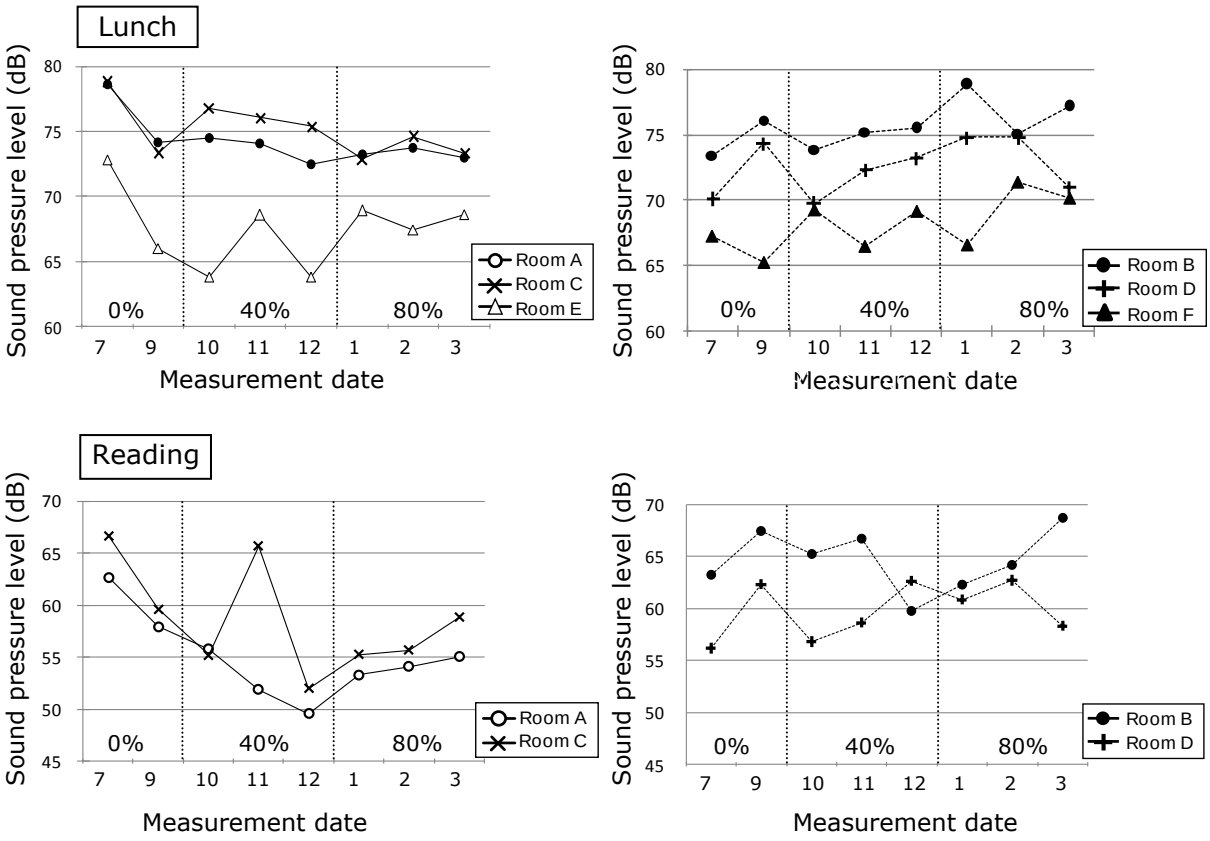


Fig. 4 Experiment 1: The change of Sound pressure levels

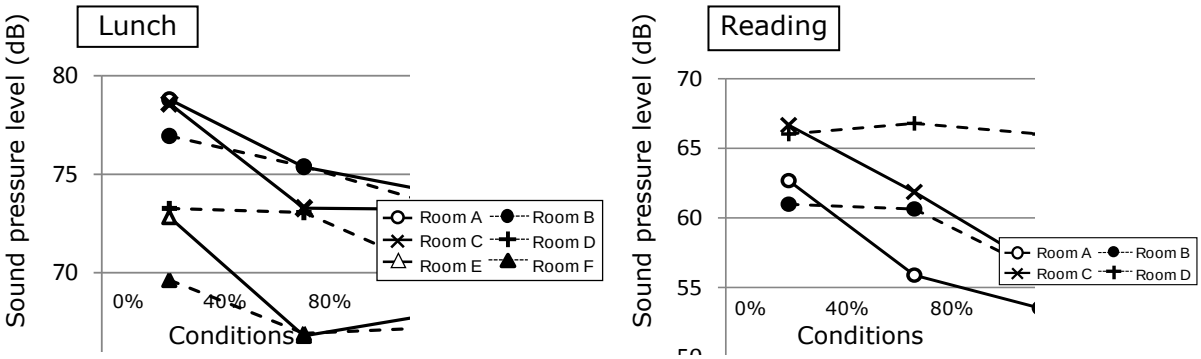


Fig. 5 Experiment 1: Sound pressure levels in each condition

absorption has an effect which decreases the L_{Aeq} in classroom.

Questionnaire

The questionnaire for teacher was carried out in March 2011 when Experiment 1 was finished, in order to obtain the psychological evaluation data for each of the three conditions. The questionnaire contents are comprehensive evaluation of the classrooms, impression of the rooms and the condition of teacher and children. Answers on each question, were rated on five graded scale, are shown in the Table 2. This result shows that teacher reported the rooms with sound absorption were better than that of without sound absorption. Furthermore, the rooms with sound absorption received positive evaluation from teacher in free writing about sound environment.

Conclusions

In this study, the effect of sound absorption on the mitigation of noisy acoustic environment of nursery school classrooms was examined through two

field studies for one and a half years. The major results are summarized as follows:

- In Experiment 1, the noise level difference with between 0% and 80% cover ratio was approximately 5 dB, which was higher than a predicted value.
- In Experiment 2, the level difference between the rooms became smaller when the condition of sound absorption was set to the same in all the rooms.

These results give clear indications of the existence of mitigating effect of sound absorption on noisy acoustic environment in nursery school classrooms. As a further research, we intend to carry out observation for action of children and measurement of noise exposure for teacher and children.

Acknowledgements

The authors would like to thank *Sakuranbo Hoikuen* ("Cherry nursery school" in English) in Kumamoto city for the cooperation and assistance to carry out this research.

References

[1] K.P. Waye et.al, (2010), "Being in a pre-school sound environment – annoyance subjective symptoms among personnel and children", Proceedings of Inter-noise 2010, DVD-ROM.
[2] L. Grebennikov, (2007), "Preschool teachers' exposure to classroom noise", Intl. J. Early Years Education 14(1), 35-44.
[3] M. Vallet et al, (2002), "Some European policies regarding acoustical comfort in educational buildings", Noise Control Engineering Journal 50(2), 58-62.
[4] WHO, (1999), Guideline for Community Noise. Website:http://whqlibdoc.who.int/hq/1999/a68672.pdf

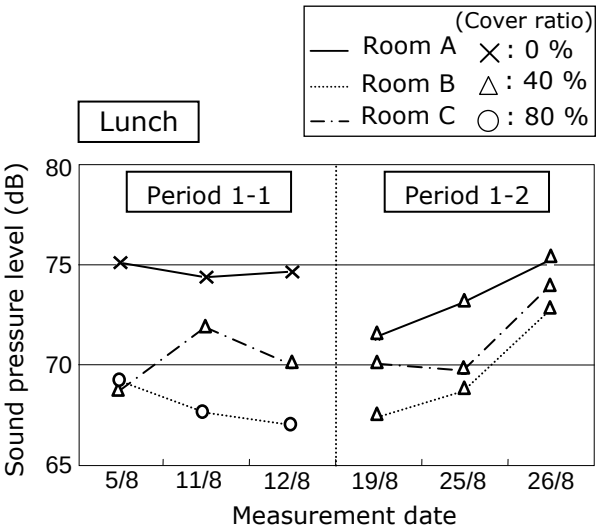


Fig6. Expriment 2: Comparison of measured Sound pressure levels (2010)

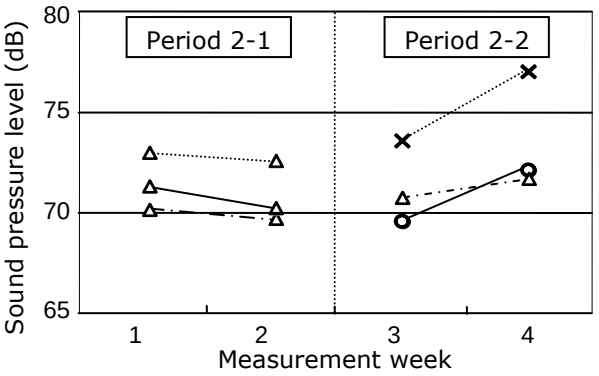


Fig7. Expriment 2: Comparison of measured Sound pressure levels (2011)

Table 2. Teacher's response

Question contents			Words
Comprehension	Fitness for childcare		-> Good
Impression of rooms	Reverberation		-> Nothing
	Ease of conversation		-> Easy
	Noise		-> Quiet
Condition	Behavior (children)		-> Calm
	Early awakenings (children)		-> Never
	Throat pain (teacher)		-> Never
	Speak loudly (teacher)		-> Never
	Feel stress at work (teacher)		-> Never

2nd International Engineering Symposium - IES 2012
(KU-MU-NITK-HCMCUT Joint Symposium) March 5-7, 2012, Kumamoto University, Japan

Community response to aircraft and road traffic noises in Da Nang City, Vietnam

Thu Lan Nguyen[1], Takashi Yano[1], Huy Quang Nguyen[1], Khanh Tuyen Nguyen[1], Hiroaki Fukushima[1], Keiji Kawai[1], Tsuyoshi Nishimura[2]
and **Tetsumi Sato[3]**

1 *Graduate School of Science and Technology, Kumamoto University, 2-39-1 Kurokami, 860-8555 Kumamoto, Japan. e-mail: linh2lan@gmail.com, nhuyquang@yahoo.com, yano@gpo.kumamoto-u.ac.jp, tuyenntk12012002@gmail.com, kopporabutai@hotmail.co.jp, kkawai@kumamoto-u.ac.jp*
2 *Graduate School of Engineering, Sojo University, 4-22-1 Ikeda, 860-0082 Kumamoto, Japan. e-mail: nisimura@cis.sojo-u.ac.jp*
3 *Faculty of Engineering, Hokkai Gakuen University Minami 26-Jo, Chuo-ku, 064-0926 Sapporo, Japan. e-mail: sato@arc.hokkai-s-u.ac.jp*

Abstract: To provide more elaborate approach to rate transportation noise annoyance across communities in Vietnam, socio-acoustic surveys on community response to aircraft and road traffic noises were conducted in residential areas around Da Nang City. The community response was obtained by face-to-face interviews during the daytime on weekends. The aircraft noise was measured for seven successive days. Road traffic noise was measured every 1 s for 24 h on the road shoulders of selected streets. The ranges of aircraft and road traffic noise exposures observed in Da Nang were from 52 to 64 dB, and from 66 to 76 dB L_{den}, respectively. Representative dose-response relationship for aircraft and road traffic noise annoyance in Vietnam has been proposed based on data obtained in Hanoi, Ho Chi Minh, and Da Nang City. It has been found that Vietnamese were more disturbed by aircraft noise but less annoyed by road traffic noise than European people. The respondents in Da Nang were found to be the most tolerant of noise among those in all the investigated cities based on the results of Community Tolerance Level.
***Keywords**: Aircraft Noise, Road Traffic Noise, Dose-response Relationship*

Introduction

Dose-response relationships for aircraft and road traffic noise annoyance have been establish for Vietnam with data obtained from surveys in Hanoi and Ho Chi Minh City [3]. The curves are in the noise exposure ranges of 48-71 dB L_{den} and 75-83dB L_{den} for aircraft and road traffic noises, respectively. When compare with the dose-response relationship derived by Miedema and Vos[1] which are used for EU noise policies, The dose-response curve for road traffic noise almost coincided with the EU's curve, while the curve for aircraft noise was slightly higher than EU's. However, it is worth noting that these findings may be influenced by the distinctive characteristics of traffic situation in surveyed cities, particularly, here is, Hanoi and Ho Chi Minh City. They are the two busiest major metropolitan areas in Vietnam with approximately 7 million inhabitants in each. The dominant source is road traffic noise which is contributed to by a huge amount of motorbikes but not cars or light trucks as in other countries. Extremely high road traffic noise exposure existed even in the vicinity of the airports.

On the other hand, though the curve for aircraft noise is in the range of primary interest of EU's policy, from 45 to 75 dB L_{den}, that for road traffic noise is in the range from 75-83 dB $L_{den,}$. It means that the road traffic curve lies outside the comparable range with EU's. All the above arguments suggest that it is necessary to accumulate data from other cities in



Fig.1. Map of survey sites in Da Nang City.

Vietnam, particularly small and medium size cities, to achieve more valid relationships for policy and regulatory purposes. Da Nang City was selected for the next target of our study. Da Nang City is located in middle of Central Vietnam, between Hanoi and Ho Chi Minh City, with 887.1 thousand habitants (April 2009). Unlike the previously surveyed cities, Da Nang City has a comparatively reasonable urban planning and transportation network without traffic overload. Surveys on effects of aircraft and road traffic noises in Da Nang are aimed to provide more elaborate approach to rate transportation noise annoyance across communities in Vietnam.

Methods

Survey sites

Da Nang International Airport is one of the three largest in Vietnam after Tan Son Nhat and Noi Bai Airports, locating 3.2 km southwest of downtown Da Nang. For the survey on aircraft noise, six sites were selected along the north to the south direction of the airport including as one site to the north (Site 6) and five other sites to the south of the airport (Site 1-5). While all target houses at Site 6 are in the alley of a populated street area, those at other sites are detached houses lying in rural and scattered-populated villages along the national highway crossing Da Nang. Unlike the surveys on aircraft noise in Hanoi and Ho Chi Minh City, which surveyed the impact of aircraft noise in both single and mixed noise environment, aircraft noise in this study is investigated as only a single source.

Six sites were selected in the urban areas of the city to the northeast of the airport at the distance that the possibility of influence of aircraft noise could be excluded (Site A-F). The sites were selected to represent various noise exposures, traffic volume, functions and scatter widely in the city. The investigated streets are diverse, including merely residential streets (Sites A, B, and F), a street of the busy trade with many shops and commercial centers, (Site D), or a mixture of both (Sites C and E). All target houses are row houses and located along the main roads of the areas (Figure 1).

Social surveys

Social surveys on community response to aircraft noise and road traffic were carried out in Da Nang City in two weekends of September 2011.

Community responses were obtained through an interview questionnaire presented as a social survey of the living environment.

Two scales—5-point verbal and 11-point numeric—constructed according to the ICBEN method were used [4].

Noise measurements

Since there was a lack of available noise data in Vietnam, all noise databases for this study were compiled using field measurements. Aircraft noise exposure was measured every 1 s for seven successive days from September 11 to 18 by using sound level meters (RION NL-21 and NL-22) at selected sites. Microphones covered with omni-weather wind screens were positioned on the rooftops of the highest houses at the sites—1.5 m above the roofs and at least 1 m away from any other reflecting surface. Road traffic noise was measured every 1 s for 24 h from September 12 to 13 on the road shoulders of selected streets. Traffic volume was counted by panel-replaying the video recordings for 10 minutes every hour.

Results and discussion

Results of social surveys

The outline of the surveys is summarized in Table 1. In total, 528 and 492 responses were obtained in the aircraft and road traffic noise surveys, respectively. The response rates were very high in both surveys: the average response rates of all sites for the aircraft and road traffic noise surveys were 84% and 80%, respectively. Some of the socio-demographic factors of the surveys are summarized and compared with the demographics of the Vietnamese population in Table 2.

The ratio of males to females in all surveys was well balanced and comparable to the ratio obtained in the Vietnam population census. 87% of respondents in the aircraft noise survey were in the age range from 20 to 60; corresponding figure for the road traffic noise survey was 86%. All of these percentages were slightly higher than that obtained in the Vietnam population census (84%) but quite comparable with corresponding figures obtained in the previous surveys in Hanoi and Ho Chi Minh City. Employed respondents constituted 61% and 53% in the two surveys, lying in between the values of the same figures of the previous surveys conducted in Hanoi and Ho Chi Minh City. These results represent the well-balanced and unification in the structure of the respondents of our study through performed surveys.

Table 1 – Outline of social survey on community response to aircraft noise and road traffic noise in Da Nang City.

	Site ID	Sample size	Response rate (%)
Aircraft noise survey	1	85	82
	2	78	75
	3	77	70
	4	99	95
	5	99	94
	6	90	85
	Total (1)/ Average (2)	(1) 528	(2) 84
Road traffic noise survey	*A*	*75*	*72*
	B	*49*	*67*
	C	93	85
	D	98	93
	E	87	83
	F	90	82
	Total (1)/ Average (2)	(1) 492	(2) 80

Table 2 – Some demographic factors of the surveys.

Items	Aircraft (%)	Road (%)	Demographics of Vietnam (%)
Gender			
Male	47	50	49
Female	53	50	51
Age			
20-39	48	48	84
40-59	39	37	
Older than 60	13	15	16
Occupation			
Employed	61	53	52
Students, housewives, retired, and unemployed	39	47	48

Traffic volumes and noise exposure

Tables 3 and 4 show the noise metrics calculated for aircraft and road traffic noise exposures at all the surveyed sites in Da Nang. The aircraft noise exposure was from 52 to 64 dB L_{den} . The lowest exposure level was found at Site 1, the farthest site to the south of the airport. The residents at Site 4, the second nearest site, were exposed to the highest exposure level of the aircraft.

The fluctuation of traffic volumes at all sites for 24 h is shown in Figure 2. There seemed to be considerable differences in traffic density between Site D and the others. The largest traffic volume at Site D reached approximately 5000 pass-bys per hour around rush hours of the city (from 5 to 6 PM). The component of the traffic vehicles in Da Nang was similar to those in Hanoi and Ho Chi Minh City in that motorbikes formed the bulk of the traffic.

The range of road traffic noise exposure observed in Da Nang was from 66 (Site C) to 76 dB L_{den} (Sites D and E). In spite of having significantly different traffic volumes, the noise exposure levels obtained at Site D and E are approximately equal.

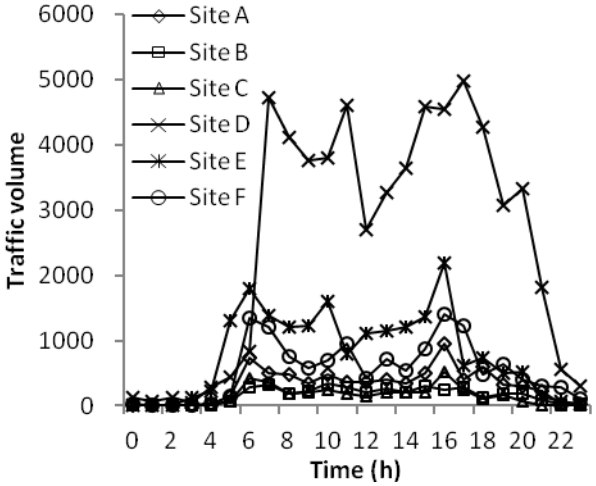


Fig.2. Traffic volumes in Da Nang City.

Dose-response relationships

A logistic regression function was applied to plot the dose-response curves for aircraft and road traffic noise annoyance in Da Nang (Figure 3). The data point shown in the figure represents a paired observation of the percentage of people highly annoyed with day-evening-night average sound level (L_{den}) at each surveyed site. Though the data points fit very well to the established curve, the curve for road traffic noise annoyance is steep. In spite of that the noise exposures vary over the range of around 10 DB, there is a great variability of observed of the percentage of highly annoyed respondents, from 0 to 24.5% (Table 4). The trend of the curve for aircraft annoyance is more stable with the percentages of the highly annoyed varying from 1.5 to 12.1% over the range of around 12 dB (except Site 6). It can easily be observed that the fit of the data points to the logistic function is poor with a very wide scatter. The data point of Site 6 lies noticeably apart from the distribution area of the other points. The outstandingly higher of the percentage of the highly annoyed at Site 6 significantly affects the trend and position of the aircraft annoyance curve. The noise exposure level at Site 6 was 59.8 dB L_{den} , lower than that of Site 3, 5, and 4 (60.2 – 63.5 dB L_{den}) but there were 33% of highly annoyed people, considerably higher than the second highest percentage of highly annoyed observed at Site 5 (12%). The background noise level defined as the 95th percentile (L_{95}) of all sites was calculated. It has been found that the background noise at Site 6 is the lowest (L_{95} = 37.7 dB), while the maximum noise level (L_{max} =112.5 dB) is the highest among all other sites (88.8-101.3 dB). These characteristics might make the aircraft noise events more noticeable; therefore, raise the nuisance to the residents at Site 6. The difference in position with the airport and the distance to downtown, as well as the residential characteristics between Site 6 and the other sites also helps to explain this. Characteristics of the reaction of residents at Site 6 to aircraft noise should be further analyzed to be elucidated.

Figure 4 shows a comparison of the dose-response relationships established for Da Nang to those for Hanoi and Ho Chi Minh City. Da Nang's curves are much lower than Hanoi's in both terms of aircraft and road traffic noises. The closer agreement was found between Da Nang and Ho Chi Minh City's curves. The dose-response

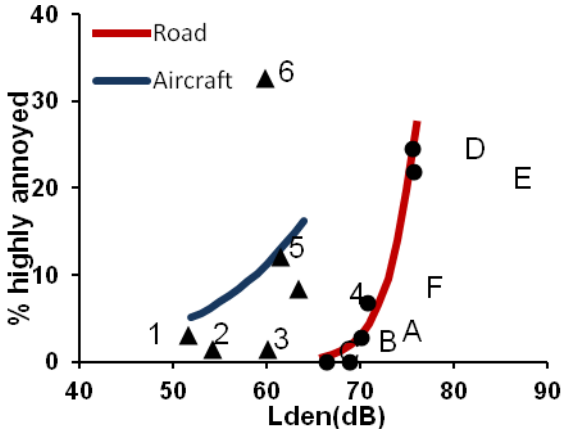


Fig.3. Dose-response relationships noise annoyance in Da Nang.

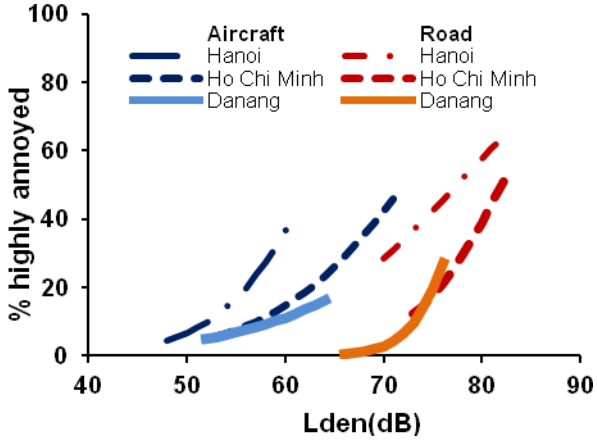


Fig.4. Comparison of the dose-response relationships established for Da Nang to those for Hanoi and Ho Chi Minh City.

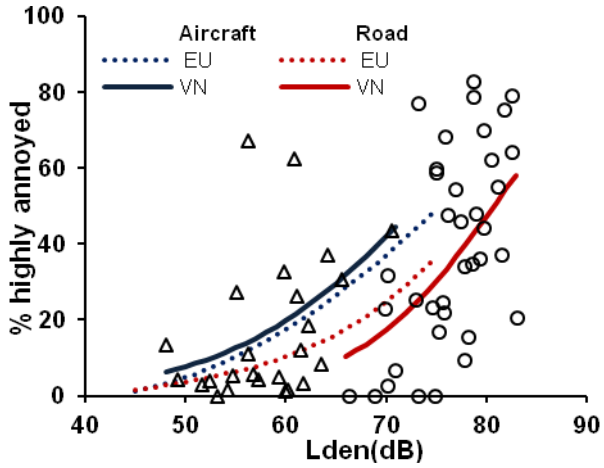


Fig.5. Comparison of the dose-response relationships synthesized from the data of Hanoi, Ho Chi Minh and Da Nang to the EU's corresponding curves.

curves for aircraft and road traffic noises of Da Nang were consistent to Ho Chi Minh City's. The separation of Hanoi's curves and the good fits of Da Nang and Ho Chi Minh's relationships have not been explained fully. However, the results can be expected considering the geography and history of the three cities. Da Nang and Ho Chi Minh City are quite similar in climate, living condition, social customs, history, etc. Finally, the synthesized curves of Da Nang, Hanoi, and Ho Chi Minh City were superimposed and fitted on to the EU curves (Fig. 5). The supplement of the data obtained in Da Nang makes the relationship for aircraft annoyance in Vietnam closer to EU's than the previously published one, but lower the position of the curve for road traffic noise. It could be argued that, at the same noise exposure level, Vietnamese were more disturbed by aircraft noise but less annoyed by road traffic noise than European people.

Conclusions

The ranges of aircraft and road traffic noise exposures observed in Da Nang were from 52 to 64 dB, and from 66 to 76 dB L_{den}, respectively. Representative dose-response relationship for aircraft and road traffic noise annoyance in Vietnam has been proposed based on data obtained in Hanoi, Ho Chi Minh, and Da Nang City. It has been found that Vietnamese were more disturbed by aircraft noise but less annoyed by road traffic noise than European people.

Acknowledgement

The present study was supported by *Grant-in-Aid* for Scientific Research C of Japan Society for the Promotion of Science (No.23560695). The authors also appreciate Dr. Son and students from Da Nang University of Technology for their support in conducting the survey and noise measurements in Da Nang City.

References

[1] European Communities, Position paper on dose-response relationships between transportation noise and annoyance. EU's future noise policy, WG-Dose/Effect, (2002).
[2] S. Fidell, V. Mestre, P. Schomer, B. Berry, T. Gjestland, M. Vallet, and T. Reid, A first-principles model for estimating the prevalence of annoyance

with aircraft noise exposure, Journal of Acoustical Society of America, 130(2), (August 2011).
[3]T.L. Nguyen, T. Yano, H.Q. Nguyen, T. Nishimura T. Sato, T.Morihara, and Y.Hashimoto, The impact of transportation noises on communities in Vietnam, Proceeding of Internoise 2011, Osaka (2011).
[4]T. Yano and H. Ma, Standardized noise annoyance scales in Chinese, Korean and Vietnamese, Journal of Sound and Vibration, 277 (3), pp.583-588, (2004).

Table 3 - Noise metrics calculated for aircraft noise exposure at all sites in Da Nang City.

Noise metrics (dB)	Site 1	Site 2	Site 3	Site 4	Site 5	Site 6
$L_{Aeq,\ day\ (07:00\sim22:00)}$	50.7	53.1	57.8	61.9	59.5	58.6
$L_{Aeq,\ night\ (22:00\sim07:00)}$	40.0	42.8	52.0	54.7	51.2	49.2
$L_{Aeq,\ evening\ (19:00\sim22:00)}$	49.8	52.5	54.9	58.5	59.3	28.2
L_{dn}	50.8	53.2	59.9	63.2	60.6	59.6
L_{den}	51.7	54.2	60.2	63.5	61.5	59.8
$L_{Aeq,24h}$	48.9	51.3	56.4	58.0	60.3	54.8
L_{95}	39.3	41.4	41.3	45.9	41.0	37.7
L_{1}	67.9	69.8	70.3	72.5	73.3	70.1
L_{MAX}	88.8	89.1	92.1	91.8	101.3	112.5
% highly annoyed	3.0	1.5	1.5	8.3	12.1	32.6

Table 4 - Noise metrics calculated for road traffic noise exposure at all sites in Da Nang City.

Noise metrics (dB)	Site 1	Site 2	Site 3	Site 4	Site 5	Site 6
$L_{Aeq,\ day\ (07:00\sim22:00)}$	68.5	67.0	65.0	73.7	73.6	68.8
$L_{Aeq,\ night\ (22:00\sim07:00)}$	60.4	59.5	56.8	66.5	63.1	61.5
$L_{Aeq,\ evening\ (19:00\sim22:00)}$	68.5	66.7	63.3	73.2	77.8	69.3
L_{dn}	69.3	68.1	65.8	75.0	73.4	70.0
L_{den}	70.2	68.9	66.4	75.7	75.8	70.9
$L_{Aeq,24h}$	66.9	65.4	63.4	72.1	71.8	67.2
L_{95}	41.5	45.3	41.5	46.6	42.8	42.5
L_{1}	76.5	76.0	73.3	80.5	82.3	77.0
% highly annoyed	2.7	0.0	0.0	24.5	21.8	6.7

2nd International Engineering Symposium - IES 2012
(KU-MU-NITK-HCMCUT Joint Symposium) March 5-7, 2012, Kumamoto University, Japan

A mapping of recognition structure based on human life history

Kaoru Ono[1] and **Yuji Hoshino** [2]

1 *Department of Civil Engineering, Kumamoto University, Kurokami, 2-39-1, Kumamoto 860-8555, Japan. e-mail:101d9401@st.kumamoto-u.co.jp*
2 *Department of Civil Engineering, Kumamoto University, Kurokami, 2-39-1, Kumamoto 860-8555, Japan. e-mail: hoshino@kumamoto-u.ac.jp*

Abstract: The background of this study is to understand what and how people remember in life, and to clarify the structure of its recognition. The aim of this study is to examine a mapping with rules defined from sentence structure. A book is selected as a research object which is assembled life histories who lived in Kumamoto city. A sentence structure is utilized for mapping. As a result, recursive elements are functioned as nodes and turning points of relationship between other elements and 'I.' It is also suggested that the perspective change is happened in the memory and weaken the connection to 'I.' Comprehensive elements shows expanse or cohesion temporally or spatially when bundling each elements collectively or continuously.

Keywords*: comprehensive elements, life history, mapping, sentence structure, recursive elements, recognition structure*

1. Introduction

In Japan, a definition of landscape is a sight of environment around human being. With this definition, a lot of studies have done in civil engineering, architecture, landscape architecture and so on. Some are focused on regional structure or recognition process.

A person's understanding of their surrounding is mostly unconscious. Almost the experiences we have while moving through and interacting with the landscapes near our homes, or life-scape, some are remembered and some are forgotten. The background of this study is to understand what and how people remember in life, and to clarify the structure of its recognition.

Sasaki Y. (2011) categorized regional landscape researches into four types according to the analysis perspective.

a) Substantial property in region

Substantial property is cleared what or how people understand the observation area as a unit of landscape. Condition of a regional environment is captured from land utilization, photographs, or contour map. Objective indexes are also adopted to understand a region. Dohi H. et al (1995) , Kubo T. et al (1985) , and Sakamoto J. et al (1996, 1998) would be example studies of this type.

b) Description of collective representation in region

Regional property is also cleared from descriptions of lyrics, discourses, maps or contour data. From these medias, understanding or assessment is done from experiences in sharing recognition or movement of visual objects. Demura Y. et al (2010), Iwanaga K. et al (1988), Kitahara T. (1990), Nii A. et al (2007), Simago S. et al (1994), Shimizu Y. and Nakamura Y. (1990), Yabe T. et al (1995), Yanagawa et al (1996) , and Zhao C and Satoh S. (2008) would be in this type.

c) Recognition process or structure in region

There is a group of studies focused on recognition process more than assessment. Recognition process or structure of community people is analyzed not only land utilization or visible data, but also question survey, caption evaluation method or text mining. Iwanaga K. and Matsumoto N. (1990), Koga T. et al (1999),

Negoshi H. and Ohuchi H. (2005), Nishimura M. et al (1992), Oishi H. et al (2006), Saito T. et al (1997), Yamaguchi M. et al (2001), Yamamoto K. et al (2005), and Watanabe S. et al (1996) would be in this type.

d) Internal aspect and external sight of people

Recognition elements or contents of landscape are found from the descriptions of personal experience, for example, literature and life history. These recognitions are personal and internal aspects, but there is a possibility to think about regions as accumulation of personal experiences. Furuya K. (1998), Hori S. et al (1988), Ikeda T. and Konno A. (1993), Ikeda T. and Ohgai A. (1993, 1994), Senda M. (1982), Yoshimura A. et al (1997), and Yoshimura A. (1998) would be examples of this type.

This thesis is focused on d) internal aspect and external sight of people. Some personal experience is represented by language expression. There are several analysis of language data extracted with sentence structure. Some is to transpose words to objective data as numerical value. Other is to illustrate diagrams or maps of recognition process or structure. There are several methods of illustration; mapping method, image mapping, hyper text model, dynamic model of landscape and so on. These illustration methods are one of valuable analysis to visualize internal aspect of people. On the other hand, rules of illustration seems depending on meanings of each word or phrase, which possibly includes interpretation of analysts. From those reasons, the aim of this study is to examine a mapping with rules defined from sentence structure.

2. Object and Method

2.1 Research Object

In this study, 'Machi ha Kioku suru (A City Remembers) ' (2004) is selected as a research object book. This book is assembled life histories of eight people who lived around Kami-tori Street, Kumamoto city. From this book, one person's life history is chosen to make a mapping as a trial.

2.2 Elements of Japanese Language

There are several differences and similarities between Japanese and English languages. Some study guide books pointed discrepancies and similarities. Japanese and English have different word orders, but word elements are almost same ; subjective noun phrase(S), predicate verb(V), objective noun phrase(O), complement noun phrase(C), and modifier(M). M is added to noun phrase in Japanese so that main elements are S, V, O and C. In this study, mapping is examined with these four elements and their relationships.

2.3 Rules for Mapping

Rules for mapping is defined from rules of sentence structure described in Fig-1. One sentence from the candidate book is used to explain this mapping rules. First of all, noun phrases and predicates are broken down from one sentence. Noun phases are component elements of mapping. Predicates are used to understand the relationship between noun phrases at the second step. An arrow is figured from O noun phrase to S noun phrase. Equal is drown from C noun phrase to noun phase or arrows. This is because C noun phrase adds information of a noun phrase or predicates. In Japanese, S is clipped in sentences. Dot lines are drawn presumptively for understanding. Single lines are also drawn to make sure which elements are in one sentence.

There are two cases to pay attention to mapping noun phrases ; recursive elements and comprehensive elements. Recursive elements are the noun phrases appeared several times in whole life history. In this case, noun phrases are unified to one noun phrase and circles are added outward. Comprehensive elements are the noun phrases including other noun phrase; for example, 'family' includes 'father' and 'mother.' To show this relationship, 'father' and 'mother' are set inside the 'family' phrase.

From those rules, mapping had done from a person's life history in Fig-2 on page 6. The life history is in Japanese so that the mapping had done in Japanese. However, in this thesis, the mapping was

translated and simplified from Japanese to English.

3.Recognision Structure in Life History

3.1 Recursive Elements ; Relationship between Elements and 'I'

From Fig-2, recursive elements and comprehensive elements are focused for discussion.

Firstly, 'I' is focused to see the recursive elements. This is because the life history is a story of 'I' and 'I' is the starting point of memory as a recursive elements.

There are 3 patterns of recursive elements in Fig-2 ; the elements which connect directly to 'I', one which connect 'I' by the intermediary of other elements, and one which have no connection to 'I.' In the cases which connect to 'I' directly or by the intermediary of other elements, the recursive elements are functioned as nodes to connect other elements to 'I.' It is also considered that the recursive elements are turning points of relationship between 'I' and other elements. The recursive elements which has no connection to 'I,' these elements are taken objectively.

Recursive elements which have connection to 'I' are picked up in Fig-3. In this case, 'father' and 'Datsun(car)' are the elements which connected directly to 'I.' Next, 'stuff,' 'second floor of the shop' and 'grandfather' connect to 'father.' At this time, those three elements are captured from the sight of 'father,' which suggests that the perspective change is happened in the memory. Also this perspective change weaken the connection to 'I.'

3.2 Comprehensive Elements ; Collective Memory with expansion

There are 25 comprehensive elements in Fig-2. Comprehensive elements also have three patterns ; single comprehension, inward comprehensive, and overlap comprehension. Single and inward comprehensions put pieces of memory together into one collective memory. In overlap comprehension, the element which connects comprehensive elements is the recursive element. This recursive element provides the collective memories as a continuum memories.

In Fig-2, the noun phrases types of comprehensive elements are mostly date or place. These types of elements shows expanse or cohesion temporally or spatially when bundling each elements.

4.Conclusion

In preceding chapter, recursive elements are functioned as nodes and turning points of relationship between other elements and 'I.' It is also suggested that the perspective change is happened in the memory and weaken the connection to 'I.' Comprehensive elements shows expanse or cohesion temporally or spatially when bundling each elements collectively or continuously. In this chapter, it is consider the recognition structure from recursive and comprehensive elements.

Fig-4 shows a recursive and comprehensive elements in a person's life history. From this mapping, it is cleared that mapping from sentence structure enables to understand a dimension of relationship between elements and 'I,' and patterns of collective memories.

By resolving and mapping a person's life history from sentence structure, one recognition structure is cleared. However, this structure shows a memory of only one person. More life histories would be needed to examine if this mapping is useful or not and if the recognition structures clarify a structure or characteristic of a region or not.

References

[1] Demura, Y et al (2010), Determination of the Domains Specified by the Highest Visual Peaks around the Higashiyama Mountains, D Journal of the Japan Society of Civil Engineering, Vol.66, No.1, pp.46-53.
[2] Dohi, H et al (1995), On the Descriptive Method of Regional Landscape Applying the Concept of Landscape Unit, Papers on City Planning, No.31, pp.645-649.
[3] Furuya, K (1998), Characteristics and Structure of Memory of Landscape Past, Journal of the Japanese Institute of Landscape Architecture, Vol.61, No.5, pp.669-674.
[4] Hori, S et al (1988), On Structure of Experienced Landscape, Journal of the Japanese Institute of Landscape Architecture, Vol.51, No.5, pp.287-292.
[5] Ikeda, T and Konno, A (1993), Study on the Method of Reading Landscape from Literature Works A case of Matsusaka settlement from the novel entitled 'The town where there is a castle,' Journal of

Architecture, Planning and Environmental Engineering, No.450, pp.121-130.
[6] Ikeda, T and Ohgai, A (1993), Study on Landscape from Literature Works - A Case of Takayama City-, Papers on City Planning, No.28, pp.583-588.
[7] Ikeda, T and Ohgai, A (1994), A Study on Landscape Described in Literature Works Received the Prize of Public Contribution of Takayama -Analysis by Context-, Papers on City Planning, No.29, pp.601-606.
[8] Iwanaga, K and Mastumoto, N (1988), A Study on Mental Scenery of Central District in Nagao City, Papers on City Planning, No.28, pp.685-690.
[9] Iwanaga, K and Matsumoto, N (1990), A Study on Mental Scenery in Urban Area -About Image Structure of Mental Scenery in Nagano-City-, Papers on City Planning, No.25, pp.451-456.
[10] Kamitori Shoei Kai (2004), Machi ha Kioku suru (A City Remembers), Kamitori Shinsyo, pp.12-17.
[11] Kitahara, T (1990), An Study on the Landscape Structure Represented in the School Songs -Case Study of Three Cities in the Mie Prefecture-, Papers on City Planning, No.25, pp.673-678.
[12] Koga, T et al (1999), Participatory Research of Townscape, Using "Caption Evaluation Method" - Studies of the cognition and the evaluation of townscape, Part 1-, Journal of Architecture and Planning (Transactions of AIJ), No.517, pp.79-84.
[13] Kubo, T et al (1985), A Fundamental Study on Organization of Neighbourhood Landscape in Great City, Osaka, Journal of the Japanese Institute of Landscape Architecture, Vol.48, No.5, pp.300-305.
[14] Negoshi, H and Ohuchi, H (2005), Visible Space by Landscape Recognition of Local Inhabitants and Its Composition, Journal of Architectural Institute of Japan, No.3, pp.102-107.
[15] Nii, A and Saito, U (2007), A Study on Sustainability of Geological Shapes from Moving View, D Journal of the Japan Society of Civil Engineering, Vol.63, No.2, pp.182-189.
[16] Nishimura, M et al (1992), Studies on the Factor of the Formation and Remembrance of Mental Scenery, Papers on City Planning, No.27, pp.721-726.
[17] Oishi, H et al (2006), A Study on the Characteristics of the Preference for Regional Landscapes Based on the Free Descriptive Answer by Subjects, Journal of Environmental Engineering (Transactions of AIJ), No.599, pp.135-142.
[18] Saito, T et al (1997), A Study on Formation Factor and Scene Characteristics of Mental Scenery in Urban Area, Papers on City Planning, No.32, pp.325-330.
[19] Sakamoto, J (1996), Typology of Macroscopic Coexisting Phenomena on the Index of Landscape and Problems on Planning -Part 1 A study of rurban area focussing on landscape feature-, Journal of Architecture, Planning and Environmental Engineering, No.487, pp.157-166.
[20] Sakamoto, J et al (1998), "Landschaft" in Rurban Area ; Characterization and Typology - Part 2 A study of rurban area focussing on landscape feature-, Journal of Architecture, Planning and Environmental Engineering, No.504, pp.127-134.
[21] Sasaki, Y (2011), Memorandum for Discussion of Regional Landscape, Conference for Architecture and Infrastructure Environment, No.7, pp.160-165.
[22] Senda, M (1982), Research on Structure of Children's Play-spaces by Investigating Primary Scenes in Memories about Playing, Transactions of the Architectural Institute of Japan, No.322, pp.108-117.
[23] Shimago, S et al (1994), A Study on the Image of Railway Station by Analyzing Descriptions of Popular Songs, Papers on City Planning, No.29, pp.589-594.
[24] Shimizu, Y and Nakamura, Y (1990), A Study on Historic Landscape in SETAGAYA-ku Tokyo, Journal of the Japanese Institute of Landscape Architecture, Vol.53, No.5, pp.205-209.
[25] Watanabe, S et al (1996), The Process of the Formation of Mental Scenery and the Practical Forms of Space, Papers on City Planning, No.31, pp.175-180.
[26] Yabe, T et al (1995), A Study on the Japanese Local Landscape Image of the School Songs, Journal of Architecture, Planning and Environmental Engineering, No.472, pp.111-122.
[27] Yamaguchi, M et al (2001), Mental Sceneries of Local Inhabitants in the Mixed Industrial and Residential Area, Papers on City Planning, No.36, pp.745-750.
[28] Yamamoto, K et al (2005), A Study on the Characteristics of the Inhabitant's Preference for Regional Landscape in Higashi-Hiroshima City, Journal of Environmental Engineering (Transactions of AIJ), No.587,pp.53-61.
[29] Yanagawa, M and Nakama, K (1996), A Study on Urban Landscapes in Comprehensive Representations -An Analysis of Edo Meisho Zue-, Papers on City Planning, No.31, pp.181-186.
[30] Yoshimura, A (1998), A Study on a Dynamic Model of Landscape through an Analysis of "Tohkan-Kikou," Journal of Japanese Institute of Landscape Architecture, Vol.61, No.5, pp.675-680.
[31] Yoshimura, A et al (1997), A Study on Dialectic Dynamism in Landscape Value Production through an Analysis of "The Narrow Road to the Deep North," Journal of Japanese Institute of Landscape Architecture, Vol.60, No.5, pp.567-572.
[32] Zhao, C and Satoh, S (2008), The Description of Town-scape Structure using "Keirou" -Focusing on the Japanese Castle Town of Yama-ate as its Speciality-, Journal of Architecture, Planning and Environmental Engineering, Vol.73, No.32, pp.2165-2172.

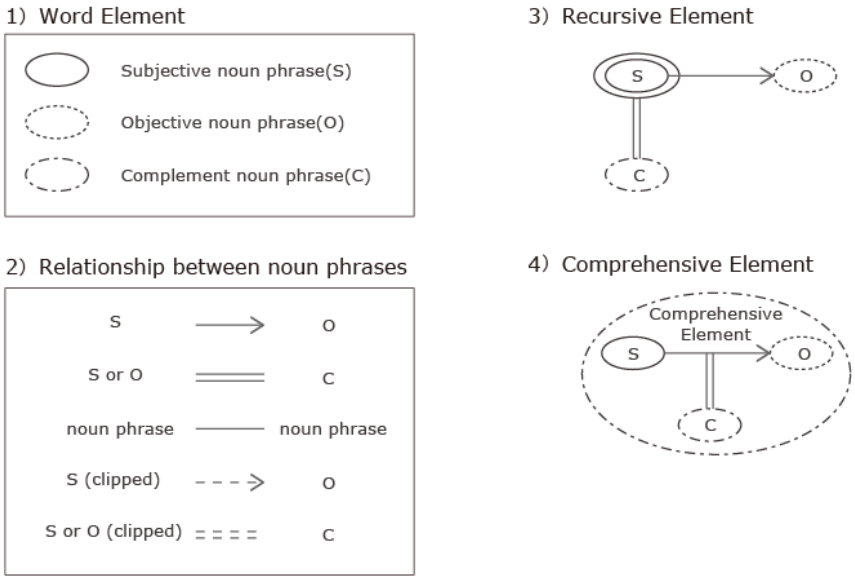


Fig.1 Rules for Mapping

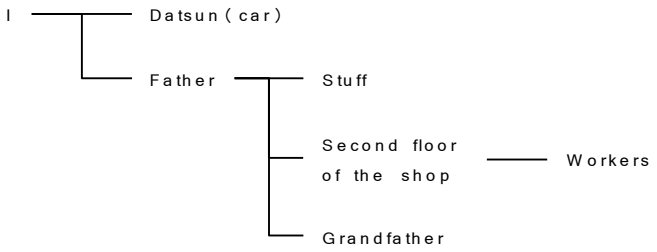


Fig.3 Recursive Elements connected to 'I'

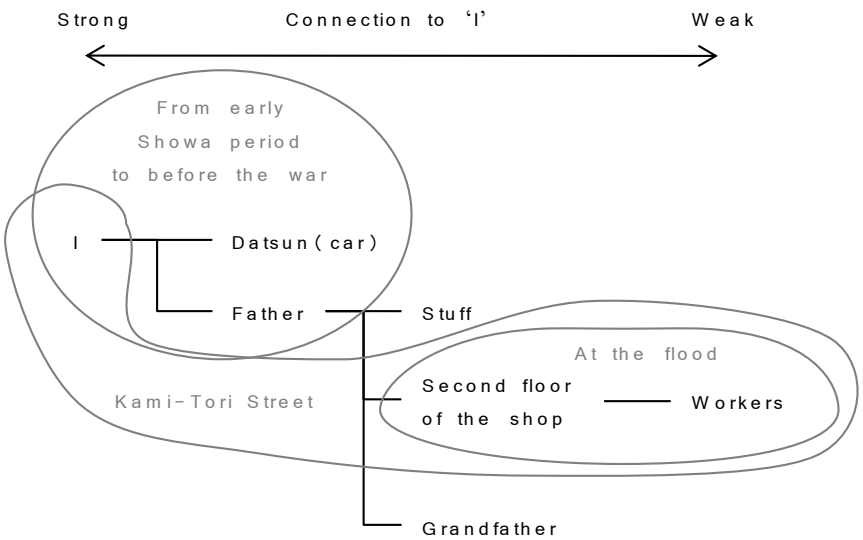


Fig.4 a recursive and comprehensive elements in a person's life history

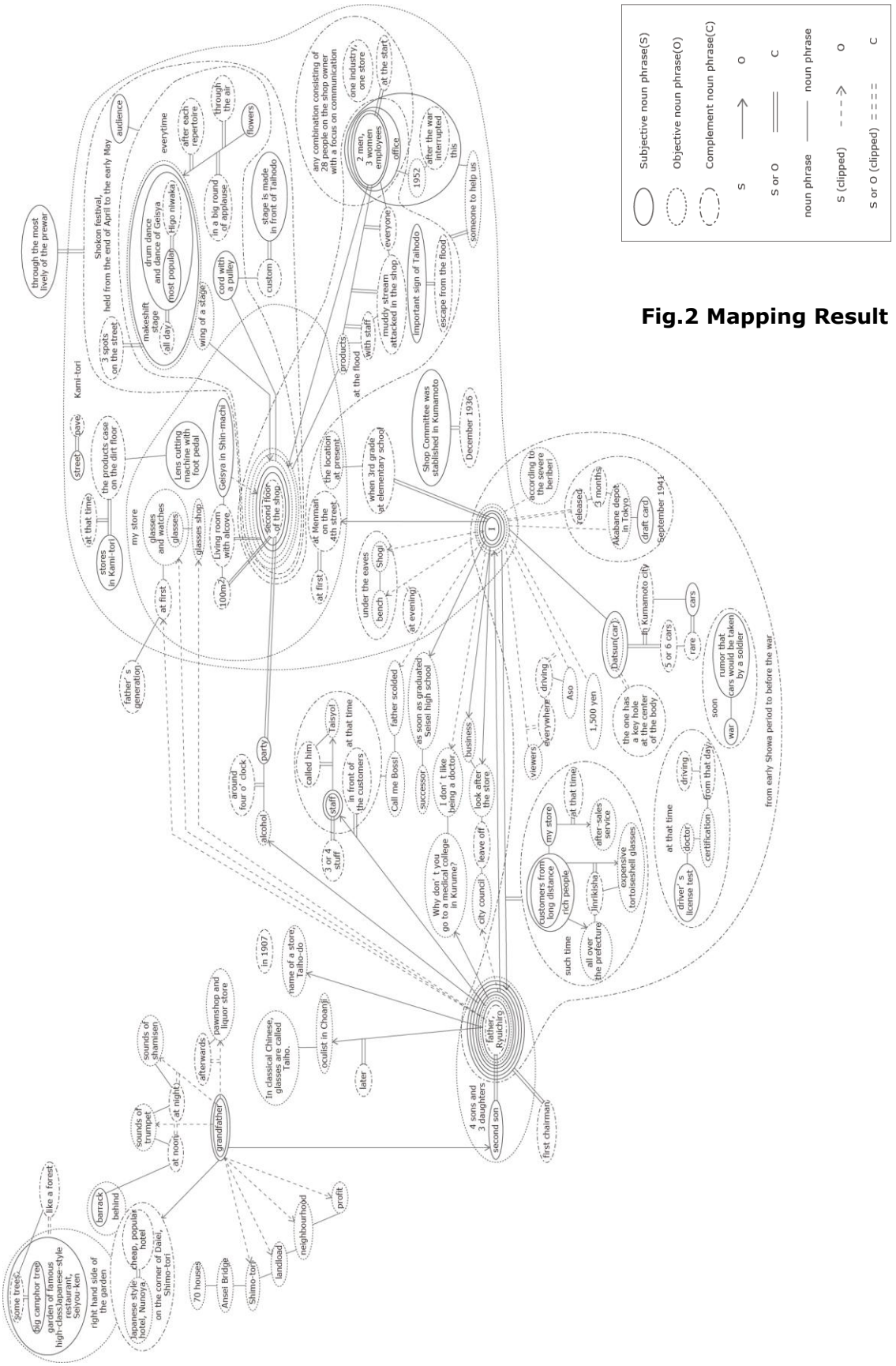


Fig.2 Mapping Result

2nd International Engineering Symposium - IES 2012
(KU-MU-NITK-HCMCUT Joint Symposium) March 5-7, 2012, Kumamoto University, Japan

The Relevance of Physical Configuration to Mental Map of Town

Deepika Shetty [1] **B. S. Bhooshan [2]**

1 *Manipal School of Architecture and Planning, Manipal University, Manipal, Karnataka 576104, India. e-mail:deepika.jeevan@gmail.com*
2 *B Shashi Bhooshan and Associates, Mysore and Proffesor, BMS college of Engineering, Bangalore, Karnataka,India. E-mail: shashi.bhooshan@gmail.com*

Abstract: Spatial design has attempted to represent the nature of society and the town is believed to be a representation of the community that inhabits it then mental maps and identity of towns have strong relation with physical configuration of built forms. The aim is to see if the level of connectivity and visual link has an impact on the mental mapping of the town structure by the inhabitant. The paper tries to identify the morphology of Barkur town in terms of spatial syntax in terms of organization principles. This is superimposed with the findings of questionnaire and maps sketched by people to describe the town by the inhabitants. In this way we are trying to identify the grammar of 811 years old town plan of Barkur.

***Keywords**:* mental mapping, vernacular town planning, Barkur town, space syntax

Introduction

Barkur is a small important historic town in South Kannada district of Karnataka. It boasts of many old buildings and streets spanning several centuries between, 1000 and 1900 AD. The people who live there seem to have strong attachment to the place and strong images about its structures and streets and localities. The question is whether this is so because of the mental attachment or because of the physical qualities of the place. How is the meaning read from the city's physical environment, vis-à-vis certain qualities of physical environment or the mental attachment due to longer stay or both? This question is relevant when we deal with traditional and vernacular environment.

Historic significance

The west coast of Indian subcontinent through legend was popularly known as 'Parasurama-ksetra' extending from Gokarna to Cape Comerin reclaimed from the sea some millennia ago. However there is historic evidence of megalithic settlement through archaeological excavations to confirm the existence of Iron Age culture. The identification of 'Olokhoira' (meaning the land of the Alupas) in Greek literature of 2nd cent AD is mentioned, which means that this culture was established before the acquisition of this nomenclature, maybe somewhere in the beginning of Christian era. In 7th and 8th century in Sanskrit work 'Prapan Chahridaya', seven territories of the west coast are mentioned including Alupa. This town was established as the capital for Alupa kingdom in 12th century as per records, though it's existence could be from 8-9th century as per the dating of some ruins. It then took the sovereignty of the Kadambas of Banavasi and total annexation of Vijaynagara Empire. During Vijaynagara rule from 1336 to 1600 AD it was the period of economic prosperity, social harmony and political consolidation. It had also seen a tremendous religious development based on tradition and convention. It is during this time that the physical manifestation of these towns can be dated; however the footprint could have been from the Alupa times.

Further, Barkur witnessed the rule of Keladi Nayaks and Haider. However after the Tipu's invasion at around 17th century

and during the British Empire the status of Barkur went downhill and today it is a small town belonging to three different panchayat. The town had ten extensions called Keris - some being named after the profession of the residents. Each Keri had a tank and number of temples. The dates of the temples vary from 9th to 14th century. [1]

Profile of the town

Barkur town today is a small town centre, with a population of around 7,000, with 1236 females per 1000 males. The literacy level is up to 99% and the total numbers of houses are 1200 of which 4% are Muslims, 22% are Christians and 78% are Hindus. Till today all the communities of the district have their main temple located in this town. Barkur is providing services with respect to education and commercial activities to surrounding 20-30 villages around. Refer Figure 1 for location and map of town.

Literature Review

Urban systems have inherent properties of physical structure and organization of built forms which closely relate to the social and political structure of people in their activities and lifestyle. The design allows certain behavioural patterns to which the people adjust and the people in turn modify their environment to suit their needs. This give and take relationship finally defines an urban form which is an integral part of the society. (*Hillier Bill, Julienne Hanson, 1984),* Perception and cognition is one aspect that has been studied through mental mapping, to understand the relationship between meaning of the space to the people and the physical entity by itself.

In the classification of urban perception Appleyard (1973) has postulated three categories.

Operational perception: when people move in a city using some elements as reference points, in their everyday life to create a working mental structure of the city.

Responsive perception: where some unique or unusual feature creates an impact in the image and generates a response from the user.

Inferential perception- the user evaluates the new data of the city with past experience from parallel situation.

Lynch in 1960 provided the five elements with which the physical element of the city was analysed which were paths, edges, districts, nodes and landmarks. He asked questions centred on passive mode of perception examining the people's reaction to contrasting environments rather than looking at more active mode where people imposed meaning upon their urban environment (*Yadav C.S.*1987). Lee (1965), Carr and Schissler (1969), Downs (1970), Golledge, Briggs and Demko (1969), Orleans (1973), Golledge and Zannaras (1973) and Ladd (1970) have further investigated the visible components of the city image and postulated that the mental maps may be viewed as an essential component of human adoption and use of a particular environment. To understand cognition where the person acquires, processes, codes, stores, recalls and decodes information of the environment to assign meanings, could be derived through from the mental image of the cognitive map or construct. The popular method of sketch maps is biased towards the sketching ability of the person as well as graphic aptitude of the individual. Hence along with sketch maps, the method of verbal way finding and photo and association and links are techniques to counter balance these biases.

Mental Mapping

A questionnaire with three parts was used. First part was about respondent's background. The second part consisted of photographic recognition of the places and buildings and some landscape features and discussion about them. The third part was to draw map of the town as the remember it. In this way the mental maps were deduced. 30 people were interviewed the profile of this is in figure 2.

Figure 3 shows references of key landmarks in maps drawn. It is noted that the streets drawn in the cross axis were mostly straight but the turn at

[1] Shetty, B. Vasanth, '**Barakuru (a metropolitan city of antiquity) Its political and cultural history'**, 1984, unpublished doctorate thesis under Mysore University

Panchalingeshwara was drawn by 90% of the people and the roads ended abruptly at the temples at Bennekudra, Mudukere and Choulikere as ends or at the waterfront though the river was not drawn by most. The district mostly followed the panchayat nomenclature of Kacchur, Hanehalli, Hosala, as used in present official documents but few old nomenclature from history like ratha beedi, Mudukere have also survived.

In the questionnaire when asked about daily routine, most liked places, places visitied by visitors, things that should change and the things that should not change. The reponse was as shown in Figure 4.The places which are most used were the cross roads also where they emphasized that they do not like the condition it is in and hence would like to improve. The most identified elements were main junction 1 Kalchapra, 2 car street shops along the old street and the main temple of the town- 3 Panchalingeshwara, then the bigger temple which had been renovated recently like 4 Bennekudra, old big temples like 5 Choulikere and 6 Mudukere, places of historical significance identified by archaeological survey of India like the 7 Kote, 8 Kathale Basadi and 9 Simhasanagudde. The rest of the places varied from person to person because they were temples belonging to a particular community and were linked to rituals performed by them. The other things referred were the conservation of environment and culture and that the people were the best part of the town.

In photograph identification as shown in figure 5, the most recognized places were front façade of Panchalingeshwara and Kalchapra which was expected. Surprising thing was that 100% recognized the old market building which has not been used for past 5 years and is not along the main road and never mentioned in questionnaire or drawn in the map as one would have expected it to be of relevance to be remembered. This shows that there are certain images of town which are there from its significance of the past which may not be reflected in the references of the present. 90% recognized small elements alongside road. Familiarity with the inside of the structures was reduced to 80% as interior elements and the houses of people along main road. The familiarity of landscape is further reduced to 50% of the river edge where the bridge ends, where the boat arrives and the plantation along the main road. The familiarity is almost 0 when it comes to buildings along the main road down south which is 40-50 years development and with no pedestrian activity.

Social Logic of Space

Space syntax analysis as introduced by Bill hillier and julienne Hanson in their book 'Social logic of space' tries to quantify and distinguish spatial configuration for its affordance[2] to various social activity.

In space syntax first spatial configuration is studied for its potential to embody social ideas then the relation is turned into measures and representation geometry of spatial structure. This allowed statistical comparison of different spatial patterns of different cultures. This developed a one city format which qualified space in quantitative terms the social and cultural content through which it expresses social meanings. This is the core argument of 'social logic of space'. (Hillier Bill, Hanson Julienne, 1984)

There are two formal ideas on which space syntax is built.

First aspect is that space is intrinsic part of human activity where his movement is linear his activity and interaction is in a convex space and his view from a point is in the form of variable shape, often spiky, visual fields called isovist (Benedikt 1979). This defines the way in which people perceive distinct spaces as reference with respect to space geometry.

Second is that space configuration is the interaction between many spaces where parts make up the whole. Configuration allows us to include different ways in which it can be experienced and hence closer to social meanings and consequences.

[2] The affordances of anything ,be it anything material or non-material, are those of its properties that enable it to be used in a particular way by a particular species or an individual member of that species. They also afford meaning and aesthetic appreciation.(Lang Jon, 1987)

Since streets are of great significance for connectivity, coming together and hence movement there is a theory of natural movement (Hillier et all, 1993) which helps us to understand cities as a socially meaningful pattern of integration and segregation.

The first step is to convert the open space into series of convex space which is defined as a polygon with no acute angles. Here the scale is of lesser significance. Also if a single space and multiple nooks and corners it is read as many spaces as it gives privacy and identity to number of activities hence an apparent singular space with undulating boundary may read as multiple space to a person in terms of its capacity to hold activities and identities.

The second aspect is movement; the axial lines drawn in the map are such that the longest straight line is drawn as long as it meets no obstruction. The meaning being that the memory of paths or noting of turns is done when the visibility is cut off. Here the distance is of secondary importance as also seen in mental maps that sometimes road distances are totally misjdged if they are straight and the roads with deep turns are elaborately drawn. Hence geometry takes priority over distance and visual link takes priority over geometry. (Hillier and Iida 2005)

It is to be noted that the physical configuration is facilitator to social behaviour however it is not necessary the society chooses to use all its features in a similar manner hence physical entity gives opportunity but society may choose to give different levels of significance to various spaces as per the need.

As in Figure 7, the convex space index indicates that the physical configuration supports the making of landmarks. However some places due to lack of any activity or landmark building is not referred to as nodes. This shows that the indexes show possibilities which may or may not be associated with meanings by the society. The dead ends are surely not referred as landmarks or nodes and the adjacency of 2 has become a node or landmark due to location of important building like Kathale Basadi.

In the convex space index as in figure 8, it is noted that the high index coincides with the roads most identified by the people including the turns. Though the turn of the road to Choulikere is a main road and it has a sharp turn it is not important in the mental maps and the index is also low. The second hierarchy landmarks were mentioned by people as points with errors in distance and description of roads and these lie in the index range of 4-9. This further emphasizes the link of the index with the mental maps.

Figure 9 refers to index of depth. For this Kalchapra is considered the beginning of depth analysis as it the main bus-stop of the town and it is also the centre of the town as part of the main crossroads from ancient times. The main landmarks lie within the depth of 5, whereas the second level landmarks lie in the depth of 6-10. The town is pedestrian friendly as most of the town is readable within the depth of 10 which means it is easy to remember the key features and location of the places. The only place which has high depth value is at the south west end which is reclaimed area and a new development and also there is no mention of this place in the mental maps or people in their daily routine.

Conclusion

In terms of familiarity of key features it is noted that age group wise 18-22 is distinctly different in terms of religious aspects and emotional attachment of temples in their daily routine. However the other age groups show similar preferences in terms of places identified and aspirations of the town.

There is a difference because of familiarity in terms of how many years the people have stayed in Barkur.

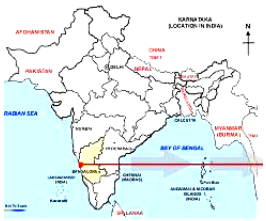
It is to be noted that age and community did not make a difference in identifying the elements of town in terms of photograph or questionnaire. Mental maps also did not show variance in terms of identification of elements in terms of age and community. What made a difference is the familiarity of the place in terms of number of years that the people visited the town. People who have been there for more than 10years of all age groups identified most of the elements of the town be it age groups of 20 or 80. The community

temples in the interior were mostly identified by residents of all age groups.

From the above observations it is noted that number of years in the town and places of daily routine affects the image of the town. Hence removing facilities of new generation from old parts of town or tendency not to upgrade facilities as per present needs may disassociate the future generation from the old town and structures. Also the physical elements of the town by the road small or big become part of the memory of the residents and changing them must be done sensitively. Hence a balanced up gradation of the old town and some new developments may make the town relevant for years to come at the same time develops distinct identity for the town.

References

1. Hillier, B. (2005) *The art of place and the science of space.* World Architecture, 185 . pp. 96-102. ISSN 09569758
2. Hillier, B. (2007) *Space is the machine: a configurational theory of architecture.* Space Syntax, London, UK. ISBN 9780955622403
3. Hillier Bill, Julienne Hanson,(1984) *'The Social Logic of Space'*, , Cambridge University Press.
4. Hillier, B. and Vaughan, L. (2007) *The city as one thing.* Progress in Planning, 67 (3). pp. 205-230. ISSN 03059006
5. Kim, Young Ook and Penn, Alan (2004) *Linking the spatial syntax of cognitive maps to the spatial syntax of the environment.* Environment and Behavior, 36 (4). pp. 483-504. ISSN 00139165
6. Naser Jack L, (1998), *'The evaluative image of the city',* Sage publications.
7. Shetty, B. Vasanth,(1984) *'Barakuru (a metropolitan city of antiquity) Its political and cultural history'*, , unpublished doctorate thesis under Mysore University
8. *Yadav C.S.*(ed.), (1987)' *Perspectives in Urban Geography- Volume Ten,* Morphology of Towns', Concept publishing company, Delhi, ISBN- 81-7022-31-7



A. Barkur (13°24'N 74°45'E)



B.

Fig1: A. Location of Barkur town In India
B.Map of Barkur

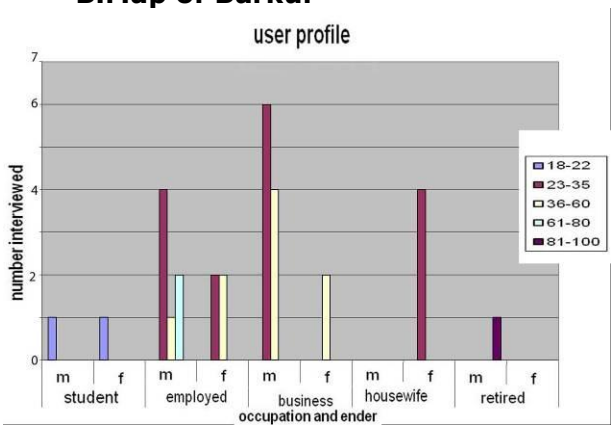


Fig2: profile of people interviewed

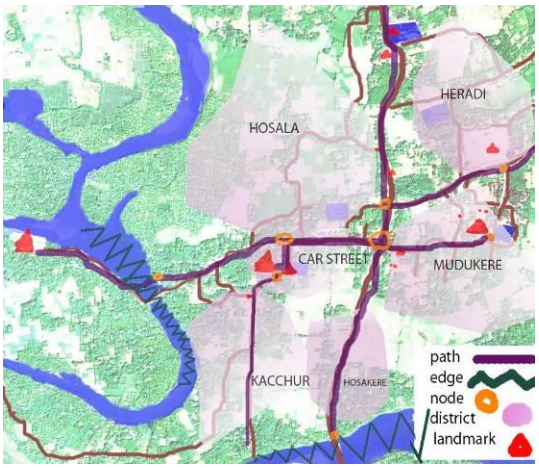


Fig3: Five elements of Lynch

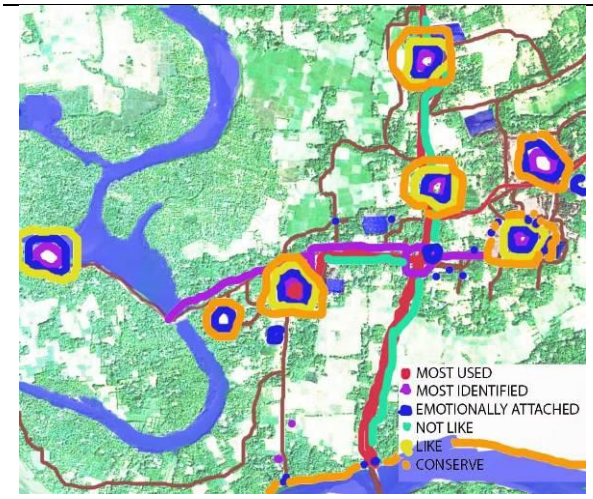


Figure 4: response of people

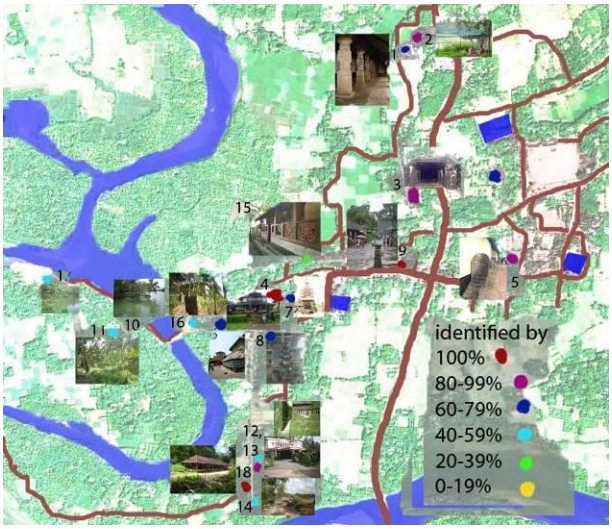
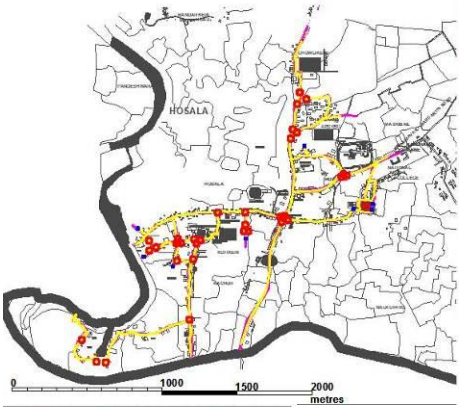


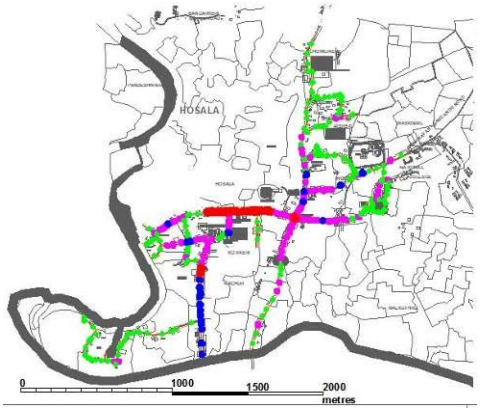
Fig 5: reponse to photoidentification



convex space adjacency index where the index indicates number of convex space it is directly linked to.
this index indicates the level of common areas of meeting is possible which develops a hierachy in spaces for various activity within the same area.

index 3- 5
index 2
index 1

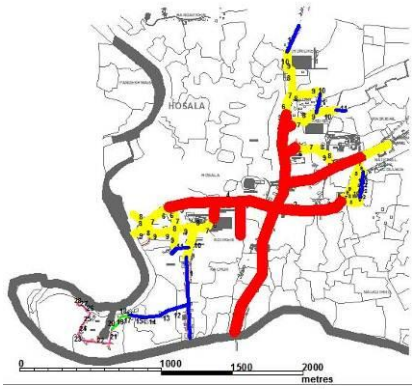
Fig7: Convex Space Adjacency Index



index from 20 and above
index 14-20
index 7-13
index 1-6

axial space index
considering the convex spaces from an axial point of view.
Each space in the system will be axially linked to a certain number of other convex spaces, perhaps in several different directions. The total number of these spaces is the axial space index of a space.

Fig8:Axial space index for connectivity



index of depth from the other villages.
this indicates the accessibility of the space from the outside hence the level of pulicness and privacy is indicated in terms of connectivity.

index 1-5
index 6-10
index 11-15
index 16-20
index 21- 30

Fig 9: Index of Depth for the town

2nd International Engineering Symposium - IES 2012
(KU-MU-NITK-HCMCUT Joint Symposium) March 5-7, 2012, Kumamoto University, Japan

Application of Digital Documentation Techniques for Conservation of a Buddhist Stupa through Virtual Reconstruction

Kailash Rao M. [1] Srikumar M. Menon [2]

1 *Manipal School of Architecture & Planning, Manipal University, Manipal – 576 104, INDIA.E-Mail : kailashrao69@gmail.com*
2 *Manipal School of Architecture & Planning, Manipal University, Manipal – 576 104, INDIA.E-Mail : srikumar.menon@gmail.com*

Abstract: In recent times, much advancement has taken place in digital reconstruction in architectural conservation and archaeology. The application of these techniques opened up new insights in understanding the intricacies involved in the field of heritage conservation. This paper discusses various challenges posed in the restoration of a rare 3rd century BC Buddhist "Stupa" at Sannati, Kanaganahalli Village, India unearthed by Archaeological Survey of India. The author has been involved in documentation of the monument and preparation of Heritage Conservation Plan and presents the different techniques of observation, data recording, condition assessment and digital reconstruction of the monument to ascertain the original form of the structure which is at present in a ruined and scattered condition. The paper throws light on the techniques of photogrammetric documentation, long range and short range laser scanning techniques and manual measurement techniques exclusively devised for this kind of situations. Also the paper compares the pros and cons of these techniques and elaborates on their applications in different contexts.

Keywords*: Buddhist Heritage, Heritage Conservation, Digital Documentation, Virtual Reconstruction, Photogrammetry.*

Introduction about Sannati stupa

Sannati, which is a relatively lesser known small village to even the well-informed common man, is a very important discovery for archaeology, art history and by and large to the Buddhist World from the excavations under taken by Archaeological Survey of India during 1998 – 2002 (Figure 1). There is no exaggeration in describing it as the rarest of rare gems in terms of missing link in completing the understanding of Buddhist heritage of the period.

The stupa built in various stages of time originally during 3rd century AD by the great Emperor Asoka and subsequently enlarged by patronage of various successors and patrons is a fine architectural marvel done in limestone. The stupa has a drum portion with lower and upper portions separated by a small *medhi* (circumambulatory path) totally measuring upto a height of the present ruins of 4m height with the limestone cladding of lower drum panels being roughly square in shape measuring 1.40m X 1.25m and four *ayaka* platforms in the cardinal directions. The *ayaka* platforms are adorned with a highly intricate relief-carved limestone panels depicting the various important Buddhist symbols, mythical representations of the great *Muchalinda* N*aga* (Figure 2) *yakshi sree*, *vajrasana* and many important iconographic representations of early Buddhist period of *theravada* or *hinayana* Buddhism.

Challenges in documentation of Sannati Stupa

The great stupa at Sannati has been covered under debris for nearly fourteen centuries and was found accidentally

during an archaeological excavation. There was continuous agricultural practice on this mound for centuries before excavation. The possible cause of dilapidation according to the field archaeologists is due to a massive earthquake that happened sometime in 6th century AD.
One can imagine the state of ruined condition of various parts of stupa from the photographs (Figure 3a 3b)and enormous challenges that it poses in documenting the stupa in "as – is" condition before any conservation efforts are made. After thorough investigations of the site conditions and initial assessment of the all the components of stupa, it has been decided to engage different methods of documentations have to be adapted for different applications. Following documentation techniques were adopted:

1. Manual measuring and recording systems
2. Photogrammetric techniques
3. Long range laser scanning techniques
4. White light scanning techniques

Main applications that were envisaged were assessment of possible full extent of stupa in its original condition, preparation of complete inventory of the material that is available at site as of today, condition of the components, mending techniques of broken members of stupa, preservation and conservation of the stupa. Apart from this, the efforts to understand the historic significance in terms of architecture of Buddhist heritage from 3rd century BC as well as iconographic, epigraphic, philosophical and spiritual aspects of the site were considered.

Manual measuring and recording system

A simple numbering system was developed dividing the entire site into four quadrants (figure 4) and each quadrant into clusters as shown in Figure 5. A detailed stone-by-stone inventory has been recorded with tabulation of physical measurements, description of the status, condition assessment and detailed photographs.

Photogrammetric data

A photo-based scanning and re-creation of the objects for detailed capturing of three dimensional data was employed. Parallel photographs were taken from specified distances and angles with calibrated cameras as shown in Figure 6 using targets of specified sizes and location for this purpose. These photographs were processed using computer-aided programs to generate a point-cloud data (Figure 7a), high-polygonal meshes were generated and superimposing of the photographic data (Figure 7b and 7c) was done to get the three dimensional model of the sculptural object (Figure 8).

Application of Photogrammetric data

The data acquired from the photogrammetric techniques is used for assessment of the exact size and quantity and primarily used to virtual assembling of the various scattered parts in corroboration with archaeological, iconographical, epigraphical and circumstantial information to re-assemble in original condition.

Long range laser scanning

The entire site measuring approximately 90m 100m size to using a Faro long range (60m range) scanner with 27 multiple station-points and finally integrated to obtain the point-cloud data to an accuracy of 2mm (Figure 9).

This enormous point-cloud data generated has been used to prepare the overall master plan for numbering and sliced up to generate information to micro-level (Figure 10, 11) to ascertain the geometry, structural details and overall condition-assessment of the stupa (Figure 12).

Applications of long range scan data

The reduced data has been very useful to obtain very great detail of dimensional information and using different software, the information has been converted into dense mesh. This information has been stitched together using digital sculpting software to ascertain the missing links to arrive at possible original state of the

sculpture. As the data available had no textures the photographs after being rectified for perspective distortion from photogrammetric data has been superimposed to get more realistic appeal.

Short range laser scanning for detailed recording

For further detailed studies of micro level information measuring 50 microns and below, a white light scanner was used. Due to enormity of the information generated, the objects were mapped using multiple scans and the data has been compiled to get very detailed information to achieve detailed dense meshes (Figure 13).

Applications of white light scan data for robotic milling

The data of short range white light scans is converted to machine program for obtaining various tool paths (Figure 14, 15) for different milling bits and using a seven-axis robotic arm milling machine, the data has been used to replicate the precious sculptural details using limestone of similar composition to the original construction material used in the ancient stupa (Figure 16).

Database preparation

The data procured using traditional manual survey techniques, photogrammetric techniques and laser scans have been compiled to prepare a data base for various applications like numbering of the artefacts, details of various components of the structure, condition-assessment of the members of structure, virtual reconstruction of the structure and reproduction of certain important sculptural members of the monument.

Conclusions

The following conclusions are deduced from this study:

- The site has been thoroughly investigated and a detailed database of the existing artifacts, structural members and ancillary members of the structure are recorded.
- A comparative compilation of the various techniques of documentations and their relative merits and demerits has been obtained.
- After studying the pros and cons of each technique, the results have been applied for appropriate remedial measures.

Acknowledgements

We wish to thank the Archaeological Survey of India for the opportunity to work on this rare and important site. We wish to specially acknowledge the enthusiastic support and guidance of Dr. V. Halakatti, Superintending Archaeologist, ASI (Dharwad Circle). We are indebted to Mr. Dakshat Kidiyoor and Ms. Sneha Bakshi for valuable fieldwork, data collection and compilation. The photogrammetric images were prepared by Easwar, 3-D Scan Solutions. Mr. Harish Pawaskar of Harish Designs carried out the laser scanning work. M/s GTP, Salem carried out the milling work. We thank the ASI staff at Sannati for their hospitality and the students of MIT, MSRIT, Polytechnic College of Raichur and BVB, Hubli for on-site assistance. We thank our colleagues and well-wishers at MSAP, Manipal for discussions.

References

[1] Alshawabkeh, Y. and Haala, N. (2004), INTEGRATION OF DIGITAL PHOTOGRAMMETRY AND LASER SCANNING FOR HERITAGE DOCUMENTATION The International Archives of the Photogrammetry, Remote Sensing and Spatial Information Sciences, Vol. XXXV, Issue 5, pp. 424-429.

[2] Grussenmeyer, P., Landes, T., Voegtle, T. and Ringle K. (2008), COMPARISON METHODS OF TERRESTRIAL LASER SCANNING, PHOTOGRAMMETRY AND TACHEOMETRY DATA FOR RECORDING OF CULTURAL HERITAGE BUILDINGS, The International Archives of the Photogrammetry, Remote Sensing and Spatial Information Sciences, Vol. XXVII, Part B5, pp. 213-218.



Figure 1: Excavation site of the great adholoka maha chaitya at Kanaganahalli



Figure 2: The great Muchilinda Naga as relief sculpture cladded to western ayaka platform

a



b



Figure 3, a, b: Present status of stupa site with its scattered architectural members

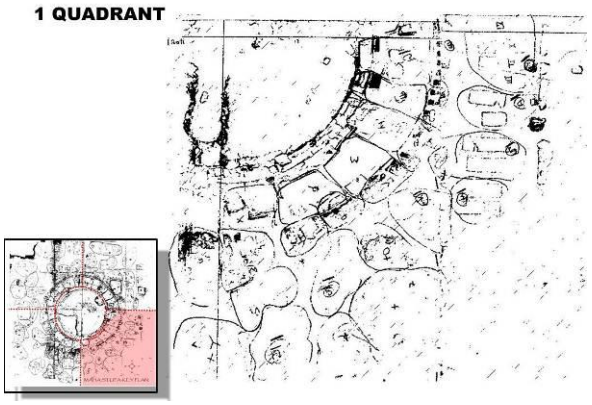


Figure 4: Showing key map of Stupa with one quadrant enlarged

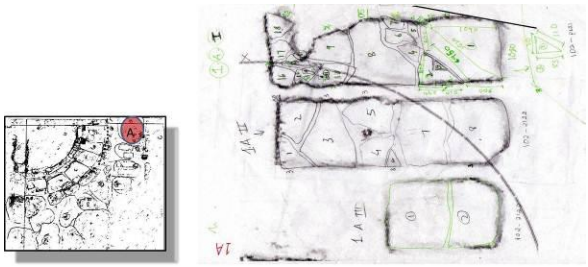


Figure 5: Key map of one quadrant and one cluster enlarged

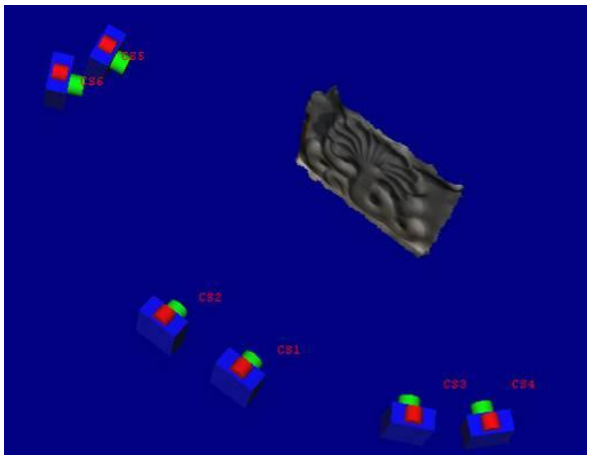
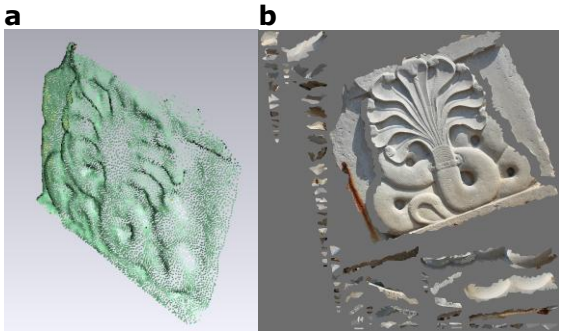


Figure 6: Technique for photogrammetric data recording

a **b**



c

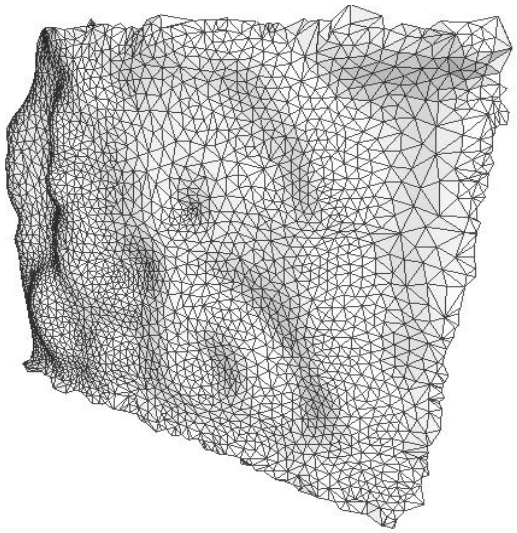


Figure 7: a: Point-cloud data generated for one of the panels b: TIFF image generated from (a) c: Mesh generated from (a)

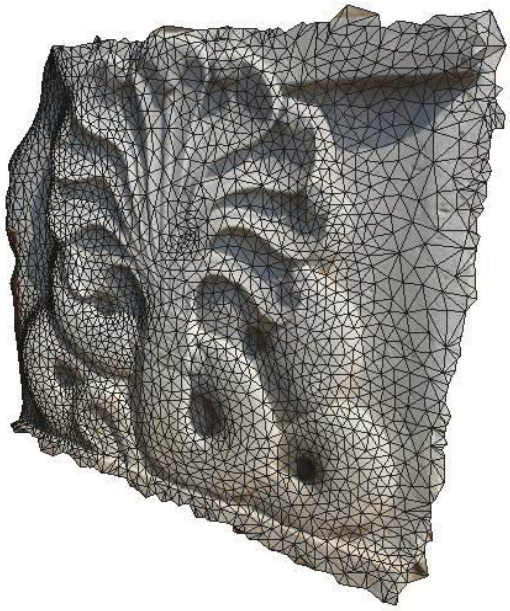


Figure 8: Superimposing of photographic information onto the mesh

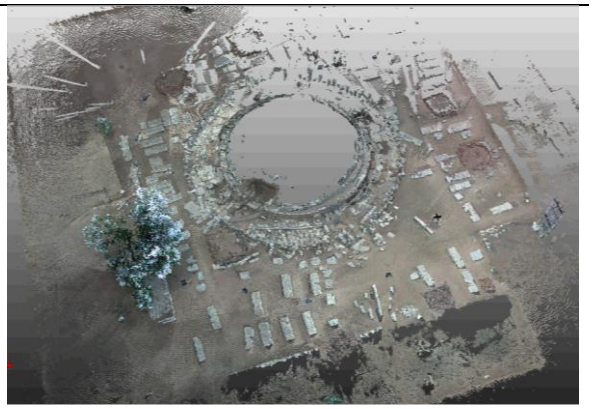


Figure 9: Image of point-cloud data obtained from long-range laser scanning



Figure 10: Sliced-up point-cloud information for a panel

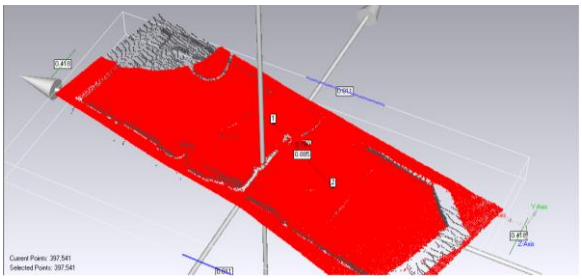


Figure 11: Point-cloud data used to ascertain dimensional information in x-, y- and z-axes



Figure 12: Photographic information superimposed for enriched visual representation



Figure 13: Detailed dense mesh of panel depicting Emperor Asoka

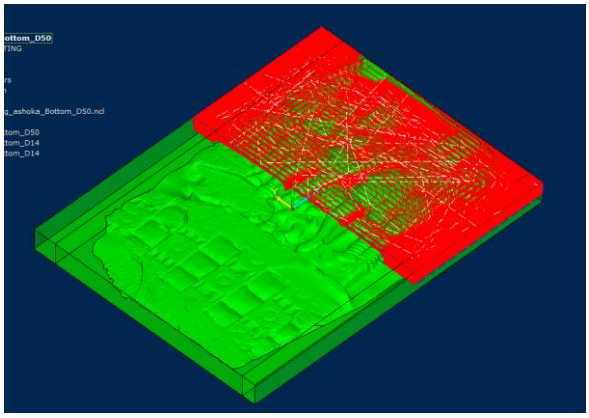


Figure 14: Machine tool-path for milling using 50mm drill bit for initial rough cut

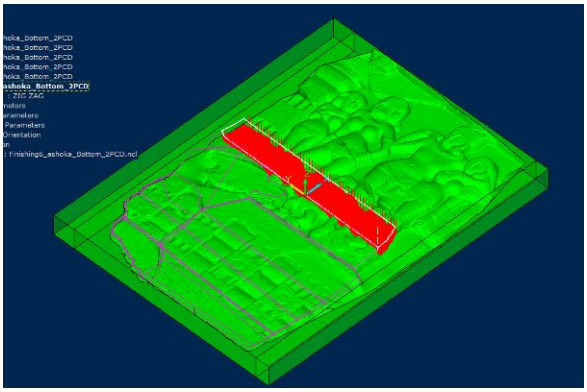


Figure 15: Machine tool-path for milling using 1mm drill bit for fine cut



Figure 16: Panel replica produced by milling

2nd International Engineering Symposium - IES 2012
(KU-MU-NITK-HCMCUT Joint Symposium) March 5-7, 2012, Kumamoto University, Japan

Bio Aesthetic Aspects of Planning for Residential Gardens in Mysore City, Karnataka, India

Padmashree Urs M.K

Manipal School of Architecture and Planning, Manipal University, Manipal–576104, Karnataka, INDIA. Email:urs_padma@yahoo.com, urs.padma@manipal.edu.

Abstract: Bio-Aesthetic planning is as a conscious planning of the Flora and Fauna with the object of beautifying the Habitat. Residential gardens form a significant component of urban green space in many cities and consequently have the potential to play a major role in the conservation of urban biodiversity. Residential gardens within developments can be tools to help repair damage done to the native ecosystem. This paper highlights the vital role played by residential gardens and thereby the significance of planning and maintaining the Bio aesthetic aspects. It aims to assess the present state of Residential gardens in the city and evaluate its potential for sustainable development. The purpose of this study is to explore the nature of the relationship between an individual and his or her garden. Bio-aesthetic planning can be attempted in new residential layouts that are developing in the outskirts of old towns or in new cities.

Keywords*: Bio Aesthetic Planning, Residential gardens, Conservation*, *Urban biodiversity, Sustainable development, Environment.*

Introduction

Greenery is important for a city to be wholesome and attractive. One of the undesirable aspects of rapid urbanization is the tendency for cities to look alike a case of drab uniformity. Many urban environs, although functional, are harsh concrete jungles with uninviting public spaces. In recent years people have become for removed from nature, with technology and science keeping him indoors most of the time. Urban residents desire trees, parks and forests for a variety of reasons. As human become more urban in his ways of living, an acute feeling of having become detached from nature sets in; and a desire to remain close to nature increases. This desire will manifest itself in the form of a widespread demand for urban greenery. Residential gardens are a small endeavor by people to stay connected with nature. They may feature specialized gardens, for exhibiting one particular type of plant, or special features, such as rockery or water features. They are also used for growing herbs and vegetables and are thus an important element of sustainability. Residential gardens are a combination of form, function, balance, individual taste, practicalities and lifestyle. An urban garden can be a wonderful oasis, a great place to relax and a source of bountiful homegrown produce.

Historical Background

Human has always tried to retain or create spaces that bring nature close to him. All ancient civilizations had huge gardens. Man's fascination for gardens dates back to the time of Adam and Eve and the Garden of Eden. The fascination continues and to this day, a small garden by one's house is the dream of many homeowners. A chance to bring in some nature is what a garden provides to a city dweller.Gardens are a small attempt by people to reconnect with nature's bounties. City developers have recognized the need for gardens in cities and now plan for them. Gardens are cultivated at all levels right from the small house to at local administration.

The Functions of Bio-aesthetics Planning

Green spaces are the lungs of cities. Gardens provide a pleasant sight for the eyes, sweet smelling flowers and fresh plants, fruits tickle our taste buds, birds that nest in their trees provide pleasant sounds for our ears and the fresh breeze blowing through, leaves a pleasant feeling on our skins. Beautiful roads and well planned parks, residential gardens and squares bring beauty to urban areas.

Trees and plants can be termed as ornaments on the body of earth which brings joy to one's mind, it can be even said that the colour given to the buildings will fade but the natural colour of nature will change according to the seasons which please our minds and bodies.

A residential or private domestic garden is the most common form of garden and is in the neighbourhood of a residence, such as the 'front or back garden'. A garden typically is located on the land within, surrounding, or adjacent to a residence. The art and craft of growing plants takes place in or around one's residence, in a space referred to as the setback. In urban lifestyle, small gardens are very popular, and may be located in the setbacks of a house, on a roof, in an atrium, courtyard, on a balcony, or as vertical garden, with a little bit of innovative landscape designing. (Fig1,2,3).Residential gardens are typically designed on a humanly modest scale, as they are most often intended for private use. The garden is designed to carry the sense of the city's urban fabric into the site.

Gardening is done on a smaller scale, primarily for pleasure, to enhance the aesthetic of dwellings, a hobby, or for income supplement, and to produce goods for the own family. Ornamental plants are grown for decorative purposes, for their flowers, foliage, or overall appearance; useful plants are grown as vegetables, fruits, herbs, leaf, for their dyes, for medicinal or cosmetic use. Garden designing involves the spatial organization of outdoor areas to meet the human needs and desires keeping in mind the climate, soil, and the air. From the residential gardens to parks, and urban landscapes, all try to integrate the cultural, social, political and environmental needs of humans.

Residential gardens are an asset to Residents. It provides spaces for leisure and passive and active recreation. The residential garden is one of the few places where people can create an environment that reflects their own needs, values and tastes. The artistic tastes of the homeowner can be through designing hardscape by Patios, terraces, seating areas, interconnecting walkways, and rotundas, gazebos are commonly used for both functional and ornamental effect. Good design combines form and function to create a unique garden–tailored to individual desires and specific site.

Courtyards are also an excellent way of bringing the outdoors in. When used for creating landscapes they bring in pleasantness and visual appeal. The small courtyard is an excellent thermal regulator. The heat absorbed by cooler surfaces and the earth beneath the courtyard during the day is re-emitted into the open sky during the night creating a pool of cool night air as this is heavier than the surrounding warm air. Courtyards maximize the use of sunlight hence reducing the electric costs. They add aesthetic to indoor environment.

Background of the Study Area

Mysore is an ancient, historical and beautiful city in India and is also the second largest in Karnataka State. Mysore is located at an altitude of 770 mtrs above MSL. Flanked by the rivers Kaveri and Kabini, The city enjoys a very salubrious climate all through the year, minimum temperature in winter is around 15 degrees Celsius and in summer the maximum temperature is around 35 degrees Celsius. The city combines beauty with diversity and is well known for its uniqueness in terms of architectural monuments, palaces and gardens and spreads across an area of 128.42 km2.

Mysore is, besides a city of long boulevards radiating from a well-defined central axis, with well recessed public buildings balanced on either side, can be a model for any town planner. But over the years due to urbanization and industrialization rapid increase in population has occurred and certain slums in the city's landscape, urban decay in one form or other have been a concern. The difficulties today are those of scale, awareness and economies of change. There is scarcely a harmony among buildings, streets and open spaces. Mysore is slowly deteriorating due to urban expansion, traffic growth and declined concerned for planning. It is better to take appropriate planning measures to conserve the greenery of the city.

The Need for the Study

Bio-aesthetic planning is not a new phenomenon. It existed even in the early decades and can be traced even to the earliest civilizations. However the planning scale was different from what is needed today. The need of this component is to fulfill the three important principles of planning i.e., safety, health and convenience. In the name of development we have simply raised the concrete jungles undermining natural greenery and there is hardly any area, which could compare reasonably with what it was originally.

Bio-aesthetic planning is important to preserve the environmentally and aesthetically sensitive areas and to protect them. The open spaces must be used for parks, residential gardens or other green spaces to determine the character, quality and aesthetic of the urban environment. The green spaces bring nature into cities and allow the citizens to live work and move. This can provide environmental up gradation along with restoration of harmony among nature, men, animals and plants.

With increase in urbanization, distance between city inhabitants and nature is increasing. The residential garden can play an important role in bridging human and nature. When a town or a city is planned, residential layouts are developed, each residence either small or big plot will be with adequate setback all around the building according to local byelaws. There domestic gardens can be designed and developed.

Our changing lifestyles dreadfully need a garden space for many reasons. It is apparent however that the majority of people in urban areas link the idea of a garden with relaxation and being in or creating a pleasant environment: it is probable that being able to look into the garden from a dwelling is as valuable as actually being in it in terms of stress relief. It is also apparent that, although, preferences and perceived benefits varied with age, gender and economic status, all but the smallest of gardens can be linked to a wide range of human benefits, and even the smallest have some value to human well-being. The environment of residential area has a closed relationship with human's living. It is not only a significant place of human activities, but also an important constituent in urban environment. Along with the development of society and economy, the residential landscape is also changing.

There are four ways in which the urban greenery is valuable: aesthetic, economic, functional and environmental.

a) An attractive greenery is aesthetically valuable because it adds beauty or is pleasing to senses. The visual beauty of home and property can be enhanced through creative landscaping. The chirping sounds that a landscape offers, like a breeze rustling the leaves in the trees or the sounds of birds or of water splashing in a fountain, enhance the aesthetic qualities of our home and town environment.

The aroma of flowers or the smell of a freshly mowed lawn and even the taste of fruit from plants that you might have in the landscape are refreshing. The sense of touch also can be an aesthetically valuable feature of the landscape.

b) The well-done urban greenery adds economic value to our home and property. The value of our home can be increased by

as much as 6 to 15 percent as a result of a good landscape. The function of the landscape is to enhance the beauty and therefore the economic value of our house. Thoughtful landscaping can also reduce energy bills by buffering seasonal temperatures. In addition, trees and shrubs can be used to act as buffer, reduce wind speed, making outdoor living area more comfortable.

c) Residential gardens offer a special functional value, too. Well-placed trees, shrubs, turf, and such other construction features increase value and usefulness of the property. A little shade in the right place, a little sun in another, a place for the kids to play, a private patio, pool, or deck - all add to the enjoyment of being outside.

d) The Residential gardens not only have functional worth, but it can enhance the environment, too. Through careful landscaping, temperatures can be buffered in the summer and winter. Glare and wind can be reduced and water can be used more efficiently. In addition, plants can help rid the air of dust and other pollutants. It provides a habitat for various kinds of wildlife.

Town planning and bio-aesthetics planning should go hand in hand. It is a precondition for bio-aesthetic planning. A city without vegetation can be likened to a desert. The younger generation must be educated regarding a new mode of living. We must improve the environment in our towns by introducing modern architecture and landscaping.

The purpose of town planning is to make urban areas look more efficient, healthier and more beautiful. It requires not only spacious well-planned streets designed as a unit but also well-planned roads, residential gardens and parks with planned planting of ornamental trees.

The Aims and Objectives

The aim of the study is to understand how the city looks like when bio-aesthetic aspects of planning are incorporated in residential areas which are important as environmental and cultural values. It also tries to frame some guidelines for proper maintenance and beautification.

The main objectives are:

- to study the growth and development of urban form as related to conservation of greenery in Mysore City;
- to analyze the existing regulations and guidelines concerning residential gardens to improve city aesthetics;
- to weave aesthetic quality into a development,
- to create an awareness about the importance of residential greens and also their continuous maintenance by land owners and
- the planning proposals regarding bio-aesthetic planning of residential greens in Mysore.

Methodology

For the preparation of this thesis, the author proposed to adopt the methodology based on specific objectives. The study is proposed to be carried out in the heritage/garden city of Mysore. The research work is beginning with reviewing the literature on urban green spaces and residential greens. For this, the necessary material will be collected from authorities concerned and also obtained through available documents. The various factors which are affecting bio-aesthetics are sought to be studied through primary survey (illustrations only) i.e. land use data, maintenance of residential gardens , violations of building byelaws and regulation, field visits and visual surveys and also secondary data and information from various sources. The policies and design guidelines proposed in other cities have to be studied and also based on inferences; planning proposals will be prepared for better and aesthetically attractive.

Scope and Limitations

Bio-aesthetics is a component in urban planning amidst several others. The intention of the study is to evolve guidelines to design better urban greenery within a sustainable city and also to establish norms of compatibility of the surrounding area. The study seek to identify the facilities to be provided, utility

improvements in a select group of residential areas to a level suited to encourage use on a local community level. Residential greens can provide wonderful opportunities for all ages to regenerate themselves and to lead full and rewarding lives. The assets children and youth need for healthy development fall into four major domains: physical, intellectual, emotional, and social.

The study will be focused on planning for residential green by protecting and preserving the beauty of the city and retaining its character. The study has been limited to exiting residential gardens in the context of the urban scenario of Mysore city. The study is designed to give planning guidelines for better maintenance and conservation and also to integrate this with its surrounding activities to ensure aesthetic quality of the city.

Present Scenario of Residential Gardens in Mysore

A considerable portion of the 'Royal City' Mysore is constituted by parks and gardens intercepted by many beautiful sylvan avenues. One of the adverse effects of the rapid and relatively unplanned growth of the so-called 'Garden City' is the frequent encroachment on gardens, parks, playgrounds and other organized open spaces and tanks/lakes. This has resulted in the problem of shrinking green areas.

Every aspect of planning and development should be infused with a concern for imaginative and effective use of open spaces and sustaining flora and fauna thereon. Mysore is poised to launch its new Master Plan aimed at beautifying the city. To promote a green environment in a residential area, the first step is to regulate development or building construction activities on the setbacks. The other is to preserve green areas in their existing condition and wherever possible to enrich and diversify them.

Planning and development of Residential Gardens

Residential gardens are a significant Component of our urban landscape. They are a vital part of urban areas as it provides remarkable depth and range of benefits. Each individual may only have a small garden but, together, the amount of green space we look after really adds up– to beautify the cities. We really can make a difference by ensuring that every available space in our front and back garden contains planting.

We need to protect our existing gardens and ensure their provision in urban expansion. In addition we must support those with access to a garden so they can tend it in a way that continues to enhance urban quality of life.

A buffer strip improves and maintains the water quality by providing a filter area to trap sediments and excess nutrients, reduce maintenance time and cost, preserves natural beauty of a setting, screen undesirable views and frames good views and provides erosion control and shoreline stabilization.

Conclusion

The following conclusions are deduced from this study:

- To create awareness about the imperatives of protecting environment and rainwater harvesting by education, training & organizations should safeguard and develop horticultural skills to ensure growth in gardening in urban areas to protect and preserve the beauty of the city.
- To give greater emphasis on protecting and enhancing gardens and green space in our cities for the benefit of the environment and future generations.
- Instead of going in for only landscaping, lawns and decorative plant, they should consciously go in for fruit bearing trees, flowering plants or even kitchen gardens which should be useful that meet the growing demand for food and food-related items including fruits and vegetables.
- A competition is to be organized for exhibiting of flowering and ornamental plants of residential

gardens and to be judged and there should be prizes for the best ones.

- It has suggested that ecological and environmental stability of Mysore should be ensured by increasing the green cover by protecting and preserving the beauty of the city and retaining its character.
- Local Planning Authorities should develop a shared vision with their local communities of residential environments & to see and develop design policies that set out the quality of development that will be expected for the local area.

Acknowledgements
The Kumamoto University, Kumamoto, Japan and Manipal University, Manipal, Karnataka, India, provided support to accomplish this work.

References

[1] Benedict, A. Mark & Edward T. McMahon (2006), "Green Infrastructure: Linking Landscapes and Communities", Island Press.
[2] Brown, D. Robert & Terry J.Gillepsie, (1995) "Micro Climatic Landscape Design", New York.
[3] Futehally, Laeeq (1998),'Gardens', New Delhi, National Book Trust, India.
[4] Gowda, Krishne and Prof. Sridhara M.V. (2000), "Open space and Green areas in Mysore City and Planning Strategies for the 21st century", Shelter, Vol.III July No 1,3 July, New Delhi, India, pp.7-12 & 22.
[5] Greenhalgh and Worpole, (1995), "Urban parks, Open Spaces and Sociability", Centre for Leisure Research at the University of Edinburgh.
[6] Hough, Michael, (1995), "Cities and Natural Process", Routledge, London.
[7] Miller,W. Robert(1997), "Urban forestry: Planning and Managing Urban Green Spaces", Prentice Hall, New Jersey, Inc.
[8] Natu, Abhijit,(2003)"Public Open Space: The Indian perspective", ARCHITECTURE Time, Space and People, May.
[9] Neginhal, S. G. (2006), "Golden Trees, Green Spaces and Urban Forestry".
[10] Prasad Devi A.G., S. Lakshiminarayan and K.S. Jagadish Chandra,(1998), "Urban Forestry for Pollution Control and Bio-aesthetic Planning in Mysore City". In Proc. of Intl. Seminar on Air and Water Pollution on Urban Environment, pp.107-110,
[11] Randhwa M. S. (1965), Flowering Trees, National Book Trust, New Delhi, India.
[11] Sundar, Nandhini (2005), "Make use of those green spaces", Deccan Herald, Mysore Edition, Mysore,India, October 14,
[12] Walker, Chris (2004), "The value of urban Parks", Washington, D.C, U.S.A.
[13] The Hindu (2005), "Mysore's Greenery under threat", Newspaper – The Hindu-Mysore Edition, May 05.
[14] The Times of India, Mysore (2006) "Initiatives for a clean city", News Paper-The Times of India-Mysore Edition, Mysore, India, June 24.







Fig 1,2,3 : Residential gardens

2nd International Engineering Symposium - IES 2012
(KU-MU-NITK-HCMCUT Joint Symposium) March 5-7, 2012, Kumamoto University, Japan

Wood: A natural choice as a green building material – A key to a sustainable future

Roshan S. Shetty

Manipal School of Architecture & Planning, Manipal University, Manipal 576104, India.
Email:rooshan22@yahoo.com, roshan.shetty@manipal.edu

Abstract: Wood's environmentally superior nature makes it the perfect material to use when building green and it is a natural choice when it comes to climate change. Wood's sustainability stems from its renewability, minimal manufacturing energy use, and few environmentally damaging Greenhouse Gases (GHG) and other air-polluting emissions both in manufacturing and over its life cycle. Life Cycle Assessment (LCA) studies show wood is better for the environment than steel or concrete in terms of consumed energy, global warming potential, air and water emissions and solid waste production. Here in this paper an attempt is made to compare the advantages of wood as a green building material over other man made building materials and also how wood use can make a significant and valuable contribution to society's desire for a more sustainable future.

***Keywords**: Wood, Climate change, sustainability, GHG, LCA, green building material*

Introduction

Wood is the only major renewable source for building material possessing substantial positive environmental attributes, having great warmth capacity and requires less energy to manufacture than any other building material. Wood is a historic, classic and durable building material that has leant longevity, aesthetics and a natural flair to buildings for thousands of years, Barbara Horwitz-Bennett and C. C. Sullivan (2008). Its superior nature makes it environmentally perfect material for use when building green.

It is a natural material derived from the living matter having special significance in nature and its environment. The wooden structures have a pleasant atmosphere also. Wood is also a natural choice of building material when it comes to climate change. Wood is one of the oldest raw materials that have been used in constructions from time immemorial to generate energy and as a building material. It is most versatile and adaptable as a building material. The structures built with wood have much better energy balance than the structures made of concrete, glass, steel or aluminium.

Unique properties of wood

Wood offers various advantages such as durability, workability, warmth, beauty, flexibility, strong in relation to weight, high strength to weight ratio, good electrical insulation, low thermal conductance, high shock and acoustic absorption capacity and excellent strength at low temperatures. Wood has high tolerance stress, earthquake movement, strong wind etc. It has an impressive mix of qualities and can be easily bent or moulded to any desired shape and is aesthetically pleasing material. Because of its unique properties, wood becomes a natural choice as a building material.

Wood - a green building material

Wood has many attributes that makes it a green building material and as smart environmental choice. Wood requires considerably less energy to manufacture, transport, construct and maintain than any other building materials. A significant amount of greenhouse gas emissions are avoided by substituting low impact wood for materials such as concrete, steel, plastic etc. which responsible for high amounts of CO_2 emissions.

Wood's sustainability stems from its renewability, minimal manufacturing energy use and few environmentally damaging greenhouse gases and other air polluting emissions both in manufacturing and over its life cycle, APA (2005). Wood is very economical, relatively simple and clean to work as a building material. It is ecologically friendly material and far superior when compared to other raw materials. Wood, in comparison with other building materials such as concrete or steel, has various advantages. The environmental superior nature of wood makes it a perfect material to use when building green.

Wood for sustainable development

As quoted by Brundtland (1987) "Sustainable development is a development pattern which focuses on efficient resource use to meet human needs while preserving the environment so that these needs can be met not only in the present, but also for future generations to come". Sustainability is also about maximizing the resources that are available locally so as not to waste, damage or exhaust them. The longevity of buildings makes it important to use the sustainable construction in order to maximise the efficiency of the building and the quality of life of the building for future generations also. The goal is to lessen the energy required to heat, cool and illuminate buildings. The growing awareness on the environment has made the building professionals find wood as a sustainable building material.

The positive effect of wood on the environment

Earlier, the factors which influenced the selection of the building materials were mostly appropriateness of the material, accessibility, availability, cost and the appearance, but now-a-days, the consumers are concerned about the impact the materials have on the environment when it comes to product selection. Both manufacturing and using wood as an industrial or building material has positive effect on the natural environment compared to other man made building materials. The environment impact of wood construction has been extensively studied by Building Research Establishment (BRE). The BRE have developed standards against which the environmental impacts and responsible sourcing of building materials and components can be assessed and certified. BRE approach heavily weights climate change relative to the other environmental factors measured, which contributes to wood's attractive environmental profile.

Trees take considerable amounts of the greenhouse gas CO_2 from the atmosphere in the course of its life and store it in the form of harmless carbon. Using wood as a building material for construction or other purposes like furniture relocates the storage effect. The studies have shown that 1 metric ton of wood stores roughly 510 kilograms of carbon, corresponding to 1.8 metric tons of CO_2 which would otherwise enhance the GHG effect in the atmosphere. Roughly 36 metric tons of CO_2 are stored in a house, made of wood. Longer the life of the wood product, the longer it holds CO_2. Making one m^3 of lumber releases mere 50 kilograms of carbon as greenhouse gas CO_2, while producing one cubic meter of Aluminium releases 22,000 kilograms (Danzer Group, Life cycle assessment, 2011).

Life Cycle Assessment of wood

Life Cycle Assessment is a process to evaluate the environmental burdens associated with a product, process, or activity by identifying and quantifying energy and materials used and wastes released to the environment; to assess the impact of those energy and materials used and releases to the environment; and to identify and evaluate opportunities to affect environmental improvements. The assessment includes the entire life cycle of the product or the material. It includes process or activity, extracting and processing raw materials; manufacturing, transportation and distribution; use, re-use, maintenance; recycling, and final disposal.

The Athena model explains the life cycle of building products. The cradle-to-gate stages of processing include forest

management and harvesting, transportation and product manufacturing. The environment impact using LCA, wood outperforms concrete, steel and glass in terms of embodied energy during the production, emission of GHGs, release of air pollutants and water pollutants and solid wastes production. The studies conducted by the Canadian Wood Council have shown that relative to the wood design, the steel and concrete designs released more solid wastes, used more resources, required more energy, emitted more GHG and discharged more water pollution refer Fig 1.

Embodied energy of wood

Every building material used in the construction has embodied energy in it, which has an impact on the environment. The embodied energy can be defined as the sum of the energy required to extract, produce, process, manufacture, transport, construct and maintain the materials used in the building applications. The balanced approach to sustainable development is to understand how the embodied energies of the building material have an impact on the environment. Studies have shown that steel conducts heat 400 times faster than wood and the high conductivity of the material causes thermal bridging which leads to increased energy usage for heating and cooling.

According to the Athena model which is developed by Canada's Athena Sustainable Material, wood is a greener choice than steel and concrete construction based on the sustainability attributes refer Table 1.
APA-The Engineered Wood Association has demonstrated that the energy required to produce one ton of wood is much less than that for other materials. Compared to the energy required to produce one ton of wood, it takes: 5 times more energy to produce 1 ton of cement, 14 times more energy to produce 1 ton of glass, 24 times more energy to produce 1 ton of steel & 126 times more energy to produce 1 ton of aluminium (Barbara Horwitz-Bennett, et al, 2008).

Wood has low embodied energy and the use of wood and wood products creates less water and air pollution. The operating and embodied energy assessment results showing the air pollution and water pollution, based on the life cycle assessment are shown in Fig 2 and Fig 3. The embodied energy in construction and maintenance of buildings with different wall materials are shown in the table 2.

Carbon footprint of wood and other building materials

A carbon footprint is a measure of the greenhouse gas emissions associated with an activity, group of activities or a product, Report ECCM (2008). The main reason for calculating a carbon footprint is to decide on how to reduce the climate change impact of a material. The term carbon neutral refers to material with a carbon footprint of zero. Wood products from sustainably harvested forests have a negative carbon footprint meaning that they act as a carbon store. The trees fix CO_2 from the atmosphere by photosynthesis as they grow and is stored as carbon within the organic matter that makes up the tress. Studies have shown that the carbon footprint of buildings can be reduced by increased use of sustainably sourced timber acting as a long term carbon store.

The carbon footprint of a wooden pallet (cradle to gate including product use phase, ECCM 2007) is shown in the Table 3 and Fig 4. The figure shows a breakup of the carbon footprint by activity and the amount of carbon stored in timber greater than emissions associated with harvesting, transportation and manufacturing. The net footprint of the wooden pallet is -28 kgs of CO_2/pallet. The study also has demonstrated that, it is possible to achieve up to 86% reduction in GHG emissions by increasing the amount of timber in buildings. The emissions reductions are achieved as timber is used to replace building materials that have high carbon intensity such as concrete, glass and steel. These materials have high GHG emissions associated with extraction, refining, processing and manufacture.

Materials like plastic, metal and concrete all require a lot of energy during

production phase. All these materials have positive carbon footprints. Wood has a negative footprint because of the carbon dioxide sequestration. The emissions associated with harvesting, transporting and processing of wood products are small related to the total amount of carbon stored in the wood. Comparing the carbon footprints for wood and non-wood products, wood product saves GHG emissions. Fig 5 shows the graph of the cradle to gate carbon footprints for materials used in construction.

The amount of carbon emitted during manufacture of Aluminium, steel and wood is shown in the Table 4. Each m^3 of wood in a building sequesters about 250 – 300 kg of atmospheric carbon which is equivalent to 0.9 – 1 tonne of CO_2. The characteristics of building materials with respect to embodied energy, carbon storage and density are shown in the Table 5.

Wood and climate change

Climate change is one of the most complex issues faced by the society. Earth's climate has been changing drastically. The effects are changes in the temperature, seasonal rainfall and violent storms. The atmosphere has been damaged by greenhouse gases emitted by human actions and the result is global warming.
Materials used in construction have varying amounts of greenhouse gases associated with the extraction, manufacture or processing and delivery. The studies have shown that the production of cement and steel alone account for over 10% of global greenhouse gas emissions annually. As new buildings become more energy efficient, the emissions associated with materials make up a greater proportion of their total climate change impact.

The United Nations Framework Convention on Climate Change – UNFCCC has contributed to the creation of mechanisms for emissions compensation around the globe. Among the sectors which contribute to reducing emissions by 2030, the construction sector is a large GHG contributor, with 30-40% of all global emissions - while the wood sector could give a fast response to an increase in Certified Emissions Reductions - CERs prices. Together they can play a major role on reducing the global climate change acceleration. When addressing the issue of wood framed houses as replacements for traditional cement-iron, there are positive impacts also on the energy and residues sector Zanetti and Casagrande, (2011)

Conclusions

1. The use of wood as a building material can make a significant and valuable contribution to the society's desire for a sustainable future.
2. The society's perception of viewing wood as not a favourable building material has to be changed tending to think with bigger problems in forestry such as deforestation and forest degradation.
3. The national treasure should be protected by Sustainable forest management practices. The practice ensures a plentiful supply of wood and wood products for construction industry and for many other uses also.
4. Wood in buildings has an important role to play with respect to climate change. Planners, developers, architects and builders are to be made aware of the climate change impacts of construction materials and should consider the same in their selection of materials for building projects.
5. The potential benefits of utilising wood products to reduce carbon dioxide emissions should be well recognized by the governmental agencies and individual consumers. The improved understanding needs to be widely communicated.
6. Many people believe that they must save trees and use other materials instead. This misunderstanding is still common. The main objective of the study is that there should be wood promotion programmes to convince the public that using wood is good, infact of great benefit to the environment.

Acknowledgements

I thank Manipal University, Manipal and Kumamoto University, Japan for the support.

References

[1] Barbara Horwitz-Bennett and C. C. Sullivan, Using Wood for Sustainable Design + Construction, Feb 2008.
[2] Building Research Establishment (BRE), www.bre.co.uk, Assessed on 11th December 2011.
[3] Lawson, W. R. et al., 1996, Timber in Building Construction: Ecological Implications Research Paper commissioned by the Timber Development Association (NSW) Limited and FWPRDC.
[4] Report of the World Commission on Environment and Development, United Nations, 1987.
[5]The Edinburgh Centre for Carbon Management (ECCM), Report, February 2008.
[6] Wood: Sustainable Building Solutions, APA – The Engineered Wood Association, September 2005, Assessed on December 2011.
[7] Zanetti, E. A. and Casagrande, E. (2011), Wood from Sustainable sources and the mitigation of Global Climate Change – Case study of social housing in Curitiba, Parana, South of Brazil, An International Conference and Exhibition on the Art and Joy of Wood, 19-22 October 2011, Bangalore, India.
[8]http://www.danzergroup.com/Life-cycle assessment. Assessed on December 2011.
[9]http://www.gdrc.org/uem/lca/lcadefine.htm. Assessed on Dec 2011.
[10] www.cwc.ca, Canadian Wood Council, Sustainable series 1-11, Assessed on Nov 2011.
[11]http://oak.arch.utas.edu.au/environment/env_prop/env_prop.asp, Assessed on Nov 2011.
[12]http://www.palletcarboncalculator.org/CarbonFootprintReport10_logo.pdf Assessed on Nov 2011.
[13]http://www.insights.co.nz/Overview.aspx Assessed on Nov 2011.
[14]http://www.tastimber.tas.gov.au, Assessed on December 2011.

Tables and Figures

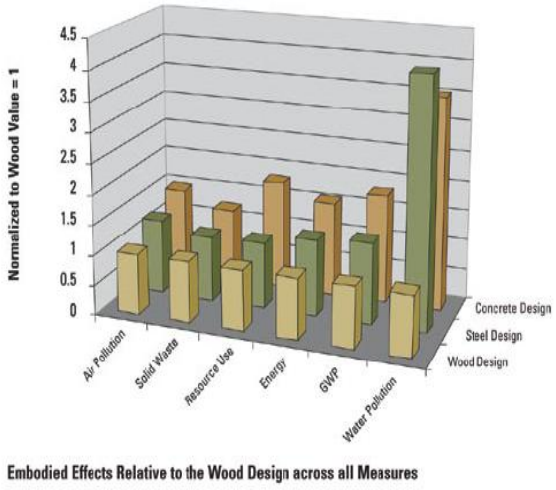


Fig.1 Life Cycle Assessment (LCA) comparison of building materials (Source: Sustainable Building Series 4, Canadian Wood Council)

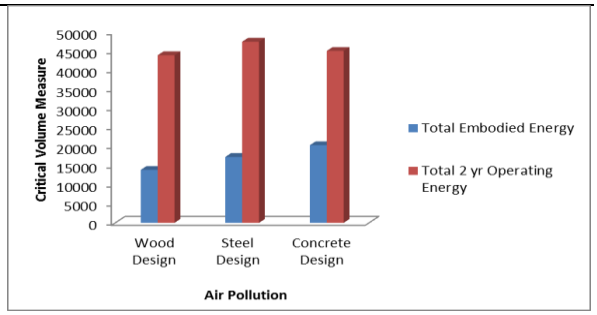


Fig 2 Life Cycle Assessment result for Air Pollution (Source: Sustainable Series 5, Canadian Wood Council)

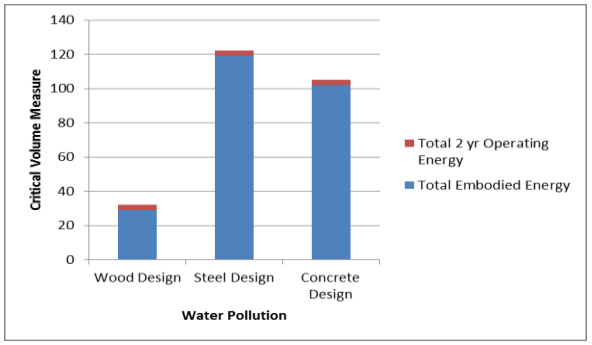


Fig 3 Life Cycle Assessment result for Water Pollution (Source: Sustainable Series 5, Canadian Wood Council)

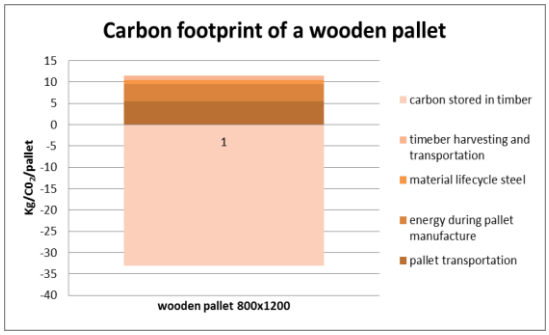


Fig 4 Carbon footprint of wooden pallet (Source: ECCM, 2007)

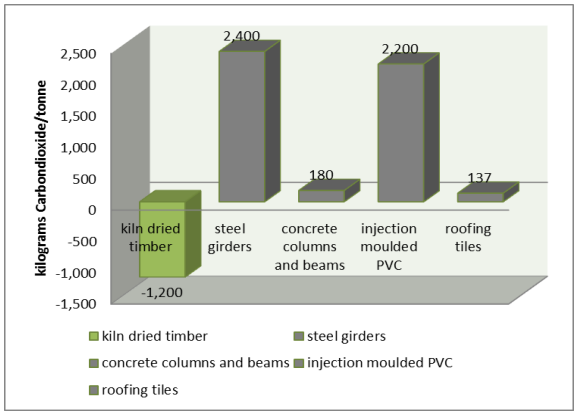


Fig 5 Graph of the cradle to gate carbon footprints for materials used in construction (Source: ECCM, 2007)

Table 1 Comparison of wood, steel and concrete construction (Source: Athena Model, Canada's Athena Sustainable Materials Institute)

Sustainability attribute	Wood	Steel	Concrete
Total energy use	Lowest	140% more	70% more
Greenhouse gases	Lowest	45% more	81% more
Air pollution	Lowest	42% more	67% more
Water pollution	Lowest	1900% more	90% more
Solid waste	Lowest	36% more	96% more
Ecological resource waste	Lowest	16% more	97% more

Table 2 Embodied energy of different wall materials (Source: Lawson et al. 1996)

Type of Construction	Energy per unit area of assembly (MJ/m^2)	Energy used to complete construction (MJ)	Energy used in maintenance over 40 years (MJ)
Timber frame, timber clad, painted	188	31020	24750
Timber frame, brick veneer, unpainted	561	92565	0
Double brick, unpainted	860	141900	0
Autoclaved aerated concrete, painted	464	76560	24750
Steel frame, fibre cement clad, painted	460	75900	24750

Table 3 Cradle to gate Carbon Footprint for materials used in construction (Source: ECCM report, 2007)

Material	$KgCO_2$/tonne	Source	Year
Kiln dried timber	-1,200	Bldg. Research Est.	1999
Steel girders	2,400	EC Technical Steel Research (BRE method)	2002
Concrete columns & beams	180	ECCM (Bldg. Info. Foundation, Finland)	2004
Injection moulded PVC	2,200	The Association of Plastics Manufacturers, Europe	2005
Roofing tiles	137	Bldg. Information Foundation, Finland	2004

Table 4 Amount of carbon emitted during production (Source: Forestry Insights)

Material	Carbon Emitted Kg/m3
Aluminium	6325
Steel	8117
Wood	-228

Table 5 Characteristics of major building materials (Source: CSAW, Tasmanian timber)

Material	Embodied energy $(mj/m^3)^1$	Carbon stored $(kg/m^3)^2$	Density $(Kg/m^3)^1$
Softwood	880	242	550
Hardwood	1550	308	700
Concrete	3180	0	2300
Steel	251200	0	7850
Aluminium	515700	0	2740

2nd International Engineering Symposium - IES 2012
(KU-MU-NITK-HCMCUT Joint Symposium) March 5-7, 2012, Kumamoto University, Japan

Gated Communities in India – An Overview

Sanghamitra Roy [1]

1 Manipal School of Architecture and Planning, Manipal University, Manipal 576104, India. e-mail:sanghamitra402@gmail.com

Abstract: The megacities of India are experiencing rise in development of gated communities. Increased income levels are prompting people to live in gated communities to ensure safety, access to urban services and quality living. This study attempts to understand various aspects of such developments and their impacts on urban areas. These are inward-looking low-density communities comprising of apartments or villas or both occupying on an average 25 acres of land for 550 residential units. Scale of development is the key factor that contributes to segregation of communities, privatization of spaces, and spatial incompatibility. It is advocated to define the physical extents of a gated community after fair understanding of the activity patterns in residential precincts of urban areas.

***Keywords**: gated communities, urban development, India*

Introduction

Urban areas of India today are facing population growth and urbanization at an unprecedented scale. India's urban population is projected to grow to about 473 million by 2021 and 820 million by 2051 as against 285 million in 2001. Every year India is adding six to seven million people to its urban areas. The fundamental question then is how to accommodate such growth in a sustainable manner. In recent times, urban areas of India particularly the megacities are experiencing a sharp rise in development of gated communities. About 40% of the gated communities studied were built in the last decade and the remaining 60% are due to be completed by this decade. Most of the gated communities are large scale developments and cater to a particular section of the population.

This study attempts to understand various aspects of such developments and their long-term impacts on urban areas and their people. The study is based on a sample of 75 gated communities located in metropolitan areas across India built mostly since 2000, interviews of people residing in such communities and government officials. The samples include projects done by leading builders across India. Data were collected through secondary sources. Since there is no single definition of gated communities, the same in this paper is limited to a group of residential units enclosed by a wall, monitored by a security system, and provided with civic amenities for exclusive use.

What are gated communities?

Gated communities have developed mostly in response to inadequate provision of security and urban services by local authorities. They offer three basic facilities. First, access to communities is restricted and controlled. They have 24-hour security system maintained by security personnel at entry-exit points and other locations within the community. Second, continuous water and power supply is ensured through private backup systems. Third, civic amenities such as clubs, shopping areas, schools, health care facilities, etc., are provided within the complex for exclusive use. Amenities are provided as an added feature and are not accountable for making of gated communities. Clearly, all these come with a heavy price tag and not everyone can afford it.

Target population

It is within the means of only the affluent to provide for their needs when local authorities cannot do so. Per capita income for urban areas in India has increased three-fold during 1990-2008 and is projected to increase four-fold during 2008-2030, McKinsey Global Institute (2010). Executives and professionals from multinational companies and technology sector prefer gated communities not only because of facilities available but also because people residing within are from similar social and economic backgrounds. Professionals returning to India too prefer such communities as life within is more predictable and often at par with living standards abroad. Even young professionals and business classes opt for the same in expectation of higher returns and also for the prestige associated with living in such communities. Some professionals who travel frequently prefer gated communities to ensure security of their property when unoccupied. Many retirees too choose to live in such communities as life inside is comparatively peaceful and hassle-free.

Location

Gated communities are located both within and outside city limits. However, due to want of space and higher land value within the city, they occur mostly in the outskirts and satellite towns. Many a times, such developments are pushed further away to make them affordable to young professionals in the age group of 25-35. Delhi National Capital Region (NCR), Mumbai, Bangalore, and Hyderabad are major destinations. Chennai, Kolkata, Jaipur, Mohali, and Pune are also not far behind. Even some of the lower order cities from all over India such as Indore, Lucknow, Mysore, Shimla, Guwahati, Belgaum, etc., triggered by specific conditions are experiencing such developments. Many non-resident Indians from Mangalore are keen to invest in gated communities for future use. A look into the projects done by five major real estate companies in India indicates that Delhi NCR houses about one third of all gated communities in India.

Residential units

Residential units in a gated community fit into two basic categories – apartments and villas. Smaller communities house exclusively either apartments or villas and larger communities often house both. The communities occupy sites ranging from about seven to 70 acres. Some of the communities are part of proposed townships covering area up to 500 acres. As observed in the samples studied, a typical apartment and a typical villa occupy approximately 250sqm and 650sqm of land area respectively. Types of residential units range from one-bedroom apartments to elaborate villas. Provision of servant's quarter is available from three-bedroom unit onwards. As shown in Table 1, three-bedroom apartments have the largest share of units beyond which the cost of apartments increases considerably. Cost of a unit varies anywhere from 30 lakhs to 4 crores and in cases when it is located in the heart of a metro city it can be as high as 19 crores. Cost depends upon floor area of the unit, its proximity to centre city and the range of amenities provided within the complex.

Issues

Gated communities are large scale developments. In many urban areas they tend to be concentrated in certain locations. For example in Gurgaon, as shown in Fig. 1, many sectors earmarked for residential development specially the ones along State Highway 13 and Southern Periphery Road are witnessing explosion of gated communities. Such large scale developments that too occurring at a fast pace and in huge numbers, often coming up in adjoining parcels, are bound to have considerable impact and far reaching effects on urban areas and society at large. For the residents, gated communities are a solution to their immediate needs and problems and therefore to them merits are substantial. They feel since they have the ability to pay for getting away from urban problems by living in gated communities, they would choose to do so. But for the non-residents, gated communities are entities that raise critical issues regarding

long-term social and spatial impacts on urban areas. Studies on gated communities in both developed and developing nations share these fundamental areas of concern, Blakely & Snyder (1997), Landman K. (2000). Following is an attempt to understand the same with regard to gated communities in India.

Segregation of communities

As noted earlier, security is a basic feature of gated communities. Residents in response to increased crime levels in urban areas attempt to segregate or cordon themselves off by means of a physical barrier so that they can remain safe within the premises. But this segregation does not necessarily make them less susceptible to crime because first, as prior research indicates physical barriers may reduce some opportunist and impulsive crime, but they may not help in reducing serious crimes like rape, assault, and murder which are mostly committed by people known to the victims, Naudé (2004). Second, residents of gated communities are exposed to crime in general as much as any other non-resident once they step out of the cordoned area. While the residents may feel secure for being in a gated community they may or may not be actually so. If security cannot be ensured, the fundamental justification for gating communities falls apart.

Gating communities for security reasons has consequences none the less. First, gating results in sorting people by design as per their social and economic parameters thus segregating particular group of people from others. This causes lack of sufficient activities within a complex which in turn limits the usual vigilance that exists naturally in communities with people from multiple age groups and backgrounds. Jane Jacobs in her classic *The Death and Life of Great American Cities* strongly suggested that a community should have people from all age groups to support wide range of activities throughout the day. Only then can residents identify strangers walking into the community and prevent crime. One may argue that in many of our cities residential segregation based on ethnicity already exists. But such segregations are not demarcated by physical barriers or separation of activities and hence do not come in the way of natural vigilance. Moreover, since these gated communities are walled up, crime committed inside may go unnoticed, Lang (1997). Second, the impact of segregation on the development of children is an emergent area of concern. In one of the most sought after elite gated communities in Bangalore, residents expressed their concerns over the limited association their children are subjected to within the premises. Third, high costs of living in cities have already pushed the low-income and even the middle-income people towards the outskirts of urban areas. As the data indicates, most of the gated communities are located in the outskirts and they trigger further outward displacement of these people. This may create social imbalance in the long run, Kundu (2006). With close to 75% of India's urban population living in low income segments and with urban areas predicted to grow even more in terms of population and employment, inclusive development in the form of new integrated townships rather than discrete gated communities may be desirable. At a time when the effort worldwide is to make zoning more flexible and induce mix of uses and compact development, gating communities is a complete reversal of approach.

Privatization of spaces

Besides security, provision of utilities and amenities are an integral part of gated communities. Smaller communities usually provide a club. Some include daily-need stores too. Larger communities include additional amenities such as health club, shopping facilities and sometimes nursery school, health centre and crèche. Still larger communities provide primary school, better medical facilities, sports facilities, and sometimes even a hotel. Most of the public amenities consume considerable land area and are exclusively for the residents. They are paid for and maintained as well by the residents. This raises an important question - even if the residents are willing to pay for the

amenities, whether they have the right to consume any quantum of land for the same for exclusive use. As in the case of Gurgaon, some sectors are becoming completely privatized as large number of gated communities are coming up in adjoining plots.

Today, urban India faces a shortage of 25 million affordable housing units which is projected to increase to 38 million by 2030 as 70% of the migrants to urban areas belong to low income group, McKinsey Global Institute (2010). Given this context, allowing a small segment of the population residing in gated communities to use large parcels of land devoted for amenities for exclusive use does not seem appropriate. Local authorities are obliged to ensure appropriate allocation of land to suit the needs of all segments of the population. Moreover, social infrastructure needs a base larger than that in an average gated community to support itself.

Spatial incompatibility

Gated communities have mostly one, sometimes two and seldom more entry-exit points. No other physical connection of the complex with the neighbouring streets exists. As seen in Fig. 2, these complexes are completely inward looking, detached from their surroundings, and impermeable. They are large-scale walled entities creating long stretches of barren streets alongside. They are unable to support activities along the streets which in turn discourage pedestrian movement, promote vehicular traffic, and make community vigilance difficult. As seen in Fig. 3, clustering of gated communities in adjoining plots adds to alienation of communities and any possibility of pedestrian activities on streets disappears. On an average gated communities house 550 residential units on a 25-acre site, that is, more than 3000 people. This is an opportunity lost.

Fundamentally, the spatial structure of a city is a result of intricate blend of its people and their activities. The moment large scale gated entities come into picture, the basic unit of design shifts from one person to a parcel of land. They cut into the fabric of a city disturbing the characteristics and normal functioning of the existing communities. As seen in Fig. 4, spatial arrangement of the gated communities is in sharp contrast to that of the existing settlement in terms of scale and pattern. Most of the Indian cities have a long standing history of development which has to be given due consideration while taking development decisions.

Moreover, development density is low in gated communities. Approximate floor area ratio (F.A.R.) consumed by sample apartment and villa complexes are 1.5 and 0.5 respectively which is less compared to standards outlined in building bye laws of municipal corporations and F.A.R. achieved in other Asian countries which ranges between 5 and 15, Pucher A. (2005). As shown in Fig. 5, there is a negative correlation between site area and F.A.R. consumed, that is, F.A.R. consumption decreases with increase in site area. This implies significant amount of buildable area remains untapped. Land is limited; there is no option but to use it judiciously.

Even site plans of many gated communities indicate mere subdivision of land into smaller plots without much attention to site planning principles that enhances quality of living. In few cases even the widths of internal roads are as much as that of a collector road.

Observations

A typical apartment building in any city housing as few as 50 households can have 24 hour security, back up for water and power supply, amenities like a small gym, a multipurpose hall, and a swimming pool as well. Such apartment buildings do not raise issues like segregation, privatization, or spatial incompatibility. Why?

Key to this is the scale of development. When a development is small enough to fit into the fabric of an existing community it will cease to disrupt community activities beyond acceptable limits and will not cause segregation even in the presence of boundary walls. Small scale developments are usually connected well with its surroundings physically, visually, and

psychologically. They tend to become an integral part of the communities. They can support activities continually at ground level, encourage people to walk and in turn increase community vigilance. Even when a development houses people belonging to a particular social or income group, if it is small in scale, it may not be dominant enough to trigger displacement of the less-privileged. Amenities in small developments are usually modest in scale and do not occupy large amount of land area. In such cases, even when the amenities are for exclusive use, the issue of inappropriate land allocation may not arise. Small scale developments also maximize consumption of F.A.R. as otherwise the project may not yield expected returns.

Any development is eligible to put up a boundary wall and monitor movement of non-residents to ensure security within the complex. As discussed, small developments do not pose major challenges while large developments do. Therefore, there has to be a threshold in terms of scale beyond which the positives inbuilt in a small development start losing ground. What then is the threshold scale for a residential development? This will depend upon the activity patterns and other functional requirements of residential communities. Detailed studies need to be conducted on the same which will provide the basis for determining the physical extents of a gated community in any given urban area.

Conclusions

This study suggests that the upper middle-class population in India prefers to live in gated communities mostly in response to inadequate provision of urban services including security by the local authorities. Added to this is the requirement of having public amenities within the complex for exclusive use. As these gated communities are large-scale inward looking entities housing people from similar social and economic backgrounds, issues related to segregation, privatization, and spatial incompatibility creep in. These developments contradict compact mixed use approach which is inherently integrated and inclusive in nature. Given that megacities of India are facing rapid urbanization, development of gated communities is likely to increase. It is therefore important to first and foremost understand whether or not gated communities contribute towards crime prevention or reduction not only within the community but in the vicinity as well. Only if there is merit to such studies, it will then be important to conduct further studies to decide upon the appropriate scale of such developments. Accordingly, guidelines can be formulated for the same that strike a balance between short-term needs of the residents and long-term issues of urban areas.

References

[1] Blakely, E J and Snyder, M G (1997), Fortress America: Gated Communities in the United States, Brookings Institution Press, Washington D.C.
[2] Kundu A (2006), Trends and Patterns of Urbanization and their Economic Implications, in India Infrastructure Report 2006, Oxford University Press, New Delhi, pp. 27-41
[3] Landman, K (2000), Gated communities and urban sustainability: Taking a closer look at the future, 2nd South African Conference on Sustainable Development in the Built Environment, Pretoria, South Africa, August 23-25.
[4] Lang, R E and Danielsen, K A (1997), Gated Communities in America: Walling Out the World?, Housing Policy Debate, Vol. 8, Issue 4, pp. 867-899
[5] McKinsey Global Institute (2010), India's urban awakening: Building inclusive cities, sustaining economic growth.
[6] Naudé, B (2004), Can Public Road Closures Reduce Crime Effectively?, Institute for Criminological Sciences, UNISA
[7] Pucher, J et al (2005), Urban Transport Crisis in India, Transport Policy, Vol. 12, No.3, pp. 92-104.

Table 1 Residential Units

Types of units	Average floor area (in sq.ft.) per unit	Average cost (in crore)	Share of units (%)
One bedroom	700	.44	2
Two bedroom	1300	.84	20
Three bedroom	1800	.96	42
Four bedroom & above	3100	2.47	23
Villa	4000	2.68	13

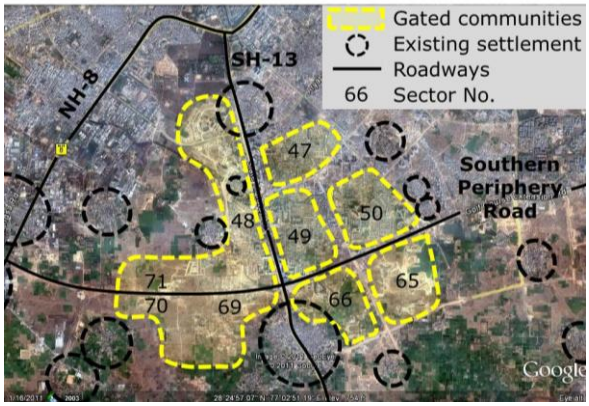


Fig.1 Location of existing and upcoming gated communities in Gurgaon, Delhi NCR

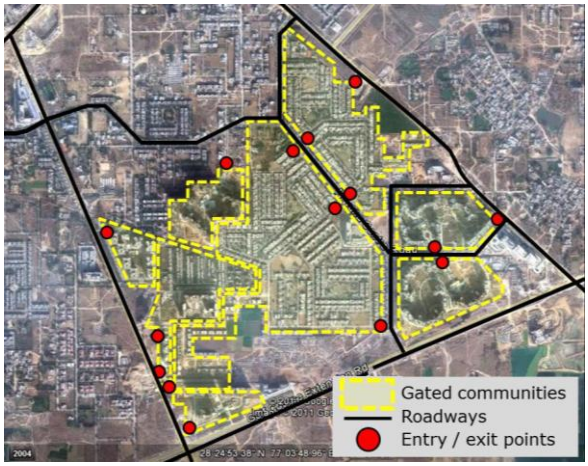


Fig.3 A cluster of gated communities



Fig.2 Interface of gated communities with adjoining streets

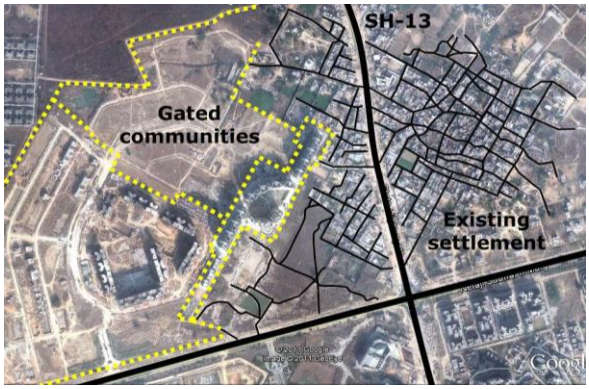


Fig.4 Contrast in spatial arrangement

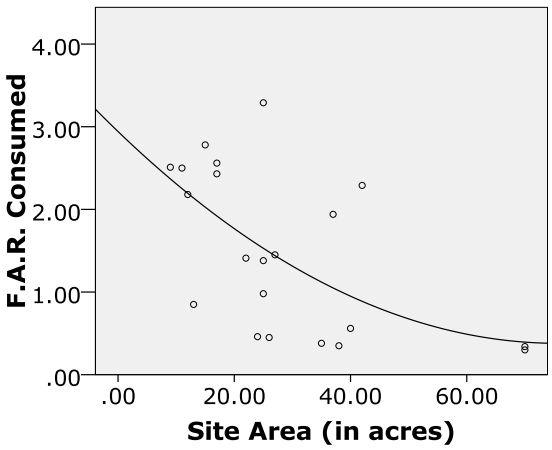


Fig.5 Correlation between site area and F.A.R. consumed

2nd International Engineering Symposium - IES 2012
(KU-MU-NITK-HCMCUT Joint Symposium) March 5-7, 2012, Kumamoto University, Japan

Strengthening imageability of an old urban core -a pilgrimage

Soumi Muhuri

Manipal School of Architecture and Planning, Manipal University, Manipal-576104, Karnataka, India. email:soumi_muhuri@rediffmail.com, soumi.muhuri@manipal.edu

Abstract: Strengthening imageability of an unplanned urban core is really very challenging. In this research paper an attempt has been made of strengthening imageability or user's perception of such an old urban core, which is also a famous religious hub of city Kolkata.
Existing set up of the study area (Kalighat temple and its vicinity)has been analysed within a broader perspective of a neighbourhood, based on its land use/activity, population, trade and commerce, tourist-pilgrims, infrastructure, built form, rent structure and overall impression.
Finally an integrated process, incorporating the concept of place branding, has been attempted to strengthen the imageability of the place, through some strategies and specific proposals for activities, built form and infrastructure with proper fiscal and management initiatives.

Keywords*: imageability, place branding, old urban quarter, pilgrimage*

Introduction

In India, all the organic cities have been developed throughout years based on people's usage, needs and beliefs. These cities are the expression of our culture or the way we live. So, unlike the planned cities these cities have problems of haphazard development, over-crowding, congestions, urban poverty, slums, poor infrastructure, environmental pollution, poor urban governance and mismanagement of urban resources. And as a result, the traditional urban quarters of these old cities are losing their social values and identities or their so called 'image' and going through a degraded built environment.
Strengthening imageability of such an urban quarter, which is a pilgrimage, is really very challenging because stakeholders attitude towards the place do not really change, as long as pilgrims come with their offerings. The pilgrims, who are very strong on their religious belief, are ready to sacrifice even their basic needs and means of comfort and therefore do not really bother about the environment and its physical setting. But with time when the nature of pilgrims change and the pilgrims become tourists-pilgrims the intangible factor of place-impression or 'imageability' of the place actually matters a lot. So, what could be the stakeholder's initiative with which they would be able to portray a better image of a place?

Place branding

"Brand is a product or service made distinctive by its positioning relative to the competition and by its personality, which comprises a unique combination of functional attributes and symbolic values" (Hankinson & Cowking 1993, p. 10). However the full brand of a place represents the feeling and function of the place including the products, activities, and special features associated with the area. So in complete branding of a place process is as important as product, where the basic objective is attracting more people and contributing to the economic growth, along with providing spaces of new experiences, which can finally change people's perception, attitude and value of the place.

About Kalighat

Kalighat is a famous religious place of Kolkata. The place is well known and attached with the city from its beginning. Even the name Calcutta (previous name of Kolkata) is said to have been derived from 'Kalighat'. The famous temple of Goddess Kali, of Kalighat is considered one of the 52 shakti peethams of India and it is also believed to be the **`Maha-pith'** as situated in combination of three important spots namely the `Keoratala smasan' (cremation ground)- in the south, `Adi Ganga' (the water channel) –in the west and `Nakuleswar Vaivav' (saimbhu Siva)- in the north-east directions.

It was 1809 when present Kali Temple was built under the patronage of Sabarna Roy Chowdhury's family of Barisha. The settlement started developing centering the temple. The market also developed along the pilgrim's path along Kalighat Road (Fig. 1), which was the old route to the temple. But it was 1920-30s when most of the buildings what we can see today came into existence. Though the area was formerly a religious cum residential area, with very little commercial establishment, because of huge number of tourists pilgrims, later on rapid development happened without much changes in infrastructure or basic amenities. So in spite of its popularity, because of inefficient infrastructure it is going through a degraded built environment, even the 'Kalighat Pat' or the kalighat painting which was once a very famous art is now about to die.

Analysis of existing set up

Imageability or people's perception cannot be strengthened without proper understanding of the morphology and the psychology of the urban core. So the analysis has been done based on various primary and secondary data sources and the outcome is as follows-

1. Activities- The area is primarily residential centering the temple and surrounding religious activities (Fig.1). The concentration of religious activity is more along the water channel. Also there is high concentration of slum (7%). Ground floor of residential and institutional buildings, are mostly used for commercial purposes. The paths leading towards the temple are consisting of numerous hawkers, encroached upon footpath and roads. Although surprisingly there are some pockets consisting of buildings, which are under utilize or vacant.

2. Population- Total population of the study area is 35000 and average household size is 4.5.Population density is very high (8974 person/sq.km.). Out of total population 26% lives in slum and 1.16% is pavement dweller. The working participation in general is very less (60% male and 20% female). Those who work are mostly (55%) involved in service sector.

3. Trade and commerce-There are about 1000 formal and 850 informal shops. The shop owners are mostly come from outside the study area.Their per day income varies between Rs. 300-800.

4. Tourist-pilgrims-Around 20000 visitors come over here regularly. On festive day it may go up to 1 lakh. Most of them come from in and around the city. They come in a group normally 3-4 persons per group. Average time spent per group is 1-2 hours. Per head average expenditure varies between Rs. 40-50. Mostly people use bus or metro rail to reach the place. Very less visitors (12%) use private car.

5. Infrastructure- Though the place attracts huge number of tourists-pilgrims but hardly offers any facilities to them. The place does not have adequate public toilet and drinking water facilities. It does not have adequate tourist lodge/ resting place, proper guiding map, signage and car parking facilities. Lack of garbage disposal and management is an addition to these problems.

6. Land price and ownership- In this area almost 80%is free hold private land. The land price is very high along the periphery roads (Fig.2). Where as the traditional settlements with narrow roads and slum pockets are lowest land price zones.

7. Built form- The area is densely built and open space is very less (11%). There are about 26% single storied structures, 54% are double storied and 20% structures are three storied and above. Among total structures 22% are semi-pucca and 2% are kuchcha (Fig.3). Again among the pucca structures, about10% are dilapidated and 12%are in intermediate condition.

8. Imageability**-**A detail imageability study (Fig.5) through cognitive map and questionnaire survey revealed that the landmarks of the place are very strong. The path leading towards temple from the main road is also very prominent because of lot of activities.

So, though the area is a very well known religious hub and a vibrant economic core of the city, it is because of unorganised activities, inadequate and inefficient infrastructure which act as repellent and create a poor impression to the larger group of tourists from far off places (within the country and abroad).

Approach towards future

With basic objective of imageability strengthening to encourage larger group of tourists from far off places some strategies and specific proposals have been adopted for future development. These are as follows-

1. Activities-

- Adaptive reuse has been proposed for underutilized buildings
- Properties belonging to Sevayets, adjacent to the temple, (which are at present in intermediate to deteriorating condition) has proposed to be reorganized and the ground floor has been proposed to be utilized for temple related functions (like rooms for pandas , ritual rooms or Bhog Distribution center).
- An artisan village has been proposed to promote traditional art and crafts (especially for Kalighat Painting).
- A slum removal project with rehabilitation package and 50% relocation within the exiting location has been proposed with proper facilities.
- Hawkers are proposed to be relocated in organized shopping arcades/shopping kiosks.
- Restricted access to Adi Ganga (water channel) has been proposed for the community as well as for the tourist pilgrims.
- New construction along Kali Temple road and Kalighat road has been proposed to have temple related shops at the ground floor and special incentives (like soft loan, tax exemption etc.) has been proposed for those construction.

2. Built form-

- To create a better street scape no front setback has been proposed for the construction along Kalighat road and Kali Temple Road.
- 3.6 meter height ground floor with uniform arcade is proposed for the new buildings with shops (fig.6).
- Sympathetic infill (having strong horizontal band, axial symmetry and arcaded shop front) has been proposed for new construction along Kalighat road and Kali temple road (fig.6).
- Since at present the temple does not have proper visibility from the main road and the path leading towards the temple is not so defined, a way finding gate is proposed to resolve the problem(fig.7).
- Hawkers, though very much part of any religious place normally secluded are tried to incorporate within the designed environment with designated space (shopping arcade), which will also act as imageable elements for the visitors.

3. Infrastructure-

- Adequate public toilet, drinking water fountain, resting place, guiding map, signage and organized parking have been proposed for tourist-pilgrims.
- Creation of green areas along Adi Ganga, has been proposed to meet

the requirements of open spaces and to protect the waterfront.

- Water conveyance system for temple waste and installation of individual plot level solid waste storage equipment with a door to door collection has been proposed for residential buildings and commercial areas.

4. Fiscal and management-
   Most of the cases proposals remain unexecuted without proper fiscal and management initiatives.

   Since a willingness to pay survey revealed that 49% visitors, 35% residents and 30% shop-owners are ready to pay for better facilities and services, therefore funds can be generated

- Through tax collection from commercial houses
- Through advertisement, publications and funding from sponsorship.
- Parking charges and fees collection for visiting artisan village, and rent of ritual rooms, lodges, rest houses etc.
- Incorporating nominal increase in household tax for additional services

Fiscal incentives could be

- Property tax relief for repair and restoration of old structures and better utilization of existing stock.
- Tax incentives for the new construction having temple related shops.
- Provision of special funds for the buildings for undergoing through changes and adoption for temple related functions.
- Special funds for rehabilitation.
- Built-up space allotment for relocation.

For proper management an active public participation by developing a multidisciplinary team, for chanalising grants and loans and monitoring the activities can be very effective.

Conclusions

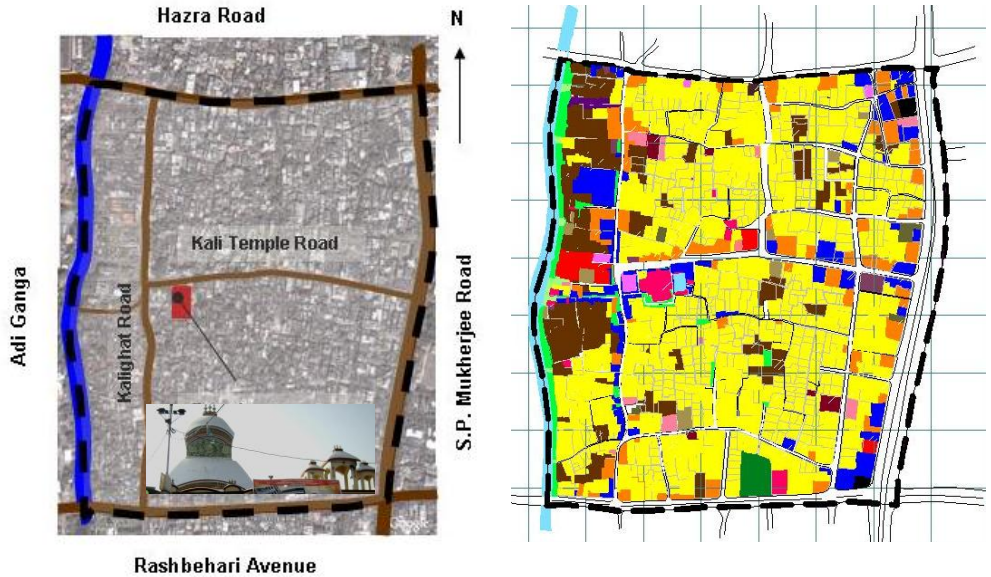
The process remains incomplete without proper attention of the users. So, to draw user's attention finally advertisement through posters or electronic medias can be created, highlighting interesting images, featured buildings, imageable elements and incorporating catchy captions, which can actually help in developing a proper brand and ultimately strengthen the imageability of the place.

Acknowledgements

I would like to thank Kolkata Municipal Corporation, West Bengal Tourism Development Corporation, Kolkata Metropolitan Development Authority, International Foundation of Sustainable Development (NGO) and Kalighat Temple Committee for sharing important data and for their immense help in this research project. I would also like to express my gratitude to Professor (Dr.) Sanghamitra Basu, Professor Kashinath Mukhopadhay and Mrs. Sabitri Halder for their extended help and suggestions.

References

[1] Alan Plattus, Donald Watson, Robert Shibley (2003), Time-Saver Standards for Urban Design, The McGraw-Hill publication.
[2] Architecture + Design (1989), Vol. VI no 1, Nov-Dec.
[3] Gordon Cullen (1996), The Concise Townscape, Publication of Architectural Press, Oxford,U.K.
[4] Henry Sanoff (1991), Visual Research methods in Design, Van Nostrand Reinhold Publication.
[5] Himanshu Burte (1995), Launching off from the Backyard, India.
[6] Jing Jing (2009), Urban Planning and Design in the context of Creative Economy --Place Branding , degree project, KTH, Department of Urban Planning and Environment Division of Urban and Regional Studies, Kungliga Tekniska högskolan, Stockholm.
[7] Kevin Lynch (1960), The Image of the City, Publication of joint center for Urban Studies, MIT, Cambridge, London.
[8] N. Collins-Kreiner and N. Kliot (2000), Geojournal, - Pilgrimage tourism in the Holy Land: The behavioural characteristics of Christian pilgrims, April.
[9] Network of Indian Cities of Living Heritage (2007), UNESCO publication.
[10] William Michelson (1975), Behavioral research methods in environmental design, Dowden Hutchison & Ross Inc. publication.



Primary Residential	45%	Socio-cultural	0.6%
Informal Residential	7%	Religious	1.1%
Industrial	0.3%	Utility-services	0.1%
Commercial	5%	Parks	0.9%
Residential+ Commercial	6%	Openspace	3.7%
Residential + Public-semi public	1.3%	Ghat	0.3%
Commercial + Public-semi public	0.5%	Under construction site	0.7%
Govt. & Semi-Govt Uses	0.2%	Transport	0.4%
Health	0.4%	Roads	22%
Education	0.5%	Waterbody	4%

Fig.1 location and land use of study area

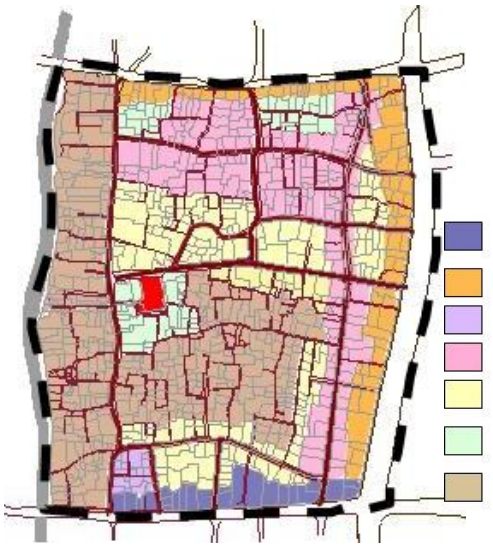


Fig.2 land price/kattah

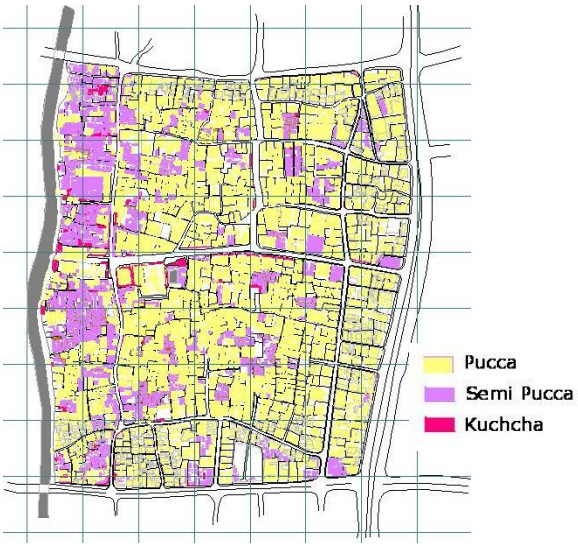


Fig.3 Building material



Fig.4 Built form



Fig.5 Imageability study

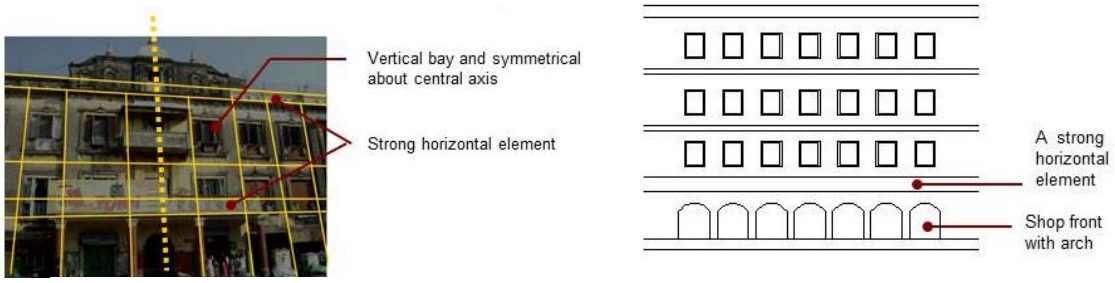


Fig.6 Proposed infill technique

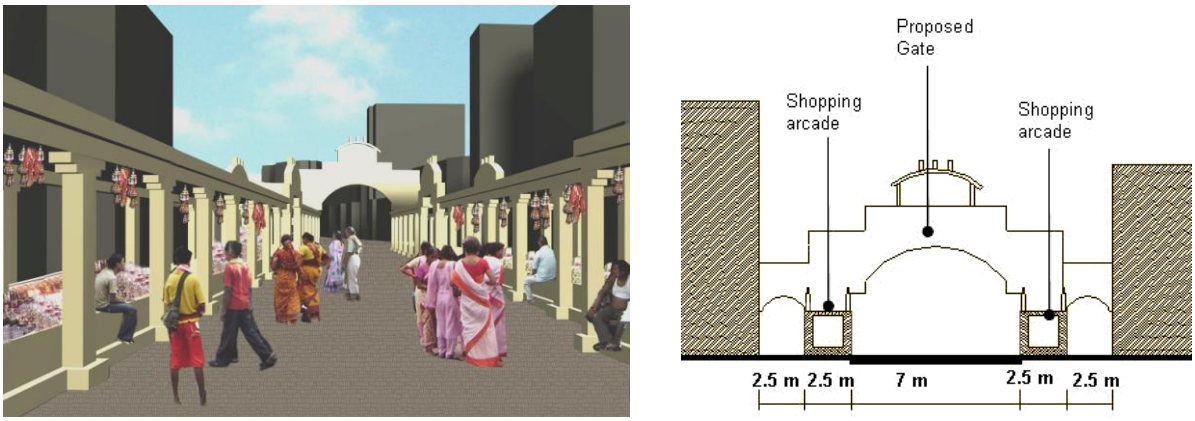


Fig.7 Proposed gate and shopping arcades

2nd International Engineering Symposium - IES 2012
(KU-MU-NITK-HCMCUT Joint Symposium) March 5-7, 2012, Kumamoto University, Japan

Primitive Invention Of Mankind - Earth Architecture; Case Study at Wayanad, S. India

Kala Choyimanikandiyil

Department of Architecture, Manipal School of Architecture And Planning, ManipalUniversity, Karnataka, India 576104.
e-mail:kalabrhm@yahoo.com, kala.cmk@manipal.edu

Abstract: Majority of the Indian population which fall below the poverty line are homeless. Scarcity of finance and increasing cost of materials and labour necessitate the scientists to research extensively on the indigenous, self-help methods practised over the years using local materials. This paper presents case studies carried out in Wayanad, hilly region in Kerala State, South India on the traditional dwellings of tribal community which are of high heritage value. These sustainable structures made mostly of mud known for its low carbon emissivity and high thermal control are built completely by laymen by methods handed down to them through generations. These historical dwellings still exist with little maintenance and minimal deterioration. This study will set a base for the fundamental research on the traditional indigenous construction techniques at Wayanad.

Keywords*: Earth Architecture, Mud Construction, Indigenous Construction Techniques, Traditional Architecture, Wattle And Daub Wall Construction, Tribal Settlements*

Introduction

Smart little gophers surely will build their village near a patch of grain where they can get their food, and close by a creek for water. They will never build their towns near willow clumps for there is where owls will be roosting. But many modern towns built for men, slope towards the bitter winter winds. Even breeze in the summertime can catch the smoke from the flax mill and pour it across our houses and into our windows (John Ormsbee Simonds and Barry W. Stake, 2006). This is not what our ancestors taught us.

The result of thousands of years of research through trial and error is Earth Architecture that we see around the globe. May it be the method using rugby ball shaped mud bricks as we see in Zaria, Nigeria (Friedrich W. Schwerdtfeger, 1982) or the mud tower houses using adobe that we find in Asir, Saudi Arabia (Kaizer Talib, 1984) or the use of wattle and daub infilling to timber framed houses in Northern Europe, everywhere there is one common material – Earth.

Man's next invention was on how to make them water resistant, termite resistant and earth quake resistant. He used all the indigenous materials like wood, lime, husk and straw along with earth to overcome each of these defects.

This paper discusses the importance of study of indigenous technique practiced on the tribal housing settlements through the ages in Wayanad, Kerala. In spite of its wide occurence in the region, very little is known about its engineering properties with respect to comfort and durability aspects. This study will contribute greatly to the urgent need of uplift in the housing sector of the poorest of the poor in the present Indian scenario.

Brief Background Of The Indian Setup

The Population density per Sq.M. of Kerala is 859 and that of Wayanad is 383 whereas in India it is 382 according to 2011, Census Data, Government of India (Table 1). As per the same Census Data the tribal population in Wayanad is 136,062 which is almost 40% of total tribal population in Kerala State (Table2).

A total of 1,943,766 of the Indian population are listed as houseless (2011,Census Data, Government of India).

From the year 1950 starting with the First Five Year Plan, Ministry Of Housing And Urban Poverty Alleviation, Government Of India is struggling hard by setting up different policies and schemes to eradicate poverty and help out the homeless. Also innumerable number of dilapidated houses will be renovated by these schemes. Even the housing policies and tribal housing schemes formulated this year by the Government Of Kerala make us aware that this study will be purposeful.

Traditional Earth Architecture In India

Mud is not only cheap but available in abundance. The statistics from UNCHS (UN- Habitat) says that 40% of the world population lives in earthen dwellings. Also while Indian statistics is referred majority of the population in India are living in earthen dwellings. Earth can achieve very high quality and durability as a building material.

In India the vernacular earth buildings were in existence since the vedic period, through medieval, feudal, Islamic and colonial times. Owing to the heritage of the subcontinent, earth architecture of India is diverse and unique to individual region. When we are talking of earth architecture of India, we are, in all probability, talking about earth walls, flooring, plastering and tiled or thatched roof.

The policies of the administration with regard to finance, planning and control of building in earth needs much to be introduced. Education in this area is given minimum considerations so far.

The traditional earthen wall construction that are generally practiced in India are listed as follows.

(a) Cob wall Construction:

The oldest method of all is cobwall construction. In this method the earth is made into required consistency and placed in horizontal layers, one on top of another. Each layer will be put on alternate days or so, after the lower layer has dried; every layer at a height of 60–90 cm. These walls are thicker at the base 45-60 cm and gradually tapering towards top. For imparting strength straw and cowdung are added to the kneaded soil.

(b) Adobe Construction

Here again the earth is made into required consistency and hand moulded into bricks of suitable sizes (normally 30 cm x 30 cm x 10 cm). These bricks after drying in the sun are laid in mud mortar to form regular walls. This is more strong than cob wall construction because the sundried bricks are used.

(c) Rammed-Earth Wall Construction

In the rammed-earth technique a vertical form work (shuttering) is made first into which wet earth is rammed, then it is left for drying for a day or so. Then the formwork is raised and a second layer of mud is rammed. This process is continued until the desired height is reached. To impart more strength small stones or straw are mixed in the earth. The wall thickness is made 30 cm x 45 cm.

(d) Wattle and Daub Wall Construction

This is a very common method practiced in different parts of India. Comparatively this is used for simpler buildings. First some vertical posts at required intervals are set into the ground. Usually timber poles or strong tree branches or whole culms of bamboos are used for posts. Next step is to create a woven rods or sticks between the posts to make some kind of a solid screen which is called wattle. In some areas wattle of intricate basketwork is also used. This is covered (daubed) on both sides with clay, sand and straw mix which is called the daub.

The paper will be incomplete if no mention is taken on the modern developments in the field of earth architecture taking place presently in India.

The Centre for Sustainable Technologies (CST) established as Centre for ASTRA (Application Of Science and Technology For Rural Areas) in 1974, is IISc's (Indian Institute of Science) interdisciplinary research and technology development centre for providing sustainable solutions regarding energy, buildings and

environment. The Centre's focus is on promoting Sustainable Technologies to suit local conditions of resource availability and habitation. This is a Centre where extensive research on stabilized mud blocks have taken place.

AUROVILLE Earth Institute is the next remarkable one in India which is at Pondicherry. This is founded by HUDCO (Housing and Urban Development Corporation), Government of India, in 1989. The institute is researching, promoting, developing, promoting and transferring earth based technologies which are cost and energy effective.

My emphasis here is to consider solely the case of traditional construction method of tribal community at Wayanad and study further at a higher level in terms of extreme sustainability. No recorded research has taken place on this topic yet.

Geographical Location And Geological Setting – Wayanad

1. Location: North-East Of Kerala State, South India
2. Co-ordinates: Between North Latitude $11^0$27' and 150 58' and East Longitude 75^0 47' and 70^0 27'.
3. Area: 2131Sq.Km. (2,12,560 hectares)
4. Reserve Forest: 20,864 hectares.
5. Altitude: From 700m.– 2100m. from sea level
6. Seasons: Cold Weather - December to February, Hot Weather – March to May, South-West Monsoon – June to September, North East Monsoon – October to November.
7. Mean Maximum Temperature: 29^0C
8. Mean Minimum Temperature: 18^0C
9. High Annual Rainfall: 3000 -4000 millimetres per year.
10. Average Annual Rainfall: 300 mm per year.
11. Relative Humidity: Maximum upto 95% during South-West monsoon period.
12. Soil Characteristics:

- Laterite Soil: This is reddish brown in color. It has a low content of Nitrogen, Phosphorous and Potash. The pH of this soil ranges between 5.5 and 6.5 and its texture is clayey loam to silty loam with 5-20% coarse fragments.
- Brown Hydromorphic Soil(BHS): This is very deep brown in color with sandy loam to clayey texture. The pH of this soil ranges between 5.2 and 6.3 and is slightly acidic in nature.
- Forest Loam: This is reddish brown in color, rich in organic matter, Nitrogen and humus and of loamy to silty loam texture. The pH of the soil ranges between 5.3 and 6.3 and is slightly acidic in nature.
- Riverine Alluvium: These are found along the rivers called Kabani and Chaliyar and their tributaries. It contains moderate organic matter, Nitrogen, Phosphorous and Potash and its texture is sandy loam to clayey loam.

13. Pre-monsoon Depth to Water Level: 1.68 – 20.16 mbgl.
14. Post-monsoon Depth To Water Level: 0.37 – 19.50 mbgl.
15. Tribal Population: Almost 15 tribal communities live in this district. Around 1.3 lakhs of tribal people live here according to the latest census.
16. Type Of Tribal Settlements:
    The remarkable ones are having walls of either Wattle and Daub type of construction or the adobe construction. The roof is mainly thatch on wooden reepers and purlins.

Case Study Of Traditional Tribal Dwellings At Wayanad

There are evidence of some caves in Wayanad even today where Paleolithic man took shelter. Most of the traditional settlements in Wayanad are situated scattered in the reserve forest areas. Bamboo is an indispensable item in the construction of traditional houses. Because of their main preoccupation of collecting forest products, traditional settlements are distributed far from each other. Changes in the ecosystem have also effected their traditional house construction as well as deforestation and new forest regulations have reduced the availability of wood and bamboo. The very primitive tribal must have then set up wooden shelters, the model of which are still existing in different parts of Wayanad

as seen in Fig.1. Similar types are set up even these days, but for a temporary use due to lack of finance. These huts are erected on slightly raised basement and mostly with bamboo collected from the same region. Most of the tribal settlements are placed on a sloping ground with the entrance of every hut in the opposite direction of the hill.

The next phase of experiment in terms of construction can be assumed as Wattle and Daub wall construction with thatch roof. The plinth of the structure is put up on slightly erected firm ground of rammed earth. Vertical posts of strong trees normally round in shape are set into the ground at the corners of the plinth. These logs are connected at their free ends by wooden beams. Also there are cross beams connecting the main beams. Struts are provided on this to support the ridge of the roof. Between the corners other vertical posts like bamboo poles are given at intervals. Onto this some mesh kind of intricate work made of twigs and bamboo slats are tied. Across all these posts woven bamboo slats are tied (Fig. 2). After that moist mud along with straw and cow dung is plastered on either side. Also carbon black obtained by burning coconut shell is added to this mixture. On the roof ridge bamboo strips are connected for rafters. On top of this the roofing materials used are either Lemon grass (Cymbopogon), Darbha grass (Desmostachya Bipinnata) or paddy straw.

This Wattle and Daub wall construction is the widely used and most popular among all the tribal settlements. Nonetheless adobe wall construction is also rarely seen in dilapidated condition (Fig. 3). This does not seem to have originated from the tribal base. But people migrated from nearby places must have introduced it.

Among all the tribal settlements the hutment colony at Pakkam village owned by Kurichiya community is a remarkable one which exist in marvelous condition even without much maintenance (Fig. 4). Only difference here is the elevated stone plinth. Everywhere a good roof overhang is provided which ideally protects the wall from rainwater seepage. These settlements are usually known as 'kudi'. The hutments in a hamlet are usually clustered in nature. The maximum number of houses found in a hamlet is 20. Average household in a hamlet is 10.2.

These days the society has accepted the brilliant antique construction technique of tribal community; the proof of which is seen in the construction of some resorts in that very region Wayanad (Fig. 5 - Fig. 9)

Conclusions

The following conclusions are deduced from this study:

- Mankind is a part of nature. Everything in nature is made for the existence of each other. Though it took ages, man became successful in making use of the indigenous materials and tried himself to provide the best shelter for himself in the easiest way to give him maximum comfort from external climate.
- The materials such as mud, bamboo, round log, wooden battens, straw, cow dung etc. provide thermal insulation.
- The method of construction and the use of materials are true reflection of their adaptation to surrounding ecology.
- This is a unique method practiced very rarely and with no input of modern materials.
- No written documentation of the method of construction is so far done on this. Nonetheless the technique is handed down through generations till date so meticulously.
- Introducing science and technology to these traditional indigenous techniques can result in wonders.
- Research has to be channelized towards further innovations regarding cost efficiency and performance with respect to strength and durability.
- The livability, healthy atmosphere and reduced cost of construction enable every individual to own a dwelling for the family.
- Educating the common public in the region about the construction technique very authoritatively will aid them to form a self-help process to build homes for everyone.

Acknowledgements
The Ministry of Education, Government of Japan and Manipal University, Manipal, Karnataka, South India provided financial support to carry out this research.

References
[1] Bernard M. Feilden (2003), Conservation Of Historic Buildings, Third Edition, Elsevier Ltd.,pp.77.
[2] Friedrich W. Schwerdtfeger (1982), Traditional Housing in African Cities: A comparative Study Of Houses in Zaria, Ibadan and Marrakech, John Wiley & Sons Ltd., Chichester, pp.76.
[3] John Ormsbee Simonds and Barry W. Starke (2006), Landscape Architecture-A Manual Of Environmental Planning And Design, IVth Edition, The McGraw Hill Companies Inc., pp.xv.
[4] Kaizer Talib (1984), Shelter In Saudi Arabia, Academy Editions, London, pp.98.
[5] Vinayachandran N. and Dr. V. S. Joji (2007), Groundwater Information Booklet Of Wayanad District, Kerala State, Central Ground Water Board, Ministry Of Water Resources, Government Of India, pp.5, 13-15.
[6] http://censusindia.gov.in/ retrieved on 16-November, 2011.
[7] http://wayanad.nic.in/ retrieved on 02-December, 2011.

Tables and Figures

Table 1. Population Data

	India	Kerala State
Total Population	1028,610,328	31,841,374
Population Density/Sq. Km	382	859
Tribal Population	84,326,240	364,189

Table 2. Population Data Of The Region Of Study

	Rural Kerala	Wayanad District
Total Population	23,574,449	816,558
Population Density/Sq.Km.	566	383
Tribal Population	350,019	136,062



Fig.1. Wooden Dwelling At Wayanad



Fig.2. Wattle and Daub Wall At Construction Stage



Fig.3. Adobe Wall Improperly Maintained



Fig.4. Hut of Tribal King At Pakkam



Fig.7. Tribal Homestay At Wayanad



Fig.5. Tribal Homestay At Wayanad



Fig.8. Tribal Homestay At Wayanad



Fig.6. Earthen Building At Banasura Resort



Fig.9. Treehouse At wayanad

ELECTRICAL, ELECTRONICS, COMPUTER ENGINEERING & RELATED FIELDS

Maximin Degree Domination Number in Graphs

S. S. Kamath[1] and Prameela Kolake[2]

1 Department of Mathematical and Computational Sciences, National Institute of Technology Karnataka, Surathkal, Srinivasnagar, Mangalore - 575 025. India. Email: shyam.kamath@gmail.com

2 Department of Mathematical and Computational Sciences, National Institute of Technology Karnataka, Surathkal, Srinivasnagar, Mangalore - 575 025. India. Email: prameela.kolake@gmail.com

Abstract: A set $D \subseteq V(G)$ of a graph G is called a *dominating set* of G if every vertex $u \in V - D$ is adjacent to at least one vertex $v \in D$. In this paper we define a maximin degree dominating set D of a graph G as a dominating set in which $\delta(\langle D \rangle)$ is maximum. The minimum cardinality of a maximin degree dominating set is the maximin degree domination number of the graph and is denoted by $\gamma_{\delta_{max}}(G)$. We discuss the basic properties of maximin degree dominating sets, maximin degree domination number of some well-known graphs, bounds on $\gamma_{\delta_{max}}(G)$ and the critical aspects of maximin degree dominiation number with respect to edges and vertices.

Keywords: *Maximin degree domination number, Domination, Total domination, Connected domination, complement of a graph, critical vertices and edges*.

Introduction

We consider here only the finite simple undirected graphs with no loops or multiple edges. For the notations and terminologies used here, the reader is referred to Harary F. (1972), unless specified otherwise. We begin with a brief introduction to domination in graphs.

Definition 1.1. *In a graph $G = (V, E)$ two vertices u and v are said to dominate each other if they are adjacent to each other in G. A set $D \subseteq V(G)$ is called a dominating set if for every vertex $u \in V - D$, there exists a vertex $v \in D$ such that u and v are adjacent. The minimum cardinality of a dominating set is called the domination number of the graph G and is denoted by $\gamma(G)$.*

In this paper we introduce a new domination parameter called the maximin degree domination number.

Definition 1.2. *A dominating set D of a graph G is said to be a maximin degree dominating set if the minimum degree of the induced subgraph $\langle D \rangle$ of D is maximum, where the maximum is taken over all the dominating sets D of the graph. The minimum cardinality of a maximin degree dominating set is called the maximin degree domination number of the graph and is denoted by $\gamma_{\delta_{max}}(G)$.*

Example:

In Fig.1. there are three maximin degree dominating sets, viz., $D_1 = \{v_1, v_3, v_4, v_5, v_6\}$, $D_2 = \{v_3, v_4, v_5, v_6\}$ and the vertex set V itself. The minimum degree of the induced subgraphs of all the above three dominating sets is 3. But among the three D_2 has minimum cardinality and hence $\gamma_{\delta_{max}}(G) = 4$ for the graph in Fig.1.

Maximin degree domination number of some well-known graphs

In this section we obtain the value of $\gamma_{\delta_{max}}$ of some class of graphs.

Lemma 2.1. For a regular graph G of order p, $\gamma_{\delta_{max}}(G) = p$.

Proof: This is immediate from the observation that in any r - regular graph G, $\delta(G - v) < r$, for any vertex v of G. □

Remark: Converse of the above lemma, however, need not be true. For example, $\gamma_{\delta_{max}}(W_n) = n$, where W_n is the wheel graph, defined as in Harary F.(1972).

Theorem 2.2. For any complete bipartite graph $K_{m,n}$, $\gamma_{\delta_{max}}(K_{m,n}) = 2\min\{m,n\}$.

Proof: Let V_1 and V_2 be the partite sets of $K_{m,n}$ with cardinalities *m* and *n* respectively. Without loss of generality, let $m \leq n$. Then the induced subgraph of the set V_1 together with any *m* number of vertices from the set V_2 forms a complete bipartite graph $K_{m,m}$ which is a regular graph. Note that addition of any vertex of $V(K_{m,n}) - V(K_{m,m})$ to the induced subgraph $K_{m,m}$ will not increase the minimum degree. But the removal of any vertex from $K_{m,m}$ decreases the minimum degree. Hence $\gamma_{\delta_{max}}(K_{m,n}) = 2\min\{m,n\}$. □

Cokayne E.J. et al. (1980) introduced the concept of total domination in graphs as follows.

Definition 2.1. *A dominating set D of a graph $G = (V, E)$ is said to be a total dominating set if every vertex of G is adjacent to at least one vertex of D. The minimum cardinality of a total dominating set is the total domination number of the graph and is denoted by $\gamma_t(G)$.*

Theorem 2.3. For any tree T, $\gamma_{\delta_{max}}(T) = \gamma_t(T)$, where $\gamma_t(G)$ is the total domination number of the graph G.

Proof: Since any subgraph H of a tree T is a forest, the minimum degree of the induced subgraph $\langle H \rangle$ of H is 0 or 1. Hence it is not possible to obtain a dominating set D of tree T such that the minimum degree of the induced subgraph $\langle D \rangle$ of D is more than 1. But by definition of the total dominating set of a graph, it is the dominating set of the graph whose induced subgraph has no isolated vertices. Hence any γ_t - set of a tree is also a $\gamma_{\delta_{max}}$ – set of the tree. Thus $\gamma_{\delta_{max}}(T) = \gamma_t(T)$, for any tree T. □

Corollary 2.3.1. For any graph G without isolates, $\gamma_t(G) \leq \gamma_{\delta_{max}}(G)$.

Proof: Without loss of generality, let us assume that the given graph G is connected. Then G contains a spanning tree, say, T. By the Theorem 2.3., we have, $\gamma_{\delta_{max}}(T) = \gamma_t(T)$. Hence the result follows. □

Proposition 2.4. If G is a graph with isolated vertices then $\gamma_{\delta_{max}}(G) = \gamma(G)$.

Proof: As the isolated vertices of a graph G must be the elements of the γ-sets of the graph G, the minimum degree of induced subgraph of any dominating set of such graphs is always 0. Thus $\gamma_{\delta_{max}}(G) = \gamma(G)$. □

Bounds on $\gamma_{\delta_{max}}$

Since $\delta(G) \leq \delta(\langle D \rangle)$, for any maximin degree dominating set D of G, every vertex v in a $\gamma_{\delta_{max}} - set\ D$ of a graph G is adjacent to at least $\delta(G)$ number of vertices of D. Hence $\delta(G)$ is an obvious lower bound for $\gamma_{\delta_{max}}(G)$. The following theorem gives a better lower bound for $\gamma_{\delta_{max}}(G)$.

Theorem 3.1. For a graph G without isolated vertices, $\gamma_{\delta_{max}}(G) \geq \left\lceil \frac{n\delta(G)}{\Delta(G)+1} \right\rceil$, where $\delta(G)$ and $\Delta(G)$ represents the minimum and maximum degrees of the given graph G respectively.

Proof: Note that in a graph G each vertex can dominate at most $\Delta(G)$ number of vertices. In a $\gamma_{\delta_{max}} - set$, every vertex is adjacent to at least $\delta(G)$ number of vertices. Thus $\gamma_{\delta_{max}}(G) \geq \left\lceil \frac{n\delta(G)}{\Delta(G)+1} \right\rceil$. □

Theorem 3.2. Let v be a vertex of a graph G without isolated vertices such that v satisfies the following conditions.

a. $\deg(v) = \delta(G)$ and
b. $N(u)$ contains at least $\delta(G)$ number of vertices of degree greater than $\delta(G)$ for all $u \in N(v)$.

Then $v \in V - D$, where D is a $\gamma_{\delta_{max}} - set$ of G.

Proof: Let $u \in N(v)$, where $\deg(v) = \delta(G)$. Suppose u satisfies the second condition in the statement of the theorem. Then the removal of the vertex v from G results in a graph G' with $\delta(G') \geq \delta(G)$. Hence $V(G) - \{v\}$ forms a maximin degree dominating set of G. This proves the theorem. □

Remark: The vertices satisfying the conditions stated in the above Theorem 3.2., belongs to $V - D$ for a $\gamma_{\delta_{max}}$-set D of G. Hence we define the following set and obtain an upper bound for $\gamma_{\delta_{max}}(G)$.

Definition 3.1. *Let G be a graph without isolated vertices. The set $M_\delta(G)$ is the set of all minimum degree vertices v of G such that $N(u)$ contains at least $\delta(G)$ number of vertices of degree greater than $\delta(G)$ for all $u \in N(v)$.*

Corollary 3.2.1. Let G be any graph without isolates. Then $\gamma_{\delta_{max}}(G) \leq |V - M_\delta(G)|$.

Theorem 3.3. Let G be a graph with minimum degree $\delta(G) \geq 1$. Let D be a $\gamma_{\delta_{max}} - set$ of G. Then $V - D$ does not contain a maximin degree dominating set of G.

Proof: Let us consider two cases.

Case 1: $V - D$ is not a dominating set of G.
Then any subset of $V - D$ can not be a dominating set of G and hence the result is true.

Case 2: $V - D$ is a dominating set of G.
Since D is a maximin degree dominating set of G, $\delta(\langle V - D\rangle) \leq \delta(\langle D\rangle)$. Suppose there exists a subset T of $V - D$ such that $|T| = |D|$ and T is a dominating set of G. Then obviously $\delta(\langle T\rangle) \leq \delta(\langle D\rangle)$. If $\delta(\langle T\rangle) = \delta(\langle D\rangle)$ then since T is a dominating set of G, the vertices of minimum degree in $\langle D\rangle$ are adjacent to some vertices of T. Then the vertices of T together with the vertices of D forms a new dominating set D' of G such that $\delta(\langle D'\rangle) > \langle D\rangle)$. This is a contradiction to the fact that D is $\gamma_{\delta_{max}} - set$ of G.

Thus T cannot be a dominating set of G. Thus $V - D$ does not contain a maximin degree dominating set of G. □

Theorem 3.4. Let D be a $\gamma_{\delta_{max}} - set$ of a connected graph G. Then D is a $\gamma - set$, $\gamma_t - set$ and a $\gamma_c - set$ of G if and only if $\langle D\rangle$ is connected and for every vertex $u_i \in D$ there exists at least one vertex $v_i \in V - D$ such that v_i is uniquely dominated by u_i.

Proof: Let D be a $\gamma_{\delta_{max}} - set$ of a connected graph G. Suppose D is a $\gamma - set$, $\gamma_t - set$ and a $\gamma_c - set$ of G. Then D satisfies the following

a. $\delta(\langle D\rangle)$ is maximum
b. $\langle D\rangle$ is connected and
c. D is the minimum dominating set of G.

Suppose D contains a vertex u such that for each vertex w in $N(u)$ there exists at least one vertex $v \in D$ where $v \neq u$, so that v is adjacent to w. Then $D - \{u\}$ forms a dominating set of G. This is a contradiction to the fact that D is a $\gamma - set$ of G.

Conversely, let D be a $\gamma_{\delta_{max}} - set$ of a connected graph G and $\langle D\rangle$ is connected. Since D is a dominating set of G and $\langle D\rangle$ is connected, $\gamma \leq \gamma_t \leq \gamma_c \leq \gamma_{\delta_{max}} = |D|$. Since for each vertex $u_i \in D$ there exists at least one vertex $v_i \in V - D$ such that v_i is uniquely dominated by u_i, $D - \{u_i\}$ is not a dominating set of G. Hence D is a minimum dominating set of G. Thus

$|D| = \gamma(G)$. Thus D is the $\gamma - set$, $\gamma_t - set$ and a $\gamma_c - set$ of G. □

Corollary 3.4.1. Let D be a $\gamma_{\delta_{max}} - set$ of a graph G without isolates. Then D is also a $\gamma - set$ and a $\gamma_t - set$ of G if and only if for every vertex $u_i \in D$ there exists at least one vertex $v_i \in V - D$ such that v_i is uniquely dominated by u_i.

Proof: Since G is a connected graph and $\delta(G) \leq \delta(\langle D \rangle)$ for any maximin degree dominating set D of G the result follows. □

Critical aspects of maximin degree domination number

Sampathkumar E. et al. (1992) introduced the critical aspects as follows:

Definition 4.1. *Let t be any parameter defined on the graph G and e be any element of graph G. Then the element e is said to be*

1. $t - critical$ *if* $t(G - e) \neq t(G)$.
2. $t^+ - critical$ *if* $t(G - e) > t(G)$.
3. $t^- - critical$ *if* $t(G - e) < t(G)$.
4. $t - fixed$ *if e belongs to every* $t - set$.
5. $t - free$ *if e belongs to some* $t - set$ *but not to all* $t - sets$.
6. $t - totally\ free$ *if e belongs to no* $t - set$.

Motivated by the above definition, we define the following

Definition 4.2. *Let e be any element of the graph G. Then the element e is said to be*

1. $\gamma_{\delta_{max}} - critical$ *if* $\gamma_{\delta_{max}}(G - e) \neq \gamma_{\delta_{max}}(G)$.
2. $\gamma^+_{\delta_{max}} - critical$ *if* $\gamma_{\delta_{max}}(G - e) > \gamma_{\delta_{max}}(G)$.
3. $\gamma^-_{\delta_{max}} - critical$ *if* $\gamma_{\delta_{max}}(G - e) < \gamma_{\delta_{max}}(G)$
4. $\gamma_{\delta_{max}} - redundant$ *if* $\gamma_{\delta_{max}}(G - e) = \gamma_{\delta_{max}}(G)$.
5. $\gamma_{\delta_{max}} - free$ *if e belongs to some* $\gamma_{\delta_{max}} - set$ *but not to all* $\gamma_{\delta_{max}} - sets$.
6. $\gamma_{\delta_{max}} - fixed$ *if e belongs to every* $\gamma_{\delta_{max}} - sets$
7. $\gamma_{\delta_{max}} - totally\ free$ *if e belongs to no* $\gamma_{\delta_{max}} - set$.

Theorem 4.1. Every element of a regular graph G is $\gamma^-_{\delta_{max}} - critical$.

Proof. Note that removal of any edge or any vertex from a regular graph G results in graph G' with $\delta(G') = \delta(G) - 1$. Hence G' contains at least two vertices, say u and v, of degree $\delta(G) - 1$. Then the subgraphs $\langle V - \{u\} \rangle$ or $\langle V - \{v\} \rangle$ will form a maximin degree dominating set of G'. Hence $\gamma_{\delta_{max}}(G') \leq |V| - 1 < \gamma_{\delta_{max}}(G)$. This proves the result. □

Theorem 4.2. Every edge of a star graph is $\gamma_{\delta_{max}} - redundant$.

Proof. Let e be any edge of the star graph $K_{1,n}$. Then the removal of e from $K_{1,n}$ results in a graph, $K_{1,n} - e = K_{1,n-1} \cup K_1$. Then $\gamma_{\delta_{max}}(K_{1,n} - e) = 2 = \gamma_{\delta_{max}}(K_{1,n})$. □

Theorem 4.3. Let G be a graph of order n such that $\gamma_{\delta_{max}}(G) < n$. If an edge $e = uv$ of G is $\gamma^+_{\delta_{max}} - critical$, then for every $\gamma_{\delta_{max}} - set\ D$, any one of the following two conditions hold.

a. $u \in D, v \in V - D$ implies $N(v) \cap D = \{u\}$.
b. $u, v \in D$.

Proof. Suppose $e = uv$ is a $\gamma^+_{\delta_{max}} - critical$ edge of the graph G. Let us assume that none of the two conditions is true for e. Then there exists a particular $\gamma_{\delta_{max}} - set$ D of G such that $u \in D, v \in V - D$ but $N(v) \cap D \neq \{u\}$. Since D is dominating set of G, we must have $|N(v) \cap D| \geq 2$. Thus v is vertex of $V - D$ which has at least two neighbors in D and hence removal of the edge e does not affect the minimum degree of the subgraph $\langle D \rangle$ and domination property of D. This is a contradiction. □

Corollary 4.3.1. For any graph G, suppose there exists a $\gamma_{\delta_{max}} - set\ D$ such that $e = uv$ is an edge of G with $u \in D, v \in V - D$ and $|N(v) \cap D| \geq 2$ then the edge e is $\gamma_{\delta_{max}} - redundant$ edge of G. □

Theorem 4.4. Let $e = uv$ be an edge of the graph G. If $u, v \in V - D$ then the edge e is $\gamma_{\delta_{max}} - redundant$.

Proof. The removal of the edge e does not affect the minimum degree of D and the domination property of D. □

Theorem 4.5. A $\gamma_{\delta_{max}} - totally\ free$ vertex v of a graph G is $\gamma_{\delta_{max}} - critical$ if and only if $V(G - v) - D$ contains a set A of vertices with $deg_{G-v}(u) \geq \delta(\langle D \rangle)$ for all $u \in A$, which are adjacent to a set $D' \subseteq D$, where D' is a dominating set of $G - v$ and $|D'| \neq |D| - |A|$.

Proof: Suppose v is a $\gamma_{\delta_{max}} - totally\ free$ vertex of G which is also $\gamma_{\delta_{max}} - critical.$ Suppose $deg_{G-v}(u) < \delta(\langle D \rangle)$ for all $u \in V(G - v) - D$. Then induced subgraph of any dominating set of $G - v$ will not have minimum degree greater than $\delta(\langle D \rangle)$. Also since v is a $\gamma_{\delta_{max}} - totally\ free$ vertex of G, removal of v from G will not affect the minimum degree of $\langle D \rangle$. Hence $\gamma_{\delta_{max}}(G - v) = |D| = \gamma_{\delta_{max}}(G)$. This is a contradiction to the fact that v is $\gamma_{\delta_{max}} - critical.$ Hence $V(G - v) - D$ contains few vertices of degree greater than or equal to $\delta(\langle D \rangle).$ Let $B = \{u \in V(G - v) - D \mid deg_{G-v}(u) \geq \delta(\langle D \rangle)\}$. Since v is $\gamma_{\delta_{max}} - totally\ free$ vertex of G, $v \notin D$ for any $\gamma_{\delta_{max}} - set\ D$ of G and removal of v form G does not affect the minimum degree of any $\gamma_{\delta_{max}} - set$ of G. Let $D' \subseteq D$ be a dominating set of $G - v$. Suppose $A \subseteq B$ be the set of vertices which are adjacent to all the vertices of D'. Then $A \cup D'$ is a $\gamma_{\delta_{max}} - set$ of $G - v.$ If $|D'| = |D| - |A|$ then

$$\gamma_{\delta_{\max}}(G - v) = |A \cup D'| = |A| + |D'| \neq |D| = \gamma_{\delta_{\max}}(G)$$

This is a contradiction to the fact that v is $\gamma_{\delta_{max}} - critical.$ Hence $|D'| \neq |D| - |A|$.

Conversely suppose v is a $\gamma_{\delta_{max}} - totally\ free$ vertex of G. Let $D' \subseteq D$ be a dominating set of $G - v$ and $V(G - v) - D$ contains a set A of vertices with $deg_{G-v}(u) \geq \delta(\langle D \rangle)$ for all $u \in A$. Suppose every vertex of A is adjacent to each vertex of D' and $|D'| \neq |D| - |A|$. Then $A \cup D'$ forms a maximin degree dominating set of $G - v$ and also

$$\gamma_{\delta_{\max}}(G - v) = |A \cup D'| = |A| + |D'| \neq |D| = \gamma_{\delta_{\max}}(G)$$

Thus v is $\gamma_{\delta_{max}} - critical.$ □

References

[1] Allan, R. B., Laskar, Renu, and Hedetniemi, Stephen (1984), A note on total domination. DISCRETE MATHEMATICS, Vol. 49, pp. 7–13.
[2] Cockyne, E.J., Dawes, R.M., and Hedetniemi, S.T. (1980), Total domination in graphs, NETWORKS, Vol. 10, pp. 211–219.
[3] Chen Xue Gang, Sun Liang, and De-Xiang Ma, (2004), Connected domination critical graphs, APPLIED MATHEMATICS LETTERS, Vol. 17, pp. 503–507.
[4] Harary, F (1972), Graph Theory. Addison Wesley, Academic Press.
[5] Haynes, T.W, Hedetniemi, S.T, and Slater, P.J, (1999) Fundamentals of domination in graphs, Marcel Dekker Inc., N.
[6] Sampathkumar, E. and Prabha S. Neeralagi (1992), Domination and neighbourhood critical, fixed, free and totally free points, SANKHYÃ: THE INDIAN JOURNAL OF STATISTICS, Vol. 54, pp. 403–407.
[7] Walikar, H.B, and Acharya, B.D (1979), Domination critical graphs. NATIONAL ACADEMY SCIENCE LETTERS, INDIA, Vol. 2, pp. 70–72.
[8] West, D. B, (2003), Introduction to Graph Theory. Prentice Hall of India, New Delhi.

Figure 1:

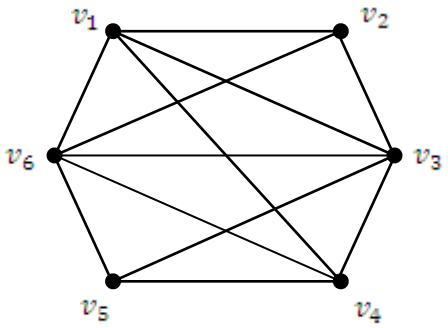


Fig. 1

2nd International Engineering Symposium - IES 2012
(KU-MU-NITK-HCMCUT Joint Symposium) March 5-7, 2012, Kumamoto University, Japan

Initial e-learning pilot system for secondary educational institutions in Tuvalu

Atufenua Maui [1] **Tony Kwato'o[2]** **Royyana M. Ijtihadia[1]**
Ronald Vetter[3] **Yoshifumi Chisaki[1]** and **Tsuyoshi Usagawa[1]**

1 *Graduate School of Science and Technology, Kumamoto University, Kurokami, 2-39-1, Kumamoto 860-8555, Japan. e-mail:maui@hicc.cs.kumamoto-u.ac.jp; royyana@hicc.cs.kumamoto-u.ac.jp;chisaki@cs.kumamoto-u.ac.jp; tuie@cs.kumamoto-u.ac.jp*
2 *Motufoua Secondary School, Vaitupu Island, Tuvalu Ministry of Education. email:tontonsekete@gmail.com*
3 *Kirwan Primary School, Townsville, Queensland, Australia. email:rvett1@eq.edu.au*

Abstract: This study presents results of an initial e-learning pilot system based on an open source Learning Management System (LMS), the Moodle 2.0, within a secondary school in Tuvalu. The recent innovations of e-learning and Information and Communication Technologies (ICTs) in the classroom have been enthusiastically met by students, teachers and administrators. The performance of students who participated in activities designed for Computer Studies and the data collected from questionnaires and surveys confirm the system's potential for improving student skills in the use of technology and their motivation towards study. This includes the potential to bridge the wide gap Tuvaluan students previously faced when entering tertiary level of education outside Tuvalu, one of the world's Least Developed Countries (LDC).

Keywords*: e-learning pilot system, Learning Management System (LMS), Secondary School, Tuvalu, Computer Studies.*

Introduction

E-learning or electronic learning has been defined in many different ways. In general e-learning is used to describe "instructional content or learning experience delivered or enabled by electronic technology," Chorng, Jung, and Yi (2004). In this case it refers to a learning process by the support of computer technology and a web based environment.

The Advisory committee for Online Learning (2001) clearly highlighted that e-learning is not a substitute for a strong relationships between teachers and learners. Rather, it can and should use to nourish, transform and enrich these relationships and promote a more active and student centered learning. Tuvalu, as one of the world's LDC, struggles to keep up with the changes provided by the rapid increase in use of information technology in education. The mode of subject delivery in schools is face to face in class with a teacher centered style.

A few crucial concern areas that the proposal pilot system was taking into consideration were with the lack of skilled man-power, the geographical remote scattered of the islands with a mean average distance of 135.8 Kilometres between the islands, and the available limited bandwidth.

Information's provided in the MoodleRoom website (2011) describes that the Moodle was the world's most used LMS amongst 300 million users around the world, which gave away the choice of trusting it once more for use as the LMS here. Moodle has many great advantages including the most important ones of no costing and easy installation.

Currently a more recent version of Moodle, the Moodle 2.0 which has very simple and interesting navigation

functions available, which is more suited to the needs of Tuvalu with their shortage of skilled manpower.

An effort to address this skilled manpower shortage was made by offering workshops to students and teachers. During these sessions their IT skills were upgraded so that they gained greater knowledge and confidence in their ability to embrace e-learning in Tuvalu. Unfortunately, a problem that was not as easy to address was that of the availability of electricity. Not having a consistent 24 hour electricity supply remained another obstacle.

The Tuvalu islands are scattered over an area of 28.5 square kilometres so gaining access to the internet is by satellite. Each island has a satellite dish in order to communicate. With the current available band width of 512kbps uplink and 1.5Mbps with more than 900 subscribers, it is obviously very slow. Therefore, providing local Moodle 2.0 servers installed in each islands institute will best serve the students for learning.

Meanwhile, many teachers and students have shown an enthusiastic interest in the e-learning system during the pilot initial stages of its implementation. Student confidence and motivation towards their studies have increased noticeably with their recent improvement in technology skills. The current innovations and proposals in relation to e-learning will greatly assist the Education Department's plans to introduce ICTs into education in an attempt to stay abreast with the rest of the world and the potential to bridge the wide gap Tuvaluan students previously faced when entering tertiary level of education inside/outside Tuvalu.

ICT in Primary Education institutions

In all the primary level of institution in Tuvalu, ICT has not yet fully introduce the extending where both students and teachers can enjoy and experience. Currently, in all the primary institutions of all the islands only about 3-5 computers and a printer has been deployed to each schools for teachers use only. These computers are to be used for typing examinations and preparing class work.

However in the capital island, Funafuti, a computer lab has been organized for also teachers only with about 8 PCs and a printer. This is the institute with the most number of student's enrolled with up to 938 according to the Tuvalu Biannual Statistical Report (2008).

ICT in secondary institutions

There are two main secondary institutes in Tuvalu. One is owned and run by the Tuvalu Church, and the other one by the Government.

The Church owned secondary institute, Fetuvalu High School (FHS) follows an England syllabus from Cambridge High in England. Motufoua Secondary School (MSS) the Government owned institute, uses the Tuvalu Ministry of Education and the Pacific Islands Education system syllabus. It was very fortunate and with great timing that ICT in secondary education has happened to begin extended to the students with the introducing of the Computer Studies (CS) subject for the Form 5 and Form 6 levels, age 16 and 17, respectively, for the first time ever in MSS history. Therefore, having implementing this e-learning within the school could be a great beginning for the CS subject history and hopefully other subjects too. Currently, there is only 1 computer laboratory with 20 PCs available for the students to use. Also another small computer room for the teacher's with only 4 available PCs at the moment.

However, the Church institute is yet to extend ICT to the students. It may be able to be that this pilot e-learning would help them witness and decide to extend ICT to students.

Augmented Foundation Program (AFP)

The AFP has been introduced by the government for students that finishes high school/senior high school students before entering tertiary level/universities. The Ministry of Education uses AFP as a filter to check eligibility for university entrance. In according to the Tuvalu Medium Term

Expenditure Framework for Education (2011) the AFP students perform poorly with a 51% completion rate. Many reasons have been raised about this issue, but the obvious one was that because of the lack of computer experiences and skills of students that causes most of them to neglected attending schools and completing their studies. In here that a digital divide gap between high school/senior high school students was witnessed.

Overview of the E-learning system implementation

The initial plan for this pilot e-learning system implementation was to have all the institutes in each islands running their own local Moodle 2.0 servers. Each school with the same level may have their similar content in their LMS. But in the main island capital a Master server with all the original contents and back ups of each updates. When dealing with updating contents, teachers need to work collaboratively between islands by the use of email via the internet connection and also with the available mail function of the Moodle 2.0 as shown in Fig. 1.

Initialization of the e-learning system

The introduction of the pilot e-learning system in Tuvalu was selected to be trialled in the government owned secondary school, MSS. One of the first decisions to be made was about the selection of subject and building the content. This was most important as a successful implementation of e-learning is dependent on successful delivery of contents by Khaled (2010).

Therefore, getting the content setup and run was simply done with this CS subject for the two forms/grade levels, form 5 and form 6 (age 16 and 17). The consistent on-going collaboration between the teacher responsible for the subject at MSS the second author, and the first author here in Kumamoto over the net by email was such that it fast-tracked the teachers skills and competency in the developing of the online content of the CS subject. Obviously there was an expectation that more subjects by other teachers could be implemented as soon as further training and workshops were completed. Therefore, the main aim of this first step was to equip the teachers and students with the skills to competently and confidently begin using the e-learning system. The one thing that is a must in according to debate results on strategies in implementing successful e-learning in LDCs, was the need for training of the teachers and students (Cavin, 2010).

Research Method

Study population items

- Students who enrolled in the CS subject, including the Form 5 & Form 6 students.
- Teachers participated in the workshop training of the Moodle 2.0
- And volunteer who participated in the online survey from the website prepared by Atufenua (2011). These volunteers are teachers, under graduate students and graduate students, the majorities are the Tuvaluan civil servants.

Sample size

- Form 5 students = 23
- Form 6 students = 22,
- Teachers = 19,
- And 59 volunteers in total from the online survey.

Sampling technique

- Convenient sampling technique was used for collecting data.

Data type

- The data are all primary data randomly collected from the LMS itself and from online survey.

Data collection tool

- Semi structured questionnaire & 5 Likert scale questionnaire.

Results and Discussions

CS Activities

The activities available and prepared for this subject were included:

- Lecture notes, Quizzes, Forums, live chat, email system, comments and finally a final survey to ask for their opinions

after this first term trial, from August 22 – November 25, 2011.

Figure 2 and 3 show the grades of students participated in the quizzes, with about 43% and 64% of the Form 5 and Form 6 students, respectively, from the total students didn't attempt all the quizzes in this study term.

Some of the main reasons are of the limited of PCs available for students to use. The lack off student's control behaviour for there were no strict policies in-line to control the students to do their works on this pilot system as compulsory and independently. Rather, they grouped up using one students account and try the quizzes and the lecture notes together for their needs of revisions and studies. This shows that some of the students' level of confidence using computers independently is still a bit low.

However, 16 of the Form 5 level students filled the end of the term survey and the results are expressed in Fig. 4.

Figure 4 shows a 100% of the students are "strongly agree" or "agree" that the LMS contributes to improving their computer skills and about 88% of them found that the system contributes a lot to their motivation and enjoyment of learning. Overall the result from the student's questionnaire is positive, which illustrates the potential influence of the LMS to the students.

The used of the comment box and forums to share their thoughts, questions and answers with each other was also well expressed in Tuvaluan in some of their comments in the comment box.

Teacher's workshop training

During this workshop training the main aim was to equip the teachers with the confidence level to competently master the Moodle 2.0 LMS.

The 19 participated teachers was given the questionnaire with the 5 Likert scale to identify their level of confidence operating the system.

In according to the pie graph in Fig. 5, 89% of the teachers are well in the "average" and the "above average" level with their confidence. However, only 11% of the staffs where feeling less confident after the training.

Online survey

This research also created a website along side with a survey to promote the pilot e-learning system in Tuvalu. Mostly the idea to see if the public/Tuvalu citizens have known about e-learning, and how strongly the support they give to the idea of having the e-learning system officially implemented in Tuvalu.

Therefore, the questionnaire adopts the similar e-learning knowledge scale in Khaled (2010).

According to the survey most of the respondents falls in the "good" knowledge of e-learning as shown in Fig. 6.

According to the survey well above 58% of the despondences are familiar with e-learning. This shows the awareness level of e-learning in the majority of respondents, which are from the Tuvalu government civil servants.

Therefore, e-learning is definitely a potential tool in the Tuvalu Government for future education system.

Conclusion

In conclusion, the results as the e-learning activities show that the pilot system was highly convincing and has been met with great enthusiasm from all areas of the education sector in Tuvalu.

The enormous advantages this e-learning system will bring to the teaching/learning process have been recognized.

The Education Department immediately requested to have an official e-learning program running in 2012 if possible. Even the teachers and students are making gestures that they look forward to having the system officially running soon.

Having the public and government civil servants support, the system will contribute in the expanding of the e-learning system knowledge to many areas in Tuvalu, in particularly in bridging the gap Tuvaluan students previously faced when entering tertiary

level of education outside Tuvalu. Also the improving of the infrastructures and having the right equipment in-place is most likely the area to consider addressing first.

Future works

- Monitoring the activities in the next academic term and compare with the current term.
- Updating of content between Moodle LMS, with the use of a synchronization technique in low band width.

References

[1] Atufenua, M. (2011). Survey, website: elearning.motufoua.info/Home_Page.html

[2] Cavin M. (2010, March 15). Strategies for Deploying eLearning in Developing Countries. Retrieved December 20, 2011, from eLearning Promise: https://edutechdebate.org/elearning-promise/strategies-for-deploying-elearning-in-developing-countries/

[3] Chorng S. Ong, Jung Y. Lai, and Yi S. Wang. Factors affecting engineers' acceptance of asynchronous e-learning systems in high-tech companies. Information & Management, 41 (6), 2004, pp. 795-804.

[4] Khaled Mahmud, E-learning for Tertiary Level Education in Least Developing Countries: Implementation Obstacles and Way Outs for Bangladesh, International Journal of Computer Theory and Electrical Engineering, Vol. 2, No.2 April, 2010, 1793-8201.

[5] MoodleRoom website, (2011). elearningstrategy Website:http:/www.moodlerooms.com/elearningstrategy/managed-open-source/moodle-core/

[6] The Advisory Committee for Online Learning. (2001). The e-learning, e-volution in Colleges and Universities. World Wide Web , 25.

[7] Tuvalu Biannual Statistical Report, (2008). Government of Tuvalu, Central Statistics Division Ministry of Finance & Economic Planning Vaiaku, Funafuti, TUVALU.

[8] Tuvalu Medium Term Expenditure Framework for Education and Health 2011-2014, Planning and Budget Department Ministry of Finance Government of Tuvalu Funafuti, September 2011

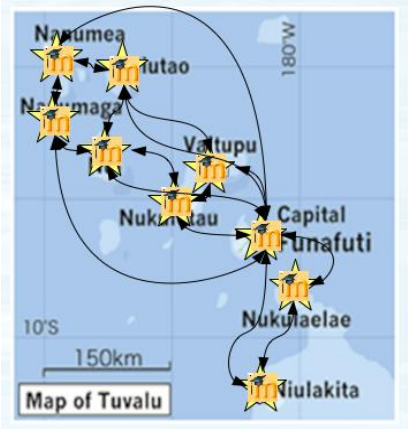


Fig. 1. This figure shows the future initial e-learning system within the Tuvalu islands, with all the Moodle 2.0 servers in each island's education institutes with the teachers' collaboration for their content updates representing by the lines connecting the Moodle 2.0 servers.

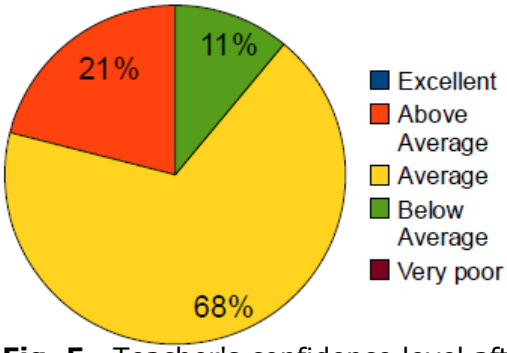


Fig. 5. Teacher's confidence level after about 4 hours of workshop training in operating the Moodle 2.0 system.

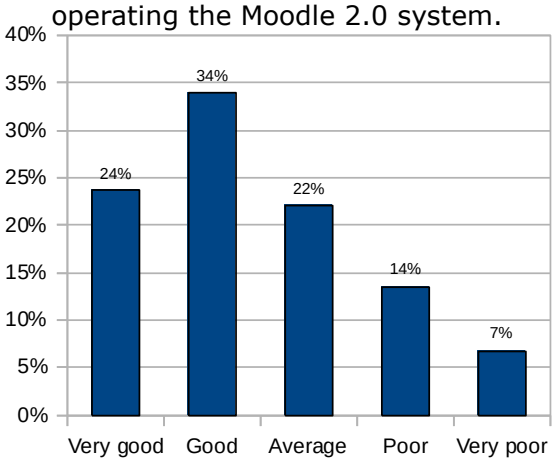


Fig. 6. Percentage of e-learning knowledge.

[redacted]	-	-	-	-	-
[redacted]	Sele Poutoa QUIZ on MS Word Processor	-	-	-	-
[redacted]	-	-	-	-	-
[redacted]	10.00	4.00	-	-	70.00
[redacted]	6.00	-	-	-	60.00
[redacted]	-	-	-	-	-
[redacted]	2.00	-	-	-	20.00
Overall average	6.31	6.43	4.50	-	60.13

Fig. 2. Form 5 quiz grades

[redacted]	-	-	-	-	-
[redacted]	-	-	-	-	-
[redacted]	-	7.50	5.56	6.00	6.25	63.26
[redacted]	8.00	10.00	8.89	10.00	8.75	91.28
[redacted]	-	-	-	-	-	-
[redacted]	-	-	-	-	-	-
[redacted]	-	-	-	-	-	-
[redacted]	-	-	-	-	-	-
Overall average	8.00	8.93	7.14	7.00	7.34	76.19

Fig. 3. Form 6 quiz grades

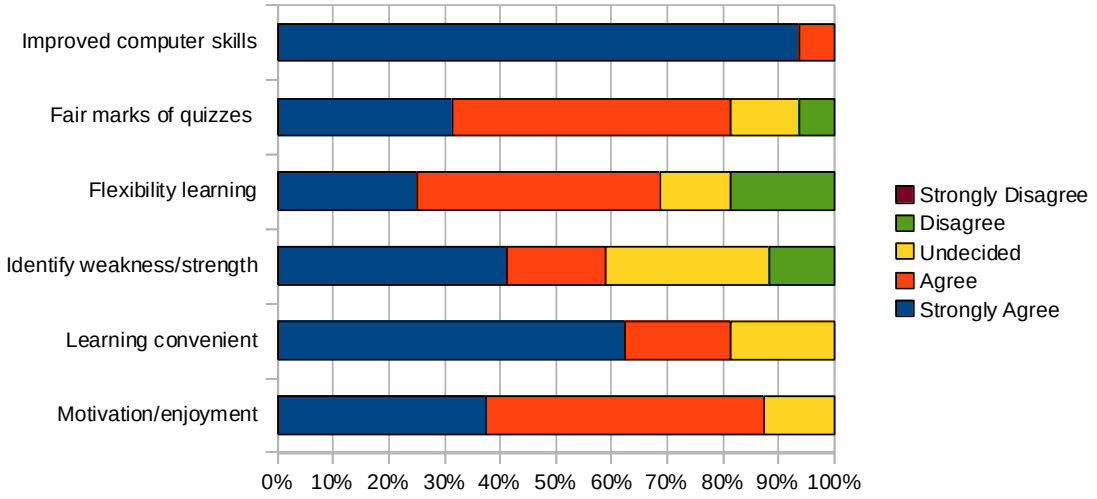


Fig. 4. Form 5 level responds to the survey.

2nd International Engineering Symposium - IES 2012
(KU-MU-NITK-HCMCUT Joint Symposium) March 5-7, 2012, Kumamoto University, Japan

20 µW, 500 kHz Continuous-Time Low-Pass Filter in 0.18 µm CMOS Process

Vasantha M.H. [1] **and Tonse Laxminidhi** [2]

1 *Department of Electronics and communication Engineering, National Institute of Technology Karnataka, Surathkal, P.O. Srinivasnagar, Mangalore- 575025, India. e-mail: vasant.iitm@gmail.com*
2 *Department of Electronics and communication Engineering, National Institute of Technology Karnataka, Surathkal, P.O. Srinivasnagar, Mangalore - 575025, India. e-mail: laxminidhi_t@yahoo.com*

Abstract: A low power continuous-time low-pass filer is presented for low voltage, low frequency applications. The filter has Cochlea architecture and is designed to have second order Butterworth response with a 3-dB frequency of 500 kHz. The transconductor, a basic building block of the filter, is chosen to have a bulk driven input stage which allows the filter to operate at DC supply as low as 0.5 V. Pseudo-differential operation is adopted for the filter in order to increase the dynamic range. Simulation results showed that the filter consume a power of 20 µW when operating at 0.5 V supply. Filter has 240 mV peak-to-peak input differential signal swing for 1% third harmonic distortion and dynamic range of 48 dB. Simulated Figure of Merit (FOM) is found to be 0.52 fJ, lowest among similar low voltage filters found in the literature.

Keywords*: bulk-driven, Cochlea filter, low-power, pseudo-differential, continuous-time.*

I. Introduction

Continuous technology feature size scaling has enabled denser and faster digital systems. In a typical System On Chip (SOC), analog and RF front end exist along with the digital circuit. Though the analog design occupies just about 5% to 10% of the total chip area, its functionality is quite important. There is need for efficient and reliable design approach to be followed in the field of analog integrated circuits.

Low-voltage supply operation is an important design issue in many integrated circuits due to low-power consumption requirements of today's major hand held and medical applications that are typically battery operated, S. Chatterjee. et al. (2007). Further the increasing use of mobile electronic products has motivated the industry towards reducing the power, especially for analog and mixed signal circuits. One of the important analog modules on a SOC is a filter performing tasks like anti aliasing, equalization etc. Filters used in biomedical applications such as ambulatory heart rate detectors and hearing aids demand small size and low power consumption. These analog parts are intended to be embedded parts of a complete on-chip analog front-end. In this paper, we focus on the design of bulk-driven low power continuous time filter.

Scaling dimensions in CMOS technology require proportional scaling in supply voltage as well. An important factor concerning analog circuit design is that the threshold voltage of transistors in future standard CMOS technologies does not scale with supply voltage and is projected to remain at about 0.25V, S. Thompson (1998). Though lower supply voltages result in lower power consumption in analog circuits for a given bias current, with reduced supply voltages, there is a need to maintain relatively larger threshold voltage in order to reduce subthreshold currents. To overcome this limitation the threshold voltage is reduced by forward biasing the body-to-source junction. As an outcome, the bulk driven

transconductance design technique is one such alternative used in low voltage analog circuit design. Bulk driven MOS transistor concept was proposed by A. Guzinski. et al. (1987). The filter presented in this paper uses the aforementioned technique in order to obtain sufficient voltage headroom at 0.5 V supply.

Transconductors (Gms)/OTAs are fundamental building blocks in analog signal processing applications and in particular Gm-C/OTA-C filters. Various architectures for simple OTA designs with single ended and differential input/output can be found in E. Sanchez. et al. (2000), Rosenfeld. et al. (2004), and Shen M.H. et al. (2010). It is found, in these designs, that power consumption is a major issue. There exits, always, a trade-off between power dissipation and frequency of operation, B. Razavi, (1998). The aim of minimizing the power consumption has put the restrictions on maximum speed that is achievable. This paper presents a low power filter with 500 kHz bandwidth, maximum among similar filters found in the literature while operating at 0.5 V. The rest of the paper is organized as follows. Section II and III discuss the implementation of the filter. In section IV the model of the filter is developed. In section V the simulation results and filter performance are given. Finally conclusion is drawn in section VI.

II. Filter architecture

The basic building block of any continuous time filter is the integrator. The integrator can be realized using Op-amps/G_{ms}/OTAs, capacitors and resistors. Popular topologies for the filters are active-RC and G_m-C. Because of the negative feedback in op-amp based RC filters, they have higher dynamic range when compared to Gm-C filters for a given power. However, the frequency of operation of active–RC filters is limited due to smaller gain bandwidth product of the op-amp. As the operating voltage scales down with scaling of dimensions in CMOS technology there is proportional reduction in operating frequency. One such active-RC fifth-order elliptic low-pass filter presented in S. Chatterjee. et al. (2005) operates at 0.5V, has a cut-off frequency of 135 kHz and dissipates 1.1mW in 0.18 µm CMOS process. Gm-C filters are capable of operating at higher frequencies but have lower dynamic range when compared to active-RC filters for a given power. The design of Gm-C low pass filters in 0.5 V regimes are not found in literature.

In this work we use Gm-C approach for the filter design with aim to push the bandwidth to 500 kHz but at the expense of dynamic range. Cochlea filter architecture shown in Fig. 1 is used to realize the second order low pass filter, I. Grech et al. (2003).

The transfer function of this circuit can be written as

$$\frac{V_{out\,(s)}}{V_{in\,(s)}} = \frac{g_{m1}g_{m2}/C_1C_2}{s^2 + \left[\frac{g_{m1}C_1 + g_{m2}C_1 - g_{m3}C_2}{C_1C_2}\right]s + \frac{g_{m1}g_{m2}}{C_1C_2}} \quad (1)$$

Where g_{m1}, g_{m2} and g_{m3} are the transconductance of the transcondcutors, C_1 and C_2 are the integrating capacitors. Comparing with the transfer function of the second order low pass prototype given in (2),

$$\frac{V_{out(s)}}{V_{in(s)}} = \frac{\omega_0^2}{s^2 + \left[\frac{\omega_0}{Q}\right]s + \omega_0^2} \quad (2)$$

the cut-off frequency ω_0 and the Quality factor Q can be written as shown in (3) and (4) respectively

$$\omega_0 = \sqrt{\frac{g_{m1}g_{m2}}{C_1C_2}} \quad (3)$$

$$Q = \frac{\sqrt{g_{m1}g_{m2}(C_1/C_2)}}{(g_{m1} - g_{m3}) + g_{m2}(C_1/C_2)} \quad (4)$$

It is clear from the expressions that the filter can be tuned for the desired frequency of operation ω_0 and quality factor Q by proper choice of transconductances and capacitances. If the transconductors, realized, are bulk-driven as is the case in this paper, the transcoductances g_m in (1), (3) and (4) will be replaced by bulk-transconductances (g_{mb}).

III. Design implementation

(a) Bulk driven Transconductor:

The bulk-driven transconductors of the Cochlea filter are realized using pseudo-differential amplifier with current-mirror load. The circuit diagram of the transconductor realized is shown in Fig. 2. In the figure, v_{ip} and v_{im} are the differential inputs and v_o is the single ended output. M1 and M2 are the PMOS input transistors and M3 and M4 form the NMOS current mirror load. The input common mode voltage of the transconductor is fixed at 0.25 V. Gates of M1 and M2 are biased to carry quiescent current of 2 µA. The total quiescent current of the differential amplifier is set at 4 µA and the input transistors are sized to have bulk transconductance 11 µS. Designed transconductor has a DC gain of 23.76 dB and UGB of 12 MHz. The transconductor consumes a power of 3 µW.

(b) Cochlea filter:

The Cochlea filter having Butterworth response is designed using the above mentioned transconductors for a cut-off frequency of 500kHz. Under ideal cinditions the values of integrating capacitors C_1 and C_2 along with the bulk transconductances decide the filter frequency response. But non-idealities of the transconductors such as parasitic capacitances, finite output and input resistances cause the frequency response to deviate from the Butterworth response. Filter response is brought back to near ideal by tuning integrating capacitors using a design centering method. Space mapping technique is found to be effective for design centering such filters, T. Laxminidhi, and S. Pavan (2007). This technique requires the entire filter to be modeled and the state space model is used in the present work.

IV. State space model of transconductor

The state space model of the filter is obtained with the help of small signal equivalent circuit of the filter. This, in turn, is derived by drawing the small signal equivalent circuit of the transconductor. Fig. 3 shows the small-signal equivalent circuit of the transconductor, where output is shorted to v_{im} terminal of the transconductor. Three state variables are required for modeling this transconductor. Source resistance R_s is included in the Fig.3 for completeness. The state space equations of the transconductor are given in equations (5) and (6).

$$\dot{x}(t) = Ax(t) + Bu(t) \tag{5}$$

$$y(t) = [0\ 0\ 1]x(t) \tag{6}$$

Where $x(t) = [v_1\ v_2\ v_{o1}]^T$ and $y(t)$ is output.

- *H*: is (3x3) matrix whose elements indicate the capacitive (or inductive) coupling among the state variables.
- *A*: is (3x3) matrix whose elements indicate the resistive coupling among the state variables.
- *B*: is (3x1) matrix whose elements indicate the resistive coupling of the state variables with the input.

The state space matrices of transconductor are written as follows.

$$H = \begin{bmatrix} C_{in}+C_{bd} & -C_{bd} & 0 \\ -C_{bd} & C_{mid}+C_{bd}+C_{gd} & -C_{gd} \\ 0 & -C_{gd} & C_{out}+C_{in}+C_{gd} \end{bmatrix} \tag{7}$$

$$A = \begin{bmatrix} -\dfrac{(R_s+R_{in})}{R_s R_{in}} & 0 & 0 \\ -g_{mb1} & -1/R_{mid} & 0 \\ -g_{m4} & 0 & -[g_{mb2}+1/R_{out}+1/R_{in}] \end{bmatrix} \tag{8}$$

$$B = \begin{bmatrix} -1/R_s \\ 0 \\ 0 \end{bmatrix} \tag{9}$$

The values of the transconductances, parasitic capacitances and resistances are obtained from DC operating point of the transconductor.

V. Results and discussion

The State space model of the filter is used for design centering the filter. The filter response is optimized for non-idealities of the transconductor by tuning integrating capacitors C_1 and C_2. The filter is tuned in the model space and the resulting optimized capacitor values are used in the

transistor level filter. The response of the tuned filter is shown in Fig. 4 and is compared with the ideal. The deviation in the filter response from the ideal is attributed to the effects of sub-threshold operation of the transistors which is, typically not taken care in small signal model of the transistors. Simulated filter has 240 mV peak-to-peak input differential signal swing for 1% third harmonic distortion

The performance of the designed filter is compared with some of the low voltage filters found in the literature and is tabulated in the Table I. The figure of merit (FOM) used for the comparison is computed using (11) T. Laxminidhi. et al. (2009). It is to be noted that all the filters with which the present work is compared have fully/pseudo differential architecture.

$$FOM = \frac{P_{diss}}{p\, Q_{\max} f_o\, DR^2} \qquad (11)$$

where P_{diss} is the power dissipation, p is the number of filter poles, $Q_{\max}$ is the maximum quality factor of the filter poles, f_o is the filter cut-off frequency and DR is the dynamic range. It can be seen that the designed filter has the lowest FOM compared to other filters found in the literature. A lower FOM indicates better power efficiency.

VI. Conclusion

A low pass 2nd order Butterworth filter using Cochlea architecture is designed for 500 kHz bandwidth with supply voltage of 0.5 V in 0.18 µm n-well standard CMOS technology. The designed pseudo-differential filter performance is compared with filters available in the literature and is found to be power efficient. From simulation results it is found that the designed filter has a dynamic range of 48 dB with power dissipation of 20 µW at 0.5 V supply voltage.

References

[1] A. Guzinski M, et al (1987), Body-driven Differential Amplifier for Application in Continuous-Time Active C-Filter, in Proceedings of the European Conference on Circuit Theory and Design–ECCTD 87, Paris, France. North Holland, pp. 315-319.

[2] B. Razavi, (1998), RF Microelectronics. Prentice Hall.

[3] E. Sanchez, et al (2000), CMOS transconductance Amplifiers, Architectures and Active Filters: A Tutorial, in IEE Proceedings Circuits, Devices and Systems, vol. 147, no. 1, IET, pp. 3–12.

[4] I. Grech, et al (2003), A 0.9 V Wide-Input-Range Bulk-Input CMOS OTA for Gm-C Filters, in Proceedings of the 10th IEEE International Conference on Electronics, Circuits and Systems, ICECS 2003, vol. 2, pp. 818–821.

[5] J. Carrillo, et al (2008), 1-V Continuously Tunable CMOS Bulk-Driven Transconductor for Gm-C Filters, in IEEE International Symposium on Circuits and Systems, ISCAS, pp. 896–899.

[6] J. Carrillo, et al (2010), On the Input Common-Mode Voltage Range of CMOS Bulk-Driven Input Stages, International Journal of Circuit Theory and Applications.

[7] J. Rosenfeld, et al (2004), A Bulk-Driven CMOS OTA with 68 dB DC Gain, in Proceedings of the 2004 11th IEEE International Conference on Electronics, Circuits and Systems, ICECS 2004, pp. 5–8.

[8] M. H. Shen, et al (2010), A 0.7-V CMOS operational transconductance amplifier with bulk-driven technique, International SoC Design Conference (ISOCC), pp. 392-395.

[9] S. Chatterjee, et al (2005), 0.5-V Analog Circuit Techniques and Their Application in OTA and Filter Design, IEEE Journal of Solid-State Circuits, vol. 40, no. 12, pp. 2373-2387.

[10] S. Chatterjee, et al (2007), Analog circuit design techniques at 0.5 V, Springer Verlag.

[11] S. Thompson, (1998), MOS scaling: Transistor Challenges for the 21st Century. MIT Microsystems Technology Laboratories.

[12] T. Laxminidhi and S. Pavan (2007), Efficient Design Centering of high-Frequency Integrated Continuous-Time Filters, IEEE Transactions on Circuits and Systems I: Regular Papers, vol. 54, no. 7, pp. 1481–1488,.

[13] T. Laxminidhi, et al (2009), Widely Programmable High-Frequency Active RC Filters in CMOS Technology, IEEE Transactions on Circuits and Systems I: Regular Papers, vol. 56, no. 2, pp. 327–336.

[14] X. Zhang, et al (2007), A novel CMOS OTA Based on Body-Driven MOSFETs and its Applications in OTA-C Filters, IEEE Transactions on Circuits and Systems I: Regular Papers, vol. 54, no. 6, pp. 1204–1212.

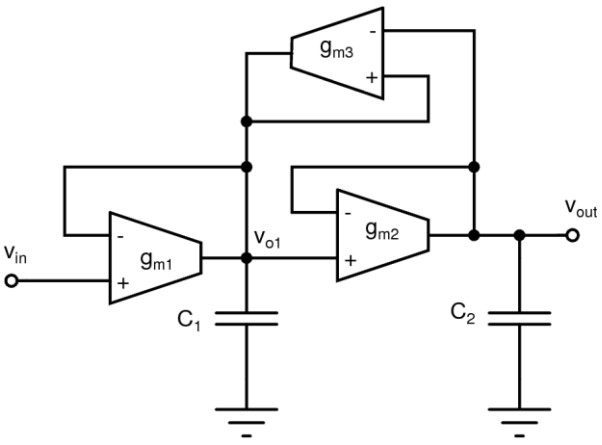


Fig. 1 Cochlea filter Architecture

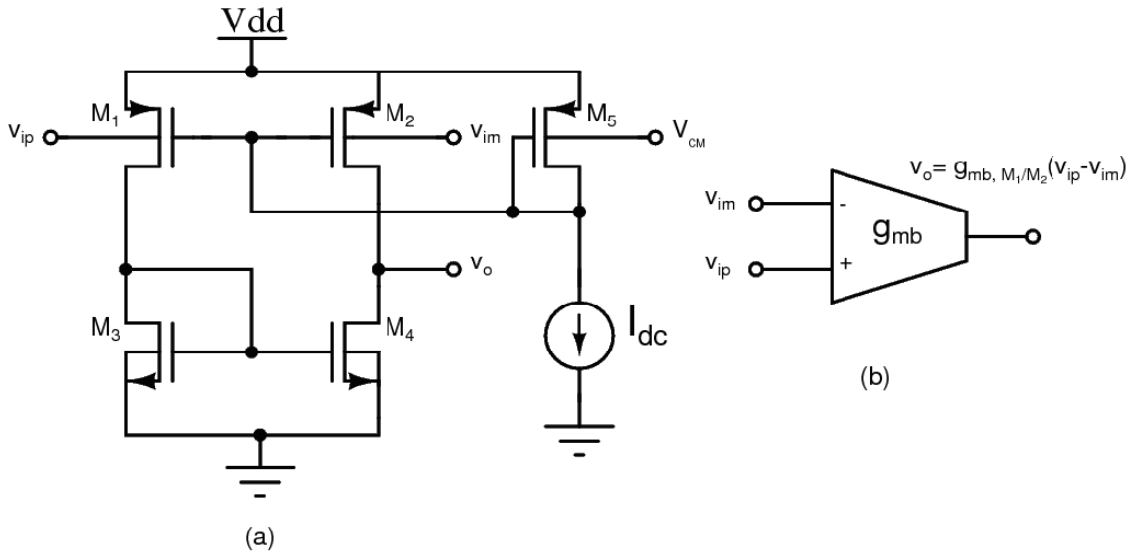


Fig. 2 Bulk driven Transconductor (a) Schematic (b) Symbol

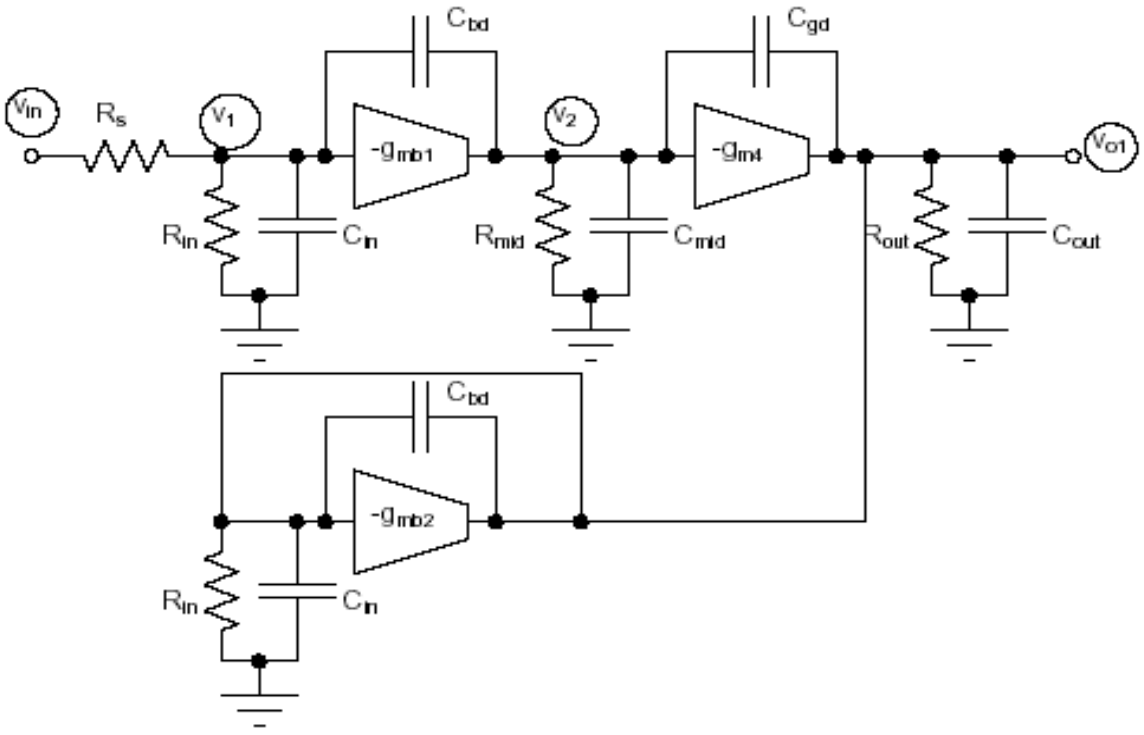


Fig. 3 Small signal equivalent circuit of the bulk driven transconductor in unity feedback configuration

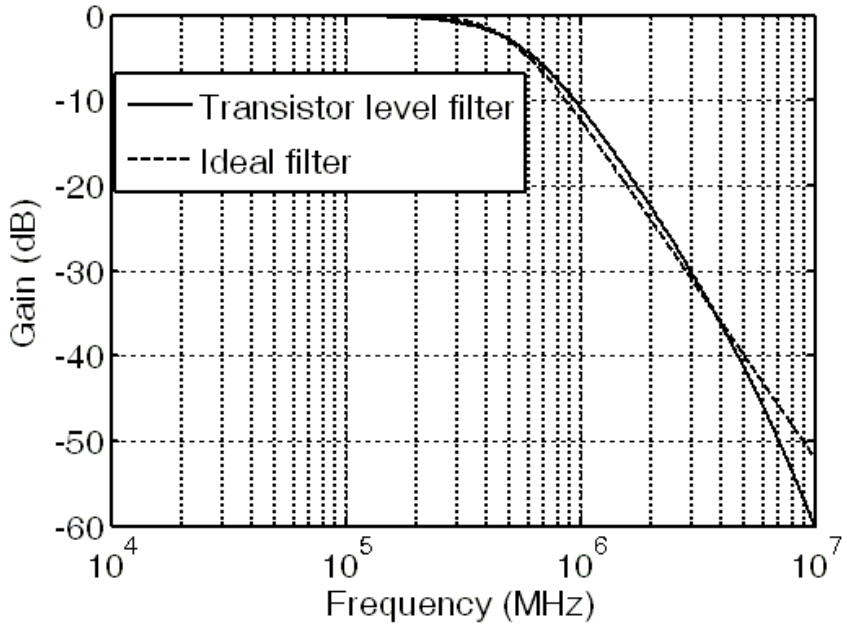


Fig. 4 Magnitude response of transistor level filter and ideal Butterworth filter

Table I Comparison with available filters in literature

Reference	Bandwidth [KHz]	Order	Supply Voltage [V]	Power [µW]	Q_{max}	Dynamic range@ 1%THD [dB]	Topology	Tech-nology	FOM [fJ]
S.Chatterjee. et al. (2005)	135	5	0.5	1100	6.2	56.6	Active-RC	0.18	0.58
X. Zhang et al.(2007)	1050	3	1.8	4070	1.99	45	Gm-C	0.18	20.53
J. Carrillo. et al. (2008)	17.5	2	1	45	0.89	63.71	Gm-C	0.35	0.62
J. Carrillo. et al. (2010)	10	2	1.5	648	0.707	62.6	Gm-C	0.35	25.18
Present work	500	2	0.5	18	0.707	48	Gm-C	0.18	0.52

2nd International Engineering Symposium - IES 2012
(KU-MU-NITK-HCMCUT Joint Symposium) March 5-7, 2012, Kumamoto University, Japan

Preserving Privacy in Data Streams Query Processing on Synopses

An Ngoc Thien NGUYEN[1] Tran Khanh DANG[1] Nam THOAI[1] Ngoc Hieu DUONG[1]

1 *Faculty of Computer Science and Engineering,*
HCMC University of Technology, VNUHCM,
268 Ly Thuong Kiet Street, District 10, Ho Chi Minh City, Vietnam.
e-mail: {annguyen, khanh, nam, dnhieu}@cse.hcmut.edu.vn

Abstract: The rapid development of sensor technologies, the broadening of information networks and the evolution of e-commerce applications are motivations for the prominent growth of data stream applications. In a similar way to other kinds of information systems, it is essential to protect privacy for owners of information streams. However, requirements of huge amounts of time and resources for query processing in real-time are challenging issues for privacy preserving solutions in data streams. In this paper, we present a modified method integrating a variable reservoir sampling technique with a k-anonymizing algorithm to protect privacy on data streams. Our suggestion provides anonymized data to give approximate query answers which are possible to accept and as good as the exact ones in many contexts.

Keywords*: Data Stream, Privacy Preserving, Query Processing, Synopsis, Sampling, Anonymity*

1. Introduction

The fleet appearance and development of modern technologies such as sensors with great sensitive degree, high-speed networks have brought about the explosion of data in recent years. Data Stream, a new outstanding class of applications with diverse special requirements, has come out to tackle the need of working on massive and evolving data volume such as IP network management, financial analysis, real-time decision support systems and telephone fraud detection, etc.

[Golab and Özsu (2003)] gave a formal definition of data stream: "A data stream is a real-time, continuous, ordered (implicitly by arrival time or explicitly by timestamp) sequence of items. It is impossible to control the order in which items arrive, nor is it feasible to locally store a stream in its entirety." Because of these attributes, stream processing always necessitates vast quantities of time and resources, especially online analyses in real-time. In addition, some streams have changes in their nature over time (This is also referred to as data stream evolution). To solve these problems, researchers propose different query processing techniques: filtering, punctuations, windowing, synopses [Maier, D. et al. (2005)]. Each of them has various features in accord with particular demands. Notwithstanding, synopsis structures have got special attention due to their cost-effectiveness and good query results in approximate query processing.

Another important issue of streaming data is privacy preservation. It is abundantly clear for data streams to contain too much private information of individuals, which can damage them when being revealed. These problems concerning privacy of customers also become more and more considered by both civilians and government organizations [European Parliament and of the Council (2002)]. There are a considerable number of researchers on these problems. Nevertheless, they have not made use of

particular features of data streams in their algorithms. They usually make the data satisfy requirements of k-anonymity and output it for a data mining engine to process.

In this paper, we want to introduce a new approach to this interesting problem that is utilizing advantages of employing synopsis constructions in the stage of query processing to improve the required time and memory while maintaining the quality of cloaking. In other words, our modified method integrates a dynamically sampling technique with a k-anonymizing algorithm to protect privacy for the data stream.

The remained of this paper is organized as follows. In the next section, we review several kinds of synopses and give an explanation for what we have chosen; section 3 gives a look on reservoir based sampling methods; section 4 talks about an anonymizing algorithm (SKY); section 5 is our proposal and the last section gives a conclusion and our future works.

2. Overview of Synopses

As mentioned in the introduction, there are many different query processing techniques on data streams to cope with requirements of time and resources. Among existing techniques, synopses get attention specially based upon interesting characteristics.

Synopses can be considered as compact representations of data streams that summarize the stream input, are maintained online at stream input rates in much less space than the full data and can be used to provide approximate answers to some class of user queries [Maier, D. et al. (2005)]. Some examples of applications using these kinds of structures are as follows: approximate query estimation, approximate join estimation, computing aggregates, data mining, etc.

[Aggarwal, C. and Yu, P. (2007)] classifies synopsis constructions into five groups:

- Sampling methods: Methods of this group are usually the simplest synopsis techniques for data streams. The basic idea is using some way to sample data in a biased or unbiased manner. Its main advantage is keeping the original form of data. As a result of that, it is relatively easy to apply for a broad range of domains with only a little change. Especially, they are usually preferred choices for multi-dimensional streams.
- Histograms: Histogram based methods are widely used for static data sets. Basically, we need to divide the data along some attribute into a set of ranges and retain the count for each bucket. The space requirement is defined by the number of buckets in the histogram. Hence, essential issues of this kind are of how to design buckets.
- Wavelets: Wavelets have been conventional methods used in a wide area of image and query processing. They give a mathematical tool for the hierarchical decomposition of functions. *Haar Wavelet* is the most popular type, which creates a decomposition of data characteristics into a compact summary including wavelet functions and basic functions [Garofalakis, M. (2009)].
- Sketches: Sketch based methods can be considered a randomized version of wavelet techniques, and are among the most space-efficient of all methods. Sketches are designed in order that the update caused by each new item is handled in the same way, almost independent of the current status of the summary. They are, therefore, especially appropriate for processing data streams and easy for parallelizing. Basically, sketches are data structures which can be represented as a linear transform of the input. In other words, if we model a relation as defining a vector or matrix, then the sketch is a product of a fixed sketch matrix and the data vector. These constructions are hard to understand intuitively and consequently necessitate defining an operation to extract the desired query results from the sketch (the division operation). Generally, this group of methods is often difficult to apply for multi-dimensional case [Cormode, G.].

- Micro-cluster based summarization: This method uses a temporal extension of *cluster feature vector* maintained online in real-time to store statistics information of micro-clusters and saves them as *snapshots* over *pyramidal time frame*. Those snapshots of micro-clusters are temporal concise summaries for answering queries in offline stages. This method is very effective for data streams having fast evolution [Aggarwal, C. et al. (2007)].

The purpose of this paper is to give a solution for privacy preservation on data streams. Data streams that need protection usually have multi-dimension (with many quasi-identifiers and sensitive columns) and are used for a wide range of queries. Accordingly, synopsis construction based upon sampling methods is the best choice for our goal. We will discuss sampling methods in more detail in the next section.

3. Sampling with Reservoir

The most famous sampling method on dynamic streams is reservoir based one. This method was presented firstly in [Vitter, J. S. (1985)] as an unbiased random way of sampling on evolving streams. To acquire an equal probability for being sampled of every data point, the author keeps a reservoir with size *n* being updated dynamically depending on changes of the stream input over time. At the very early stage, the reservoir is filled up with *n* first items of the stream. Subsequently, whenever a new one arrives, it is inserted into the reservoir with probability $n / (t + 1)$. In order to make room for the new item, any of the current ones in the reservoir are removed with equal probability. We can compute the probability at which each item of the stream after processing (t+1) ones is sampled as below:

$$n/(t+1).[n/t\,.\,(n-1)/n] + [1–n/(t+1)].(n/t) = n/(t+1)$$

For further details, you can see in [Vitter, J. S. (1985)].

Based on the above method, many other reservoir based algorithms have been suggested with various improvements such as Concise Sampling, Reservoir Sampling on a Moving Window, Min-Wise Sampling and Biased Reservoir Sampling.

All streams requiring privacy preservation are relevant to human beings who have changes gradually in trends, characteristics (e.g. distribution) and consequently make the stream evolve with time. In such cases, a temporal biased sampling way is better than an unbiased random way in providing good approximate answers. Because of that reason, we choose Biased Reservoir Sampling method in [Aggarwal, C. (2006)] to lay the foundation for our approach.

The paper [Aggarwal, C. (2006)] has proposed two algorithms for sampling in a biased way: *fixed reservoir sampling* and *variable reservoir sampling*. In our approach, we use *variable reservoir sampling* to make use of the capacity of the reservoir owing to the law of large numbers. The following algorithm presents the main idea of sampling in that paper:

> ***Algorithm 1****. We start off with an empty reservoir with capacity $n = p_{in}/\lambda$, and use the following replacement policy to gradually fill up the reservoir. Let us assume that at the time of (just before) the arrival of the t-th point, the fraction of the reservoir filled is $F(t) \in [0,1]$. When the (t+1)-th point arrives, we add it to the reservoir with insertion probability p_{in}. However, we do not necessarily delete one of the old points in the reservoir. We flip a coin with success probability F(t). In the event of a success, we randomly pick one of the points in the reservoir, and replace its position in the sample array by the incoming (t+1)-th point. In the event of a failure, we do not delete any of old points and simply add the (t + 1)-th point to the reservoir. In the latter case, the number of points in the reservoir (current sample size) increases by 1.* [Aggarwal, C. (2006)]

To have a variable reservoir, we adjust *Algorithm 1* as follows: let n_{max} be the total available space for the reservoir; start off with $p_{in} = 1$ and use *Algorithm 1* to add points to the reservoir (that means we "pretend" to have a fictitious reservoir with size equal $p_{in}/\lambda \geq n_{max}$); until n_{max} is reached, we decrease p_{in} by a factor of $(1 – 1/n_{max})$, eject a fraction of $1/n_{max}$ points

and continue the process of adding points according to *Algorithm 1*. We repeat adding points and reducing pin until $pin = n_{max} . \lambda$. As proved in the paper, sampled data points using the above variable reservoir satisfy the property that a temporal biased sample $S(t)$ at the time of arrival of the t-th point in the stream is defined as a sample such that the relative probability $p(r, t)$ of the r-th point belonging to the sample $S(t)$ (of size n) is proportional to $f(r, t) = e^{-\lambda(t-r)}$. Function $f(r, t)$ is the bias function for r-th point at the arrival of the t-th point. (For proving, please refer to [Aggarwal, C. (2006)]).

4. Anonymizing with k-anonymity

K-anonymity is a well-known technique in solving privacy problems. Its core idea is making each tuple in a dataset indistinguishable from at least k-1 other tuples. Recent techniques usually generalize data on attributes of quasi-identifiers to anonymize data and *Domain Generalization Hierarchies* (DGH for short) are visual structures to show this generalization (see Fig.1).

We opt for SKY [Li, J. et al. (2008)] thanks to its efficient running time and easiness in design. The key component of this algorithm is Specialization Tree (SP Tree) which is directed. We assume that each quasi-identifier attribute $q_i \in \{q_1,\ldots, q_m\}$ has a pre-defined DHG_i. Each node of SP tree is a vector $<v_1 \ldots v_m>$, of which v_i is drawn from the DHG_i. There is a directed edge from *u* to *v* in SP tree if:

- $\exists\, j \in 1,\ldots,m$ such that DHG_i contains the edge $v(q_j) \rightarrow u(q_j)$.
- For all other $i \in 1,\ldots,m$ and $i \neq j$, $v(q_i) = u(q_i)$.

SP tree and DGHs are constructed before SKY starts at the first time point. After that, when a new tuple t arrives, SKY finds the most specific generalization node g for it. If g is a work node (that means the number of tuples belonging to g is greater than or equal k), t is anonymized with g and output immediately. Otherwise, if the size of g's holding area is k after adding t, all tuples of g are anonymized with g and returned out and then g is marked as a work node. In the worst case, which means g still does not meet the k-anonymity property even after receiving t, tuples of g are stored temporarily in the buffer (see Fig.2 for full algorithm).

5. Anonymizing Algorithm using Biased Sampled Synopsis

As mentioned in previous sections, our goal is a proposal for preserving privacy by employing a dynamic reservoir based sampling method with a k-anonymizing algorithm. Specifically, our approach samples the stream input by the variable reservoir sampling method (described in *Algorithm 1*) and then anonymizes them by SKY. In words of one syllable, we construct and maintain an anonymized dynamic sample synopsis. Users' queries will be processed on that concise summary without disclosing sensitive information. Furthermore, properties of the biased reservoir ensure the freshness of the answers.

Observing Fig.3, we see a visual model for the presented process. We modify and add new components to the original abstract architecture for a data stream management system in [Golab, L. and Özsu, M. T. (2003)]. Firstly, the stream is sampled through the Sampling unit and anonymized by the Anonymizing unit before being inserted into Anonymized Sample Storage.

Before introducing details of our algorithm, we define a data structure containing an anonymized data point of the reservoir: *{t: tuple; g: node of SP tree to anonymize; i: index}*. As the maximum available space for the reservoir is n_{max}, i's have values from 0 to (n_{max} – 1). Moreover, we extend SP tree nodes to structures:*{g: label of node; c: count of points linked with this node; l: list of linked point indexes in the reservoir}*.

Each point in the reservoir may have one of two states, hidden or displayed. A point is only displayed after it is anonymized with some node of SP tree. Fig.4 shows our entire algorithm. *Algorithm 2* is a modified implementation of *Algorithm 1* at positions of procedures ADD and REMOVE.

This algorithm helps us to sample data points of the stream in a temporal biased way. Once being sampled, the point is added to the reservoir with the hidden status by default and linked to a node of SP tree. Depending on the current status of that node, the point is anonymized immediately or waits until the node archives k-anonymity condition. On the other hand, once being removed from the reservoir, a data point is processed safely by REMOVE procedure to remain the k-anonymity condition on the reservoir after dropping. If the SP tree node of the deleted point is violated after its removing, the other points will be processed by ADD procedure to anonymize again. The function PROCESS_DELTA is used to check whether a point waiting for being anonymized expires or not. If yes, then anonymizes it with the nearest more general parent node that is satisfying the k-anonymity.

6. Summary

In a nutshell, we suggest a new approach integrating advantages of synopses using sampling and k-anonymity algorithm SKY to construct and retain an anonymized temporal dynamic compact summary for query processing. This method not only helps to prevent information from revealing but also keeps approximate answers as good as possible over the evolving streams. For future work, we will implement this algorithm and make experiments on real-world datasets.

Acknowledgements

This research is partly supported by JICA via SUPREM-HCMUT project.

References

[1] Aggarwal, C. (2006), On Biased Reservoir Sampling in the Presence of Stream Evolution, Proc. 32nd International Conference on Very Large Database, pp. 607-618.
[2] Aggarwal, C. and Yu, P. (2007), A Survey of Synopsis Construction in Data Streams, Data Streams: Models and Algorithms, Springer US, pp. 169-207.
[3] Aggarwal, C. et al. (2007), On Clustering Massive Data Streams: A Summarization Paradigm, Data Streams: Models and Algorithms, Springer US, pp. 10-38.
[4] Cormode, G., Sketch Techniques for Approximate Query Processing, Foundations and Trends® Journal, Now Publishers, pp. 1-64.
[5] European Parliament and of the Council (2002), Directive 2002/58/EC of 12 July 2002 concerning the Processing of Personal Data and the Protection of Privacy in the Electronic Communications Sector, Official Journal L201, pp. 37-47.
[6] Garofalakis, M. (2009), Wavelets on Streams, Encyclopedia of Database Systems, Springer.
[7] Golab, L. and Özsu, M. T. (2003), Issues in Data Stream Management, ACM SIGMOD Rec., Vol. 32, No. 2, pp. 5-14.
[8] Li, J. et al. (2008), Anonymizing Streaming Data for Privacy Protection, Proc. IEEE 24th International Conference on Data Engineering, pp. 1367-1369.
[9] Maier, D. et al. (2005), Filtering, Punctuation, Windows and Synopses, Stream Data Management, Springer, pp. 35-58.
[10] Vitter, J. S. (1985), Random Sampling with a Reservoir, ACM Transactions on Mathematical Software, Vol. 11, No. 1, pp. 37–57.

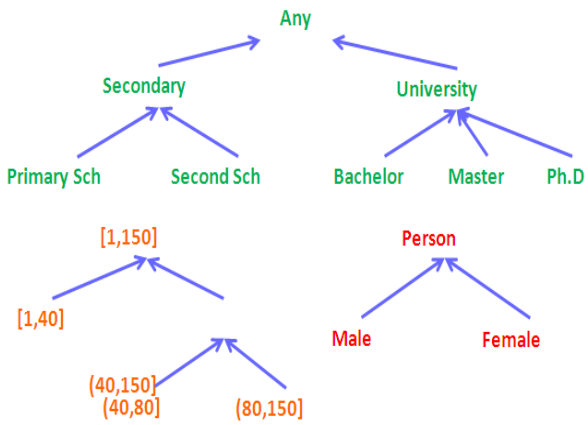


Fig.1 Examples of Domain Generalization Hierarchies

Algorithm SKY
Input: Stream S, specialization tree Sptree,
parameter k of k-anonymity, parameter δ of δ-constraint
Output: Anonymized tuples
1. WHILE (True)
2. Read a new tuple t from S;
3. Search Sptree from the root until reach a node g,
which is the most specific node that contains t;
4. IF (g is a work node)
5. Anonymize tuple t with g and ouput it;
6. ELSE
7. Insert t into g's buffer $FS(g)$;
8. IF($FS(g)$ satisfies k-anonymity)
9. Anonymize and output $FS(g)$ with g;
10. Label g as a work node;
11. Drop $FS(g)$;

Fig.2 SKY Algorithm

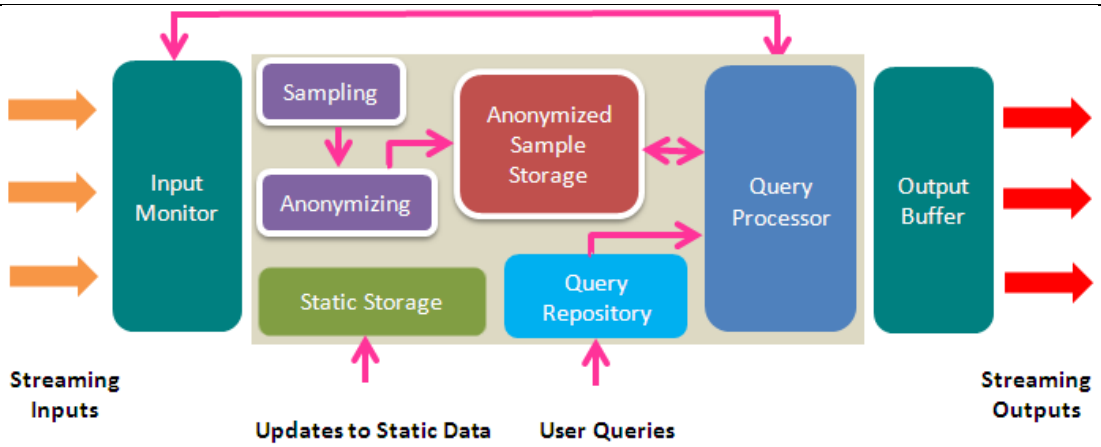


Fig.3 Modified Architecture for Anonymization

Algorithm 2. **Variable reservoir sampling**

Input: Stream **S**, **SP tree**, k-anonymity factor **k**, Reservoir size $\mathbf{n_{max}}$, Bias rate **λ**, Limiting time **δ**

```
1.  Set up SP tree, the reservoir R[n_max], k, δ
2.  p_in := 1;
3.  θ := n_max * λ;
4.  n_now := 0;
5.  While (NOT eof) Do
6.      t := READ_NEXT_ITEM(S);
7.      a := RANDOM(0,1);
8.      If (a ≤ p_in) Then
9.          b:=TRUNC((p_in/λ– 1)*RANDOM(0,1));
10.         If (b < n_now) Then
11.             REMOVE(b);
12.             ADD(b, t);
13.         Else
14.             If (n_now = n_max & p_in ≥ θ) Then
15.                 p_in := p_in * (1 – 1/n_max);
16.                 If (p_in < θ) Then
17.                     p_in := θ;
18.                 End If;
19.                 REMOVE(n_max – 1);
20.                 n_now := n_now – 1;
21.             End If
22.             n_now := n_now + 1;
23.             ADD(n_now – 1, t);
24.         End If;
25.     End If;
26. End While;
27. PROCESS_DELTA(δ);
```

Procedure 1. ADD(index i, item r)

```
1.  R[i].t := r;
2.  Search SP tree from the root until
    reach a node h, which is the most
    specific node that contains r;
3.  h.c := h.c + 1;
4.  ADD_TO_LIST(i, h.l);
5.  If (h.c ≥ k) Then
6.      ANONYMIZE(R[i].t, h.g);
7.      DISPLAY(R[i].t);
8.  Else If (h.c = k-1) Then
9.      For Each j in h.l Do
10.         ANONYMIZE(R[j].t, h.g);
11.         DISPLAY(R[j].t);
12.     End For;
13. End If;
```

Procedure 2. REMOVE(index i)

```
1.  If (R[i].t hidden || R[i].g.c ≥ k+1)
2.  Then
3.      R[i].g.c := R[i].g.c -1;
4.      REMOVE_OFF_LIST(i, R[i].g.l);
5.      HIDDEN(R[i].t);
6.  Else
7.      R[i].g.c := 0;
8.      For Each j in R[i].g.l Do
9.          HIDDEN(R[j].t);
10.         REMOVE_OFF_LIST
                (j, R[i].g.l);
11.         ADD(j, R[j].t);
14.     End For;
15. End If;
```

Fig.4 Anonymizing Algorithm using Biased Sampled Synopsis

2nd International Engineering Symposium - IES 2012
(KU-MU-NITK-HCMCUT Joint Symposium) March 5-7, 2012, Kumamoto University, Japan

Charging method for an electric vehicle using a computerized ultra fast charger at recharge stations in India

Hafeez Basha R[1], Raju A[2] and **Nikhil Prakash P[3]**

[1]Department of Electronics & Computer Engineering, K L University, Guntur District, Andhra Pradesh, INDIA Email: hafeezbasha@kluniversity.in, hafeezbasha@gmail.com
[2]Department of Applied Mechanics, National Institute of Technology (NIT-Karnataka) Surathkal, Post Srinivasnagar, Mangalore DK, Karnataka, INDIA Email: rajucits@gmail.com
[3] IP & Science Department, Thomson Reuters, Hitec City, Madhapur, Andhra Pradesh, INDIA Email: nikhilprakash.puntikoora@thomsonreuters.com

ABSTRACT: Electric transportation infrastructure is gaining a renewed interest over gasoline powered vehicles due to the non-renewable nature of the fuel, rise in petroleum prices and environmental impacts like smoke and sound pollution. There is a rise in average monthly sales in India according to Ministry of New and Renewable Energy, due to which the Government has initiated to increase the number of electric recharge stations by installing facilities at all the existing petroleum and gas stations in India. This initiative would be fruitful only when the users can get their electric vehicles recharged within minutes at recharge stations. But the most commonly-heard criticisms of electric vehicles are that their batteries take too long to recharge though they store a large amount of energy. This paper presents a charging method using a computerized ultra fast charger which employs a genetic algorithm trained generalized regression neural network which can be set-up at recharge stations. Hardware realizations of the method are also discussed that significantly reduces the charging time. Experimental results reveal that the ultrafast charger is efficient and suitable for recharge station, and it scarcely deteriorates the battery energy storage capability when compared with the conventional charger.

KEYWORDS: Battery charger, ultra fast charging, GRNN controller, RISC

INTRODUCTION:

Fossil fuels like coal, oil, petrol, etc are non-renewable sources of energy that are within human time-scales and take many years for the nature to produce it again. The IC engine vehicles are dependent on such exhaustible fuels which may perish in the years to come. Due to huge demand for oil, the petroleum prices are increasing.

Table-1 Rise in Petrol Prices in India

Month & Year	**Price** (Indian Rupees)
November 2011	73
June 2011	67
January 2011	62
August 2010	56
October 2009	51
May 2009	47
December 2008	44

In spite of endeavor of many years on and improvement of gasoline engine based vehicles, the environmental pollution due to exhaust gases still exist. The electric vehicles produce no exhaust gas, and are silent, thus being suitable for the travelling of vehicle in an area which should be free from noise or in an environment protection area. But the common conceptions of electric vehicles driven by electrically powered motors are that they run slowly, limited battery capacity which also takes too long to get recharged and suitable for short distance transport. However progress in modern technologies has accomplished a substantial increase in the speed of the electric vehicles and performance of secondary batteries such as lead acid storage batteries, nickel-metal hydride storage batteries and lithium-ion secondary batteries have been improved in these days.

Bangalore based "Reva Electric Car Company" (now Mahindra Reva Electric Vehicles Private Limited) was the first company to introduce an electric vehicle worldwide. It has recorded a three-fold rise in average monthly sales in the year 2011, boosted by incentives announced by the Ministry of New and Renewable Energy. The Government of India has initiated to increase the number of electric recharge stations by installing facilities at all the existing petroleum and gas stations in India. The charging stations are also installed at convenient places throughout the country across Delhi and Chandigarh at parking lots, taxi stands, driveways and garages. This initiative would be fruitful only when the users can get their electric vehicles recharged within minutes at recharge stations.

Electrical Vehicle Charging Station:

It is an electric recharge point which is connected to an electrical grid and supplies electric energy to recharge electric vehicles. The battery capacity of a fully electric vehicle is 20kWh which provides electrical autonomy of 150 km. In an average the electrical vehicle may have to be recharged every three days. The time taken for charging by different configurations of power supply is shown in Table-1.

Table-2 Charging time with respect to power

Power in Kilo Watts	Voltage in Volts	Current in Amps	Phase	Electricity Kind	Charging time
3.3	230	14	Single	AC	6-8 hours
10	400	16	Three	AC	2-3 hours
7	230	32	Single	AC	3-4 hours
24	400	32	Three	AC	1-2 hours
43	400	63	Three	AC	20-30 mins
50	400	125	-	DC	20-30 mins

According to Table-2 the charging station providing 3.3 kW of power will take more than eight hours to recharge a secondary battery. This type of charging is commonly used for recharging electric vehicles at home or work, but not suitable for refueling in the middle of a trip. High power charging stations which require industrial-type electric service can reduce the battery charging time significantly. DC fast rate also called as level-3 charging stations can supply about 62.5 kW where the battery can be recharged in just 30 mins.

In this paper a method of charging a battery of an electric vehicle is discussed using computerized Ultra-fast charger which can recharge a secondary battery in 17 minutes 30 seconds. The method involves supply of current pulses, measuring the off-load voltage of the battery between current pulses, determining voltage drop during second pulse of current, and stopping the supply of current pulses once the peak value is reached.

The Ultrafast charger includes an intelligent controller that can measure input parameters like voltage & temperature along with associated gradients and determine the charging current as output. The battery current can also be used to estimate the amount of charge remaining in the battery. By including more parameters better performance can be achieved, however this will increase the computational complexity making the circuitry more complicated.

In this circuit design the temperature and its associated gradients are included since it can be easily computed using the past and current values of the measured temperature. The voltage gradient is necessary to verify the fully charged state of the secondary battery. The charge current should be properly reduced during later phases of charging depending on the two control parameters T and dT/dt. In this way an optimal charging current within the safety limit will always be supplied without any battery damage.

General Regression Neural Networks:

Neural Networks grew out of research in Artificial Intelligence. General regression neural networks (GRNN) perform regression where the target variable is continuous. It is able to approximate any functional relationship between a set of independent and dependent variables. GRNN is similar to multilayer back propagation neural network structurally and has number of input nodes

equal to the number of predictor variables. GRNN also has a number of hidden units where the number of hidden nodes is well defined. The hidden-to-output weights are just the target values, so the output is simply a weighted average of the target values of training cases close to the given input case.

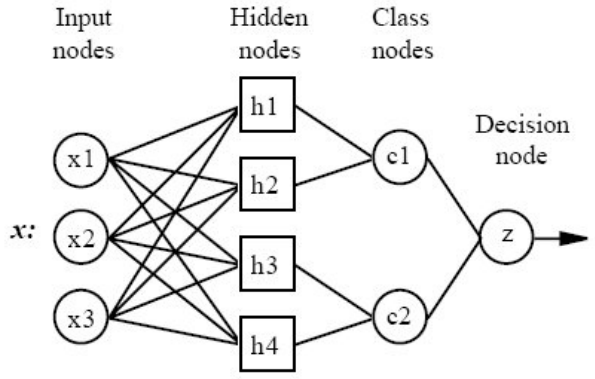


Figure-1 Architecture of a GRNN Network

Input layer: The input neurons standardize the range of the values by subtracting the median and dividing by the interquartile range. The input neurons then feed the values to each of the neurons in the hidden layer.

Hidden layer: This layer has one neuron for each case in the training data set. The neuron stores the values of the predictor variables for the case along with the target value. The resulting value is passed to the neurons in the pattern layer.

Pattern layer / Summation layer: There are only two neurons in the pattern layer. One neuron is the denominator summation unit which adds up the weight values coming from each of the hidden neurons, the other is the numerator summation unit that adds up the weight values multiplied by the actual target value for each hidden neuron.

Decision layer: The decision layer divides the value accumulated in the numerator summation unit by the value in the denominator summation unit and uses the result as the predicted target value.

GRNN is also a solution to realization of an ultra fast charger, since charging the battery naturally involves its inherent nonlinearities. The GRNN can approximately determine the charging current (I_c), temperature (T) and temperature gradient (dT/dt). The output of GRNN, given the inputs x, is the weighted combination of the functional distance between the input data and the center of the basis function in the second (hidden) layer.

The charging current I_c is given by

$$I_c(x) = \frac{\sum_{i=1}^{N} y_i \mathrm{RBF}(\|\mathbf{x}, \mathbf{x}_i\|)}{\sum_{i=1}^{N} \mathrm{RBF}(\|\mathbf{x}, \mathbf{x}_i\|)}$$

Where $x \in R^N$ is, in general, an input vector of dimension *N.* RBF stands for Radial Basis Function, $\| . \|$ denotes the Euclidean norm, y_i are weights or parameters of the network, $x_i \in R^N$ are known as the centers of radial basis function and *N* is number of centers.

$x = [T_i, (dT/dt)_i]^T$ where T_i and $(dT/dt)_i$ denote i^{th} temperature and i^{th} temperature gradient.

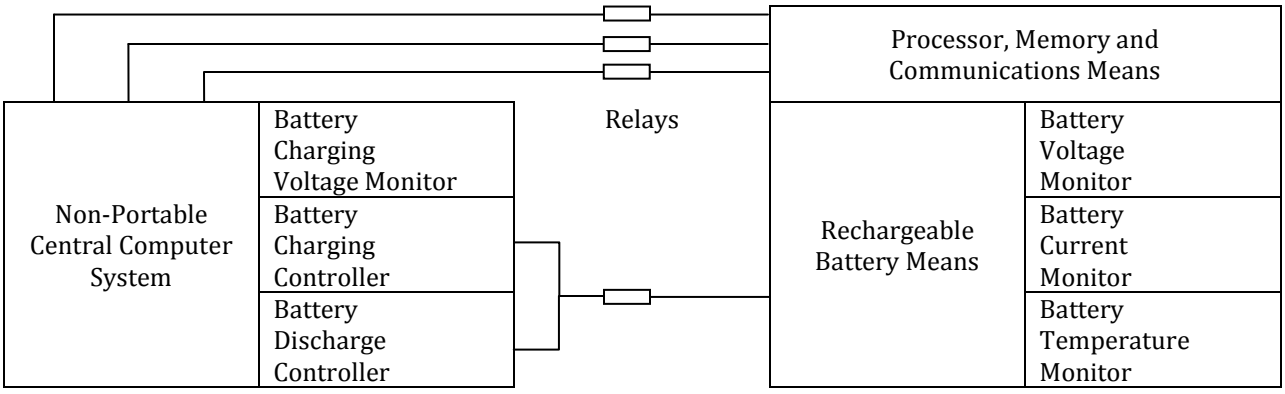


Figure-2 Central Computer Controlled Charging System

Ultrafast Charger Structure:

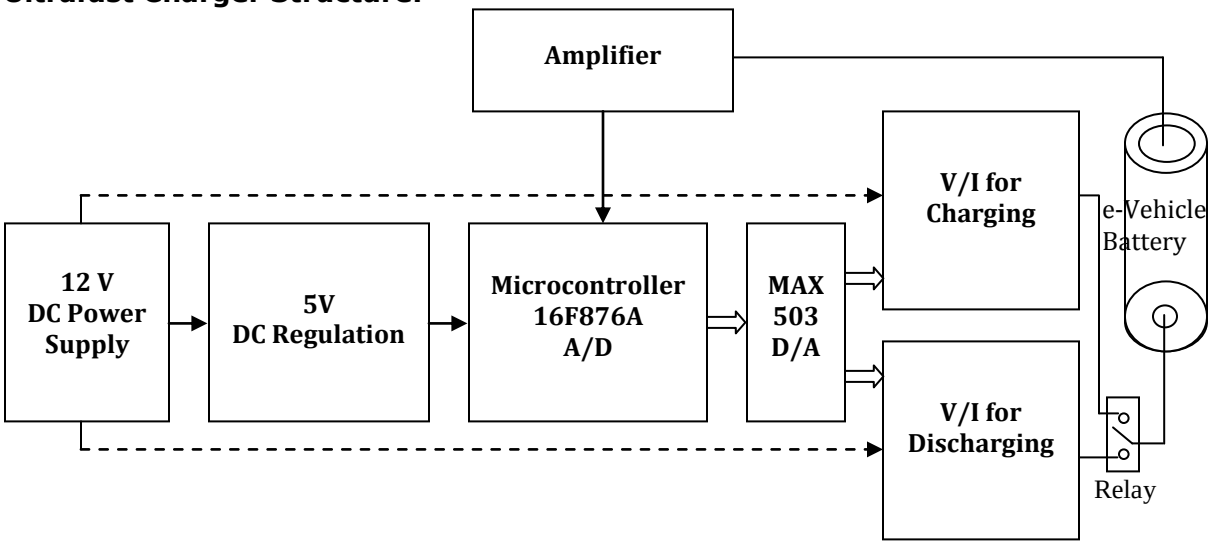


Figure-3 Structure of an ultrafast charger suitable for electric vehicle charging

The ultrafast charger [1] is realized on a low cost 10 bit reduced instruction set computing 16F876A microcontroller with 8kb programmable memory & A/D converter. The additional hardware circuitry includes a voltage control current source, battery temperature and voltage detector, D/A converter, and two V/I converters. The figure-3 shows the structure of an ultrafast charger suitable for electric vehicle charging.

The battery temperature is measured by a thermistor which acts as temperature sensor; the data is converted and fed to a microcontroller via a built in A/D converter [5]. The temperature gradient d*T*/d*t* is computed using a unit delay, where both *T* and d*T*/d*t* are used as control inputs and charging current is performed in the microcontroller. MAX 503 D/A converter [6] converts the charging current data to an analog voltage, which is fed to V/I converter [7] in order to produce proper charging current supplied to the secondary battery.

Microcontroller 16F876A A/D Converter: The microprocessor examines the sequence of ratios to determine the peak value, in response to which fast-charging of battery is terminated. The battery remains on trickle charge until it is removed from the battery charger. The predetermined amount of charging is calculated by the microprocessor and is stored in read-only memory.

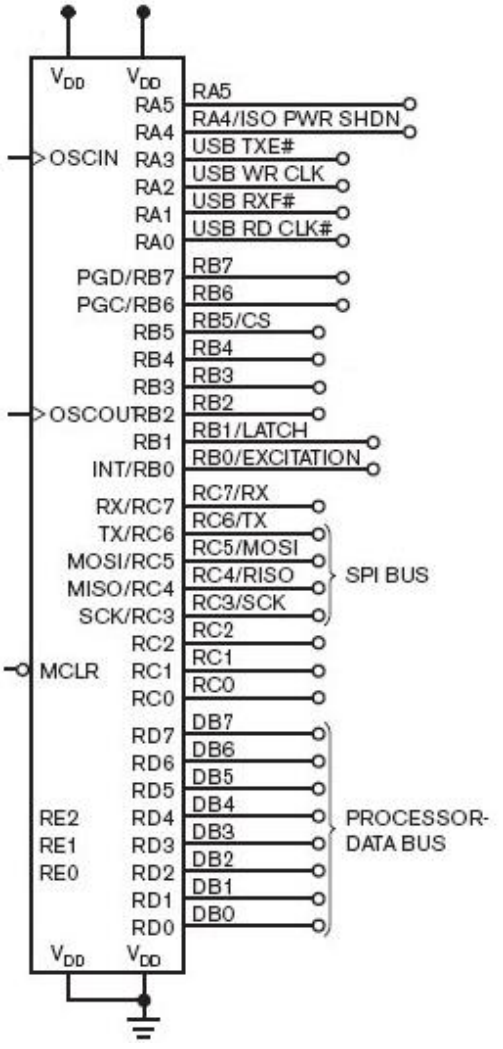


Figure-4 16F876A A/D Converter

MAX 503 D/A Converter: It is a low-power, 10-bit, voltage-output digital-to-analog converter [6] that uses single 5V or dual ±5V supplies. This device has an internal voltage reference plus an output buffer amplifier. Operating current is only 250µA from a single 5V supply, making it ideal for portable and battery-powered applications. In addition, the shrink small-outline package (SSOP) measures only 0.1 square inches, using less board area than an 8-pin DIP. 10-bit resolution is achieved through laser trimming of the DAC, op amp, and reference. No further adjustments are necessary.

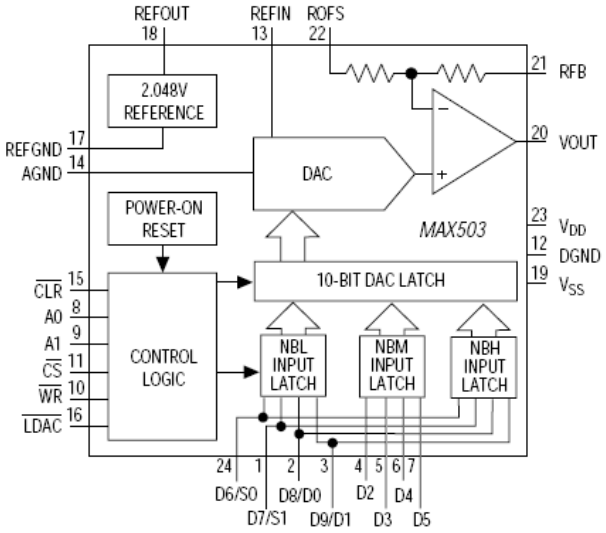


Figure-5 Circuit diagram of MAX 503 Digital to Analog Converter

Internal gain-setting resistors can be used to define a DAC output voltage range of 0V to +2.048V, 0V to +4.096V, or ±2.048V. Four-quadrant multiplication is possible without the use of external resistors or op amps. The parallel logic inputs are double buffered and are compatible with 4-bit, 8-bit, and 16-bit microprocessors. For a hardware and software compatible 12-bit upgrade, refer to the MAX530 data sheet. For D/A with similar features but with a serial data interface, refer to the MAX504 / MAX515 data sheet.

XTR111 Voltage to Current Converter: It is a precision V/I converter [7] designed for analog signals. The ratio between input voltage and output current is set by a single resistor R_{SET}

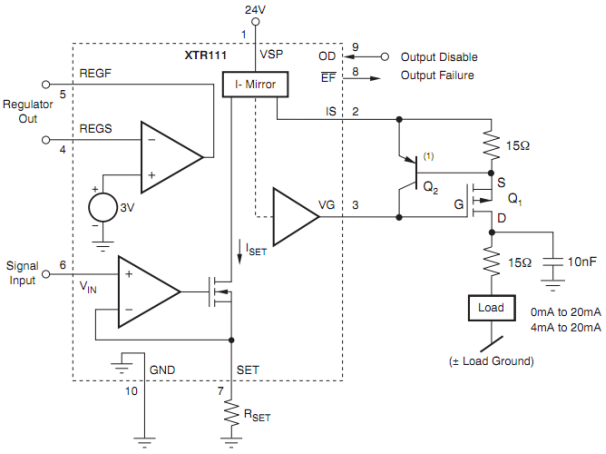


Figure-6 Circuit diagram of XTR111 Voltage to Current Converter

It includes an external P-MOSFET transistor which ensures high output resistance and a broad compliance voltage range.

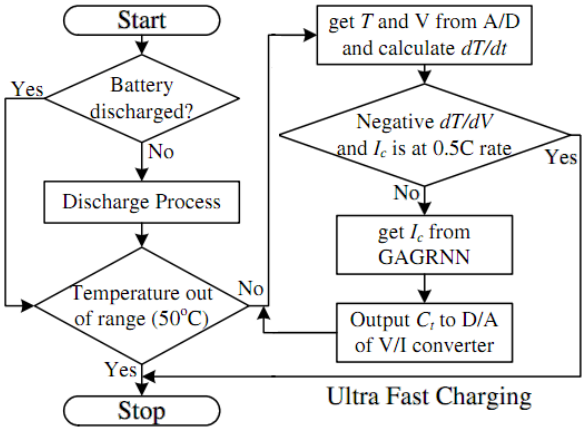


Figure-7 Software flow chart for Ultra fast charging

The above figure shows the software flow chart of the GRNN trained ultrafast charger for charging electric vehicles.

Results:

The trained GRNN controller was simulated using MATLAB and experimentation of the hardware prototype to determine number of neurons in the hidden layer. Experiments were conducted to check the performance of charger with different number of neurons in the hidden layer. Initially the battery was charged using a conventional charger with a constant current.

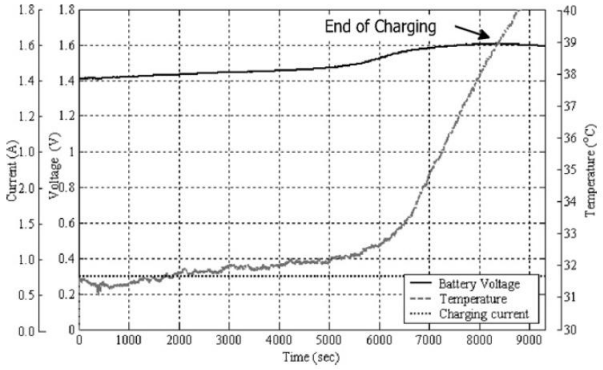


Figure-8 Characteristics of Voltage, Current and Temperature with respect to Time for a conventional charger

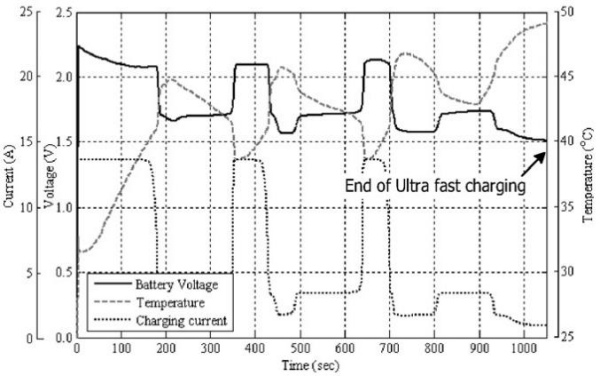


Figure-9 Characteristics of Voltage, Current and Temperature with respect to Time for GRNN trained ultrafast charger

The battery when charged using an ultrafast charger implied drastic reduction of charging time. The below figure shows the Characteristics of Voltage, Current and Temperature with respect to Time for GRNN trained ultrafast charger for electric vehicles.

Advantages:

The training procedure for GRNN is simple and fast, prediction is unique with good mathematical background. Also the GRNN controller can attain ultrafast charging while avoiding battery damage.

Conclusions:

The Ultrafast charger when compared to conventional chargers can recharge the electric vehicle in less than 18 minutes. The proposed charger is proved to be efficient and suitable for recharge stations in India. The Government and related private investments should initiate this technology transfer and setup this element in an infrastructure that can supply electric energy to electric vehicle secondary batteries.

References:

[1] Panom P, Phaophak S, Noppadol K, Khamron S, Phinyo W, and Wiwat K "Low cost RISC implementation of intelligent ultra fast charger for Ni-Cd battery" 2007 Elsevier Ltd.

[2] Edward J. Rzempoluck "Neural network data analysis using Simulnet" ISBN 0-387-98255-8 Springer-Verlag New York, 1998

[3] Khosla A, Kumar S, Aggarwal KK. ''Fuzzy controller for rapid nickel–cadmium batteries charger through adaptive neuro-fuzzy inference system (ANFIS) architecture''. In: Proceedings of the NAFIPS 2003 Conference, 2003. p. 540–544.

[4] Ullah Z, Burford B, Dillip S. Fast intelligent battery charging: neural fuzzy approach. IEEE Aero Electron Syst Mag 1996; 11:26–34.

[5] 28/40/44-Pin Enhanced Flash Microcontroller Microchip PIC16F87XA handbook June 2009

[6] Maxim Low-Power, Parallel-Input, Voltage-Output, 10-Bit D/A Converter handbook November 2008

[7] Precision Voltage to Current Converter / Transmitter Texas Instruments handbook June 2011

Experimental Evaluation of Recovery Algorithms of TCP in Wireless Networks

Vikash Kumar, Annappa B, Mohit P. Tahiliani

manju.vikash145@gmail.com, annappa@ieee.org, tahiliani.nitk@gmail.com

Centre for Wireless Sensor Networks, Department of Computer Science and Engineering,

National Institute of Technology Karnataka Surathkal

Abstract

Communication network is growing in many dimensions including number of users, protocols and infrastructure. Transmission Control Protocol (TCP) accounts for approximately 90% of the Internet traffic in both wired and wireless networks. The most effective mechanism of this protocol is, its ability to provide reliable, bi-directional and virtual channel between two hosts in the network. This paper presents the experimental comparisons of three TCP variants namely, TCP Selective Acknowledgment (SACK), TCP Forward Acknowledgment (FACK) and TCP Selective Negative Acknowledgment (SNACK) running over similar traffic. We have used throughput to highlight the performance differences between these variants of TCP. Simulations are carried out using Network simulator. Our simulation results show that, Negative Acknowledgment and its error recovery procedure makes TCP SNACK to outperform both SACK and FACK in wireless networks.

Keywords- TCP; SNACK; SACK; FACK; performance; throughput

1 Introduction

TCP Tahoe [1] implementation uses cumulative acknowledgment, indicating that receiver has received all of the data up to the acknowledged byte. This property leads to limit the ability of the sender to detect more than one loss per RTT. TCP SACK [2] uses selective acknowledgment which provides information about several packet losses within a single feedback message. It is based on the ability of the receiver to report successfully delivered data packets; which is realized by standardizing selective acknowledgment option. It can inform the sender up to four ordered received data blocks. This saves the unnecessary retransmission of data packet that is not lost, but apprehended by sender as packet loss due to cumulative acknowledgment. In contrast, TCP FACK [3] uses additional information to handle error and number of outstanding packets which makes it better over TCP New Reno and SACK. SNACK [4] uses negative acknowledgment with bitmap scheme which is highly efficient than SACK and FACK. It is capable of specifying a large number of holes in an efficient manner. Receiver provides full image of its buffer to the sender in a single acknowledgment. It was introduced for TCP congestion control in wireless networks but now used extensively in high BDP (Bandwidth Delay Product) networks as well.

In this paper, we illustrate the efficiency of SNACK TCP over SACK and FACK TCP in wireless network. Simulations are done using NS-2. Our tests are carried out in two network topology with five and ten TCP connections and in accord to the IEEE 802.11 wireless networks specification. We use throughput as our metric to highlight performance

differences between TCP SNACK, FACK and SACK in wireless networks.

The remainder of the paper is organized as follows: Section 2 describes the mechanisms of TCP SACK, FACK and SNACK in detail. Section 3 shows simulation setup and methodology. Section 4 demonstrates results and analysis of the experimental result. Finally Section 5 concludes the paper.

2 TCP Variants

2.1 TCP SACK

Traditional TCP specification implements cumulative acknowledgment i.e. the receiver acknowledges the last in-order data packet. Since only in-order delivered packets are acknowledged, the sender remains ignorant of out-of-order delivered packets. This leads to spurious re-transmissions and wastage of network resources.

Mathis et al. [3] addresses the problem of limited information available in cumulative acknowledgment by extending and standardizing the selective acknowledgment (SACK) option. The receiving TCP provides an image of the set of non-contiguous data blocks currently residing in its buffer to the sender. Using this information sender retransmits only data which has been lost. The receiver awaits the receipt of data to fill the gaps in sequence space between received blocks.

Each contiguous block of data queued at the receiver is defined in the SACK option by two 32-bit unsigned integers see (Fig. 1) and specified as:

- Left edge of the block: specifies first sequence number of the block.
- Right edge of the block: specifies last sequence number of the block.

A SACK option which specifies *n* blocks has a total length of 8 * n + 2 bytes. As a result, SACK option can contain at most four blocks of data received in order. This number is further reduced by the use of additional TCP options like *timestamp* [5] etc. In wireless scenario where packet drop rate is high, this limitation of receiver heavily affects the efficiency of network and it degenerates the original problem of TCP.

2.2 TCP FACK

It defines recovery procedure, which unlike the Fast Recovery algorithm of standard TCP, uses additional available information available in SACK to handle error recovery (flow control) and the number of outstanding packets (rate control) in two separate mechanisms.

TCP FACK uses selective acknowledgment to indicate losses which provides a means of timely retransmission of data. The FACK sender retains information about retransmitted data packet for at least one RTT. It maintains three special state variables: (1) *H,* the highest sequence number of all data packets- all data packets with sequence number less than *H* have been sent at least once. (2) *F*, the forward-most sequence number of all acknowledged data packets. (3) R, the number of retransmitted data packets. The relation *H-F+R* gives a reliable estimate of outstanding data packets in the network and is used by sender to decide whether or not to send a new portion of data. The FACK option has been an embedded part of the Linux Kernel since the 2.1.92 version.

2.3 TCP SNACK

TCP SNACK merges the capabilities of both TCP SACK and Negative Acknowledgment (NAK). TCP receiver informs sender about the data that it did not receive. It is capable of specifying a large number of holes in a bit efficient manner. As in SACK, SNACK uses option field in TCP header to convey the SNACK information. The detailed structure is shown in (Fig. 2).

Every gap in sequence number is represented as *hole*. *Hole offset* specifies the starting location of the first hole and the size of the *hole* is specified in *Hole length* field. Both the offset and length values are expressed in terms of number of Maximum Segment Size (MSS) unit. *Bit vector* maps the sequence space of the receiver buffer beyond the end of the block specified by first hole. When receiver gets out-of-order data packets, it invokes the SNACK option, scan the buffer and send the option in next ACK. Sender in a single ACK gets all the information about the lost data packets. Sender aggressively retransmit the lost packets and sets the expected recovery sequence number as the highest sequence number sent so far to keep track of the recovery segment in error recovery phase.

For every duplicate ACK in error recovery phase congestion window is increased by one. For every further loss of packet sender checks the SNACK option and updates the expected recovery sequence number. Sender remains in the error recovery phase till the acknowledgment of all the outstanding data packets up to expected sequence number is received. This is particularly very efficient in wireless scenario where packet error rate are relatively high and large number of out-of-order packets reach at receiver side

3 Simulation setup and methodology

This section describes the simulation setup and methodology used for analyzing the performance of TCP SACK, FACK and SNACK. Simulation set up as shown in (Fig. 3) is analogous to the one designed in [6].

Simulation is carried out by varying:

1. TCP connections: 5 and 10.
2. Error rate: 1% to 5%.
3. 802.11 MAC: 802.11, 802.11b, 802.11g.

Other simulation parameters are described in Table 1. The metric used to compare the performance of SACK, FACK and SNACK is *throughput*. *Throughput* is defined as average number of successfully delivered packets in a network per second.

4 Results and Analysis

Fig. 5-7 and 8-10 shows the results for wireless network with 5 TCP connections and 10 TCP connections respectively

It is observed that TCP SNACK consistently achieves higher *throughput* and outperforms SACK and FACK in both scenarios (Fig.5 through FIG.10). Unlike SACK, SNACK receiver informs sender about the expected data packet which were not received. Thus SNACK sender retransmits all the data packets which were lost and recovers the data faster as compared to SACK and FACK. This feature of SNACK is very important, particularly in wireless scenario where large numbers of out-of-order packet arrive at receiver side. The receiver acknowledges a correctly received segment whether or not it arrives in correct sequence. SNACK sender use expected recovery sequence number to have account of retransmitted packets and updates it with every receipt of acknowledgment, thus avoiding unnecessary retransmission.

Although TCP FACK has an efficient recovery algorithm than SACK, its *throughput* is almost same as that of SACK. Moreover it is pointed by Mathis et al. [3] that overall performance of FACK and SACK will be same for the environment where packet loss will not exceed half the congestion window size.

Table 2 and Table 3 summarizes the percentage improvement in *throughput* of TCP SNACK as compared to SACK and FACK. SNACK performance improves significantly with the increase of TCP connection. This shows the effectiveness of SNACK especially when

there are large numbers of TCP connections in wireless network.

5 Conclusion

Wireless networking has grown multiple folds in last two decades. Researcher community has shown great interest to improve the performance of wireless networks. Packet drop, Out-of-order Arrival of data packets at receiver side, Timely retransmission of lost packets are some of the key issues in the wireless networks.

In this paper we have investigated the data recovery algorithm implemented by TCP SACK, FACK and SNACK. We calculated *throughput* with varying error rate to simulate real world wireless network traffic. It is observed that SNACK shows overall 6.80% and 12.83% *throughput* improvement in 5 TCP connections and 10 TCP connections respectively in wireless scenario.

It is observed that *throughput* degrades with the increase of error rate. It is because of the premature invocation of SNACK option by receiver. Thus to improve the efficiency, enabling of SNACK option must be delayed to considerable amount of time before sending SNACK acknowledgment. But still SNACK recovery algorithm can be further improved, such that sender has much accurate estimation of lost or corrupted data packets.

References

[1] V. Jacobson (1988), Congestion avoidance and control, ACM SIGCOMM, pp. 314–329.
[2] M. Mathis, J. Mahdavi, S.Floyd and A. Romanov (1996), RFC2018-TCP Selective Acknowledgment Options, RFC.
[3] M. Mathis and J. Mahdavi (1996), Forward acknowledgement: refining TCP congestion control, in Proc. conference on applications, technologies, architectures, and protocols for computer communications (SIGCOMM), New York, NY, USA, pp. 281–291.
[4] Rung-Shiang Cheng, Hui-Tang Lin (2007), Improving TCP Performance with Bandwidth Estimation and Selective Negative Acknowledgment in Wireless Networks, Journal of Communications and Networks, vol. 9, no. 3, pp. 236-246.
[5] V. Jacobson, R. Braden and D. Borman (1992), TCP Extensions for High Performance, RFC 1323.
[6] H. Balakrishnan et al. (1997), A comparison of mechanisms for improving TCP performance over wireless links, IEEE/ACM Trans. Networking, vol. 5, no. 6, pp. 756 769.

Table 1 Parameters used in simulation

Parameter	Value
Antenna	OmniAntenna
Radio Propagation Model	Two Ray Ground
Routing Protocol	DSDV
Queue Type	DropTail
Queue Limit	50
Number of Wired Nodes	6
Number of Base Station	1
Number of Wireless Node	1
Error Rate	1–5 %
Simulation Time	150 seconds

Table 2 Throughput improvement of SNACK with 5 TCP connections

	Bandwidth	Improvement (%)
802.11	2 Mbps	3.89
802.11b	11 Mbps	6.06
802.11g	54 Mbps	6.80

Table 3 Throughput improvement of SNACK with 10 TCP connections

	Bandwidth	Improvement (%)
802.11	2 Mbps	5.17
802.11b	11 Mbps	10.2
802.11g	54 Mbps	12.83

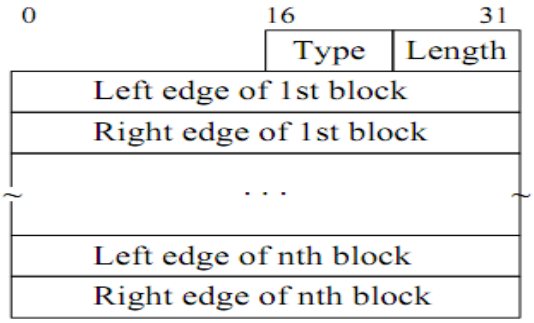
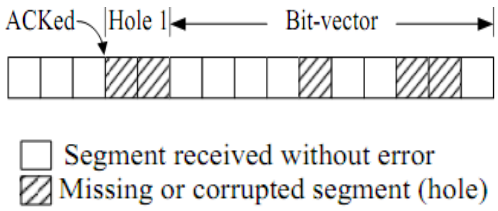
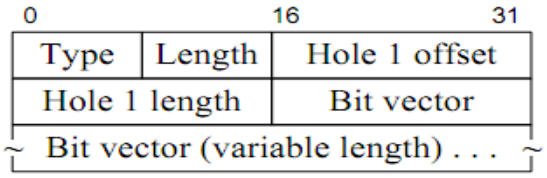


Fig. 1 Structure of SACK option [4]



(a)



(b)

Fig. 2 SNACK example: (a) Receiver side buffer, (b) SNACK segment when bit-vector is used [4]

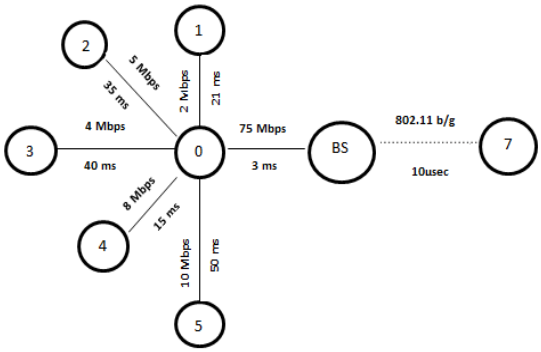


Fig. 3 Simulation diagram

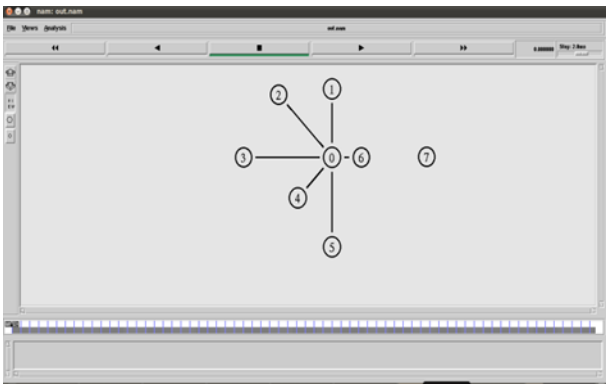


Fig. 4 Snapshot of simulation of TCP SNACK, FACK and SACK

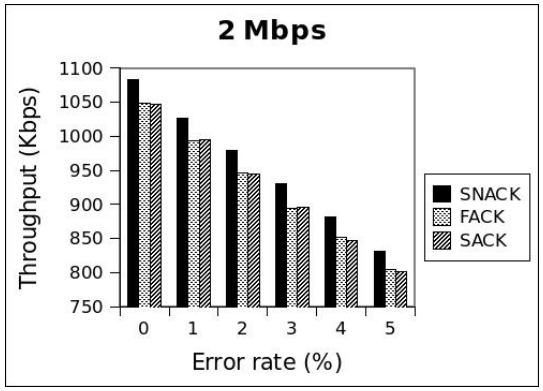


Fig. 5 Throughput vs. Error rate for 5 TCP connections

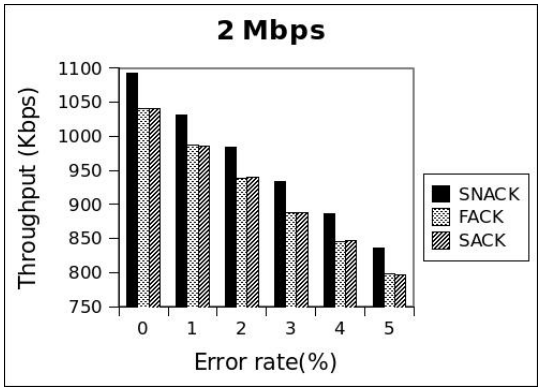


Fig. 8 Throughput vs. Error rate for 10 TCP connections

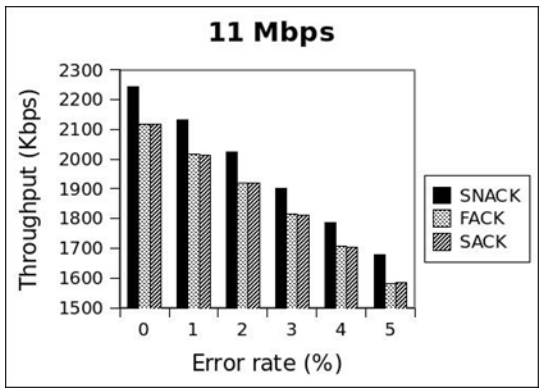


Fig. 6 Throughput vs. Error rate for 5 TCP connections

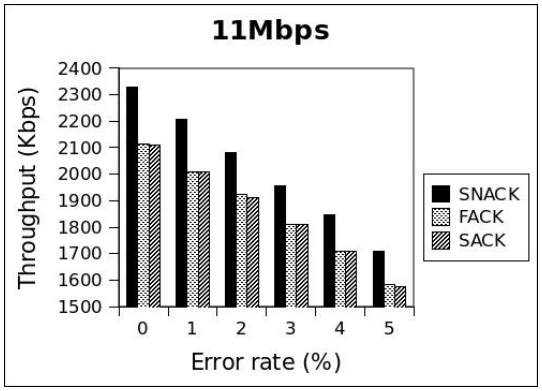


Fig. 9 Throughput vs. Error rate for 10 TCP connections

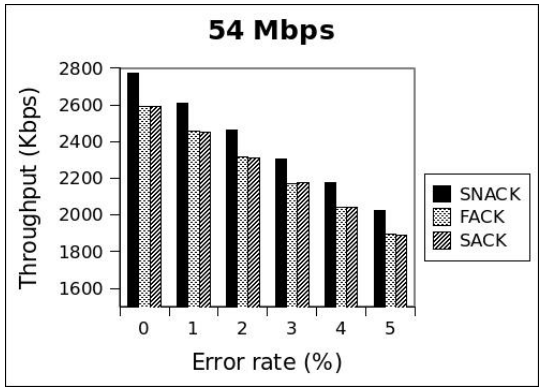


Fig. 7 Throughput vs. Error rate for 5 TCP connections

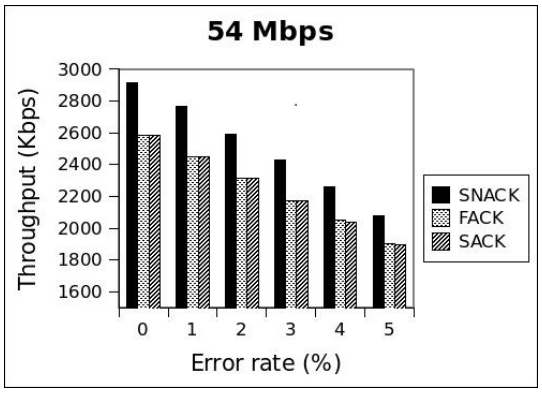


Fig. 10 Throughput vs. Error rate for 10 TCP connections

2nd International Engineering Symposium - IES 2012
(KU-MU-NITK-HCMCUT Joint Symposium) March 5-7, 2012, Kumamoto University, Japan

Machine Learning Based Intrusion Detection Systems using RSC

Sanoop Mallissery [1] **Shahana Sathar [2]**

1 *Department of Information and Communication Technology, Manipal Institute of Technology, Manipal University, Manipal, Karnataka 576 104, India. e-mail: sanoop.m@manipal.edu*
2 *TIFAC Core in Cyber Security, Amrita School of Engineering, Amrita University, Coimbatore, Tamil Nadu, 641 112, India. e-mail: shahanasathar@gmail.com*

Abstract: The main function of Intrusion Detection System (IDS) is to protect the information and network system by analysing and predicting the behaviours of users. These behaviours will be considered an attack or a normal behaviour. Recently machine learning based Intrusion Detection systems have been subjected to extensive researches, because they can detect both misuse and anomaly. Most of existing IDS use all features in the network packet to look for known intrusive patterns. Some of these features are irrelevant or redundant. In this paper Rough Set Classification (RSC) algorithm, is used to rank features and extract for detecting intrusions and generate intrusion detection models. Feature ranking is a very critical step when building the model. Rough Set Theory is used to pre-process the data and reduce the dimensions. RSC creates the intrusion (decision) rules using the reducts as templates. Finally we compared RSC with SVM, CART and ID3 on KDD Cup '99 dataset.
Keywords*: Intrusion Detection System, Rough Set Classification, Support Vector Machine, Classification and Regression Tree, Iterative Dichotomiser 3*

Introduction

Intrusion Detection Systems (IDS) are software or hardware systems that automate the process of monitoring and analyzing the events that occur in a computer network, to detect malicious activity. Since the severity of attacks occurring in the network has increased drastically, Intrusion Detection Systems have become a necessary addition to security infrastructure of most organizations. Intrusion detection allows organization to protect their systems from the threats that come with increasing network connectivity and reliance on information systems.

This paper will examine the use of machine learning algorithms in intrusion detection. The system can then decide on a course of action: it may do anything from giving a simple alert message to taking action against the intrusion. This paper examines the difference between a rough set based, a SVM, a CART and a decision tree to determine the relative strength and weaknesses of using these approaches. The purpose is to give an evaluation of the performance of these algorithms that will allow someone who wishes to use one of these approaches to understand how accurate the approach is and under what condition it works well.

Related Works

A number of researchers have done work in intrusion detection. Since it is difficult to cover all the previous research works, only some of the papers are compiled in this part. Many researchers developed IDS by using different approaches. Most agree that central part of IDS is the detector module and its underlying principle of operation. Hence the literature survey is divided in to three parts: the first part deals with the general detection methodologies like anomaly and detection approaches, the second part covers recently proposed solutions such as visualization and combined or integrated approach, Ajith A. and Johnson T. (2005).

Another successful and widely used network based intrusion detection system is Bro. One of unique features of Bro is that, it is designed to cope up with the attacks that attack the IDS itself. It monitors packet traffic entering and leaving the target network. For other services, Bro records information for all connection attempts. If the number of connection attempts for these services exceed N, this source is also identified as a scanner. The list of services and N are configured in various policy scripts implemented by Bro. These policies can also contain signatures of well-known types of attacks, Paxson V. (1998).

Machine learning algorithm offer a generalization over the statics based anomaly detection systems. Machine learning algorithms can be used to "learn" the normal behavior of the subject automatically. Machine learning algorithms work with a few exemplar instances, called training set and the output of the algorithms will be a set of hypothesis which describes the training set effectively. Machine Learning includes a number of advanced statistical methods for handling regression and classification tasks with multiple dependent and independent variables. These methods include Support Vector Machines (SVM) for regression and classification, Naive Bayes for classification, and k-Nearest Neighbors (KNN) for regression and classification. SVM method performs regression and classification tasks by constructing nonlinear decision boundaries. Because of the nature of the feature space in which these boundaries are found, Support Vector Machines can exhibit a large degree of flexibility in handling classification and regression tasks of varied complexities. There are several types of Support Vector models including linear, polynomial, RBF, and sigmoid, Srinivas M. et al. (2002). Naïve Bayes is a well established Bayesian method primarily formulated for performing classification tasks. Given its simplicity, i.e., the assumption that the independent variables are statistically independent, Naive Bayes models are effective classification tools that are easy to use and interpret. Naive Bayes is particularly appropriate when the dimensionality of the independent space (i.e., number of input variables) is high (a problem known as the curse of dimensionality). For the reasons given above, Naïve Bayes can often outperform other more sophisticated classification methods. A variety of methods exist for modeling the conditional distributions of the inputs including normal, lognormal, gamma, and Poisson. K-Nearest Neighbors is a memory-based method that, in contrast to other statistical methods, requires no training (i.e., no model to fit). It falls into the category of Prototype Methods. It functions on the intuitive idea that close objects are more likely to be in the same category. Thus, in KNN, predictions are based on a set of prototype examples that are used to predict new (unseen) data based on the majority vote (for classification tasks) and averaging (for regression) over a set of k-nearest prototypes (hence the name k-nearest neighbors).

The KDD Cup '99 dataset was created by processing the TCP dump portions of the 1998 DARPA Intrusion Detection System (IDS) Evaluation dataset, created by Lincoln Lab under contract to DARPA, Richard L. et al. (2000). Since one cannot know the intention (benign or malicious) of every Connection on a real world network (if we could, we would not need research in intrusion detection), the artificial data was generated using a closed network, some proprietary network traffic generators, and hand-injected attacks. It was intended to simulate the traffic seen in a medium sized US Air Force base (and was created in collaboration with the AFRL in Rome, NY, which could be characterized as a medium sized US Air Force base). 1998 DARPA intrusion detection dataset was acquired from nine weeks of raw TCP dump data for a Local Area Network (LAN) simulating a typical U.S. Air Force LAN and four main categories of attacks: DoS, Probe, U2R, R2L, Mahbod T. et al. (2009).

Rough Set

Rough sets have been introduced as a tool to deal with inexact, uncertain or vague knowledge in artificial intelligence applications, Pawalk Z. (1991). Rough set concept can be defined quite generally by

means of topological operations, interior and closure, called approximations, Pawalk Z. (2002).

Suppose we are given a set of objects U called the universe and an indiscernibility relation $R \subseteq U \times U$, representing our lack of knowledge about elements of U. For the sake of simplicity we assume that R is an equivalence relation. Let X be a subset of U. We want to characterize the set X with respect to R. To this end we will need the basic concepts of rough set theory given below.

The lower approximation of a set X with respect to R is the set of all objects, which can be for certain classified as X with respect to R (are certainly X with respect to R).

The upper approximation of a set X with respect to R is the set of all objects which can be possibly classified as X with respect to R (are possibly X in view of R).

The boundary region of a set X with respect to R is the set of all objects, which can be classified neither as X nor as not X with respect to R.

Now we can give the definition of rough sets.

Set X is crisp (exact with respect to R), if the boundary region of X is empty.

Set X is rough (exact with respect to R), if the boundary region of X is nonempty.

Thus a set is rough (imprecise) if it has nonempty boundary region; otherwise the set is crisp (precise). The approximations and the boundary region can be defined more precisely. To this end we need some additional notation.

The equivalence class of R determined by element x will be denoted by $R(x)$. The indiscernibility relation in certain sense describes our lack of knowledge about the universe. Equivalence classes of the indiscernibility relation, called granules generated by R, represent elementary portion of knowledge we are able to perceive due to R. Thus in view of the indiscernibility relation, in general, we are an able to observe individual objects but we are forced to reason only about the accessible granules of knowledge.

Let $I = (U, A \cup \{d\})$ be an information system, where U is the universe with a non-empty set of finite objects. A is a non-empty finite set of condition attributes, and d is the decision attribute (such a table is also called decision table). Where $\forall a \in A$ is a corresponding function with $f_a : U \to V_a$, where V_a is the set of values of a. $P \subseteq A$, then there is an associated equivalence relation.

$$IND(P) = \{(x, y) \in U \times U \mid \forall a \in P, \; f_a(x) = f_a(y)\} \quad (1)$$

The partition of U is generated by $IND(P)$ and it's denoted by using U/P. If $(x, y) = IND(P)$, then x and y are indiscernible by attributes from P. The equivalence classes of the P-indiscernibility is relation are denoted by $[x]_{\underline{P}}$. Let the P-lower approximation $\underline{P}X$ and P-upper approximation $\overline{P}X$ of set X can be defined as:

$$\underline{P}X = \{x \in U \mid [x]_{\underline{P}} \subseteq X\} \quad (2)$$

$$\overline{P}X = \{x \in U \mid [x]_{\underline{P}} \cap X \neq \phi\} \quad (3)$$

Let $P, Q \subseteq A$ be equivalence relations over U, then the positive, negative and boundary regions can be defined as:

$$POS_P(Q) = \bigcup_{X \in U/Q} \underline{P}X \quad (4)$$

$$NEG_P(Q) = U - \bigcup_{X \in U/Q} \overline{P}X \quad (5)$$

$$BND_P(Q) = \bigcup_{X \in U/Q} \underline{P}X - \bigcup_{X \in U/Q} \overline{P}X \quad (6)$$

The positive region of the partition U/Q with respect to P, $POS_P(Q)$ is the set of all objects of U that can be certainly classified to blocks of the partition U/Q by means of P. Q depends on P in a degree k $(0 \le k \le 1)$ denoted $P \Rightarrow_k Q$.

$$k = \gamma_P(Q) = \frac{|POS_P(Q)|}{|U|} \quad (7)$$

If $k = 1$, Q depends totally on P, if, $0 < k < 1$ and Q depends partially on P and if $k = 0$ then Q does not depend on P. When P a set of condition is attributes and

Q is the decision, $\gamma_P(Q)$ is the quality of classification.

The goal of attribute reduction is to remove redundant attributes so that the reduced set provides the same quality of classification as the original, Pawalk Z. (2002). The set of all reducts is defined as:

$$RED = \{R \subseteq C \mid \gamma_R(D) = \gamma_C(D), \forall B \subset R, \gamma_B(D) \neq \gamma_C(D)\} \quad (8)$$

A dataset may have many attribute reducts. The set of all optimal reducts is:

$$\mathrm{Re}d_{\min} = \{R \in \mathrm{Re}d \mid \forall R' \in \mathrm{Re}d, |R| \leq |R'|\} \quad (9)$$

Decision Rules

An expression $c:(a=v)$ where $a \in A$ and $v \in V_a$ is an elementary condition (atomic formula) of the decision rule which can be checked for any $x \in X$. An elementary condition c can be interpreted as a mapping $c: U \rightarrow \{true, false\}$ .A conjunction C of q elementary conditions is denoted by $C = c_1 \wedge c_2 \wedge \ldots. \wedge c_q$. The cover of a conjunction C denoted by $\bar{C}$ or $|C|_A$, is the subset of examples that satisfies the conditions by C , $\bar{C} = \{x \in U : C(x) = true\}$ which is called the support descriptor. If K is the concept, the positive cover $\bar{C}_k = \bar{C} \cap K$ denotes the set of positive symbols covered by C . A decision rule r for A is any expression of the form $\varphi \Rightarrow (d = v)$ where $\varphi = c_1 \wedge c_2 \wedge \ldots. \wedge c_q$ is a conjunction, satisfying the positive cover of $\varphi \neq \phi$ and $v \in V_d$, V_d is the set of values of d . The set of attribute-value pairs occurring in the left hand side of the rule r is the condition part, Pred(r), and the right hand is the decision part, Succ(r).

An object $u \in U$ is matched by a decision rule $\varphi \Rightarrow (d = v)$ if u supports both the condition part and the decision part of the rule. If u is matched by $\varphi \Rightarrow (d = v)$ then we say that the rule classifies u to decision class v . The number of objects matched by a decision rule $\varphi \Rightarrow (d = v)$, denoted by Match(r), is equal to $card(|\varphi|_A)$. The support of the rule $card(|\varphi|_A) \cap |d = v|_A$ is the number of objects supporting the decision rule. The accuracy and coverage of a decision rule $\varphi \Rightarrow (d = v)$ are defined as:

$$\alpha_\varphi(D) = \frac{card(|\varphi|_A \cap |d = v|_A)}{card(|\varphi|_A} \quad (10)$$

$$K_\varphi(D) = \frac{card(|\varphi|_A \cap |d = v|_A)}{card(|d = v|_A)} \quad (11)$$

Algorithm for Induction of Minimum Set of Decision Rules

The LEM2 (algorithm of Learning from Examples based on Rough Sets) was proposed to extract a minimum set of decision rules. Let K be a nonempty lower or upper approximation of a concept, C is an elementary condition, and C is a conjunction of such conditions being a candidate for the condition part of the decision rule, $C(G)$ denotes the set of conditions currently considered to be added to the conjunction C . Rule r is characterized by its condition part. The LEM2 algorithm follows a heuristic strategy for creating an initial rule by choosing sequentially the 'best' elementary conditions according to some heuristic criteria. Then learning examples that match this rule are removed from consideration. The process is repeated iteratively while some learning examples remain uncovered in that series, Grzymala-Busse (1997). The resulting set of rules covers all learning examples.

The global strength defined in Eq. 12 for rule negotiation is a rational number in [0, 1] representing the importance of the sets of decision rules relative to the considered tested object. Let us assume that $T = (U, A \cup \{d\})$ is a given decision table, u_t is a test object, $Rul(X_j)$ is the set of all calculated basic decision rules for T , classifying objects to the decision $X_j(v_d^j = v_d)$, $MRul(X_j, u_t) \subseteq Rul(X_j)$ is the set of all decision rules from $Rul(X_j)$ matching tested object u_t . The global strength $GS(X_j, u_t)$ of decision rule set $MRul(X_j, u_t)$ is defined as:

$$\frac{card(\bigcup_{r\in MRul(X_j,u_t)} |\Pr ed(r)|_A \cap |d = v_d^j|_A}{card(|d = v_d^j|_A} \quad (12)$$

To classify a new case, rules are first selected matching the new case. The strength of the selected rule sets is calculated for any decision class, and then the decision class with maximal strength is selected, with the new case being classified to this class. The quality of the complete set of rules on a dataset with size n is evaluated by the classification accuracy: n_c/n where n_c is the number of examples that have been correctly classified.

Table 1 gives an idea about the features of KDD 99 dataset and a complete listing of the set of features defined for the connection records.

Rough Set in KDD

Rough sets theory was introduced as a mathematical tool for data analysis. It does not need external parameter to analyze and make conclusions about the datasets. Rough sets offer many opportunities for developing many Knowledge Discovery methods using partition properties and discernibility matrix. The features selected after RST operations is given in Table 2.

Discretization is the process to transform continuous features into qualitative features. A continuous feature could be partitioned into many subintervals, Ron K. and Mehran S. (2006). In reducing the number of features it is expected that the ones that are redundant and irrelevant will be deleted, Lian et al. (2004).

Fig.1 shows the general scheme of RSC algorithm. RSC creates the intrusion (decision) rules using the reducts as templates. After reducts generation, the detection rules are automatically computed subsequently. The rules generated have the intuitive "IF-THEN" format, which is explainable and very valuable for improving detector design. Experiments were designed to test the rules detection performance, Rung C. et al. (2009). For detection rules auto-generation, here present the use of rough set classification for this task. It includes three phases. In preprocessing phase the raw data is first partitioned into three groups: DoS attack detection dataset, Probe attack detection dataset, U2R and R2L attack detection dataset. For each dataset, a decision system is constructed. Each decision system is subsequently split into two parts: the training dataset and the testing dataset. In training phase rough set classifier is trained on each training dataset of three different types of attacks (DoS, Probe, U2R & R2L). Each training dataset uses the corresponding input features and fall into two classes: normal (+1) and attack (−1) and the testing phase that measure the performance on testing data.

Performance Analysis

The comparison results of RSC algorithm with SVM, CART, and ID3 is done using KDD Cup'99 intrusion detection data set is given in Table 3. From the table we can conclude that RSC algorithm has high detection performance level than SVM, CART, and ID3 with reduced feature set. Table 4 showing the performance of RSC algorithm carried out on three types of attacks.

Conclusions and Future Work

It is very valuable to get both high detection rate and explainable rules since this can improve our knowledge about the nature of the intrusion. In this thesis we use rough set classification (RSC) for intrusion detection system (IDS) feature ranking and intrusion detection rules generation. Intrusion detection using RSC can yield both explainable detection rules and high detection rate for some attacks. Feature ranking using RSC for IDS is simple and fast and also done a performance analysis with CART, ID3 and SVM.

References

[1] Ajith Abraham and Johnson Thomas (2005), "Distributed intrusion Detection System:A Computataional Approach," IDEA Group Inc. Publishers, USA, pp: 105-135.

[2] Grzymala-Busse (1997), "A new version of the rule induction system LERS", Journal of Fundamenta Informaticae Vol. 31, Issue 1, pp: 27-39.

[3] Lian-hua, Guan-hua and YU Lang (2004), "Intrusion detection using rough set classification",

Journal of Zhejiang University Science, ISSN 1009-3095.
[4] Mahbod Tavallaee, Ebrahim Bagheri, Wei Lu, and Ali A. Ghorbani (2009), "A Detailed Analysis of the KDD CUP 99 Data Set", Proceedings of the 2009 IEEE symposium on Computational Intelligence in Security and Defence Applications(CISDA).
[5] Richard P. Lippmann, David J. Fried, Issac Graph, Joshua W. Haines, Kristopher R. Kendall, David McClung, Dan Weber, Seth E. Webster, Dan Wyschogrod, Robert K. Cunningham, and Marc A. Zissman (2000), "Evaluating intrusion detection systems: The 1998 DARPA off-line intrusion detection evaluation", In Proc. of the DARPA Information Survivability Conference and Exposition, Los Alamitos, CA. IEEE Computer Society Press.
[6] Ron Kohavi and Mehran Sahami (2006), "Error-Based and Entropy-Based Discretization of Continuous Features", KDD-96 Proceedings.
[7] Rung-Ching Chen, Kai-Fan Cheng, and Chia-Fen Hsieh (2009), "Using Roughest and Support Vector Machine for Network Intrusion Detection", International Journal of Network Security & Its Applications (IJNSA), Vol.1 No.1.
[8] Srinivas Mukkamala, Guadalupe Janoski and Andrew Sung (2002), "Intrusion Detection: Support Vector Machines and Neural Networks", Proceedings of IEEE International Joint Conference on Neural Networks, pp.1702-1707.
[9] Vern Paxson (1998), "Bro: A System For Detecting Network Intruders In Real-Time", In Proc. of the 7th USENIX Security Symposium.
[10] Zdzislaw pawalk (1991), "Rough Sets: Theoretical Aspects of Reasoning about Data", Kluwer Academic Publishers.
[11] Zdzislaw pawalk (2002), "Rough set theory and its applications", Journal of telecommunications and Information Technologies.

Table 1 KDD CUP '99 Features

No	Features	No	Features
1	Duration	22	is_guest_login
2	protocol_type	23	Count
3	Service	24	srv_count
4	Flag	25	serror_rate
5	src_bytes	26	srv_serror_rate
6	dst_bytes	27	rerror_rate
7	Land	28	srv_rerror_rate
8	wrong_fragments	29	same_srv_rate
9	Urgent	30	diff_srv_rate
10	Hot	31	srv_diff_host_rate
11	num_failed_logins	32	dst_host_count
12	logged_in	33	dst_host_srv_count
13	num_compromised	34	dst_host_same_srv_rate
14	root_shell	35	dst_host_diff_srv_rate
15	su_attempted	36	dst_host_same_src_port_rate
16	num_root	37	dst_host_srv_diff_host_rate
17	num_file_creations	38	dst_host_serror_rate
18	num_shells	39	dst_host_srv_serror_rate
19	num_access_files	40	dst_host_rerror_rate
20	num_outbound_cmds	41	dst_host_srv_rerror_rate
21	is_host_login		

Table 2 Features after RST Operations

No	Features	No	Features
1	Duration	16	rerror_rate
2	protocol_type	17	same_srv_rate
3	src_bytes	18	diff_srv_rate
4	dst_bytes	19	srv_diff_host_rate
5	wrong_fragments	20	dst_host_count
6	num_failed_logins	21	dst_host_srv_count
7	logged_in	22	dst_host_same_srv_rate
8	num_compromised	23	dst_host_diff_srv_rate
9	root_shell	24	dst_host_same_src_port_rate
10	num_root	25	dst_host_srv_diff_host_rate
11	num_file_creations	26	dst_host_serror_rate
12	num_shells	27	dst_host_srv_serror_rate
13	num_access_files	28	dst_host_rerror_rate
14	Count	29	dst_host_srv_rerror_rate
15	serror_rate		

Table 3 Comparison of RSC with CART, ID3 and SVM

No. of Features	Algorithm	Classification (%)
41	CART	84.62%
41	SVM	92.42%
41	ID3	84.62%
29	RSC	98.18%

Table 4 Experiment Results of RSC based IDS

No. of Features	Category	Classification (%)
29	DoS	99.90%
29	Probe	99.23%
29	U2R and R2L	99.68%

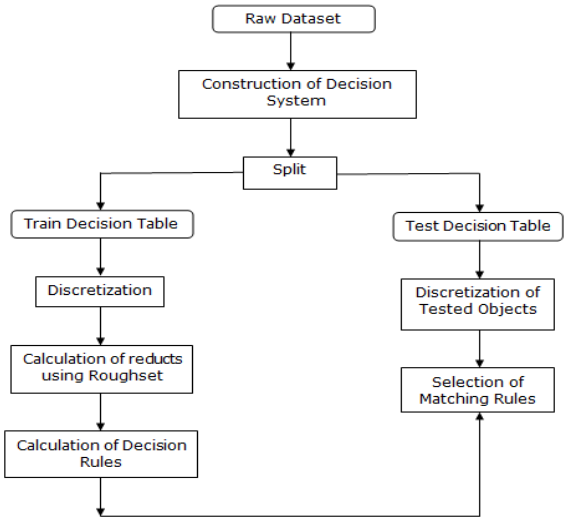


Fig.1 General Scheme of RSC Algorithm

2nd International Engineering Symposium - IES 2012
(KU-MU-NITK-HCMCUT Joint Symposium) March 5-7, 2012, Kumamoto University, Japan

Complexity Analysis of Simulink Models to Improve the Quality of Outsourcing in an Automotive Company

Jeevan Prabhu [1] **Alexander Serebrenik [2]** **Sanjay Singh[3]**

1 *Department of Information and Communication Technology, Manipal Institute of Technology, Manipal University, Manipal, Karnataka 576 104, India. e-mail: jeevan.prabhu@manipal.edu*
2 *Department of Computer Science, Technical University of Eindhoven, Netherlands. e-mail: a.serebrenik@tue.nl*
3 *Department of Information and Communication Technology, Manipal Institute of Technology, Manipal University, Manipal, Karnataka 576 104 India. e-mail: sanjay.singh@manipal.edu*

Abstract: *Usage of software in automobiles is increasing rapidly and since software development is not the core business of automobile industry, outsourcing the development activity of the software is gaining more importance. Quality of the outsourced product depends on products functionality, testability, maintainability etc. All these aspects are directly or indirectly depend on the implementation activity performed by the supplier. The main idea proposed in this paper is to identify delicate parts of the design, which are complex and can be prone to errors during implementation. We define the metrics which can be applied to the design documents and validate them by generating the code from the designs. These results can be used to identify the complex functionalities in the code and help the company to perform more rigorous testing on those parts.*

Keywords*: Outsourcing, Quality, Design, Metrics, Testing*

Introduction

Outsourcing of software development work is an important activity carried out by many companies. It is done mainly because of the engineering challenges and also because the outsourced activity is not a central part of the core business. Outsourcing has both advantages and disadvantages. The major advantages are lower development costs, access to talent, increased capacity, decreased time to market etc., Carmel E and Tija P [2007]. At the same time problems related to communication and quality of the product may arise.

Geographical distributions and cultural differences between the outsourcer and the service provider can lead to lot of complications, especially in the transfer or hand-over moments. Also different development practices and skill levels may further add to the complexities. Outsourcing of software development and management activity is carried out both in the IT industry and beyond. In automotive industry also, outsourcing is gaining importance. The use of software for the automobiles is increasing every day and hence outsourcing of this software is also increasing. Many new innovative functions in automobiles are enabled and driven by software. The rapid increase of software and software based functionality has given rise to various challenges for the automotive industries, Grimm K [2003], Heinecke H [2005]. The company outsourcing the software for the various functionalities has to ensure that the software delivered is of good quality. The outsourcing company has to follow a systematic method to

assess the quality of outsourced systems and should be in a position to assure quality of the product to the customers.

This paper proposes a new approach to improve the quality of outsourcing in the case of automotive industry. It mainly gives insights on assessing the design models based on model's complexity and also it gives a method to improve the testing process by prioritizing the test cases.

Current Approach of the Automotive Company

The automotive company has an Engine System Department which is responsible for constructing the Simulink models [*http://www.mathworks.co.kr/access/helpdesk/help/toolbox/ Simulink / simulink_product_page.html*] of the requirements. The Engine System Department gets the requirements from the pre-engine departments for various functionalities in natural language. The Simulink models are given to the supplier who develops the binaries for the chips and delivers back to the company. The Fig.1 shows the detailed process of outsourcing carried out in the automotive company.

Problems Faced By Automotive Company

As the company is outsourcing the software implementation activity, it is unaware of the quality aspects considered by the supplier. Also it has limited amount of time to test the delivered product from the supplier. It does not want to lose its customers' confidence by delivering poor quality products. Hence it wants to gain more control over the systems quality by performing more critical testing and deliver high quality engines to the customer.

Hence it is desirable to have a method by which they can get an indication of the product quality and they can gain more confidence about the products they deliver. This paper aims at finding a new method on which the automotive company can rely upon.

Hence we try to answer the following research questions.

- How can we measure the complexity of the Simulink design models?
- How can we validate the measured complexity of the models?
- Can we prioritize the tests using the above results?
- How can the automotive company make use of these results?

Assessment Process

The proposed approach aims at identifying the possible defects in implementation. Testing is the process by which the automotive company can know the possible defects or problems in the implementation. To do an effective testing, the automotive company should be able to predict the hot spots in the implementation where the errors or bugs can occur. Hence the new process of outsourcing is proposed in the Fig.2. This is the method to identify the delicate parts of the implementation, so that more importance is given to such parts during testing.

Fig.2 depicts the activities to be carried out at both the automotive company and the suppliers' side. The automotive company uses the Simulink models to calculate the model metrics using the structure of the model. The calculated model metrics can be validated by generating the source code from the model and then comparing the source code metrics with the model metrics. The calculation of model metrics and source code metrics are discussed in the later sections. Based on these model complexity metric values, we prioritize the design modules. This can serve as a valuable input to the risk analysis phase which will then reflect in the improvement of the testing strategy by prioritizing the test cases.

Fig.2 also shows the comparison of the source code metrics from the supplier with the model metrics. This will be useful to have a better idea of the suppliers' source code and identify the complex modules before the software is actually delivered.

Software Complexity
Software complexity is a term that includes various properties of a piece of software which affect internal interactions. The properties can be related to design, implementation, testing, maintenance etc. Software complexity measurement is an area of software engineering concerned with the measurement of factors that affect these properties.

This paper mainly focuses on identifying the structural and procedural complexities at the design level. We try to measure the complexities involved in the design of the system which will further reflect in the implementation.

Model Metrics
Model metrics are mainly concentrating on the design complexity of the system. Since design complexity will reflect in the implementation activity, it is important to identify the complex modules at the design phase and handle them. The design of the system will be in the form of a model. In our case we try to assess the design models which are in the form of Simulink models. Simulink models are commonly used in the designing the systems such as aerospace and defense, automotive industries, medical instrumentation, communications, electronic and signal processing.

Metrics selection
An examination of the literature on the measurement of software complexity provides us with various metrics like cyclomatic complexity, McCabe T J [1976], Halstead metrics, Halstead M H [1977], Henry Kafura metrics, Henry S M, and Kafura D G, [1981], lines of code, Henry S and Selig S [1990], depth of nesting, Piwowarski P [1982], OO complexity metrics like depth of inheritance, number of classes, and weighted methods per class, Etzkorn L, Bansiya J,Davis C [1999].

We have selected the complexity metrics based on following criteria

- Metrics should be for imperative or procedural programming paradigm
- Metrics should be applicable to Simulink design models.

Applying metrics to model
Based on the metrics selection criteria we could select two metrics for our evaluation i.e. Halstead metrics and Cyclomatic complexity

Model Halstead metrics
We apply the Halstead metrics to the Simulink models by calculating the number of operations taking in the model. The definition of an operator and operator are as follows.

i. Operator of the model
Any block in the model which has one or more incoming lines and has one or more outgoing lines is an Operator.

ii. Operand of the model
Any incoming line to an operator is an Operand.

The general procedure followed to calculate the number of operators and numbers of operands are

- Eliminate all the blocks which give the inputs to the model.
- Eliminate all the blocks which act as Outputs for the model.
- Count the blocks remaining after the above two steps which act as operators. Also count the number of distinct blocks which act as distinct operators.
- Count the all the inputs to the remaining blocks which act as operands. Also count the number of distinct inputs which act as distinct operands.
- Once the operators and operands are calculated, the Halstead metrics are calculated using the general formulae.

Model Cyclomatic Complexity
We apply the McCabe complexity definition to the model to find its complexity. We will concentrate on those parts of the model which implement the control flow in the model. In particular we find decision blocks in the model which directs the flow of information.

The basic decision blocks are 'IF-Else block', 'Switch block', 'While block' and 'For Iterator block' which are available in Simulink block library [*http://www.mathworks.co.kr/access/helpdesk/help/toolbox/Simulink/simulink_product_page.html*].

Source Code Metrics

The method of validation involves generating the source code for the target model and then using a suitable metric tool, calculating the source code metric values. The source code metric values are then compared with the model metric values. The metric values may coincide or they may have a relation between them or there may be no relation.

For code generation we used a MATLAB plug-in, Real time work shop which generates the C code from the model.

Applying metrics to Simulink models

The metrics defined for design models and source code need to be applied for a set of Simulink models. Hence we construct three models which include set of operational blocks and a set of decision blocks to check how the model complexity and the source code complexity vary with each other. First we consider a relatively complex model with many operational and conditional blocks. We generate code for the model and calculate both the model and source code metrics. The results are shown in the Table 1. We could find that there exists a relation between the model metrics and source code metrics.

Metric Tools used

- Understand: It is a static analysis tool for measuring various metrics including the cyclomatic complexity [*http://www.scitools.com/*].
- Testwell CMT++: We use this metric tool to calculate Halstead metrics. [*http://www.verifysoft.com/en_cmtx.html*].

Case Studies

Here we discuss two case studies which are from an automotive company. The case studies are the design documents which are developed in the automotive company and are given to a supplier to implement.

Metric Results Comparison And Analysis

The case study models have various modules which specify the functionalities. Each module is evaluated by calculating the model and source code metrics from them.

In Table 2, N1 and N2 are the total number of operators and total number of operands. n1 and n2 are the total number of distinct operators and total number of distinct operands. We calculate the N and n values separately for all the modules since all the Halsted metrics are based on these values.

Next we find correlation between the model and source code metrics. Since for the cyclomatic complexity, the model metrics maps exactly to the source code metrics, we do not need any other analysis. For the Halsted metrics, we use Spearman's Rank Correlation method, Richard G L [2007]. It assesses how well the relationship between two variables can be described using a linear function.

Table 3 shows that there is a strong positive co-relation between the Halstead model metric and Halsted code metric. The correlation between the total number of operators and operands of model and code is +0.84 and between total number of distinct operators and distinct operands of model and source code is +0.87. Both of them are calculated at 1% significance level, Richard G L [2007].

Prioritizing the Tests

Testing is process which involves the mapping of requirements to the implementation. In this research work we prioritize the modules by assigning a rank to the modules based on their complexity. Higher the complexity lower the rank assigned.

First we assign rank for the modules based on their cyclomatic complexity. After that for the Halstead metrics we have to assign the ranks for

N and n separately then the final rank for Halstead metrics is calculated by taking the average of the two ranks.

While measuring final complexity, we have considered both of them equally important. We decided that the final rank for the modules is assigned by calculating the average of both cyclomatic metrics rank and the Halstead metric rank. If the average rank calculated for two modules coincides then both of them will have same priority and hence any one of them can be considered first. The values calculated are shown in the Table 4.

Suggestions to an Automotive Company

- The automotive company will get an indication of the complexity of the modules implemented by the supplier
- If the automotive company gets the final source code metrics from the supplier, then comparing the model metrics with those metrics will give a clear picture about the deviation of the metrics. Based on the amount of deviation between the metrics, the company can instruct the supplier to handle the implementation.
- We estimated the complexity of every module in the design. These modules will be reflected in the test cases also. Hence the complexity values of the modules are used to prioritize the modules

Conclusion

The proposed method shows how to calculate the complexity of the design. This will help the automotive company to assess their design before its implementation and also it will help the company to instruct their supplier to do necessary modifications in the implementation. This will help in improving the quality of product and also the confidence of the company about the product.

We prioritize the test cases based on the complexity values of the design. This will help the company to improve the testing process by concentrating on the delicate parts of the implementation and thus improving the quality of testing.

Future Work

Though we have shown the relation existing between the model metrics and source code metrics, it is for only two set of case studies. For any statistical analysis more the sample data more accurate the results will be. Hence to make the results more precise we recommend considering more set of case studies and performing the analysis.

For the analysis we have considered two metrics which satisfy the defined constraints. But there is scope for defining more metrics for the Simulink models and then they can also be used as quality measure

The model metrics which we have defined are calculated manually for the models. Further work can be done to develop a tool which calculates these metrics automatically.

References

[1] Carmel E, and Tija P (2007), "Offshoring Information Technology: Sourcing and Outsourcing to a Global Workforce", Cambridge University Press.

[2] Etzkorn L, Bansiya J, Davis C (1999), "Design and code Complexity metrics for OO classes", Journal of Object oriented programming, vol 12, pp. 35-40.

[3] Grimm K (2003), "Software Technology in an Automotive Company-Major Challenges", Proc ICSE, pp. 498-505.

[4] Halstead M H (1977), "Elements of Software Science", North-Holland, New York.

[5] Heinecke H (2005), "Automotive System Design Challenges and Potential", In Proceedings of the Conference on Design, Automation, and Test in Europe, IEEE Computer Society, Washington, DC, pp. 656-657.

[6]Henry S and Selig S (1990), "Predicting Source-Code Complexity at the Design Stage," IEEE Software, pp. 36-44.

[7] Henry S M, and Kafura D G (1981), "Software Structure Metrics Based on Information Flow", IEEE Transactions on Software Engineering, vol. SE-7, pp.510-518.

[8] McCabe T J (1976), "A Complexity Measure", IEEE Transactions on Software Engineering, vol. SE-2, pp. 308-320, Dec. 1976.

[9] Piwowarski P (1982), "A nesting level complexity measure", SIGPLAN , pp. 44-50.

[10] Richard G L (2007), "An Introduction to Statistical Concepts", Second Edition, Lawrence Erlbaum Associates Inc., NJ.

[11] Simulink Basic Tutorial: http://www.mathworks.co.kr/access/helpdesk/help/toolbox/ simulink/simulink_product_page.html

[12] Testwell CMT ++ Metric Tool: http://www.verifysoft.com/en_cmtx.html
[13] Understand Metric Tool: http://www.scitools.com/

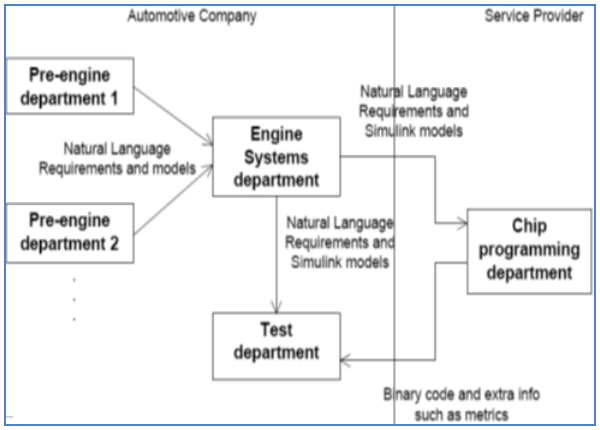


Fig 1 Overview of Outsourcing Process

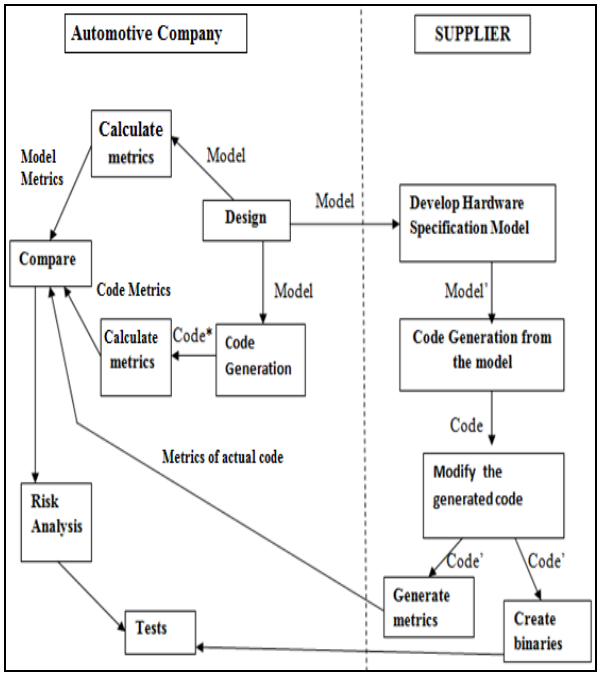


Fig 2 New Approach for Outsourcing

Table 1 Metric Values Comparison

Module Name	Model Metrics			Code Metrics		
	Cyclomatic	Halstead		Cyclomatic	Halstead	
		N1+N2=N	n1+n2=n		N1+N2=N	n1+n2=n
Complex Model	7	53	37	7	256	66
Semi complex	3	41	33	3	111	43
Simple	2	18	16	2	65	31

Table 2 Model and source code metric values of the case studies

Case Study	Module Name	Model Metrics			Code Metrics		
		Cyclomatic	Halstead		Cyclomatic	Halstead	
Case study 1			N1+N2=N	n1+n2=n		N1+N2=N	n1+n2=n
	Module A	1	19	14	1	56	25
	Module B	3	48	38	3	372	72
	Module C	3	29	24	3	141	43
	Module D	4	64	51	4	253	58
	Module E	3	15	12	3	72	31
	Module F	1	20	18	1	133	42
	Module G	2	26	21	2	145	47
	Module H	2	40	34	2	240	54
	Module I	3	17	14	3	95	39
	Module J	3	21	20	3	74	34
	Module K	2	25	21	2	123	37
	Module L	7	50	39	7	392	62
Case study 2							
	Module M	5	26	11	5	366	54
	Module N	5	26	11	5	366	54

Table 3 Correlation between Halsted Model and Source Code Metrics

	Correlation between model(N) and code(N)	Correlation between model(n) and code(n)
Spearman's Rank correlation Coefficient	+0.84	+0.87

Table 4 Final Rank of Modules

Case Study Modules	Average Rank	Final Rank
Module A	10.50	12
Module B	3.00	3
Module C	4.00	4
Module D	1.50	1
Module E	7.50	10
Module F	10.00	11
Module G	7.00	8
Module H	6.00	7
Module I	5.75	6
Module J	5.50	5
Module K	7.25	9
Module L	1.50	2

2nd International Engineering Symposium - IES 2012
(KU-MU-NITK-HCMCUT Joint Symposium) March 5-7, 2012, Kumamoto University, Japan

Round Robin Approach to Intrusion Detection System on SNMP

Ekansh Jitendra Gupta[1] **Mayank Nayar**[2] and **Raunaq Akhauri**[3]

1 *Department of Information & Communication Technology, Manipal Institute of Technology, Manipal,Udupi 576104, India. E-mail :gupta.ekansh@gmail.com*
2 *Department of Information & Communication Technology, Manipal Institute of Technology, Manipal,Udupi 576104, India. E-mail :maynayar@gmail.com*
3 *Department of Information & Communication Technology, Manipal Institute of Technology, Manipal,Udupi 576104, India. E-mail :raunaq.90@gmail.com*

Abstract: In this digital era, where online presence in every form has turned into a necessity, Information Security can't be neglected. One of the most important features of computer networks, Intrusion Detection System (IDS) is an important key to Network Security. Most network devices support *Simple Network Management Protocol (SNMP)* because it is active by default. An SNMP Attack can result in the network being mapped, and traffic can be monitored and redirected. Our work deals with the analysis of packets. The payload of the packet is checked for different signatures, thereby identifying malicious content. To keep up with the constantly changing packet signatures, the system would analyse the payload repeatedly for new signatures and update it into the existing database, alerting the system about the attack as and when an intrusion is detected. The paper is a research on development of general and symmetric methods for Intrusion detection. The idea is continuous mining of data and its analysis for new patterns of attacks.
Key terms: IDS, SNMP, packet analysis, attack signature, pattern recognition, data mining

Introduction

Intrusion Detection System (IDS) is device or a computer application designed to monitor a network or a system for malicious activities, packet or policy violations and traffic pattern. Some systems may attempt to stop an intrusion attempt but this is neither required nor expected of a monitoring system. The goal of the device or the application is identifying possible incidents, logging information about them, and reporting attempts to the network or system administrator.

IDS basically sniff data-> store data tag-> decrypt information-analysis data-> determine attacks-> alert system. This is taken care by the monitoring and detection system of the IDS.

The part of preventing attacks is taken care by the Intrusion Prevention System (IPS). IDS and IPS together are known as IDPS and work together to give the system or network a full care over attacks.

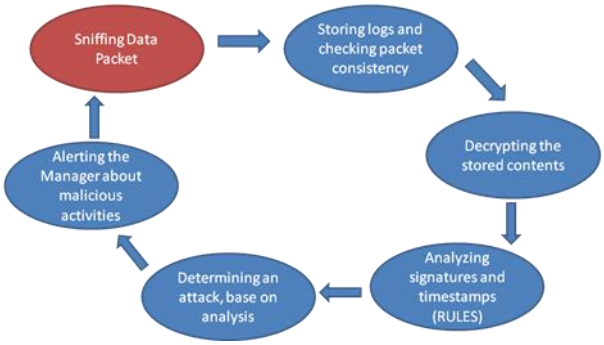


Figure 1: Basic IDS working principle

There are two types to Intrusion Detection Systems:

- Statistical anomaly-based IDS
- Signature-based IDS

A statistical anomaly-based IDS determines normal network activity like

bandwidth used, protocols used, ports and devices generally connect to each other and alert the administrator or user when traffic is detected which is anomalous(not normal).
Signature based IDS monitors packets in the Network and compares with pre-configured and pre-determined attack patterns known as signatures. The issue is that there will be lag between the new threat discovered and Signature being applied in IDS for detecting the threat. During this lag time your IDS will be unable to identify the threat. The pre-determined attacks are known as rules.

This study is based on Rule Based anomaly detection in the Signature-based IDS.

Basics of Signature-based IDS

Rules
Rules are sets of instructions to be followed to engage traffic on a specific network.
They are independently built for each protocol separately. They are checked sequentially (one by one) for different protocols and headers.
Rules are a necessity to check for the flow of control of the system. Any and all anomalies can be identified if sufficient types of rules are applied over a system.
Rules are structures for Firewall implementation, i.e. it is necessary to have rules to firewall data flow over network.

A general example of Rule
<STATUS/FLAG> <PROTOCOL> <SRC IP> <DEST IP> <TRAFFIC DIRECTION> <SRC PORT> <DEST PORT> <OPTIONS>

Here,
- STATUS/FLAG – the type of action to be performed when a rule or anomaly is detected.
- PROCOTOL – the protocol type used for the packet frame.
- SRC IP – IP address of the sender.
- DEST IP – IP address of the receiver.
- TRAFFIC DIRECTION – direction in which the packets are sent i.e. into the network (->) out from the network (<-) or in both directions (<>)
- SRC PORT – the port number used by the sender.
- DEST PORT – the port number used by the receiver.
- OPTIONS – Extra features to check for packet data, header violations and specifying special alert detections to different kind of attacks.
- Options include several options like msg, sid, offset, depth, content, metadata etc.

Rule Concept
Rules are handled in a specific way by the algorithm or the configuration file running in the background. Specific attack patterns are recognised from the vulnerabilities of the protocols, systems, packet formats and time synchronizations and these patterns are stored in files as rules.

Salient features of rules:
- Rules can be defined for different types of attacks, such as backdoor, chat, dns, dos, finger, ftp, icmp, imap, mysql, netbios, policy, certificate etc.
- Each rule is added to a header file depending on the type of rule.
  Type can be defined as the specific signature used to attack on the system.
  i.e. all backdoor related rules are put into the file for backdoor rules.
- These rule files or headers are now included in the intrusion configuration file (CONF) or IDS algorithm file.
- Now the IDS has to check for all the rule files included in the CONF file and has to also check for a all the rules included in one header file.

Extended Rule Concept
Inspite of the features in rules and rule testing techniques normally implemented, there are shortcoming and disadvantages of using the normal technique. Hence, to fasten the approach and to get results efficiently new features are to be added into the algorithm.
Extensions in the rules are as follows:
- All network PROTOCOLS have a different RULE HEADER.

A RULE HEADER can be defined as a file storing similar kind of rules or attack patterns.

- All miscellaneous type rules or attack types have a different rule header.
- The Algorithm or Configuration file [A/C] contains all types of rule headers. A user can edit the A/C and include specific header for speeding up the execution process.
- Depending on the network traffic only few headers can be included to look for attacks concerned with the network specifics.
- Threats are divided on the basis of PROTOCOL, IP, PORT, DATA, SEQUENCE, TIME-STAMP & OPTIONS.
- The Round Robin approach checks different kinds of RULE HEADERS one after the other, on a Round Robin basis to find a solution.
  The headers are queued in a Round Robin Queue before they are processed.
- The queue has a specific slot size [*ss*] for all headers.
- Specific types are attacks which are more prominent then the others and require more time for processing then the others.
  So we assign a window size [*ws*] to each header.
  The *ws* is a multiple of the *ss* and each header is assigned a *ws.*
  Each header has a *ws* amount of time in the queue.

Note: These ws can the set by the Network Administrator on the basis of the network requirement, traffic details and attack pattern.

x	x	x	x	x	…	…	x

Figure2: Slot Queue with 8 slots denoted by x.

>> All slots are of equal sizes (*ss*)
>> The slot window size (*ws*) has to be the multiple of the slot size (*ss*)
i.e. a is a window size then
a=Mx
where, M is a positive integer
>> The slot has to be of fixed length based on the rule executed.
It is not on time based but rule execution based.
x equals to execution of ONE rule and not any fixed time interval.
The slot sequence queue has different ws for different headers.

Adaptive Features – Priority based

For the application or device to be robust and durable the system should be adaptive with time.
To make this system adaptive the algorithm implements priority in the system. This priority changes with use of the system and matures with time. The system becomes fast for the usual attacks as they are tested first.

The basic features of the priority based algorithm are:

- As the algorithm starts, it allocates an array for priority of the headers. The algorithm increases the count in this array as it finds a rule match or hit.
- On the basis of priority the algorithm matures itself.
- On the basis of priority the headers are divided into classes.
- Classes range from A to Z and each class has a different time interval for execution time.
- Headers with highest priority or count are put into class A and the one with lowest priority into class Z.
- Each Header is put in a class based on priority and each class has a different interval for running.
- Class A is in the front of the queue and Class Z and the last.
- Hence the headers with the highest priority are processed first and then the headers with the lower priority are checked.
- This approach is adaptable as it changes with the network to which the algorithm is operating and to the generally defaulted rules as it bases its queue on the basis of priority which keeps on changing with each rule hit, hence in a general case the algorithm works well with the priority system.

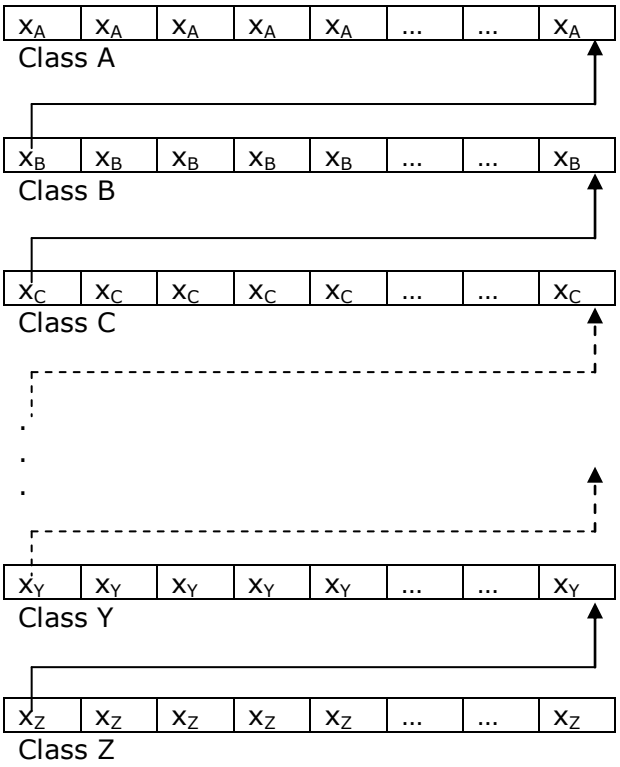


Figure 3: Priority based system

As you can see the queue is divided into parts based on the classes. Class A gets the processor first and Class Z at last. Hence the rule header defaulted mostly is processed first and the rule defaulted least is processed at the end.

Additional Options for Protocol Specific use

The rules implemented are protocol based, i.e. rules have to have a protocol, and hence additional options can be added to the basic algorithm on specific protocols.

Example: DNS has a specific header as shown below:

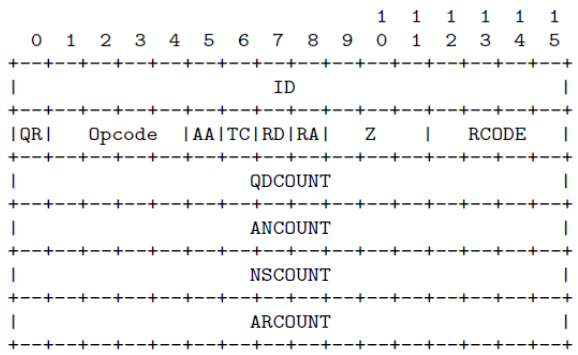


Figure 4: DNS packet header.

The header has fields like ID, QR, Opcode etc.
These fields are used to check for the anomalies in the packet which can account for an attack.

Hence all the fields need to be checked for the anomalies and for these checks additional options are added in the algorithm to optimise it for specific protocols.

Implementation on SNMP

Simple Network Management Protocol has a protocol header with fields like version, community string, request id, error, error id, data sequence (object id, object value).

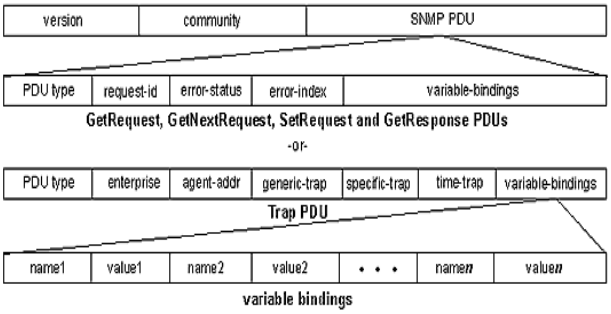


Figure 5: SNMP Header

Features of additions options on SNMP:

- For these different field anomalies or attacks the algorithm again has to be slotted or divided into slots.
- The window size (ws) in each of the headers is divided into number on slots called the mini-slots (ms). These *ms* are used for checking for specific field rules.
- As per the normal approach all the fields are checked sequentially but this algorithm takes it to the next level and follows the round robin approach in field checks too.
- Each rule is not checked sequentially but again on a round robin basis. Hence at first only one rule is checked for a specific field and then one rule is checked for another field, so the algorithm is consistent in checking around for different type of rules.

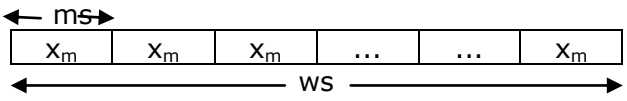


Figure 6: shows a window slot with mini-slot. Each field rule is put in the mini-slot and hence finally a window slot is made.

The idea is to look for anomalies in different parts of the packet at a faster rate. Checking different parts of the packet adds a random advantage of finding an anomaly.

For an SNMP packet:

- The fields in the SNMP packet are needed to check if we write all the rules sequentially. Then all rules of the version will be checked first and then of community string and at last for variable binding. Therefore if an anomaly is present in variable binding then a normal sequential processing will take a lot of time to find a result.
- This approach fastens the search by randomizing the process and not going sequentially. The algorithm searches for anomalies in all the fields on a round robin bases.

Example: If the problem is in the MIB then the approach will check for the MIB much faster than normal approach.

Advantages of the System

- Attacks are random approaches for breaching into the security of a network and planting malicious data into the network, hence sequential search cannot work and this random approach over anomalies is better.
- As the Algorithm is slot based and uses round robin approach hence it makes a successful detection in much less time or faster than the sequential approach, increasing the data rate of the network.
- The priority feature of the algorithm enables the administrator to detect anomalies which are common to the network in a much faster way then any regular approach.
- As the priority is adaptive and keeps on changing with the anomaly hit rate and network traffic the algorithm changes its rule sequence and still remains fast and apt on the slot queue.
- The checking on the fields of different protocols is followed on the basis of round robin approaches and hence the protocol based mini-slot queuing improves the efficiency of the algorithm.
- The approach does not concentrate on one type of header for all the time but checks different types of headers in a round robin way, making the approach more efficient.

Limitations and Shortcomings

- If an attacker proceeds sequentially, then the attack packet will take a lot of time in finding out an anomaly in the last part of the first header type and hence can cause DDOS (data denial of service), causing network unavailability. A Similar problem occurs if the attacker tries the same thing as mentioned in the previous scene, with the field in the mini-slots and again causes DDOS.
- The algorithm requires advanced hardware for efficient processing.
- The algorithm is complex to implement.

Conclusions

The system implemented above is a fast and efficient approach for implementing Intrusion Detection System on a network or system. The Approach can also be implemented on specific Protocols (as shown above) and used to find specific field attacks in a protocol.
The approach is robust to time as it matures itself used a dynamic priority based system.

References

[1] John McHugh, Alan Christie, and Julia Allen, "Defending Yourself: The Role of Intrusion Detection Systems", IEEE Sofware, September/October 2000.
[2] Fredrik Valeur, Giovanni Vigna, Christopher Kruegel,Richard A. Kemmerer, "A Comprehensive Approach to Intrusion Detection Alert Correlation", IEEE Transaction on Dependable and Secure

Computing, VOL. 1, NO. 3, July-September 2004.
[3] Robiah Yusof, Siti Rahayu Selamat, Shahrin Sahib,"Intrusion Alert Correlation Technique Analysis for Heterogeneous Log", IJCSNS International Journal of Computer Science and Network Security, VOL.8 No.9, September 2008.
[4] BELL94b Bellovin, S., and Cheswick, W."Network Firewalls." IEEE Communications Magazine, September 1994.
[5] CHAN02 Chang, R. "Defending Against Flooding-Based Distributed Denial-of-Service Attacks: A Tutorial." IEEE Communications Magazine, October 2002.

CHEMICAL ENGIEERING, BIOTECHNOLOGY & RELATED FIELDS

2nd International Engineering Symposium - IES 2012
(KU-MU-NITK-HCMCUT Joint Symposium) March 5-7, 2012, Kumamoto University, Japan

Studies on the Production of Camptothecin from an Endophytic Fungi *Fusarium Sp*

Sogra Fathima B, Krishna Kumar A J, Raj Mohan B

Department of Chemical Engineering, National Institute of Technology Karnataka, Surathkal, Mangalore 575025, India. email:fathi_bio@yahoo.co.in

Abstract:
Camptothecin (CPT) a monoterpene alkaloid is a potent natural anticancer drug usually extracted from *Nothapodytes foetida* (Icacinaceae) a medicinal plant inhabitant of Western Ghats, India. Several efforts have been made to enhance its production quantitatively. In the present study endophytic fungi *Fusarium sp* was isolated from explants of *Nothapodytes foetida* and identified based on morphological characteristics. The presence of CPT was analyzed chromatographically and confirmed by comparing with authentic standards. The growth kinetic studies were carried out and the kinetic parameters were estimated using Exponential and Monod model.

Keywords: Camptothecin, Endophytic Fungi, *Fusarium sp*, Growth kinetics, *Nothapodytes foetida*

Introduction

Camptothecin (CPT), a pentacyclic quinoline alkaloid (Fig. 1) was first isolated from the wood of *Camptotheca acuminate* (Nyssaceae) by Wall et al. (1966). CPT is naturally distributed in several plant families of the order Asterids as reported by Larsson (2007). Among these, leaves and stem bark of *Nothapodytes nimmoniana* (Grahm) Mabb. (Icacinaceae), a small tree in southern India, accumulate the highest content of CPT in the range (0.3–0.5%) Ramesha et al. (2008). The primary action mechanism of CPT is by virtue of inhibiting the intranuclear enzyme topoisomerase-1, which is required in DNA replication and transcription during molecular events Hsiang et al. (1985). *Nothapodytes foetida* (*Mappia foetida*) commonly called "Kalagur" is a medium sized medicinal plant that grows widely throughout India including the northwestern Himalayan agro climatic region as well as Southern Konkan forests. The best suited habitat for this medicinal plant is found in the northwestern Ghats of India Cooke (1967).

Plants are commonly a host to multitude of microbes including endophytes which may influence the production of plant's metabolites and may also be capable of producing metabolites that are similar to those produced by the host plants Rehman et al. (2008).

Since the discovery of endophytes in Darnel, Germany in 1904, various investigators have defined endophytes in different ways which are usually dependent on the perspective from which the endophytes were being isolated and subsequently examined by Tan R. X and Zou W. X (2001). A widely accepted definition of endophytes i.e., "Microbes that colonize living, internal tissues of plants without causing any immediate, overt negative effects" is given by Bacon and White (2000). It has been estimated there may be as many as 1.5 million different fungal species on our planet by Hawksworth and Rossman (1987). Of these only about 10% have been discovered and described and nearly 1% is examined for their production of secondary metabolites. A major contribution is thought to be made by endophytic fungi which are found mostly in all plant families of different climatic

regions of the world. Thus endophytic fungi are considered to be rich and reliable source of genetic diversity with novel and undescribed species Narayan et al. (2006). The demand for natural secondary metabolites is increasing and hence there is an immediate need for finding a significant alternative source for consistent supply of important chemical compounds like Camptothecin.

The objectives of the present study are: (i) To check the potentiality of the isolated endophytic fungi from *Nothapodytes foetida* as a source for CPT production, (ii) To observe the growth kinetics of endophytic fungi and predict the kinetic parameters using mathematical models.

Experimental studies

Collection of plant material

Nothapodytes foetida synonym for *N.nimmoniana (*Hombe Gowda et al., 2002) was collected from Agumbe forest of South Karnataka. The plant material was identified and authenticated on the basis of botanical characteristics by an experienced Botanist. Disease free parts of the plants like stem, twigs and leaves were cut with a sterile scalpel and stored at 4ºC in a sterile plastic bag prior to the isolation process.

Isolation and Identification of Endophytic Fungi

The endophytic fungal culture used in this study was isolated from leaves, twigs and stem of medicinal plant *Nothapodyte foetida*. The plant samples were surface sterilized by using the method described by Suryanarayanan et al. (1998). The surface sterilized plant segments were evenly spaced in petri dishes (9 cm diameter) containing potato dextrose agar (PDA) medium amended with chloramphenicol 150 mg/L. The petri dishes were sealed using Parafilm™ and incubated at 26±1°C in a light chamber with 12 hours of light followed by 12 hours of dark cycles. The petri dishes were monitored every day to check the growth of endophytic fungal colonies from the plant segments. As and when the hyphal tips emerged out from plant segments they were isolated and sub-cultured and brought to pure culture by serial sub-culturing. The same procedure without surface sterilization was used as negative control to check for contamination by fungi. Purity of the isolates was checked by preparing microscopic slides of every isolate by standard methods of microscopy.

Screening Of Endophytic Fungi For Camptothecin Production

Endophytic isolates obtained were screened for the production of camptothecin. Each organism isolated in this study was grown in fungal growth liquid media containing dextrose (4%) and peptone (1%). Agar plugs containing mycelium were used as inoculum. The Erlenmeyer flasks with growth media and fungus were grown for 14 days at 28$\pm$2° C under shaking conditions at 150 rpm. After every 24 h, three flasks of 9 isolates were separately sacrificed and harvested. The culture fluid was filtered through four layers of cheesecloth followed by Whatman No.1 filter paper. The filtered broth extracted with organic solvent dichloromethane. The organic phase was collected and the solvent was then removed by evaporation under reduced pressure at 35°C using rotary vacuum evaporator as given by Strobel et al. (1996b). All of the prepared extracts were subjected to TLC with standard camptothecin (Sigma, United States) for detection of Camptothecin.

Extraction of Camptothecin

The positive isolates of endophytic fungus for CPT production was grown in 250 mL of Erlenmeyer flasks containing 100 mL of Sabouraud dextrose broth and incubated for 14 days on shaker with 150 rpm at 28$\pm$2°C. The mycelium of endophytic fungi was separated from the fermentation broth by filtration. For extraction of camptothecin from mycelium, the procedure described by Shweta et al. (2010) was followed. The mycelia were dried to constant moisture content at 60° C for 96 hr in a hot air oven. The dried samples were ground to fine powder using pestle and mortar. About 0.1 g of fine tissue powder from each of the samples was extracted in 10 ml of 61 % ethanol at 60° C in a shaking water bath. After

cooling to room temperature, the extract was centrifuged at 10,000 rpm for 10 min at 10 °C (Remi cooling centrifuge, India). The supernatant was passed through a 0.22 µ filter (Tarsons, India) and analyzed for the presence of CPT. The extraction procedure for broth followed was that of Strobel et al. (1996b) as described earlier. Further the extracts were analyzed by chromatographic separation and spectroscopic analyses.

Chromatographic Analysis

Thin Layer Chromatography (TLC) analysis was carried out on Merck 0.25mm silica gel plates 1mm (20cmx20cm) developed in a solvent system comprising of chloroform-methanol(v/v) in the ratio 6:4, 7:3, 9:1 and 8:2. Camptothecin procured from SIGMA was also run along with the samples as standard.

Liquid Chromatography/ Mass Spectrometry (LC/MS) analysis of the extracts was performed using BDS HYPERSIL C 18 reverse phase column with a mobile phase consisting of 40% acetonitrile and 60% water with 0.1% trifluroacetic acid in a gradient mode at a flow rate of 0.2 mL/min, run time of 60 mins and injection volume of 10µL. After each run the column was washed and re-equlibrated.

Microbial Growth Kinetics

Understanding the growth of microbes is an important key step for optimal production of bio products. Growth kinetic study of the fungal isolates was done by conducting shake flask experiment on incubatory shaker 150 rpm for a period of 14 days at 28±2°C in presterilized 250 ml Erlenmeyer flasks consisting of 4% dextrose and 1% peptone. Agar plugs impregnated with mycelia were used as inoculums. The first sample was collected immediately after inoculation and subsequent samples were harvested in the interval of 3 days. Biomass is filtered from the fermentation broth and dry weight of biomass is measured to estimate the yield.

Theoretical studies

Modelling

The first step in modelling a fermentation process is selecting a suitable mathematical expression for microbial growth. In this work, kinetics of fungal growth is described using unstructured model. In general a fungus appears to be in a filamentous or pellet form under submerged conditions.

Exponential model

Growth of the fungi in filamentous form was observed to follow the exponential law. It has been found that individual hypha grows at the tips of the mycelia only, with a linear extension rate. Exponential growth is maintained by continuous branching of hyphae Van Suijdam et al. (1982). The growth of various fungi in accordance with exponential law was reported by (Pirt et al., 1975)

$$X = Xo\ exp(\alpha t) \qquad (1)$$

Where, X is mass of mycelium/cm^3 at time t, and α is a constant (specific growth rate).

Monod Model

Monod (1942) described the growth of microorganism based on substrate consumption, which is used to describe the relation between the specific growth rate (µ) and the concentration of substrate and essentials nutrients (S). It is given as

$$\mu = \mu max * S/(ks + S) \qquad (2)$$

Where μmax is maximum specific growth rate achieved when $K_s << S$, where K_s is the limiting nutrient concentration corresponding to the half maximum growth rate (Barclay et al., 1993). The yield of biomass with respect to substrate consumption ($Y_{x/s}$) is given as

$$Y_{x/s}=X-Xo/So-S \qquad (3)$$

The rate of biomass generation and the rate of substrate consumption in a batch culture can be given as

$$\frac{dX}{dt} = \mu \max S X/(Ks + S) \qquad (4)$$

Substituting equation (3) in (4) and for substrate concentrations and integrating we get the following expressions

$$\mu max\, t = \left(\frac{Ks\, Yx/s}{Xo+So\, Yx/s}+1\right)\ln\left(\frac{X}{Xo}\right)-\left(\frac{Ks\, Yx/s}{Xo+So\, Yx/s}\right)\ln\left(\frac{Xo+So\, Yx/s-X}{Xo+So\, Yx/s-X0}\right) \quad (5)$$

Using equation (5) we can predict kinetic parameters such as μ_{max}, K_s and $Y_{x/s}$ using non linear regression analyses (Barclay et al., 1993).

Results and Discussion

Endophytic fungi are prospective producers of an abundant and dependable source of bioactive and chemically novel compounds with potential for exploitation in wide variety of medical, agricultural and industrial arenas. They are a poorly investigated group of microorganisms that represent secondary metabolites having an immense impact on modern medicines, since about 40% of prescription drugs are based on them. Rajesh et al, (2011)

Organism characteristics

Fungal isolates from the plant samples of *Nothapodytes foetida* in this study was identified as *Fusarium oxysporum* by analysing mycological characteristics. Cottony spongy white aerial mycelia produce pale pink which later changed to dark violet pigment (Fig. 2a & b). It is one of the well known properties of *Fusarium oxysporum.* It is found to produce both macroconidia and microconidia. (Fig 2 c) The observed morphological characteristics of the identified species are compared with the reports of Booth (1970) and description in a *Fusarium* manual book John and Brett (2006).

Analysis of Camptothecin

Initial screening of isolates for the production of CPT was done by thin layer chromatography. The fungal compound had a chromatographic property identical to the authentic CPT in a solvent system of chloroform and methanol (8:2 v/v). Rf value in the range of 0.56-0.59 was observed under a shortest wavelength.

LC/MS analysis demonstrated near equivalence retention time between the isolated camptothecin and the standard material (Fig. 3 a& b). MS validation of the fungal CPT compared that of the standard is shown in (Fig 3 c & d). The authentic camptothecin yielded MH^+ at m/z (349.38) and $M+MH^+$ at m/z (697.07). The fungal CPT yielded characteristic fragment peaks $M+CO_2-H$ at m/z (391.41) and M+M at m/z (696.32) which showed 100 percent relative abundance.

Kinetic and modelling

The experimental result for growth of fungi was simulated using two models. The parameters estimates for exponential model are X_0=2.01 and α=1.48 and for Monod model are X_0=0.1267, μ_{max}=1.2124, K_s=3.2045 and Y_{xs}=0.1113. By comparing two models with experimental result, it is evident that Monod model predicts kinetic parameter with minimum sum of square weighted residuals. Exponential model initially over predicts the growth of fungi and it also observed to attain stationary phase after long time intervals.

Conclusion

The use of endophytic fungi opens up new areas of biotechnological exploitation which leads to the necessity of isolation and cultivation of these organisms. In the present study *Fusarium sp* has shown to be a suitable alternative for the production of Camptothecin. However large scale production of secondary metabolites still needed to be improved.

Acknowledgement

We thank and wish to express our gratitude to Dr. G. K Bhat, retired Prof of P P College, Udupi and also Dr. Johnpaul Muthumary, CAS University of Madras for encouragement and suggestions.

References

[1] Bacon C W and White J F (2000), Microbial Endophytes, Marcel Dekker Inc., New York, pp.341-388.

[2] Barclay et al (1993), Modelling the Growth Kinetics of *Phanerochaete chrysosporium* in Submerged Static Culture. Applied and Evironmental Microbiology, pp. 1887-1892

[3] Booth C (1970), Fusarium oxysporum. CMI descriptions of pathogenic fungi and bacteria. Kew, Surey, England.

[4] Cooke T (1967), Flora of The Presidency of Bombay, Botanical Survey of India, vol. 1, pp.220-225

[5] Hawksworth D C and Rossman A Y (1987), Where are the undescribed fungi? Phytopathology. 87: 888-891.

[6] Hombe Gowda H C et al (2002), Breeding types in *Nothapodytes nimmoniana* Graham. *Curr. Sci.*, 83: pp.1077–1078.

[7] Hsiang Y H et al (1985), Camptothecin induces protein-linked DNA breaks via mammalian DNA topoisomerase-I. *Journal of Biological Chemistry*, 260: 14873-14878
[8] John F.Leslie and Brett A.Summerell (2006). The Fusarium Laboratory Manual, Blackwell Publishing
[9] Larsson S (2007). The new chemosystematics: phylogeny and phytochemistry. Phytochemistry 68:2903–2907.
[10] Narayan et al (2006), Diversity of endophytic fungi associated with *Taraxacum coreanum* and their Antifungal activity.Mycobiology 34(4): 185-190.
[11] Pirt S J (1975), Principles of Microbe and Cell Cultivation. Blackwell Scientific publications, Oxford
[12] Rajesh K et al(2011), Endophytes-Mines of pharmacological therapeutics, World Journal of Science And Technology 1(5);127-149.
[13] Rehman S et al (2008), An Endophytic *Neurospora sp*. from *Nothapodytes foetida* producing Camptothecin. Applied biochemistry and microbiology, vol. 44, 225-231
[14] Shweta S et al (2010), Endophytic fungal strains of *Fusarium solani*, from *Apodytes dimidiata* E. Mey. ex Arn (Icacinaceae) produce camptothecin, 10-hydroxycamptothecin and 9-methoxycamptothecin. *Phytochemistry*.; 71: 117-122.
[15] Suryanarayanan T S et al (1998), Foliar fungal endophytes from two species of mangrove *Rhizophora.* Canadian journal of Microbiology 44: 1003-1006
[16] Strobel et al (1996b), taxol from *Pestalotiopsis microspora*, an endophytic fungus of *Taxus wallachiana*; Microbiology 142: pp.435-440.
[17] Strobel G A and Daisy B (2003), Bioprospecting for microbial endophytes and their natural products. Microbiol. Mol. Biol. Rev. vol 67, pp.491-502
[18] Tan R X and Zou W X (2001), Endophytes: a rich source of functional metabolites. Nat. Prod, Rep 18, pp.448-459
[19] Van Suijdam J C (1982), Unstructured Model for Growth of Mycelial Pellets in Submerged Cultures. Biotechnology and Bioengineering, Vol. XXIV, p. 177-191
[20] Wall M. E (1966), Plant antitumor agents. I. The isolation and structure of camptothecin a novel alkaloidal leukemia and tumor inhibitor from *Camptotheca acuminata*. *Journal of the American Chemical Society*, 88: pp.3888-3890

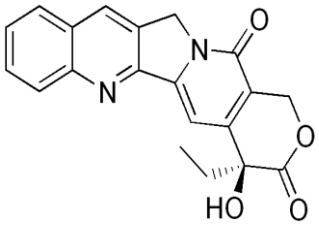


Fig. 1 Structure of Camptothecin

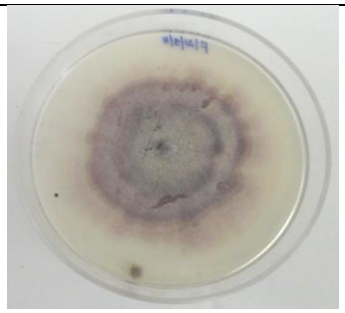


Fig. 2a *Fusarium oxysporum* grown on PDA (front view)

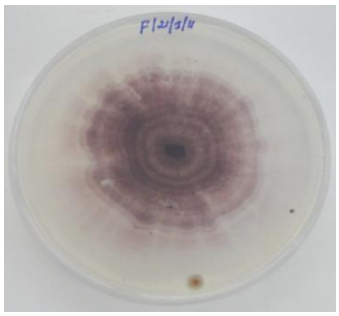


Fig. 2b *Fusarium oxysporum* grown on PDA (back view)



Fig. 2c Microscopic view of microconidia and macroconidia of *Fusarium oxysporum*

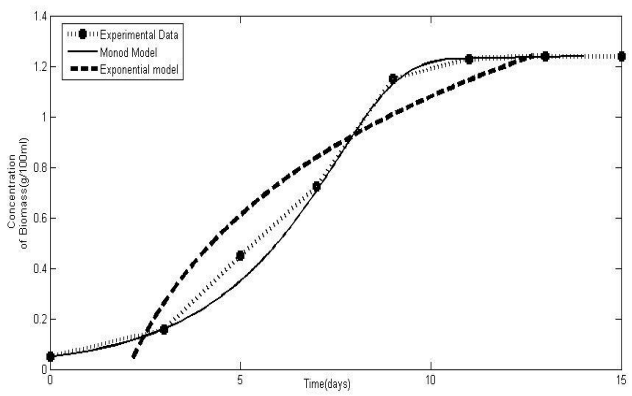
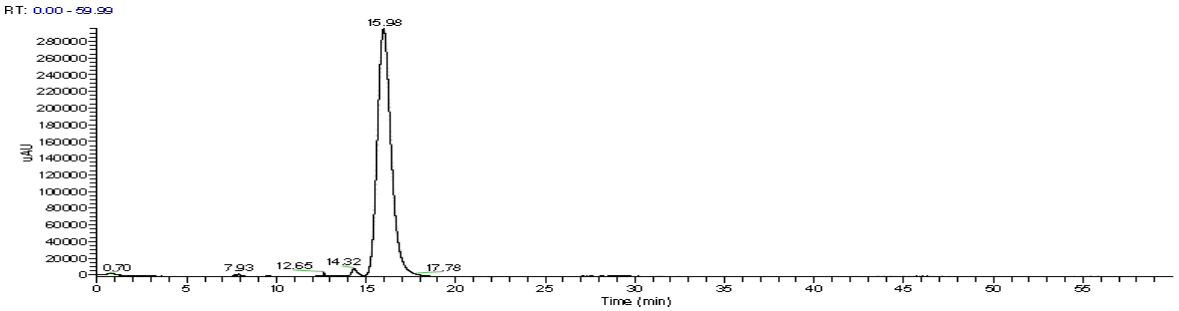
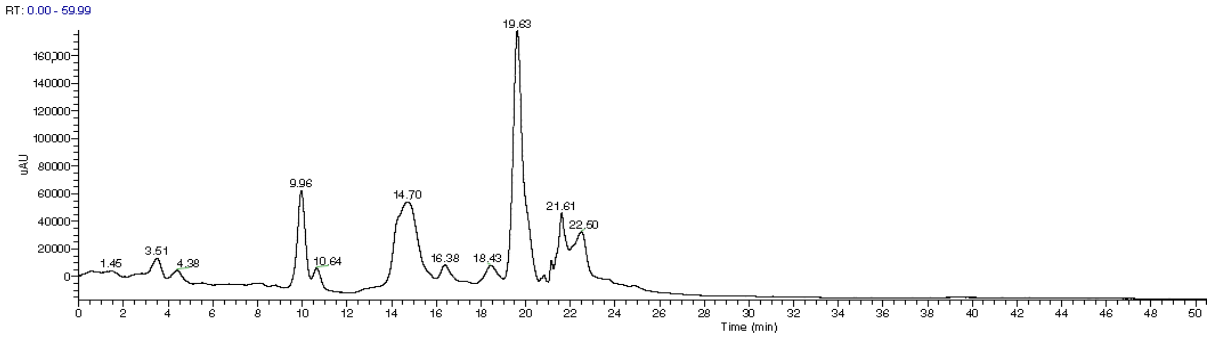


Fig. 4 Growth Kinetics of *Fusarium oxysporum*

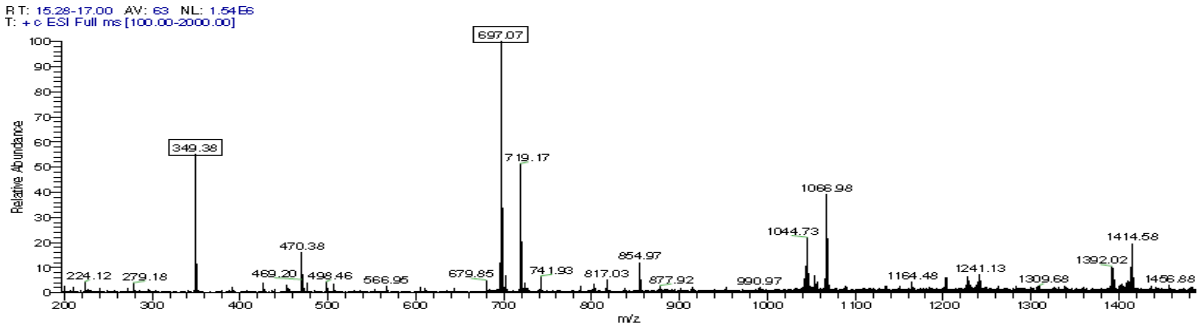
(a)



(b)



(c)



(d)

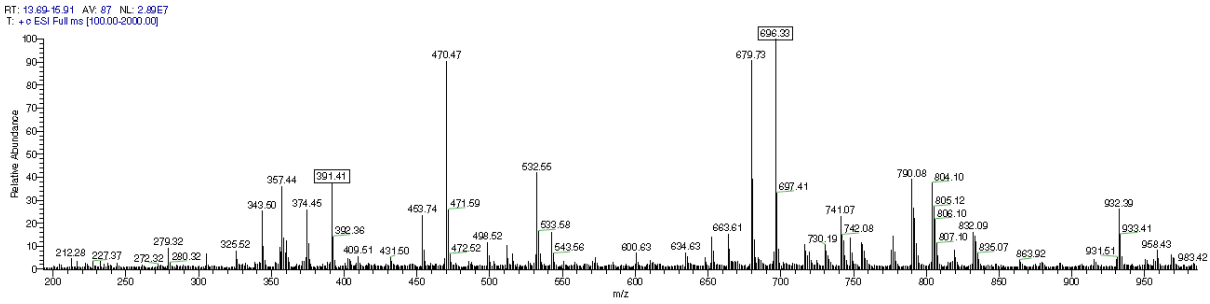


Fig. 3 Liquid chromatography profile of Camptothecin standard (a), fungal Camptothecin (b)

Mass spectra of authentic Camptothecin (c) and fungal CPT (d)

2nd International Engineering Symposium - IES 2012
(KU-MU-NITK-HCMCUT Joint Symposium) March 5-7, 2012, Kumamoto University, Japan

Isolation of halophilic bacteria for ectoine, xylanase, cellulase production from agro-wastes

Pooja Shivanand [1] **Gopal Mugeraya [2]** and **Hitesh Chhabra[3]**

1 *Department of Chemical Engineering, National Institute of Technology Karnataka, Surathkal, Mangalore 575025, India. email:Pooja.shivanand@gmail.com*
2 *Department of Chemical Engineering, National Institute of Technology Karnataka, Surathkal, Mangalore 575025, India. email:gopalmugeraya@yahoo.com*
3 *Department of Chemical Engineering, National Institute of Technology Karnataka, Surathkal, Mangalore 575025, India. Hitesh.chhabra88@gmail.com*

Abstract: Several strains of biopolymer (xylan, inulin and cellulose) degrading bacteria were isolated from sea coasts and solar salterns of coastal Karnataka. HPLC analysis showed that Strain PS6 showed high yields of ectoine (64 mg/g dcw) in MM63 media using untreated wheat bran as the medium component. Alkaline and enzymatic pre-treatment of wheat bran was carried out. However, the strain exhibited optimal growth and ectoine production on untreated residue. Xylanase and cellulase activity was assayed by DNS method for those strains which gave a halo zone of clearance on plates stained with Congo-red dye. In the alkaline range (pH 8.5), strain PS3 yielded 1.2 U/ml of xylanase in MM63 medium and yielded sufficient amounts of xylanase in agro-residue media. Strain PS47 was found to produce higher yields of cellulase (0.14 U/ml) at a neutral pH of 7.1. The activity readings on agro-residue media were comparable. Both xylanase and cellulase exhibited stability over a wide range of NaCl concentrations.

Keywords*: ectoine, xylanase, cellulase, halophilic bacteria, saltern, agro-waste*

Introduction

Halophiles are microorganisms that adapt to moderate and high salt concentrations. They are found in all three domains of life: Archaea, Bacteria and Eukarya. Halophilic *Bacteria* grow over an extended range of salt concentrations (3-15% NaCl, w/v and above) unlike the truly halophilic *Archaea* whose growth is restricted to high saline environments Ventosa A. et al. (1998).

Ectoines produced by halophilic bacteria protect biomolecules like DNA, protein and enzyme and are used in advanced buffer systems, cosmetics and skin-care creams. Saline hydrolases like xylanases and cellulases which come under the category of biofuel enzymes have potential applications in several saline fermentation processes.

Few reports are available on the usage of renewable agricultural resources for growth and metabolite production by halophiles. Halophilic bacteria capable of utilizing cheap renewable agricultural wastes could be exploited as an economic alternative to existing production processes.

Isolation of halophilic bacteria

Bacterial isolation was done by the serial dilution plating technique on mineral salt medium (MSM) containing in g/l: $NaNO_3$-2, K_2HPO_4-0.5, $MgSO_4.7H_2O$-0.2, $MnSO_4.H_2O$-0.02, $FeSO_4.7H_2O$–0.02, $CaCl_2.2H_2O$-0.02 NaCl-60, in 1000 ml water using each of the polymeric substrates – xylan and cellulose (0.5% w/v) as sole carbon source. The bacteria growing on these biopolymer medium would harbor the potential enzyme machinery to degrade the polymers and utilize them for growth and multiplication.

The bacterial cultures took around 72-96 h to grow in broth and 5-7 days to appear as

colonies on the agar plates. Most of the isolates appeared as small pin-pointed colonies on the agar surface. Many cultures showed orange-yellow pigmentation which is typical characteristic of halophilic bacteria.

Ectoine production

Growth studies of halophilic bacteria were conducted in MM63 medium containing in g/l: KH_2PO_4-13.61, KOH-4.21, $(NH_4)_2SO_4$-1.98, $MgSO_4.7H_2O$–0.25, $FeSO_4.7H_2O$-0.0011, NaCl-60, and Glucose-5 in 1000 ml water. The growth curve studies are shown in Fig. 1.

After a period of time when sufficient growth was attained, the cells were centrifuged at 8,500 rpm for 20 min at 20 ºC. The cells pellets were dried and lyophilized. The compatible solutes (ectoine) were extracted from dried biomass pellet by using a modified Bligh and Dyer technique, Bligh and Dyer (1959). Several strains produced ectoine as shown in Fig. 2.

Later the halophilic bacteria were grown in MM63 medium were the carbon source glucose was replaced by biopolymers like xylan, CMC, chitin and carob at 0.5% (w/v) level. Out of all the strains PS6 (Gram negative rod) was able to produce ectoine on all the polymers (Fig. 3) and was selected for further studies on wheat bran.

Wheat bran was procured for the local market. It was subjected to alkaline and enzymatic hydrolysis. The purpose is to remove lignin and increase the porosity of the materials. Pretreatment solubilises hemicelluloses and decreases crystallinity of the substrate. Compared to acid or oxidative reagents, alkali treatment appears to be the most effective method in breaking the ester bonds between lignin, hemicellulose and cellulose and avoiding fragmentation of hemicellulose polymers Gasper, M. et al. (2007). A possible advantage of using halophilic bacteria is that the salt created after neutralization does not need to be removed and for haloalkaliphiles the neutralization step can be avoided.

For alkaline treatment, wheat bran mixture was ground to particles of 0.5 – 1 cm. For de-lignification, 100 ml of these agro-residues taken in 1 L Erlenmeyer flasks were soaked in 1% NaOH and autoclaved at 121 ºC for 20 min. After the alkali treatment, the materials were washed with tap water until neutral and oven-dried. Treated substrates were passed through 0.5 mm screens for use as medium component.

For enzymatic treatment, a freeze-dried enzyme mixture was procured from Senzyme (Troisdorf). After treatment at 50 ºC and pH 7.1, both residue and hydrolysate was used in the MM63 medium. The results of ectoine production of PS6 on alkaline and enzyme-hydrolysed wheat bran are shown in Fig. 4. PS6 was found to utilize untreated wheat bran for growth and efficient production of ectoine. Hence pretreatment and neutralization, two cost-intensive steps can be avoided which is significant from industrial view-point.

Xylanase production

Strains grown on xylan were screened for xylanase activity. After incubation of the plates for 2-3 days, zones of hydrolysis were visualized by staining the plates with aqueous solution of 0.1% (w/v) Congo red for 15 min, and then destained with 1 M NaCl. The agar plates showed zone of clearance around the colonies and wells incubated with culture supernatants indicating the hydrolytic activity, when flooded with 0.1% Congo red solution.

Production studies were carried out in 50 ml media taken in 250 ml Erlenmeyer flasks for 96 h at 30 ºC and 150 rpm. For enzyme assay oat-spelt xylan was used as the substrate. The enzyme activity was determined by measuring the release of reducing sugars during the enzyme substrate reaction using the dinitrosalicylic acid method, Miller, G. L. (1959). One unit (U) of activity was defined as 1 µmol of xylose equivalent released per minute at 50 ºC and pH 8.5. The values were determined from the xylose standard curve. PS3 (Gram positive coccus) was found have larger clearance zone on the

plate. It also gave higher activity with DNS test and hence was used for studies on polymer.

The activity of PS3 on MM63 with xylan, treated and untreated wheat bran and rice bran are discussed in Fig. 5. The activity (1.2 U/ml) was higher in xylan medium. Yeast extract and peptone seemed to have a positive influence on xylanase activity. The activities on wheat bran (0.24 U/ml) and rice bran (0.08 U/ml) were lower. However the concentration of agro-residues along with yeast extract and peptone can be optimised to get better yields of xylanase activity. Wahyuntari, B et al. (2009) reported maximum xylanase production of 0.23 U/ml from *Bacillus* sp. AQ-1 in LB supplemented with 0.5% oat spelt xylan medium.

To check the NaCl stability of xylanase the crude enzyme was pre-incubated for 1 h at different concentrations of NaCl ranging from 0.5 M to 4 M. 1 ml of this enzyme was used to in the assay mixture. The xylanase exhibits stability over a wide range of NaCl concentrations (Fig. 6). The activity was reduced to around 50% of the initial value at 3 M NaCl. Truly halophilic enzymes which need at least 12.5% (w/v) NaCl for high activities are less suitable in saline fermentation processes. Therefore, in saline fermentation processes, halotolerant enzymes, which are active both at low and high concentrations of NaCl, are needed.

Cellulase production

Strains grown on CMC as sole source of carbon in MM63 at 6% (w/v) NaCl were screened for Cellulase activity using the Congo red dye-staining protocol discussed above. For quantitative measurements, production studies were carried out in 50 ml media taken in 250 ml Erlenmeyer flasks for 96 h at 30 ºC and 150 rpm. For enzyme assay CMC was used as the substrate. The enzyme activity was determined by measuring the release of reducing sugars during the enzyme substrate reaction using the dinitrosalicylic acid method Miller, G. L. (1959). One unit (U) of cellulase activity is defined as 1 µmol of glucose released per minute at 50 ºC and pH 7.1. The values were determined from the glucose standard curve. PS47 (Gram positive coccus) was found have larger clearance zone on the plate. It also gave higher activity with DNS test and hence was used for studies on agro-residues.

The activity of PS47 on MM63 with CMC, treated and untreated wheat bran and rice bran are discussed in Fig. 7. The activity (0.14 U/ml) was higher in the medium containing CMC with yeast extract and peptone. The activity on wheat bran (0.12 U/ml) was quite comparable to enzyme production on CMC showing that the bacterium is capable of using the agro-residue efficiently for enzyme production. Strain PS47 was able to grow and produce cellulase on rice bran yielding 0.074 U/ml along with yeast extract and peptone.

Deka, D. et al. (2011) reported the enzyme activity of *Bacillus subtilis* AS3 in the unoptimised CMC medium to be 0.07 U/ml. By optimising the medium further (CMC, peptone and yeast extract) a six fold increase in enzyme activity was obtained (0.43 U/ml). It has been reported recently that *Bacillus* sp. (DUSELR 13) and *Brevibacillus* sp. (DUSELG 12) isolated from gold mine produced maximum CMCase activity 0.12 U/ml and 0.02 U/ml, respectively under optimised conditions, Rastogi, G. et al. (2010).

NaCl stability of cellulase was determined as described above. PS47 cellulase exhibited stability over a wide range of NaCl concentrations (Fig. 8). Even in the presence of 4 M NaCl over 60% of the initial activity was retained. These halotolerant enzymes constitute an excellent model for structural adaptations that permit them to be active over a wide range of salt concentrations. Although halophilic enzymes display identical enzymatic functions as their non-halophilic counterparts, they have different properties, including stability and activity at different range of salinity, Amoozegar, M. A. et al. (2007).

Conclusions

The following conclusions are deduced from this study:

- Strain PS6 strain produced higher amount of ectoine (64 mg – 75 mg ectoine per gram dry cell weight) in MM63 medium using untreated wheat bran. This novel study shows the ability of the halophilic bacterium to utilize *bio-polymers* in the *synthetic medium* for growth.
- Ectoine production from halophilic bacteria using untreated lignocellulosic agricultural wastes (wheat bran) is significant from industrial viewpoint since pretreatment of agro-wastes and neutralization, two cost-intensive steps, can be avoided.
- Strain PS3 was shown to produce higher amounts of xylanase (1.2 U/ml) on xylan. The strain exhibited xylanase activity when grown on different agro-wastes like wheat bran and rice bran
- Strain PS47 showed substantial amounts of cellulase (0.141 U/ml) on CMC and the activities were comparable to the ones produced on media supplemented with agricultural residues (0.11 U/ml on wheat bran).
- Yeast extract and peptone are shown to have a significant effect on enzyme secretion.
- Both cellulase and xylanase (crude enzyme) exhibited NaCl stability. While PS3 xylanase lost around 50% of the initial activity at 3 M NaCl, PS47 cellulase retained over 60% activity even at 4 M NaCl. Both these enzymes have optimal activity at 50 ºC, by far, exhibiting thermostability.

The study assumes significance in the ability of halophilic bacteria to utilise cheap lignocellulosic biopolymers (agro-wastes) to produce optimum levels of high value products like compatible solutes and saline hydrolases, thereby contributing towards the limited information available with regards to industrial applications of halophilic bacteria and adding value-addition of agro-wastes.

Acknowledgements

DAAD India, provided financial support to carry out a part of this research at Institute for Microbiology and Biotechnology, University of Bonn, Germany.

References

[1] Amoozegar, M A et al (2007), A rapid method of lipid extraction and purification, Microbiology Research, Vol. 162, pp. 369-377.
[2] Bligh, E G and Dyer W J (1959), A rapid method of lipid extraction and purification, Canadian J Biochem & Physiology, Vol. 37, pp. 911-917.
[3] Deka, D et al (2011), Enhancement of Cellulase Activity froma New Strain of *Bacillus subtilis* byMediumOptimization and Analysis with Various Cellulosic Substrates, Enzyme Research, doi:10.4061/2011/151656.
[4] Gasper, M et al (2007), Corn fiber as a raw material for hemicellulose and ethanol production. Process Biochem, Vol. 42, pp. 1135-1139.
[5] Miller, G L (1959), Use of dinitrosalicylic acid reagent for determination of reducing sugar, Analytical Chemistry, Vol. 31, pp. 426-428.
[6] Rastogi, G et al (2010), Characterization of thermostable cellulases produced by *Bacillus* and *Geobacillus* strains, Bioresource Technology, Vol. 22, pp. 8798-8806.
[7] Ventosa, A et al (1998), Biology of moderately halophilic aerobic bacteria, Microbiol Mol Biol Rev, Vol. 62, pp. 504-544.
[8] Wahyuntari, B et al (2009), Effect of pH, Temperature and Medium Composition on Xylanase Production by Bacillus sp. AQ-1 and Partial Characterization of the Crude Enzyme, Microbiology, Vol. 3, pp. 17-22.

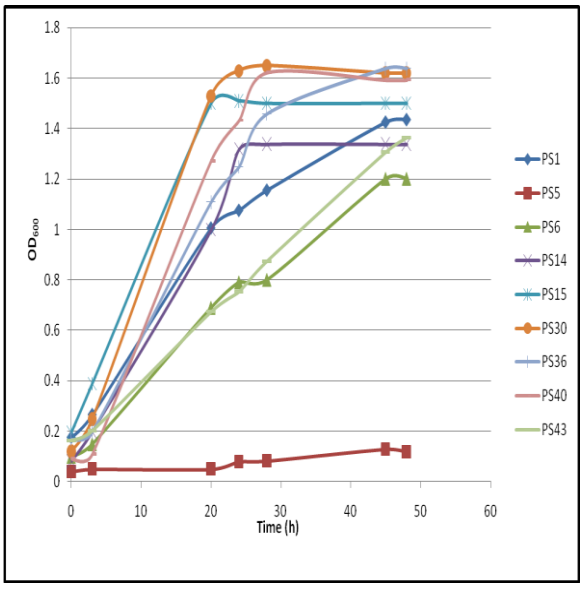


Fig.1 Growth studies of bacterial strains on MM63 pH 7.1, 6% w/v NaCl.

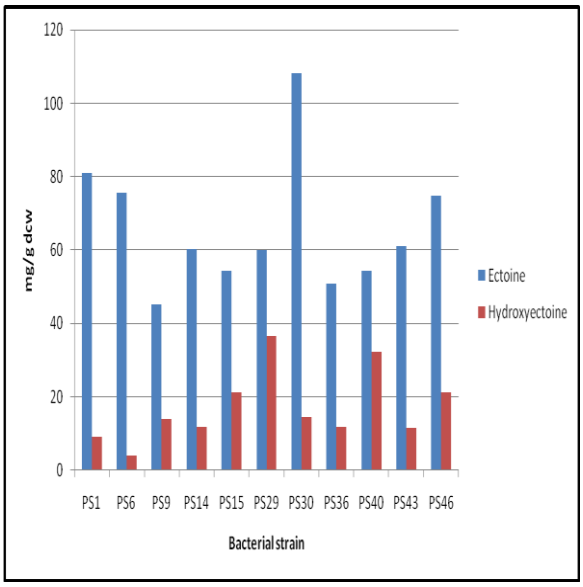


Fig.2 Ectoine and hydroxyectoine production by bacterial strains.

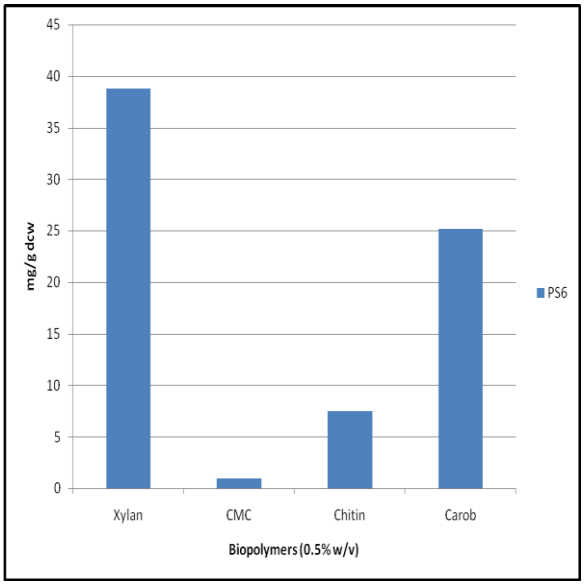


Fig.3 Ectoine production of PS6 on different biopolymeric substrates.

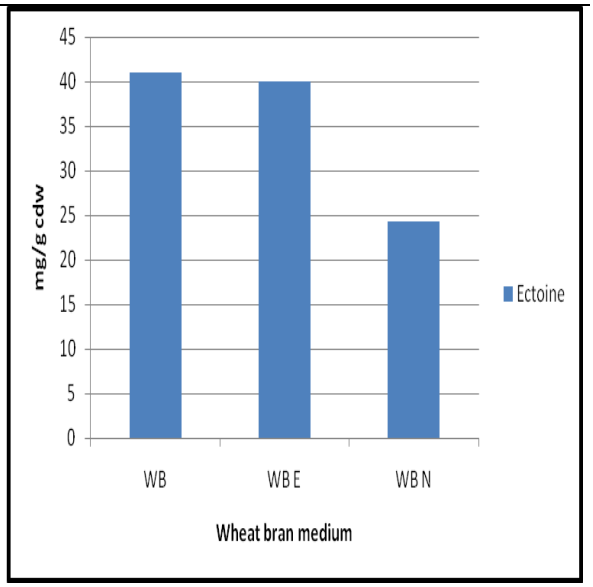


Fig.4 Ectoine production by PS6 on pretreated wheat bran media- WB: Control flask containing 1% (w/v) wheat bran in MM63 at 6% (w/v) NaCl), WBE: 1% enzyme hydrolysed wheat bran in MM63, WBN: 1% alkali hydrolysed wheat bran in MM63.

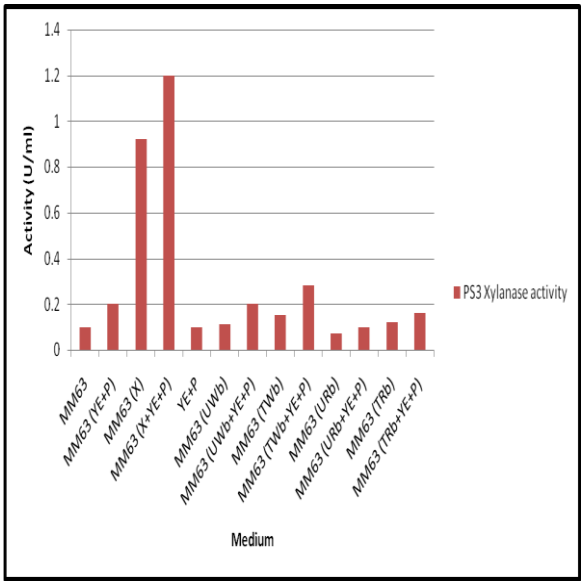


Fig. 5 Xylanase activity of PS3 in MM63 medium substituted with biopolymers: YE-yeast extract, P-peptone, UWb-untreated wheat bran, TWb-treated wheat bran, URb-untreated rice bran, TRb-treated rice bran.

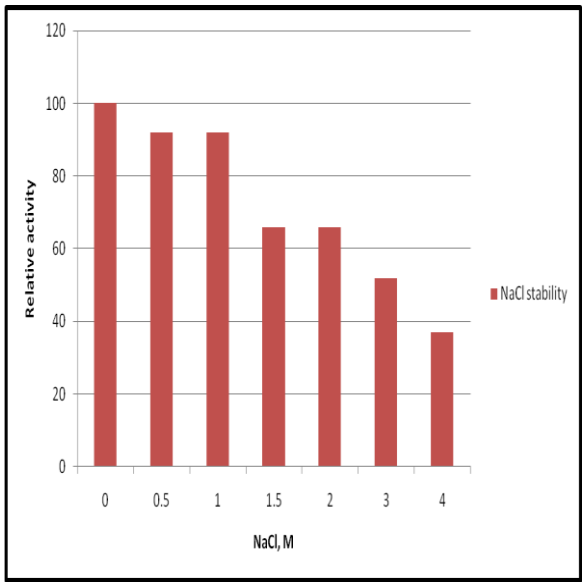


Fig. 6 NaCl stability of PS3 xylanase.

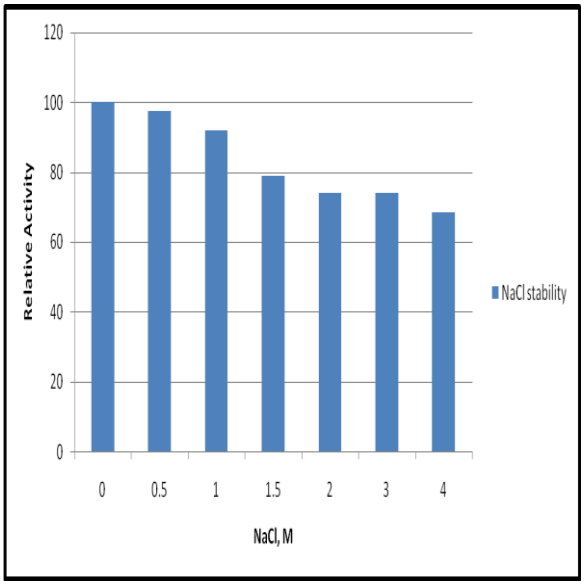


Fig. 8 NaCl stability of PS47 cellulase.

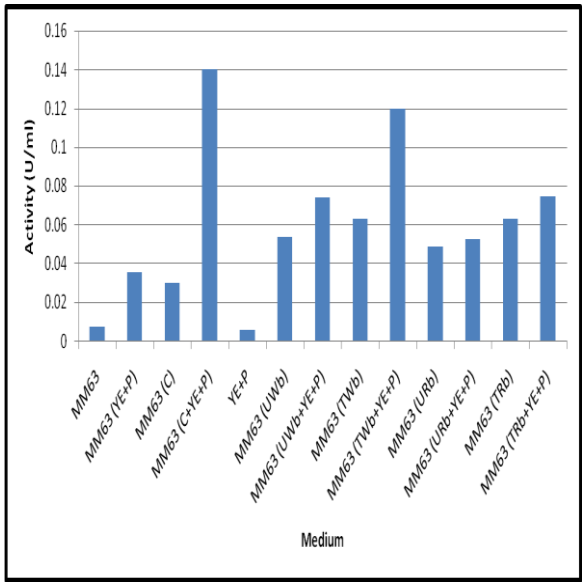


Fig. 7 Cellulase activity of PS47 in MM63 medium substituted with biopolymers: YE-yeast extract, P-peptone, UWb-untreated wheat bran, TWb-treated wheat bran, URb-untreated rice bran, TRb-treated rice bran.

2nd International Engineering Symposium - IES 2012
(KU-MU-NITK-HCMCUT Joint Symposium) March 5-7, 2012, Kumamoto University, Japan

Research on Wastewater Treatment by Expanded Granular Sludge Bed (EGSB) Reactor Using Polyvinyl Alcohol (PVA) Carrier

Vu Dinh Khang [1*] and Nguyen Tan Phong [1]

[1]Faculty of Environment, Ho Chi Minh City University of Technology, 268 Ly Thuong Kiet, District 10, Ho Chi Minh city, Vietnam. Email : khangmt04@gmail.com*
[1] Faculty of Environment, Ho Chi Minh City University of Technology, 268 Ly Thuong Kiet, District 10, Ho Chi Minh city, Vietnam. Email : tanphong69@yahoo.com

Abstract: The pilot-scale of expanded granular sludge bed reactor (EGSB) has more advantage than UASB. The ration of height to width of EGSB is 4 to 10, so that it has more time to contacting between wastewater and granular sludge. Additionally, with the high velocity, granular sludge are expanded and the hydraulic mixing is intensified giving granules more chances to contact with wastewater. This pilot-scale was operated under mesophilic (30-35^{o}C) condition and with the low strength wastewater (0.8-1g COD/L) for over 150 days. The effluent recirculation water to feed water is set 100%-200%. PolyVinyl Alcohol (PVA) is used like a nucleus of granular sludge. PVA has porous structure, so that it has the appropriate structure to immobilize and expand anaerobic microorganism. After 2 months star up and contacting to construct granular, the pilot-scale can be removed COD from 50% to 78% and the COD loading was increased up to 7.2 kg COD/m^3.day.

Keywords: PolyVinyl Alcohol*, Anaerobic process, EGSB reactor, Granular sludge, Biological carrier.*

Introduction

The anaerobic treatment has been rapidly developed since the late 1960s. Lettinga told that anaerobic treatment process makes mineral compounds such as ammonium, phosphate, or sulfide and needs additional post treatment for a sustainable environmental protection can be met. Anaerobic treatment has a lot of advantages such as low energy consumption, low production of waste biological solids, storage ability unfed for many months, low nutrients and chemicals requirements, great removal at even high loading rate, pathogen removal, improving dewaterbility and producing energy gases. Seung J. Lim, (2009). Anaerobic biofilm processes, such as up-flow anaerobic sludge blanket (UASB), fluidized bed and fixed bed, are widely accepted as a proven technology for the methanogenic treatment of organic wastewater. The main advantage of this system is the high-rate treatment of wastewater, related to the good retention of anaerobic bacteria by formation of biofilm or granular sludge. Lettinga, 1995 &Speece, (1996). However, most of organic wastewater is discharged at a moderate temperature and with a low or medium organic strength. Rebec *et al*., 1999; Angenent *et al*.,(2001). EGSB (Expanded Granular Sludge Bed) reactor was developed to improve the wastewater-biofilm contact via expanding the sludge bed and increase hydraulic mixing by effluent recirculation system As a result, the EGSB reactor show sufficient process performance for treatment of low strength wastewater (ethanol and volatile fatty acid containing wastewater) with 0.8-1.0 g COD/L. Kato *et al.,* (1994, 1997); Rebec, (1998). In this study, this anaerobic process was operated under mesophilic (30-35^{o}C) condition. The effluent recirculation was used to increase contact

wastewater- sludge. In this pilot-scale, the property of granular sludge impact on effect treatment and sludge discharge. Poly vinyl Alcohol (PVA)-gel is used like carrier and immobilize bacterium in itself. The porous structure of PVA-gel allows substrates, microorganism to diffuse into the internal pores where treatment processes are carried out by the entrapped cells . In-Soung Chang, (2005).

Materials and Methods

In this study, there are two pilot-scales operate on the parallel conditions, One has PVA carrier and one without PVA carrier. The schematic diagram of an EGSB reactor is shown in (Fig.1). A pilot-scale consists two sections, column section (with 6.0L volume) and gas-solids separators (GSS) section (with 2.5L volume). Total height of pilot-scale is 120 cm, include 100cm column and 20 cm GSS. Inside and outside diameter of cylinder column are 8.8cm and 9.0 cm. The total volume of pilot-scale reactor is 8.5L. Cylinder column is transparent mica material. There are three sampling ports with arranged 30cm per port on column. The up-flow velocity was set depending on the organic loading rate needed; the effluent recirculation was set to maintain the OLR needed. Anaerobic activate sludge for star- up was obtained from biogas plant using muck livestock wastewater. The sludge and PVA carrier volume using in the reactor (for PVA reactor) to column section volume were 30% and 20%, respectively.

PVA carrier has special structure molecule to capture bacterial. Poly Vinyl Alcohol has two different types of hydrogen bonding compete with each other in the each other solution. The first is the inter molecular hydrogen bonding in PVA molecules and the other is hydrogen bonding between water and hydroxyl groups in PVA molecules. If the inter strength of hydrogen bonding between water and PVA exceeds the strength of hydrogen bonding between the hydroxyl groups in PVA (inter-molecular hydrogen bonding), PVA could be dissolved in water. Consequently, strong hydrogen bonding between inter-molecules makes the F-series PVA difficult to dissolved in water. In-Soung Chang; Chi-II Kim and Byeong-Uk Nam (2005). The suitable PAV in this study is F-series. It has porous beehive structure, molecular weight 1.04g/cm^3, bead diameter 2-3mm.

Feed water using in this study was a aquaculture wastewater, it was collected from a aquaculture processing market in the suburbs of Ho Chi Minh city. The main products are from freshwater fish. Feeding of wastewater to the reactors was diluted concentration to needed before. After that, diluted wastewater was started immediately with granular sludge. The COD concentration of original wastewater ranged from 3.0 to 6.0 g/L. After dilution, ranged from 0.6 to 1.1 g/L. The average concentration of sulphate ; total Nitrogen ranged from 11 to 21,8 and from 49 to 87.5 mg/l, respectively. The pH of influent was ranged from 6.3 to 6.85.

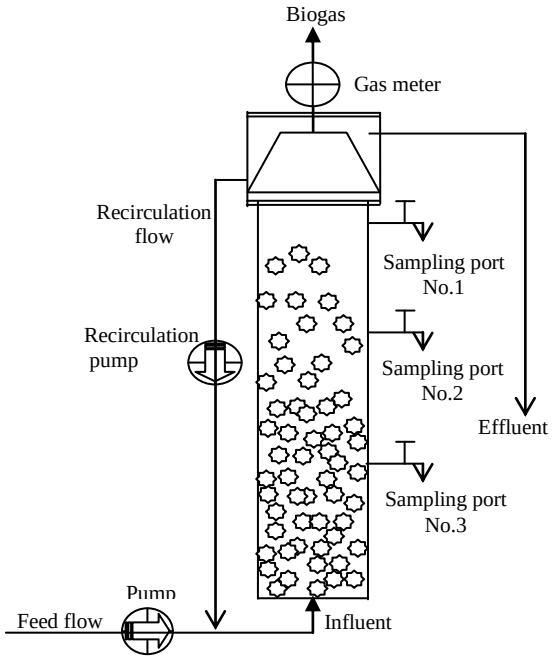


Fig.1 Schematic Diagram of an EGSB reactor

Analyse activity was carried out as soon as starting-up the lab-scales. Routine analyses of influent and effluent wastewater were conducted from Monday to Friday every week. The influent and effluent were sample for COD concentration; pH; alkalinity; total suspended solid (TSS); volatile fatty acid (VFA); analyses. The BOD_5; TN; TP were conducted on Monday, Tuesday and Friday. Additionally, the retain sludge properties sometimes were analysed by

detecting MLSS; SVI index; granular sludge size and colour. Granular sludge was sampled for scanning electron microscopic (SEM) observation. Uemura, S. And Harada, H. (1993). The gas produced was metered by gas meter equipment.

Table 1: Parameter and Method analyse

Parameter	Method
COD	Standard Methods 5220B
pH	pH meter
Alkalinity	Standard Methods 2330-B
MLSS	Standard Methods2540-E
TSS	Standard Methods 2540-D
VFA	Standard Methods 5560-C

The EGSB reactor was operated at five organic loading rates (OLR): 4 (star-up); 6; 10; 14 and increased stepwise up to 18 kg COD/m^3/day by reduce the hydraulic retention time (HRT) from 6 hour to 1.3 hour on the mesophilic (30-35^{o}C) condition (Fig.2). The influent COD concentration was stabilized 0.8-1.0g COD/L.

Results & Discussion

Those two similar reactors (Fig.3) were operated on the same conditions be compared the effective treatment.

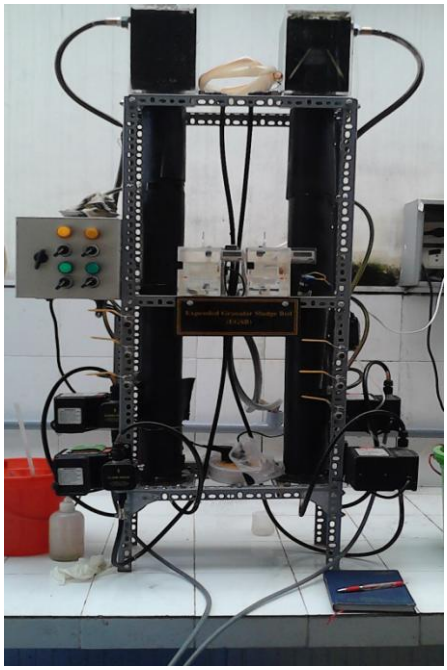


Fig.3 Two similar reactor EGSB

The star-up OLR process needed more time than others. (Fig.4). This is the important stage to contact and immobilize microorganism on PVA carrier. The stage was terminated after effluent COD concentration reach more 80 percents and stabilizing.

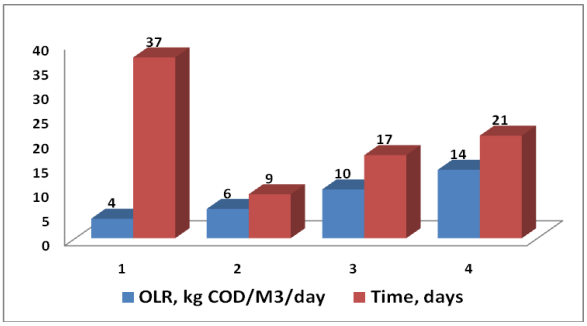
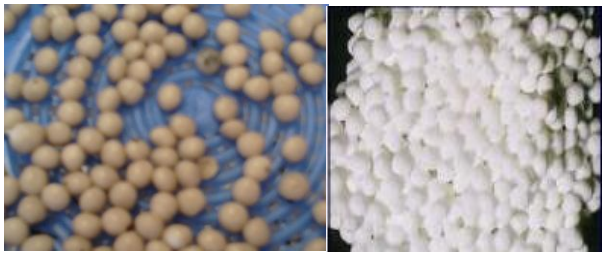


Fig.4 Time needed for each OLR

After 37 days, granular PVA carrier had biofilm on surface. White colour was changed to dark brow, and deep brow.



a) b)

Fig.5. a) PVA carrier at day 37
b) Original PVA

The effluent COD concentration of lab-scale with PVA carrier was strong reduced at the end of each OLR.(Fig.6)

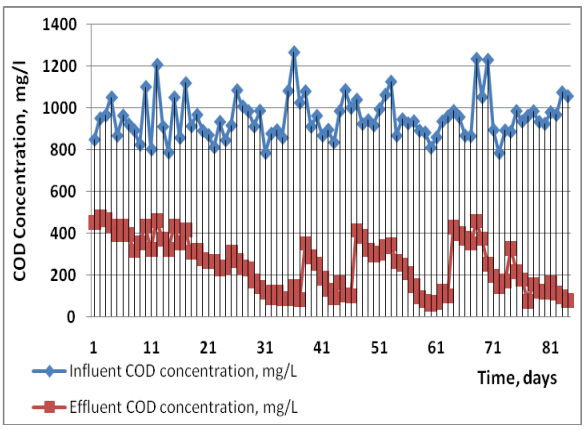


Fig.6 The effect of COD treatment - lab-scale PVA carrier.

Compare with the lab-scale without PVA carrier (Fig.7), the lab-scale with PVA was more slowly adaptableness. It needed more time to take form the structure granular sludge around PVA's surface. As a result, at the star-up OLR, the effluent COD of it was higher.

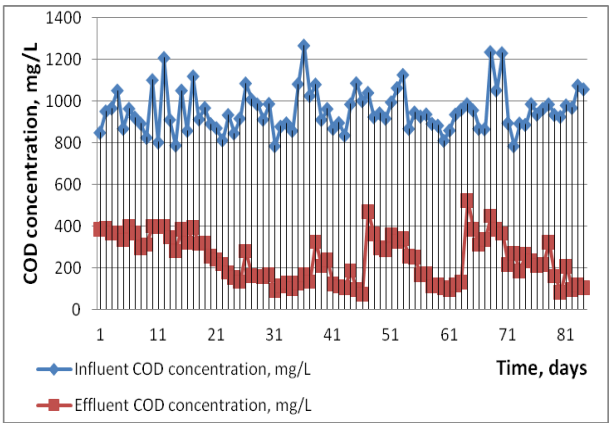


Fig.7 The influent and effluent COD - lab-scale without PVA carrier.

There was not much different effect of COD removal of two reactor. At the beginning of OLR4, the effluent COD of lab-scale with PVA carrier higher than without PVA carrier, but at the next organic loading rates it was always lower.(Fig.8)

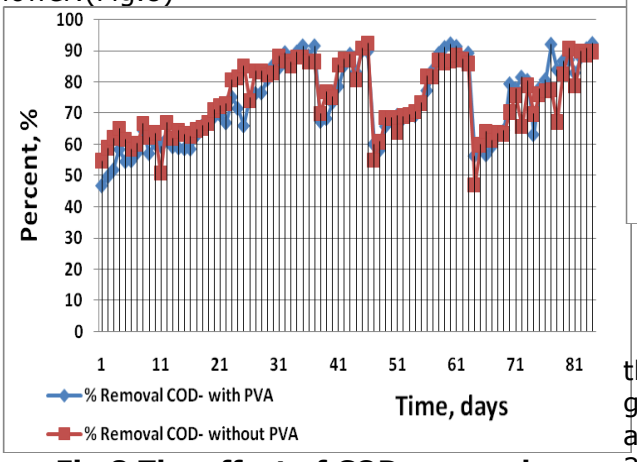


Fig.8 The effect of COD removal

pH factor impact strongly on anaerobic treatment process. The favourable pH value for this process range from 6.8 to 7.4. This range is optimum condition to growing up the methanobacterium. Leslie Grady,C.P.JR (1999). The figure 9 and 10 show that, almost effluent PH values were higher than influent Ph values. This is the good sign of the anaerobic process. There were chances of ph value at the beginning of each OLR. When OLR step up higher, the VFAs would be increased. Leslie Grady,C.P.JR (1999). The pH value would be decreased when the VFAs increase higher the methane transforming capacity.

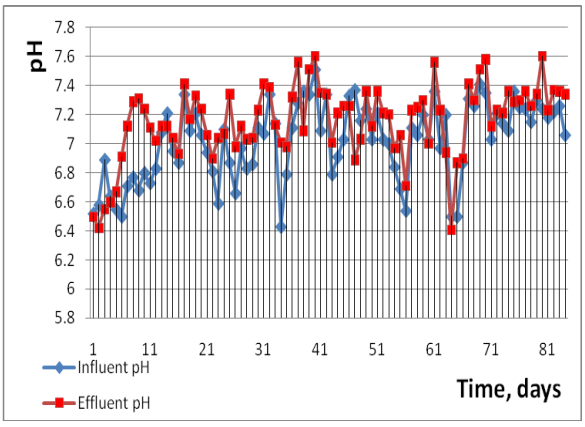


Fig.9 The influent and effluent pH - lab-scale with PVA carrier.

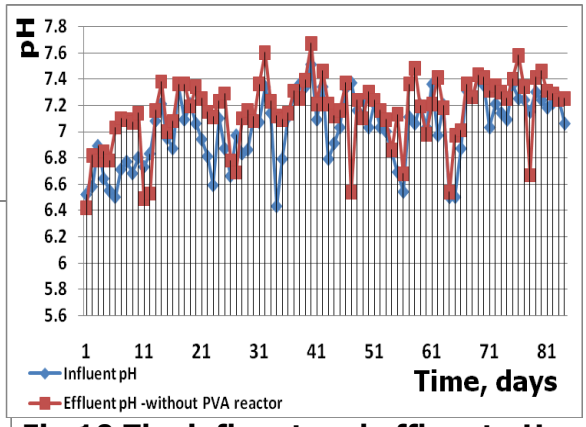


Fig.10 The influent and effluent pH - lab-scale without PVA carrier.

With the high CO_2 content (typically in the range from 30 to 50 percent) in the gas produced in anaerobic treatment, alkalinity concentrations in the range from 2000 to 4000 mg/L $CaCO_3$ are typically required to maintain the pH at or neutral. Metcalf and Eddy,(2003).

In the influent wastewater, the level of alkalinity needed is seldom available, but may be generated in some cases by the degradation of protein and amino acids. The requirement to purchase chemicals for ph control can have a significant impact on economics of anaerobic treatment.

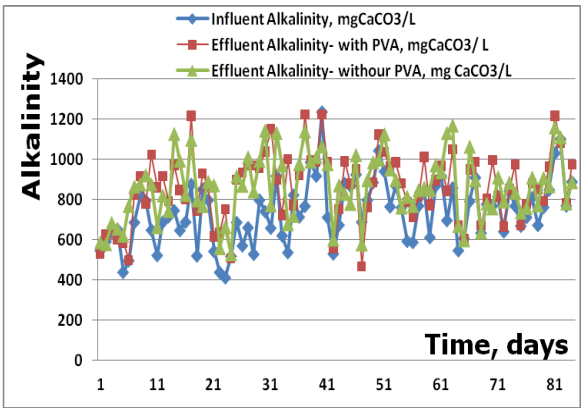


Fig.11 The influent and effluent Alkalinity

The relationship between pH and alkalinity is controlled by the bicarbonate chemistry as below:

$$\frac{[HCO_3^-][H^+]}{[H_2CO_3]} = K_{al}$$

Where, K_{al} = first acid dissociation constant, which is a function of ionic strength and temperature. Metcalf and Eddy,(2003).

In this study, influent wastewater had maintained the characteristic origin.

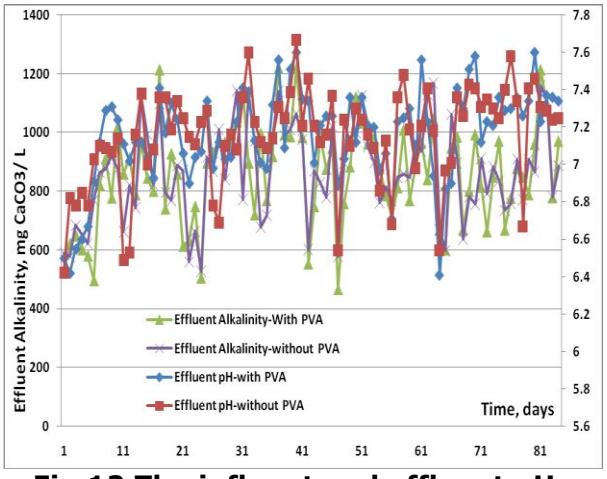


Fig.12 The influent and effluent pH and Alkalinity

Low alkalinity value can be the signal of the reducing pH strongly. Figure 12 show that effluent alkalinity and pH can have the cause relation.

The EGSB reactor operate at high velocity and with high recycle ratio, so that it enables the EGSB reactor to contact granules with wastewater enough, but sludge could be lost by effluent flow. With PVA as nucleus of granular sludge, effluent TSS could be reduced significant.

Figure 13 shows that, the effluent TSS of lab-scale with PVA carrier was lower than lab-scale without PVA carrier. TSS removal could reach to 82%.

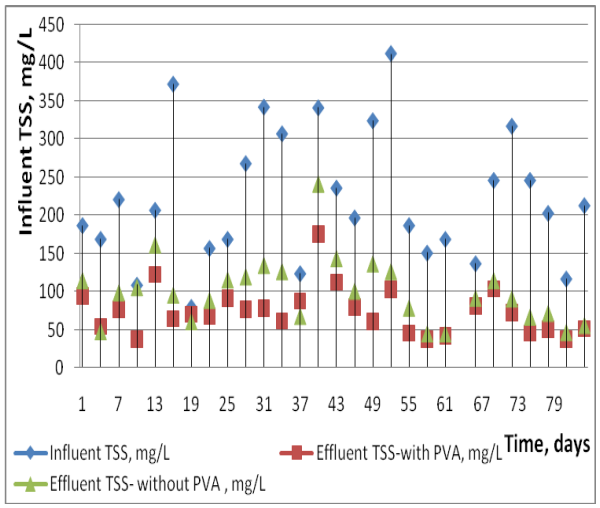


Fig.13 The influent and effluent TSS of two lab-scales.

Conclusions

This present shows that the efficiency of this lab-scale EGSB reactor using PVA carrier for removal COD of low strength wastewater with low HTR range from 6h to 1.3h. Effluent TSS and sludge retain got highly and stably.

In this study, the sludge and PVA carrier volume using in the reactor (for PVA reactor) to column section volume were 30% and 20%, respectively. The research needed more case-study on another ratio for more knowledge.

Acknowledgements

The authors wish to thank laboratory of Faculty of Environment, Ho Chi Minh City University of Technology. This study is supported by JICA's Project, Japan.

References

[1] In-Soung Chang a, Chi-Il Kim a, Byeong-Uk Nam (2005), The influence of poly-vinyl alcohol (PVA) characteristics on the physical stability of encapsulated immobilization media for advanced wastewater treatment, attach.

[2] Kato, M.T., Field, J.A. and Lettinga, G. (1994 &1997), The Anaerobic treatment of low strength

wastewater in UASB and EGSB reactors. Wat Sci Tech.,
[3] Lettinga, G.(1995), Anaerobic Digestion and Wastewater Treatment Systems.
[4] Lettinga, G.; Field, J.; van Lier,J.; Zeeman, G.; and Hulshoff Pol, L.W. (1997), Advanced Anaerobic Wastewater Treatment in the near Future. Water Sci. Tech.
[5] Leslie Grady, C. P. JR and et al. (1999), Biological wastewater treatment. ISBN: 0-8247-8919-9. Marcel Dekker, Inc.
[6] Metcalf and Eddy. (2003),Wastewater engineering treatment and reuse. ISBN 7-302-05857-1/X_42. Mc Graw Hill Companies, Inc.
[7] Rebec, S., van Lier, J.B., Lens, P., Stams, A.J.M., Dekkers, F., Swinkels, K.T.M. & Lettinga, G,(1999). Psychrophilic anaerobic treatment of low strength wastewaters. Wat. Sci. Tech.
[8] Sung J. Lim (2009), Comparisons Between the UASB and the EGSB Reactor, Korea.
[9] Uemura, S. and Harada, H. (1993), Microbial characteristics of methanogenic sludge consortia developed in thermophilic UASB reactor. Appl. Microbiol. Biotechnol.
[10] Yoochatchaval, Ohashi, A, Harada, H, Yamaguchi, T and Syutsubo, K, (2008), Characteristics of Granular Sludge in an EGSB Reactor for Treating low Strength Wastewater, nt. J. Environ. Res., 2(4): 319-328.

2nd International Engineering Symposium - IES 2012
(KU-MU-NITK-HCMCUT Joint Symposium) March 5-7, 2012, Kumamoto University, Japan

BIC model coupled with DOE to simulate supercritical fluid extraction of 10-DAB III from Taxus Wallichiana Zucc

Nguyen Quang Duy[1], Chau Ngoc Do Quyen[1], Phan Dinh Tuan[1], Mitsuru Sasaki[2], Motonobu Goto[3], and **Le Thi Kim Phung[1]**

1 *Faculty of Chemical Engineering, Ho Chi Minh University of Technology, Vietnam*
2 *Graduate School of Science and Technology, Kumamoto University, Japan*
3 *Bioelectrics Research Center, Kumamoto University, Japan*

Abstract: Supercritical CO_2 was employed to extract 10-deaccetylbaccatin III - a precursor for preparing Paclitaxel. The overall extraction curve was described with the mathematical model based on the concept of broken and intact cells (BIC). The BIC model could describe the extraction curve with high agreement to the experimental data. The information of external mass transfer coefficient at distinct experimental setting is important data for simulating the overall extraction curve. In this work, to predict the effect of process parameters to the rate of extraction process, the mass transfer between core solute and free solute in solid phase was estimated using empirical correlation. Design of experiment (DOE) with quadratic order model with central composite design was used to propose the correlation of mass transfer coefficient in solid and extraction parameters including pressure, temperature and flow rate. The supercritical fluid extraction of 10-deaccetylbaccatin III (10-DAB III) from Taxus Wallichiana Zucc was simulated basing on the integration of mathematical model and statistical model. The developed SFE simulation tool can be complete the calculation to predict the rate of the extraction process affected by the input process parameters.
***Keywords**:* Supercritical fluid extraction, mathematical modelling, 10-DAB III, Paclitaxel, BIC

Introduction

In recent years, supercritical fluid extraction (SFE) has been recommended as an innovative technique for the separating of pharmaceutical compounds from natural plant derivative (Julian Martínez 2003) due to its non-toxic, non-flammable properties and low impact on human and environment. Its advantages are the absence of solvent residues and the easy control of process selectivity, which are the relevant characteristics for pharmaceutical, cosmetic and food industries (Subra, Castellani et al. 1998). It is important to model the SFE of the essential oil to obtain access to optimum operating conditions.

The mathematical modeling of experimental data of SFE has the objective of determining parameters for process design, such as equipment dimensions, solvent flow rate, and particle size, to make possible the prediction of the viability of SFE processes on an industrial scale, through the simulation of overall extraction curves (Subra, Castellani et al. 1998).

Extraction from solids consists of dissolution of extractable material within the matrix and transfer to the bulk fluid (Sovová 2005). To describe the time-dependent curves thus obtained, several approaches have been proposed in the literature: empirical, diffusion-based and differential mass balance integration. The empirical model considers the extractor as a 'black box'. In the diffusion model, the particles of solid matrix are now considered as a unit of extraction. The extractable material is uniformly distributed within the particles, which are assumed to be spherical and porous. The third approach takes into account not only the particle characteristics via porosity and diameter, but also the bed properties. Extraction is described regarding a local dissolving rate, intraparticle diffusion and an external mass transfer. It reflects the various mechanisms that contribute to the overall behavior of an extraction process (Sovová 2005; Machmudah, Sulaswatty et al. 2006).

The broken and intact cell (BIC) model proposed by Sovová was based on differential mass balance integration and has been successfully applied in the extraction of oils from different kind of matrices (Sovová 2005).
In this work, the BIC model was applied for modeling the SFE of 10-DAB III from cultivated *Taxus Wallichiana Zucc*. The adjustable parameter has been used and the mass transfer coefficients in the solid phase were obtained by fitting of the experimental data. The modeling results were applied to evaluate the effects of pressure, temperature on the extraction.

Material and experimental

The air – dried leaves of 5 year old *Taxus Wallichiana Zucc* cultivated in Dalat, Vietnam was milled and stored in dry condition until use.
Paclitaxel and 10 DAB III standard was obtained from Aldrich Sigma, SC-CO_2 was carried out with high purity carbon dioxide (99.95%, Singapore), ethanol as co-solvent was from Merck Chemical, USA.
Supercritical carbon dioxide extraction of 10-DAB III was conducted in a Thar SFE – 100 supercritical fluid extraction systems. For each extraction, 20g material was loaded into the extraction vessel. The SC-CO_2 extraction of 10-DAB III was performed by means of a dynamic extraction procedure. For evaluating the effects of operating pressure and temperature on the process kinetics and model parameters, extraction pressure and temperature were analyzed in 3 levels: 98bar, 220bar, 342bar and 308K, 323K, 338K, respectively.
HPLC system (Agilent) was employed to analyze the concentration of 10 DAB III in the extract at the wavelength of 230 nm with mobile phase as acetonitrile – water at the ratio 35:65 v/v.

Mathematical model

The BIC model was developed using the following assumptions (Sovová 2005):
The solute is assumed to be homogeneously distributed in untreated particles that arranged as packed bed in the extractor.
The particles contain broken cells near the surface and intact cells in the core. The volumetric fraction of broken cells in the particles is r ($0 < r < 1$).
The solute from broken cells is transferred directly to the fluid phase, while the solute from intact cells diffuses first to broken cells and then to the fluid phase. Mass transfer from broken cells to the solvent is characterized by fluid phase mass transfer coefficient (k_f) that is by several orders of magnitude larger than the solid phase mass transfer coefficient (k_s) related to the diffusion from intact cells to broken cells.
The extraction bed characteristics, void fraction and surface area, are not affected by the reduction in the solid mass during the extraction, and fluid density is not affected by the solute dissolved in the solvent
Equilibrium of solutes in the fluid phase and the solid phase with broken cells is established before the extraction starts, while the concentration in the intact cells is equal to the original concentration in the untreated material.
Mass balance equations for the solute in the fluid phase, solid phase with broken cells and intact cells are written as following (Sovová 2005):

$$\boldsymbol{\rho_f \varepsilon}\ \frac{\partial y}{\partial t} + \boldsymbol{U}\frac{\partial y}{\partial \square}\ = \boldsymbol{k_f a_0 \rho_f}\ \boldsymbol{y^* - y} \qquad (1)$$

$$\boldsymbol{r\rho_s}\ \boldsymbol{1-\varepsilon}\ \frac{\partial x_1}{\partial t} = \boldsymbol{k_s a_s \rho_s}\ \boldsymbol{x_2 - x_1}\ - \boldsymbol{k_f a_0 \rho_f}\ \boldsymbol{y^* - y} \qquad (2)$$

$$\boldsymbol{1-r}\ \boldsymbol{\rho_s}\ \boldsymbol{1-\varepsilon}\ \frac{\partial x_2}{\partial t} = -\boldsymbol{k_s a_s \rho_s}\ \boldsymbol{x_2 - x_1} \qquad (3)$$

The extraction curve is calculated as(Sovová 2005):

$$E = Q\ \int_0^t y|_{h=H}\, dt \qquad (4)$$

Phase equilibrium between the fluid-phase and the solid phase with broken cells is given by the discontinuous equilibrium function(Sovová 2005):

$$y^*\ x_1\ = y_s \text{ for } x_1 > x_t$$
$$y^*\ x_1\ = Kx_1\ for\ x_1 < x_t\ ; Kx_t < y_s \qquad (5)$$

The discontinuity occurs at the transition concentration x_t which is equal to matrix capacity for interaction with the solute. At solid phase concentrations lower than x_t all solute interacts with matrix and phase equilibrium is determined by partition coefficient, K. At the concentrations higher than x_t the solid phase contains also free

solute whose equilibrium fluid phase concentration is equal to the solubility y_s.
The finite differential method was employed for integrated numerically the model equations. The continuous extraction bed is represented by a series of *n* mixers, where n is a sufficiently large number. The model equations thus are transformed to the set of ordinary differential equations and solved numerically using Runge – Kutta method.
Average absolute relative deviation (AARD) was employed for investigating the model - experiment deviation. At each point, the AARD is calculated by:

$$\boldsymbol{AARD}\ \% = \frac{\mathbf{1}}{\boldsymbol{n}} \sum_{\boldsymbol{i=1}}^{\boldsymbol{n}} \frac{\boldsymbol{D_{exp} - D_{cal}}}{\boldsymbol{D_{cal}}} \mathbf{.100} \qquad (6)$$

Results and discussion
The calculated extraction curve and experimental data were plotted in Fig. 1. For investigating the model properties, four supercritical fluid extraction assays varied in pressure and temperature were taken into account. Generally, the model gave good agreement with the experimental data, both for the first part and curve portion of OEC as well as the transaction point. The model parameters and the fitting parameters were shown in Table 1.
As the first portion of extraction curve occurs in straight line, the extraction was at equilibrium state. Therefore, the external mass transfer resistance can be negligible. This behaviour can be estimated by an analytical solution with the hypothesis that the external mass transfer resistance is close to zero. For the first part of OEC, the mass flow of solute within solid matrix is negligible. The model equation is then:

$$\frac{\partial Y}{\partial \tau} + \frac{\partial Y}{\partial Z} + \frac{\mathbf{1}}{\Gamma}\frac{\partial X_1}{\partial \tau} = \mathbf{0} \qquad (7)$$

Numerical integrating of model equation would provide the extraction yield as a first order function of dimensionless extraction time.
The second extraction period is controlled by solute diffusion from intact cells to broken cells. Due to the large values of internal mass transfer resistance, $\boldsymbol{\Theta_i}$, the number of mixers $\boldsymbol{n}$ in model equations does not affect the calculated extraction rate. That the calculated free solute concentration in solid matrix $\boldsymbol{X_1}$ remains a constant value indicates solutes – matrix interaction. Therefore, the extraction process is mainly governed by the internal mass transfer within the solid matrix.
The partition coefficient or the equilibrium constant of solute concentration in fluid phase and solid phase is shown in Table 1 The calculated equilibrium curve is shown in Fig. 2.
Two levels of partition coefficient were distinguished from Table 2. The greatest value of equilibrium constant was obtained at higher pressure (220bar) at any temperature (313K, 333K). The effect of pressure on equilibrium phase thus is pronounced whilst that of temperature is negligible. This behaviour is agreed with the effects of extraction pressure and temperature on solubility of solutes in supercritical fluid.

Internal mass transfer evaluation
Due to the structure of solid matrix is not described generally; the calculated mass transfer coefficient in solid phase is just valid for a distinct experimental setting. This behavior is a major drawback for simulating the overall extraction curve because we would have no information on the mass transfer within the solid matrix. Therefore, it is expected to propose a correlation for estimating the data of internal mass transfer coefficient versus operating condition. In this research, quadratic order model with central composite design was employed for investigating the correlation of internal mass transfer coefficient and operating parameters including extraction pressure, temperature and flow rate.
The different formulations of the factorial design consisted of all possible combinations of three factors at all levels and were conducted in a fully randomized order. The three-level face-centered design was used to evaluate both the main and the interaction effects of the operating conditions on the internal mass transfer coefficient. To determine the experimental error, the experiment at the center point was replicated three times on different days. The matrix of the experiments and the response results for every experiment are listed in Table 3, and sorted by standard order (StO) for easier comparison. It was shown that in the investigated

domain, the value of responses was great varied. To investigate the effects of the experimental factors on internal mass transfer, the experimental data were analyzed by using statistical analysis.

Analysis of variance (ANOVA)

For the statistical analysis of experimental results, enter method was used to calculate the estimated coefficients of the polynomial functions of response surfaces for internal mass transfer coefficient. To quantify the effect of operating parameters to internal mass transfer coefficient, coefficients of all factors of each model were calculated.

The regression coefficient of polynomial functions of response surfaces:

$k_s a_s$=0.00047-1.9E-07P-2.7E-06 T-1.7E-06 Q+5.38E-10PT+4.02E-09P^2+1.46E-08Q^2

It was shown that the mainly factors affect to the internal mass transfer are pressure, the solvent flow rate and temperature, the interaction of pressure and temperature and the square of temperature and flow rate. It is observed that internal mass transfer increase with pressure at any temperature levels. The highest internal mass transfer is obtained at greatest extraction pressure and temperature. The results have good agreement with reported data in prior art. The regression equation thus will allow us to estimate the value of internal mass transfer coefficient at given operating condition. It would provide important data for simulating the OEC.

Simulation of overall extraction curve

The data of overall extraction curve is not only needed for predicting the extraction yield and concentration profile but also required for design and scale up purposes. The information obtained from OEC would be expected to provide data on optimized extraction time, operating condition, and further is the ratio of mass of loaded material to total amount of solvent used.

In order to simulate of overall extraction curve, following additional data are required:

-Operating condition including extraction pressure, temperature, and solvent flow rate.

-Information of loaded material including density, porosity, particle size and loaded mass.

-External mass transfer coefficient in fluid phase which can be estimated using Sherwood correlation based on data of physical properties, pack bed parameters and mass transfer diffusivity.

-Internal mass transfer coefficient in solid matrix phase which can be calculated using the correlation proposed in chapter 6 of this work. This value is limited for the operating condition ranged from 98bar – 342bar of pressure, 7g/min – 23g/min of flow rate and 308K-338K of temperature.

-Initial partition of broken and intact cell.

The overall extraction curve thus is obtained by integrating the model equations. Calculated OEC shown in Fig.3 was varied in pressure and temperature to investigating those effects on extraction yield. The temperature and flow rate were set to 313K and 15g/min for investigating 3 pressure assays: 300bar, 250bar and 100bar.

The obtained data would provide the information of suitable operating parameters. For e.g., the calculated OEC at 100bar, 313K, 15g/min has the linear portion followed by a curve portion. Due to the slope of the curve portion is significant low, the increase of extraction yield is negligible from the point of 25g/g solvent used. The extraction assays thus can be finished at which the solvent consumption reach to 25g/g without any significant effect on the extraction yield.

Based on the information of solvent consumption, we would be able to distinguish the target flow rate and extraction time. The effects of pressure and temperature are also reflected quantifiably in the calculated OEC so that we can operate the process at desired conditions.

All of model parameters such as mass transfer in fluid and solid phase, solvent density and viscosity, solubility are integrated in correlation with operating conditions. Therefore, optimization problem would be formulated and solved numerically.

Conclusions

The overall extraction curve was modelled within a mathematical model based on the

concept of broken and intact cell. The model is a versatile tool for the SFE simulation as it includes flexible relationships both for phase equilibrium and flow pattern. The model with solute – matrix interaction is valid for describing the OEC. The internal mass transfer coefficient was calculated by fitting to the experimental data.

Quadratic order model with central composite design was employed for the formulation of empirical correlation of internal mass transfer coefficient and operating condition including pressure, temperature and flow rate. The mutual effect of operating parameters to extraction yield and kinetic data within the regression equation is agreed with the one characterized by extraction mechanism.

The regression equation is a mathematical tool for estimating the data of internal mass transfer at desired value of operating parameters which are in investigated range whilst the solid structure is not generally defined. This is a completely new approach and expected to be applied for other products.

In terms of the model and empirical correlation of internal mass transfer coefficient, the supercritical fluid extraction of 10-DAB III was simulated. The simulation tool is very useful for optimizing the extraction process where the operating condition and extraction time can be identified.

Acknowledgements work was supported financially by Jica-Suprem through Project No.B1-4/B2-4 and B3-7

References

[1.] Chung-sung tan, s.-k. l. a. d.-c. l. (1988). "Fluid-Solid Mass Transfer in a Supercritical Fluid Extractor." The Chemical Engineering Journal **38**(1): 17-22.

[2.] Julian Martínez, A. R. M., † Paulo T. V. Rosa, Márcia O. M. Marques,‡ and M. Angela A. Meireles (2003). "Multicomponent Model To Describe Extraction of Ginger Oleoresin with Supercritical Carbon Dioxide." Industrial and Engineering Chemistry Research **42**(5): 1057–1063.

[3.] Machmudah, S., A. Sulaswatty, et al. (2006). "Supercritical CO2 extraction of nutmeg oil: Experiments and modeling." The Journal of Supercritical Fluids **39**(1): 30-39.

[4.] Maria Dolores Macías-Sánchez, C. M. S., Miguel Rodríguez Rodríguez, and E. M. d. l. Ossa (2009). "Kinetics of the supercritical fluid extraction of carotenoids from microalgae with CO2 and ethanol as cosolvent." Chemical Engineering Journal **150**(1): 104-113.

[5.] Martinez, J. L. (2008). Supercritical Fluid Extraction of Nutraceuticals and Bioactive Compounds, CRC Press.

[6.] Owen J. Catchpole, M. B. K. (1994). "Measurement and Correlation of binary diffusion coefficients in near critical fluids." Industrial and Engineering Chemistry Research **33**(1): 1827 - 1837.

[7.] Robert C.Reid, J. M. P., Bruce E. Poling (1987). The properties of Gases and Liquids, McGraw-Hill, Inc.

[8.] Sovová, H. (2005). "Mathematical model for supercritical fluid extraction of natural products and extraction curve evaluation." The Journal of Supercritical Fluids **33**(1): 35-52.

[9.] Subra, P., S. Castellani, et al. (1998). "Extraction of [beta]-carotene with supercritical fluids: Experiments and modelling." Journal of Supercritical Fluids, The **12**(3): 261-269.

Table 1. Partial coefficients

No.	Pressure (bar)	Temperature (K)	K	$x_{1,0}$ (w/w)
1	140	313	0.1247	0.0040
2	300	333	0.1645	0.0036
3	140	333	0.1202	0.0042
4	300	313	0.1617	0.0037

Table 3. Experiment of design data

StO	Z_1	Z_2	Z_3	Y_1	Y_2
	P	T	Q	Yield	$k_s a_s$
1	140	313	10	2.812	2.6E-06
2	300	333	10	3.523	3.17E-06
3	140	333	10	2.624	2.33E-06
4	300	313	10	3.421	2.83E-06
5	140	333	20	3.235	3.12E-06
6	300	313	20	5.111	4.08E-06
7	140	313	20	3.171	3.74E-06
8	300	333	20	5.296	6.3E-06
9	98	323	15	1.808	1.15E-06
10	342	323	15	4.008	4.47E-06
11	220	308	15	3.542	2.33E-06
12	220	338	15	4.219	4.16E-06
13	220	323	7	2.605	1.88E-06
14	220	323	23	4.818	4.42E-06
15	220	323	15	3.561	2.49E-06
16	220	323	15	3.572	2.49E-06
17	220	323	15	3.650	2.49E-06
18	220	323	15	3.488	2.49E-06
19	220	323	15	3.553	2.49E-06
20	220	323	15	3.588	2.49E-06

Table 2. Fitting parameters

P (bar)	T (K)	Q g/min	y_s (g/g)	r	γ (g/g)	Γ	$k_s a_s$ (1/s)	$k_f a_o$ (1/s)	Θ_i	Θ_e
8	323	15	0.0002	0.569	1.083	0.152	1.15E-06	2.527	2535.7	0.0034
342	323	15	0.0004	0.570	2.068	0.345	2.49E-06	1.921	611.3	0.0018
220	308	15	0.0004	0.565	1.953	0.317	2.33E-06	2.072	692.1	0.0023
220	338	15	0.0005	0.572	1.741	0.309	4.16E-06	2.198	434.4	0.0025
220	323	7	0.0006	0.560	1.849	0.896	1.88E-06	1.279	421.5	0.0019
220	323	23	0.0003	0.559	1.849	0.148	4.42E-06	3.182	589.7	0.0025
220	323	15	0.0005	0.555	1.849	0.368	4.47E-06	2.314	380.5	0.0022

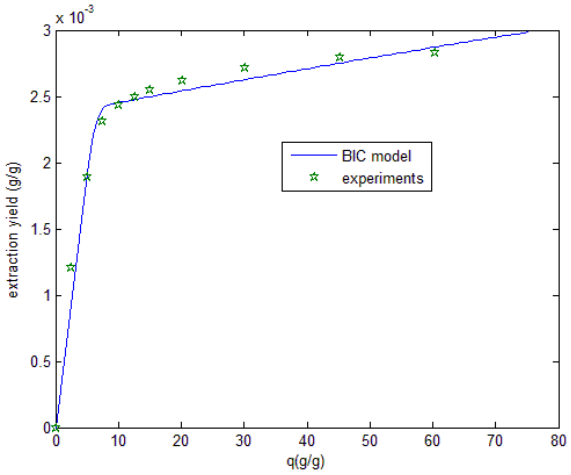


Fig.1. Fitting of calculated OEC to experimental data

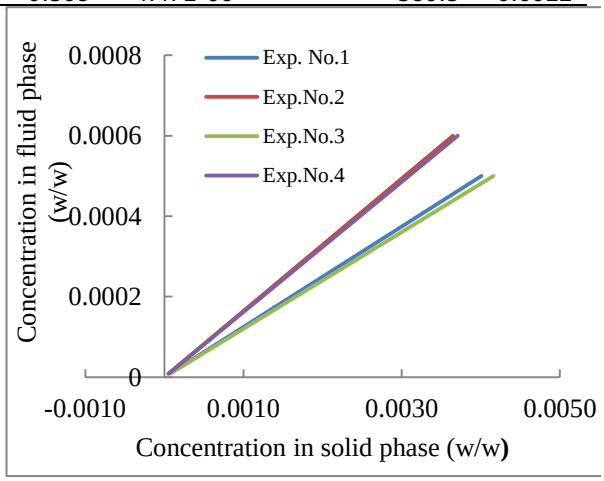
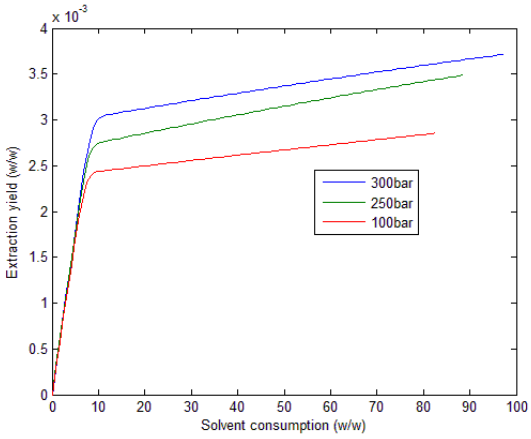
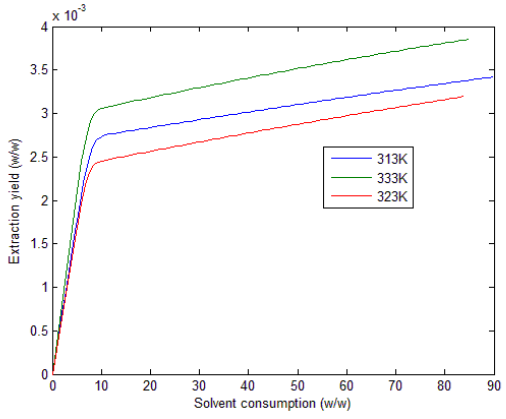


Fig.2. Calculated equilibrium curve



Calculated OEC at T=313K, Q=15g/min



Calculated OEC at P=300bar, Q=15g/min

Fig. 3 Calculated OEC varied in P and T

2nd International Engineering Symposium - IES 2012
(KU-MU-NITK-HCMCUT Joint Symposium) March 5-7, 2012, Kumamoto University, Japan

Optimization of conditions for extraction of collagen from the skin of *Pangasius hypophthalmus* by response surface methodology

Le Thi Thu Huong[1] Phan Ngoc Hoa [1] Nguyen Hoang Dung [1] and Phan Dinh Tuan [1]

[1] Department of Chemical Engineering, Ho Chi Minh City University of Technology, Vietnam, 268 Ly Thuong Kiet St., Dist.10, Hochiminh City, Vietnam. Email: lethuhuong1976@yahoo.com

Abstract: Collagen has been used widely in the production of pharmaceutical and cosmetic products. Fishbased collagen has still more advantages than other sources of collagen and becomes an object of interested researches recently. Extraction and some properties of collagens from the skin of *Pangasius hypophthalmus* fish were investigated. Pepsin enzyme and acetic-acid solution was used as an extracting solvent. The optimal conditions for collagen extraction were determined by response surface methodology. The effects of four independent variables (pepsin enzyme content, acetic-acid concentration, liquid/solid ratio, and temperature) on the extraction yield of collagen from *Pangasius hypophthalmus* skin were evaluated. The optimal conditions to obtain the highest yield were determinded as follows: a pepsin enzyme content of 0.25%, a acetic-acid concentration of 0.75 M, a liquid/solid ratio of 80, a temperature of 13.87 ^{o}C. The predicted yield was 73% which was in agreement with the actual value ($P<0.05$). The molecular weights of α_1, α_2 and β chains in collagen were estimated to be 115 and 125 and 240 kDa, respectively.

***Keywords**: fish collagen, extraction, pangasius hypophthalmus fish*

Introduction

Collagen is the most abundant protein in vertebrates making up approximately 30% of total protein. Collagen is a major component of connective tissue, muscle, teeth, bone and skin. There are 19 types of collagen, lableed I-XIX. Collagen is composed of three similarly sized triple helix polypeptid chains. Each chain contains about 1000 amino acid residues in size and has an average length of 300nm and diameter of 1.4 nm. Collagen has a repetitive primary sequence of which every third residue is glycine. The sequence of the polypeptide chain can be described as Gly-X-Y, in which X and Y are often found to be proline and hydroxyproline forming a left-hand super helix with the other two chains (Whitford, 2005).

Collagen has been used in the biomedical, pharmaceutical (Lee et al.,2001), food and cosmetic industries (Kim and Mendis, 2006; Senaratne et al., 2006).

Response surface methodology is a statistical method that use quantitative data from an appropriate experimental design to determine or simultaneously solve multivariate equation (Triveni, Shamala and Rastogi, 2001). Besides, this experimental methodology can generate a mathematical model and optimize the process level (Bas and Boyaci, 2007; Yang, Zhao, Shi, Yang, & Jiang, 2008). So far, available publications on collagen extraction with response surface methodology are very limited. The objective of this work was to investigate the effects of above four variables on the yield of collagen solution extracted from the skin of *Pangasius hypophthalmus* fish by response surface methodology.

Optimization of the extraction was also performed.

Experimental

Material

The skins of *Pangasius hypophthalmus* fish were supplied by the Viet An Company in An Giang province in Vietnam. Pre-treatment method was adopted from Le Thi Thu Huong *et al.* (2010). After removing remained flesh, the skins were washed in cold water, packed in PE bag and kept storage under -20^{o}C.

Collagen extraction

The skins of *Pangasius hypophthalmus* fish were first defrosted, washed, drained and dipped in LASNa 0.5% in 6 hours. Then they were dipped in H_2O_2 1% in NaOH 0.05N solution in 2 hours to remove lipid, minerals, colorants, and odorants. After that, they were cut into smaller pieces using scissors. The small pieces of the skin were extracted with acetic acid and pepsin solution. Pepsin enzyme content, acetic acid concentration, the ratio of liquid/solid and temperature were chosen as variables with different levels. The extract was filtered out with filter cloth and this was followed by vacuum-filtering with a Whatman No.1 filter paper. The collagen was precipitated by adding NaCl to the final concentration of 0.9M. The resulting sediment was collected by centrifuging at 12,000 rpm for 30 min. The collagen precipitate was dissolved in solution of 0.5M acetic acid with the solid/ liquid ratio of 1/10 (w/v), then dialysed against 0.1M acetic acid distilled water sequentially. The collagen was obtained by freeze-drying and this was followed by removing lipid from crude collagen with supercritical carbon dioxide.

Box-Behnken design

Response surface methodology was employed for experimental design, data analysis and model building with software Design Expert 8.0.6 Trial. A Box-Behnken design with four variables was used to determine the response pattern and then to establish a model (Box & Behnken, 1960; Quang, Yang, Du, & Yi, 2008). Four independent variables used in this work were pepsin enzyme content (X1), acetic acid concentration (X2), liquid/solid ratio (X3) and temperature (X3), with three levels for each variable, while the dependent variable was the extraction yield of collagen. The symbols and levels are shown in Table 1. Six replicates at the central point of the designed model were used to estimate the pure error sum of squares. Experiments were randomised to maximise the effects of unexplained variability in the observed response, due to extraneous factors.

Table 1 Box-Behnken design and the response for extraction yield of collagen from *pangasius hypophthalmus* skin

Exp	X_1 (%)	X_2 (M)	X_3	X_4 (deg C)	Yield (%)
1	0.25	0.25	20.00	3.00	30.6
2	0.75	0.25	20.00	3.00	31.8
3	0.25	0.75	20.00	3.00	35.6
4	0.75	0.75	20.00	3.00	34.7
5	0.25	0.25	80.00	3.00	37.6
6	0.75	0.25	80.00	3.00	39.5
7	0.25	0.75	80.00	3.00	36.3
8	0.75	0.75	80.00	3.00	38.9
9	0.25	0.25	20.00	17.00	46.8
10	0.75	0.25	20.00	17.00	45.8
11	0.25	0.75	20.00	17.00	46.9
12	0.75	0.75	20.00	17.00	45.8
13	0.25	0.25	80.00	17.00	60.8
14	0.75	0.25	80.00	17.00	53.6
15	0.25	0.75	80.00	17.00	69.2
16	0.75	0.75	80.00	17.00	61.1
17	0.50	0.50	50.00	10.00	59.6
17	0.50	0.50	50.00	10.00	45.7
17	0.50	0.50	50.00	10.00	60.7
17	0.50	0.50	50.00	10.00	56.4
17	0.50	0.50	50.00	10.00	60.7
17	0.50	0.50	50.00	10.00	56.6
18	0.15	0.50	50.00	10.00	69.2
19	0.85	0.50	50.00	10.00	40.5
20	0.50	0.15	50.00	10.00	60.5
21	0.50	0.85	50.00	10.00	68.4
22	0.50	0.50	7.57	10.00	59.4
23	0.50	0.50	92.43	10.00	62.4
24	0.50	0.50	50.00	0.10	15.3
25	0.50	0.50	50.00	19.90	50.4

Gel SDS-polyacrylamide (SDS-PAGE) electrophoresis

SDS-PAGE gel electrophoresis was performed (Laemmli, 1970) using the Buffer System, a mini- PROTEAN Tetra cell manufactured by BIORAD. The resolving gel was 7% and stacking gel was 5%. After electrophoresis, gel was dyed by 0.05% (w/v) Coomassive blue R-250 in 15% methanol and 5% (v/v) acetic acid. Then the gel was dipped in the solution of 30% (v/v) methanol and 10% (v/v) acetic acid to remove the color. The molecular mass of collagen protein was determined using a standard protein scale, ranging from 75 kDa to 250 kDa.

Scanning electron microscopy

Collagen samples was diluted to equal concentrations of 3 mg/ml with milliQ water, were coated on clean glass coverslips and air dried at room temperature in clean air flow of a laminar flow hood. Dried samples were then platinum coated and examined in SEM 7410F – JMS – JEOL – Japan, at 50.000x magnification.

Results

Effect of pepsin enzym content, acetic-acid concentration, liquid/solid ratio and temperature on the extraction yield of collagen.

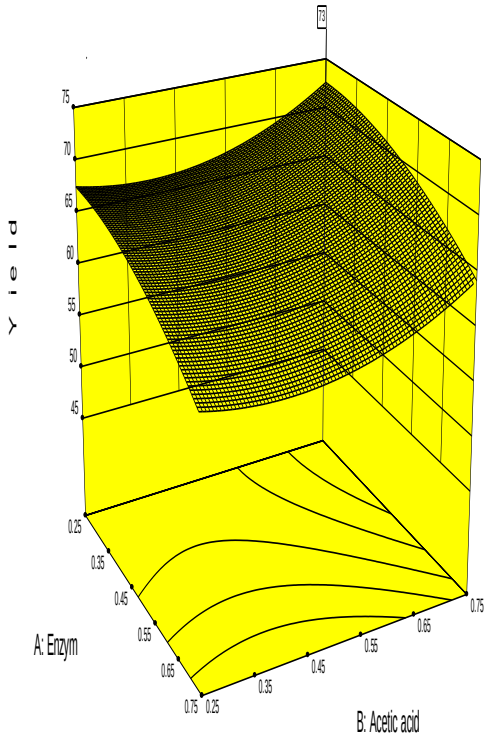


Fig.1 Response surface plot showing the effect of pepsin enzym content and acetic-acid concentration on the extraction yield of collagen. The ratio L/S was constant at 80; the temperature was constant at 13.87°C.

The effects of pepsin enzym content and acetic-acid concentration on the extraction yield of collagen from *pangasius hypophthalmus* skin are shown in Fig.1. The extraction yield of collagen was decreased with the increase of pepsin enzym content. The extraction yield was slightly decreased when the acetic-acid concentration increase to a certain value (approximately 0.30 to 0.51 M) thereafter increased. The effect of liquid/solid ratio on the extraction yield of collagen is shown in Figs.2 and 3. The extraction yield of collagen was increased when the liquid/solid ratio increase.

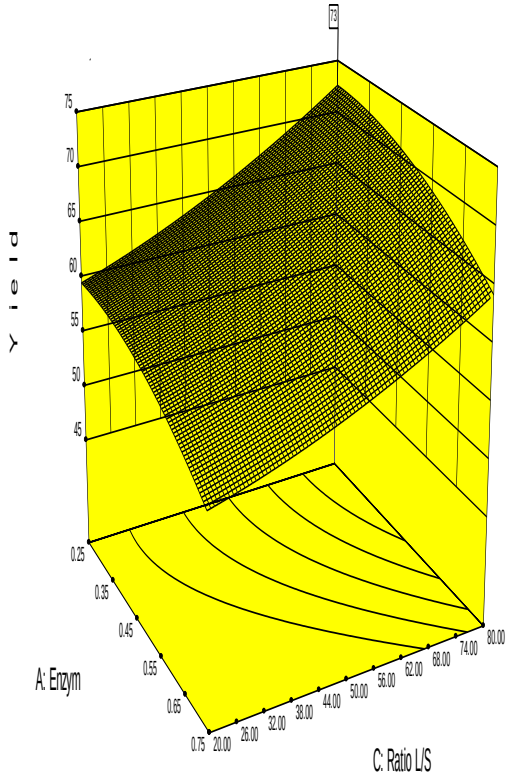


Fig.2 Response surface plot showing the effect of pepsin enzym content and ratio L/S on the extraction yield of collagen. The acetic acid concentration was constant at 0.75M ; the temperature was constant at 13.87°C.

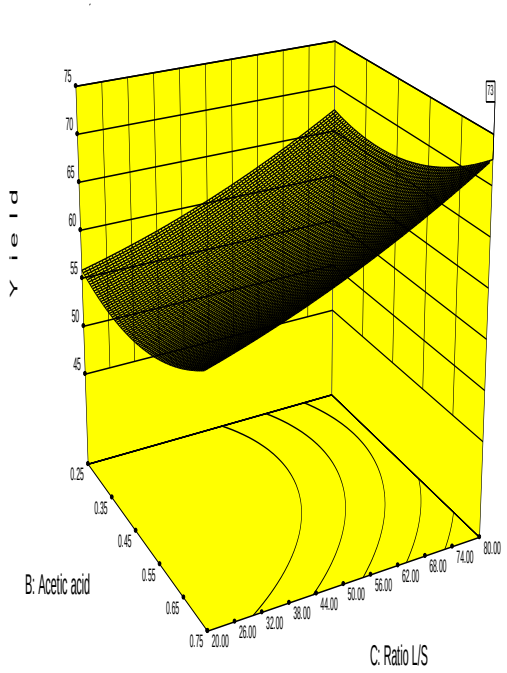


Fig.3 Response surface plot showing the effect of acetic-acid concentration and ratio L/S on the extraction yield of collagen. The pepsin enzym content was constant at 0.25% ; the temperature was constant at 13.87°C.

Model fitting and optimization

The mathematical model representing the extraction yield of collagen as a function of the independent variables within the region under investigation was expressed by the following equation:

$$Y = 51.17-2.66X_1 +1.66X_2 +4.16X_3 +9.73X_4 -0.15X_1X_2 -0.56X_1X_3-1.39X_1X_4 +0.38X_2X_3 +0.0.63X_2X_4 +2.49X_3X_4 -1.93X^2_1 +2.87X^2_2 +1.09X^2_3 -12.93X^2_4 \quad (1)$$

Where Y is the extraction yield of collagen, whereas X1, X2, X3 and X4 are the code variables for pepsin enzym content, acetic-acid concentration, liquid/solid ratio and temperature, respectively.

The analysis of variance for the response surface quadratic model of the extraction yield collagen from *pangasius*

hypophthalmus skin was shown in Table 2. The P-value of the model was less than 0.0003; meanwhile, the lack of fit value of the model was 0.4819 which was not significant. These two values confirmed that the model fitness was good.

By analysis of variance, the R^2 value of this model was determined to be 0.89, which proved that the regression model defined the true behavior of the system.

By prediction with computing program, the optimal conditions to obtain the highest yield of collagen were determined as follows: a pepsin enzym content of 0.25%, a acetic-acid concentration of 0.75 M, a liquid/solid ratio of 80, a temperature of 13.87 ^oC. After extraction under these optimal conditions, the extraction yield of collagen was 72.8±0.3% and this value was not significantly different from the predicted value 73% within 95% confidence interval.

This result indicated that there was abundant collagen in *pangasius hypophthalmus* skin. The extraction yield of collagen from *pangasius hypophthalmus* skin is higher than the extraction yield of Carp fish skin *Cyprinus carpio* ASC (41.3%) (Rui Duan et al.,2009) and higher than the extraction yield of big-eyed snapper PSC (65.03%) (Sitthipong Nalinanon et al., 2007) for 24h.

Table 2 Analysis of variance for the response surface quadratic model of the extraction yield collagen from *pangasius hypophthalmus* skin

Source	Sum of Squares	df	Mean Square	F	p
Model	4213.74	14	300.98	7.26	0.0003
Residual	580.73	14	41.48		
Lack of fit	431.66	10	43.17	1.16	0.4819
Pure error	149.07	4	37.27		
Total	5166.47	29			

SDS-polyacrylamide (SDS-PAGE) gel electrophoresis

The electrophoresis patterns of the samples are shown in Fig.4. Collagen displayed one γ band (300 kDa), one β band (240 kDa), and two α bands (α_1-115 kDa and α_2 -125 kDa). These patterns were similar to those of pepsin soluble collagen from the skin of Grass carp (Yan et al, 2007) and chanel cat fish (Liu et al, 2007).

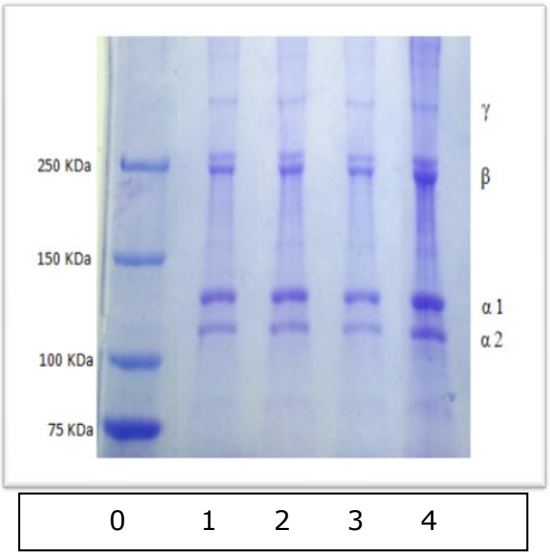


Fig.4 SDS-PAGE pattern of pepsin-solubilized collagen from *pangasius hypophthalmus* skin. Lane: 0, protein markers; 1-2-3-4, pepsin-solubilized collagen.

Scanning electron microscopy

The scanning electron micrograph at 50,000x magnification are shown in Fig.5. the surface morphologies of the collagen there were fibril networks with a rough membranous structure for the collagen membrane, the same as the surface morphology of the collagen membrane of bovine (Zhongkai Zhang et al., 2005).

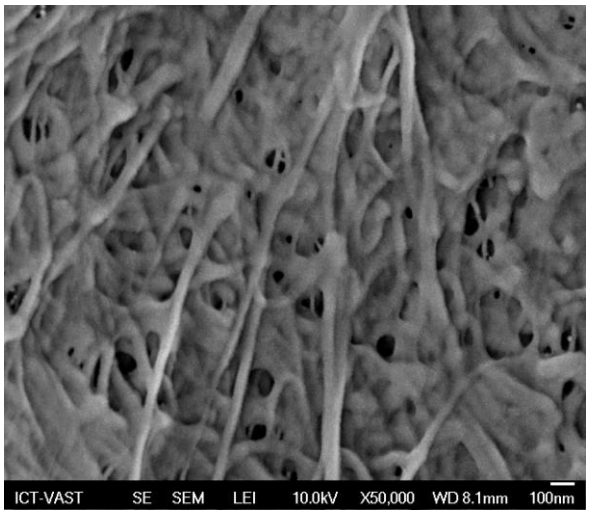


Fig.5 Surface morphologies of the collagen from *pangasius hypophthalmus* skin observed by SEM.

Conclusions

The following conclusions are deduced from this study:

- The effects of four variables (pepsin enzym content, acetic-acid concentration, liquid/solid ratio and temperature) on the extraction yield of collagen from the skin of *Pangasius hypophthalmus* fish by response surface methodology. The optimal conditions to obtain the highest yield were determinded as follows: a pepsin enzym content of 0.25%, a acetic-acid concentration of 0.75 M, a liquid/solid ratio of 80, a temperature of 13.87 ^{o}C. The predicted yield was 73% which was in agreement with the actual value ($P<0.05$).
- The results of research on the structural characteristics of collagen show that, surface morphologies of collagen was fibril pattern. The large amount of type I collagen having subunit composition α_1, α_2, and β.
-

Acknowledgements

This research was financial support by JICA

References

[1] Bas, D., & Boyaci, I. H (2007), Modeling and optimization I: Usability of responce surface methodology, Jounal of Food Engineering, Vol.78, pp 836-845.
[2] Box, G. E. P., & Behnken, D. W (1960), Some new three level design for study of quantitative variables, Technometric, Vol.2, pp 455-475.
[3] Kim, S.K. and E. Mendis (2006), Bioactive compounds from marine processing byproducts- a review, Food Research Intl, Vol.39, pp 383-393.
[4] Lee, C.H et al (2001), Biomedical applications of collagen, Inter.J. of Pharma, Vol.221, pp 1-22.
[5] Le Thi Thu Huong, Nguyen Ngoc Truong, Nguyen Hoang Dung, Phan Dinh Tuan (2010), Treatment of Tra fish *(pangasius hypophthalmus)* skin for collagen extraction, *Journal of Science and Technology, Vol. 48*, 6A, pp 319-328.
[6] Liu, H et al (2007), Studies on collagen from the skin of channel catfish (*Ictaurus punctaus*), Food Chemistry, Vol. 101, pp 621-625.
[7] Rui Duan, Junjie Zhang, Xiuqiao Du, Xingcun Yao and Kunihiko Konno (2009), Properties of collagen from skin, scale and bone of carp (*Cyprinus carpio*), *Food Chemistry*, Vol.112, pp 702-706.
[8] Senaratne, L. S et al (2006), Isolation and characterization of collagen from brown backed toadfish (*Lagocephalus gloveri*) skin, Bioresource Tech, Vol.97, pp 191-197.
[9] Sitthipong Nalinanon, Soottawat Benjakul, Wonnop Visessanguan and Hideki Kishimura (2007), Use of pepsin for collagen extraction from the skin of bigeye snapper (*Priacanthus tayenus*), *Food Chemistry*, Vol.104, pp 593-601.
[10] Triveni, R et al (2001), Optimised production and utilization of exopolysaccharid from Agrobacterium radiobacter, Processing Biochemistry, Vol.36, pp 787-795.
[11] Wang, L. Z et al (2008), Optimisation of supercritical fluid extraction of flavonoids from *Pueraria lobata*, Food chemistry, Vol.108, pp 737-741.
[12] Whitford, D. (2005), Protein structure and function, John Wiley & Sons Ltd., 528p.
[13] Yan, Z., et al (2007), Isolation and partial characterization of pepsin-soluble collagen from the skin of grass carp *Ctenopharyngodon idella*, Food chemistry, Vol. 103, pp 906-912.
[14] Yang, B et al (2008), Effect of ultrsonic treatment on the recovery and DPPH radical scavenging activity of polysaccharides from longan fruit pericarp, Food chemistry, Vol. 106, pp 685-690.
[15] Zongkai Zang, Guoying Li and Bi Shi (2005), Physicochemical properties of collagen, gelatin and collagen hydrolysate derived from bovine limed split wastes, Journal of the Society of Leather Technologists and Chemists, Vol.90, pp23.

2nd International Engineering Symposium - IES 2012
(KU-MU-NITK-HCMCUT Joint Symposium) March 5-7, 2012, Kumamoto University, Japan

Neural Network Modeling of Urea Release from Briquettes

M Ramananda Bhat[1] **D V R Murthy[2]** and **M B Saidutta[3]**

1 Department of Chemical Engineering, MIT, Manipal 576119, India.
email: bhatchem@gmail.com
2 Department of Chemical Engineering, NITK, Surathkal, Mangalore 575025, India.
email: dvrmvzm@gmail.com
3 Department of Chemical Engineering, NITK, Surathkal, Mangalore 575025, India.
email: saidutta.mb@gmail.com

Abstract: Urea briquettes are extensively used in agricultural fields since loss of urea occurring is minimized. However since briquettes dissolve in about 8-10 hours, high concentration of urea develops around the shrinking briquette. Large deviations observed in the case modeling urea release from uncoated briquettes by shrinking core and semi infinite models could be minimized by subjecting the same set of data to empirical modeling technique such as Artificial Neural Networks (ANN). In the case of uncoated briquette data, ANN model with one hidden layer containing ten neurons provided the best fit.

Keywords: urea, briquette, soil, ANN model.

Introduction

Rice is the most important food crop in the developing countries of Asia, where population densities are very high and overall dietary levels are not adequate. In South and Southeast Asia, rain fed and irrigated transplanted rice occupies nearly two-thirds of the rice growing area and produces more than 80% of the paddy (Savant and Stangel, 1990). In these areas, prilled urea conventionally applied by farmers is very inefficiently used by transplanted rice largely because of serious losses (up to 60% of the applied N) via ammonia volatilization, denitrification, leaching and surface runoff (Kesava, 1987). In order to minimize N loss, especially due to denitrification, historically the Japanese have used different ways of deep placing nitrogenous fertilizer. In 1975, International Fertilizer Development Corporation proposed the use of large sized, cost effective briquetted form of urea which could achieve the same agronomic benefits as achieved through the Japanese concept of deep point placement of N fertilizer in transplanted rice fields (Savant and Stangel, 1990).

The commercially available urea briquettes are commonly used in certain parts of Asia and these briquettes are known to reduce the loss of N and increase agricultural yield per unit weight of applied fertilizer (Narayan and Paul, 1998). However, urea briquettes *per se* are not slow release fertilizers, since they dissolve in about 8-10 hours in wet soil, producing high concentration of urea around the shrinking briquette (Murthy et al., 2011b).

Shrinkage and dissolution of uncoated briquettes in wet soil could be modeled using different approaches. Shrinking core model focuses upon the reduction in size/weight of the briquettes and correlates the various soil/medium parameters with size/weight of briquettes and time/duration. Concentration of urea developed in the wet medium is ignored and resistance is assumed to exist in the core containing high concentration of urea surrounding the shrinking solid. Although a

reasonably good prediction from this model can be obtained in case of low clay soils, in the case of high clay soils, large deviations can be observed. This is because of lack of free soil solution in the case of wet high clay soils. Semi infinite model correlates the time dependant urea concentration developed from shrinking briquette in the wet soil with various soil parameters. However, large deviations can be observed between the experimental soil concentration and the model predicted soil concentration profile irrespective of type of soil (Murthy et al., 2011b). Attributable reasons for the deviations could be the assumption of unchanging size of briquettes and experimental concentration measurement errors.
In this paper, data of unreleased urea vs. time, from experiments conducted in various soils and moisture contents, is modeled using Artificial Neural Network (ANN) techniques.

Materials and methods
Urea concentration was measured in this study by the colorimetric method outlined by Marc and Jacques (2006). Urea concentration in wet soil as reported includes urea present in soil solution plus the quantity adsorbed on solid particles per gram of wet soil. Commercial urea briquettes are ellipsoidal in shape, weigh about 2.1g and have a urea content of about 98.5%. Three different soils were used in the study, viz. silty clay, loam and silt loam. These soils were characterized as per the Indian Standards. Their properties are listed in Table 1.

Experimental
The uncoated briquettes were subjected to release in wet soils. For uncoated briquettes, experiments were conducted in loam, silt loam and silty clay soils. Moisture contents (m, g-moisture/ g-dry soil) were 0.05, 0.10, 0.2, 0.3 and 0.4 for loam, 0.2, 0.3 and 0.4 for silt loam soil, while for the silty clay soil moisture contents were 0.2, 0.3, 0.4 and 0.55.
For a known quantity of dry soil, required quantity of water was added; equal quantity of the prepared wet soils soil was transferred to a series of plastic columns, covered by plastic film to prevent evaporation and incubated for 24 hours.

One urea briquette was placed at a depth of 5 cm in each of the plastic column and allowed to dissolve and shrink. At regular intervals of time, shrunk briquette was withdrawn from different column and analyzed for unreleased quantum of urea.
Uncoated briquettes shrank uniformly with time. At lower moisture contents, the differences in the urea release from the uncoated briquettes were almost independent of the type of soil; however at higher moisture contents, slower release was observed in the silty clay soil. Parameters affecting the urea release from the uncoated briquettes depended on time, moisture and clay content of the soils taken up.

Modeling
Data required of unreleased urea vs. time for the modeling were obtained from Murthy et al.,(2011a) for each of the moisture content. Clay content of soil as determined is presented in Table1.

Artificial Neural network (ANN)
One of the more popular soft computing techniques, Artificial Neural Network (ANN), is used as a problem solving tool. ANN is a collection of interconnecting computational elements, which function like neurons in biological brain. It has the ability to model processes by learning from input and output data, without mathematical knowledge of the process. ANN tools are extensively used in almost all fields of engineering to model the experimental data and use the developed network to predict output (Dabhade et al., 2008). In the field of slow release studies, dissolution and diffusion of pharmaceutical products are extensively studied by this technique (Takayama et al., 2000; Goh et al., 2002; Sun et al., 2003). Du et al., (2008) used ANN to predict nitrate release from polymer coated fertilizers.
Feed forward back propagation type network was used for modeling urea release from briquettes. For the present work, Levenberg-Marquardt algorithm was chosen to perform training since it was found to give the most accurate and rapid

results. The ANN modeling work was carried out using the *nntool* function of the software Matlab 2007b. Topology of ANN was three layers viz. one input layer, one hidden layer and one output layer. Input layer was set at purelin transfer function. By trial and error, number of neurons and transfer function in the hidden layer was varied and RMSE was noted in each case. Number of neurons in the hidden layer giving least RMSE was chosen to represent the model.

Modeling Uncoated briquettes

For modeling the experimental data of uncoated briquettes, the fractional urea release (i.e., 1-fraction of unreleased urea) has been found to give the best result with ANN technique. The input parameters for the modeling the data are time, moisture content and fractional clay content as mentioned in the experimental section.

ANN Model

About 40% of the representative data was used for modeling. The data converged in about 30 epochs. Ten neurons with logsig transfer function were found to give the best result.

Plot of outputs from the ANN model vis-à-vis the experimental data for the entire range of data are shown in Figure 1.

Variation of RMSE with the number of neurons with logsig transfer function is shown in Figure 2.

In the case of ANN, both the types of errors (RMSE and Mean Absolute Error) are lower and R^2 value is higher. Based on these results, it can be concluded that ANN technique gives a better representation of the released urea from uncoated briquettes. In contrast with the shrinking core model and Semi infinite model (Murthy et al., 2011a), the ANN model predicted values compared very well with the experimental data.

Conclusions

Artificial Neural Network technique was employed to model the data of unreleased urea from the wet soil experiments conducted in various soils. In the case of urea release from uncoated briquettes, the ANN model provided a good fit for the data in comparison with the reported semi infinite and shrinking core model predictions. Ten neurons with logsig transfer function was found to provide best results in the cases of urea release from uncoated briquettes.

References

[1] Dabhade, M.A., Saidutta, M.B. and Murthy, D.V.R. (2008). Modeling of phenol degradation in spouted bed contractor using Artificial Neural Network (ANN), Chemical Product and Process Modeling, 3(2), 1-14.

[2] Du C., Zhou J., Shaviv A. and Wang H. (2004). Mathematical model for potassium release from polymer coated fertilizer, Biosystems Engineering, 88(3), 395-400.

[3] Goh, W.Y., Lim, C.P., Peh, K. K. and Subari, K. (2002)., Application of a recurrent neural networks to prediction of drug dissolution profiles, Neural computing and Applications, 10,311-317.
Indian Standards, IS 2720 (1985). Methods of Test for soils, Bureau of Indian Standards (BIS), New Delhi-110002, India.

[4] Kesava Rao, K. (1987). Large Granule and Slow Release Urea- A state of art report, Indian Institute of Science, Bangalore.

[5] Levenspiel Octave, *Chemical Reaction Engineering*, 1998, 3rd edition, John Wiley and Sons, New York.

[6] Marc P. and Jacques G. (2006). Handbook of soil Analysis-Mineralogical, Organic and Inorganic Methods, Springer, Netherlands.

[7] Murthy D.V.R., Ramananada Bhat and Saidutta M.B. (2011a). Slow release studies on commercial urea briquettes in loam and silty clay soils of Karnataka, India, International Journal of Earth Science and Engineering, Volume 04, N0.2, 351-356.

[8] Murthy D.V.R., Ramananada Bhat and Saidutta M.B. (2011b).Modeling of urea release from briquettes using semi infinite and shrinking core models, Chemical Product and Process Modeling: Vol. 6: Iss. 1, Article 17.

[9] Narayan K.S. and Paul J.S. (1998). Urea briquettes containing diammonium phosphate: a potential new NP fertilizer for transplanted rice, Nutrient cycling in Agroecosystem, 51, 85-94.

[10] Savant N.K. and Stangel P.J. (1990). Deep placement of Urea supergranules in transplanted rice: Principles and practices, Fertilizers Research, 25, 1 - 83.

[11] Sun Y.,Peng Y.,Chen, Y. and Shukla, A.J. (2003). Application of ANN in the design of controlled release drug delivery systems, Advanced Drug Delivery Reviews,55, 1201-1215.

[12] Takayama, K., Morva, A., Fujikawa, M., Hattari, Y., Obata, Y. and Nagai, T. (2000). Formula optimization of theophylline controlled release tablets based on artificial neural networks, Journal of controlled release, 68, 175-186.

Notations

ANN	Artificial Neural Network
C	fractional clay content
RMSE	root mean square error
t	time, h

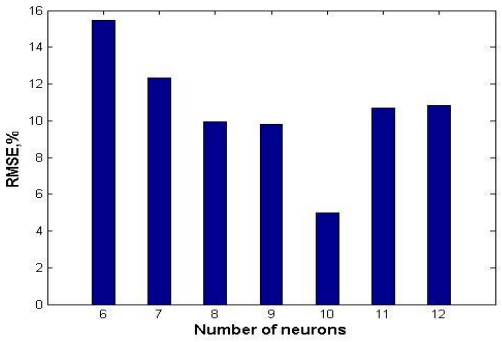


Fig.2 RMSE vs. number of neurons for uncoated data

Table 1 Properties of various

Characteristic	silty clay	loam	silt loam
Clay content, %	51	13	5
Saturation moisture, $\frac{g-moisture}{g-dry\ soils}$	0.55	0.40	0.40
pH	8.19	5.17	6.02
Organic carbon, %	0.582	0.323	0.0

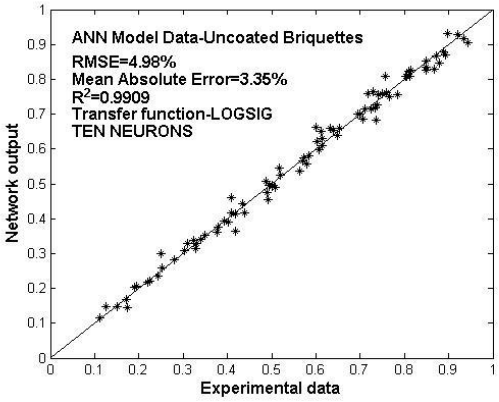


Fig.1 ANN output vs. experimental output for uncoated briquette data

2nd International Engineering Symposium - IES 2012
(KU-MU-NITK-HCMCUT Joint Symposium) March 5-7, 2012, Kumamoto University, Japan

Use of granular activated carbon for the enhancement of phenol removal from wastewater by Electrocoagulation

Rajesh Pachimatla [1] and B. Prasad [2]

1 *Department of Chemical Engineering, Manipal Institute of Technology, Manipal 576104, India. Email : rajeshp.33@gmail.com*
2 *Department of Chemical Engineering, Indian Institute of Technology Roorkee, Roorkee 247667, India. Email:basefch@iitr.ernet.in*

Abstract: The results in this study shows that Electro Coagulation (EC) process using Aluminium plates as sacrificial anodes strongly depends on pH, current density, operating time, inter-electrode distance, initial concentration and adsorbent Granular Activated Carbon (GAC) dosage. At nearly neutral pH, effective removal was achieved and both electrochemical reduction reaction at the cathode surface and adsorption on $Al(OH)_3$ floc mechanisms were responsible for phenol exhaustion. Increasing current density in a range 7.8 to 25 mA/cm^2 enhances the removal efficiency from 72.4% to 90.2%. By addition of adsorbent GAC the removal efficiency of phenol significantly increased at lower current densities and operating time, with 15.5% more than the conventional EC process under the same operating conditions.

***Keywords**:* Electrocoagulation, adsorption, phenol removal, GAC, Aluminium electrode

Introduction

Phenolic compounds are one kind of pollutants listed by the Environmental Protection Agency (EPA) (EPA, 1981) as priority pollutants because of its toxic nature, oxygen demand in receiving water and objectionable to drinking water [Lin et al. (1999)]. Phenols are released into environment mainly by effluents discharged in oil refineries, coke, petrochemicals, iron and steel, pulp and paper, paints and pharmaceutical industries [Somnath M. et al. (2007)]. These are harmful to aquatic life and humans even at low concentrations (5-25 mg/L) and harmful to use and reuse of our national resources [Yousef et al. (1999)]. Various techniques have been employed for treatment of phenols including precipitation, ion exchange, adsorption, distillation, solvent extraction, advanced oxidation processes and bioremediations [Ratna et al. (2004)]. Traditional treatment processes such as biological treatments are not very effective for degradation of phenol due to their high toxicity. Owing to its stability and solubility in water, the degradation of this compound to a level of safety is very difficult, Leanardo et al. (2008).

Recently, advanced oxidation processes (AOPs) have attracted much attention, since they can be used effectively to treat wastewater containing phenols [Xiao-yan et al. (2004)]. Recent work on EC proved that it is very effective compared with conventional chemical coagulation in removing contaminants from water characterising ease of operation, no requirement for chemical use, amenability to automation and reduced sludge production in amount and toxicity [Scott K. et al. (1995)].

However, electrocoagulation in large scale is facing difficulties in operation and high cost for treatment of phenol effluents, especially in developing countries. Taking these criteria into consideration, it is obvious that more inexpensive and effective approaches need to be found [Cabala B. et al. (2009)]. In this present study adsorption process using GAC has been coupled with EC to treat phenol wastewater to get judicious results. The removal of phenol from aqueous solution

was investigated using vertically oriented parallel plate aluminium electrodes. The effect of wastewater characteristics such as initial pH, current density, treatment time, sodium chloride concentration and GAC adsorbent concentration on the removal efficiency is explored and determined the optimum operational conditions.

Theory

Coagulation is achieved by charge neutralization and destabilization of negatively charged colloids by cationic hydrolysis products of Al^{3+} ions and then aggregation of the destabilized phase leads to form flocs [Mouedhen G. et al. (2008)]. The electrochemical processes that occur on the anode and on the cathode surfaces are represented in Equations (1) and (2). On the anode, aluminum dissolution and oxygen evolution can compete. On the cathode, hydrogen evolution is the main expected reaction which favours the flotation of aggregates, so allowing an easier removal [Guohua G. et al. (2004)].

Anode: $Al_{(S)}{}^{0} \rightarrow Al_{(aq)}{}^{3+} + 3e^{-}$ (1)

Cathode: $3H_2O_{(l)} + 3e^{-} \rightarrow \frac{3}{2} H_{2(g)} + 3OH_{(aq)}{}^{-}$ (2)

Depending upon the solution pH and time of electrolysis, $Al_{(aq)}{}^{3+}$ and OH^- ions generated by electrode reactions (1) and (2) react to form various monomeric species such as $Al(OH)^{2+}$, $Al(OH)_2{}^{+}$, $Al_2(OH)_2{}^{4+}$, and $Al(OH)^{4-}$ and polymeric species such as $Al_6(OH)_{15}{}^{3+}$, $Al_7(OH)_{17}{}^{4+}$, $Al_8(OH)_{20}{}^{4+}$, $Al_{13}O_4(OH)_{24}{}^{7+}$, and $Al_{13}(OH)_{34}{}^{5+}$, which transform finally into $Al(OH)_3$ according to complex precipitation kinetics [Chen G. et al. (2004)].

Solution reaction:

$$Al_{(aq)}{}^{3+} + 3H_2O \rightarrow Al(OH)_{3(s)} + 3H_{aq}{}^{+} \quad (3)$$

Freshly formed amorphous $Al(OH)_{3(s)}$ have large surface areas and contain less bound water which is beneficial for a rapid adsorption of soluble organic compounds and trapping of colloidal particles. Finally, these flocs are removed from aqueous solution by sedimentation or floatation and this process is enhanced by bubbles formed at electrodes [Bayramoghlu M. et al (2004)].

Electrocoagulation Test

The EC cell used in this study was a plexiglass rectangular container having the dimensions (12 cm ×12 cm ×18 cm). The performance of the cell was evaluated in batch mode. The experimental setup is shown in Figure 1. Vertically oriented parallel Al plates are used as sacrificial anode as well as cathode having dimensions of the electrodes 8cm×8 cm×1mm. The two electrodes were separated by a distance of 1 cm. During electrolysis, the current density was maintained constant by using a voltage regulator. For each run, 2 L of phenol solution was placed into the cell. The electrolyte, NaCl, was added to the phenol solution at the required concentration (2 g/L), then the current density was adjusted to the desired value and electrolysis was conducted for a certain time. Samples were drawn periodically during each experiment, filtered to separate the sludge then were analyzed for phenol concentration.

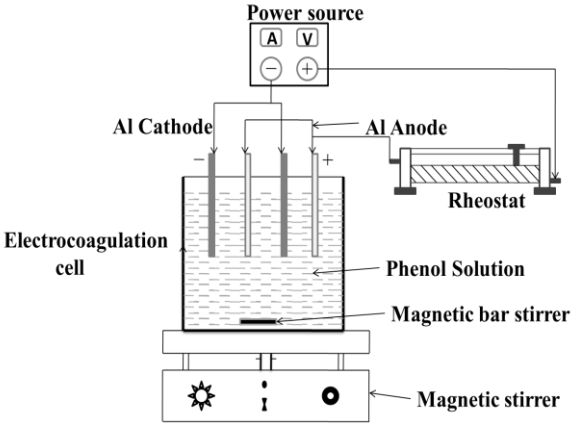


Figure 1. Experimental setup

Results and Discussions

Effect of Initial pH

It has been established that in EC process the current efficiency as well as solubility of metal hydroxide strongly depends on pH of wastewater to be treated. The results as shown in Figure 2., explains that maximum efficiency of phenol removal was at neutral conditions i.e. pH 7. It was also

observed that efficiency was very low either at low pH or high pH. This can be explained as at low pH aluminium hydroxide does not precipitate due to its amphoteric character and at high pH, $Al(OH)_4^-$ forms which is soluble and useless for adsorption of phenol. Therefore, further increase in initial pH of wastewater would decrease the phenol removal efficiency. EC also exhibits some pH buffering capacity in alkaline medium due to the dissolution reactions of aluminum and its hydroxide as $Al(OH)_4^-$ which are alkalinity consumers [Adhoum et a. (2004)].

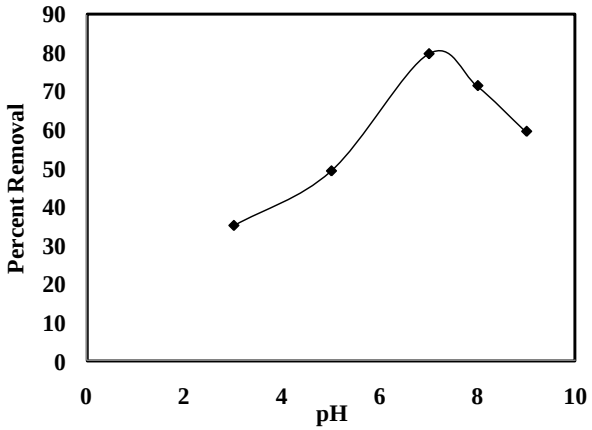


Figure 2. Effect of Initial pH on percentage removal of phenol [Initial concentration = 100 mg/L , Inter-electrode distance = 1cm; time = 120 min; NaCl = 2g/L]

Effect of NaCl Concentration

In the present study, NaCl concentration was varied in the range from 1 to 2.5 g/L to increase the ionic conductivity of the solution in order to minimize energy consumption. And also, the presence of chloride ions break the passive oxide layer on electrode surface by pitting corrosion, hence it increases the availability of aluminum hydroxide in the solution and improves the efficiency of phenol removal [Golder AK. et al. (2007)] which was shown in Figure 3. As shown in Figure 3, Energy consumption decreased from 0.466 kWh/g to 0.348 kWh/g phenol removed with increasing NaCl from 1 to 2.5 g/L. This shows economical importance of the presence of NaCl.

Effect of Inter-electrode Distance

The effect of electrode distance on phenol removal efficiency was shown in Figure 4, optimal distance was found as 1cm. With increase in the value of electrode gap

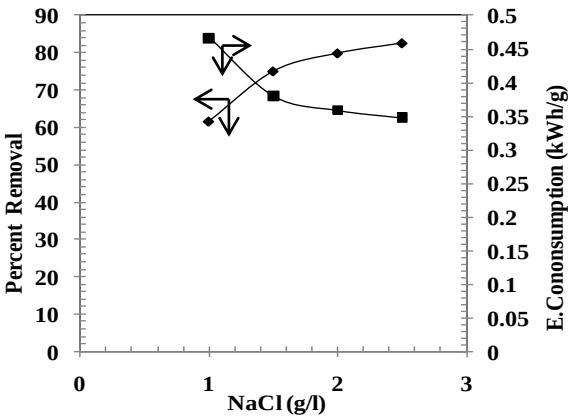


Figure 3. Influence of NaCl concentration on % Removal and Energy consumption [Initial concentration = 100 mg/L; Inter-electrode distance = 1cm; time = 120 min; NaCl = 2g/L; pH = 7].

between anode and cathode, the electrolysis voltage increases owing to the ascent of the electrolyte resistance. With increasing distance, less interaction occurs between the Al ion and hydroxyl ions. In the other words, decrease of both the local concentration and the electrostatic attractions are the reasons for decrease in the removal of phenol.

Effect of Current Density and Operating Time

Current density is the most important parameter for controlling the reaction rate in all electrolysis processes. For determining the influence of operating

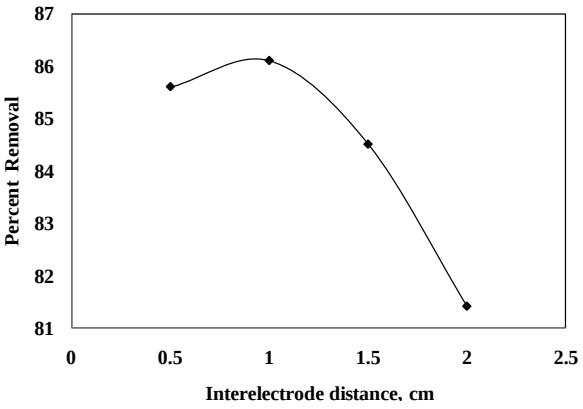


Figure 4. Effect of Inter-electrode distance on phenol removal efficiency [Initial concentration = 100 mg/L; time = 150 min; NaCl = 2g/L; pH = 7].

time and current density, experiments were carried out at pH 7 with initial phenol concentration 100 mg/L in the presence of 2 g/L NaCl. Figure 5 shows the effect of current density, c.d, on EC, which depicts removal efficiency increases with increasing operating time. This is because, increase in current density not only increases the dissolution rate of Al but also bubble production rate and the size and growth of $Al(OH)_3$ flocs which can influence the treatment efficiency of the electrocoagulation. It has been found that, maximum removal efficiency of phenol are 90.2, 86.1, 78.2 and 72.4 % for current densities of 25, 20.31, 14.06 and 7.8 mA/cm^2 respectively after 150 min of operating time without addition of GAC. Further increase in current density may decrease the removal efficiency by effecting the solubility of Al in the solution due to increase in the temperature of the solution [Adhoum et al. (2004)]. However, no such effects were observed in the recent study.

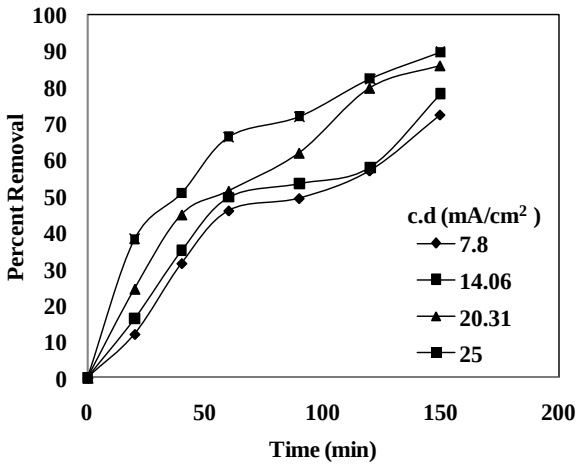


Figure 5. Effect of Current density and Operating time on phenol removal efficiency [Initial concentration = 100 mg/L; Inter-electrode distance = 1cm; time = 150 min; NaCl = 2 g/L; pH = 7].

Effect of Initial phenol concentration

Figure 6, shows, as the concentration increased the phenol removal efficiency decreased. This investigation shows that the percentage removal was gradually decreased from 96.4 to 38% as the phenol concentration increased from 50 to 250 mg/L under the optimum operating conditions. This is because of the formation of insufficient hydroxide complexes to coagulate the greater number of phenol molecules at higher concentrations [Kobya M. et al. (2006)]. But by increasing the concentration of phenol the energy consumption per gram of phenol removed will decreased from 0.745 kWh/g to 0.375 kWh/g of Phenol as phenol concentration increased from 50 to 250 mg/L as shown in Figure 6.

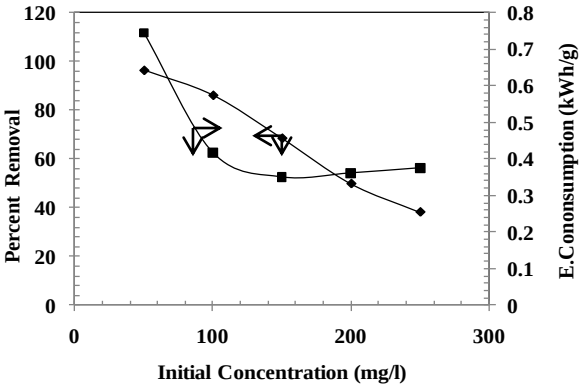


Figure 6. Effect of Initial phenol concentration on % Removal and Energy consumption [Initial concentration = 100 mg/L; Interelectrode distance = 1 cm; time = 150 min; NaCl = 2g/L].

Effect of adsorbent dosage

In order to study the effect of GAC on phenol removal efficiency by EC process, the batch operations were performed. The entire runs were performed at room temperature and in each run 2 L of the phenol solution was poured into the electrolytic cell. The dosage range of GAC (50 – 250 mg/L) was added into the phenol aqueous solution, which was first crushed and screened with 850 micron size sieve. Figure 7 and Figure 8 shows the Effect of GAC dosage at optimum pH 7 after 30 min and 120 min at 7.8 and 25 mA/cm^2 respectively. The percentage removal of phenol was increased as adsorbent dosage increased keeping all other parameters constant.

- By the addition of GAC in the dosages of 50, 100, 150, 200 and 250 mg/L at current density 25 mA/cm^2, increases the efficiency by the amount of 13.95, 19.95, 22.7, 26.2 and 28.8 percentages respectively after 30 min of process in comparative to EC without GAC.

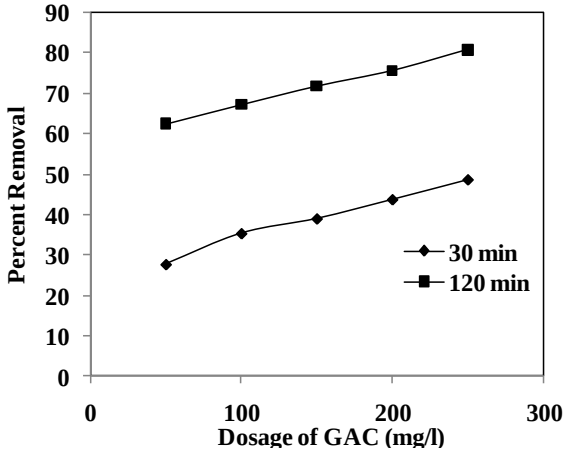


Figure 7. Effect of GAC Addition on % phenol removal after 30 and 120 min [Initial concentration = 100 mg/L; c.d = 7.8 mA/cm^2; Inter-electrode distance = 1cm; NaCl = 2g/L; pH = 7].

Similarly, after 120 min of process the increase in efficiencies were found to be 3.8, 4.6, 6.7, 9.1 and 14.4 percentages respectively as shown in Figure 7.

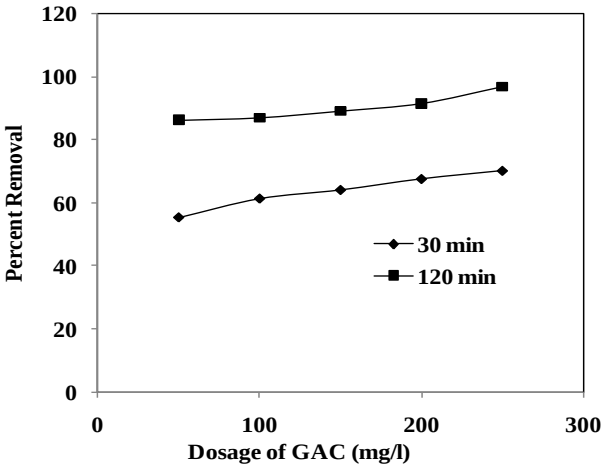


Figure 8. Effect of GAC Addition on % phenol removal after 30 and 120 min [Initial concentration = 100 mg/L; c.d = 25 mA/cm^2; Inter-electrode distance = 1cm; NaCl = 2g/L; pH = 7].

- It has been found that 97% phenol removal was achieved at an adsorbent dosage of 250 mg/L whereas there has been only 82.4% phenol removal without adsorbent under the same operating conditions (Initial Concentration = 100 mg/L; c.d.= 25 mA/cm^2; Time = 120 min). Therefore, it has been confirmed that addition of adsorbent increases the extent of phenol removal.
- It was also observed that a percentage removal of 70.1 was achieved in 30 min of operating time with an adsorbent dosage of 250 mg/L whereas at an adsorbent dosage of 50 mg/L, only 55.25% removal was observed under the same operating conditions. Therefore, it has been concluded that addition of adsorbent not only enhances the process of electrocoagulation but also reduces the operating time.

Characterization of sludge

The sludge produced in EC process was dried in hot air oven at 110^{o}C temperature for 4 hr and crushed into powder for determining morphology and elemental composition. Figure 9 shows Scanning electron micrograph (SEM) images of sludge produced after EC treatment with addition of GAC along with EDAX analysis , which

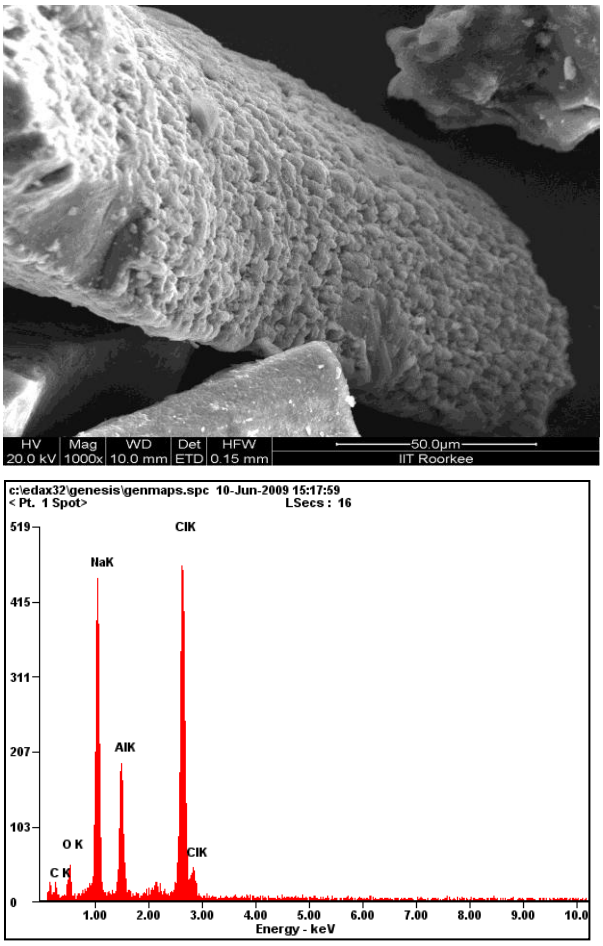


Figure 9. SEM and EDAX analysis of sludge produced in EC process with GAC addition.

are used to compare the composition of the elements in weight percentage and atomic percentages. It was interesting to note that the sludge produced by EC without addition of GAC at optimal conditions contains carbon 36.55%, oxygen 17.89% and aluminum 18.35% (% Wt), whereas sludge produced in EC process with addition of GAC contains carbon 59.86%, oxygen 21.67% and aluminum 12.13% (% Wt). The results shows that by addition of GAC it increases the phenol removal from solution which is indicated by increase in percentage of carbon and oxygen, and also shows that aluminum consumption decreases for the same operating condition with higher percentage removal efficiency. Therefore, the process of EC coupled with addition of GAC is found to be more economical by reducing operating time and electrode consumption.

Conclusion

In light of the obtained results, it has revealed that phenol removal efficiency is enhanced by sweep coagulation and adsorption. It was concluded that phenol removal efficiency was more at initial pH 7. Increase in current density and NaCl resulted in increase in the phenol removal. While it decreases with the increase in initial phenol concentration. And also found that NaCl concentration is an important factor for reducing energy consumption. Energy consumption decreased from 0.466 kWh/g to 0.348 kWh/g of phenol with increase in NaCl dosage from 1 to 2.5 g/L as shown in the results. The addition of GAC as adsorbent resulted in significant increase in the removal rate of phenol at lower densities and operating time than conventional EC process. Hence, decreasing the energy consumption and electrode consumption. The experimental results with addition of GAC shows that the highest percentage removal 97% was achieved for 120 min operating time and current density of 25 mA/cm^2 which was approximately 15% more compared with conventional EC process. It can be concluded from this study that EC with addition of GAC is a promising technique for phenol removal.

References

1. Adhoum, N. and Monser, L. (2004). Decolourization and removal of phenolic compounds from olive mill wastewater by electrocoagulation. Chem. Engg and Processing, 43 (10), 1281–1287.
2. Bayramoglu, M., Can, O.T., Kobya, M. and Sozbir, M. (2004). Operating cost analysis of electrocoagulation of textile dyer wastewater. Sep. Purif. Tech., 37, 117-125.
3. Cabala, B., Tsyntsarski, B., Budinovab, T., Petrov, N., Parra, N.B. and Ania, C.O. (2009). Improved phenol adsorption on carbons after mild temperature steam reactivation. J. Hazard. Mater.
4. Chen, G. (2004). Electrochemical technologies in wastewater treatment. Sep. Purif. Tech., 38, 11–41.
5. Golder, A.K., Samanta, A.N. and Ray, S. (2007). Removal of trivalent chromium by electrocoagulation. Sep. Purif. Tech., 53, 33-41.
6. Guohua, C. (2004). Electrochemical technologies in wastewater treatment. Sep. Puri, Tech., 38, 11–41.
7. Kobya, M., Demirbas, E., Can, O.T. and Bayrmoglu, M. (2006). Treatment of levafix orange textile dye solution bye electrocoagulation. J. Hazard. Mater., B132, 183-188.
8. Lin, C.H. and Tseng, S.K. (1999). Electrochemically reductive chlorination of Penta-Chlorophenol using a high over potential zinc cathode. Chemosphere, 39, 2375–2389.
9. Mouedhen, G., Feki, M., De-Petris, W.M. and Ayedi, H.F. (2008). Behaviour of aluminum electrodes in electrocoagulation process. J. Hazard. Mater., 150, 124–135.
10. Ratna, K.P., Sanjeev, C., Kartic, C.K. and Mahajan, S.P. (2004). Removal of arsenic from water by electrocoagulation. Chemosphere, 55, 1245–1252.
11. Scott, K. (1995). Electrochemical Processes for Clean Technology. The Royal Society of Chemistry, London.
12. Somnath Mukherjee., Sunil Kumar., Amal Misra, K. and Maohong Fan. (2007). Removal of phenols from water environment by activated carbon, bagasse ash and wood charcoal. Chem. Eng. J., 129, 133–142.
13. Yousef, M A. and Nabil, S.A. (1999). Electrochemical oxidation of phenol using graphite anodes. J. Sep. Sci. and Tech., 34(4), 699-708.
14. Xiao-yan, L., Yu-hong, C., Yu-jie, F., Zhao-ming, X. and Ji-Dong, G. (2005). Reaction pathways and mechanisms of the electrochemical degradation of phenol on different electrodes. J. Water Res., 39, 1972–1981.
15. Leonardo, S. A., Rocha-Filho, R., Nerilso, B., Sonia, R. B., Garcia-Garcia, I. and Vicente, M. (2008). Degradation of phenol using Co- and Co, F-doped PbO_2 anodes in electrochemical filter-press cells. J. Hazard. Mater., 153, 252–260.

2nd International Engineering Symposium - IES 2012
(KU-MU-NITK-HCMCUT Joint Symposium) March 5-7, 2012, Kumamoto University, Japan

COMPARISON OF LAM-DONG AND PHU-YEN DIATOMITE AS RAW MATERIALS FOR FILTER AID MANUFACTURE

Tran Duy Hai, Mai Thanh Phong*

Faculty of Chemical Engineering, Ho Chi Minh City University of Technology
268 Ly Thuong Kiet Str., Dist. 10, Ho Chi Minh City
* Corresponding author**:** mtphong@hcmut.edu.vn

Abstract: Diatomite (or kieselguhr) is deposit of skeletal remains of single-cell water plants (diatom algae). Diatomite can be used as raw materials for production of several products, such as filter aids, fire-bricks, adsorbents, etc. Two major deposits of diatomite in Vietnam are in Phu-Yen and Lam-Dong province. This study aims to study preparation of filter aids from Lam-Dong and Phu-Yen diatomite. The raw materials and the filter aids were characterized by using X-ray fluorescence spectrometer, scanning electron microscope and instrumentally measured color coordinates. Effects of raw material characteristics on process of filter aid preparation were considered. Results of beer filtration tests with the obtained filter aids were also presented in this paper.

Keywords*: diatomite, filtration, filter aids, calcination*

1. INTRODUCTION

Chemically, diatomite is essentially amorphous hydrated or opaline silica ($SiO_2.nH_2O$) with varied amounts of impurities such as clay minerals, organic matters, silica sand and metal salts. The level of soluble impurities in diatomite affects its end-use properties [1, 2]. Diatomite can be used as raw material for production of several products, such as filter aids, fire-bricks, adsorbents, … Thuene and Bellet [1] brought standard compositions of diatomaceous filter aids as follows: SiO_2 > 85% w/w, CaO < 1% w/w and Fe_2O_3 < 1.5% w/w.

Diatomite reserve of Vietnam is quite large, mainly in two provinces: Phu-Yen (90 million tons) and Lam-Dong (8.9 million tons). In Vietnam, diatomite has mostly been used as adsorbents to treat water from aquacultural ponds. Hence, the value of Vietnam diatomite is limited. Filter aids used for beer filtration in Vietnam are completely covered by products imported from other countries such as China, Japan [3].

Properties of the raw diatomite affect filter aid manufacture process. This work aims to compare Lam-Dong and Phu-Yen diatomite as raw materials filter aid manufacture.

2. EXPERIMENTAL

2.1. Chemicals and material

Chemicals: Chemicals used in this work are H_2SO_4 (95-98% w), NaCl (> 99.9% w) purchased from Guangdong Guanghua Sci-Tech Co., Ltd, China.

Diatomite: Raw diatomites were collected from Dai-Lao valley in Lam-Dong province and Xuan-An district in Phu-Yen province with copious shapes and sizes.

2.2. Analytic instruments

Chemical compositions of calcined diatomite were determined by X-ray fluorescence (XRF) spectrometer - No 113388/ 410031 XD, Germany, Error ± 1%.

Scanning electron microscope (SEM) was used to photograph surface microstructure.

The whiteness index and yellow index of filter aids were calculated following ASTM E 313-00 standard.

The beer color was calculated from the absorbance measured by T70+ UV-VIS spectrometer - No. 18-1815-01-0001, England.

2.3. Experimental procedures

2.3.1. Acid treatment

Raw diatomites were wet ground in an attrition mill for 1h using alumina balls. The slurry was dried at 90-105 ^{o}C for 2-3 h, then screened through sieve 0.25 mm apertures and leached in H_2SO_4 solution at 90-95 ^{o}C. The acid treatment was executed by means charging 10 g of diatomite into 200 ml of H_2SO_4 solution, which was continuously stirred at 500 rpm for 6 h using a magnetic stirrer [3]. After that, diatomite was filtered and washed by clean water till H_2SO_4 was completely removed. This treatment process can be repeated depending on the chemical composition of the diatomite.

2.3.2. Flux calcination

Fluxing agents used in this study was NaCl. Fluxing agent was mixed in diatomite with different contents (3, 4, 5% w/w). The mixtures were calcined in the furnace at 900 ^{o}C for 90 minutes [3]. In order to reach the desired temperature, the furnace was heated up from the ambient temperature with a rate of 10 ^{o}C/min. During flux calcination, the diatoms become white in color, and fuse together; also some amorphous silica gets converted to crystalline silica. After calcinations, the products were sieved to remove slag and coarse particles.

2.3.3. Beer filtration tests

The filtration tests utilized a funnel connected to a vacuum system. The pore diameter of filter paper is 37 μm. The filtration area is 0.0009618 m^2. Beer filtration tests were conducted to evaluate effects of the obtained filter aids on filtration process. pH value and turbidity of clarified beer were determined in these tests.

Beer color was calculated by formula below:

$$X = 25.D.A_{430nm} \text{ (EBC)}$$

where, D is the dilution factor, and A_{430nm} is the absorbance at 430 nm in 1 cm.

The increase in pressure across the filter was observed over time. During filtration, vacuum pressure stabilized at 700 mmHg.

A defined amount of diatomite filter aid was mixed in 20 ml of clean water and admitted into the filter funnel and filtered to make a precoat. At the end of this filtration, another amount of diatomite filter aid was mixed in 200 ml beer at 2-6 ^{o}C to make a bodyfeed and admitted into the funnel. The filtration time was started record. After filter duration, the filtration was stopped and recorded volume of clarified beer. The filtration rate was estimated according to the Bazhal [2] method and the related equation given below:

$$v = \frac{W}{F.t}$$

where, v is filtration rate ($hl.m^{-2}.h^{-1}$), W is the volume of the filtrate (hl), F is the effective filter paper surface (m^2) and t is the filtration time (h).

3. RESULTS AND DISCUSSION

3.1. Properties of the raw diatomites

Chemical compositions of the raw diatomite are present in Table 1.

Table 1. Chemical compositions of the raw diatomites collected from Lam-Dong and Phu-Yen

Origin of diatomite	Chemical compositions				
	SiO_2	Fe_2O_3	CaO	Al_2O_3	L.O.I
From Lam-Dong	52.9	5.32	0.43	22.9	19.8
From Phu-Yen	70.1	4.32	0.19	10.8	12.5

Based on data in Table 1 it could be seen that SiO_2 content of Phu-Yen diatomite is much higher then what of Lam-Dong diatomite. Impurity contents of Phu-Yen diatomite, such as Fe_2O_3, Al_2O_3 and CaO are lower compared to Lam-Dong diatomite. Loss on ignition (L.O.I) of Phu-Yen diatomite is also lower compared to Lam-Dong diatomite. This proves that disintegrative impurities (such as organic matters, clay minerals, etc) in the raw diatomite of Phu-Yen are lower compared with Lam-Dong. Consequently, the Phu-Yen diatomite is better the Lam-Dong diatomite.

SEM images of the raw Phu-Yen and Lam-Dong diatomite were also shown in

Fig. 1. In Fig. 1a, impurities completely cover outside structure of the Lam-Dong diatomite. In order to clearly observe diatomite pore, the Lam-Dong diatomite must be treated in acid solution. Meanwhile, porous structure of the raw Phu-Yen diatomite could be seen in Fig. 1b. However, the most pores are intercepted in impurities.

3.2. Straight calcination

SiO_2 of Lam-Dong diatomite is too low to prepare filter aid. Therefore, it must be pretreated to enrich SiO_2 before calcination. For Phu-Yen diatomite, due to higher SiO_2 content, a first attempt was to calcine without acid pretreatment. The results (Table 2) show that Fe_2O_3 content of the calcined diatomite is still high. This may influence the filtrate. To enrich SiO_2 content and reduce impurities, the raw diatomite was treated in acid solution as described above. The treated diatomite was then calcined without fluxing agents at 900 °C. Chemical compositions of the acid treated and the calcined diatomite are presented in Table 2.

According to the chemical composition standard given by Thuene and Bellet [1] for diatomite filter aids, is better to treat Lam-Dong diatomite for 30h and Phu-Yen diatomite for 6h in acid solution.

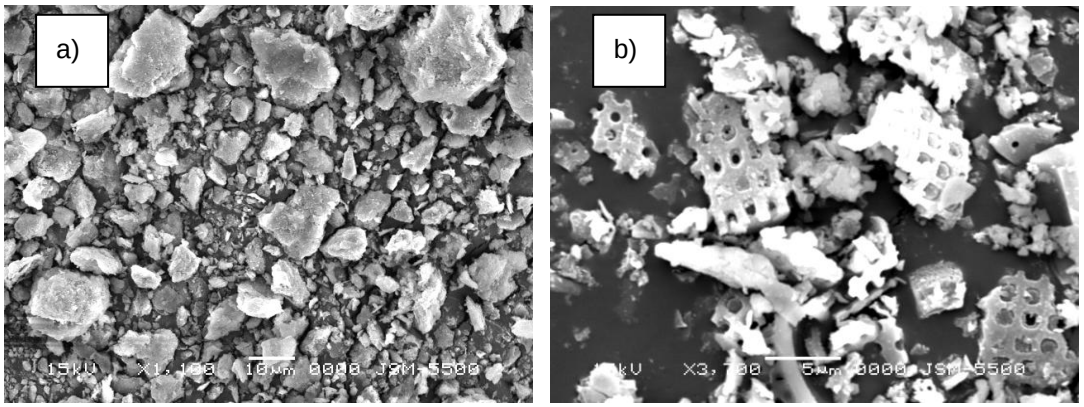


Figure 1. SEM images: a) Raw Lam-Dong diatomite and b) Raw Phu-Yen diatomite

Table 2. Chemical compositions of the straight calcined diatomite

Compositions	Lam-Dong diatomite		Phu-Yen diatomite		
	30h (1)	30h-calcined (2)	6h (1)	6h-calcined (2)	Raw-calcined (3)
SiO_2	81.7	89.6	93.8	97.7	82.1
Fe_2O_3	0.89	0.94	0.39	0.45	4.79
CaO	0.04	0.09	0.03	0.04	0.19
Al_2O_3	6.73	3.00	1.13	1.25	11.8
Color index	-	YI = 28.1	-	WI = 63.4	-

Note: (1) diatomite treated in 6M H_2SO_4. (2) diatomite calcined at 900°C with acid pretreatment. (3) diatomite calcined at 900°C without acid pretreatment. YI and WI are yellowness and whiteness index.

After acid treatment, the diatomites were calcined to become filter aids. SEM images of the filter aids are shown in Fig. 2. In SEM images, it could be seen cylindrical and plateaus particles in Lam-Dong diatomite; meanwhile, plane and ear-ring in Phu-Yen diatomite.

3.3. Flux calcination

Purpose of using fluxing agents is to increase whiteness, the stableness of the structure and permeability for filter aids.

The straight-calcined diatomite is brick yellow in color due to the oxidation of iron. When calcined with fluxing agents, the color of the diatomite is improved due to the formation of the complex alkali-aluminum-iron silicates.

Based on color indexes presented in Table 2, it could be seen that the treated Lam-Dong diatomite must be calcined with fluxing agents to improve filter aids color.

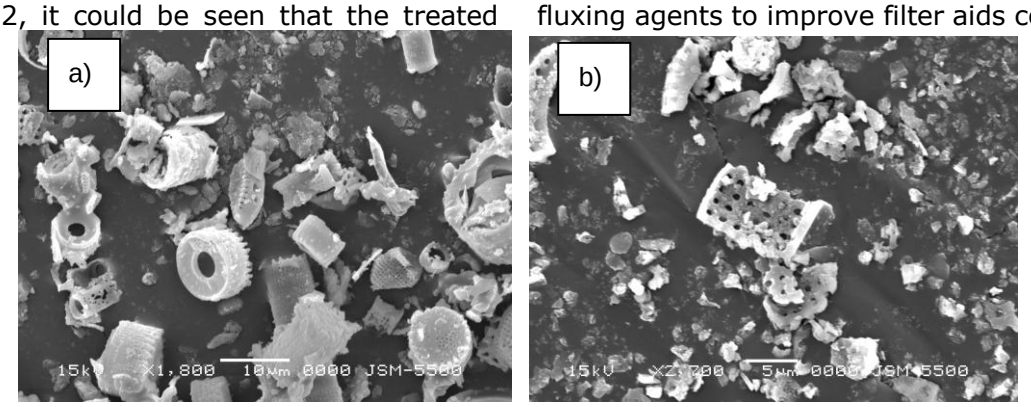


Figure 2. SEM images of the filter aids based on a) Lam-Dong diatomite and b) Phu-Yen diatomite

Meanwhile, the obtained filter aid by straight calcination of the treated Phu-Yen diatomite was white.

Color indexes of the flux calcined diatomite are presented in Table 3.

Table 3. Whiteness indexes (*WI*) of the flux calcined diatomites

Types of diatomite	Flux calcined Lam-Dong diatomite		
	3% w/w	4% w/w	5% w/w
WI	57.6	63.4	67.6

When the diatomite was calcined in NaCl, the filter aid is not only whiter but also increased stableness of diatomite structure. It could be proved in Fig. 3. In this SEM image, the surfaces of frustules show clean and clear pores. The morphology of the frustules and the origin geometry of the pores are exposed.

The filter aids obtained from straight calcination of the treated Phu-Yen diatomite (S-PY), treated Lam-Dong diatomite (S-LD) and flux calcination with 5% w/w of NaCl of the treated Lam-Dong diatomite (F-LD) were selected for beer filtration tests.

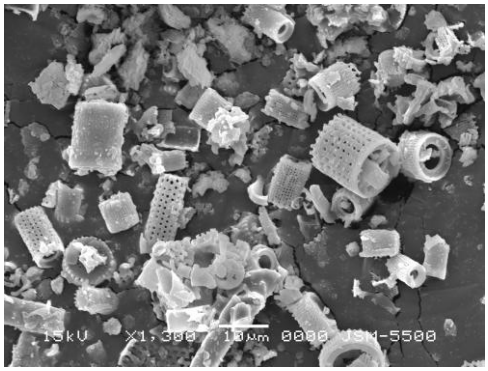


Figure 3. SEM image of the calcined diatomite with 5% w/w of NaCl

3.4. Beer filtration tests

In order to evaluate effects of filter aids on filtration, beer filtration tests were performed. Several properties of the filtrates are shown in Table 3.

Table 3. Clarified beer properties (15 minutes of the filtration time) (500 g/m^2 precoat and 2 g/l bodyfeed)

Type of the filter aids	Parameter			
	pH	Beer color (EBC)	Average filtration rate (hl.m^{-2}.h^{-1})	Beer taste and flavor
S-PY	5.5	4.8	7.38	Normal
S-LD	5.4	4.7	3.91	Normal
F-LD	5.4	7.2	5.10	Normal

From Table 3, it can be observed that pH value of the clarified beer is almost unaffected by filter aids. The results also show that using NaCl as fluxing agent can

increase considerably the clarified beer color. This effect may be due to calcination, the NaCl united with several material oxides and coursed out of the skeletal pores. The pore diameters tend to maximum limits, which make condition for small solids to pass. In addition, the NaCl could react with some materials and create minute solid particulates, which go down with clarified beer.

Effects of the NaCl fluxing agent on average filtration rate are studied by using S-LD and F-LD filter aids in beer filtration process. Using NaCl as fluxing agent can increase average filtration rate from 3.91 to 5.10 $hl.m^{-2}.h^{-1}$. Data in Table 3 can also show that the filter aid made from Phu-Yen diatomite can improve the average filtration rate much more than compared to what made from lam-Dong diatomite.

4. CONCLUSIONS

The raw diatomite from Lam-Dong is not suitable for direct manufacture of filter aids. Therefore, it should be pretreated with acid to enrich SiO_2 and reduce impurities before calcination to produce filter aids. The obtained results show that it is better to leach Lam-Dong diatomite for 30h and Phu-Yen diatomite for 6h in 6M H_2SO_4 solution to get diatomite suitable for filter aids preparation. NaCl could be used as a flux agent for calcination of Lam-Dong diatomite to improve color as well as filtration rate. Ultimately, Phu-Yen diatomite is better Lam-Dong diatomite in terms of raw materials for filter aid manufacture.

Acknowledgments: The financial support by JICA through SUPREM project is acknowledged

REFERENCES

1. S D J Inglethorpe, Industrial Minerals Laboratory Manual Diatomite*. British Geological Survey.* Technical report WG/92/39, Mineralogy and Petrology Series (1993).
2. Luc Fillaudeau et al., Water, wastewater and waste management in brewing industries. *Journal of cleaner Production* 14 (2006) 463-471.
3. Tran Doan Minh Dang, Preparation of filter aids based on Lam-Dong diatomite. Master thesis, Ho Chi Minh City University of Technology (2011).
4 S.C.A. Franca, Beneficiation of Brazilian diatomite for filtration application industry. *SME annual meeting*, Feb. 25-27, Phoenix, Ariona (2002).
5. Richard B, Nielse, Diatomaceous earth filter aid and method for its manufacture. *United States Patent*, No 4,142,968 (1979).
6. Ian L Ward, Wort & Beer Clarification Manual. *Brewers Wholesale Supply*, Rhode Island 02840.
7. Sanja Martinnovic, Preparation of filter aids based on diatomites. *Int. J. Miner. Process*. 80 (2006) 255-260.
8. K.Niemsch and Th. Heinrich, Raible-Test for Evaluation of Filtration Properties. *Journal of the Institute of Brewing*, Volume 106, No. 5 (2000).
9. R.Alex Speers et al., Effects of b-Glucan, Shearing and Environmental factors on the Turbidity of Wort and Beer. *Journal of the Institute of Brewing. Publication no*. G-2003-0925-137 (2003).
10. Hossam, Diatomite: Its Characterization, Modifications and Applications. *Asia journal of Materials Science* **2** (**3**) (2010) 121-136.
11. Christophe Peuchot - Testing of filter media for liquid filtration-introduction and review. *Institute of Filtration and Techniques of Separation*, BP 40292, 4707 Agen, France (2006).
12. George Asante Nyamekye et al., Filter aids made from low permeability diatomite. *United States Patent Application Publication*, No. US 2010/0248953 A1 (2010).
13. Doug Stewart el al., Development and Assessment of a Small-Scale Wort Filtration Test for the Prediction of Beer Filtration Efficiency. *Journal of The Institute of Brewing*, Volume 106, No. 6 (2000).

2nd International Engineering Symposium - IES 2012
(KU-MU-NITK-HCMCUT Joint Symposium) March 5-7, 2012, Kumamoto University, Japan

Application of ultrasound and hemicellulase preparation to acerola juice processing

Nguyen Thi Xuan Lan [1] **Vuong Thi My Thanh** [1] and **Le Van Viet Man** [2]

1 *Tien giang center for Technology and Biotechnology, Vietnam. email: nguyenthi_xuanlan1983@yahoo.com.vn*
2 *Department of Food Technology, Ho Chi Minh City University of Technology, Vietnam. email: lvvman@hcmut.edu.vn*

Abstract: Acerola mash was subsequently treated by ultrasound and hemicellulase preparation. The sonication conditions were previously optimized and fixed. The conditions of enzymatic treatment were investigated and optimized. The optimal concentration of hemicellulase preparation and biocatalytic time were 0.59%v/w and 69.5 min, respectively. Under these conditions, the extraction yield achieved maximum of 93.77%. The level of reducing sugars, total acids, vitamin C, total phenolics, antioxidant activity evaluated by 1,1-diphenyl-2-picrylhydrazyl (DPPH), and 2,2'-azinobis-(3-ethylbenzothiazoline-6-sulfonic acid) (ABTS) methods of the obtained juice was 47.05%, 59%, 16.40%, 34.92% and 39.33% (DPPH), 43.16% (ABTS) higher than that of the control without ultrasound and hemicellulase treatment.

***Keywords**:* acerola, hemicellulase, juice, ultrasound

1. Introduction

Nowadays, ultrasound is considered to be an emerging and promising technology for industrial food processing. The use of power ultrasound significantly improved the extraction of different bioactive compounds such as phenolics (Ya-Qin Ma et al. (2009)), lycopene (Zhang Lianfu, Liu Zelong (2008)), anthocyanin (B. K. Tiwari et al (2009)). Mechanical effects of ultrasound provided a greater penetration of solvent into cellular materials and improved mass transfer (T.J. Mason et al. (1996)).
Extraction is an important operation in juice processing. Conventionally, hydrolase preparations such as pectinase, hemicellulase and cellulase have been widely used in juice production for enhancement in juice yield (M.K. Bhat (2000)). Recently, some previous studies indicated that combined sonication and hydrolase treatment increased both extraction yield and product quality in the production of grape juice (Le Ngoc Lieu, Van Viet Man Le (2010)) and guava juice (Le Thi Thuy et al. (2011)).

Acerola is a tropical fruit rich in vitamin C and antioxidant activity. Our previous study showed that the use of hemicellulase preparation in acerola mash treatment highly improved the juice yield and quality (Vuong Thi My Thanh et al. (2011)). This paper focused on application of the combined ultrasound and hemicellulase method to acerola juice processing. The acerola mash was firstly sonicated with optimal conditions (Dang Bui Khue et al. (2010)) and subsequently treated by hemicellulase preparation. The objective of this study was to determine optimal conditions of hemicellulase treatment of acerola mash in the combined ultrasonic and enzymatic method and to compare the quality of the acerola juice extracted from different treatment methods.

2. Materials and method

2.1. Materials

- Acerola (*Malpighia glabra L.*) was purchased from Go Cong co-operative, Tien Giang. Acerola fruits were washed and crushed to reject seeds in a crusher

(Panasonic MJ-70M, Malaysia). The intermediate product was grinded again in a blender. Acerola pulp was stored in a freezer at -18°C until use.
- Hemicellulase preparation Viscozyme L. (Novozyme, Denmark) was used in this study. This preparation contains mostly β-1,3 glucanase and 1,4 xylanase. The catalytic temperature and pH of this enzyme preparation are 55°C and 4.5, respectively. The activity of Viscozyme L was 100 fungal beta-glucanase (FBG)/g (Novozymes A/S - Krogshoejvej 36 - 2880 Bagsvaerd – Denmark (2010)).

2.2. Experimental methods

2.2.1. Procedure for acerola juice processing in the laboratory

Distilled water was added into acerola mash with the ratio of 2:1 (w/w). The pH of this mixture was adjusted to 4.5. Samples of 40g diluted acerola mash were taken and placed into beakers for each assay.
The acerola mash was sonicated at 40°C with ultrasonic power of 3.75W/g for 100s (Dang B. K. et al. (2010)). Sonication was performed with a horn type ultrasonic probe with frequency of 20 kHz (Sonics and Materials. Inc, VC750, USA). During the ultrasonic treatment, the temperature of samples was adjusted by using a water bath. The samples were then added with Viscozyme L and incubated at 55°C for hemicellulase treatment. At the end of the treatment, the mixture was filtered via a vacuum filter. The obtained filtrate was centrifuged at 10000 rpm for 20 min by a centrifuge (Sartorius 3K30, Switzerland) and the solution obtained was used for further analysis.
Control samples without ultrasonic and/or enzymatic treatments were also carried out.

2.2.2. Effects of concentration of hemicellulase preparation on extraction yield

In this experiment, the concentration of Viscozyme L preparation was varied (0, 0.2 , 0.4, 0.6, 0.8, 1.0%, v/w) while the biocatalytic time was fixed at 60 minutes.

2.2.3. Effects of biocatalytic time on extraction yield

The treatment time in this experiment was changed: 0, 30, 60, 90 and 120 min. The concentration of Viscozyme L preparation was selected from the results obtained in section 2.2.2.

2.2.4. Optimization of enzymatic treatment conditions of acerola mash by response surface methodology

The experiments were carried out according to a central composite design with 2 factors and 5 levels. A randomised, quadratic central composite circumscribed (CCC) response surface design was used to study the effect of hemicellulase concentration and biocatalytic time on the extraction yield. The complete design consisted of 13 experimental points including 4 factorial points, 4 axial points and 5 center points. The software Modde version 5.0 was used to generate the experimental planning and to process data.

2.2.5. Comparison of quality of acerola juice extracted from different treatment methods

Four treatment methods for acerola mash were performed:
Method 1: Control sample without ultrasonic and enzymatic treatment (C).
Method 2: Ultrasonic treatment (UT).
Method 3: Enzymatic treatment (ET).
Method 4: Combined ultrasonic and enzymatic treatment (UET).
In this experiment, the ultrasonic treatment conditions in methods 2 and 4 were described in section 2.2.1. The enzymatic treatment conditions in method 3 were chosen from the results of our previous study (Vuong Thi My Thanh et al. (2011)). The enzymatic treatment conditions in method 4 were selected from the results of section 2.2.4.
The obtained juice was used for analysis of reducing sugars, total acidity, vitamin C, total phenolics and antioxidant activity.

2.3. Analytical methods

- Extraction yield was calculated according to the content of soluble compounds in the extracted juice and the content of solids in the original material (Le Ngoc Lieu, Van Viet Man Le (2010)).
- Reducing sugars were determined by spectrophotometric method using 3,5-dinitrosalicylic acid reagent (Le Ngoc Lieu, Van Viet Man Le (2010)).
- Total phenolics were quantified by spectrophotometric method using Folin-Ciocalteu reagent (Le Ngoc Lieu, Van Viet Man Le (2010)).
- Total acidity was evaluated by titration method using 0.1 N NaOH solution and phenoltalein indicator. The result was expressed in equivalent of tartaric acid content (g/L), (Le Ngoc Lieu, Van Viet Man Le (2010)).
- Vitamin C was determined by HPLC method (Tran Bich Lam (2006)).
- Antioxidant activity: Antioxidant activity of acerola juice were determined by DPPH and ABTS methods (Roberta Re et al. (1999)).

2.4. Statistical analysis

All experiments were performed in triplicate. The experimental results obtained were expressed as means ± SD. Mean values were considered significantly different when $P < 0.05$. Analysis of variance (ANOVA) was performed using the software Stagraphic centurion XV.I

3. Results and discussion

3.1. Effect of concentration of hemicellulase preparation on extraction yield

Table 1 shows that the ultrasonic treatment of acerola mash increased extraction yield of 2.6% in comparison with the control sample without any treatment. Increase in extraction yield by sonication in acerola juice processing was lower than that in grape juice (Le Ngoc Lieu, Van Viet Man Le (2010)) and guava juice (Le Thi Thuy et al. (2011)) processing.

Table 1 Effect of concentration of hemicellulase preparation on extraction yield

Enzyme concentration (%, v/w)	0^1	0^2	0.2	0.4	0.6	0.8	1.0
Extraction yield (%)	75.8 ±0.63^a	77.8 ±1.34^b	87.3 ±1.09^c	93.8 ±0.47^e	92.5 ±0.80^{de}	93.8 ±0.89^e	92.8 ±1.06^{de}

Values with different small letters are significantly different at $P < 0.05$.

0^1: control sample without ultrasonic and enzymatic treatment.

0^2: control sample with ultrasonic treatment and without enzymatic treatment.

However, the combined ultrasound and hemicellulase preparation method significantly improved the yield of acerola juice. Increase in concentration of hemicellulase preparation from 0 to 0.4% v/w augmented highly the acerola juice yield. Maximum extraction yield achieved 93.8% when the hemicellulase concentration was 0.4%v/w. Higher concentration of hemicellulase preparation did not improve the juice yield. It was due to the limitation of extracted compounds in the fruit material used in the experiment (Le Thi Thuy et al. (2011)).

As a result, the hemicellulase concentration of 0.4% was chosen for the next experiment.

3.2. Effect biocatalytic time on extraction yield

When the time of hemicellulase treatment increased from 0 to 60 min, the extraction yield increased 24.6% in comparison with that in the control sample without any treatment (Table 2). Hemicellulases broke down hemicellulose in plant tissue and facilitated juice extraction from cellular cytoplasm (Demir N (2001)). Nevertheless, longer biocatalytic time did not improve the juice yield.

Consequently, the biocatalytic time for the acerola juice extraction was 60 min.

Table 2 Effect of biocatalytic time on extraction yield

Treatment time (min)	0^1	0^2	30	60	90	120
Extraction yield (%)	71.7±0.62[a]	73.6±0.78[b]	80.8±1.74[c]	89.4±1.28[d]	88.8±0.76[d]	89.6±1.95[d]

Values with different small letters are significantly different at P < 0.05.
0^1: control sample without ultrasonic and enzymatic treatment.
0^2: control sample with ultrasonic treatment and without enzymatic treatment.

3.3. Optimization of hemicellulase treatment conditions of acerola mash by response surface methodology

A concentration of Viscozyme L. of 0.4% v/w and a biocatalytic time of 60 min were selected as central conditions in the optimization. The experimental planning and results of extraction yield are presented in Table 3.

Table 3 Experimental planning and results of extraction yield in the combined ultrasound and hemicellulase treatment of acerola mash

Run	X_1 - Hemicellulase concentration (%, v/w)	X_2 - Bio -catalytic time (min)	Yield (%)
1	0.2	30	82.68
2	0.6	30	93.92
3	0.2	90	84.75
4	0.6	90	94.52
5	0.1172	60	83.93
6	0.6828	60	96.36
7	0.4	17.58	87.52
8	0.4	102.42	94.72
9	0.4	60	94.39
10	0.4	60	93.91
11	0.4	60	94.03
12	0.4	60	94.00
13	0.4	60	94.57

Multiple regression analysis was performed on the experimental data and the final predictive equation (1) obtained is as given below:

$$Y = 94.18 + 3.94\ X_1 + 1.31\ X_2 - 1.6\ X_1 * X_1 - 1.3\ X_2 * X_2 \quad (1)$$

Where Y, X_1 and X_2 were the extraction yield (%), the hemicellulase concentration (%v/w) and biocatalytic time (min), respectively.

According to analysis of variance, the F-value was 2.22 times higher than the F listed value. The regression model was therefore significant ($p<0.05$). The estimated effect of each variable and their interaction on the extraction yield are presented in Table 4.

Table 4 Estimated effect of independent variables on extraction yield in the combined ultrasound and hemicellulase treatment of acerola mash

Factor [a]	Effect	Standard error	P
X_1	3.93998	0.413846	0.0000295
X_2	1.31218	0.413846	0.0156924
$X_1 \times X_1$	-1.61546	0.362385	0.00294364
$X_2 \times X_2$	-1.30249	0.362385	0.00880752

X_1: Hemicellulase concentration, X_2: Time of hemicellulase treatment (min); P indicates significance of linear regressions; [a] Significant factors at 95% of confidence level.

X_1 was considered as dominative effect. Three variables X_2, X_1^2, X_2^2 were estimated as significant effect but the interaction term X_1*X_2 was not. The effect of hemicellulase concentration on the extraction yield in acerola juice processing was stronger than the effect of biocatalytic time.

Figure 1 indicates the three-dimensional surface plots according to Eq. 1. From the model, the optimal conditions were the enzyme concentration of 0.59% v/w and the time of 69.5 min, at which the model predicted a maximum response of 96.7%. Three replicates were then performed for measuring the extraction yield under optimal conditions. The obtained extraction yield was 93.77% ± 0.65. The experimental values were nearly similar to the predicted value from the model.

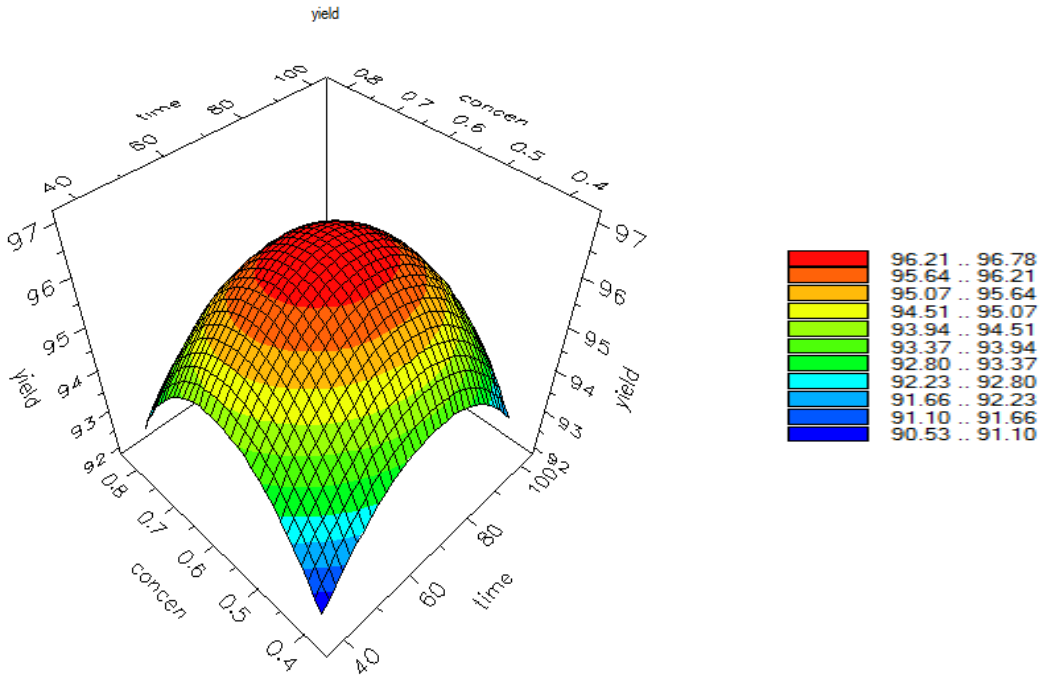


Fig. 1 Fitted surface for yield of hemicellulase treatment of acerola mash as a function of enzyme concentration and treatment time

3.4. Comparison of extraction yield and quality of acerola juice obtained from different treatment methods

Table 5 shows that among 4 methods tested, the combined ultrasonic and enzymatic treatment (method 4) gave the highest extraction yield. In addition, the concentration of different nutrients in acerola juice from the combined method was similar or significantly better than that from other treatment methods. The level of reducing sugars, total acidity, vitamin C, phenolics and antioxidant activity evaluated by DPPH and ABTS methods was 47.05%, 59.00%, 16.40%, 34.92% and 39.33% (DPPH), 43.16% (ABTS), respectively higher than that in the control sample without any treatment (method 1). Similar observation was recently mentioned by researchers who used the combined ultrasound and pectinase treatment in grape juice (Le Ngoc Lieu, Van Viet Man Le (2010)) and guava juice (Le Thi Thuy et al. (2011)) production.

Table 5 Quality of acerola juice obtained from different treamnet methods of acerola mash treatment

Physico-chemical characteristic	C	UT	ET	UET
Yield (%)	69.40±0.94[a]	71.78±0.76[b]	92.43±0.65[c]	93.77±0.65[d]
Reducing sugar (g/L)	43.23±0.58[a]	47.68±0.58[b]	59.93±0.46[c]	63.57±0.47[d]
Total acidity (g tartaric/L)	5.10±0.52[a]	6.30±0.00[b]	7.20±0.00[c]	8.10±0.00[d]
Vitamin C (g/L)	16.02±0.26[a]	16.12±0.25[a]	18.25±0.23[b]	18.64±0.036[b]
Total phenolics (g GAE/L)	7.64±0.32[a]	8.27±0.17[b]	9.64±0.26[c]	10.30±0.38[d]
Antioxidant -DPPH method (mmolTEAC/L)	65.60±3.30[a]	68.00±1.39[a]	80.40±1.59[b]	91.40±1.39[c]
Antioxidant -ABTS method (mmolTEAC/L)	74.60±0.92[a]	80.20±2.71[b]	91.80±1.39[c]	106.80±4.33[d]

Values with different small letters in the same row are significantly different at P < 0.05.

4. Conclusions

The combined ultrasound and hemicellulase treatment of acerola mash improved both juice yield and quality. This combined method could be used not only in juice production but also in extraction of different bioactive compounds from plant and animal resources. The use of ultrasound and hemicellulase preparation in industrial extraction was therefore very potential.

Acknowledgements

The authors wish to thank JICA (Japan International Cooperation Agency) for the financial support for this research project.

Reference

[1] B. K. Tiwari et al. (2009), Effect of sonication on retention of anthocyanins in blackberry juice, Journal of Food Engineering, Vol. 93, No.2, pp.166-171.
[2] Dang Bui Khue et al (2010), Simultaneous treatment of Acerola by ultrasound and pectinex concentration and pectolytic time by response surface methodology, International conference of food research (ICFR) 2010, Malaysia, Nov. 22-24.
[3] Demir N et al. (2001), The use of commercial pectinase in fruit juice industry- Part 3: Immobilized pectinase for mash treatment, Journal of Food Engineering, Vol.47, No.4, pp. 275-280.
[4] Le Ngoc Lieu, Van Viet Man Le (2010), Application of ultrasound in grape mash treatment in juice processing, Ultrasonics Sonochemistry, Vol.17, No.1, pp.273–279.
[5] Le Thi Thuy et al. (2011), Consecutive treatment of guava (*psidium guajava*) mash with ultrasound and pectinase preparation in juice processing: Optimization of pectolytic treatment by response surface methodology, Journal of science and technology, Vol.49, No.5A, pp.261-267.
[6] M. K. Bhat (2000), Research review paper: Cellulase and related enzyme in biotechnology, Biotechnology Advances, Vol. 18, No. 5, pp. 355-383.
[7] Novozymes A/S - Krogshoejvej 36 - 2880 Bagsvaerd - Denmark, Valid from 2010-02-25. Product Data Sheet of Viscozyme L and information Sheet of Viscozyme pH and temperature curves.
[8] Roberta Re et al. (1999), Antioxidant activity applying an improved ABTS radical cation decolorization assay, Free Radical Biology & Medicine, Vol.26, No. 9/10, pp. 1231-1237.
[9] Tran Bich Lam, 2006, Food analysis practicing, National University HCM city, Vietnam, pp. 47 – 67.
[10] T.J. Mason et al. (1996), The uses of ultrasound in food technology, Ultrasonics Sonochemistry, Vol.3, No.3, pp. S253-S260.
[11] Vuong T. M. T. et al. (2011), Application of hemicellulase preparation to Acerola *(Malpighia emarginata DC.)* mash treatment in juice processing Journal of science and technology, Vol.49, No.5A, pp.283-289.
[12] Ya-Qin Ma et al. (2009), Simultaneous extraction of phenolic compounds of citrus peel extracts: Effect of ultrasound, Ultrasonics Sonochemistry, Vol.16, No.1, pp. 57–62.
[13] Zhang Lianfu, Liu Zelong (2008), Optimization and comparison of ultrasound/microwave assisted extraction (UMAE) and ultrasonic assisted extraction (UAE) of lycopene from tomatoes, Ultrasonics Sonochemistry, Vol.15, No.5, pp.731-737.

2nd International Engineering Symposium - IES 2012
(KU-MU-NITK-HCMCUT Joint Symposium) March 5-7. 2012. Kumamoto University. Japan

Use of Koji in production of fish sauce from the waste of fishery processing plant

Do Minh Hien [1], Huynh T. Truc Hang [1], Huynh T. Viet [1], Phan N. Hoa [1], Nguyen T. Thu Ha [1], Nguyen T. Hang [2], Shindo Jo [3] and **Nguyen Hoang Dzung [1]**

1 *HCMC University of Technology, Vietnam*
2 *University of Food Industry, Vietnam*
3 *Kagoshima University, Japan*

Abstract: Fish sauce is an important ingredient in Vietnamese cuisine and is widely consumed in other Asiatic countries. Traditionally, fish sauce fermentation process may take up to a year to complete. The aim of this study was to investigate on the possibility of using koji to accelerate the fermentation process in producing fish sauce from the waste of fishery processing plants. In order to reduce the off-flavor, a fat removing step has been applied. Parameters such as pH, amino-type nitrogen, total soluble solids, were monitored regularly during the fermentation process. Amino acid composition was analyzed at the end of the fermentation process. The accelerated process was able to produce fish sauce comparable to comercial fish sauce regarding to flavour and nutrition qualities. This procedure took only 12 days to complete.

***Keywords**: koji, fish sauce, waste of fishery processing plants*

Introduction

Fish sauce is an important ingredient in Vietnamese cuisine and is widely consumed in Southeast Asia. Traditionally, fish sauce is a condiment derived from fermented fish. It can be served during the cooking process, and also be used as a dipping condiment.

With the huge network of fishery processing plants which, each day, produce a lot of wastes, the south of Vietnam actually confronts with the environmental issues. In order to resolve this problem, new technologies can be applied to transform wastes of processing plants into added value products such as collagen and fish sauce (Lopetcharat et al., 2001; Morimura et al., 2002).

In Japan, fish sauce has been driven out by soy sauce with a moderate taste and smell. Few of fish sauces may be found in Japan as characteristic products of specific region. Recently, these products have been rediscovered, because of renewed consumer interest in authentic taste and traditional foods. Fish sauce has been applied in a variety of processed products in Japan and the amount of imported fish sauce has been increasing year after year. Thus, a lot of Japanese food companies are interested in production or import of fish sauce.

Some encouraging results have been achieved during previous studies in frame of the first phase of JICA project. Thank to the collaboration with Kagoshima University, especially with Prof. Shindo Jo, we can produce the fish sauce from the residue (head, backbone) of basa and/or tra fish.

However, further studies focused on increasing the protein content, reducing the fish smell, improving the fish sauce flavor and removing fat from the final product should be carried out in order to optimize the technology and produce fish sauce on a small scale.

Materials and Methods

Materials

Koji

Koji was used to accelerate the fermentation process. Koji was prepared from soybean, wheat flour and *Aspergillus*

oryzae culture. Dried soybean was purchased from local supermarket, No. 8 wheat flour was obtained from Dai Phong Wheat Co. Ltd. *Aspergillus oryzae* culture was gracefully given by Kagoshima University, Japan.

Preparation procedure for Koji is shown in Fig.1. Dried soybean was soaked in water for 8 h (the weight ratio of soybean to water was fixed at 1/2) and steamed for 75 min at 105 – 110 ^{o}C. At the same time, the wheat flour was roasted at 150 ^{o}C for 30 min. After cooling the ingredients to ambient temperature, the cooked bean and roasted flour were mixed at ratio of 1/1 (w/w).

Aspergillus oryzae culture was added to the mixture in a ratio of 1/5,000 (w/w) and incubated in a temperature chamber (Memmert). The incubation temperature and time was adjusted according to three stages: at 35 ^{o}C for 12 h, 28 ^{o}C for 6 h and 26 ^{o}C for 60 h (Hariono et al., 2005).

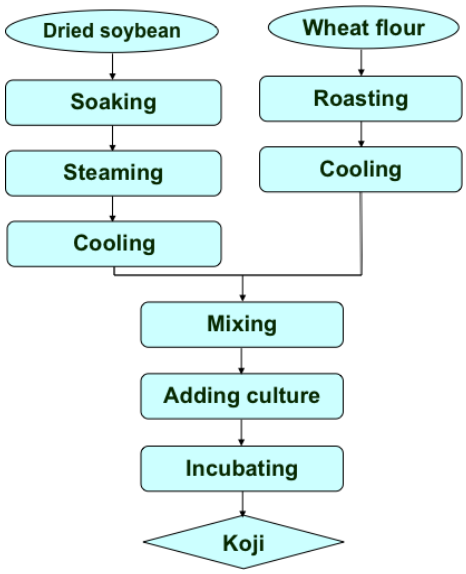


Fig.1 Preparation procedure for Koji

Fish waste

Present fish waste used to produce fish sauce on a Lab scale was collected from AGIFISH Co. (An Giang Province, Vietnam). The fish waste was the residue of basa fish after filleting. All of the leftover parts (head, backbone, tail, internal organs...) have been used in this study.

The fish waste was cut into small piece (1÷2 cm in max size), washed with cold water before material storage in a freezer. The material was sampled for analysis of total protein, moisture, crude fat and ash. Carbohydrate content was estimated by the following formula: carbohydrate content = 100% - (% moisture + % total protein + % crude fat + % ash). The chemical constituents of raw material were protein 12.7 ± 0.8 %, moisture 55.4 ± 1.7, crude fat 13.6 ± 1.4 %, ash 13.3 ± 0.9 % and carbohydrate 5.0 ± 1.9 % (w/w). It can be affirmed that the fish waste with 12.7 % (w/w) protein content was a potential raw material for fish sauce production.

Salt

Salt for producing the fish sauce was purchased from local supermarket. It contained 99.6% NaCl.

Methods

Fat removing process

This step was necessary to remove the high lipid component (13.6 %) to reduce off-flavour in the final product. The raw material was unfreezed at ambient temperature. The raw material was then washed with cold water (in triplicate) and heat treated to remove fat. Method of heat treatment were varied: steaming at 105 – 110 ^{o}C for 20 min, boiling at 100 ^{o}C for 20 min with the ratio of 2/3 (w/w, material to water) and water soaking at 80 ^{o}C for 20 min with the same ratio of material to water. After heat treatment, the material was drained to remove excess water and cooled to 30 ^{o}C for further analysis and fish sauce preparation. The pre-treated samples were analysed of crude fat.

Preparation of fish sauce

Koji and salt were added to the pre-treated material. Ratio of salt and koji to material were varied in 2 experiments. In the first experiment, the ratio of salt to material was varied: 1/20, 2/20, 3/20, 4/20 and 5/20 (w/w) while the ratio of koji to material was fixed at 1/5 (w/w). In the second experiment, the ratio of koji to material was varied: 2/20, 3/20, 4/20, 5/20 and 6/20 (w/w) while the ratio of salt to material was selected from the result of the first experiment.

The fish sauce fermentation was carried out at 37 °C for 16 days. During the fermentation, the mixture was stirred daily to increase process yield and sampled for analysis of pH, amino-type nitrogen and total soluble solids contents every 2 days.
At the end of the fermentation, the whole fermented mixture was filtered with cheesecloth. Liquid obtained from the filtration was heated to 80 °C for 15 min and sampled to analyse of amino acid composition.

Analytical methods
Moisture content was determined by drying until a constant weight using an infrared moisture analyser (SCALTEC. Germany). Amino-type nitrogen content was determined by ninhydrin colorimetric method. Total soluble solids was determined by using hand refractometer. Crude fat content was quantified by Soxhlet method (AOAC 960.39). Crude fat was extracted from solid samples for 16 h with petroleum ether in a Soxhlet apparatus. Ash content was determined by heating the sample at 600 °C in an oven (AOAC 930.30). Amino acid composition was determined using high pressure liquid chromatography (HPLC).

Fat removal yield calculation
The fat removal yield was calculated according to the following formula: Fat removal yield (%) = {1 - [weight of fat in the residual material (g)/ weight of fat in the material before fat removal (g)]} x 100.

Statistical analysis
The experiments were performed in triplicate. The data were analysed by using one-way Analysis of Variance with significant level of 5% (α = 0.05). All values are means of triplicate determination ± standard deviation.

Results and discussion

Fat removing process
The fat removal yield of samples pre-treated with 3 methods of heat treatment are shown in Fig.2. Steam or hot water was used. Liquid phase containing fat and other organic matters was cooled to ambient temperature. Fat was separated from liquid phase by sedimentation. The liquid was reused for fish sauce preparation.
In the pre-treatment of fish waste with soaking in hot water, steaming or boiling, 45.4%, 52.8% or 62.8% of fat were removed respectively. It can be concluded that the appropriate method for fat removal was boiling at 100 °C for 20 min.

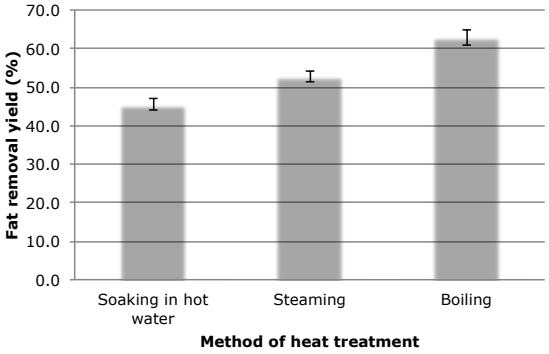


Fig.2 Effect of heat treatment on fat removal yield

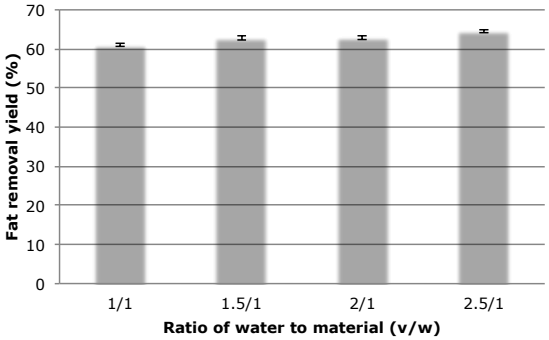


Fig.3 Effect of ratio of water to material on fat removal yield

In order to increase efficiency the removal of fat from fish waste, the ratio of water to material was varied: 1/1, 1.5/1, 2/1, 2.5/1 (v/w). The fat removal yield of samples are shown in Fig.3. Increasing the amount of water augmented the fat removal yield from 61% to 64.6%. However, an insignificant change in fat removal yield was observed when the ratio was increased from 1.5/1 to 2/1 (v/w). With the ratio of 2.5/1. the samples have the highest fat removal efficiency but the final fish sauce can be diluted by a large amount of water. Therefore, the ratio of 1.5/1 (v/w, water to material) was suitable

ratio for removing fat. With this method, the residual fat content was reduced to 5.1%.

Changes in chemical composition during fermentation process

Changes in pH, amino-type nitrogen and total soluble solids during fermentation process is shown in Fig.4. The pH of samples decreased when the fermentation period prolonged from 2 to 16 days.

Microorganisms generally increase during the early fermentation stage and then decrease gradually as fermentation time is extended (Saisithi et al., 1966; Ijong and Ohta, 1996). During fermentation process, *Aspergillus oryzae* mould produces a variety of enzymes which degrade insoluble materials to soluble products (Chae et al., 1989). Protein is broken down to peptides and amino acids. Consequently, the amino-type nitrogen content of samples increased strongly during early periods and then increased slightly relative to protease production of mould. An insignificant change in amino-type nitrogen content was observed when fermentation period was extended. The same change was observed in total soluble solids contents of samples. The total soluble solids increased until a certain extent, then stabilized. The results in Fig.4 show that 12 days was a suitable hydrolytic time for fermentation period.

Effect of ratio of salt to fish waste

Salt inhibits the growth of undesirable microorganisms. However, high salt concentration also inhibits the growth of mould. Amino-type nitrogen content increased when ratio of salt to material was increased from 1/20 to 3/20 (w/w) and decreased when higher salt concentration was used. Amino-type nitrogen content decreased with extending fermentation period because of the growth of undesirable microorganisms in some samples. Therefore, the ratio of 3/20 (w/w, salt to material) was suitable ratio for fish sauce fermentation.

Effect of ratio of koji on fish waste

The amino-type nitrogen content of samples increased when increasing the ratio of koji to material from 2/20 to 4/20 (w/w). An insignificant change in amino-type nitrogen content was observed when the ratio of koji to material increased even more (4/20, 5/20 and 6/20, w/w). Thus, the ratio of 1/5 (w/w, koji to material) was used for further investigation on fish sauce production. Similar results were previously observed by other researcher who used koji preparation to accelerate fish sauce fermentation process (Lopetcharat et al., 2001; Shil et al. 2003; Hariono et al. 2005; Uchida et al., 2005; Xu et al., 2008).

Amino acid composition of fish sauce

Products during fermentation, amino acids and peptides, have a considerable effect on the sensory characteristics of fish sauce. The free amino acid profile in the fish sauce is shown in Table 1.

Similar free amino acid profile was observed by Park et al. (2002) who determined taste-active components for a typical first-grade Vietnamese fish sauce.

The essential amino acid components obtained were composed mainly of isoleucine, lysine, methionine, threonine, valine, leucine, phenyalamine, histidine and moderately of tyrosine and arginine.

The overall flavour of fish sauce mainly depends on the balance of all amino acids. Glutamic acid, threonine, alanine, valine, histidine, proline, tyrosine, cystine and methionine are taste-active components contained in fish sauce (Park et al., 2002). Glutamic acid, responsible for palatable umami taste, was the most abundant in produced fish sauce. It accounted for 35.9% of the total amino acid content of fish sauce. Threonine, alanine and histidine were responsible for fish sauce-like taste (Park et al., 2002).

The total amino acids concentration of the fish sauce prepared in this study are lower in comparison to those of commercial products. This may be due to the fact that the fish waste contained less protein than whole fish.

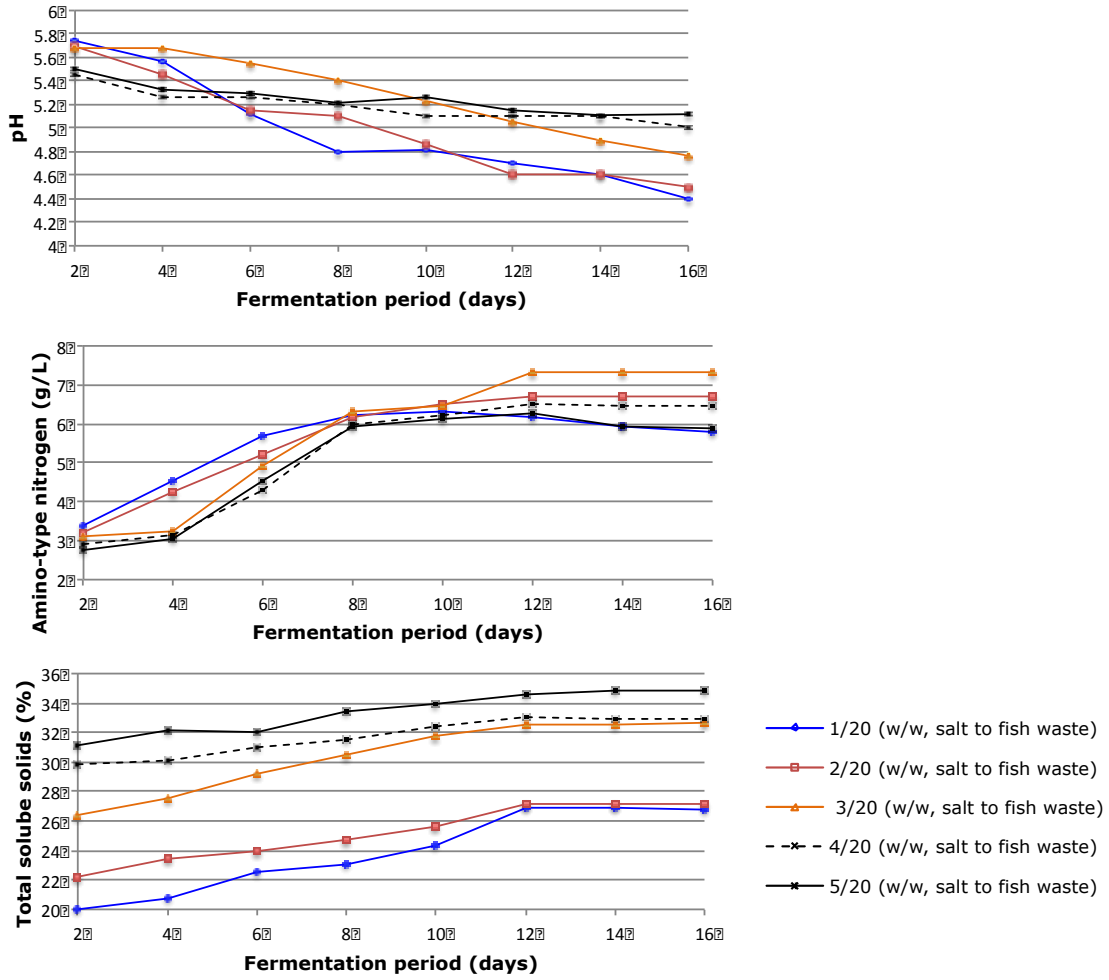


Fig.4 Effect of salt content on pH, amino-type nitrogen and total soluble solids of fish sauce

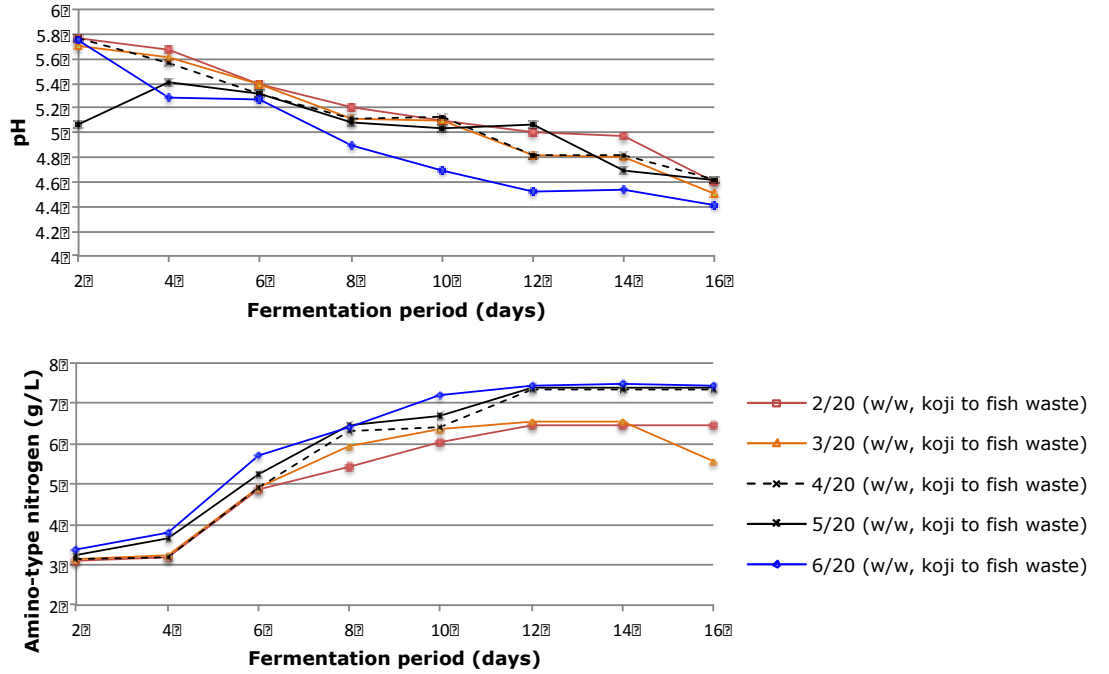


Fig.5 Effect of koji content on pH and amino-type nitrogen of fish sauce

Table 1 Free amino acid composition of fish sauce

Amino acid	Content (mg/Kg)
Leucine	567.6
Isoleucine	9432.7
Lysine	1545.7
Methionine	929.5
PhenylAlanine	512.8
Threonine	917.6
Valine	818.8
Tryptophan	210.8
Arginine	50.9
Histidine	498.2
Glutamic acid	21766.0
Alanine	2140.8
Aspartic acid	5482.5
Glycine	743.9
Proline	487.0
Serine	353.7
Tyrosine	124.6
Cystine	178.5

Conclusions

The following conclusions are deduced from this study:

- For fish sauce preparation, the fat removal process was carried out by boiling at 100 ^{o}C for 20 min. The suitable ratio of water to material was 1.5/1 (v/w). The residual fat content in material was reduced to 5.1%.

- For accelerating fermentation process, koji should be used with ratio of 1/5 (w/w, koji to material) and the suitable ratio of salt to material was 3/20 (w/w). This method took only 12 days to complete the fermentation process as compared to 6 – 12 month fermentation of traditional fish sauce.

- It is possible to produce fish sauce with acceptable qualities in flavour and nutrition from basa and/or tra fish wastes. Fish sauce obtained from mentioned procedure have pH of 5.0, amino-type nitrogen content of $7{,}55 \pm 0{,}58$ % (w/w), brown color and the same amino acid profile to traditional fish sauce.

- Obtained fish sauce had lower amino-type nitrogen content in comparision to traditional products. Thus, ultrafiltration to increase amino-type nitrogen content should be further investigated.

Acknowledgements

This study has been supported by the JICA SUPREM-HCMUT project. for which the authors feel deeply grateful.

References

[1] Chae, S K et al (1989), Effects of soy sauce kiji ad commercial proteolytic enzyme on the acceleration fish sauce production, Korean J. Food. Sci. Technol., Vol. 21, pp. 639–48.
[2] Hariono I et al (2005), Use of koji and protease in fish sauce fermentation, Singapore J Pri Ind, Vol. 32, pp. 19-29.
[3] Ijong GG and Ohta Y (1996), Physicochemical and microbiological changes associated with Bakasang processing - A traditional Indonesian fermented fish sauce, J. Sci. Food. Agric., Vol. 71, pp. 69-74.
[4] Kilinc B (2003), Fish sauce technology, EU J Fish Aquatic Sci., Vol. 20, No. 1, pp. 263–272.
[5] Lopetcharat K et al (2001), Fish sauce products and manufacturing: a review food, Reviews International, Vol. 17, No. 1, pp. 65–88.
[6] Morimura S et al (2002), Development of an effective process for utilization of collagen from livestock and fish waste, Process Biochemistry, Vol. 37, pp. 1403–1412.
[7] Official Methods of Analysis of AOAC International, 17th Edition, Edited by William Horwitz, AOAC International (2000).
[8] Park J et al (2002), Taste-active components in a Vietnamese fish sauce, Fish. Sci., Vol. 68, pp. 913–920.
[9] Saisithi P et al (1966), Microbiology and chemistry of fermented fish, J. Food Sci., Vol. 31, No. 1, pp. 105-110.
[10] Shih I-L et al (2003), Microbial reclamation of fish processing wastes for the production of fish sauce, Enzyme and Microbial Technology, Vol. 33, pp. 154–162.
[11] Uchıda M et al (2005), Effects of soy sauce koji and lactic acid bacteria on the fermentation of fish sauce from freshwater silver carp Hypophthalmichthys molitrix, Fish Sci., Vol. 71, No. 2, pp. 422–430.
[12] Xu W, et al (2008), Biochemical changes associated with fast fermentation of squid processing by-products for low salt fish sauce, Food Chemistry, Vol. 107, pp. 1597–1604.

Comparative studies on the total anti-oxidant activity of certain plant species unique to Western Ghats of India

Farhana K[1], Pavithra G S[2], Raj Mohan B[3]

1. *Department of Chemical Engineering, National Institute of Technology Karnataka, surathkal, Mangalore 575025, India. Email : farna2312@gmail.com*
2. *Department of Chemical Engineering, National Institute of Technology Karnataka, Surathkal, Mangalore 575025, India. Email: pavithra.gs@gmail.com*
3. *Department of Chemical Engineering, National Institute of Technology Karnataka, surathkal, Mangalore 575025, India. Email : rajmohanbala@gmail.com*

Abstract

The Western Ghats of India are amongst the world's biodiversity hotspots and are richly credited with varied kind of vegetation of high medicinal value. In this paper, three plant species (*Bridelia scandens, Leea indica* and *Wattakaka volubilis*) that are commonly found in the forest belts of Western Ghats (Karnataka, India) are chosen to study their antioxidant activity. The antioxidants interrupt radical-chain oxidation processes and form low activity radicals, which are easily removed from the organism. This improves general health, helps cell rejuvenation and prevents cancer. Although synthetic antioxidants are efficient in preventing oxidation, only a few of them are currently approved for use because of their potential toxicity and carcinogenicity. The plant extracts are prepared using methanol as solvent by microwave-assisted extraction (MAE) process. The parameters, time and solvent concentration, for extraction optimized by central composite rotate design (CCRD) software ranged between 4-5 minutes and 55-60% respectively. The total antioxidant activity was measured by FRAP method and total phenolic content was measured by F-C assay. The antioxidants Rutin, Quercetin and Coumaric acid were found to be present as indicated by high performance liquid chromatography (HPLC).

Key words: Antioxidants, Biodiversity, Flavanoids, Free radicals, Microwave extraction (MAE), Phenolics, Plant extracts, Western Ghats.

Introduction

Western Ghats and its importance

The Western Ghats is considered as one of the global biodiversity hot-spots. It is endowed with some of the magnificent forests in the country. The Western Ghats comprises of over 5000 vascular plants, of which about 30% are endemic to the Ghats. The heterogeneous condition which is affluent all along the ranges and regions of the Western Ghats makes it an ideal ground for the luxurious growth of plants with therapeutic value (medicinal plants of Western Ghats, Suja.A IISc). World Health Organization recognizes that medicinal plants play an important role in the health care of about 80 percent of World population in developing countries and depend largely on traditional medicines (Farnsworth et al. 1988). The rest of the 20 percent also depend substantially on the plant-based medicines. Plants have evolved the ability to synthesize chemical compounds that help them defend against attack from a wide variety of predators such as insects, fungi and herbivorous mammals. By chance, some of these compounds, whilst

being toxic to plant predators, turn out to have beneficial effects when used to treat human diseases. Such secondary metabolites are highly varied in structure; many are aromatic substances, most of which are phenols or their oxygen-substituted derivatives.

Plant Species

Bridelia scandens (BS) belongs to the family Euphorbiaceae. It is distributed in the warm regions of India and Southeast Asia. This plant is used for its antimicrobial and antioxidant activity (Kotigadde et al, 2005 and Senthil Kumar et al, 2010). Its bark is traditionally used by the locals for the treatment of asthma, intestinal worms and cough. *Leea indica* (LI) belongs to Leeaceae family. It is a shrub which is found in Western Ghats of India and in tropical and subtropical countries. It is claimed to have some medicinal values such as anticancer, antidiabetic, antidiarrhoeal, antidysenteric, and antispasmodic based on local uses (Burkill, 1966; Omar et al, 1984; Chatterjee et al, 1994 and Prajapat et al, 2003). *Wattacaka volubilis* (WV) belongs to the family of Asclepiadaceae. It is a large climber with green flowers. It is found in India and Southeast Asia. Its root extract is used by the locals on snake bites and leaves are applied on boils and abscesses to promote suppuration (Latha et al, 2009).

Microwave Assisted Extraction (MAE)

Microwave Assisted Extraction utilizes the energy of microwaves leading to faster movement of molecules resulting in rapid heating of the sample and solvent (Eskilsson et al. 2000 and Buldin et al. 2000). It has been demonstrated that MAE can be an effective alternative to conventional extraction of bio-active phytochemicals (Zhang et al. 2009, Yang et al.2005, Zhang et al. 2004, Jaitak et al. 2009 and Deng et al. 2009). Compared with Soxhlet extraction and ultra-sound extraction, MAE is a rapid method with higher yield and less solvent consumption (Wang et al, 2011).

With the help of above information we undertook the comparative studies on the total antioxidant activity in leaf extracts of the above described plants. The microwave extraction process was employed to extract the compounds into methanol solvent.

Materials and Methods

Sample preparation

Fresh leaves of all the three plant species *(Bridelia scandens, Leea indica* and *Wattakaka volubilis*) were procured from the forest of Western Ghats (Moodubidre, Udupi district of Karnataka), which were thoroughly washed and shade dried for four days. The dried leaves were ground to fine powder before extraction.

Reagents

Methanol (HPLC grade), 300 mM acetate buffer (3.1 g CH_3COONa and 16 ml CH_3OOH) of pH 3.6, 10 mM TPTZ (2, 4, 6-tripyridyl-s-triazine) solution in 40 mM HCl, 20 mM $FeCl_3 \cdot 6H_2O$ solution, ascorbic acid (Sigma-Aldrich), acetonitrile (HPLC grade), Trichloro acetic acid (HPLC grade), Gallic acid, Sodium carbonate, Folin ciocateau solution, Rutin (Sigma Aldrich), Quercitin (Sigma Aldrich) and p-Coumaric acid (Sigma Aldrich).

Extraction of antioxidants

QAsh 1800 Microwave ashing system from Questron Technologies Corp., Canada was used for extraction. The ground sample was mixed with methanol of HPLC grade of various concentrations in the ratio 1:10 (w/v). The extraction proceeded according to the preset programs of the microwave oven. The extracted solution was filtered using 0.45 microns filter prior to further analysis.

Total anti-oxidant activity assay

Total antioxidant activity is measured by ferric reducing antioxidant power (FRAP) assay (Benzie and Strain, 1999). The standard curve was obtained using ascorbic acid (between 200 and 1200 µM). The fresh working solution was prepared by mixing acetate buffer, TPTZ solution and ferric chloride solution in the ratio 10:1:1 respectively. Plant extracts (100 µL) were mixed with 3 ml of the FRAP solution and incubated for six minutes. Absorbance of ferrous tripyridyltriazine complex was taken at 593 nm using spectrophotometer (Hitachi U-2000, Double beam spectrophotometer, Tokyo, Japan) after 6 minutes of incubation. The FRAP was calculated using standard curve and the results were expressed in µM Ascorbic acid/g dry mass.

Total Phenolic content assay

0.5 ml of extract was mixed with F-C reagent (diluted in water 1:10 v/v) and incubated for 5 minutes at room temperature. 4 ml of Na_2CO_3 (75 g/l) was added and re-incubated for 30 minutes. The absorbance of the colored product after the incubation period was measured at 765nm. The calibration curve was obtained using Gallic acid as standard (0-250 mg/l).

HPLC Analysis

Reverse phase HPLC (Dionex, NJ, USA) was carried out to determine the presence of Rutin, Quercitin and Rosmarinic acid. C18 silica gel column was used as stationary phase. Mobile phase comprised of acetonitrile and trichloro acetic acid in water (75:25). 20µl of sample was injected and run for 15 minutes at a wavelength of 254 nm with the flow rate of 1.5 ml/minute of mobile phase.

Results and Discussion

Optimization of MAE conditions

The contour and surface plots obtained using Response Surface Methodology is as shown in Figure 1, 2 and 3. The optimum values for MAE parameters such as extraction time and solvent concentration are tabulated in Table 1. The coefficients of the variables and confidence level P (95%), as in Table 2 show that both variables significantly influence the extraction process.

Total Phenolic content

It has been demonstrated that phenolic compounds are the major source of antioxidants in plants (Stephen C Grace, 2005). Using the optimized MAE conditions, the phenolic content in BS, LI and WV was found to be 764.265, 1150.5739 and 245.358 mg gallic acid/g of dry mass of plant tissue. Comparing the three species, the antioxidant activity in terms of phenolics is found to be the highest in LI.

HPLC analysis

The presence of Rutin, Quercetin and Coumaric acid was confirmed by HPLC analysis using the pure standards. Rutin (RT: 0.941) with an area of 38.818 was found in BS with relative abundance of 99.26%. In LI, quercetin and coumaric acid (RT: 1.050) were present with the peak area of 1.258 and relative abundance of 5.19%, however the highest peak at retention time of 0.861 could not be determined due to the non-availability of the standard compound. WV showed the presence of Rutin (RT: 0.960) and quercetin (RT: 1.064) with relative abundance of 83.03% and 8.91% respectively. The chromatograms are as shown in Figure 4 (a), (b) and (c).

Conclusion

Comparative studies were done on three plants species, viz BS, LI and WV, unique to Western Ghats, for their antioxidant activity. The extracts obtained from MAE were analyzed for their antioxidant activity by FRAP method. The optimal

value for extraction time and solvent concentration in MAE ranged between 4-5 minutes and 55-60% respectively using CCRD. Under these conditions both antioxidant activity and total phenolic content was found to be the highest in LI when compared to BS and WV. HPLC at 254 nm has indicated that Rutin, Quercetin and Coumaric acid are the major antioxidants present in all the three plants. Besides the known peaks, one unknown peak at retention time of 0.861 minutes at a higher relative abundance in LI indicated the presence of a compound which may be contributing to antioxidant activity. With the help of advanced techniques, many more potential compounds could be found out. Further these antioxidants can find their application in pharmaceuticals and neutraceuticals after suitable purification.

Acknowledgments

We deeply thank Dr.Subramanyam of Alva's Ayurvedic College for helping us procuring the plants and Dr. S.Anandhan Metallurgical and Materials engineering Dept. NITK for his technical assistance. We also thank Mr. Harish Poojary for assisting in carrying out HPLC analysis. Finally we thank all the PG students and Research Scholars, Chemical engineering dept. NITK for their support throughout the project.

References

[1] A. Chatterjee and S. C. Prakashi, *The Treatise on Indian Medicinal Plants*, vol. 3, NISCAIR, New Delhi, India, 1994.
[2] A. G. Lattif, I. M. Omar, I. M. Said, and A. Kadri, "A multivariate approach to the study of medicinal plants inMalaysia," *Journal of the Singapore National Academy of Science*, vol. 13, pp. 101–105, 1984.
[3] Buldini PL, Ricci L, Sharma JL (2000) JChromatogrA975:47–70
[4]Deng JC, Xiao XH, Li GK, Ruan GH. Application of microwave- assisted extraction
[5] D. Senthil Kumar, A. Kottai Muthu, D. Satheesh Kumar and R. Manavalan., Scholars Research Library.,Der Pharma Chemica, 2010, 2(2): 195-201
[6] Eskilsson CS, Bjorklund E (2000) J Chromatogr A 902:227–250
[7] H. Burkill, *A Dictionary of the Economic Products of the Malay Peninsula*, Crown Agents, London, UK, 1966.
[8] Jaitak V, Bandna SB, Kaul VK. An efficient microwave-assisted extraction process of stevioside and rebaudioside-A from Stevia rebaudiana (Bertoni). Phytochem Anal, 2009, 20: 240–245
[9] Latha et al. Natural product radiance., vol 8(2) 2009 pp 137-141
[10] Li H, Chen B, Zhang ZH, Yao SZ. Focused microwave-assisted solvent extraction and HPLC determination of effective constituents in Eucommia ulmoides Oliv. (E. ulmodies). Talanta, 2004, 63: 659–665
[11] N. D. Prajapati, S. S. Purohit, A. K. Sharma, and T. Kumar, *A Handbook of Medicinal Plants—A Complete Source Book*, Agrobios, Jodhpur, India, 2003.
[12] S. Kotigadde, S. Jose, A. Zachariah, P. Premanathan and KG. Bhat. J Commun Dis., 2005, 37(2), 135-7.
[13] Stephen C Grace, Phenolics as Antioxidants, Blackwell Publishing Ltd. 2005, 141-159
[14] WANG GuiHua, SU Ping, ZHANG Fan, HOU XiangYan, YANG Yi & GUO ZhenKu. Comparison of microwave-assisted extraction of aloe-emodin in aloe with Soxhlet extraction and ultrasound-assisted extraction, Science China,Chemistry, 2011: 231-236
[15] Yang Y, Hou XY, Guo ZK. Microwave-assisted extraction of aloin from fresh aloe leaves. Chem J Chinese U, 2005, 25: 1627–1630
[16] Zhang F, Yang Y, Su P, Guo ZK. Microwave-assisted extraction of rutin and quercetin from the stalks of Euonymus alatus (Thunb.) Sieb. Phytochem Anal, 2009, 20: 33–37

Tables and Figures

Figure 1 (a): Contour and surface plot of BS

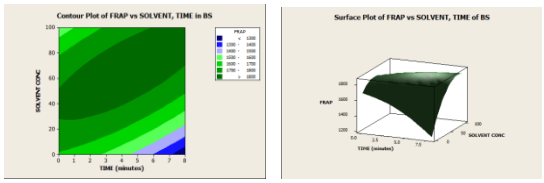


Figure 1 (b): Contour and surface plot of LI

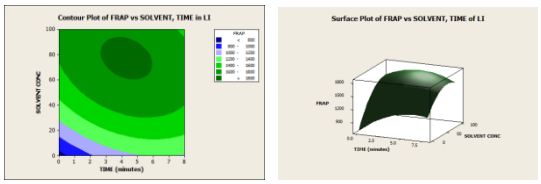


Figure 1 (c): Contour and surface plot of WV

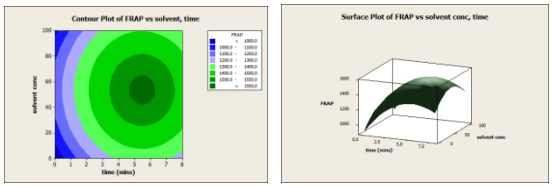


Table 1: Optimized values of parameters by CCRD

Plant species	**Extraction time**	**Solvent Concentration**
BS	4.1264	60.2726
LI	4.0292	60.8906
WV	4.8072	53.5629

Table 2 (a): Coefficients and confidence level of BS

***Bridelia scandens* (BS)** R-sq=92.4%		
Term	**Coefficient**	**P**
Constant	1833	0.000
Time	-46.43	0.049
Solvent	109.76	0.001
Time*Time	-77.28	0.029
Solvent*Solvent	-193.71	0.000
Time*Solvent	187.14	0.028

Table 2 (b): Coefficents and confidence level of LI

***Leea Indica* (LI)** R-Sq = 91.5%		
Term	**Coefficient**	**P**
Constant	1739.61	0.000
Time	98.81	0.067
Solvent	316.90	0.000
Time*Time	-189.92	0.024
Solvent*Solvent	-283.13	0.004
Time*Solvent	-130.00	0.437

Table 2 (c): Coefficients and confidence level of WV

***Wattacaka volubilis* (WV)** R-sq 86.5%		
Term	Coefficient	P
Constant	1527.96	0.000
Time	167.6237	0.003
Solvent	26.90	0.492
Time*Time	-229.44	0.004
Solvent*Solvent	-189.08	0.010
Time*Solvent	-1.43	0.991

Figure 4(a): Chromatogram of BS

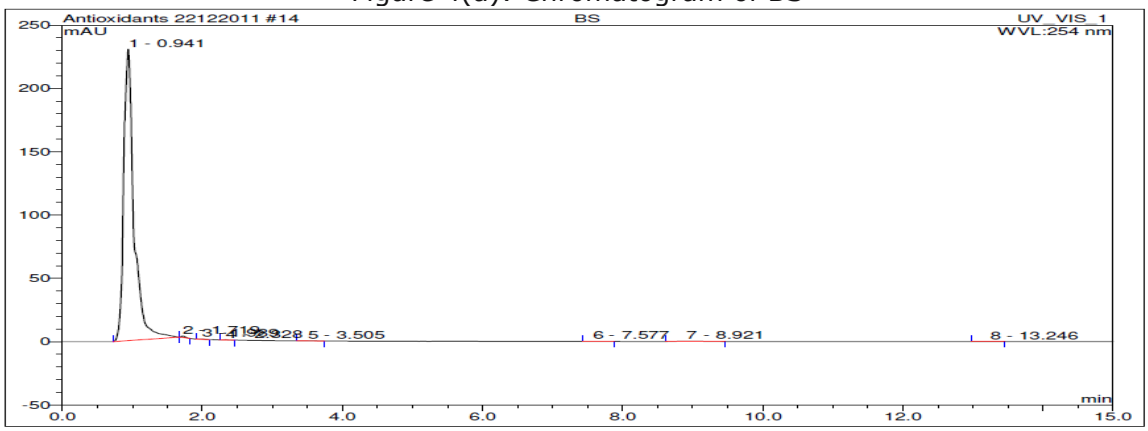


Figure 4(b): Chromatogram of LI

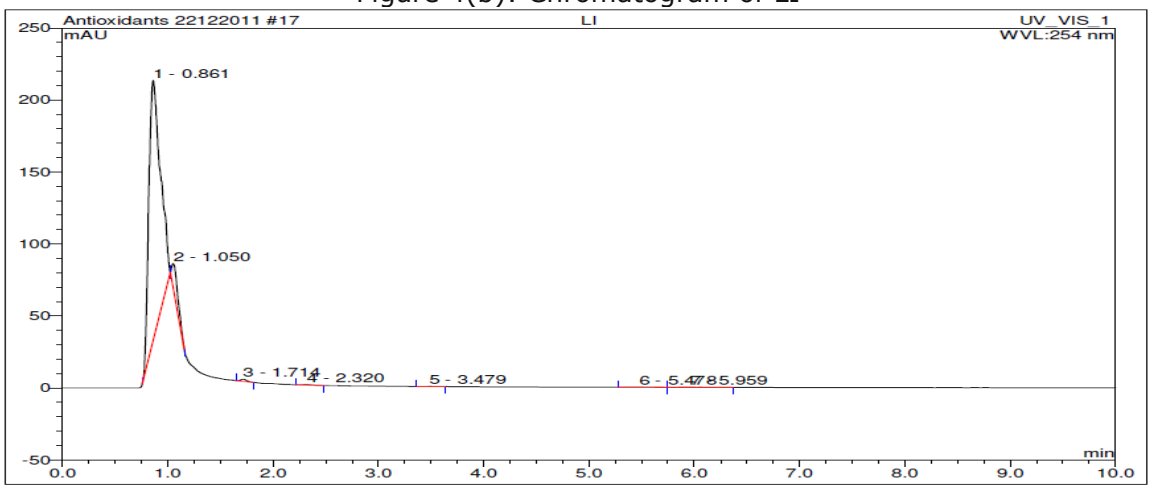
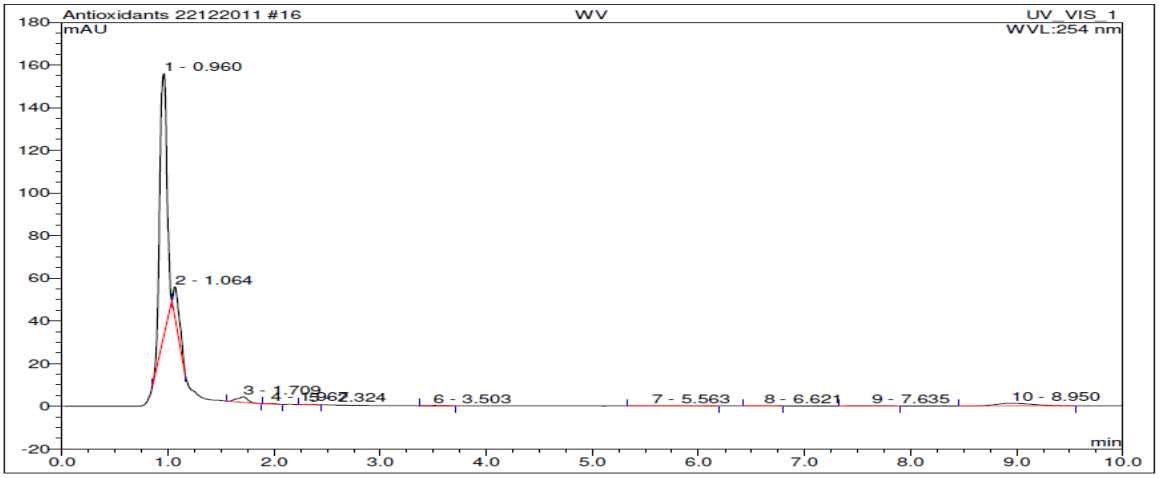


Figure 4(c): Chromatogram of WV



2nd International Engineering Symposium - IES 2012
(KU-MU-NITK-HCMCUT Joint Symposium) March 5-7, 2012, Kumamoto University, Japan

Removing of Nitrogen from Landfill Leachate by Single-Stage Using Anammox and Partial Nitritation (SNAP) with Acrylic Pile Fabrics as Biomass Carrier

Pham Van Sung [1*] and Nguyen Tan Phong [1]

[1]Faculty of Environment, Ho Chi Minh City University of Technology, 268 Ly Thuong Kiet, District 10, Ho Chi Minh city, Vietnam. Email: pvsung0509@gmail.com*
[1] Faculty of Environment, Ho Chi Minh City University of Technology, 268 Ly Thuong Kiet, District 10, Ho Chi Minh city, Vietnam. Email: tanphong69@yahoo.com

Abstract: Single-stage nitrogen removal using anammox and partial nitritation (SNAP) process is the novel technology for nitrogen removal in wastewater which has high nitrogen and low organics concentration in recent years. The research has been studied and presented in this paper. One reactor with volume 3.7 liters and Acrylic Pile Fabrics as attached biomass carrier was used. The synthetic influent, simulating mature landfill leachate, contained ammonium concentrations from 50 to 200 mg-N/l. Operation parameters such as HRT, DO, pH were 10h, 0.5-2.5 mg/l and 7.5-8.0, respectively. The temperature element was not controlled and was affected by ambient temperature condition, which was ranging 27-35.5^{o}C. With the nitrogen, loading rate was 0.2 kg-N/m^3/day, the ammonium conversion was 90% and total nitrogen removal efficiency achieved 78%.

Keywords: *SNAP, anammox, partial nitritation, acylic pile fabrics, landfill leachate*

Introduction

In 1995, the first experimental determination of anaerobic ammonia oxidation was described by researches of the Deft University of Technology, Mulder et al. (1995). The disappearance of ammonium was observed in a denitrifying fluidized bed reactor located at Gist – brocades (Deft, the Netherlands). Both nitrite and ammonium consumption increased with concomitant gas production. The authors concluded that a biological process in with ammonium is anaerobically oxidized to denitrogen gas with nitrite serving as the electron acceptor had occurred, and gave this process the name 'anammox'. The anammox process showed in Fig.1.

In the anammox process, ammonia and nitrite together converted into nitrogen gas by single autotrophic bacterium, but via a completely different metabolic pathway from conventional nitrification/denitrification.

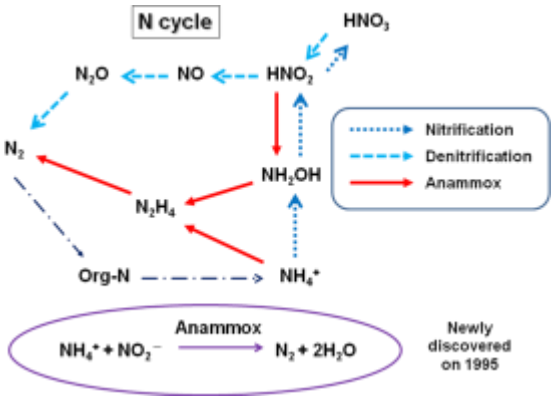


Fig.1 Nitrogen cycle and the anammox process

The anammox process enables autotrophic biological nitrogen removal that does not require organic substances, suggesting that it might be applicable to nitrogen removal from wastewater that contains high levels of nitrogen as ammonia but little organic matter, instance as the secondary-treated landfill leachate. Because the nitritation and anammox reactions are autotrophic and do not require organic matter, no addition of organic substances is required. However, if the organic content of wastewater is high, pretreatment may be required. The reaction equation of anammox process is expressed in Eq.1.

$$1.0NH_4^+ + 1.32NO_2^- + 0.066HCO_3^- + 0.13H^+ \rightarrow 1.02N_2 + 0.26NO_3^- + 0.066Biomass + 2.03H_2O \quad (1)$$

In the partial nitritation process, about half of the ammonia converted to nitrite, which results in reduced oxygen demand. The theoretical oxygen demand under optimum nitritation conditions is 43% of that need for complete nitrification. Since ammonia-oxidizing bacteria and anammox bacteria have low yield, there is little sludge production.

Partial nitritation (PN) of ammonium (NH_4) to nitrite (NO_2) needed to achieve a suitable influent for the anammox process. According to the anammox stoichiometry, 1.32 grams NO_2-N consumed per gram NH_4-N removed, Strous et al. (1998). Thus, optimal performance of PN for its coupling with the anammox process requires 57% oxidation of NH_4 to NO_2. This PN conversion is done by ammonia-oxidizing bacteria (AOB) are represented in Eq.2.

$$NH_4^+ + 1.5O_2 \rightarrow NO_2^- + H_2O + 2H^+ \quad (2)$$

The combination of the two conversion steps (Eq.5): partial nitritation (Eq.3) and anammox (Eq.4) can carried out in separate tanks or in a single tank.

$$2NH_4^+ + 1.5O_2 \rightarrow NH_4^+ + NO_2^- + H_2O + 2H^+ \quad (3)$$

$$1NH_4^+ + 1.32NO_2^- \rightarrow 1.02N_2 + 0.26NO_3^- + 2H_2O \quad (4)$$

$$1NH_4^+ + 0.85O_2 \rightarrow 0.44N_2 + 0.11NO_3^- + 1.43H_2O + 1.14H^+ \quad (5)$$

Typical systems with separate tanks include SHARON (Single reactor system for High Ammonium Removal Over Nitrite) – Anammox, Dongen et al. (2001), and PN – Anammox. Single-stage nitrogen removal processes such as OLAND, Kuai et al. (1998) and Pynaert et al. (2003), and CANON (Completely Autotrophic Nitrogen removal Over Nitrite), Sliekers et al. (2002) and (2003), in which anammox and PN occur in a single tank, were developed recently to reduce the footprint of reaction tanks and the operational costs for separate processes. In Kumamoto University, during long-term experiments on a separate PN process using an attach-immobilized reactor packed with net type acrylic resin fiber carrier, an unexpected nitrogen removal effect was observed. This new ammonium removal process was named SNAP (Single-stage Nitrogen removal using Anammox and Partial nitritation, Lieu et al. (2005) and (2006). SNAP-PN and anammox reactions occurred simultaneously in one reactor-Wholly autotrophic nitrogen removal with the advantages: removal of ammonium in absence of organic carbon, saves 100% organic carbon source and more than 50% oxygen.

In comparison to the conventional nitrification/denitrification method, partial nitritation/anammox mode to eliminate the ammonia from wastewater reduces 85% of the oxygen requirement, 100% of the carbon requirement, and 83% of the biosolids production, Daigger et al. (2011). This leads to a significant decrease in operational costs. In addition, by-products do not include greenhouse gases. Therefore, anammox is a key technology for development of more economical and energy efficient ammonia treatment systems in the future. So that, this study was tried to carried out the SNAP process and evaluated its performance with the synthetic influent imitating old landfill leachate with using Acrylic Pile Fabrics as biomass carriers.

Materials and methods

Experimental set-up and operational strategy

Figure 2 describes the schematic diagram of SNAP reactor system.

The SNAP reactor had a liquid volume of 3.7 liters which had an inner diameter of 10.5 cm and useful height of 43 cm. The

$NaHCO_3$ solution used to control the pH in the reactor and air was immersed from the bottom of the reactor.

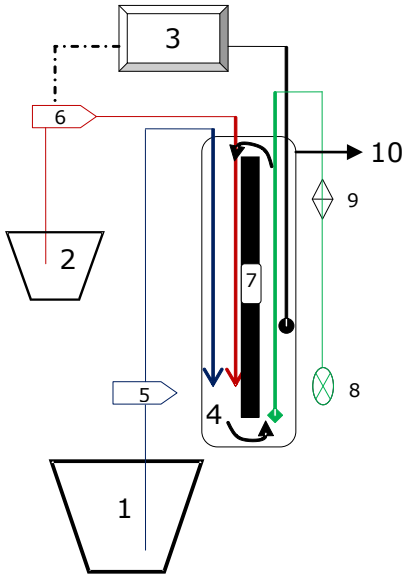


Fig.2 Schematic diagram of SNAP reactor
1.Influent tank, 2.$NaHCO_3$ solution, 3.pH controller, 4.Reactor, 5.Influent pump, 6.$NaHCO_3$ pump, 7.Biomass carriers, 8.Air pump, 9.Air-controlling valve, 10.Effluent

The pH, hydraulic retention time (HRT) and dissolved oxygen (DO) were controlled to achieving nitritation and SNAP process.

pH = 7.5 – 8.0
HRT = 10 – 12h
DO = 0.5 – 2 mg/l

The temperature element was not controlled and was affected by ambient temperature conditions which were ranging 27-35.5°C

Operating of SNAP process divided to two stages:

Stage I start-up: Seed sludge was introduced in the reactor. Influent containing low nitrogen concentration was fed to the reactor. Nitrogen gas was applied for circulation until all of sludge was attached on the biomass carriers. Then, nitrogen gas was stopped when activated sludge was introduced and air was used for circulation.

Stage II: Increase nitrogen concentration in influent wastewater to achieved nitritation and SNAP process.

Influent wastewater and seed sludge

Influent was synthetic wastewater simulating old landfill leachate that had high nitrogen concentration (from 50 mg/l to 200 mg/l) and added the trace inorganic components such as K^+, Na^+, Ca^{2+}, Mg^{2+}, Fe^{2+}.

Table 1 Composition of synthetic wastewater

Composition	Unit	Concentration
NH_4Cl	(mg-N/l)	50 – 200
$NaHCO_3$	(mg/l)	160
$KHCO_3$	(mg/l)	160
KH_2PO_4	(mg/l)	43
$MgSO_4.7H_2O$	(mg/l)	328
$CaCl_2.2H_2O$	(mg/l)	235
$FeSO_4.7H_2O$	(mg/l)	16
Na_2.EDTA	(mg/l)	16
$C_8H_5O_4K$	(mg/l)	38
Na_2SO_3*	(mg/l)	160

* Used to control the DO in influent of synthetic wastewater.

Two kinds of sludge were the activated sludge and the anammox sludge that seeded in this reactor with ratio as 4:6 (MLSS). Total of seed sludge was 1.5 g/l (MLSS).

The anammox sludge and activated sludge got from Kumamoto University-Japan and Tan Binh wastewater treatment plant, Ho Chi Minh, Viet Nam, respectively.

Biomass carriers

The newly biomass carrier was a product of Japan that was used setting up in this reactor as Acrylic Pile fabrics. Biomass carriers had two the same layers. Every layer was inserted with a length and a wide of 37 and 10 cm, respectively. Acrylic Pile Fabrics were used had 21.08g of total weight.



Fig.3 Photo of Acrylic Pile fabric as biomass carrier

The biomass carriers were fixed on steel bracket and were packed in the SNAP reactor and that show in Fig.4.



Fig.4 Photo of bracket biomass carriers

Analytical methods

Using Standard Methods for the Examination of Water and Wastewater (USA) to analyses NH_4-N, NO_2-N and NO_3-N:

NH_4-N: 4500-NH_3-B Preliminary Distillation Step

NO_2-N: 4500-NO_2^--B Colorimetric Method

NO_3-N: 4500-NO_3^--B Cadmium Reduction Method

Total nitrogen was defined by TCVN 6638:2000 (National Technical Regulation Viet Nam), Catalytic digestion-devarda alloy.

pH was controlled by pH controller BL 931700, Hanna-England and the Oxi 3210 Set-DurOx 325-3, England to measured DO in the reactor.

Results and discussions

Results of introduced seed sludge (start-up)

First, the anammox sludge was inserted into the reactor. After 24h circulating with the nitrogen gas, all of anammox sludge attached on the biomass carrier with the reactor. Then, the activated sludge was implanted, used the air for circulating, after 3 days, 95% activated sludge attached on biomass carriers with the SNAP reactor.



Fig.5 Photo of biomass carrier after the anammox sludge was inserted into the reactor

Ammonium conversion efficiency

The efficiencies of ammonium conversion in the start-up stage with 0.2 kg-N/m^3/day as nitrogen loading rate were quite high, special with the highest efficiency was 89.61% on day 57. This can be explained by the biomass on Acrylic Pile fabrics of SNAP reactor was quite good, thus limited the sludge to escaped from reactor.

Through stage II, the nitrogen loading rate was increase to 0.4 kg-N/m^3/day, the ammonium nitrogen conversion efficiencies had reduced. This can be explained by the SNAP biomass has not enough yet to respond for ammonium concentration at this nitrogen loading rate. After, the highest conversion efficiency reached 66.43% on day 86. This showed that SNAP sludge was adapted progressively with the higher concentration of ammonium.

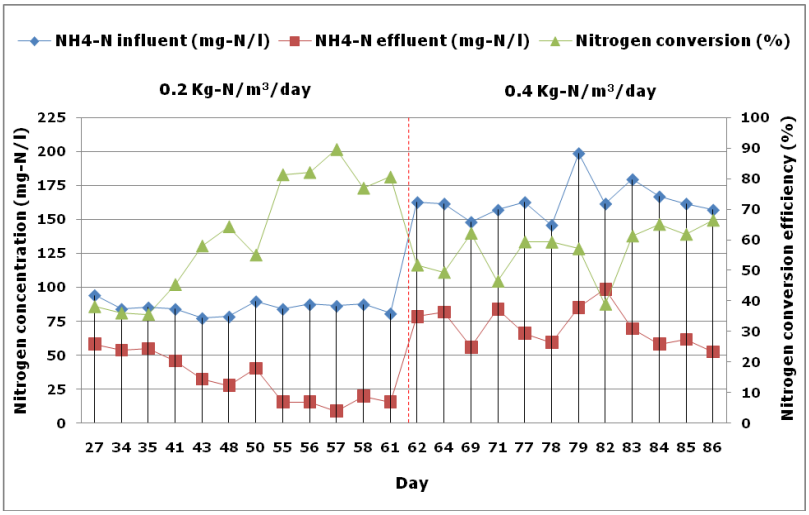


Fig.6 Changes of ammonium nitrogen concentrations and nitrogen conversion efficiencies

Total nitrogen removal efficiency

In stage start-up with 0.2 kg-N/m^3/day as nitrogen loading rate, the highest efficiency of total nitrogen (TN) was 77.93% on day 57. This can be explained by anammox biomass was accommodated well together with the good conversion of ammonium oxidation bacteria (AOB).

On the stage II, the nitrogen loading rate was increase to 0.4 kg-N/m^3/day, the total nitrogen removal efficiency was reduced together with the low conversion of ammonium oxidation bacteria. The highest total nitrogen removal efficiency reached 58.57% on day 86.

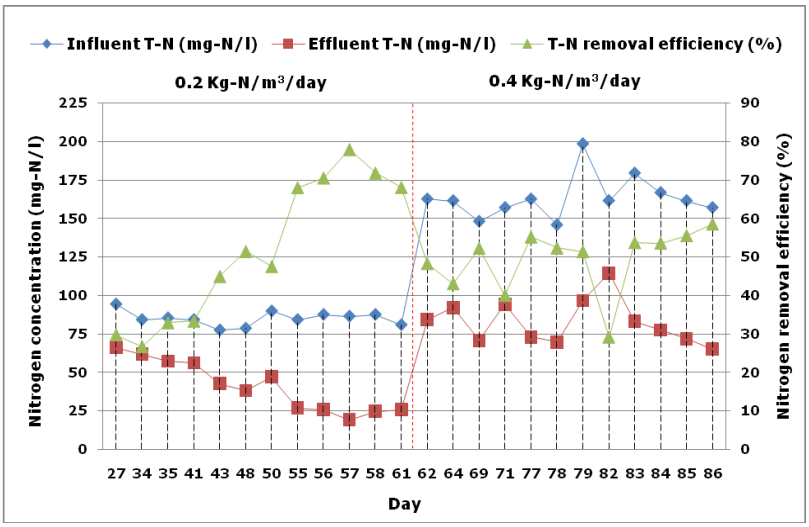


Fig.7 Changes of total nitrogen concentrations and nitrogen removal efficiencies

Ammonium nitrogen conversion to nitrate

In two stages of operation, the ammonium conversion percentages were lower 11%. The highest conversion was 10.51% on day 61 and the lowest conversion was 0.22% on day 35. The control of operation parameters in SNAP reactor to inhibited nitrite oxidation bacteria (NOB) to reduced the formation of nitrate in effluent. This was the purpose of SNAP process.

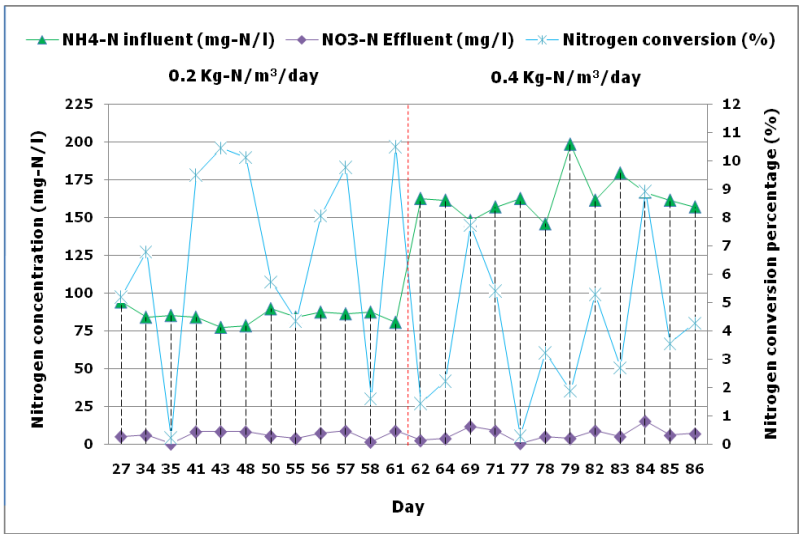


Fig.8 Ammonium nitrogen conversion to nitrate

Conclusions

The following conclusions are deduced from this study:

- Biomass attached on the Acrylic Pile Fabrics carrier was good.
- Ammonium conversion efficiencies were fairly good with highest conversions were 89.61% and 66.43% in the nitrogen loading rate of 0.2 kg-N/m^3/day and 0.4 kg-N/m^3/day, respectively.
- Nitrogen removal efficiencies reached highest were 77.93% and 58.57% in the nitrogen loading rate of 0.2 kg-N/m^3/day and 0.4 kg-N/m^3/day, respectively.
- The highest conversion of ammonium to nitrate was 10.51% through two stages. This showed the efficiency of operational control.

Acknowledgements

The authors wish to thank laboratory of Faculty of Environment, Ho Chi Minh City University of Technology. This study is supported by JICA's Project, Japan.

References

[1] Daigger, G.T., Sanjines, P., Pallansch, K., Sizemore, J., Wett, B., (2011), Implementation of a full-scale anammox-based facility to treat an anaerobic digestion sidestream at the Alexandria Sanitation Authority Water Resource Facility, In Proc. WEF-IWA Nutrient Recovery and Management Conf., pp.2386-2401.

[2] Kuai, L. and Verstraete, W., (1998), Ammonia removal by the oxygen-limited autotrophic nitrification-denitrification system, App. Environ. Microbiol, Vol.64, No.11., pp.4500-4506.

[3] Lieu, P.K., Hatozaki, R., Homan, H. and Furukawa, K., (2005), Single-Stage Nitrogen Removal Using Anammox and Partial Nitritation (SNAP) for Treatment of Synthetic Landfill Leachate, Japanese. J. Wat. Treat. Biol., Vol.41, No.2, pp.103-112.

[4] Lieu, P.K., Homan, H., Kurogi, A., Kawagoshi, Y., Fujii, T. and Furukawa, K., (2006), Characterization of Sludge from Single-Stage Nitrogen Removal Using Anammox and Partial nitritation (SNAP), Japanese. J. Wat. Treat. Biol., Vol.42, No.2, pp.53-64.

[5] Mulder, A., van de Graaf, A.A., Robertson, L.A. and Kuennen, J.G., (1995), Anaerobic ammonium oxidation discovered in a denitrifying fluidized bed reactor, FEMS Microbiology Ecology, Vol.16, pp.177-184.

[6] Pynaert, K., Smets, B.F., Wyffels, S., Beheydt, D., Siciliano, S.D. and Verstraete, W., (2003), Characterization of an Autotrophic Nitrogen-Removing Biofilm from a Highly Loaded Lab-Scale Rotating Biological Contactor, App. Environ. Microbiol, Vol.69, No.6, pp.3626-3635.

[7] Sliekers, A.O., Derwort, N., Gomez, J.L.C., Strous, M., Kuenen, J.G and Jetten, M.S.M., (2002), Completely autotrophic nitrogen removal over nitrite in one single reactor, Wat. Res., Vol.36, pp.2475-2482.

[8] Sliekers, A.O., Third, K.A., Abma, W., Kuenen, J.G. and Jetten, M.S.M, (2003), Canon and anammox in a gas-lift reactor, FEMS Microiol., Vol.218, pp.339-344.

[9] Strous, M., Heijnen, J.J., Kuenen, J.G., and Jetten, M.S.M, (1998), The sequencing batch reactor as a powerful tool for the study of slowly growing anaerobic ammonium-oxidizing microorganisms, Appl. Microbiol. Biotechnol, Vol.50, pp.589-596.

[10] Van Dongen, U., Jetten, M.S.M. and van Loosdrecht, M.C.M, (2001), The SHARON-Anammox process for treatment of ammonium rich wastewater, Wat. Sci. Tech, Vol.44, No.1, pp.153-160.

2nd International Engineering Symposium - IES 2012
(KU-MU-NITK-HCMCUT Joint Symposium) March 5-7, 2012, Kumamoto University, Japan

Nitrogen Removal from Landfill Leachate by Single-Stage Using Anammox and Partial Nitritation (SNAP) with BioFix as Biomass Carrier

Dao Vinh Loc[1*] and Nguyen Tan Phong[2]

[1] Faculty of Scientific Environment, Yersin Da Lat University, Da Lat, Viet Nam.E-mail: vinhloc278@gmail.com or dvloc_mt@yersin.edu.vn*
[2] Faculty of Environment, Ho Chi Minh City University of Technology, Ho Chi Minh, Viet Nam.E-mail: tanphong69@yahoo.com or ntphong@hcmut.edu.vn

Abstract: Single-stage nitrogen removal using anammox and partial nitritation (SNAP) is the new technology for removing nitrogen in wastewater that has high nitrogen and low organics concentration in recent years. In this study, using the reactor had volume 3.7 liters and the biomass carrier was the BioFix. The synthetic influent wastewater is used to simulating old landfill leachate. Ammonium concentration from 50 to 100 mg-N/L. Operating factors such as HRT, DO, and pH were 10, 0.5-2.5 mg/l, and 7.5-8.0, respectively. The temperature was not controlled and was affected by ambient temperature which was from 27-35.5^{0}C. With the nitrogen loading rates was 0.2 kg-N/m^3/day, the ammonium conversions was 73% and total nitrogen removal efficiencies reached 63%.

Keywords: *SNAP, anammox, partial nitritation, bioFix, nitrogen removal*

Introduction

The high concentration of nitrogen that is present in wastewater pose serious threat to environmental protection. It contributes to undesirable eutrophication in rivers and stream. A common adverse effect is eutrophication caused by assimilation of nitrate by algae. The overgrowth of algae (algal bloom or red tide) may cause taste and odor problems in water sources and filter clogging and excessive chlorine demand at water treatment facilities, consequently resulting in economic loss and health hazard as nitrate can cause methemoglobinemia in infants. No deaths of humans have been attributed by red tide, but people may euxperience respiratory irritation (coughing, sneezing, and tearing).

Therefore nitrogen has to be removed from wastewater before discharge into the environment. In Viet Nam, there was regulation of discharge requirement for nitrogen that promulgated by Ministry of Natural Resources and Environment, the discharge limits of total nitrogen (T-N) and nitrogen -ammonia (N-NH_3) depending on conditions of the receiving source for industrial wastewater are from 15-30 mg/l and 5-10 mg/l, consequently (National Technical Regulation on Industrial Wastewater QCVN 24: 2009/MNRE).

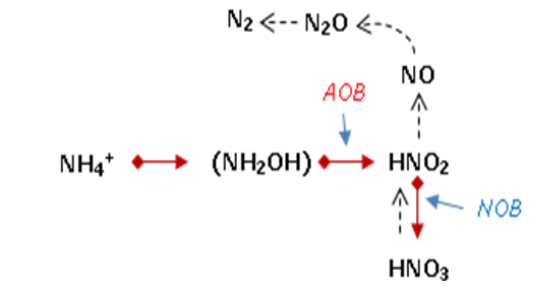


Fig. 1 Nitrification-denitrification technology to removing nitrogen

Conventional nitrification-denitrification technology to removing nitrogen but it is not feasible due to high operation and maintenance costs, requirement of skilled operators, etc.
Since the late 1990s, the discovery of anaerobic ammonium oxidation (anammox) has opened up a new approach for treatment of wastewater having high ammonium. This discovery overcomes the disadvantages of conventional treatment.

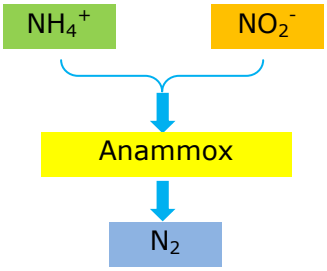


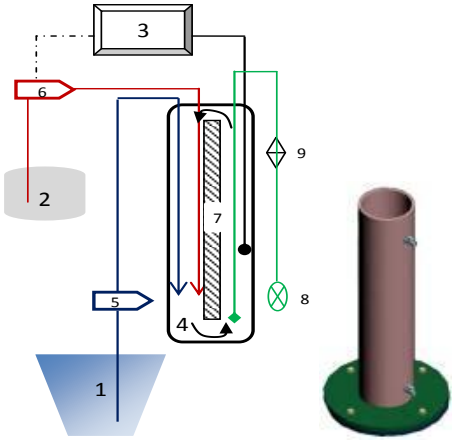
Fig. 2 The anammox process

The anammox process is the partial nitritation (PN) combines anammox to removing nitrogen. The first partial nitritation step produces a half amount of nitrite from influent ammonium by ammonia-oxidizing bacteria (AOB) (Eq. 1).
$NH_4^+(100) \rightarrow NH_4^+(50) + NO_2^-(50)$ (Eq.1)
To achieving the partial nitritation and avoiding produce of nitrate (NO_3^-) need some conditions, as follows: low dissolved oxygen concentration (DO), Yang et al., (2010); high temperature, Magris et al., (2007) and free ammonia concentration (FA), Anthonisen et al., (1976). And the second step, the anammox bacteria converters ammonium and nitrite to gaseous nitrogen (Eq. 2), Schemidt et al., (2003).
$1NH_4^+ + 1.32NO_2^- \rightarrow 1.02N_2 + 0.26NO_3^- + 2H_2O$
The combination of the two conversion steps (Eq.3) can be carried out in separate tanks or in single tanks.
$1\ NH_4^+ + 0.85\ O_2 \rightarrow 0.44\ N_2 + 0.11\ NO_3^- + 1.43\ H_2O + 1.14\ H^+$ (Eq.3)
Several novel processes bases on this approach have been developed such as SHARON-ANAMMOX (Single reactor system for High Ammonium Removal Over Nitrite), Kuai et al., (1998) and Pynaert et al., (2003), CANON (Completely Autrotrophic Nitrogen remove Over Nitrite), Sliekers et al., (2002 and 2003), SNAP (Single-stage Nitrogen removal using Anammox and Partial nitritation), Lieu et al., (2005), etc.
The SNAP is the new ammonium removal process that was developed in Kumamoto University with conditions in Japan. In this study, we investigated the potential of SNAP using Biofix as biomass carriers with conditions in Viet Nam.

Experiment

❖ Experimental set-up

The reactor had a liquid volume of 3.7 liters. The inner diameter and useful height were 10.5 cm and 43 cm, respectively. Air was spurge from the bottom of the reactor. Using $NaHCO_3$ solution to control the pH value.



(b)

(a)

Fig.3 Schematic diagram of reactor (a) and the 3D model of reactor (b)

1.Influent tank 2.$NaHCO_3$ solution
3.pH controller 4.Reactor
5.Influent pump 6. $NaHCO_3$ pump
7.Biomass carrier 8. Air pump
9.Air-controlling valve

❖ Influent wastewater

Influent was synthetic wastewater that had high nitrogen concentration (from 50 mg/l to 200 mg/l) and added the trace inorganic components such as K^+, Na^+, Ca^{2+}, Mg^{2+}, Fe^{2+}.

❖ Seed sludge

Two kinds of sludge were the activated sludge and the anammox sludge that seeded in the reactor with ratio as 4:6 (MLSS). Total of seed sludge was 1.5 g/l (MLSS).

The anammox sludge and activated sludge got from Kumamoto University, Japan and Tan Binh wastewater treatment plant, Viet Nam, respectively.

Table 1 Composition of synthetic wastewater *

Composition	Unit	Concentration
NH_4Cl	(mg-N/l)	50 – 200
$NaHCO_3$	(mg/l)	160
$KHCO_3$	(mg/l)	160
KH_2PO_4	(mg/l)	43
$MgSO_4.7H_2O$	(mg/l)	328
$CaCl_2.2H_2O$	(mg/l)	235
$FeSO_4.\ 7H_2O$	(mg/l)	16
Na_2.EDTA	(mg/l)	16
$C_8H_5O_4K$	(mg/l)	38
Na_2SO_3**	(mg/l)	160

* Lieu, et al. (2007) **Controlling the DO in influent of synthetic wastewater

❖ **Biomass carrier**

The newly biomass carrier was a product of NET Co, Ltd, Japan as Biofix. The parameters of Biofix are show in Table 1. The Biofix was fixed by steel frames and it can remove easily. Weight of using biomass carrier was 37.4g.

Table 2 Parameter of Biofix carrier *

Parameter	Unit	Value
Specific yarn length	m/m^3	23,324
Specific surface area	m^2/m^3	146,5
Yarn diameter	mm	2

** Provided by the manufacturer*



Fig.4 Photos of Biofix and steel frames fixed the biomass carriers

❖ **The conditions of operation**

The pH, hydraulic retention time (HRT) and dissolved oxygen (DO) were controlled to achieving partial nitritation and SNAP.

- pH = 7.5 – 8.0
- HRT = 10
- DO = 0.5 – 2 mg/l

The temperature was not controlled as ambient temperature from 24^0C-33.5^0C.

❖ **Analytical methods**

Using Standard Methods for the Examination of Water and Wastewater (USA) analyses NH_4-N, NO_2-N and NO_3-N:

- NH_4-N:4500-NH_3-B Preliminary Distillation Step
- NO_2-N:4500-NO_2^-B Colorimetric Method
- NO_3-N:4500-NO_3^--B Cadmium Reduction Method

Total nitrogen was determined by TCVN 6638:2000 (National Technical Regulation Viet Nam), Catalytic digestion-Devarda alloy.

Using the pH controller BL 931700 (Hanna-England) to controlled pH value. Using the Oxi 3210 Set-DurOx 325-3, England to measured DO in the reactor.

Results and discussion

❖ **Seed sludge**

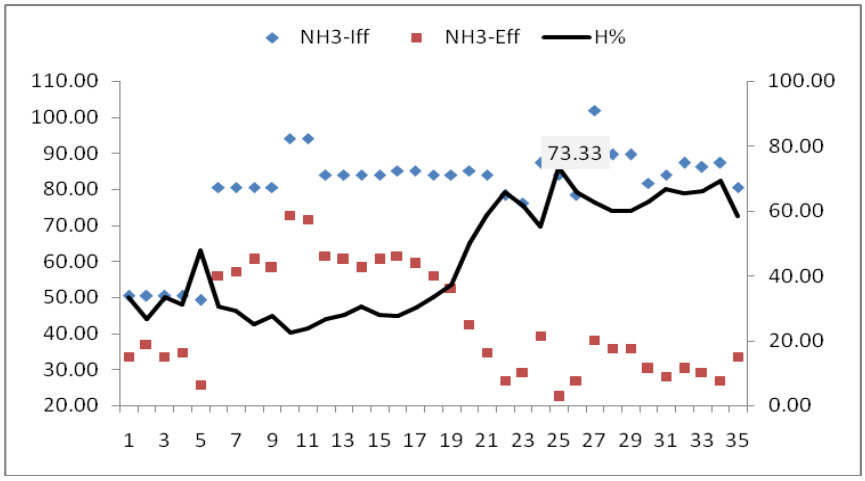
First, the anammox sludge was introduced into the reactor. After 24h used the nitrogen gas for circulating, all of anammox sludge attached on the biomass carrier. Then, the activated sludge was implanted, used the air for circulating, after 3 days, 90% activated sludge attached on Biofix carrier.



Fig.5 Photos of biomass carriers after the anammox sludge was introduced into the reactor

❖ **Ammonium oxidation**

The capacity of ammonium oxidation increases follows influent ammonium concentration. With 50 mg/l of ammonium concentration, the maximum of capacity ammonium oxidation was 47.73%. When the ammonium concentration was increased to near 100 mg/l, it was 73.33% on 25 days' operation. However, this value was not stable. It can be explain by the effects of time and condition operation. The average temperature changed from 27^0C to 35.5^0C in the morning and in the afternoon, respectively and the time of operation was 35 days. Besides, the pH value in reactor regular varies from 7.5 to 8.0. These reasons can be inhibit activity of bacteria, especially ABO and NOB.

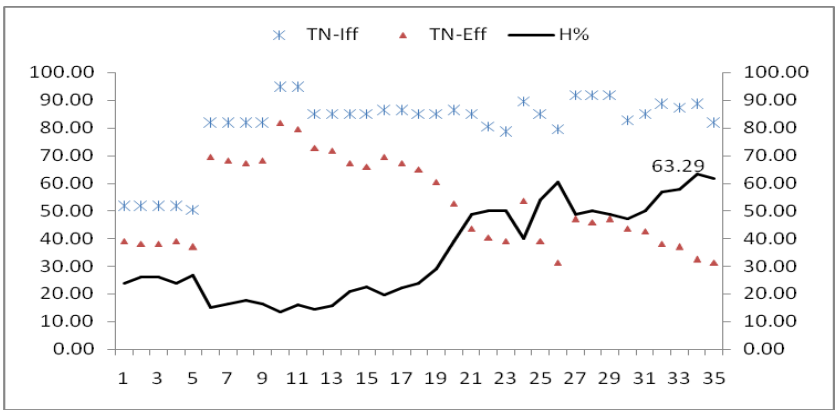


NH3-Iff: Influent Ammonium concentration;
NH3-Eff: Effluent Ammonium concentration; H%: Ammonium oxidation performance

Fig.6 Ammonium oxidation performance

❖ **Nitrogen removal performance**

Nitrogen removal performance was not high, only 63.29%. It may be cause effect of some factors. First of all, the time operation of system was not long, so the growth of bacteria was not stable and good. On the other hand, influent ammonium concentration and nitrogen loading rate was low, lower 100 mg/l and only 0.2 kg-N/m^3/day, respectively. Nevertheless, the nitrogen removal performance increase gradually. To evaluate performance of nitrogen remove needs more time and higher ammonium concentration.



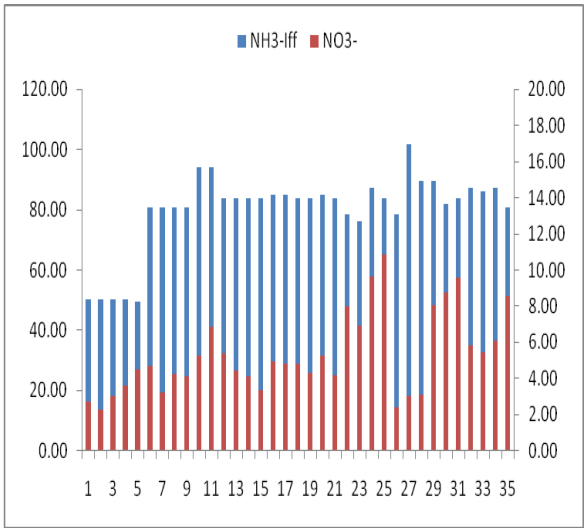
TN-Iff: Influent total nitrogen concentration;
TN-Eff: Effluent total nitrogen concentration; H%: Nitrogen removal performance

Fig.7 Nitrogen removal performance

❖ **The nitrate (NO_3^-) concentration**

The effluent nitrate (NO_3^-) concentration depends on the influent ammonium (NH_3) concentration as well as the time operator of system, but it was not much, only near 6.67% in comparison with the influent ammonium (NH_3) concentration and 11.24% against the effluent total nitrogen concentration.

With low DO in reactor (around 1.25 mg/l) inhibited activity of NOB. Therefore, the percentage of effluent nitrate was low. But it helps to appreciate effect of NOB with partial nitritation.



NH3-Iff: Influent ammonium concentration
NO3-: Effluent nitrate concentration

Fig.8 The nitrate (NO_3^-) concentration

Conclusion

Some withdrawal conclusions are as follows:

- Total nitrogen removal is 63.29% after 35 days of operate.
- The ammonium conversions efficiency 73.33% with 100 mg/l initial concentration of ammonium.
- The nitrate concentration makes up around 11.24% against initial total nitrogen concentration.

Acknowledgements

The authors wish to thank laboratory of Faculty of Environment, Ho Chi Minh City University of Technology. This study is supported by JICA's Project, Japan.

References

[1] Anthonisen et al., (1976), Inhibition of nitrification by ammonia and nitrous acid. J Water Pollut. Control Fed, No.48, pp. 835-852.
[2] APHA, AWWA, WPCF (2004), Standard methods for the examination of water and wastewater, 19th edition, Washington DC, USA.
[3] Kuai, L. et al., (1998), Ammonia removal by oxygen-limited autotrophic nitrification-denitrification system, App. Environ. Microbiol. , No.64, pp. 4500-4506.
[4] Lieu, P.K et al., (2005), Single-Stage nitrogen removal using Anammox and Partial Nitritation (SNAP) for treatment of synthetic landfill leachate, Japanse. J. Wat.Treat.Biol., No.41, pp. 103-112.
[5] Magris et al., (2007), A model for the simulation of the SHARON process: pH as a key factor. Environ. Technol, No.28, pp. 255-265.
[6] Pynaert et al., (2003), Characterization of an Autotrophic nitrogen-removing biofilm from a highly loaded lab-scale rotating biological contactor, App. Environ. Microbiol, No.69, pp. 3626-3635.
[7] QCVN 24: 2009/MNRE (2009), National Technical Regulation on Industrial Wastewater, Viet Nam.
[8] Schimidt, I. et al. (2003), New concepts of microbial treatment processes for the nitrogen removal in wastwater, FEMS Microbiol. Rev., No.27, pp. 481-492.
[9] Sliekers et al., (2002), Completely autotrophic nitrogen removal over nitrite in one single reactor, Wat. Res, No.36, pp. 2475-2482.
[10] Sliekers et al., (2003), Canon and Anammox in a gas-lift reactor, FEMS Microil., No.218, pp. 339-344.
[11] TCVN 6638:2000 (2000), National Technical Regulation: Catalytic digestion-Devarda alloy, Viet Nam.
[12] Yang et al. (2010), High rate partial nitrification treatment of reject wastewater. J Biosci.Bioeng., No.110, pp. 436-440.

Microwave-Assisted Extraction and Identification of Antioxidants from *Nerium oleander* and Determination of its Total Activity

Pavithra G S[1], Farhana K[2], Raj Mohan B[3]

1 *Department of Chemical Engineering, National Institute of Technology Karnataka, Surathkal, Mangalore 575025, India. Email: pavithra.gs@gmail.com*

2 *Department of Chemical Engineering, National Institute of Technology Karnataka, Surathkal, Mangalore 575025, India. Email: farna2312@gmail.com*

3 *Department of Chemical Engineering, National Institute of Technology Karnataka, Surathkal, Mangalore 575025, India. Email: rajmohanbala@gmail.com*

ABSTRACT

Antioxidants are substances which can prevent or slow down the oxidative damage caused by free radicals. Synthetic antioxidants used in food industry have several side effects and hence there is a need for the cost effective production of natural antioxidants in large quantity. Natural Antioxidants are usually extracted from various parts of plants using modern techniques. The microwave-assisted extraction (MAE) is found to be the most promising technique which has certain advantages like improved efficiency, reduced extraction time and low solvent consumption. Leaves of *Nerium oleander* (two varieties, pink and white flowered) were chosen as the potential sources of antioxidants and their extracts were studied for total antioxidant activity by FRAP method. The significant rupture of the plant tissues by microwave irradiation was examined using Scanning Electron Microscopy (SEM). The optimized conditions of MAE using central composite rotate design were, extraction time: 4.148 and 5.5758 min; solvent concentration: 46.732% and 70.889% for NOP and NOW respectively. The optimum extraction temperature was found to be 50^0C for both the extracts. The compounds Rutin in NOW and Rosmarinic acid in NOP extracts were found in abundance as indicated by liquid chromatography mass spectrometry (LC-MS) analysis.

Key words: *Antioxidants, Activity, Free radical oxidation, Microwave-assisted extraction (MAE), Nerium oleander, Phytochemicals*

Introduction

Anti-oxidant: Antioxidants interfere in the oxidation process by reacting with free radicals and scavenging reactive oxygen. Oxidation of fats and oils leading to rancidity is a major concern for food industries. A variety of synthetic anti-oxidants have been used in food industries, viz. Butylated hydroxyanisole, butylated hydroxytoluene, ethoxyquin and propyl gallate, etc. to protect food from rancidity. However these synthetic anti-oxidants are known to cause cancer and liver disease in the consumers (Fukushima et al. 1983, Fukushima et al. 1986 and H. Witschi, 1986). Hence consumer demand for natural and healthy products has been increasing in recent years. Phenolics and flavanoids are the natural anti-oxidants found in abundance in variety of fruits, vegetables and leaves.

Nerium oleander: Native to the Mediterranean region, Iran, the Indian subcontinent and southern China, it is

widely cultivated as an ornamental shrub or as an informal hedge in warm-temperate and dry subtropical regions, and as a plant for the conservatory in cooler climates. When ingested, it is highly poisonous to humans, pets, livestock and birds due to the presence of cardiac glycosides (Oleandrin). Its sap has been used as rat poison. There are reports that long-term use of oleander may have positive effects in patients with leiomyosarcoma, Ewing's sarcoma, prostate or breast cancer although reliable research in humans has not yet been performed. Peruvoside, a heart-active substance in yellow oleander kernels (similar to the drug digoxin) is taken orally for congestive heart disease in adults, whereas the dosage limits have not been prescribed for oleanderin (1). Isoquercitrin, Lauric-Acid, Oleanolic-Acid, Quercetin, Rutin, Stigmasterol, Ursolic Acid are the main anti-oxidants present in *N. oleander* (Dr. Duke's Phytochemical and Ethnobotanical Databases). Efficient procedures for the extraction of these natural anti-oxidants from *N. oleander* are yet to be developed for increased commercial appeal.

Microwave Assisted Extraction (MAE): MAE process utilizes the energy of microwaves to cause molecular movement and rotation of liquids with a permanent dipole leading to a very fast heating of the sample (Eskilsson et al. 2000 and Buldin et al. 2000). It has been demonstrated that MAE can be an effective alternative to conventional extraction of bio-active phytochemicals (Zhang et al. 2009, Yang et al.2005, Zhang et al. 2004, Jaitak et al. 2009 and Deng et al. 2009). Compared with soxhlet extraction and ultra-sound extraction, MAE is a rapid method with higher yield and less solvent consumption (Wang et al, 2011).

Materials and Methods

Sample preparation

Freshly collected *N. oleander* (white and pink varieties, indicated as NOW and NOP respectively) leaves from the vicinity of NITK campus were thoroughly washed, oven-dried (at 50^0C for 48hrs), finely ground into powder and stored.

Extraction process

The powdered samples of *N. oleander* were subjected for MAE with methanol as a solvent using QAsh 1800- Microwave Ashing System, flushed with nitrogen gas (ESAB Nitrogen 230 bar service, USA) at 1kg/cm^2 pressure. The samples were mixed with the different concentrations of methanol (in distilled water, v/v). The extracts were filtered using Whatmann 1 filter and used for further analysis.

Total anti-oxidant activity

Total antioxidant activity of the extracts was measured by ferric reducing antioxidant power (FRAP) assay (Benzie and Strain, 1999). The stock solutions to conduct FRAP assay include 300 mM acetate buffer (3.1 g CH_3COONa and 16 ml CH_3OOH) - pH 3.6, 10 mM TPTZ (2, 4, 6-tripyridyl-s-triazine) solution in 40 mM HCl, and 20 mM $FeCl_3 \cdot 6H_2O$ were prepared. The fresh working solution was prepared by mixing the above mentioned solutions in the ratio 10:1:1 respectively. The plant extracts of 100 µL each were mixed 3 ml of the FRAP solution and incubated for 6 min. Absorbance of the colored product (ferrous tripyridyltriazine complex) was read at 593 nm using UV spectrophotometer (Hitachi U-2000, Double beam spectrophotometer, Tokyo, Japan). The calibration curve was obtained using Ascorbic acid standard and it was found to be linear. Results were expressed in µM Ascorbic acid/g dry mass.

Central Composite Design

The operating variables like temperature, time and solvent concentration for MAE was optimized using Central Composite experimental design technique. The optimum conditions were evaluated using a response surface design with five replicates of the central point. Contour

and surface plots were also obtained from the design software.

Scanning Electron Microscopy

The significant change in the cell structure, after MAE, was examined under Scanning Electron Microscope (JSM-6380LA, Analytical Scanning Electron Microscope, Japan). The dried plant samples before and after extraction were made conductive by sputtering a thin film of gold on their surface using JFC-1600 Auto Fine Coater. Images were taken at a magnification of 800X and voltage of 20kV.

Liquid Chromatography - Mass Spectrometry (LC-MS)

Leaf extracts were analyzed in reverse phase LC (Thermo Finnigan Surveyor, USA) and Mass Spectrometry (Thermo LCQ Deca XP MAX, USA) using Xcaliber software. All samples were filtered through 0.45 µm filters (Millipore (India) Pvt. Ltd) and 10 µl of the filtrates were loaded into LC-MS system for analysis phytochemicals that are responsible for antioxidant property. The stationary phase consisted of BDS HYPERSIL C-18 column (reverse phase), 5µm diameter, 250x4.6 mm length. Acetonitrile: 0.1% trichloroacetic acid (75:25) was used as mobile phase. The samples were run for 60 minutes at 250 nm, 27^0 C oven temperature of the column, and at 0.3 ml / min flow rate and the compounds were detected using HPLC PDA / UV detector. The eluted compounds were then analyzed in ESI-MS at a source voltage of 4.5 kV and capillary temperature of 275^0 C. Helium gas at a flow rate of 1mL/min was used as nebulizer.

Results and Discussion

Preliminary Investigation of MAE

The preliminary investigation of the MAE was carried out to identify the parameters that influence the extraction process. The efficiency of extraction depends on the irradiation time and power applied which dictates the temperature inside the system (Villar et al. 2004). The preliminary investigation made on the MAE conditions has indicated that the anti-oxidant activity of the extracts were mainly dependent on the extraction time, hold temperature and concentration of solvent (methanol in distilled water, v/v). In addition, it also indicated that the highest activity was obtained for both plant extracts at 50^0C for the given range of time and solvent concentrations. Hence, the optimum temperature was fixed at 50^0C for the further experiments.

Optimization of MAE condition for extraction by CCRD

The Central Composite Rotate Design technique was used to minimize the number of experiments. A complete design of experiments consisting of 13 experimental points including five replications of the center points was used. The regression model was developed using the results of the design experiments which is as indicated in equation 1 and 2 for NOP and NOW respectively:

$$Y=1723.85 + 41.8736X_1 + 0.616552X_2 - 3.88524X_1^2 - 6.65517E\text{-}04\ X_2^2 - 0.145X_1X_2 \quad (1)$$

$$Y=1698.44 + 38.2016X_1 + 0.951363X_2 - 6.71344X_1^2 - 0.0282517X_2^2 - 0.54785X_1X_2 \quad (2)$$

Where, Y=FRAP, X_1= extraction time and X_2= solvent concentration

The analysis of variance for these models is given in Table 1. The whole model that include linear level ($a<0.05$), quadratic level ($a<0.05$) reached a significant value whereas the cross product level ($a>0.05$) was not significant for NOP. Even though the cross product level of NOP was marginally insignificant, it can be neglected as its influence over extraction process is low. Interestingly, all levels are significant ($a<0.05$) in case of NOW.

The response surface methodology was used to determine the optimum conditions for maximum extraction of antioxidants using MAE at constant temperature (50^0C). The optimal MAE conditions were obtained as, NOP: extraction time- 4.148

min; solvent concentration-46.732%., NOW: extraction time- 5.5758 min; solvent concentration-70.889%. The contour and surface graphs of RSM are given Figure 1. Under these conditions, the experimental FRAP value for NOP and NOW were found to be 1830 and 1845 µM Ascorbic acid/g dry mass of plant tissue respectively and is in good agreement with the predicted values using the polynomial model (1829.9461 and 1844.7416 µM Ascorbic acid/g dry mass respectively).

Effect of MAE on structure of the plant cell

The micrograph of the NOP and NOW samples were examined under SEM to determine the differences in the structure of the cells before and after extraction. Figure 2 reveals the significant rupture of the cells during MAE process, leading to the direct migration of the antioxidants into the surrounding solvent. Similar results were demonstrated by Liao et al (2007). This supports the fact that MAE is a rapid method of extraction when compared to conventional methods.

LC- MS analysis

The analysis of LC-MS revealed that the major antioxidant components in the sample are Rosmarinic acid (Molecular Weight: 360) and Rutin (Molecular Weight: 610) in NOP and NOW respectively. The mass spectra for the extracts, shown in figure 3 (a) and (b) reveal that the above antioxidants scored high values of relative abundance (100). From the figures it is also evident that the spectral result is in good relation with the Duke's database.

Conclusion

An efficient procedure using MAE, followed by LC-MS was developed for the rapid extraction and analysis of anti-oxidants from *N. oleander* leaves. The maximum yield of antioxidants was obtained at extraction time of 4.148 and 5.5758 min; solvent concentration of 46.732% and 70.889% for NOP and NOW respectively and extraction temperature of 50^0C for both. LC-MS indicated that Rutin in NOW and Rosmarinic acid in NOP were the potential anti-oxidants present in the leaf extracts at a relative abundance of 100. The rupture of the cells during extraction as shown by SEM analysis clearly indicates that MAE is a rapid method of extraction. By MAE the yield of antioxidants can be maximized with minimum energy and solvent consumption. With a suitable purification technique, *N. oleander* leaf extracts can serve as a potential source of natural antioxidants and eventually replace the synthetic anti-oxidants used in food industries.

Acknowledgments

We gratefully thank the faculty and PG students of Department of Chemical Engineering, Chemistry and Materials Engineering, NITK-Surathkal. We also thank Dr. M. Rajyalakshmi, Asst. professor, BMS College of Engineering, for her technical assistance.

References

(1) Allnutritionals.com., Nutritional Health Information and Tools. http://allnutritionals.com /natural-products /oleer-nerium-oleer-thevetia-peruviana.php

(2) Buldini PL, Ricci L, Sharma JL (2000) JChromatogrA975:47–70

(3) Deng JC, Xiao XH, Li GK, Ruan GH. Application of microwave- assisted extraction coupled with high-speed counter-current chromatography for separation and purification of dehydrocavidine from Corydalis saxicola Bunting. Phytochem Anal (2009) 20: 498–502

(4) Dr. Duke's Phytochemical and Ethnobotanical Databases., Chemicals and their Biological Activities in: Nerium oleander L. (Apocynaceae) – Oleander

(5) Eskilsson CS, Bjorklund E (2000) J Chromatogr A 902:227–250

(6) H. Witschi, Food Chem. and Toxicol. 24 (1986) 1127.

(7) Iris. F.F. Benzie and J.J. Strain., Ferric Reducing Anti-oxidant Power Assay: Direct

Measure of Total Antioxidant Activity of Biological Fluids and modified Version for Simultaneous Measurement of Total Antioxidant Power and Ascorbic Acid Concentration, Methods in Enzymology 299 (1999): 15-27.
(8) Jaitak V, Bandna SB, Kaul VK. An efficient microwave-assisted extraction process of stevioside and rebaudioside-A from Stevia rebaudiana (Bertoni). Phytochem Anal (2009) 20: 240–245
(9) K. Imida, S. Fukushima, T. Shivai, M. Ohtani, K. Nakanish, N. Ito, Carcinogenesis 4 (1983) 885.
(10) Li H, Chen B, Zhang ZH, Yao SZ. Focused microwave-assisted solvent extraction and HPLC determination of effective constituents in Eucommia ulmoides Oliv. (E. ulmodies). Talanta (2004) 63: 659–665
(11) N. Ito, M. Hirose, G. Fukushima, H. Tauda, T. Shira, M. Tatematsu, Food Chem. Toxical 24 (1986) 1071.
(12) Villar P, Callej´on M, Alonso E, Jim´enez JC, Guira´um A (2004) Anal Chim Acta 524:295–304
(13) Wang GuiHua, Su Ping, Zhang Fan, Hou XiangYan, Yang Yi & Guo ZhenKu. Comparison of microwave-assisted extraction of aloe-emodin in aloe with Soxhlet extraction and ultrasound-assisted extraction, Science China,Chemistry, (2011) 231-236
(14) Yangzhao Sun, Xiaojun Liao, Zhengfu Wang, Xiaosong Hu, Fang Chen. Optimization of microwave-assisted extraction of anthocyanins in red raspberries and identification of anthocyanin of extracts using high-performance liquid chromatography – mass spectrometry. Eur Food Res Technol (2007) 225:511–523
(15) Yang Y, Hou XY, Guo ZK. Microwave-assisted extraction of aloin from fresh aloe leaves. Chem J Chinese U (2005) 25: 1627–1630
(16) Zhang F, Yang Y, Su P, Guo ZK. Microwave-assisted extraction of rutin and quercetin from the stalks of Euonymus alatus (Thunb.) Sieb. Phytochem Anal (2009) 20: 33–37

FIGURES AND TABLES

Source	P (NOP)	P (NOW)
Regression	0.000	0.000
Linear	0.037	0.001
Square	0.000	0.000
Interaction	0.093	0.003

Table 1**:** Analysis of Variance for FRAP

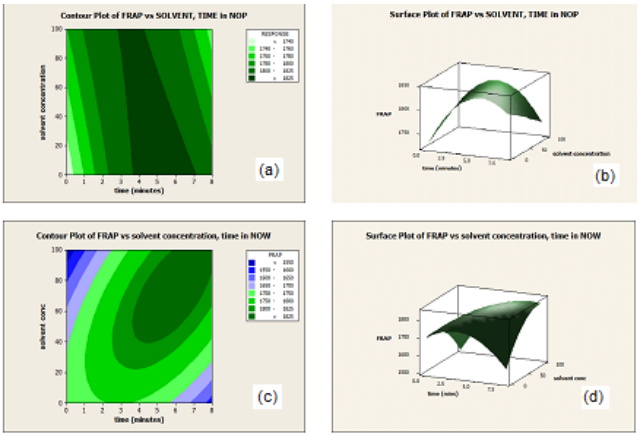


Figure 1 (a) and (c) - contour plots, (b) and (d) - surface plots of NOP and NOW respectively

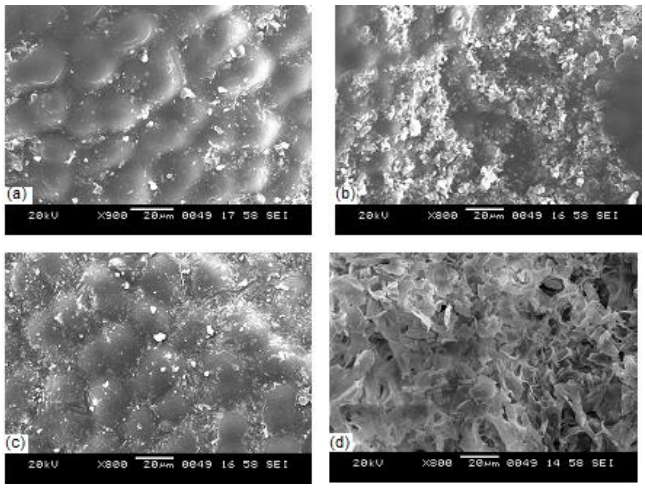


Figure 2: SEM images; (a) and (c) - cellular arrangement before extraction, (b) and (d) - rupture of cells after extraction in NOP and NOW respectively

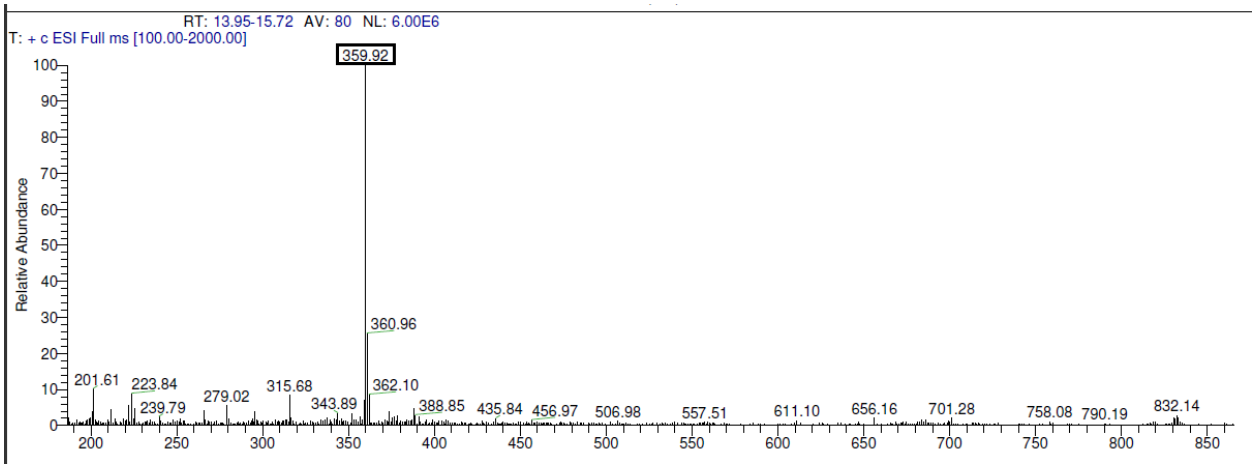


Figure 3(a): Mass spectra of NOP leaf extracts

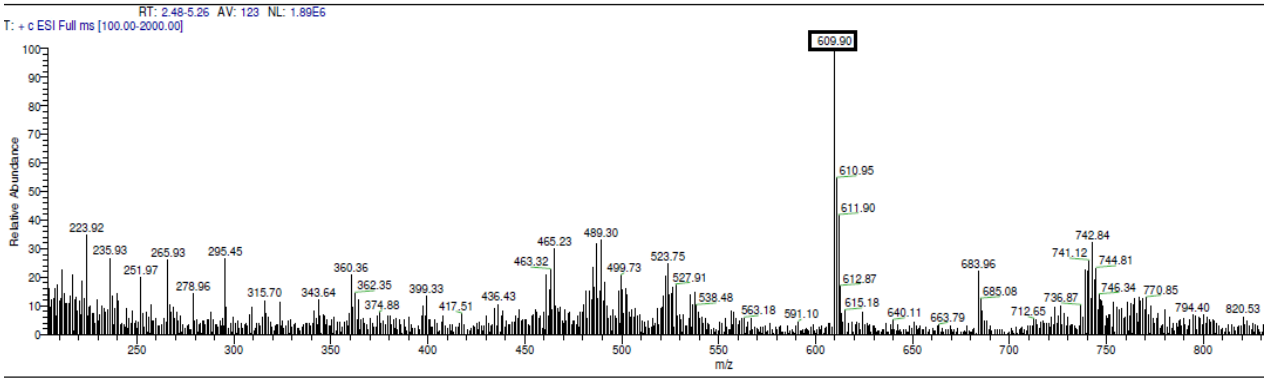


Figure 3(b): Mass spectra of NOW leaf extracts

2nd International Engineering Symposium - IES 2012
(KU-MU-NITK-HCMCUT Joint Symposium) March 5-7, 2012, Kumamoto University, Japan

Effect of Culture Conditions on the Production of Laccase by an Unidentified Basidiomycete-F-35b

Gopal Mugeraya , Akshata Hoskeri and **Harisha Poojary***

Department of Chemical Engineering, National Institute of Technology Karnataka, Surathkal, Mangalore 575025, India. Email: harishjarkala@gmail.com

Abstract: In the present study we report the production of laccase by an unidentified basidiomycetous fungus F-35b in liquid culture conditions. The isolate F-35b showed laccase activity of 2360.4 U/l in the defined liquid medium on 8th day of incubation period. Temperature 30°C and a pH of 8.0 were found to be the optimum for laccase production. The influence of different carbon sources, nitrogen sources and inducers were tested for the production of the enzyme. Production of laccase was enhanced when glycerol, xylan and sodium gluconate were used as carbon sources. The strain showed enzyme activity of 5633.33 U/l using Sodium gluconate. Organic nitrogen sources like peptone and yeast extract enhanced the laccase production. Enzyme activity of 7158.33 U/l was obtained using peptone. However, there was no much enhancement in the enzyme titer when inorganic nitrogen sources were used in the medium. Among the inducers, 2,5 xylidine and ferulic acid enhanced the laccase activity of the fungus.

Keywords*: Laccase, Basidiomycete, 2,5-xylidine, Sodium gluconate, ferulic acid, Xylan.*

Introduction

Laccase(benzenediol:oxygen oxidoreductase, EC 1.10.3.2) belongs to the small group of enzymes called the blue multi copper oxidases. Laccase is widely distributed in higher plants and fungi. In fungi, laccase is present in Ascomycetes, Deuteromycetes, Basidiomycetes and is particularly abundant in many white-rot fungi that degrade lignin. Laccases have been subject of intensive research in the last decades due to their broad substrate specificity (Shraddha R et al. 2011).

Laccases find wide commercial applications due their broad substrate specificity. Such applications include the detoxification of industrial effluents, mostly from the paper and pulp, textile and petrochemical industries, polymer synthesis, bioremediation of contaminated soils, wine and beverage stabilization. Laccases are also used as catalysts for the manufacture of anti-cancer drugs and even as ingredients in cosmetics. Recently, the utility of laccases has also been applied to nanobiotechnology (Gianfreda et al.,1999, Couto and Herrera, 2006, Desai and Nityananda,2011).

Most of laccases reported thus far are of fungal origin, especially from white rot fungi such as *Phlebia radiata, Pleurotus ostreatus and Tramates versicolor*. Many of the *Trichoderma* species extensively studied as sources of cellulases have been also reported as sources of laccases*. T.atroviride, T. longibrachiatum, T. harzanium* are some of those *Trichoderma sp*. studied as laccase sources. Beside these, *Phanerochaete chrysosporium, Theliophora terrstrus, Stereum ostrea, Lenzitis betulina and Pycnoporus species* are some of the important basidiomycetes which have been reported as the sources of laccases (Desai and Nityananda, 2011)

In the present study, a basidiomycetous fungus, was isolated and studied for its laccase production. The effects of pH, temperature, various sources of carbon and nitrogen and inducers were evaluated on the production of laccase.

Materials and Methods

Isolation, Screening and Production of laccase

The fungus was isolated from the decaying wood source from a village forest of (Mangalore) Karnataka. 2% malt extract agar (MEA) was used for the isolation. The fungus was then screened for its laccase production on solid agar media containing guaiacol as an indicator (Reddy B. R. et al. 2008). Laccase positive reaction was observed based on the visualization of brown zones in the plates due to the oxidative polymerization of guaiacol by the laccase.

The production of laccase by the isolate was further confirmed in the defined liquid medium. A slightly modified LMM medium (Dhouib A. et al. 2005) was used for this study. Composition of medium were (g/l): glucose(10.0), ammonium tartarate(2.0), KH_2PO_4(1.0), $MgSO_4.7H_2O$(0.5), KCl(0.5), yeast extract(1.0), $CuSO_4.5H_2O$(150µM), and 10mg/l of trace elements containing per litre of distilled water: EDTA(0.5g), $FeSO_4$(0.2g),$ZnSO_4.7H_2O$(0.01g),$MnCl_2.4H_2O$ (0.003g), H_3BO_4(0.03g), $CoCl_2.6H_2O$(0.02g), $CuCl_2.2H_2O$(0.001g),$Na_2MoO_4.2H_2O$(0.003g). Four mycelial agar plugs (of 7mm dia) from actively growing colony were used to inoculate 15ml of medium in 100ml Erlenmeyer flasks. The flasks were incubated at 30°C on a rotary shaker (150 rpm). The flasks were withdrawn in duplicates at an interval of every two days till fourteen days for the measurement of enzyme activities and biomass.

Effect of temperature and pH

Fifteen milliliters of modified LMM medium was dispensed into 100ml Erlenmeyer flask and sterilized, inoculated with four 7mm agar disc plugs of the white-rot fungus and incubated at 23°C to 37°C for 8 days.

To study the Influence of pH, fifteen milliliters of the LMM medium was dispensed into 100ml Erlenmeyer flask and pH adjusted by using 0.1N HCl and 0.1N NaOH to 4.0, 5.0, 6.0, 7.0, 8.0, 9.0 and sterilized (Adejoye O.D. et al.2009), then inoculated with four 7mm agar discs of the fungus and incubated at 30°C for 8 days. Thereafter, the culture mycelium was harvested and the mycelium free filtrate was used to determine laccase activity.

Influence of medium components

Carbon and nitrogen sources

The influence of different carbon and nitrogen sources was studied by one-factor-at-a-time method. The LMM medium was supplemented by replacing glucose with other carbon sources such as glycerol, carboxymethyl cellulose, mannitol, lactose, cellobiose, sodium gluconate, xylan and sucrose. Different nitrogen sources such as inorganic (sodium nitrate, ammonium nitrate, ammonium chloride and the nitrogen source of original medium), and organic (yeast extract, peptone, asparagine and urea) were employed to select the best nitrogen source. In these experiments, the initial yeast extract was eliminated from the LMM medium.

Inducers

Inducers like cuprous sulphate, Phenol red, guaiacol, gallic acid, veratryl alcohol, 2,5-xylidine, ferulic acid, ethanol were tested for their ability to enhance laccase enzyme production. The original LMM medium was supplemented with above said inducers at a concentration of 1mM and flasks were incubated in similar growth conditions.

Analytical methods

Laccase assay

Laccase activities were measured spectrophotometrically (GBC) using 2,2'-azino-bis(3-ethylbenzthiazoline-6-sulphonic acid (ABTS) (Sigma) as a substrate with an absorbance coefficient value of 36000/M/cm at 420nm. One unit (U) of laccase activity was defined as the amount of enzyme catalyzing the production of one micromole of colored product per min per ml (Tian X. et al. 2008).

Results and Discussion

In the present study, a pure culture of a fungus F-35b was isolated from a decaying wood substrate. The isolate, when grown on solid screening medium containing guaiacol, developed a brown color zone. This is due to the polymerization of guaiacol in the

presence of extracellular fungal laccase, which is the characteristic of phenol oxidation in the solid media (Fig.1).
Shake flask studies on laccase production profile in laccase basal medium (LMM) showed that the isolate F-35b produced appreciable amounts of laccase extracellularly. Maximum production of laccase activity of 2360.42 U/l was reported on 8th day (Fig. 2).

Effect of Incubation temperature and medium pH

Temperature showed significant effect on extracellular laccase activity of F-35b. An increase in the temperature from 25°C to 30°C increased the laccase activity and further increment in temperature up to 37°C reduced the laccase production. Highest Laccase activity of 2162.33 U/l was observed at 30°C (Fig.4). Increase in laccase yield was observed form 4.0 to 8.0. Further increase in pH reduced the laccase activity (Fig.3). The highest laccase activity of 4612.5 U/l was observed at pH 8. Similar observations were made by Gbolagade et al. (2006) on *Pleurotus florida* and by Adejoy et al. (2009) in Nigerian edible mushroom *Schizophyllum commune (fr.)*. Change in pH may alter the three –dimensional structure of the enzymes (Pointing S.B. et al. 2005). For these reasons, enzymes are known to be active over a certain pH range.

Influence of medium components

Among the different carbon sources tested, sodium gluconate resulted in very high production of the enzyme with activity of 5633.33 U/l on 10th day after inoculation. Glycerol and Xylan resulted in 3914.6 U/l (4th day) and 2729.17 U/l (6th day) respectively. Sucrose resulted in 3541.67 U/l on 8th day after inoculation. Carbon sources like lactose, carboxymethyl cellulose and cellobiose resulted in only moderate production of the enzyme, while mannitol was not efficiently used for laccase production by F-35b (Fig. 5). Many previous investigations on different fungi also support our findings that, the presence of specific C source increases the laccase titre (Adejoye, O.D. et al. 2009, Couto S.R. et al. 2006), Niku-Paavola et al. 1990, Shraddha R. et al. 2011).

Another factor reported to be essential for efficient laccase production is the nature of the nitrogen sources for fungal cultivation (Eggert C. et al. 1996, Kaal et al. 1995). Figure 6 shows the results of influence of nitrogen sources on laccase production by F-35b. Among the nitrogen sources used in the study, Peptone and yeast extract amended medium resulted in high production of laccase with activities of 6135.42 U/l and 4537.5 U/l respectively on 8th day after inoculation. An increasing production was found in both the cases till the 14th day. Urea resulted in reduced production of laccase. However, compared to the organic nitrogen sources, inorganic nitrogen sources, when used as the sole nitrogen source were not efficiently used for the production of laccase by F-35b. Among the inorganic nitrogen sources tested, sodium nitrate resulted in a relatively high production of laccase with an activity of 3287.5 U/l on 14th day after inoculation. Ammonium nitrate and ammonium chloride reduced both growth and production of laccase in F-35b. Saravanakumar et. al (2010) also observed that laccase production was enhanced in the presence of organic nitrogen source in *Pleurotus species.*, Higuchi (1990), Cullen (1997) reported Laccase and other ligninolytic enzyme activity increased due to carbon and organic nitrogen. The role of these compounds in the regulation of enzyme synthesis depends not only on the physiology of the tested fungi but also the medium composition (Couto and Herrera, 2006).

Different inducers were tested for their ability to enhance laccase production in F-35b. The dynamics of laccase biosynthesis by F-35b in the presence of the inducers is shown in figure 7. It was found that phenol red and gallic acid did not exhibit any inducing effect on the production of laccase by F-35b. On the other hand 2,5- xylidine and ferulic acid in the media increased the production of laccase. 2,5- xylidine increased laccase production to 1328.08 U/l while ferulic acid increased the production to

1399.23 U/l on the 4th day after inoculation. In the basal media having no such inducer the organism produced only 453U/l of laccase activity in 4th day. Hence there was approximate three-fold increase in the laccase titre was observed when the basal medium was supplemented with either 2,5-xylidine or ferulic acid. Increase in copper sulphate concentration in the medium to 0.5 g/l drastically reduced the growth and laccase production in F-35b. According to the literature, the amount of copper required to enhance laccase production varies greatly among fungi—generally within the range 0.003–40µg Cu/ml. Converse to our results, there are also reports that higher concentrations (5 mM CuSO4 or 320µg Cu/ml) effectively stimulate laccase synthesis (Dhouib A. et al. (2005). Tavares et al. (2005)], established the significance of induction on *T.versicolor* culture for laccase production using $CuSO_4$ and 2,5-xylidine as inducers. Palvannan and Sathishkumar (2008), found that copper sulfate induced the production of laccase in *P.flourida* NCIM 1243.

Conclusion

The present study reveals that the fungal isolate F-35b is a potential laccase producer. The isolate produces high titer of the enzyme at high pH value around 8 and temperature of 30°C. Production of the enzyme was further influenced by the carbon and nitrogen sources as well as the inducers used. However, further optimization is to be carried out to enhance laccase production by F-35b. Laccase, thus produced can be used for several biotechnological applications.

References

[1] Adejoye, O D and Fasid, O I (2009), Effect of cultural conditions on biomass and laccase production in submerged medium by *schizophyllum commune* (fr.), a Nigerian edible mushroom, EJEAFChe, Vol. 8, No. 11, pp. 1186-1193.

[2] Barbosa, A M et al (2007), Influence of nutrients on enhancing laccase production by *Botryospaheria rhodina* MAMB-05, J. Int. Micrbiol., Vol. 10, pp. 177-185.

[3] Couto S R. and Herrera J L T (2006), Industrial and biotechnological applications of laccases: A review, Biotechnology Advances, Vol. 24, pp. 500–513.

[4] Desai S S and Nityananda C (2011), Microbial Laccases and their applications: A review, Asian Journal of Biotechnology, Vol. 2, No. 3, pp. 98-124.

[5] Dhouib A et al (2005), Autochthonous fungal strains with high ligninolytic activities from Tunisian biotopes. Afr. J. Biotechnol., Vol. 4, No. 5, pp. 431-436.

[6] Eggert, C U Temp and Eriksson K E L (1996), The ligninolytic system of the white rot fungus *Pycnoporus cinnabarinus*, purification and characterization of the laccase, Appl. Environ. Microbiol., Vol. 62, pp. 1151-1158.

[7] Galhaup C and Haltrich D (2001), Enhanced formation of laccase activity by the white rot fungus *Trametes pubescens* in the presence of copper, Appl Microbiol Biotechnol, Vol.56, No.2, pp.225–232.

[8] Gbolagade J et al (2006), Optimization of submerged culture conditions for biomass production in *Pleurotus florida*, a Nigerian fungus, Afr. J. Biotech. Vol. 5, No. 16, pp. 1464-1469.

[9] Gianfreda L et al (1999), Laccases: a useful group of oxidoreductive enzymes, Bioremediation Journal, Vol.3, No.1, pp. 1–25.

[10] Golovlevaa L A et al (2008), New efficient producers of fungal laccases, Appl Biochem Microbiol, Vol. 44, No. 1, pp.73–77.

[11] Higuchi, T (1990), Lignin biochemistry: biosynthesis and biodegradation, Wood Sci Technol, Vol. 24, pp. 23–63.

[12] Niku-Paavola, M L et al (1990), The effect of culture conditions on the production of lignin modifying enzymes by the white rot fungus *Phlebia radiate*. J.Biotechnol, Vol. 13, pp. 211-221.

[13] Palvannan, T and Sathishkumar P (2010), Production of laccase from *Pleurotus florida* NCIM 1243 using Plackett–Burman Design and Response Surface Methodology, Journal of Basic Microbiology 2010, Vol. 50, pp. 1–11.

[14] Pointing, S B et al (2005), Screening of basidiomycetes and xylariaceous fungi for lignin peroxidase and laccase gene-specific sequences, Mycol. Res. 109:115-124.

[15] Reddy B R et al (2008), Screening and assessment of laccase producing fungi isolated from different environmental samples. Afr. J. Biotechno, Vol.7, No. 8, pp. 1129-1133.

[16] Reddy, B R et al (2008), Screening and assessment of laccase producing fungi isolated from different environmental samples. Afr. J. Biotechno., Vol. 7, No. 8, pp. 1129-1133.

[17] Shraddha, R et al (2011), Laccase: Microbial Sources, Production, Purification, and Potential Biotechnological Applications, Enzyme Research. Article ID 217861, pp. 1-11.

[18] Tavares, A P M et al (2006), Optimization and modeling of laccase production by *Trametes versicolor* in a bioreactor using statistical experimental design, Appl. Biochem. Biotech., Vol. 134, No. 3, pp.233-248.

[19] Thurston C F (1994), The structure and function of fungal laccases, Microbiology, Vol.140, No.1, pp.19–26.

[20] Tian X et al (2008), comparative study on the determination assay for laccase of *Tramates* sp., *Afr. J. Biochem. Res*., Vol.2, No. 8, pp. 181-183.

FIGURES and TABLES

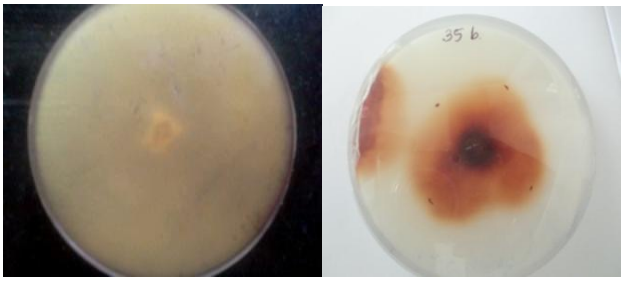


Fig.1. Photograph showing the oxidative polymerization of guaiacol to form reddish brown zones in the media. The plate on the left side is the 'control' without indicator, and plate on the right side is the 'test' with indicator.

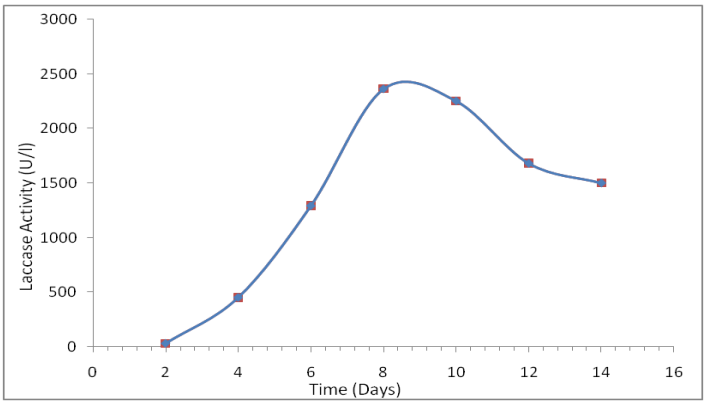


Fig.2. Time course of laccase activity of F-35b in liquid culture. Data points represent the means of two replicates.

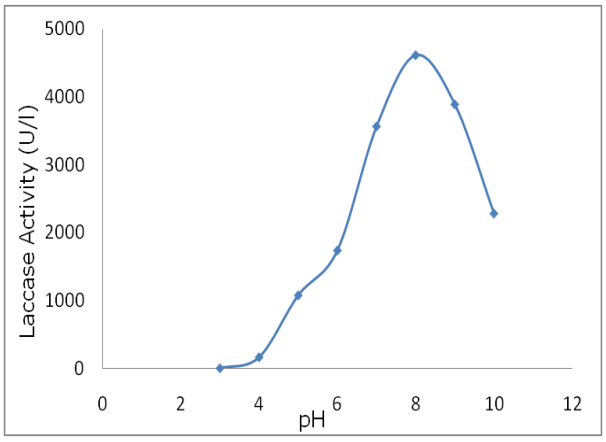


Fig.3. Effect of different medium pH on laccase production by F-35b

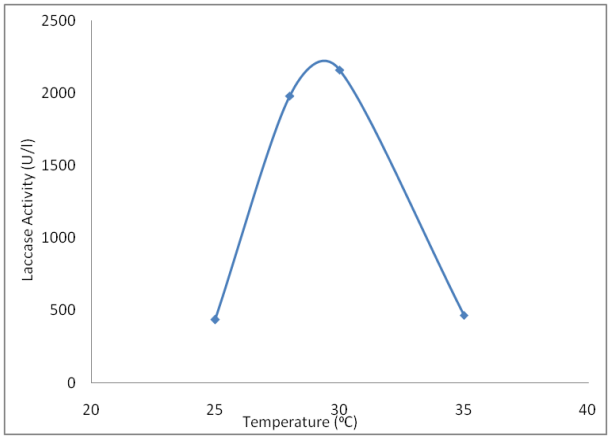


Fig.4. Effect of incubation temperature on laccase production by F-35b

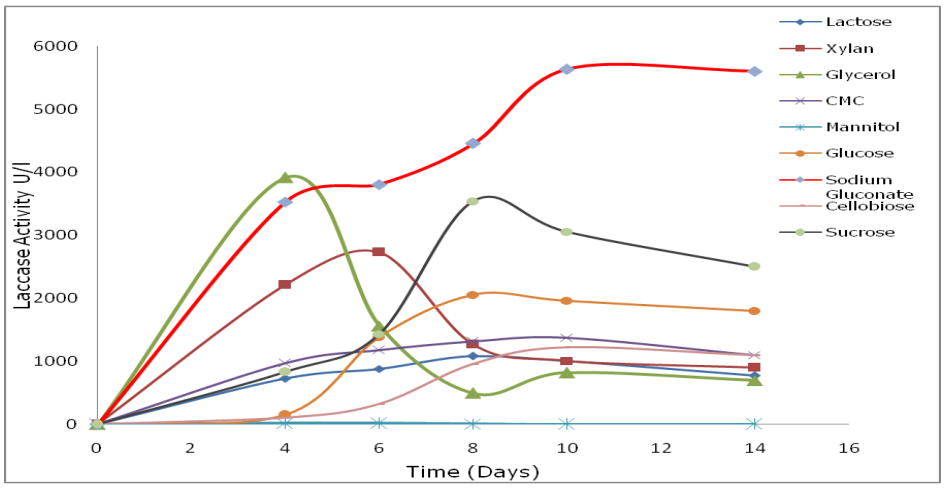


Fig.5. Influence of Carbon sources on production of laccase by F-35b. Data points represent the means of two replicates.

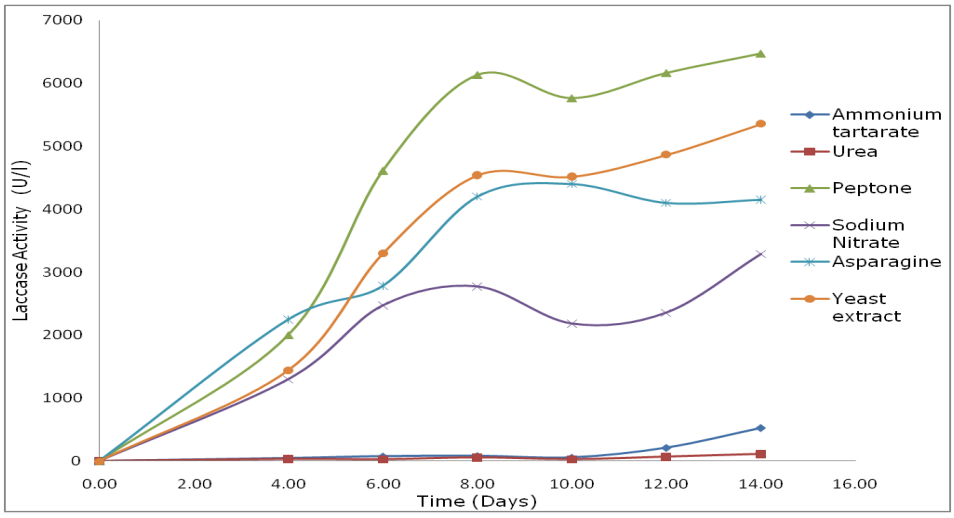


Fig.6. Influence of Nitrogen sources on production of laccase by F-35b. Data points represent the means of two replicates.

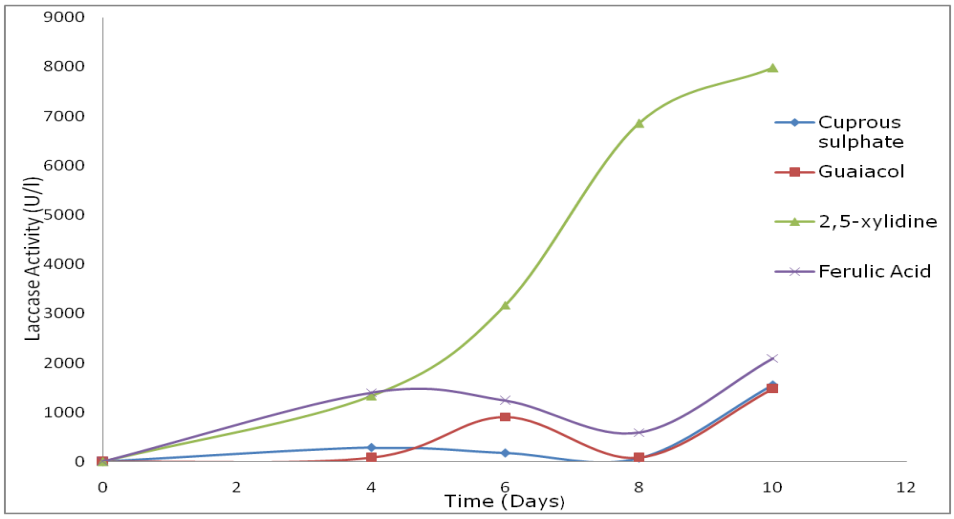


Fig.7. Influence of different inducers on production of laccase by F-35b. Data points represent the means of two replicates.

2nd International Engineering Symposium - IES 2012
(KU-MU-NITK-HCMCUT Joint Symposium) March 5-7, 2012, Kumamoto University, Japan

Detoxification of Phorbol esters from Jatropha Seed Cake by White Rot Fungi

Sampath S Muddada, Ramesh Ramanujam, Chaitanya Kilaparthi, Harisha Poojary and Gopal Mugeraya

Department of Chemical Engineering, National Institute of Technology, Karnataka, Surathkal, Mangalore 575025, India. Email : muddada.ss@gmail.com

Abstract: Jatropha is a small shrub plant which grows wildly in the tropics and sub-tropics. The seeds of the Jatropha plants are the major source of biodiesel fuel currently being used in India, Thailand, and other Southeast Asian countries. The production of bio-diesel from *Jatropha carcus* seeds yields to a large amount of seed cake which is generated as by-product. The cake was found to be a good source of proteins and other nutrients. However, in addition to this, the cake also contains various ant-nutrients which if properly processed could be used to replace most conventional feedstuffs. One of the major toxic substances present in the cake is phorbol esters which restricts its utilization as livestock feed. The safe or meaningful disposal and utilization of this major by-product necessitates the degradation of these phorbol esters. Most of the toxins can be removed either by chemical or physical methods while phorbolester is the most difficult toxin to be detoxified by these methods. Hence biological methods are found useful in detoxifying phorbol esters. In the present study we describe the degradation of phorbol esters by five different types of white rot fungi namely; *Peniophora sp hpF-04*, *Phellinus noxius hpF-17*, *Phanerochatae chrysoporium,* unknown isolates *F-16* and *F-35.* The detoxification was done by solid state fermentation process and the analysis of phorbol esters were carried out by HPLC methods. It was found that all the fungi used in the study were able to detoxify the phorbol esters.

***Keywords**:* Phorbol esters, white rot fungi, Jatropha, Solid state fermentation, HPLC.

Introduction

Jatropha is a tough woody plant that can grow in arid conditions unsuitable for most food crops. Its seeds are poisonous and produce oil that's unfit for human consumption but can be converted to biodiesel fuel. In 2007 Goldman Sachs cited Jatropha curcas as one of the best candidates for future biodiesel production. It is resistant to drought and pests, and produces seeds containing 27-40% oil, averaging 34.4% (Rakshit et al., 2008). Currently the oil from Jatropha curcas seeds is used for making biodiesel fuel in Philippines and in Brazil, where it grows naturally and in plantations in the Southeast, and the North/Northeast Brazil. Likewise, Jatropha oil is being promoted as an easily grown bio-fuel crop in hundreds of projects throughout India and other developing countries.

Jatropha seeds generate large quantum of residual de-oiled seed cake with an average rate of 500gm cake per Kg of seed used, while the oil is an excellent bio-diesel feedstock. The average chemical composition of de-oiled seed cake is; protein(60%), fat (0.6%), ash (9%), fibre (4%) and carbohydrates (26%) (Belewu et al.,2010). However, deoiled *Jatropha carcus* seed cake cannot be used as animal feedstock, due to the presence of various anti-nutrients such as trypsin inhibitor, lectin, tannins, saponins, phytate and phorbol esters. All these anti-nutrients but except phorbol esters can be removed either by chemical or physical methods (Joshi et al.,2011). The complex structure of phorbol esters cannot be digested by

animal digestion system which restricts its use as feed for animals. However, if it is left to decay as such will create environmental problems (Ahmed and Salimon, 2009).

Removal of phorbol esters is currently an important issue to be addressed. Various methods (physical, mechanical and chemical) of detoxification are well documented in literature (Aderibigbe *et al.,* 1997 Makkar and Becker, 1999). However, the biological method (Cocktail of fungi) of detoxification is still at its infancy except for the reports of some workers (Peace and Aladesanmi, 2008, Belewu *et al* 2010) who used different fungi for the fermentation of Jatropha cake. These authors noted increased crude protein content and reduction of the fibre content of the inoculated samples while some anti-nutritional factors were removed/reduced in the inoculated samples.

Hence, in the presence study, we evaluated the efficacy of five basidiomycetous fungi for detoxification of phorbol esters (PE) present in Jatropha seed cake kernel by using solid state fermentation (SSF).

Materials and methods

Isolation of organisms

Five fungi used in this study were *Peniophora sp hpF-04, Phellinus noxius hpF17, Unknown-F16, Unknown-F35, Phanerochatae chrysosporium NCIM 1090.* Four Fungi obtained from the laboratory of Chemical Engineering, NITK, Surathkal, which were isolated from the decaying wood source. *Phanerochatae chrysosporium* was procured from NCIM, Pune.

Sub-culturing of the fungi

Sub-culturing of the fungus was carried out using 2% malt extract agar. The medium was prepared, autoclaved and poured to sterile Petri plates. The mycelium of the respective fungi was placed on to the solid agar media and the plates were incubated for 6-7 days at 30^{o}C in dark. The cultures were refrigerated at 4^{o}C until they are used.

De-oiling of *Jatropha carcus* seeds:

The seed kernels were finely powdered using motor and pestle. A known amount of powdered kernel was taken in a 100ml beaker and sufficient amount of petroleum ether was added. The solution is mixed well and placed in an electrical Oven maintained at 40-60^{o}C for 30 minutes for the removal of oil. The process is called defatting. After 30 minutes the solution is taken and defatted cake is separated from the oil using a muslin cloth (Joshi et al., 2011).

Acclimatization of the fungi: To check the ability of the organisms to grow in the presence of phorbol esters of *Jatropha carcus* seed kernel was checked by growing the fungi in malt extract agar media supplemented with 1% de-oiled Jatropha cake kernel. This process also acclimatizes the organism to grow in the presence of phorbol esters of Jatropha cake kernel. Agar plugs of 9mm from the actively growing mycelia of the respective malt extract plates were taken and inoculated on to plates containing acclimatized media. The plates were incubated for 6-7 days at 30^{o}C in dark. The fungal culture from these plates was used to inoculate the solid substrates.

Detoxification of *Jatropha carcus* kernel seed

Detoxification of phorbol esters was carried out by under solid state fermentation process. 10g of the de-oiled cake was taken in 100ml Erlyn-Meyer flasks. The flasks were autoclaved and labeled accordingly with fungi to be inoculated. The respective inoculum was prepared by homogenizing 10 agar plugs from acclimatizing agar plates in 50ml of malt extract broth and 5ml of the homogenized culture was used to inoculate the flasks. The flasks were incubated at 30^{o}C in incubator for 15 days. Six flasks were maintained for each of the organism and flasks were removed on 7th day, 11th day and 15th day in duplicates. The phorbol esters were extracted from these

flasks. A control was maintained in the same condition without the fungus.

Extraction of phorbol esters

The phorbol esters from unfermented and fermented *J.carcus* seed cake were extracted using methanol as described by Joshi et al. (2011). To the content of the flask sufficient amount of methanol was added and the flasks were kept in an orbital shaker at 200 rpm for 5-10 minutes. The mixture was then transferred to centrifuge tubes and centrifuged at 6000 rpm for 20 minutes to separate the solid mass. The clear supernatant was collected into clean storage vials for HPLC analysis.

Determination of phorbol esters:

The phorbol ester contents of the fermented and unfermented flasks were analyzed and quantified using HPLC equipped with UV detector. A reverse phase C18 column [5um particle size, 4.6X250 mm i.d] was used in the present study. The solvents used were: water and acetonitrile with 20% water (A) and 80% acetonitrile (B). The column was initially washed with distilled water. Separation was performed at room temperature (25^{o} C) with a flow rate 1.3 ml/min. The eluted peak was monitored at wavelength of 275nm. The percentage of degradation was calculated by comparing the peak area of the fermented samples with that of the control by using following formula (Joshi et al., 2011).

% degradation of PE = R= $(p_c - p_t)*100/p_c$
Where p_c is the phorbol ester in the control, P_t is the phorbol ester of the tested.

Results and discussions

In the present study, detoxification of phorbol esters from *Jatropha carcus* seeds were carried out by using five different fungi belonging to the group of basidiomycetes (Fig.1). These fungi are generally regarded as 'mushrooms'. Most of these fungi produce complex set of extra cellular enzymes capable of degrading lignin, a complex bio-polymer present in wood. The enzymes are also referred to as ligninolytic enzymes which are highly non specific and have the ability to degrade most of the hazardous chemicals including, complex hydro carbons, pesticides, dyes, poly-phenols, esters etc. Hence, these fungi were selected for detoxification of phorbol esters in the present study.

In the presence of de-oiled cake, in solid pates all the fungi showed very good growth. The fungi started growing within second day incubation at 30^{o}C. These observations show that the fungi have the ability to grow on de-oiled cake by using it as a substrate.

In the solid state substrate, no other media components were provided but still organism showed the growth. The growth of the organism started within second day and continued till 14 days. Among the five fungi, the fungi *Phellinus noxius hpF17* and *Peniophora hpF04* showed highest mycelial growth than others. It was found the fungi hpF16 was slow growing in the presence of cake.

Phorbol esters of the flasks were extracted through methanol after 15 days of SSF. The phorbol esters were then quantified using HPLC. The peak eluted at 1.13 minutes was considered as ester peak as the same peak was observed in the case of control sample. The splitting and decrease in area of the peak was observed with the incubation days which confirms the degradation of the phorbol esters. However, in the control sample no such behaviour was observed. The amount of phorbol esters were quantified based on the peak area. The detoxification was then measured based on the decrease in area/or absence of peaks at that retention time. Although internal standard used, it was not detected and separated through the present HPLC operating system (fig.2).

Maximum percent of detoxification was achieved on the case *hpF-35*, an unknown isolate where the phorbol esters were completely detoxified on day 15th. *P.chrysoporium* showed almost complete detoxification of 99.98% within similar

days of incubation period (table.1). Next to these *P.noxius hpF 17* showed detoxification of about 93.64% on 15th day. *Peniophora hpF04* also showed 89.50% of detoxification. In the case of unknown *F16* very low levels of detoxification of 54.06 % was observed. However, it was found from the study that all the fungi were unable to detoxify the phorbol esters completely in 7 days of incubation period. Hence further optimization studies are required to fasten the detoxifying process and also to study the reaction mechanisms involved in the detoxification process.

Development of bioprocesses for bioremediation and biological detoxification of agro-industrial residues has been the main focus of SSF research in current years (Joshi et al.,2011). SSF has been useful in eliminating/reducing saponin from whole soybean tempe by Rhizopus oligosporus(Fenwick and Oakenfull, 1983); hydrogen cyanide from cassava peel by *Rhizopus sp*. (Ofuya and Obilor, 1994); caffeine and tannins from coffee husk by *Aspergillus sp*. (Brand et al., 2000); phytic acid from rapeseed meal by *Aspergillus niger* (El-Batal and Karem, 2001); gossypol from cotton seed by *Candida tropicalis* (Zhang et al., 2006) and tannin from creosotebush by *Aspergillus niger* (Belmares et al., 2009) aoxification from Jatropha cake kernael using *Pseudomonas aeruginosa* Pse (Joshi et al.,2011).

Conclusion

The study reveals that the fungi used are able to detoxify the phorbol esters present in the Jatropha seed cake. It could be concluded that incubation of Jatropha curcas kernel cake with white rot fungi is promising as it reduced the phorbol ester contents of the cake significantly so as to make a renewable feedstuff for livestock animals.

References

[1] Ahmed and Salimon (2009), Phorbol Ester as Toxic Constituents of Tropical *Jatropha Curcas* Seed Oil, European Journal of Scientific Research,Vol.31, No.3, pp.429-436.

[2] Belew M A and Belewu K Y (2005), Cultivation of Mushroom (*Volvariella volvacea)* on Banana leaves, Afr Journal of Biotechnol, Vol.4 No.12,pp. 1401-140

[3] Belewu M A et al (2006), Potential application of fungal biotechnology on the nutritional evaluation of Saw dust- Gliricidia mixture by rat, Research. J. Biotech., vol. 1, No. 2, pp.36-39.

[4] Belewu M A et al (2010), Response of Goat to Fungi (*Rhizopus oligosporus, Rhizopus nigrican*) treated *Jatropha curcas* kernel cake, Archives of Applied Science Research,Vol. 2, No.4, pp. 255-261.

[5] Belmares R et al (2009), Composition and fungal degradation of tannins present in semiarid plants, E.J.E.A.F.Che., Vol. 8, No.2, pp.312–318.

[6] Brand D et al (2000), Biological detoxification of coffee husk by filamentous fungi using a solid state fermentation system, Enzyme Microb. Technol.,Vol. 27,pp. 127–13.

[7] El-Batal A I and Karem, H A (2001), Phytase production and phytic acid reduction in rapeseed meal by *Aspergillus niger* during solid state fermentation, Food Res. Int., Vol.34, pp.715–720.

[8] Fenwick D E and Oakenfull D (1983), Saponin content of soybeans and some prepared foods, J. Sci. Food Agric., Vol. 32, pp.273–278.

[9] Joshi C et al (2011), Degradation of phorbol esters by *Pseudomonas aeruginosa* PseA during solid-state fermentation of deoiled *Jatropha curcas* seed cake, Bioresource Technology, Vol 102, pp. 4815–4819.

[10] Makkar et al (1997), Studies on Nutritive Potential and Toxic Constituents of Different Provenances of *Jatropha curcas*, Journal of Agriculture Food Chemistry, vol.45,pp. 3152-3157.

[11] Makkar, et al (2009), Removal and degradation of Phorbol esters during pre-treatment and transesterification of *Jatropha curcas* oil, J. Am. Oil Chem. Soc., Vol. 86, No.1, pp. 173–181.

[12] Ofuya C O and Obilor S N (1994) The effects of solid-state fermentation on the toxic components of cassava peel, Process Biochem., Vol. 29, No.3, pp. 25–28.

[13] Rakshit, K D et al (2007), Extraction, Transesterification and Process Control in Biodiesel in the diet of Lactating Goat, Pakistan J. Nutrition,Vol. 9, No.3, pp.284-286.

[14] Zhang W et al (2006), Optimization of process parameters for reduction of gossypol levels in cottonseed meal by *Candida tropicalis* ZD-3 during solid substrate fermentation. Toxicon., Vol 48, pp.221–226.

Figures and tables



Fig.1. Growth of the fungi in MEA plates

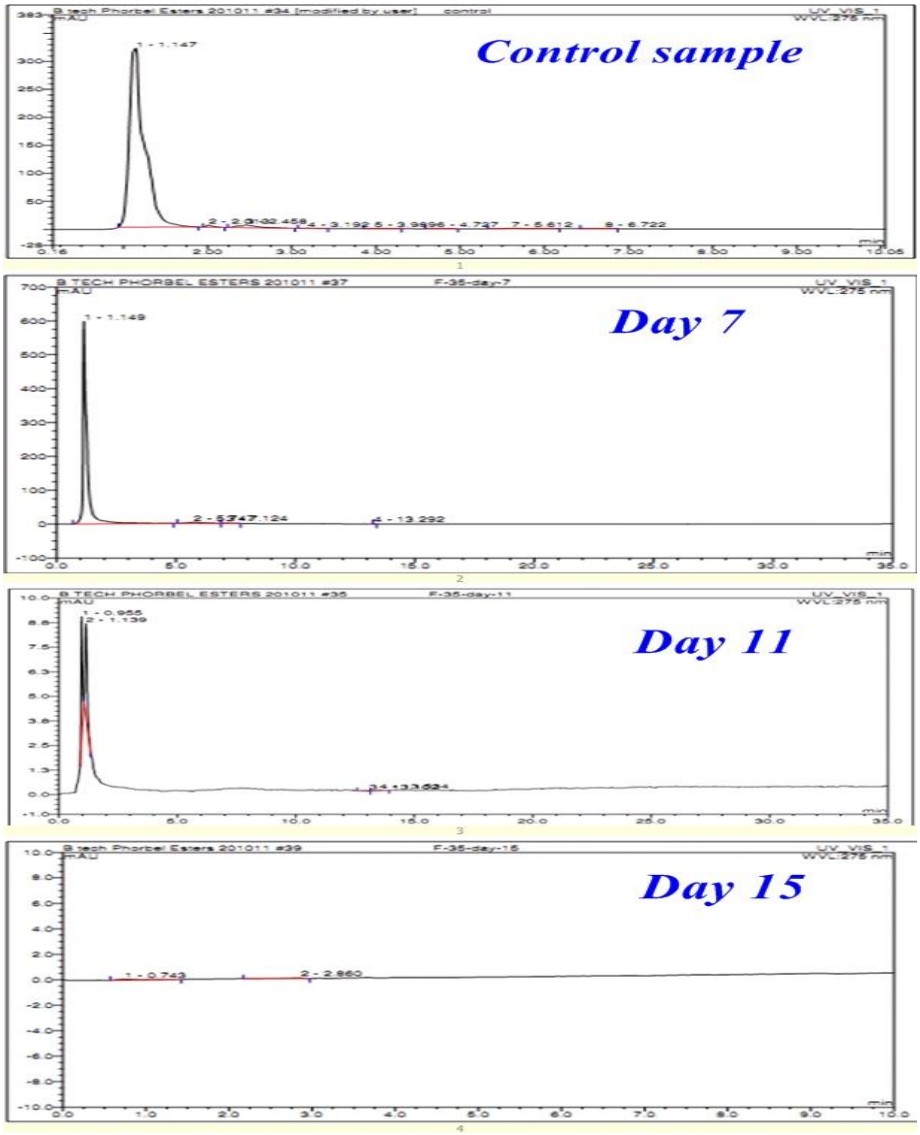


Fig.2. HPLC chromatogram of the Jatropa seed cake treated with the fungus-*Unknown* hpF35. The Control sample is untreated cake without fungal inoculation. Day 7, day 11 and day15 represents the incubation days at which samples were withdrawn from solid state fermentation for HPLC analysis.

Table.1. Percentage degradation of phorbol esters through HPLC studies

Fungi	Incubation days	Area (mAU*min/g)	Area difference (mAU*min/g) (Control-control)	% Degradation
CONTROL		825.15	--	--
Peniophora sp hpF04	7	816.51	8.64	1.049
	11	247.605	577.545	69.99
	15	86.594	768.556	89.50
Phellinus noxius hpF17	7	623.44	201.71	24.44
	11	67.512	757.638	91.8
	15	52.44	772.71	93.64
Unknown-F35	7	548.37	276.8	66.4
	11	233.68	591.47	71.66
	15	0	825.15	100.00
P. chrysoporium	7	500.9	324.25	39.29
	11	304.47	520.68	63.10
	15	0.16	824.99	99.98
Unknown-F16	7	742.11	83.04	10.06
	11	643.779	181.37	21.98
	15	454.03	371.51	54.06


2nd INTERNATIONAL ENGINEERING SYMPOSIUM
– IES2012
(KU-MIT-NITK-HCMCUT Joint Symposium)
MANIPAL